THE INFLUENCE OF DEPOSITIONAL ENVIRONMENT AND DOLERITE INTRUSIONS ON THE QUALITY OF COAL

A Study of the Twistdraai Mine Area
near Secunda, Southeastern Transvaal

by

Harald Hermann Bernd Hagelskamp

Submitted in partial fulfilment of the requirements

of the degree of

DOCTOR SCIENTIAE

in the

Faculty of Science of the

University of Pretoria

Pretoria

December 1987

Digitised by the Department of Library Services in support of open access to information, University of Pretoria, 2021.

I, Harald Hermann Bernd Hagelskamp, hereby declare that this thesis is my own original work, that all assistance and sources of information have been acknowledged, and that this work has not been presented to any other university for the purpose of obtaining a higher degree.



Digitised by the Department of Library Services in support of open access to information, University of Pretoria, 2021.

ABSTRACT

The objective of the present study is to establish the influence of syngenetic (sedimentary environment) and of epigenetic (dolerite intrusions) factors on the quality of coal. The effect of dolerite intrusions is investigated in order to develop a prediction method for the location of such dykes and sills within the seam. Both factors are dealt with separately, but their respective impacts on the exploration and mining phases of a coalfield are compared.

The sedimentary environment was established by identifying and describing eight vertically successive lithofacies associations. They are each laterally continuous and represent a certain depositional phase throughout the study area. These are related to sedimentary processes, from which a three-dimensional paleoenvironmental model is derived. Subsequently coal distribution and quality parameters are linked to the depositional features of the model.

The identified depositional phases commenced with subglacial, glaciofluvial and glaciolacustrine settings, with associated Gilbert-type deltas. These are followed by meandering and minor braided fluvial settings, characterized by laterally and vertically highly variable lithofacies, in which the main coal-bearing strata were formed.

Coal distribution and quality parameters (ash, volatile matter and calorific value) are closely related to paleoenvironmental characteristics. Major changes of coal distribution and quality parameters are mainly associated with active and abandoned channels and these properties are less variable in floodplain settings.

The effect of dolerite intrusions on the quality of coal is investigated by analysing a series of coal samples, which were taken at certain distance intervals from a dyke/coal contact. The analytical procedures include maceral analysis, vitrinite reflectivity measurements, proximate analysis, ultimate analysis and inorganic geochemistry of the coals and dolerites by means of XRF spectrometry.

The lateral extent of metamorphic affects of the dolerite intrusions on the parameters of the coal are largely restricted to the width of the visually distinguishable contact aureole. Petrographic composition mainly changes due to the formation of natural coke; ultimate and proximate analysis results are primarily dependent on the petrographic composition of the unaltered coals. With increasing metamorphism they change in accordance with the rank increase and corresponding loss of volatile matter in the coals. Major and trace element concentrations become more variable with decreasing distance from an intrusion; however, little significant depletion or enrichment tendencies are noticeable. Metasomatic processes are most probably limited to an increased formation of carbonates in the cindered coals along the dyke. The vitrinite reflectivity proves to be the most

Digitised by the Department of Library Services in support of open access to information, University of Pretoria, 2021.

sensitive parameter in the search for an anlytical tool for the prediction of intrusions. In apparently unaffected coals a distinct reflectivity gradient is discernible from bottom to top of the seam. This gradient becomes enhanced and may even be partially inverted in proximity to an intrusion.

The sedimentary processes are found to be of more regional importance in respect to their impact on the type and grade of a coal. Intrusions only have very localized effects and determine small-scale variations in the rank of the surrounding coals. They necessitate, however, more attention in view of the short and medium-term mine planning.

Digitised by the Department of Library Services in support of open access to information, University of Pretoria, 2021.

UITTREKSEL

Die doel van die huidige studie was om die invloed van singenetiese (sedimentêre omgewing) en epigenetiese (dolerietintrusies) faktore op die gehalte van steenkool vas te stel. Die effek van dolerietintrusies is ondersoek met die doel om 'n voorspellingsmetode te ontwikkel vir die vasstelling van die posisie van gange en plate in 'n steenkoollaag. Hierdie twee faktore word afsonderlik behandel, maar hulle relatieve uitwerking op die eksplorasie- en mynboufases van 'n steenkoolveld word ook vergelyk.

Die sedimentêre omgewing is vasgestel deur agt vertikaal-opeenvolgende litofasiesassosiasies te identifisier en te beskryf. Elkeen van hulle is lateraal standhoudend en verteenwoordig 'n bepaalde fase van afsetting dwarsdeur die studiegebied. Hierdie fases hou verband met sedimentêre prosesse en vorm die basis vir die afleiding van 'n drie-dimensionele paleo-omgewingsmodel. Aansluitend is die steenkoolverspreiding en gehalte-parameters in verband gebring met die afsettingskenmerke van die model.

Die geidentifisierde afsettingsfases het begin in 'n subglasiale, glasiofluviale en glasiolakustriene omgewing met die gepaardgaande Gilbert-deltas. Dit is gevolg deur kronkelstroom- en ondergeskikte vlegstroom-omgewings wat gekenmerk word deur lateraal en vertikaal hoogs veranderlike litofasies waarin die steenkooldraende lae ontstaan het.

Steenkoolverspreiding en gehalte-parameters (as, vlugstofinhoud en verhittingswaarde) toon 'n nou verwantskap met die kenmerke van die paleo-omgewing. Die belangrikste veranderings in steenkoolverspreiding en in gehalte-parameters gaan hoofsaaklik gepaard met aktiewe en verlate stroomkanale; in vloedvlakte-omgewings is hierdie eienskappe minder veranderlik.

Die invloed van dolerietindringings op die gehalte van die steenkool is ondersoek deur die ontleding van 'n reeks steenkoolmonsters op bepaalde afstande vanaf die doleriet-steenkoolkontak. Die analitiese prosedures wat gevolg is, sluit maseraalanalise, reflektiwiteitsmetings op vitriniet, kortanalise, elementanalise en anorganiese geochemie van die steenkool en die doleriet deur middel van XRF-spektrometrie in.

Die laterale verspreiding van die metamorfe invloed van die dolerietintrusies op die steenkooleienskappe is grootliks beperk tot die wydte van die visueel-onderskeibare oureool. Die petrografiese samestelling verander hoofsaaklik as gevolg van die vorming van natuurkooks; die waardes van element- en kortanalises is in die eerste plek afhanklik van die petrografiese samestelling van die onveranderde steenkool. Met toenemende metamorfose verander die element- en kortanalisewaardes in ooreenstemming met die toename in rang en die ooreenstemmende verlies aan vlugstof in die steenkool. Hoof- en

Digitised by the Department of Library Services in support of open access to information, University of Pretoria, 2021.

spoorelementkonsentrasies word meer wisselvallig met vermindering in afstand na die intrusie, maar geen betekenisvolle af- of toenames kan waargeneem word nie. Metasomatiese veranderings is waarskynlik beperk tot karbonaatvorming in die sinterkool langs die gang. Die reflektiwiteit van vitriniet is tot dusver onteenseglik die mees sensitiewe veranderlike wat moontlik gebruik kan word om die aanwesigheid van intrusies te voorspel. Selfs in skynbaar ongeaffekteerde steenkool kan 'n duidelike reflektiwiteitsgradient van die onder- na die bokant van 'n steenkoollaag gesien word. Hierdie gradient word groter, en kan selfs gedeeltelik omkeer, naby die intrusie.

Die sedimentêre prosesse skyn grootliks van regionale belang te wees sover dit die tipe en graad van die steenkool betref. Intrusies het oor die algemeen slegs plaaslike invloed en lei tot klein-skaalse wisselings in die rang van die steenkool. Hulle vereis egter 'n groter mate van aandag met die oog op kort- en mediumtermyn mynbeplanning.

Digitised by the Department of Library Services in support of open access to information, University of Pretoria, 2021.

ACKNOWLEDGEMENTS

The initial suggestion to undertake this study originates from Prof. C.P. Snyman of the Department of Geology, University of Pretoria (UP). He and Dr. P.G. Eriksson (UP) were my supervisors, to whom I am grateful for much helpful advice, discussion and assistance throughout the study.

Financial support for this project was obtained from the National Energy Programme of the CSIR (South African Council of Scientific and Industrial Research).

The author owes special thanks to SASOL (Suid-Afrikaanse Steenkool-, Olie- en Gas-Korporasie, Bpk.), who owns the Secunda Collieries and who agreed to the use and publication of all available data from previously and recently drilled boreholes, as well as analytical data which were obtained during the study. The help and advice from all the geologists at the Secunda Colleries, especially Messrs. P.P.A. Steyn, B. Hosking, and D. Kruger, is very much appreciated.

Thanks is particularly due to Mr. M.C.J. van Vuuren and Mr. J.M. Barnard as well as Dr. F. Kruzcewski of the NICR (National Institute for Coal Research), who greatly supported this study by providing analytical facilities and many helpful discussions.

The author is also grateful to Mr. S. Naidoo from TCOA (Transvaal Coal Owners Association), who provided facilities and manpower for the sample preparation. Mrs. I. Cornelius of the Geography Department of the University of Pretoria contributed through the draughting of most of the figures.

Digitised by the Department of Library Services in support of open access to information, University of Pretoria, 2021.

TABLE OF CONTENTS

ACKNOWLEDGEMENTS V
LIST OF FIGURES IX
LIST OF MAPS XIV
LIST OF TABLES XVI

1. INTRODUCTION 1

1.1. General Geology 3
1.2. Previous Work on the Sedimentology of South African Coalfields 7
1.3. Previous Work on Dolerite Intrusions in South African Coalfields 8
1.4. Objectives of the Study 10

2. DATA ACQUISITION AND METHODS OF INVESTIGATION 13

2.1. Sedimentological and Lithostratigrapic Working Methods 14
2.1.1. Underground Mapping of Sedimentary Structures 14
2.1.2. Sedimentary Petrography (Grain Size Distribution) 15
2.1.3. Sedimentary Petrography (XRD Analyses) 15
2.1.4. Sedimentary Petrography (Glauconite Occurrences) 18
2.1.5. Paleo-pH Determinations 19
2.2. Macropetrography of the No. 4L Seam 19
2.3. Micropetrography of the No. 4L Seam 21
2.4. Coal Parameters 24
2.5. Sampling of Dolerites and Thermally-affected Coals 24
2.6. Analysis of Dolerites 28
2.7. Analysis of Thermally-affected Coals 29
2.7.1. Maceral Analyses 29
2.7.2. Vitrinite Reflectivity 30
2.7.3. Proximate Analyses 30
2.7.4. Ultimate Analyses 31
2.7.5. CO_2 Correction 31
2.7.6. XRF Spectrometry 32

3. LITHOSTRATIGRAPHIC DESCRIPTION 34

3.1. Pre-Karoo Topography 34
3.2. LFA 01: Dwyka Formation Diamictites and Shales 37
3.3. LFA 02: Sedimentary Rocks below the No. 2 Coal Seam 42
3.4. LFA 03: The No. 2 Coal Seam 45
3.5. LFA 04: Sedimentary Rocks between the No. 2 Coal Seam and the Main Coal Zone 47
3.5.1. Summary of LFA's 02 to 04 50
3.6. LFA 05: The Main Coal Zone 54
3.6.1. The No. 3 Coal Seam 54

Digitised by the Department of Library Services in support of open access to information, University of Pretoria, 2021.

3.6.2. Parting between No. 3 and No. 4L Coal Seams 60
3.6.3. The No. 4L Coal Seam 62
3.6.4. Parting between No. 4L and No. 4U Coal Seams 68
3.6.5. The No. 4U Coal Seam 71
3.6.6. Summary of LFA 05: The Main Coal Zone 75
3.7. LFA 06: Sedimentary Rocks between No. 4U and No. 5 Coal Seams 76
Basal Portion - Upper Portion - Total Thickness
3.8. LFA 07: The No. 5 Coal Seam 81
3.9. LFA 08: Sedimentary Rocks above the No. 5 Coal Seam 81
3.10. Clay Minerals and Carbonates of the Karoo Sedimentary Rocks
at the Twistdraai Coalfield 85
3.11. Results of Glauconite Petrography 89
3.12. Paleo-pH Results 96
3.13. Micropetrography of the No. 4L Coal Seam 96

4. MODEL OF DEPOSITIONAL ENVIRONMENT 104

4.1. General Aspects of Coal-forming Environments 106
4.2. Pre-Karoo Topography 107
4.3. Event 01 108
4.4. Event 02 109
4.5. Event 03 111
4.6. Event 04 111
4.6.1. Summary of Events 01 to 04 115
4.7. Event 05: The Main Coal Zone 116
4.7.1. The No. 3 Coal Seam 116
4.7.2. Parting between No. 3 and No. 4L Coal Seams 119
4.7.3. The No. 4L Coal Seam 121
4.7.4. Parting between No. 4L and No. 4U Coal Seams 123
4.7.5. The No. 4U Coal Seam 127
4.7.6. Summary of Event 05: The Main Coal Zone 127
4.8. Event 06 128
4.9. Event 07 130
4.10. Event 08 130
4.11. Discussion of Possible Marine Influence in the Paleoenvironment 131
4.11.1. Clay Minerals and Carbonates 132
4.11.2. Glauconite 134
4.11.3. Paleo-pH Results 136
4.12. Discussion of the Micropetrography of the Coals 137
4.13. Summary and Discussion of the Model 139

Digitised by the Department of Library Services in support of open access to information, University of Pretoria, 2021.

5. THE EFFECT OF THE DEPOSITIONAL ENVIRONMENT ON COAL QUALITY PARAMETERS 145

5.1. The Ash Content 145
5.2. The Volatile Matter Content 147
5.3. The Calorific Value 149

6. THE EFFECT OF DOLERITE INTRUSIONS ON THE QUALITY OF COAL 153

6.1. Field Relations, Petrography and Chemistry of the Dolerites 153
6.2. Petrographic Description of the Coals 156
6.2.1. Micropetrography of the Coals 158
Qualitative Results - Quantitative Results
6.3. Vitrinite Reflectivity 164
6.4. Proximate Analyses 171
Moisture - Ash - Carbon Dioxide - Volatile Matter
6.5. Ultimate Analyses 177
Carbon - Hydrogen - Nitrogen - Sulphur
6.5.1. Calorific Value on the Basis of Carbon and Hydrogen Contents 183
6.6. Inorganic Geochemistry of the Coals 183
6.6.1. Regional Trends in Element Distribution 187
6.6.2. Element Distribution in Unaltered Coals 188
6.6.3. Element Distribution in Thermally-affected Coals 203
6.7. Discussion of Dolerite Occurrences 205
Mode of Occurrence - Width of Contact Aureole
6.8. Discussion of Coal Petrography, Reflectivity and Chemistry 206
Micropetrography of Coals - Rank Parameters - Proximate Analyses - Inorganic Constituents of Unaltered Coals - Inorganic Constituents of Thermally-altered Coals

7. SUMMARY AND CONCLUSIONS 213

REFERENCES 216
LIST OF APPENDICES 226

Digitised by the Department of Library Services in support of open access to information, University of Pretoria, 2021.

LIST OF FIGURES

The first number of each figure indicates the chapter in which it is referred to for the first time.

Fig. 1.1 Geological map of the northeastern Karoo Basin, showing the location of the study area (modified after VISSER, 1984). 1

Fig. 1.2 Coalfields of South Africa (modified after MEHLISS, 1985). 2

Fig. 1.3 Two east-west cross-sections of the Twistdraai Mine area (see figure 1.4 for locality). 5

Fig. 1.4 Map of the borehole distribution over the Twistdraai Mine and the traces of the east-west cross-sections in figure 1.3. 6

Fig. 2.1 Map of special localities that are referred to in the text. 16

Fig. 2.2 Underground plan of parts of the Twistdraai mine, with suboutcrop of the dolerites against the No. 4L coal seam and with the sampling localities marked **A** to **H**. 25

Fig. 2.3 Diagram illustrating the division of the seam into seam benches and the method of their sampling at each measured channel at localities **B** to **H** (for locations see figure 2.2). 27

Fig. 3.1 Generalized sequence of lithofacies associations (LFA's) in the study area. 35

Fig. 3.2 Sample of diamictite of the Dwyka Formation in LFA 01. Subangular clasts are less than 5cm in diameter and cemented by a grey to blue matrix. The red band in the bottom half of the core consists of a mixture of coarse-grained mixed clasts with a fine to very fine matrix of similar composition. 38

Fig. 3.3 Sample of interlaminated siltstone and shale facies with dropstones, in LFA 01. 38

Fig. 3.4 Sample-profile from borehole **A** (see figure 2.1 for location) with lithologic description and grain size distribution histograms of LFA 02. 43

Fig. 3.5 Two sample-profiles from boreholes **A** and **D** (see figure 2.1 for location) displaying the variability in lithology and thickness of LFA 04. 48

Fig. 3.6 Samples of (a) interlaminated shales and siltstone, (b) bioturbation and (c) soft sediment deformation structures within LFA 04. 49

Fig. 3.7 Four type-profiles of LFA 05 (the main coal zone), each one being representative for a respective depositional region within the study area (see map 5.1) 55

Digitised by the Department of Library Services in support of open access to information, University of Pretoria, 2021.

Fig. 3.8 Sample-profiles of macropetrographic seam sections of the No. 4L coal seam. A comparison of two drill core profiles with four profiles measured underground in the Twistdraai Mine (see figure 2.1 for localities of all profiles). 63

Fig. 3.9 Diagram illustrating roof structures of seam No. 4L in the southwestern corner of the mine (see figure 2.1 for locality). Plan (right) delineates the braided pattern of these structures. The two cross-sections illustrate the symmetrical (Type A) and asymmetrical (Type B) shapes of these sandstone bodies which protrude from the roof of the seam. 72

Fig. 3.10 Sample-profile from borehole **A** (see figure 2.1 for locality) with lithologic descriptions and grain size distribution histograms in the upper portion of LFA 06. 77

Fig. 3.11 Lithostratigraphic columns of borehole **C** (see figure 2.1 for locality) with plotted XRD-results of quantitative clay mineral and carbonate analyses, also showing the results of the paleo-pH determination. 87

Fig. 3.12 Lithostratigraphic column of borehole **B** (see figure 2.1 for locality) with plotted XRD-results of quantitative clay mineral and carbonate analyses. 88

Fig. 3.13 Photomicrographs of (a) flaky massive glauconites filling interstitial grain spaces, (b) glauconite formation on edges and cleavages of an altered biotite, (c) glauconite as a pseudomorph after mica minerals (arrow), (d) glauconite filling cell cavities of higher plants and (e) glauconite as rounded grains and filling foraminiferal tests in Cretaceous sandstones, Germany. 90

Fig. 3.14 X-ray diffractograms of glauconites from the Transvaal Coalfields. Pattern A: the diffractogram of the whole sample; Pattern B: of selected orientated glauconite grains; Pattern C: of orientated and glycolated glauconite grains; Pattern D: after heating of the orientated sample at 600°C. 93

Fig. 3.15 Ternary diagram of FeO, K_2O and Al_2O_3 for glauconite analyses of this study, compared to results found in the literature. 95

Fig. 3.16 Typical (a) fine-grained and (b) coarse-grained carbominerites , mainly comprising inertodetrinite and semifusinite of varying reflectivity, as well as minor occurrences of vitrintite. Oil immersion at 500x magnification. 97

Fig. 3.17 Distribution of cellular, detrital and massive macerals in all samples of sections **59, 61** and **62** (see figure 2.1 for location). 99

Digitised by the Department of Library Services in support of open access to information, University of Pretoria, 2021.

Fig. 3.18 Distribution of high and low reflecting inertinite and vitrinite in all samples of sections **59, 61** and **62** (see figure 2.1 for location). 100

Fig. 3.19 Three representative profiles from sections **59, 61** and **62** of the No. 4L coal seam showing the cyclicity of the relative distribution of vitrinite and low and high reflecting inertinite within the lithotype bands. 101

Fig. 3.20 Three representative profiles from section **59, 61** and **62** of the No. 4L seam showing the cyclicity of the relative distribution of massive, detrital and cellular macerals within the lithotype bands. 102

Fig. 4.1 Diagram of the chronological succession and spatial relationship of all eight events. The right hand part of the diagram shows an unscaled east-west section through the coalfield, with the spatial inter-relationships of the various processes that controlled the succession of events. 105

Fig. 4.2 Three fence diagrams through the eastern pre-Karoo paleovalley (see figure 2.1 for position of profiles). 122

Fig. 5.1 Distribution of the ash content **(a.d.)** in the coals in the No. 4L seam. 146

Fig. 5.2 Distribution of the volatile matter content **(d.a.f.)** of the coals in the No. 4L seam. 148

Fig. 5.3 Distribution of the calorific value **(a.d.)** of the coals in the No. 4L seam. 150

Fig. 5.4 Distribution of the calorific value **(d.a.f.)** of the coals in the No. 4L seam. 151

Fig. 6.1 Schematic cross-section illustrating how dolerite dykes intersect a coal seam, (A) either widening in the seam or (B) bifurcating. 154

Fig. 6.2 Photomicrographs of coke from the contact (a) and from 4m distance (b). The coke on the contact has compressed vesicles while coke from 4m distance has open uncompressed vesicles. Both photomicrographs at 200x magnification under oil immersion. 160

Fig. 6.3 Photomicrograph of devolatilization vesicles aligned in a "pearl string" manner, presumably along former bedding planes. 161

Fig. 6.4 Average maceral composition of unaltered coals (left) and of thermally metamorphosed coals (right) at sampling locality **C.** 163

Fig. 6.5 V-class distribution of samples of unaffected coals from channels **E, F, G** and **H.** 164

Fig. 6.6 Diagram illustrating the increase in average vitrinite reflectivity per channel at sampling locality **B.** Inset diagrams show reflectivity profiles of each channel. 166

Digitised by the Department of Library Services in support of open access to information, University of Pretoria, 2021.

Fig. 6.7 Diagram illustrating the increase in average vitrinite reflectivity per channel at sampling locality **C.** Inset diagrams show reflectivity profiles of each channel. 167

Fig. 6.8 Diagram illustrating the increase in average vitrinite reflectivity per channel at sampling locality **D.** Inset diagrams show reflectivity profiles of each channel. 168

Fig. 6.9 Reflectograms of each sample from channel **C4**, which illustrates the wide range and bimodal distribution of reflectivity values in the samples of this channel, due to partial metamorphism. 170

Fig. 6.10 Moisture and ash (a.d.) contents of unaffected and of metamorphosed coals in an east-west cross-section through all sampling localities (compare figures 2.2 and 2.3 for localities). 172

Fig. 6.11 Volatile matter (d.a.f./CO_2) and CO_2 contents of unaffected and of metamorphosed coals in an east-west cross-section through all sampling localities (compare figures 2.2 and 2.3 for localities). 174

Fig. 6.12 A comparison of the volatile matter (d.a.f.) content without correction for CO_2 (upper diagram) and with the correction (lower diagram) for unaffected and metamorphosed coals at locality **C.** 175

Fig. 6.13 A comparison of the carbon (d.a.f.) content without correction for CO_2 (upper diagram) and with the correction (lower diagram) for unaffected and metamorphosed coals at locality **C.** 178

Fig. 6.14 Carbon (d.a.f./CO_2) and hydrogen contents and H/C atomic ratio of unaffected and of metamorphosed coals in an east-west cross-section through all sampling localities (compare figures 2.2 and 2.3 for localities). 180.

Fig. 6.15 Nitrogen (d.a.f.) and sulphur (d.a.f.) contents and calorific value (MJ/kg) (d.a.f.) of unaffected and of metamorphosed coals in an east-west cross-section through all sampling localities (compare figures 2.2 and 2.3 for localities). 182

Fig. 6.16 Diagrams illustrating the effect of the "ash-factor" correction on the element concentrations (locality **B**). Note that for both elements concentrations increase, where the ash content of that specific sample is below average (18.08% a.d.). 185

Digitised by the Department of Library Services in support of open access to information, University of Pretoria, 2021.

Fig. 6.17 Vitrinite content, proximate analyses and element concentrations of the individual seam benches (A - F) relative to a normative average value of each parameter of all unaffected coals (>16m sampling distance from intrusion). The normative value is given as "1". The scale for depletion and enrichment ratios is from 0 to 2 or from 0.8 to 1.2. 189

Fig. 6.18 Concentrations of mainly allogenic elements of unaffected and of metamorphosed coals in an east-west cross-section through all sampling localities (compare figures 2.2 and 2.3 for localities).

(a) $\%SiO_2$; $\%Al_2O_3$; $\%TiO_2$ 193

(b) $\%SiO_2$ + Al_2O_3; $\%K_2O$; Th (ppm) 194

(c) Zr (ppm); Y (ppm); Nb (ppm) 195

(d) Cr (ppm); V (ppm); Rb (ppm) 196

(e) $\%Na_2O$; %FeO 197

Fig. 6.19 Concentrations of mainly lithophile authigenic elements of unaffected and of metamorphosed coals in an east-west cross-section through all sampling localities (compare figures 2.2 and 2.3 for localities).

(a) %CaO; %MgO 198

(b) $\%P_2O_5$; Sr (ppm); Ba (ppm) 199

(c) Cl (ppm); F (ppm) 200

Fig. 6.20 Concentrations of mainly chalcophile authigenic elements of unaffected and of metamorphosed coals in an east-west cross-section through all sampling localities (compare figures 2.2 and 2.3 for localities).

(a) Zn (ppm); Cu (ppm); Ni (ppm) 201

(b) Co (ppm); Ga (ppm); Mo (ppm) 202

Digitised by the Department of Library Services in support of open access to information, University of Pretoria, 2021.

LIST OF MAPS

The first digit of each map number refers to the respective LFA that is illustrated thereon. The second digit indicates either single layers or cumulative thicknesses of several layers within one LFA, or refers to a map showing a present-day topography of an interface between two LFA's. Maps that are referred to in the interpretation chapter have the same numbering as their counterparts in the description chapter; the suffix **M** indicates that the maps emphasize specific features of the depositional **M**odel.

Map 0	Pre-Karoo paleotopography (contour interval in meters above sea level).	36
Map 1.1	Isolith map of Dwyka Formation diamictites (contour interval in meters).	39
Map 1.2	Isolith map of Dwyka Formation shales (contour interval in meters).	40
Map 1.3	Present-day post-Dwyka topography (contour interval in meters above sea level, corrected for dolerite sills within LFA 01).	41
Map 2	Isopach map showing the geometry of LFA 02 (contour interval in meters).	44
Map 3	Isopach map showing the geometry of LFA 03 (the No. 2 coal seam) (contour interval in meters).	46
Map 4.1	Isopach map showing the geometry of LFA 04 (contour interval in meters).	51
Map 4.2	Isopach map of cumulative thickness of LFA's 02 to 04 (contour interval in meters).	52
Map 4.3	Present-day topography at top contact of LFA 04 (contours in meters above sea level, corrected for dolerite sills in underlying LFA's); (shadings illustrate geometry of LFA 04)	53
Map 5.1	Isopach map showing the geometry of LFA 05 (the main coal zone) (contour interval in meters).	56
Map 5.2	Distribution and isolith map of shales and siltstones (contour interval in meters) in the floor of the No. 3 coal seam.	57
Map 5.3	Distribution and isopach map of the coal in the No. 3 seam (contour interval in centimeters).	58
Map 5.4	Distribution and isolith map of shales which abut and overlie the No. 3 coal seam (contour interval in centimeters). The dotted line indicates the outline of the underlying No. 3 coal seam.	59
Map 5.5	Distribution and isolith map of the sandstone parting between No. 3 and No. 4L coal seams (contour interval in meters).	61
Map 5.6	Isopach map of the No. 4L coal seam (contour interval in centimeters).	65

Digitised by the Department of Library Services in support of open access to information, University of Pretoria, 2021.

Map 5.7 Distribution and isolith map of clastic lenses in the bottom one third of the No. 4L coal seam (contour interval in centimeters). The dotted line indicates the outline of the underlying No.3 coal seam. 66

Map 5.8 Distribution and isolith map of clastic lenses in the top one third of the No. 4L coal seam (contour interval in centimeters). 67

Map 5.9 Isopach map showing the geometry of the total parting between No. 4L and No. 4U coal seams (contour interval in meters). 69

Map 5.10 Distribution and isolith map of gritstones in the roof of the No. 4L coal seam (contour interval in meters). 70

Map 5.11 Distribution and isolith map of shales in the floor of the No. 4U coal seam (contour interval in centimeters). 73

Map 5.12 Isopach map of the No. 4U coal seam (contour interval in centimeters). 74

Map 6.1 Isopach map showing the geometry of LFA 06 (contour interval in meters). 79

Map 6.2 Distribution and isopach map of the siltstone-shale-coal facies in the top portion of LFA 06 (contour interval in centimeters). 80

Map 7 Isopach map of LFA 07 (the No. 5 coal seam) (contour interval in centimeters). 82

Map 3.M Paleoenvironmental interpretation of Event 03. Thicknesses of LFA 03 (contour interval in meters) are shown superimposed over thick LFA 02 sandstone body. 112

Map 4.1.M Paleoenvironmental interpretation of Event 04, based on thicknesses of LFA 04 (contour interval in meters). 114

Map 5.2.M Paleoenvironmental interpretation of shales and siltstones in the floor of the No. 3 coal seam (contour interval of the shale and siltstone thicknesses given in meters). 117

Map 5.3.M Paleoenvironmental interpretation of the coal of the No. 3 seam. 118

Map 5.5.M Paleoenvironmental interpretation of the sandstone parting (contour interval in meters) between No. 3 and No. 4L coal seams. This map indicates the spatial coexistence of the last Event 04 sediments with the early sediments of Event 05. It thus gives the lateral distribution of all lithological units forming the immediate floor rocks of coal seam No. 4L. 120

Map 5.6.M Paleoenvironmental interpretation of the No. 4L coal seam. 124

Map 5.9.M Paleoenvironmental interpretation of the parting between No. 4L and No. 4U coal seams (contour interval in meters). 126

Digitised by the Department of Library Services in support of open access to information, University of Pretoria, 2021.

LIST OF TABLES

The first number of each table indicates the chapter in which it is referred to for the first time.

Table 1.1 Stratigraphy of the Karoo Sequence in the northeastern half of the Main Karoo Basin (compiled after SACS, 1980). 3

Table 2.1 Lithotypes of humic coals (after STACH et al., 1982, p171). 20

Table 2.2 Maceral groups and macerals of humic coals (after STACH et al., 1982, p90). 21

Table 2.3 Macerals grouped according to their reactivity in the coking process (after STEYN and SMITH, 1977). 22

Table 2.4 Maceral group classification used in this study and its correlation with other classification systems. 23

Table 2.5 List of elements analysed, with the corresponding instrumental set-up. 28

Table 2.6 List of major and trace elements in coal, classified according to their association with organic and inorganic matter (after BOUSKA, 1981; VALKOVIC, 1983). 33

Table 3.1 Detailed, summarizing lithostratigraphic table of the sequence of lithofacies associations at the Twistdraai Mine. 84

Table 3.2 Chemical analyses and ionic composition of various glauconites from the Transvaal Coalfields compared to analyses taken from the literature. 94

Table 3.3 Average maceral composition of the No. 4L coal seam in sections 59, 61 and 62. The complete set of results is given in appendix 3a and 3b. 98

Table 6.1 Geochemical analyses of unaltered dolerites and "white trap" dolerites in comparison with analyses of other Karoo dolerites (major elements in %, trace elements in ppm). 156

Table 6.2 Average maceral composition of each seam bench, sorted by sampling localities. For localities **B**, **C** and **D** the average petrographic composition for cindered and for unaltered coals is given separately. 162

Table 6.3 Mean vitrinite reflectivity (%ROV) per bench and per channel. 165

Table 6.4 Five selected sample analyses, showing the effect of different methods of correction of % carbon (d.a.f.) for CO_2. In the last column a comparison is given for % carbon (d.a.f.) of coals of the same rank, but through normal coalification (after TEICHMULLER, 1971). 177

Digitised by the Department of Library Services in support of open access to information, University of Pretoria, 2021.

Table 6.5 Average inorganic geochemical results of Twistdraai coals compared to results of other South African coals. 187

Table 6.6 XRD analyses of clay minerals on some selected coal samples, in percentage of the whole coal (analysed by NICR). 190

Table 6.7 Some selected correlation coefficients that are referred to in the text. Correlation coefficients are given seperately for each seam bench. The complete set of correlation matrices is listed in appendices **19** to **23.** 191

Digitised by the Department of Library Services in support of open access to information, University of Pretoria, 2021.

1. INTRODUCTION

The Twistdraai Mine near Secunda (Fig. 1.1) was chosen as a study area for the present project. It is one of the four Secunda Collieries which serve the coal liquefaction plants of SASOL II and III. This mining area belongs to the southeastern Highveld Coalfields and lies about 130km southeast of Johannesburg, and 100km south of the Witbank and Middelburg Coalfields. The extent of the study area is about 20km in an east-west direction and 10km in a north-south direction. The present-day topography is slightly undulating with an average altitude of 1600m above sea level.

South African coal deposits were estimated at 110852 million tons (Mt) in 1983 and the economically exploitable reserves were calculated at 56034Mt (DEPARTMENT OF MINERAL AND ENERGY AFFAIRS, 1985). The production figures for 1984 total 151.11Mt, of which 27.9Mt came from the Secunda Collieries and 30.1Mt were made available for export (MEHLISS, 1985). The bulk of South Africa's coal reserves are low grade (high in ash) compared to coal qualities worldwide. Therefore, more than half of the annual production is used in power stations, and only minor amounts are of a sufficiently high grade to be used in coking processes or to meet the quality demands of the export market.

The history of systematic coal mining in South Africa began in the late 1880's and had the main objective of providing fuel for the

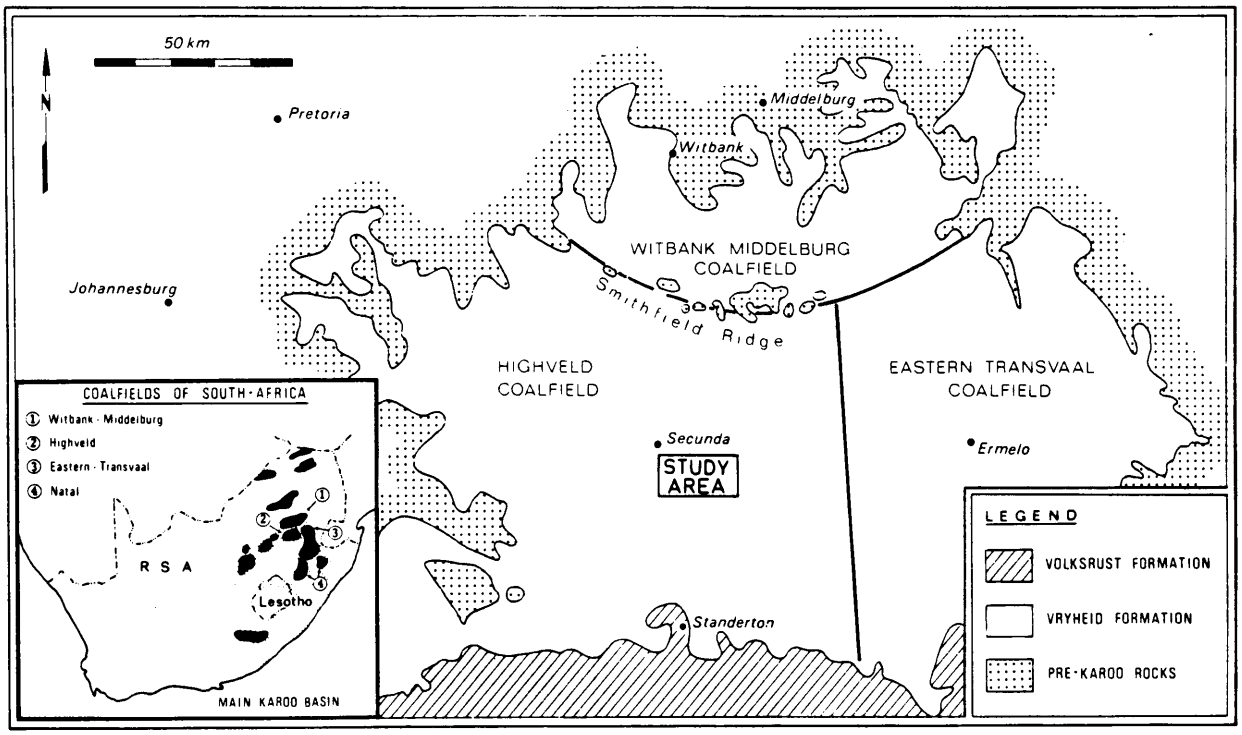


Fig. 1.1 Geological map of the norhteastern Karoo Basin, showing the location of the study area (modified after VISSER, 1984)

Digitised by the Department of Library Services in support of open access to information, University of Pretoria, 2021.

newly-found gold and diamond fields in the Transvaal, Cape Province, and Orange Free State. The first important coalfields were developed in the districts of Witbank, Middelburg, and Vereeniging, and these remained the main coal-producing areas in the country up to the present (Fig. 1.2). These coal deposits were attractive for their thick seams and shallow overburden, which led to open-cast mining since the 1960's. Due to the early developments and intensive mining in these districts, most of the analytical data recovered were from these coal deposits. Other coal mining areas, developed since World War II, are mainly in the northern and southeastern Transvaal, to which the Highveld Coalfield belongs. Relatively little research has been carried out on the latter coal deposits.

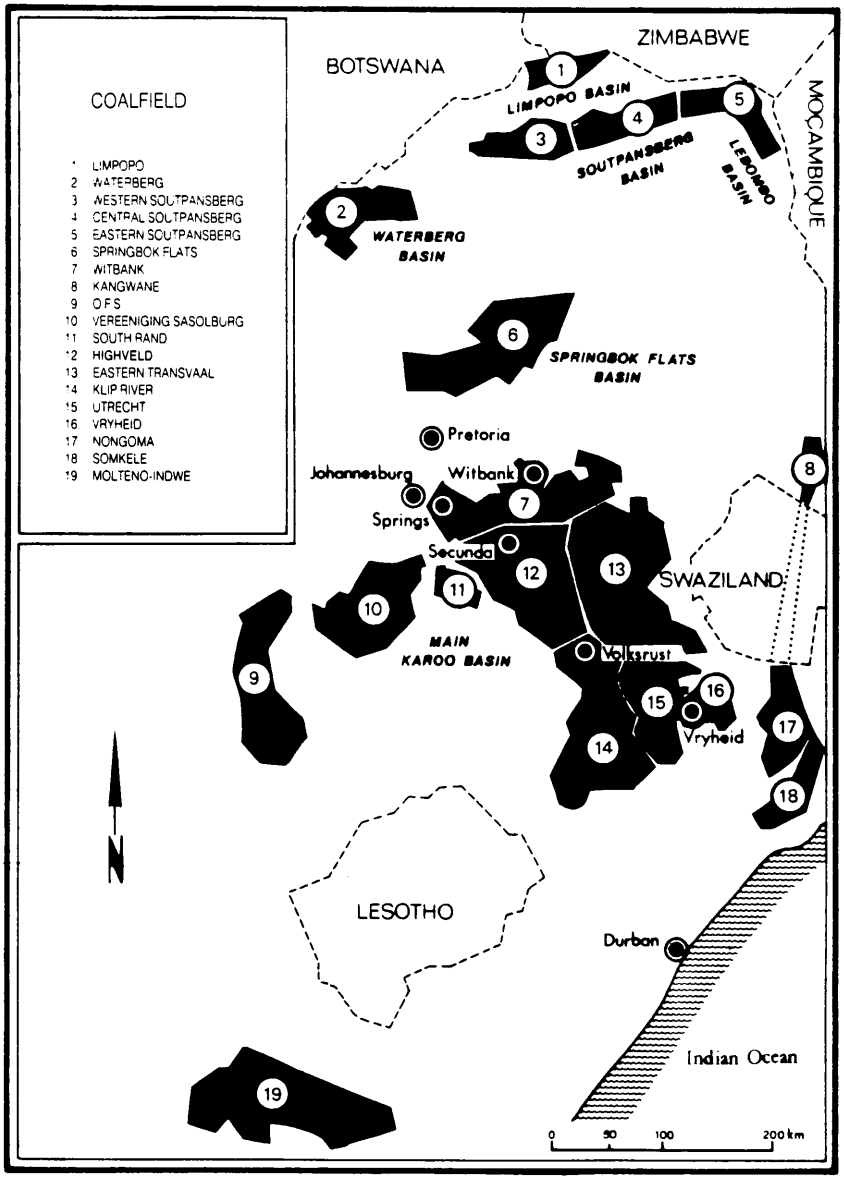


Fig. 1.2 Coalfields of South Africa (modified after MEHLISS, 1985)

Digitised by the Department of Library Services in support of open access to information, University of Pretoria, 2021.

1.1. General Geology

The Main Karoo Basin extends over a large portion of South Africa. The sedimentary rocks therein represent a depositional episode lasting from the Permo-Carboniferous glaciation of Southern Africa (Dwyka Formation), through an intracratonic basinal and marine phase (Ecca Group), to a period of terrestrial sedimentation with increasing aridity (Beaufort Group; Molteno, Elliot and Clarens Formations) (Table 1.1). The Jurassic Drakensberg volcanic rocks cap this sedimentary sequence and were fed by many dykes and sills, which affected the coal measures of the Vryheid Formation of the Ecca Group (TANKARD et al., 1982).

Of particular interest in this study are the Dwyka Formation and the Ecca Group. After the northward retreat of the Dwyka ice sheets, remnant glacial valleys with a north-south orientation reflected the major directions of earlier ice movement (TANKARD et al., 1982, p368-369). These features of the pre-Karoo Sequence topography controlled later sedimentation and, particularly, peat deposition (CAIRNCROSS, 1980; LE BLANC SMITH, 1980).

The subsequent basinal sedimentation which occurred during Ecca times comprised a marine paleoenvironment with flysch-type deposition in the south and a gently subsiding shelf platform towards the northeast (RYAN, 1968). The platform facies along the northeastern

Table 1.1 Stratigraphy of the Karoo Sequence in the northeastern half of the Main Karoo Basin (compiled after SACS, 1980).

INTERNATIONAL		GROUP	FORMATION	
150 Mill. y. Jurassic	KAROO SEQUENCE		Drakensberg ± 187 Mill. y.	Dolerite dykes & sills within the study area are regarded as part of the Drakensberg volcanism
195 Mill. y. Triassic			Clarens Elliot Molteno	
225 Mill. y. Permian		Beaufort		
		Ecca	Volksrust Vryheid * Pietermaritzburg	* present in study area
285 Mill. y. Upper Carboniferous			Dwyka *	
Pre-Karoo rocks :		Transvaal Sequence		2 300 - 2 000 Mill. y.
		Ventersdorp lavas		±2 300 Mill. y.
		Witwatersrand Supergroup		2 700 - 2 350 Mill. y.

Digitised by the Department of Library Services in support of open access to information, University of Pretoria, 2021.

margin of the Ecca Basin produced widespread clastic, fluviodeltaic deposits, which were fed from the north and which wedge out into the siltstones and mudstones of the offshore facies towards the south (HOBDAY, 1978).

The Twistdraai Mine is situated along this northeastern margin of the Karoo Basin. Therefore the cover of Karoo rocks is relatively thin here, averaging about 200-230m, compared to several thousand meters of sedimentary rocks further south (TANKARD et al., 1982; RYAN, 1968). The underlying pre-Karoo rocks mainly belong to the lavas of the Ventersdorp Supergroup and the sedimentary strata of the Transvaal Sequence and the Witwatersrand Supergroup (Table 1.1).

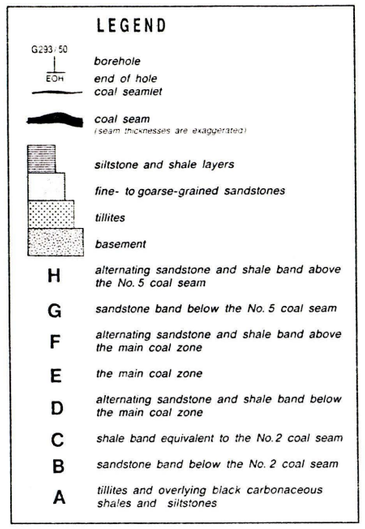
The Karoo sedimentary rocks of interest in this study range from Dwyka Formation diamictites at the base to the coal-bearing Vryheid Formation of the Ecca Group at the top. The Ecca sedimentary rocks comprise various gritstones, sandstones, siltstones and shales. The basal 80-130m of these sedimentary rocks exhibit sporadic seamlets and traces of coalified plant debris (Fig. 1.3). Above this the main coal zone contains the economic seam No. 4L, and the seams No. 3 and No. 4U which are of minor economic importance in this area. Another non-coal-bearing sequence of 40m follows and is overlain by seam No. 5, which is also not economic in the Twistdraai Coalfield.

Dolerite dykes and sills related to the Drakensberg volcanism occur irregularly throughout the entire coalfield. A few dykes segment the coalfield on a regional scale; one of these determines the southern mining boundary at Twistdraai (Fig. 1.4). Three phases of dolerite intrusion into this coalfield can be distinguished on the basis of their chilled margins and tectonic effects. The three dolerite sills are named B4, B6, and B8 and intruded into the coalfield in this order. Dolerite B8 is located close to the coal seams and cuts through them in numerous places and in an erratic manner.

The present-day surface topography is closely related to the underlying geology. Where dolerite sills crop out, erosion leaves a hill, and where Ecca sediments occur, shallow valleys have been formed.

The Karoo sedimentary rocks are virtually flat lying over the entire coalfield (Fig. 1.3). A fault zone of 500-1000m width crosses the western half of the study area. It trends southwest-northeast and forms a narrow graben structure with a downthrow of 8m on the western fault and about 30m on the eastern one (Fig. 1.4). This has displaced the northwestern portion of the study area by approximately 22m compared to the rest of the area.

Digitised by the Department of Library Services in support of open access to information, University of Pretoria, 2021.



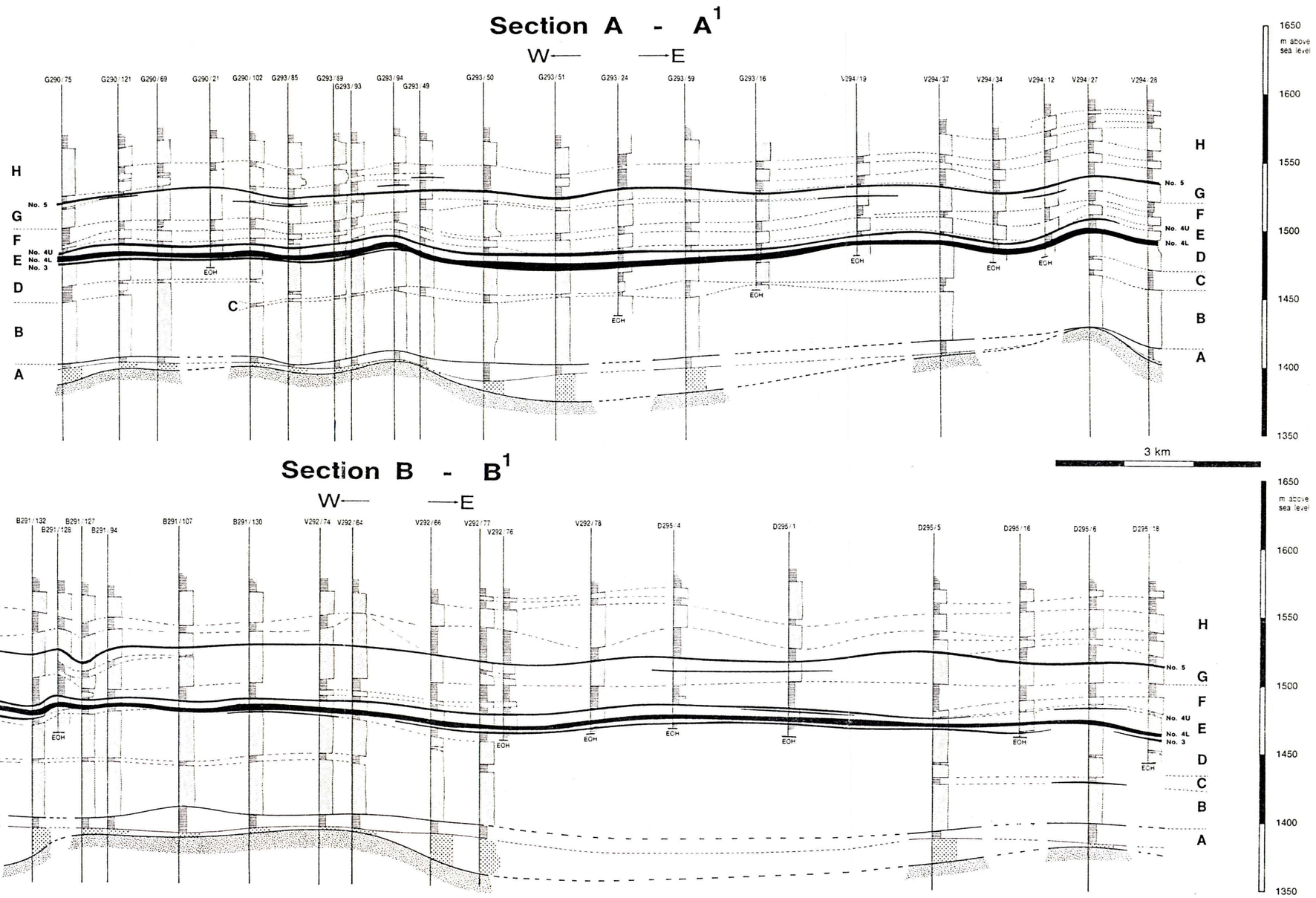
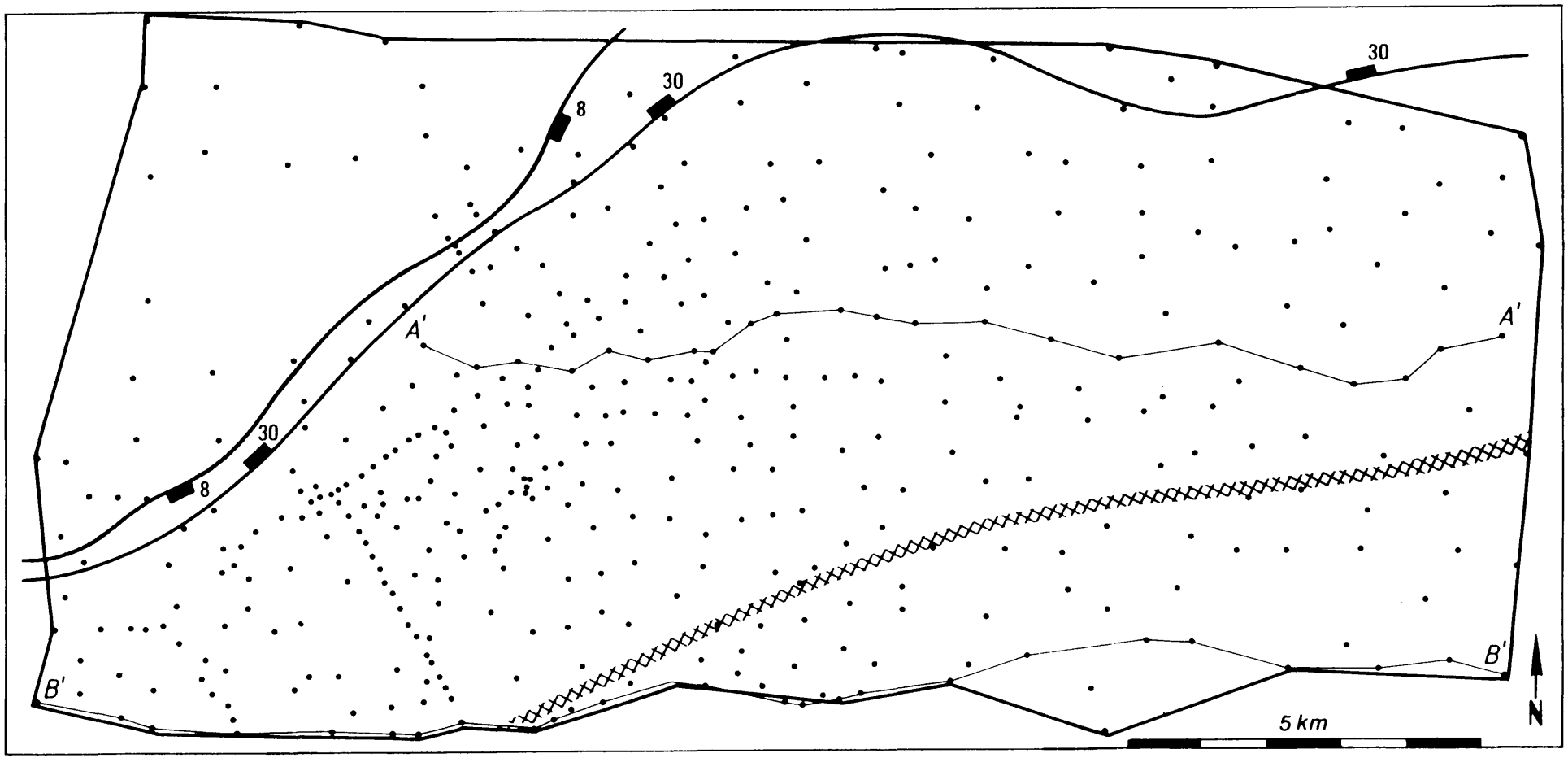


Fig. 1.3 Two east-west cross-sections of the Twistdraai Mine area (see figure 1.4 for locality).

Digitised by the Department of Library Services in support of open access to information, University of Pretoria, 2021.



LEGEND:

8 fault (with metres displacement)

Assumed trend of main dolerite dyke

Borehole site

A - A' traces of east-west

B - B' cross-sections in figure 1.3

Fig. 1.4 Map of the borehole distribution over the Twistdraai Mine and the traces of the east-west cross-sections in figure 1.3.

Digitised by the Department of Library Services in support of open access to information, University of Pretoria, 2021.

1.2. Previous Work on the Sedimentology of South African Coalfields

In the past numerous authors have dealt with the stratigraphy of the Karoo Sequence in general, as well as emphasizing the coal-bearing strata of the Ecca Group. Among the early contributors were WYBERGH (1928) and DU TOIT (1954). DU TOIT gave a comprehensive introduction to the stratigraphy of the Karoo Sequence with an emphasis on the origin of the coals within the Ecca Group. More recent summaries are provided by TRUSWELL (1977) and TANKARD et al. (1982).

WYBERGH (1928) was the first to describe the coalfields of South Africa in terms of their detailed stratigraphy, followed by PLUMSTEAD (1957) who provided petrographical and palinological descriptions of South African coals and developed the first theories about their origin. SNYMAN (1961) gave a detailed record of petrographical studies of South African coals and compared these to other Gondwana coals, and, more specifically, to Northern Hemisphere coals. LE ROUX (1985) recently applied computer-aided statistical methods to correlate coal seams from the Witbank, Bethal and Breyten areas on the basis of their coal properties.

RYAN (1968) and STRATTEN (1970) collected detailed stratigraphic data on the coal-bearing portion of the Karoo Sequence. STRATTEN concentrated on ice movement during the Dwyka glaciation. RYAN worked on the Ecca and Beaufort Groups and subdivides the Ecca into a northern, southern, central and western facies. He also gave comprehensive paleo-current data of the Ecca sedimentary sequence.

Many authors recently formulated depositional models for the coal-bearing strata in the northeastern Karoo Basin. In some cases coal distribution and coal characteristics are related to these depositional models.

HOBDAY (1973) suggested a deltaic depositional model for the Vryheid Formation in the Muden and Tugela Ferry area, southeast of Vryheid (Fig. 1.2). Based on upward-fining and upward-coarsening tendencies, which were derived from Markov analyses, CADLE and HOBDAY (1977) proposed that fluvial cycles (upward-fining) occur above thick deltaic sequences (upward-coarsening) in northern Natal and the southeastern Transvaal. Coal-bearing strata in the eastern Karoo Basin are related to upper delta plain and braided stream deposition on alluvial plains by HOBDAY (1978). Many of the succeeding studies are based on a fluviodeltaic model.

LE BLANC SMITH (1980) was the first to develop a descriptive nomenclature for lithofacies associations in the Witbank Coalfield. His system subdivides the Karoo coal-bearing strata into genetic sequences of strata (GSS's) and genetic increments of strata (GIS's). Applying this system, LE BLANC SMITH postulated a paleoenvironmental model which comprises an initial Dwyka paraglacial setting with

Digitised by the Department of Library Services in support of open access to information, University of Pretoria, 2021.

glaciofluvial and glaciolacustrine deposits. Throughout the coal-bearing zone of the Ecca Group a repetitive sequence of shallow water high-constructive deltaic deposits and subsequent braided river sediments from an upper delta plain are recognized (LE BLANC SMITH and ERIKSSON, 1979; LE BLANC SMITH, 1980). Major marine transgressions are regarded to be indicated by glauconite-bearing sandstones.

CAIRNCROSS (1979 and 1980) suggested that sedimentary rocks containing the No. 2 seam in the Witbank Coalfield reflect vertically-accreting, upward-fining cycles formed in anastomosing streams with vegetation-stabilized river banks, in an overall glaciogene setting. High-constructive lobate deltas (Gilbert-type deltas) appear to be local phenomena in the Witbank Coalfield and occur between seams No. 4U and No. 5 (CAIRNCROSS and WINTER, 1984). This upward-coarsening deltaic cycle is directly underlain and overlain by a coal seam. VAN VUUREN (1983) suggested, that a mainly meandering fluvial environment controlled the deposition of the coal-bearing strata in the Highveld Coalfield.

Further paleoenvironmental studies of the coalfields in the northeastern Karoo Basin have been carried out by HOBDAY et al. (1975), STEYN (1976), WHATELEY (1980), and STANISTREET et al. (1980). More generalized analyses were given by FALCON (1977), CADLE (1979), and TAVERNER-SMITH and MASON (1985).

LE BLANC SMITH (1980) discussed depositional controls over coal distribution on a regional scale. CAIRNCROSS (1979 and 1980) gave a general account on a local scale of the influence of depositional environment on coal characteristics such as ash content and volatile matter content.

1.3. Previous Work on Dolerite Intrusions in South African Coalfields

The Karoo dolerites are hypabyssal equivalents of the Drakensberg Group which terminated the geological history of the Karoo Sequence in the form of basaltic lava flows. Their K-Ar age varies between 154-190my (BURGER and COERTZE, 1971), which is approximately 150my after the presumed deposition of the coal seams (TANKARD et al., 1982). Contemporaneous analogs to these dolerites are found in all the other Gondwana continents (McDOUGALL, 1963; LEAMAN, 1975; KHORASANI, 1983; SHRIVASTAVA et al., 1983).

The general characteristics of the Karoo dolerites in South Africa have been described by BLIGNAUT and FURTER (1952), WALKER and POLDERVAART (1949) and BLIGNAUT (1952). Therefore, if not stated otherwise, this short review is based on these authors' publications.

Dolerites occur as undulating sills and dykes. The sills are

Digitised by the Department of Library Services in support of open access to information, University of Pretoria, 2021.

generally assumed to have intruded earlier than the dykes. Thicknesses of these intrusions vary from 10-100m, but extremes of less than 1m and up to 1000m are found. The dykes, which are of minor importance in most coalfields, specifically in the present study area, are subvertical. They appear to be more abundant in the massive sandstones of the Lower Beaufort Group (Table 1.1) than in the thinly bedded sandstones and siltstones of the Ecca Group, where sills dominate.

Dolerite sills transgress through the sedimentary horizons at any angle up to vertical. Being strongly undulating, they may form "domes" or "basins" and typically form the hill tops of the present-day undulating Highveld topography. These sills do not appear to favour certain sedimentary horizons as pathways of intrusion, but are remarkably persistent in thickness over large areas. HAMILTON (1983) reports chaotic-anastomosing dyke-sill complexes of similar intrusions in Australian coalfields.

There is no consensus about the age relation of the dolerites to the Drakensberg lavas. Based on paleomagnetic data, GRAHAM et al. (1962) arrived at the conclusion that the two igneous events are largely contemporaneous. However, the sills and dykes are generally not regarded to be the feeders of the lavas but to be a succeeding phase of igneous activity (WALKER and POLDERVAART, 1949), the evidence being the chilled margins of some dykes that intruded the basalts. The mechanism of intrusion is one of displacement and replacement as discussed by HAMILTON (1983). The weight of the thick basalt lavas is presumed to have pressed onto the underlying emptied magma chamber, which then collapsed. As a result the remaining magma intruded into cracks and bedding planes of the overlying sedimentary rocks (WALKER and POLDERVAART, 1949).

The metamorphism of the surrounding country rocks is mainly confined to heat effects; no reports of pneumatolitic activity are known to the author. The zone of contact metamorphism is considerably wider along dykes than along sills and is characterized by baking of the sandstones and change in colour of the shales. The dolerites themselves experienced endometamorphism, specifically where they are in contact with coal seams, which is indicated by altered feldspar phenocrysts and the formation of a "white trap" (KISCH and TAYLOR, 1966; ROBERTS, 1987).

The specific metamorphic effect of dolerite intrusions on coal is governed by the maximum temperature of the intrusion, the period of cooling of the magma and also depends on the rank of the coal prior to the intrusion (KHORASANI, 1983). TEICHMÜLLER (1973) observed all stages of natural coke-formation along a basaltic intrusive sheet of 0.7m width. In comparison to normally metamorphosed coals of the same carbon content, the natural coke was enriched in moisture and oxygen but depleted in hydrogen and volatile matter. Compared to technical coke it is poor in large vesicles. Mean maximum vitrinite reflectivity

Digitised by the Department of Library Services in support of open access to information, University of Pretoria, 2021.

is 12.2% and the difference of mean maximum to mean minimum vitrinite reflectivity can be up to 9.8%.

DUTCHER et al. (1966) found similar results and considered hydrogen content and maximum vitrinite reflectivity the most reliable indicators of alteration. Physical changes in heat-affected coals are contortion of the bedding, prismatic fracturing and vesiculation; the latter suggests a temperature of above 400°C.

According to ROBERTS (1987) the changes in the coals are restricted to the formation of natural coke and pyrolytic carbon and by variations in the rank parameters and major and trace element concentrations of the coals. Most of the alteration appears to be confined to the coals in the thermometamorphic aureole. LE ROUX (1985) suggested an exponential decrease of the mean maximum reflectance of vitrinite ($\overline{R}OV_{max}$) with an increase in the ratio of D/T (where D is the distance from the dyke and T the thickness of the dyke).

VAN VUUREN and QUASS (1982) found an enrichment of volatile matter of the coal at a transition point some distance away from the intrusion. This is ascribed to the migration and accumulation of tarry matter which had been released from the coal adjacent to the dyke. Carbon dioxide is enriched in the proximity of a dyke, which is attributed to secondary deposition of carbonates precipitating from percolating groundwater.

1.4. Objectives of the Study

Previous work on the Karoo coal deposits in South Africa has concentrated on the establishing of depositional models. The subsequent link between such models and the properties and distribution of the coal has mostly been discussed in a general way and on a regional scale. The following key questions thus remain:

* **To what extent does the depositional paleoenvironment influence the grade and type of coal on a local scale, i.e. within an area covered by 10-30 years of mine planning?**
* **In what way do dolerite dykes and sills influence the rank of the coal?**

The terms grade, type and rank of a coal are used according to the definitions given by SNYMAN et al. (1983).

Both key questions aim at improving coal exploration and mine planning. To date extensive exploration drilling programmes are the main investigative tool of coal mining companies in South Africa, whether they are prospecting, or evaluating operating mines. Their aim is to establish the extent and quality of the coal seams, as well as

Digitised by the Department of Library Services in support of open access to information, University of Pretoria, 2021.

the location of dolerite sills and dykes. Therefore, it is necessary to first develop a model of the depositional paleoenvironment of the coal swamps. This includes answering the following supplementary questions:

* How did the paleoenvironment develop throughout the progressive sedimentation of the Karoo rocks in and around the study area?

* Were the ancient coal swamps situated in a fluvial, a deltaic or a coastal lagoonal environment?

* How did the Eh- and pH-values change throughout the deposition of the Karoo rocks, and were there lateral changes in Eh- and pH-values, especially during the growth of the coal swamps?

* What was the salinity of the waters throughout the deposition, and did it change considerably, especially during, and shortly after the swamp-developing periods?

The first two questions can mainly be solved by interpreting the available borehole data. The second question, especially, is important, as the type of environment has an impact on the geometry of a coal seam and on the lateral variation of the coal characteristics (FIELDING, 1985). The third question aims at establishing the preservational conditions for the peat and the influx of clastic material by freshwater streams. Both determine type and grade of the coal, which will be reflected, respectively, by the maceral composition and the ash content.

The last question arose during literature studies, as macroscopically identified glauconite and bioturbation (LE BLANC SMITH, 1980; STANISTREET et al., 1980) led previous workers to the assumption that the South African coalfields experienced several major ingressions of marine waters from the southern parts of the Karoo Basin.

The subsequent step in answering the first key question will be to relate the coal properties to specific features of the model. This mainly entails outlining the quantitative and qualitative characteristics of the coal properties, with emphasis on their spatial distribution. These properties include ash content, volatile matter content and calorific value.

The second key question aims to improve the understanding of the three-dimensional relationship between rank parameters and chemical properties of the coal, on the one hand, and petrographic as well as geometric characteristics of dolerite dykes and sills, on the other. Test results of coal samples will be related to the sampling distance from the dolerite as well as the thickness and petrography of these

Digitised by the Department of Library Services in support of open access to information, University of Pretoria, 2021.

sills.

After answering both key questions the impact on exploration and direct mine planning will be as follows:

* Once a depositional model is set up and linked to the coal characteristics, it will enable a reduction in drilling to gain additional analytical data. This will influence the long term mine planning (10-30 years and more).

* At present most of the drilling in the study area is done in order to detect dolerite dykes and sills. A reliable, but expensive method is horizontal in-seam drilling (STEYN, 1983). Therefore, finding a link between dolerite characteristics and coal characteristics can help to reduce this drilling, and will subsequently influence the short to medium term mine planning (a few days up to 5 years).

Digitised by the Department of Library Services in support of open access to information, University of Pretoria, 2021.

2. DATA ACQUISITION AND METHODS OF INVESTIGATION

The main source of data for the establishment of the depositional model is the logs of some 400 boreholes that were drilled in the study area over the past two decades (Fig. 1.4). The great majority of the drill holes penetrated the entire Karoo Sequence present in this area. Underground mapping provided additional detailed information on sedimentary structures in the roof rocks of the mineable seam.

Seam profiles were measured and sampled from various places in the mine; these provide insight into the effect of the surrounding sediments and their depositional paleoenvironments on the coal seam itself. In addition thin sections, mainly from arenaceous rocks within the sedimentary sequence, were examined to determine their mineral content and grain size distribution. A series of borehole samples was taken in order to determine the clay mineral composition by means of X-ray diffraction (XRD) analysis. A number of shale and siltstone samples were subjected to paleo-pH determinations. Finally, coal petrography was utilized to help establish the paleoenvironmental conditions as well as to relate coal properties to depositional features. The data on coal parameters which were compared to the features of the depositional model were provided by SASOL.

In order to investigate the influence of dolerite intrusions on coal, it was initially intended to choose three sampling localities at dolerites of different thicknesses and to relate these to the extent of coal metamorphism and to the vertical displacement of the coal seam. However, the dolerite sills and dykes that are exposed underground at Twistdraai show little variation in thickness and only in a few cases do they cause considerable displacement, up to several meters, of the sedimentary rocks. These localities were unfortunately inaccessible at the time of the study. Therefore it was decided to sample at eight localities which lie in an area of approximately $1x2km^2$.

The doleritic intrusions in the study area occur both as sills and dykes. They are generally considered to be sills that follow an undulating path through the sedimentary sequence. Most dolerite intrusions, specifically all those under investigation here, intersect the coal vertically. For that reason the dolerite intrusions will be referred to as dykes irrespective of their attitude below and above the seam.

Digitised by the Department of Library Services in support of open access to information, University of Pretoria, 2021.

2.1. Sedimentological and Lithostratigraphic Working Methods

The reconstruction of the sedimentary history of the study area was approached by developing a three-dimensional model of the sedimentary rocks at the mine. Cross-sections were constructed from the available borehole data (Fig. 1.4). From these it became apparent that most of the sediments in the coalfield were laterally persistent or sheet-like. Subsequently, vertical lithofacies associations (referred to as LFA's) were identified and their characteristics defined. These LFA's were then correlated from borehole to borehole in order to establish their lateral relationships. During this phase of the study the author had the opportunity to log several borehole cores himself, which were drilled in various parts of the study area during 1985. Although there were several attempts to standardize the logging procedure, the detail of previous loggings remained dependent on the subjective methods of many different workers. Also the restricted time and intensive drilling programme at certain stages of the exploration diminished the accuracy and detail of these logs. However, most of the previous logs were of comparable standard and detail and could thus be compared to the recent boreholes logged by the author.

The final step involved the compilation of isopach plans of each LFA, as well as present-day elevation maps of some interfaces between LFA's. The contour plans were constructed both manually and by utilization of the Surface II Graphics System (SAMPSON, 1975), in conjunction with the computer service of the University of Pretoria. In addition, some plans were constructed showing the lateral distribution of single facies of the LFA's, especially in the floor and roof rocks of the coal seams. On the basis of this correlation and the supplementary petrographic work an interpretation of the paleoenvironmental conditions was carried out. As a result, maps of different paleodepositional stages were compiled that are based on LFA maps. These maps indicate the contemporaneous inter-relationship of vertically successive LFA's and their different environmental implications in various parts of the study area.

2.1.1. Underground Mapping of Sedimentary Structures

The underground mapping of sedimentary structures was mainly concerned with features visible in the roof rocks of seam No. 4L, and to a minor extent with clastic sediment structures within the seam itself. The structures mapped in the roof are elongated sandstone bodies of 5-15m width and 30-50cm thickness which have a convex downward bulging shape. They cause local diminishing of the total seam thickness and are only reported from the southwestern corner of the

Digitised by the Department of Library Services in support of open access to information, University of Pretoria, 2021.

mine (Fig. 2.1) and from adjoining areas of the adjacent Brandspruit Mine (Mr. B. Hosking, 1985, pers. comm.). The strike of current ripple crests was also measured and, subsequently, from their orientation and the pattern of the mapped sandstone bodies, paleocurrent directions could be determined.

In-seam clastic lenses were only measured in the eastern corner of the mine (Fig. 2.1) in order to establish their thickness and lateral extent. All results from the underground mapping are incorporated in the lithostratigraphic descriptions (especially sections 3.6.3. and 3.6.4.).

2.1.2. Sedimentary Petrography (Grain Size Distribution)

Borehole A, from the centre of the study area (Fig. 2.1), was chosen to sample mainly arenaceous rocks for a sedimentary petrographic study. The reason for this step was that some arenaceous rock units provide little macroscopic information for further differentiation and are therefore often named 'massive' in previous borehole logs.

Thin sections were cut and polished in order to determine associated minerals and the bounding conditions of the grains. The main emphasis was placed on grain shapes (i.e. their roundness and elongation) as well as on grain size distribution within a sample. Subsequently the average grain size variation from sample to sample gave an additional aid to determine upward-coarsening and upward-fining sequences.

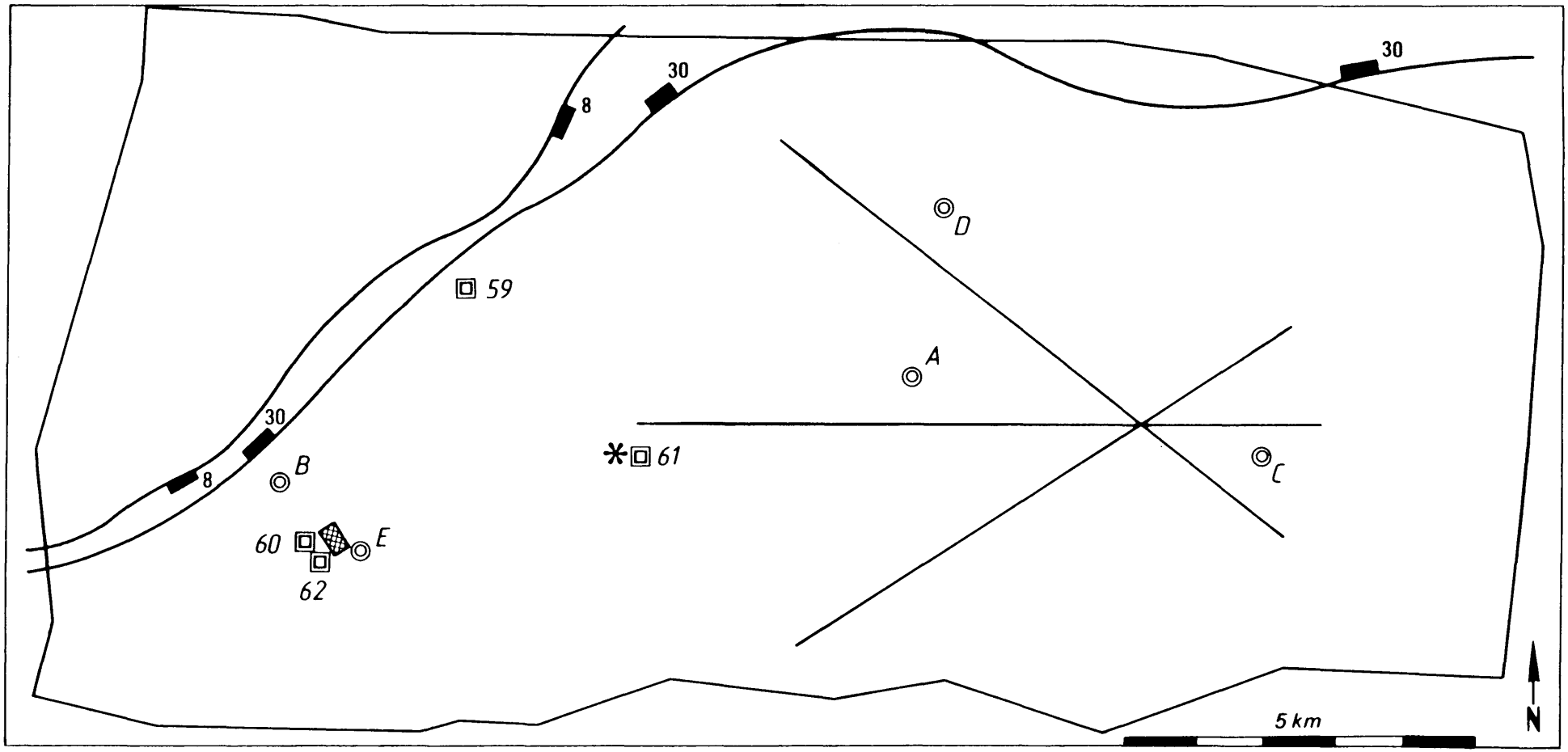
Within each thin section approximately 200 grains were measured at a 100x magnification and classified to enable histograms of grain size distributions to be drawn. The weighted mean grain size was then calculated. The results are incorporated into the lithostratigraphic descriptions in sections 3.3 and 3.7.

2.1.3. Sedimentary Petrography (XRD Analyses)

Two boreholes (B and C in figure 2.1) were sampled for X-ray diffraction analysis of their clay mineral composition and carbonate content. The illite-kaolinite ratio and its variation throughout the sedimentary sequence were of particular interest.

Both borehole cores were sampled at one meter intervals from the base of the Karoo sedimentary rocks until about 20m above the No. 5 coal seam. This yielded 137 samples from borehole B and 114 from borehole C. The samples were analysed at the XRD facility of the NICR (National Institute for Coal Research) of the CSIR, applying their preparation and measuring procedures. The measurements were taken

Digitised by the Department of Library Services in support of open access to information, University of Pretoria, 2021.



LEGEND :

Area in the mine where roof structures were mapped underground (see section 3.6.4)

Locality in the eastern part of the mine where clastic lenses in the coal seam were observed and measured (see section 3.6.3).

A - E Boreholes mentioned in text

59 - 62 Mining sections mentioned in text (see section 3.6.3)

Position of fence diagrams in figure 4.2

8 fault (with metres displacement)

Digitised by the Department of Library Services in support of open access to information, University of Pretoria, 2021.

under Cu-K_α radiation (λ =1.542Å). The sample material was ground to less than 63µm and only randomly oriented powder samples were mounted. Each holder was measured while rotating underneath the incident beam in order to compensate for preferential orientation of the clay minerals. A continuous scan at a speed of $2\theta = 3^{o}$ per minute was taken and the integral underneath each peak, diminished by the integral of the background, was calculated by an IBM PC program.

For each sample one holder of the pure sample material was run over a range of $2\theta = 33^{o}$ for a qualitative analysis. Thereafter the samples were grouped together, according to their clay mineral composition, into a

* kaolinite group,
* kaolinite-illite group,
* illite-montmorillonite group and
* illite-montmorillonite-kaolinite group.

This was done in order to optimise the measuring time for all samples during the subsequent quantitative analyses. These were carried out with two mounted holders of a mixture of lithium fluoride (LiF) (as an internal standard) and the sample material, in a mass ratio of 1:2. Finally, the measured percentages of each mineral in the two holders per sample were averaged.

The relative amounts of illite, illite-smectite and kaolinite in an argillaceous rock are indicative of the environment in which the rock was initially deposited (GRIM, 1968). The important environmental factors that control the clay mineral ratios are pH-value and salinity of the water during deposition. GRIM refers to results from MILLOT (1942), that out of 26 sediment samples of lagoonal origin 23 were illite- and smectite-dominated. Kaolinite was completely absent in 19 samples and did not exceed 30% in the remaining 7 samples. On the other hand, sediments of lacustrine origin revealed a dominance of kaolinite, whereas the cumulative amount of illite, smectite and chloritic mica ranged from 0-30%. Other authors referred to by GRIM (STRAHL, 1958; PRYOR and GLASS, 1961) find similar results, namely:

* clays deposited in a fresh water environment are mainly kaolinitic, and

* clays from a marine to brackish environment are predominantly illitic and smectitic.

For these reasons and because the question of marine influence upon South African coal deposits is widely discussed (LE BLANC SMITH, 1980), the XRD investigation was added to this study programme. It is considered to be another means to help establish the

Digitised by the Department of Library Services in support of open access to information, University of Pretoria, 2021.

paleoenvironmental conditions for the deposition of the coal-bearing sediments in the Twistdraai area, and may help to detect marine influences within that paleoenvironment.

2.1.4. Sedimentary Petrography (Glauconite Occurrences)

Glauconite in the roof rocks of coal seams has generally been accepted as an indicator for marine transgressions throughout the Transvaal Coalfields (CADLE, 1979; CAIRNCROSS, 1980; LE BLANC SMITH, 1980). BURST (1958a), similarly MILLOT (1970) and McRAE (1972), distinguish between the mineral glauconite, based on chemical composition and lattice structure, and a green, earthy pelletal glauconitic material. The latter is usually described by field geologists, working macroscopically or with a binocular microscope, as glauconite. This second approach has apparently been chosen in the previous descriptions of the glauconite occurrences in the Transvaal Coalfields.

For a complete determination, however, x-ray diffractometry, chemical analysis and microscope analysis should be combined in the study of glauconites (GALLIHER, 1939), including a correlation of their occurrences with the depositional environment of the sedimentary basins wherein the mineral was formed. It is thus not reliable to derive a marine environment solely on the basis of glauconite occurrences. A combination of these techniques has been adopted in this study in order to investigate the green, earthy pelletal and granular glauconite of the Transvaal Coalfields. Their generation will be tied into the existing depositional model of this area with focus on the Twistdraai Coalfield.

Five samples (A - E) of glauconitic sandstones were collected, one of which came from coal-bearing sedimentary rocks near Middelburg (C) and the others from the Twistdraai Mine. Two of the samples (A and B) originate from the immediate roof rocks of the No. 4L coal seam. The samples were compared to a glauconite-rich green sandstone from the Cretaceous in Northern Germany.

Thin sections of all samples are described petrographically. Glauconite grains were chemically analysed by electron microprobe, each grain four times. From the average of these analyses structural formulae were calculated on the basis of 20 O and 4 (OH), taking a micaceous crystal lattice into account. The Fe content is given as ferrous iron, as only total Fe could be determined. H_2O was calculated by the difference between 100% and the total of the analysis.

Glauconite from sample B was chosen for x-ray diffraction analysis because of its relatively large grain sizes. The x-ray diffractograms were made on a Seifert MX III diffractometer with Cu-K_α radiation (λ = 1.54178Å), using a Ni-filter, at 30mA/30kV over a range

Digitised by the Department of Library Services in support of open access to information, University of Pretoria, 2021.

of $2\theta = 5\text{-}90^{\circ}$. One portion of the sample was pulverized and prepared for a randomly oriented specimen. From another portion glauconite grains were selected by hand under a binocular microscope and milled to prepare an oriented sample. This was subsequently measured untreated, after treatment in ethylene glycol vapour at 70°C over night and eventually after heating at 600°C for 1 hour.

2.1.5. Paleo-pH Determinations

The same series of samples taken from borehole C (Fig. 2.1) for the XRD investigation was utilized to determine paleo-pH values throughout the sedimentary sequence. The method applied is described by BENNETS (1965) and BREDELL (1983) who have used it to determine the paleo-pH of South African flint clay deposits.

10g of powdered sample material (<63µm) was added to 25ml of distilled water and shaken intensively for 60 seconds. Then the pH of this mixture was measured with a 'Zeiss pH-meter 300' and glass electrode over a period of 30-60 seconds. For 20 out of the 114 samples the measuring procedure was repeated after 10 minutes and after 24 hours in order to determine the reliability and consistency of the first set of measurments. As the fluctuation was not greater than +/-0.2, the procedure was considered to be sufficiently consistent.

Paleo-pH determinations of flint clays have been correlated to the mineral and chemical composition of these clays by BREDELL (1983). MILLOT (1970) refered to paleo-pH values determined from argillaceous sediments, presuming that no adjustment took place during diagenesis. His results indicate that kaolinite-rich sediments lie in the range of pH3 to pH7, and that sediments with micaceous minerals vary from pH7 to pH9. In the present study pH values were determined in an attempt to support proposed paleoenvironmental reconstructions.

2.2. Macropetrography of the No. 4L Seam

Sections 60 and 62 are situated in the southwestern portion of the Twistdraai Mine. Five seam profiles from section 62 and two from section 60 were taken and compared to three profiles each from sections 59 and 61, situated in the northern and eastern parts of the mine, respectively. All three areas are approximately 4-5km apart from each other (Fig. 2.1). Within each mine section the profiles were taken at distances of 25-50m from one another.

The macropetrographical descriptions of the seam profiles were

Digitised by the Department of Library Services in support of open access to information, University of Pretoria, 2021.

Table 2.1 Lithotypes of humic coals (after STACH et al., 1982, p171).

Lithotype	Macroscopically recognizable features
Vitrain	bright, black, usually brittle, frequently with fissures
Clarain	semi-bright, black, very finely stratified
Durain	dull, grey or grey-black, hard, rough surface
Fusain	silky lustre, black, fibrous, soft, quite friable

done according to the standards of the ICCP (International Committee of Coal Petrography). However, lithotypes were not differentiated at a minimum thickness of 10mm as required by the ICCP. The reason for this lies in the drastic lateral changes of the lithotypes which do not allow a reasonable correlation of the different profiles. Thus, only bands showing major lithotype changes were distinguished, according to the descriptive system for humic coals as laid down in STACH et al. (1982, p171) (Table 2.1). The terms vitrain, clarain and durain correspond to the expressions bright coal, mixed coal and dull coal, respectively. For the present study the term durain was subdivided, to specify a lithotype named 'lustrous durain', which has the hardness and rough massive surface of the durain defined by STACH et al. (1982), but which has a metallic and greasy lustre. The clarain was subdivided into a clarain in the sense of STACH et al. (1982) (Table 2.1) and a bright or dull clarain, depending on the abundance of vitrain or durain stringers, respectively. Where appropriate, torbanite was distinguished from carbonaceous shales.

Coal lithotypes mainly reflect the environmental conditions during and shortly after peat deposition (STACH et al., 1982). These conditions depend on the following environmental factors (STACH et al., 1982, p219):

* ecological conditions of the swamp; including Eh/pH values, salinity, groundwater level,
* climate at the time of peat deposition,
* peat-forming plant community, which in turn is controlled by both previous factors,
* degree of biochemical coalification.

Digitised by the Department of Library Services in support of open access to information, University of Pretoria, 2021.

Therefore, a petrographical characterization of coal samples allows a paleoenvironmental reconstruction of the peat swamp. By only taking the first factor into account, fusain forms under shallow water conditions with frequent or even permanent exposure to the atmosphere. Vitrain and clarain are indicative of almost permanent flooding at comparatively shallow depths, whereas durain originates from areas with deeper water cover. Eh and pH values and salinity control bacterial activity within the peat swamp and subsequently also peat preservation and the lithotype composition of the coal (STACH et al., 1982, p31-36 and p285-291).

2.3. Micropetrography of the No. 4L Seam

From each measured profile up to 12 samples were taken, each representing a lithotype interval within the seam profile. For each sample a polished particulate section was prepared according to the procedure described by STACH et al. (1982, p295) and in the International Handbook for Coal Petrology, compiled by the ICCP (1971).

The samples, which were taken from the seam profiles in sections 59, 61 and 62, were analysed for their maceral composition according to ICCP standards. The relevant microscopic procedures and the distinction of macerals are also described by STACH et al. (1982, p308&312) (Table 2.2). The maceral groups are determined by the grey shadings and partly by the habit of the macerals, whereas the macerals of one group are mainly distinguished from one another by their habit and texture.

Table 2.2 Maceral groups and macerals of humic coals (after STACH et al., 1982, p90).

Maceral Group	Maceral	Submacerals
Vitrinite	telinite	
	collinite	telocollinite
		desmocollinite
	vitrodetrinite	
Exinite	resinite	
	cutinite	
	sporinite	
	liptodetrinite	
Inertinite	fusinite	
	semifusinite	
	sclerotinite	
	macrinite	
	micrinite	
	inertodetrinite	

Digitised by the Department of Library Services in support of open access to information, University of Pretoria, 2021.

Table 2.3 Macerals grouped according to their reactivity in the coking process (after STEYN and SMITH, 1977).

reactive macerals:	Vitrinite group (equivalent to STACH *et al.*, 1982) Exinite group (equivalent to STACH *et al.*, 1982)
semireactive macerals:	low reflecting inertinites, which include low reflecting semifusinite, low reflecting macrinite and low reflecting inertodetrinite.
inert macerals:	high reflecting inertinites, which include fusinite, high reflecting semifusinite, high reflecting macrinite and high reflecting inertodetrinite.
Sclerotinite and micrinite (equivalent to STACH *et al.*, 1982) are counted separately.	

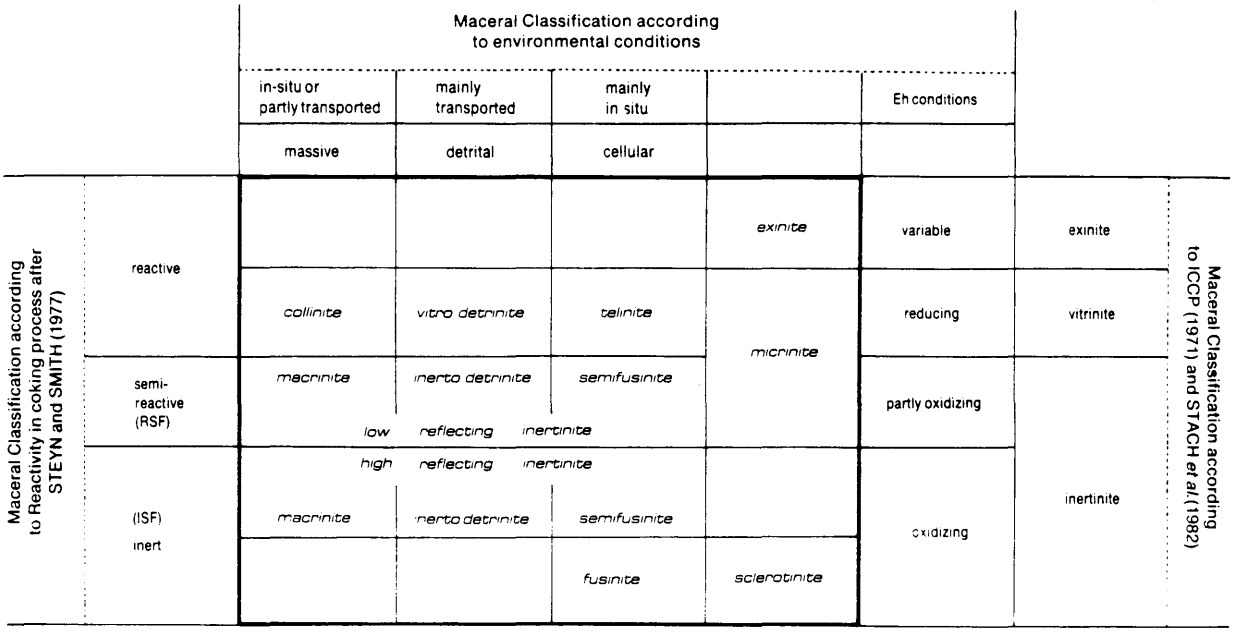
In South African coals the maceral semifusinite is commonly divided into the submacerals 'reactive semifusinite' (RSF) and 'inert semifusinite' (ISF) (STEYN and SMITH, 1977). However, here the term semifusinite signifies a wider range of macerals that may include macrinite and inertodetrinite (HAGELSKAMP, 1983). This further distinction was developed for the determination of coking properties of South African coals and is not an international standard procedure. The main purpose of this maceral analysis is to quantify the contents of reactive, semireactive and inert components in a coal with respect to its properties in the coking process (Table 2.3).

In this study the maceral analysis is mainly meant to provide indications of the depositional conditions of the peat. To a minor extent an indication of possible technical utilization can be derived. A combination of the previously mentioned group maceral classifications was adopted in an attempt to suit both purposes. The flexibility of this system is based on the subdivision of the vitrinite group macerals according to STACH *et al.* (1982) and the ICCP (1971); the inertinite group macerals are divided into low and high reflecting components after STEYN and SMITH (1977). The exinites are quantified separately because of their minor occurrence in South African coals (SNYMAN, 1961) and their resulting subordinate significance.

Thus, the macerals are grouped according to their habit and texture into massive, detrital and cellular components (Table 2.4). This classification indicates the degree of authochtony of the coals, whether the peat was rafted or formed *in situ*. Massive and cellular structures are considered to indicate no or very little transportation, whereas the detrital macerals were rafted over longer distances before redeposition and may possibly even have been wind-blown in the case of inertodetrinite (STACH *et al.*, 1982, p283).

Digitised by the Department of Library Services in support of open access to information, University of Pretoria, 2021.

Table 2.4 Maceral group classification used in this study and its correlation with other classification systems.



A maceral grouping based on the grey shading (or relative reflectivity) of the macerals serves to distinguish between vitrinitic, low reflecting inertinitic and high reflecting inertinitic macerals. These would correspond with the reactive, semireactive and inert macerals of STEYN and SMITH (1977), respectively. In this grouping the exinite group macerals, micrinites and sclerotinites are excluded. The relative reflectivity of the macerals in a coal sample is mainly the result of the oxidation and preservation conditions (STACH et al., 1982, p225-283). These in turn are determined by water depth, by the influx of fresh water and by exposure to air, either in situ or during transport of peat particles.

The technological properties indicated by this type of maceral analysis lie in the grouping according to the reactivity of the macerals during the coking process. On the other hand, the reactivity for gasification processes is largely dependent on the proportion of macerals with relatively high H/C atomic ratios and high volatile matter contents, such as the exinite group macerals and micrinite. These already comprise relatively large proportions of hydrocarbons such as alkanes and terpenes, which were derived from waxes, fats and resins from the cuticles, spores and resins of the plants. An abundance of vitrinite group macerals would indicate a higher degree of aromatization and oxidation of the molecular structure of the coal; consequently this indicates a lower hydrogen content (STACH et al., 1982, p223-283). Gasification and liquefaction would be adversely affected to an even higher degree by the presence of large amounts of strongly oxidized and aromatizised inertinite group macerals (WHITEHURST et al., 1980, p80).

Digitised by the Department of Library Services in support of open access to information, University of Pretoria, 2021.

2.4. Coal Parameters

Two coal parameters that are dependent on environmental conditions during peat deposition are ash content (grade) and maceral composition (type). Carbon content, calorific value, and volatile matter content are partly dependent on the maceral composition, and partly on the degree of regional coalification (rank) and local heating by intrusive bodies.

Only analytical data of coal seam No. 4L were utilized for this part of the study, as this is the economic seam and it extends over the entire study area. The ash content on an air dry basis (a.d.), carbon content (a.d.), calorific value (a.d.) and volatile matter content on a dry and ash-free basis (d.a.f.) were provided by SASOL.

For a number of borehole samples the calorific value had not been determined. Here an empirical formula of Mr. M.C.J. VAN VUUREN (1985, pers. comm.) was used to determine the calorific value (a.d.) from the moisture content and the ash content (a.d.) of the sample:

$$CV = f - \%moist - 0{,}41 * \%ash\ (a.d.) \quad [MJ/kg]$$

where f = 36.3 for Witbank No. 2 and No. 4 seams
f = 36.6 for Witbank No. 5 seam
f = 36.9 for anthracite

This formula is only applicable to South African coals. For this study the f-value for Witbank No. 2 and No. 4 seams was chosen, because these seams correspond to that in the present field area.

2.5. Sampling of Dolerites and Thermally-affected Coals

Four of the sampling localities (A, B, C and D) are situated adjacent to dolerite dykes. The other four (E, F, G and H) are further away from the dykes. They, however, link the localities B and D to unaffected coal in a cross-section of approximately 1km between two intrusions (Fig. 2.2). At locality A only samples of the dyke were taken, whereas both dolerite and coal samples were collected from localities B, C and D. From localities E, F, G and H only coal samples were obtained.

Two samples of dolerite were taken within the approximately 10cm wide contact zone adjacent to the seam on either side of each investigated dyke. A third sample was taken from the central portion

Digitised by the Department of Library Services in support of open access to information, University of Pretoria, 2021.

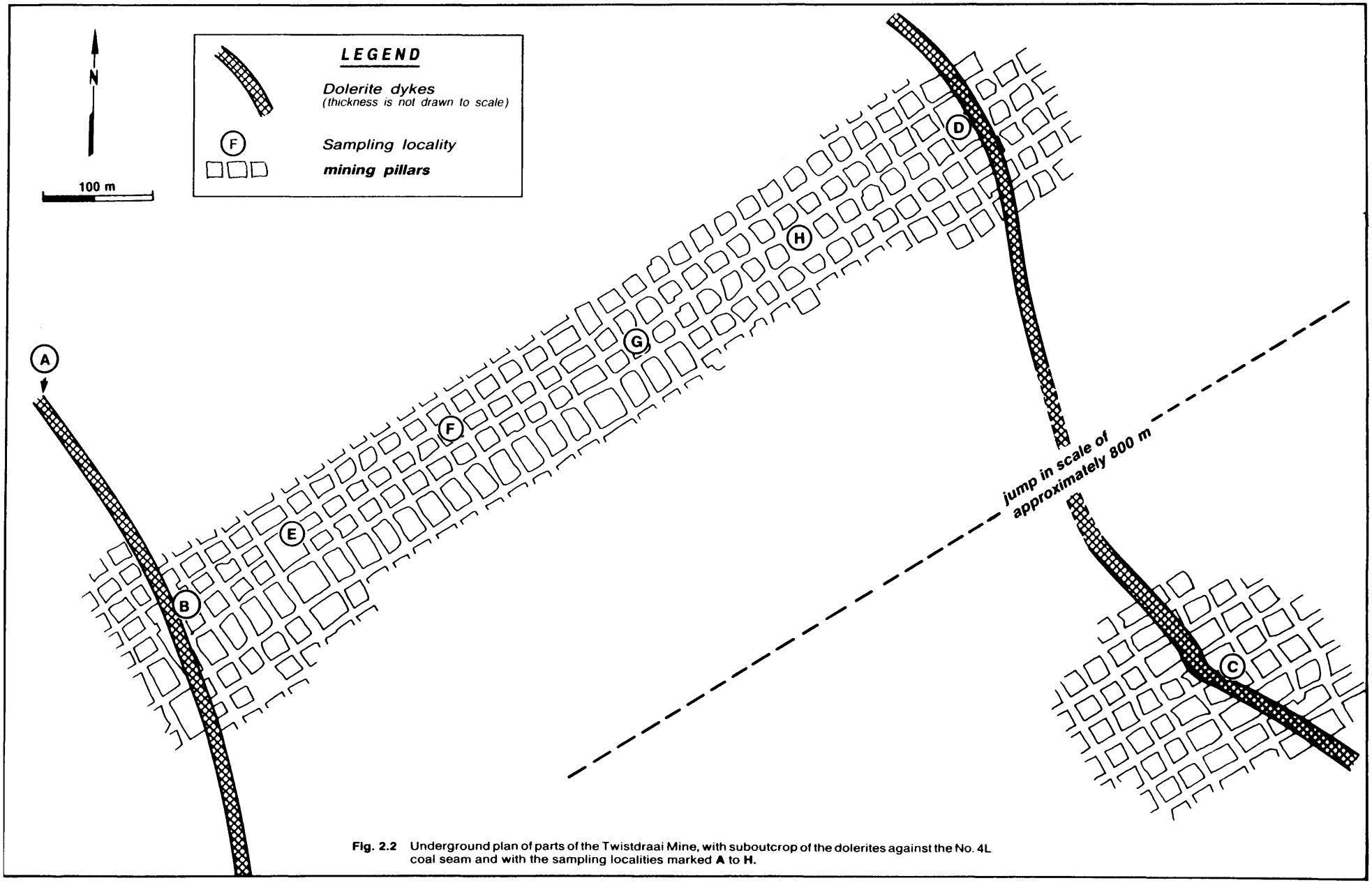


Fig. 2.2 Underground plan of parts of the Twistdraai Mine, with suboutcrop of the dolerites against the No. 4L coal seam and with the sampling localities marked **A** to **H**.

Digitised by the Department of Library Services in support of open access to information, University of Pretoria, 2021.

of each intrusion. For comparison, four dolerite samples were also taken from a drill core in the proximity of the underground sampling sites. These samples were taken at a distance of about 100m above the seam and are thus not regarded to have been affected by the coal.

The sampling procedure for the coal followed a set pattern at all localities. Seam channels from the proximity of a dyke were measured and sampled at 0, 2, 4, 8, 16 and 32m distances away from the intrusion. The two most distant channels at locality C had to be shifted further away from the dyke (Fig. 2.3), as the coal was mined out at the planned sampling sites. At localities B and D an additional channel at 10m from the dyke was introduced, because the thermometamorphic aureole had a width of about 9m at these two localities. Thus additional control points from either side of the margin of the contact zone are obtained (Fig. 2.3). At localities E to H only one channel was measured and sampled.

Each channel was divided into six samples, representing seam benches that are defined by major coal lithotype bands. The basis of distinguishing these seam benches is the same as that discussed in section 2.2. However, less detail is applied here, for practical reasons.

The samples are numbered A to F from bottom to top. At locality B the channels were divided into only five seam benches (samples A to E), of which benches A to D correspond to their equivalents at other localities. Benches E and F, however, are grouped together as E at locality B, because the seam portion above bench D is thinner than at other localities. An exceptional bench Z was distinguished in the bottom of the channel at locality G. Here the seam is about 0.5m thicker than elsewhere, which is attributed to the formation of additional coal at the bottom of the seam within a localized depression in the floor.

All channels had a width of 20-40cm. For every 10cm of bench thickness, approximately 0.5-1kg of material was collected. Rock dust, which is sprayed on the coal face as a safety measure to prevent coal dust explosions, was brushed off before sampling and it was attempted to break out large pieces of fresh coal to minimize contamination.

In total 138 coal samples and 17 dolerite samples were collected. The sample coding for the coal is explained by the following example:

D 8 C

D : sampling locality **D**.

8 : channel at distance **8m** from dyke;
this is ommitted for samples from localities E to H, as only one channel was sampled there.

C : sample **C** in that channel, representing the third seam bench from the bottom.

Digitised by the Department of Library Services in support of open access to information, University of Pretoria, 2021.

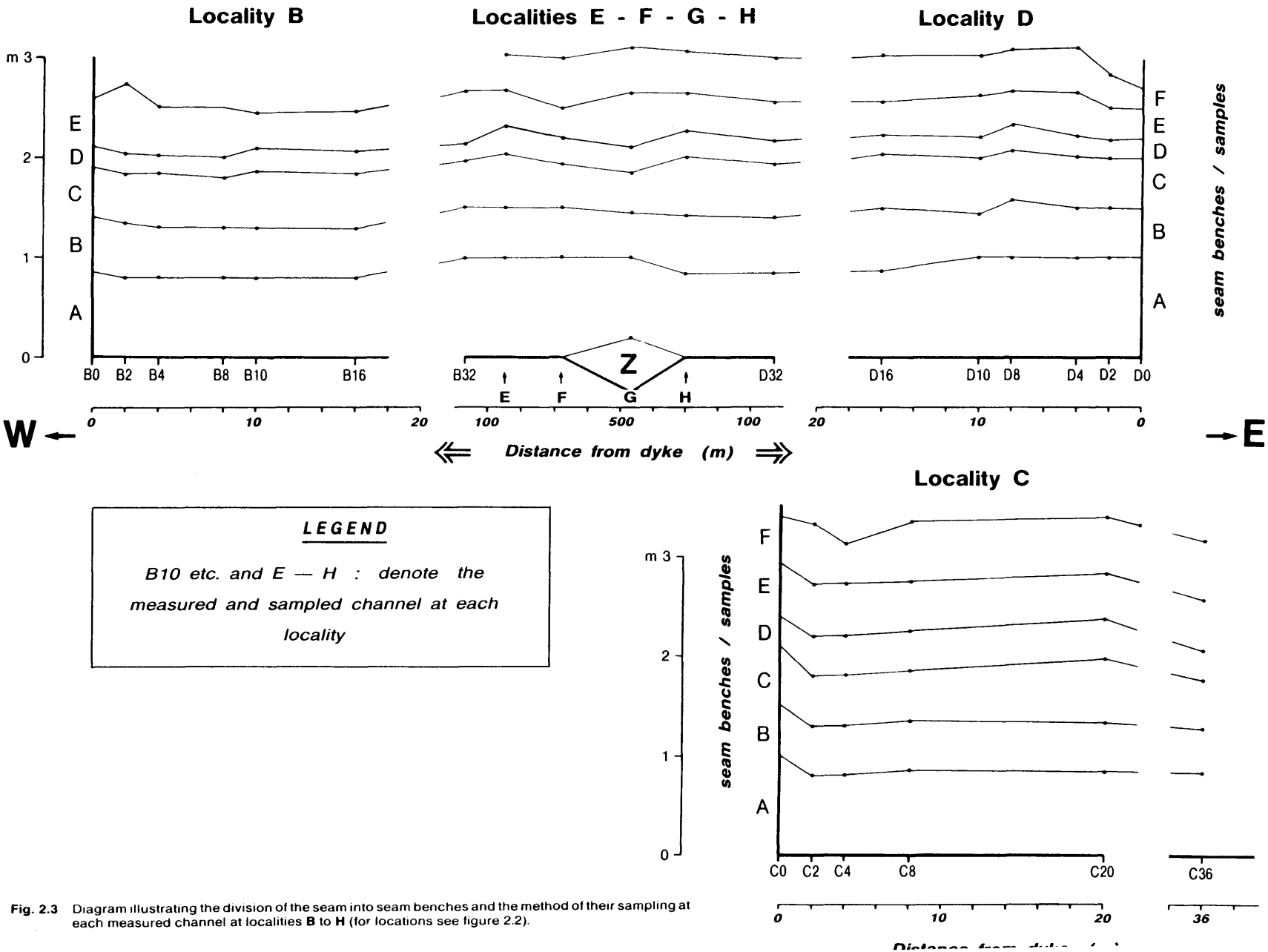


Fig. 2.3 Diagram illustrating the division of the seam into seam benches and the method of their sampling at each measured channel at localities **B** to **H** (for locations see figure 2.2).

Digitised by the Department of Library Services in support of open access to information, University of Pretoria, 2021.

2.6. Analysis of Dolerites

All dolerite samples were prepared for petrographical description and for analysis by XRD and XRF. The instrumental setting and 2Θ range for the XRD is the same as that described in section 2.1.4 for the glauconite investigation.

Determination of major and trace element contents was done with an ARL 8420 XRF spectrometer, with a Rh-end-window tube, operated at 50A/50kV. Table 2.5 lists all elements that were determined, the 2Θ position of the respective analysing peak, as well as the analysing crystal and detector combination for each element.

Norrish fusion discs (NORRISH and CHAPPELL, 1977) for major element analyses were prepared from 0.1886g of ashed air-dried sample material, 1.0000g spectroflux and 0.0134g of $NaNO_3$. The LOI was determined once for each sample after ashing over night.

Table 2.5 List of elements analysed, with the corresponding instrumental set-up.

Element K_α-line	Peak Position 2Θ	Analyzing Crystal	Detector
Si	109.21	PET	FPC-6
Ti	86.14	LIF200	FPC-6
Al	145.12	PET	FPC-6
Fe	57.52	LIF200	FPC-6
Mn	62.97	LIF200	FPC-6
Mg	20.13	AX06	FPC-1
Ca	100.22	LIF200	FPC-6
Na	24.29	AX06	FPC-1
K	136.69	LIF200	FPC-6
P	141.03	GE	FPC-6
Cr	69.36	LIF200	FPC-6
Ni	48.67	LIF200	FPC-6
Zn	41.83	LIF200	FPC-6
Cu	45.03	LIF200	FPC-6
Ni	48.67	LIF200	FPC-6
Co	52.84	LIF200	FPC-6
Ga	38.95	LIF200	SC
Mo	28.90	LIF220	SC
Nb	30.44	LIF220	SC
Zr	32.10	LIF220	SC
Y	33.87	LIF220	SC
Sr	35.85	LIF220	SC
Rb	37.99	LIF220	SC
U *	37.30	LIF220	SC
Th *	39.23	LIF220	SC
Pb **	28.26	LIF200	SC
Cr	107.06	LIF220	FPC-6
V	123.26	LIF220	FPC-6
Ba *	87.14	LIF200	FPC-6
Sc	97.68	LIF200	FPC-6
S	110.64	Ge	FPC-6
Cl	92.72	Ge	FPC-6
F	37.77	AX06	FPC-1

AX06 = 56Å synthetic multilayer crystal
FPC-6 = 4um polypropylene window
FPC-1 = 1um polypropylene window
* L_α-line
** L_β-line

Digitised by the Department of Library Services in support of open access to information, University of Pretoria, 2021.

For the trace element analyses briquettes of 15g powdered sample material, bound with a few drops of "Moviol" (a PVC binding agent) were pressed at 10t/inch^2 for about 2 minutes.

2.7. Analysis of Thermally-affected Coals

All coal samples were subjected to maceral analysis, vitrinite reflectivity measurements, proximate and ultimate analyses and XRF spectrometry of major and trace elements. The only calculated parameters are the H/C atomic ratio (VAN KREVELEN, 1961) and the calorific value; the latter is based on the hydrogen and carbon contents determined in the ultimate analyses. Both proximate and ultimate analyses were done by the NICR according to the relevant ASTM (American Standards for Testing Materials) and ISO (International Standards Organization) procedures, as described by KARR (1978). XRF analyses were carried out with the ARL 8420 XRF spectrometer of the Department of Geology at the University of Pretoria.

2.7.1. Maceral Analyses

Maceral analyses were done on all samples, except for those samples from channels at the contact of the intrusions. In these samples the distinction of macerals proved to be very difficult and often impossible due to the high degree of alteration and even coke-formation and dilatation of the sample material.

The analyses were carried out according to the ICCP norms. However, only vitrinite, low and high reflecting inertinites (as discussed in section 2.3), micrinite, exinite and natural coke particles were distinguished. Micrinite and exinite were counted separately because they were expected to be temperature-sensitive (STACH *et al.*, 1982, p283-284).

Coke particles were quantified with respect to the extent of coke-formation and this was correlated with the maceral composition of the unaltered coals in the same lithotype band. In this regard, besides typical natural coke with flow structures or mosaic texture and vesicles (CRELLING and DUTCHER, 1968), all macerals that showed early signs of devolatilization in the form of vesicles were classified as natural coke.

On each sample 400 points were counted on one polished particulate mount at 500x magnification, under oil immersion in polarized light.

Digitised by the Department of Library Services in support of open access to information, University of Pretoria, 2021.

2.7.2. Vitrinite Reflectivity

Generally only the mean random vitrinite reflectivity ($\overline{R}OV$) was measured. However, in those samples close to the dykes (4m and less), the mean maximum reflectivity ($\overline{R}OV_{max}$) was determined, as the anisotropy of the vitrinite ($\overline{R}OV_{max} - \overline{R}OV_{min}$) was more than 0.2%. The measurement of $\overline{R}OV_{max}$ was especially difficult in coals adjacent to a dyke, due to the mosaic textures of many of the thermally altered vitrinite particles. For each sample 20 points were measured, thus accumulating between 100 and 120 points per channel depending on the number of samples taken. For channels C4 and C2, 50 points per sample were measured, because of the relatively wide V-class distribution of these samples. The measurements were done under oil immersion and 500x magnification, with monochromatic light at 546+/-10nm (green). The measuring diaphragm was set at 15µm. Reflectivity standards of glass at values of 0.34, 0.54, 0.76, 0.98, 1.33, 1.60, 2.02, 2.50 and 3.04% were used.

2.7.3. Proximate Analyses

These analyses include the determination of the percentages of moisture, ash, volatile matter, fixed carbon and CO_2. The volatile matter and moisture contents, as a measure of rank, are sensitive to thermal alteration. Although ash varies widely with coal type and depositional conditions, it can also be expected to change relative to the unaffected coal, as some of the organic material is lost during the thermal metamorphism.

Proximate analysis does not normally include the determination of CO_2. It derives from carbonates in the mineral matter of the coal and is driven off during the determination of volatile matter and carbon content. However, it causes erroneous results in these analyses (KARR, 1978), which must be corrected for. Major amounts of carbonates may also cause the retention of pyritic and organic sulphur as $CaSO_4$, thus also influencing the results of the ash determination. The effective retention of sulphur is, however, not readily assessed and depends on the total sulphur and the $CaCO_3$ contents of the analysed sample (VAN VUUREN and QUASS, 1982). With low sulphur contents (generally below 2%) the chemical retention of sulphur becomes quantitatively irrelevant and makes a correction unneccessary (Mr. M.C.J. VAN VUUREN, 1987, pers. comm.).

The determination of mineral CO_2 is, however, relevant for the correction of the volatile matter and carbon analyses, and becomes especially important in thermally-affected coals, which often contain a considerably increased amount of carbonates (KISCH and TAYLOR, 1966). The volatile matter and carbon content will be dealt with on a

Digitised by the Department of Library Services in support of open access to information, University of Pretoria, 2021.

d.a.f. basis after correction for CO_2 (d.a.f./CO_2).

2.7.4. Ultimate Analyses

Ultimate analyses comprise the determination of the percentages carbon, hydrogen, nitrogen, sulphur and oxygen. Specifically C, H and N, although partially dependent on the original plant constituents and their preservation conditions, are to a great extent rank parameters for coal (VAN KREVELEN, 1961; STACH et al., 1982).

The general analytical procedures are also dealt with in detail in the respective ASTM and ISO guidelines (KARR, 1978). The H determination, in particular, is generally corrected for inherent moisture, but not for water of constitution from clay minerals. The latter, however, normally plays a minor role due to the small proportion of clay minerals in the whole coal, and is therefore not corrected for.

The calorific value (CV) can be calculated by means of an empirical formula derived from the Seyler diagram (SNYMAN et al., 1983); the empircal formula was suggested by VAN VUUREN (1987, pers. comm.) and is based on carbon and hydrogen values after CO_2 correction:

(1) $CV_{d.a.f.}$ (MJ)=1.63*%$H_{d.a.f.}$ +0.519*%$C_{d.a.f.}$ -17.6

The H/C atomic ratio indicates the nature of the original organic material and also the rank and the coalification path of a certain coal (VAN KREVELEN, 1961). For subbituminous and high-volatile bituminous coals the O/C ratio changes considerably, whereas changes in the H/C ratio only become significant in coals of the medium volatile bituminous to the anthracite and meta-anthracite stages of rank (TISSOT and WELTE, 1978). The H/C ratio also gives an indication of the aromaticity of a coal and increases with rank (BOUSKA, 1981). The H/C ratio is of great significance to the present problem and will be calculated from the CO_2-corrected results and compared to type, rank and distance from dyke.

2.7.5. CO_2 Correction

The correction for CO_2 to the volatile matter values and the carbon content is done according to the following two formulae, taken from BS 1016 (British Standards 1016 - on the reporting of results):

Digitised by the Department of Library Services in support of open access to information, University of Pretoria, 2021.

(1) $\%VM_{d.a.f.} = (\%VM_{a.d.} - \%CO_2) * 100/(100 - \%moist - \%ash)$

(2) $\%C_{d.a.f.} = (\%C_{a.d.} - 0.273 * \%CO_2) * 100/(100 - \%moist - \%ash)$

Equation (2), however, only takes into account that the CO_2 from the carbon determination is contaminated by CO_2 derived from carbonate minerals. It is, therefore, thought not to be sufficient to merely subtract the appropriate carbon ratio of the CO_2(a.d.) from the %C(a.d.) and then normalize to 100 on a moisture- and ash-free basis. Provision should also be made for the diluting effect of the CO_2 derived from carbonate minerals on the original coal, by applying the following modification to equation (2):

(3) $\%C_{d.a.f.} = (\%C_{a.d.} - 0.273 * \%CO_2) * 100/(100 - \%moist - \%ash)$

$* 100/(100 - \%CO_2)$

The effect of this modification is that the C content is increased compared to its uncorrected d.a.f. value. The values for H, N and S remain unaffected, because they are independent of the CO_2 content. Oxygen, which is not determined, but which is calculated by the difference of the sum of percentages C, H, N and S from 100, will, however, decrease accordingly.

2.7.6. XRF Spectrometry

Major element compositions were determined on Norrish fusion discs of the coal ashes. From the results a mass absorption coefficient (m.a.c.) was calculated for the coal sample including the organic constituents, which was simplistically regarded as equal to the LOI. Subsequently, trace element analyses were carried out on briquettes of powdered moisture-free coal. The instrumentation was the same as that for the dolerite analyses described in section 2.6. NBS 1632a, SARM 19 and SARM 20 were used as standard reference materials for coal. They were all briquetted in the same way as the samples analysed.

The suite of trace elements that were determined for this study is partly dependent on the instrumental set-up of the XRF facility in the Department of Geology at the University of Pretoria. On the other hand, the elements were selected and classified according to their

Digitised by the Department of Library Services in support of open access to information, University of Pretoria, 2021.

affinity for organic material, their ralative abundance in coal compared to their presence in the average crustal material, their volatile behaviour and their association with the mineral matter in the coal (NICHOLLS, 1968; CHATTERJEE and POOLEY, 1977; GLUSKOTTER et al., 1977; VALKOVIC, 1983) (Table 2.6).

The samples were prepared for briquetting following the procedure described by WILLIS and HART (1985). They were first crushed and then milled to less than 75um in an agate grinding vessel of a swingmill for about 12 minutes. After drying at 110°C for at least 4 hours, 32g of sample was weighed out and mixed thoroughly in a tumble mixer with 8g of Hoechst micropulverized binding wax. The mixture was then pressed into a pellet in a 40mm diameter die under 15t/inch^2 pressure. The pressure was applied for about 5min and then slowly released to prevent fracturing of the sample due to sudden release (VAN ZYL, 1982). The large amount of sample material, in comparison to powdered samples for ordinary rock analyses (e.g. 15g for dolerites), results in a thick pellet of approximately 3-4cm height, which then provides the infinite thickness neccessary in specimens of such low m.a.c. like coal (WILLIS and HART, 1985).

Norrish fusion discs were prepared from the ashed air-dried sample material at the same ratios as the dolerite samples. The loss on ignition (LOI) for coal samples was determined from 2g of sample, weighed into a crucible. The material was dried at 110°C over night and the moisture content determined by weight difference. During the subsequent ashing process the sample was heated up to 500°C over 1 hour and the temperature was kept constant for 1 hour. The temperature was then increased to 815°C and again kept constant for 1 hour, after which the final temperature of 950°C was applied for 2 hours. After cooling the crucible in a desiccator, the LOI was determined gravimetrically. Each sample was ashed four times in this manner to control the repeatability of the procedure.

Table 2.6 List of major and trace elements in coal, classified according to their association with organic and inorganic matter (after BOUSKA, 1981; VALKOVIC, 1983).

strongest association with organic matter in decreasing order: Ga, Ti, V, Ni, Cr, Co, Y, Mo, Cu, Zn
more abundant in coal than in average crustal material: Cl
volatile elements: F, Pb
in association with inorganic matter in coal: Zn, Cu, Ni, Co, Mn, Mg, Mo, Y, Ba, Sr, Br, Cr, V

Digitised by the Department of Library Services in support of open access to information, University of Pretoria, 2021.

3. LITHOSTRATIGRAPHIC DESCRIPTION

The description of the sedimentary sequence at the Twistdraai Mine is based on a concept of vertical lithofacies associations. The term 'lithofacies' is used in a strictly observational sense (READING, 1982, p4). It was further chosen to describe lithofacies associations (LFA's) rather than lithofacies alone, as the association of two or more different facies gives additional evidence to improve the subsequent environmental interpretation.

In this study the LFA's are taken as distinct vertical sedimentary rock units within the total sequence of Karoo sedimentary rocks at the Twistdraai Mine. The term LFA is used in a descriptive sense; each LFA is to be regarded as an equivalent to a genetic increment of sedimentation, as for example used by SIEPKER (1986). The lithofacies that are grouped together in each LFA are associated either as randomly interbedded facies or as facies in a sequential order. The transitions between facies are mostly gradational, seldom sharp and rarely erosional. The transitions of LFA's, however, are always sharp or gradational over a vertical distance of not more than a few centimeters, and in some cases a hiatus may even be recognized.

The concept of vertical LFA's was chosen because the sedimentary rocks in the study area are mainly sheet-like and a profile of each LFA therefore represents a certain phase of deposition throughout the coalfield. This implies little lateral variation of the LFA's and relatively constant thickness over the study area. However, a single facies within an association may only occur locally. The facies within one LFA are described on the basis of their lithology, their sedimentary and biogenic structures, their spatial distribution and their association with one another.

A series of eight LFA's has been established for the Twistdraai Mine Area (Fig. 3.1). All eight are developed within their defined range of variability over the entire coalfield.

In the following sections the characteristics of each LFA will be outlined. A lithological description of the sedimentary rocks as well as the main features of their vertical and lateral distribution within the study area will be given.

3.1. Pre-Karoo Topography

The present-day pre-Karoo Sequence floor is commonly referred to as the pre-Karoo topography; in the study area the elevation of this surface shows a slightly undulating relief and a general decrease in elevation from north to south, from about 1420m to 1360m above present-day sea level (Map 0). The average slope is 4.24m/km. Two

Digitised by the Department of Library Services in support of open access to information, University of Pretoria, 2021.

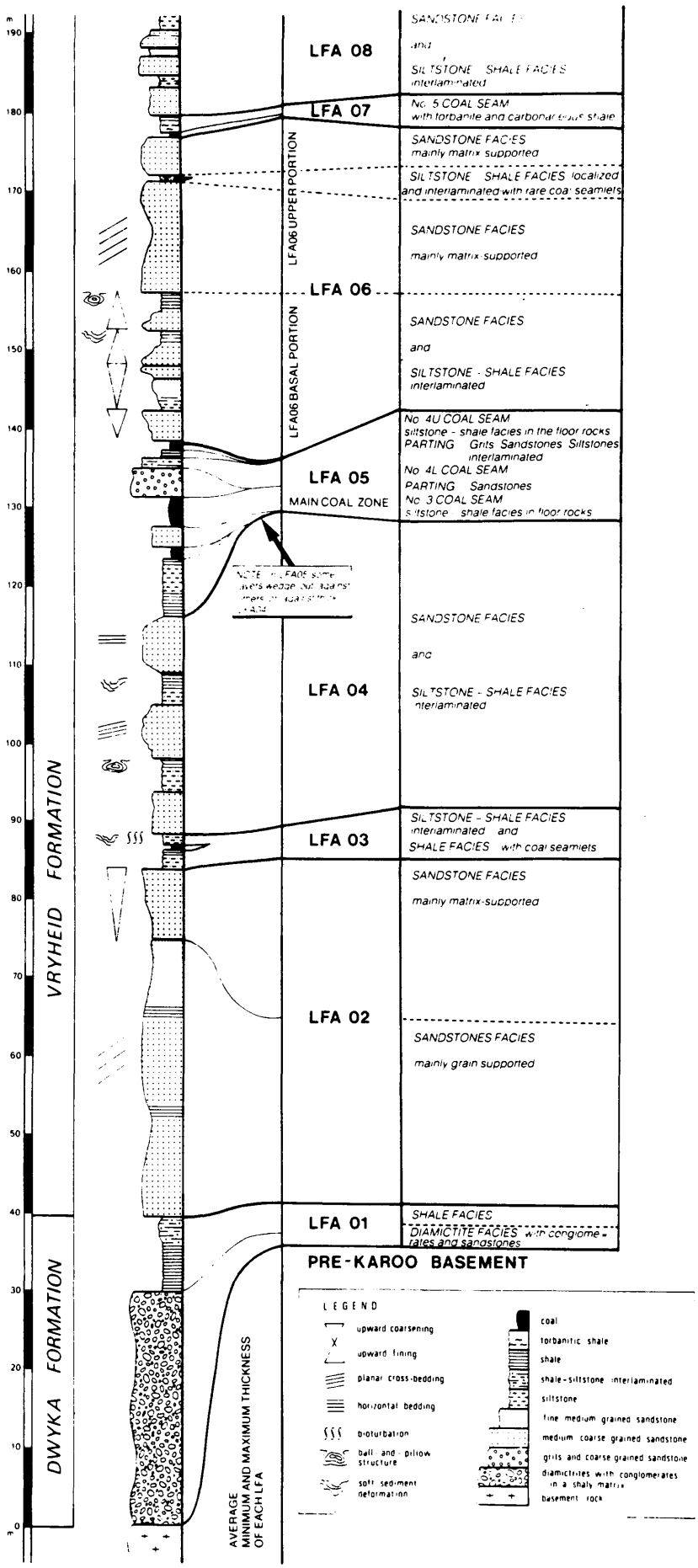
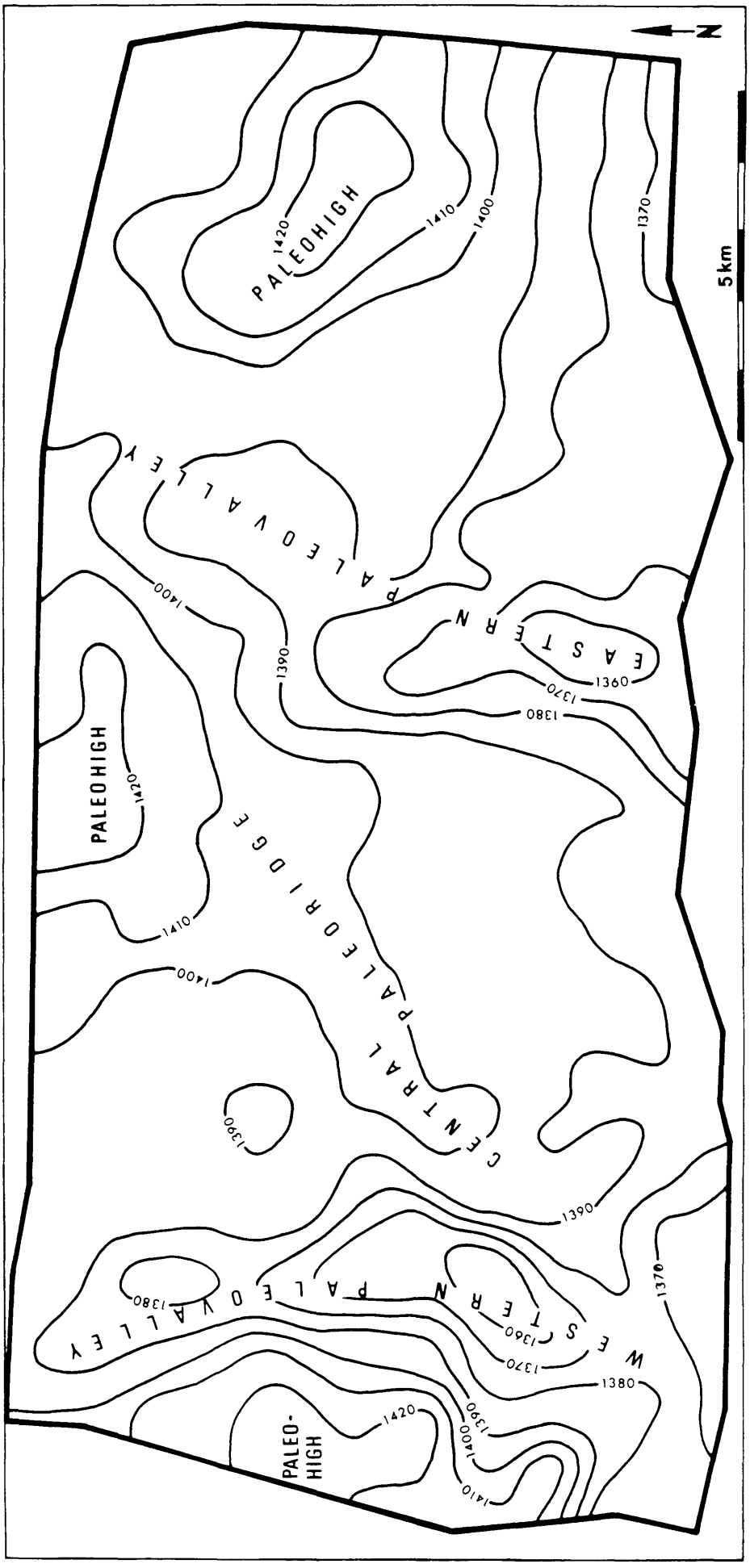


Fig. 3.1 Generalized sequence of lithofacies associations (LFA's) in the study area.

Digitised by the Department of Library Services in support of open access to information, University of Pretoria, 2021.



Map 0 Pre-Karoo paleotopography (contour interval in meters above sea level).

Digitised by the Department of Library Services in support of open access to information, University of Pretoria, 2021.

north-south trending paleovalleys are outstanding topographical features. The western one is 1-2km wide with relatively steep flanks towards the west and east and drops down to 1340m. The eastern one is about 4-5km wide, has a gently sloping eastern and a steep western flank, and drops down to 1360m. The deepest parts of the western valley occur where it intersects with the southwest-northeast trending fault zone.

The paleohighs in this region have present-day elevations of approximately 1420m above sea level and are situated in the west, the east, and in the central northern parts of the study area. A central ridge slopes down to 1390m in a southwesterly direction, parallel to the fault zone (Map 0).

3.2. LFA 01: Dwyka Formation Diamictites and Shales

This LFA comprises a diamictite facies, with lesser matrix-supported conglomerates and coarse-grained sandstones, as well as a shale facies, with occasional siltstone and sandstone interbeds. Both facies can alternate, but the diamictites and associated rocks generally occur as a massive layer underneath the shales. The shale facies is grouped with the Dwyka Formation diamictites due to a common gradational transition between the two rock types and also because the top contact of the shales is often abrupt. They do not belong to the Pietermaritzburg Formation, as this stratigraphic unit is not defined for this part of the northeastern Karoo Basin (SACS, 1980, p538&560).

The diamictite facies is generally massive and has a blue to grey, fine- to medium-grained sandy matrix (Fig. 3.2). Subangular clasts reach diameters of up to 200mm. The fragments are mostly spherical or slightly elongated and have grain sizes between 10mm and 50mm. No preferential layering or even imbrication can be detected from the borehole cores. The clasts comprise quartzite, granite, diorite, and andesite rock fragments. The diamictites are locally interbedded with, or grade up into, reworked, matrix-supported gritstones and coarse sandstones. They may thus form several upward-fining sequences. The shales and mudstones, interbedded with the diamictites, are mostly blue to grey in colour and have scattered varved layering and soft sediment deformation structures. Their contacts with the coarser facies are either sharp or gradational over a few centimeters. In some instances their top contacts with the diamictites are erosional.

The shale facies, which overlies the diamictites, is black, mostly carbonaceous and locally contains layers of siltstone with dropstones (Fig. 3.3). Interbedded coarse sandstones with ball-and-

Digitised by the Department of Library Services in support of open access to information, University of Pretoria, 2021.



Fig. 3.2 Sample of diamictite of the Dwyka Formation in LFA 01. Subangular clasts are less than 5cm in diameter and cemented by a grey to blue matrix. The red band in the bottom half of the core consists of a mixture of coarse-grained clasts with a fine to very fine matrix of similar composition.

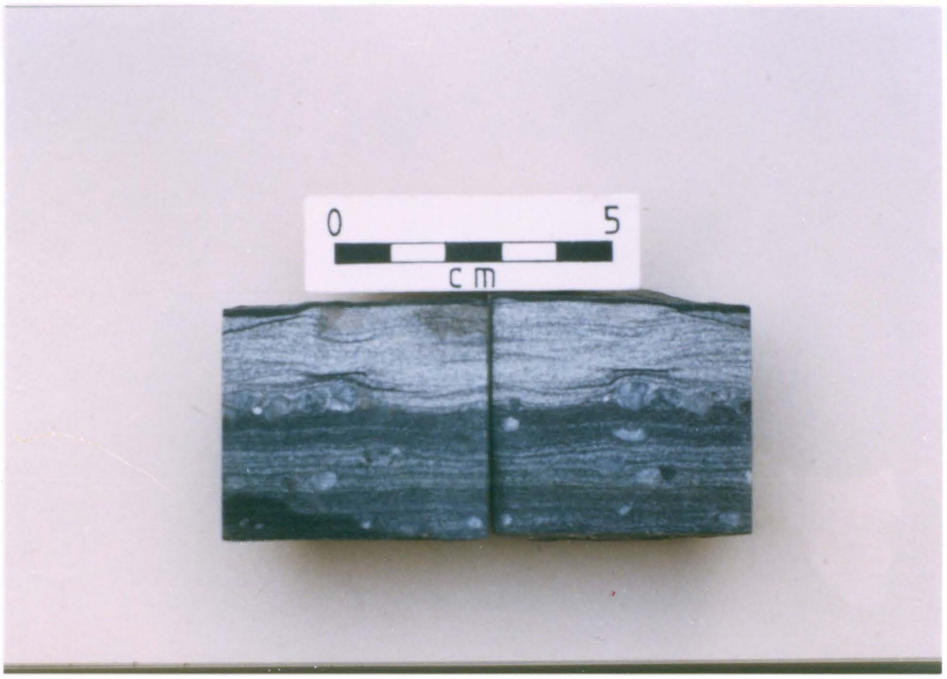
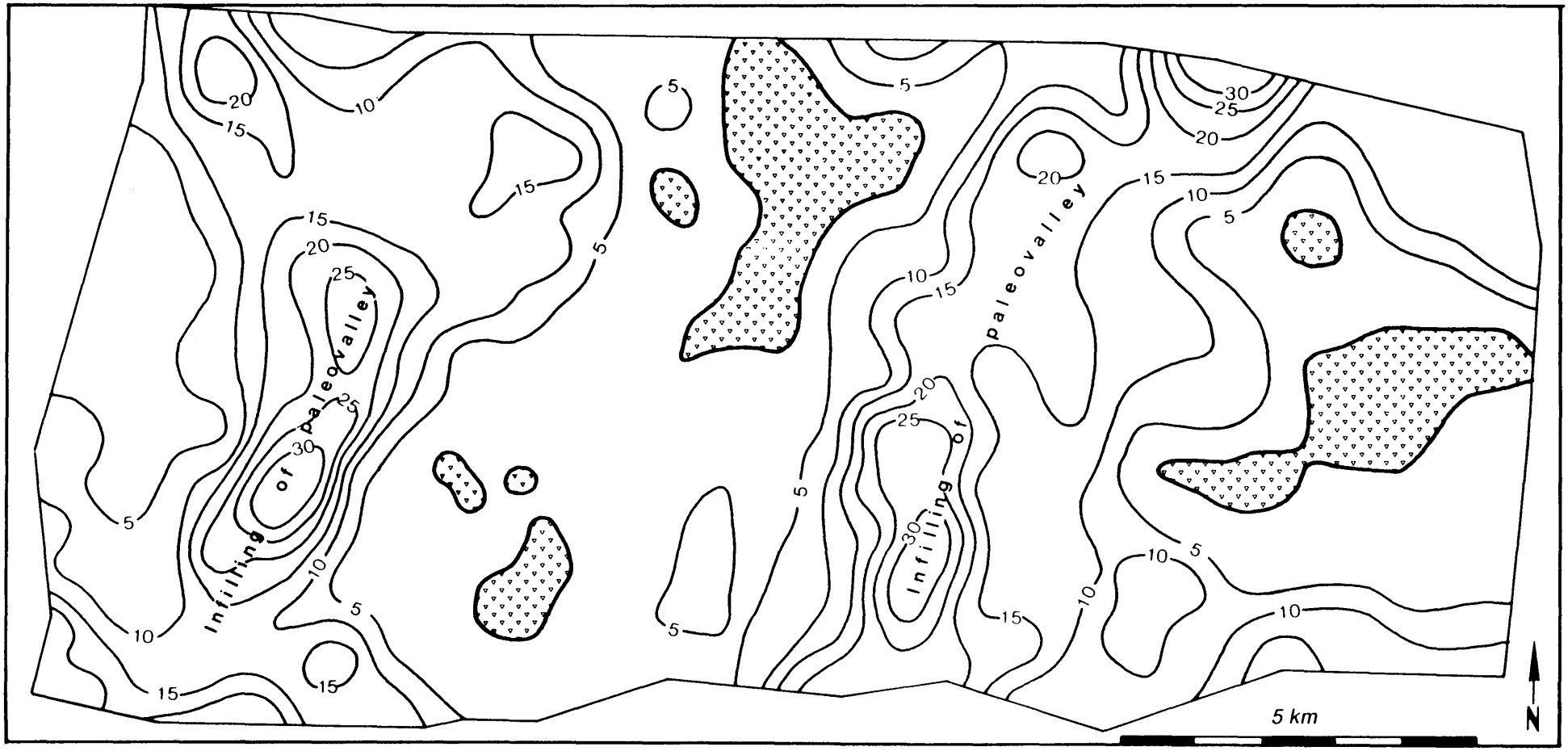


Fig. 3.3 Sample of interlaminated siltstone and shale facies with dropstones, in LFA01.

Digitised by the Department of Library Services in support of open access to information, University of Pretoria, 2021.

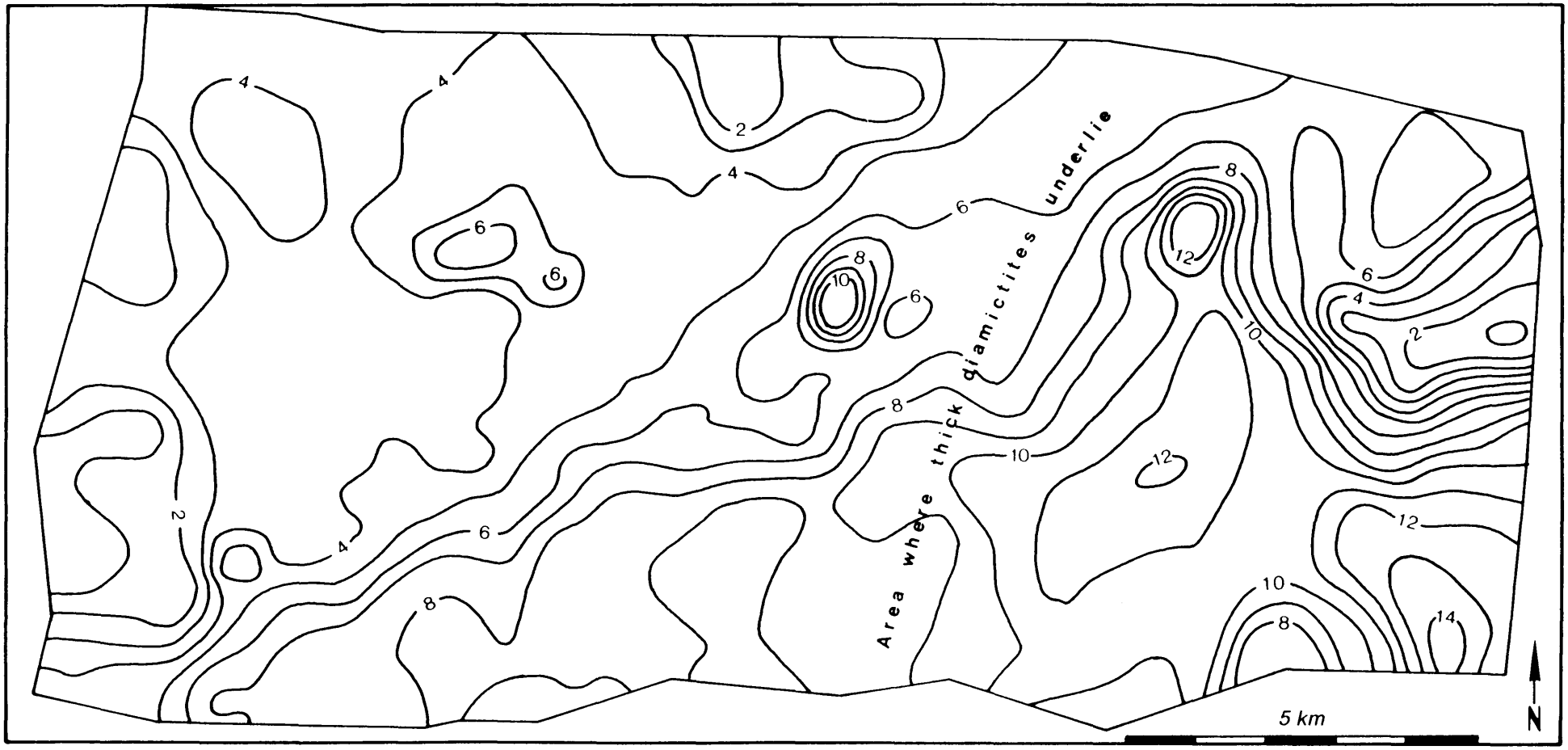


LEGEND

Areas where diamictites are not developed.

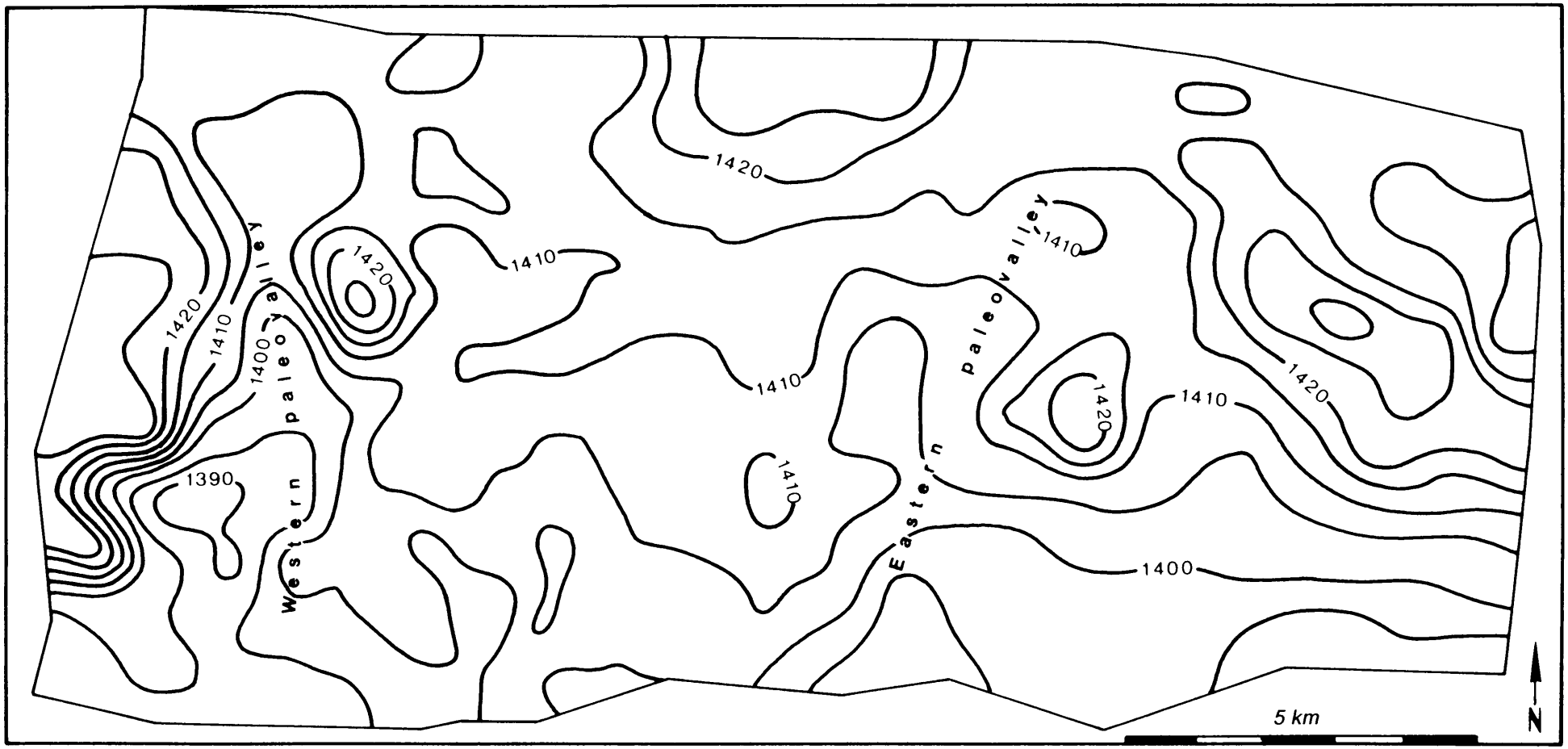
Map 1.1 Isolith map of Dwyka Formation diamictites (contour interval in meters).

Digitised by the Department of Library Services in support of open access to information, University of Pretoria, 2021.



Map 1.2 Isolith map of Dwyka Formation shales (contour interval in meters).

Digitised by the Department of Library Services in support of open access to information, University of Pretoria, 2021.



Map 1.3 Present-day post-Dwyka topography (contour interval in meters above sea level, corrected for dolerite sills within LFA 01).

Digitised by the Department of Library Services in support of open access to information, University of Pretoria, 2021.

pillow structures, as well as bioturbation increase towards the top of this layer. Rare coal fragments (<5mm) and finely disseminated pyrite and mica occur in this lithofacies.

Occurrences of the diamictite facies are concentrated in the paleovalleys of the pre-Karoo topography. From maximum thicknesses of 50m and 30m in the western and eastern paleovalley, respectively, they thin out rapidly over the paleohighs; here, in places, the diamictites are absent. Thickness trends within this facies are dominantly north-south oriented (Map 1.1).

The shale facies is generally more evenly distributed and throughout most of the area thicknesses range from about 3-8m. Thicker shales are found overlying the diamictites of the eastern paleovalley (Map 1.2), with maximum thicknesses up to 14m occurring over the eastern flank of this valley and overlying parts of a paleohigh in the pre-Karoo paleotopography. The general trend of the shale isopach contours is east-west; over the eastern paleo-valley, however, a north-south tendency remains (Map 1.2).

The present-day post-Dwyka topography reveals a less undulating surface than the pre-Karoo topography, with a more gentle north-south slope (2.42m/km). Paleohighs are more subdued compared to those of the pre-Karoo surface. The paleovalleys have gained 40-50m in elevation due to their being filled up. The eastern paleovalley, in particular, became almost level with the central paleoridge, whereas the western one still remains as a depression in the post-Dwyka surface (Map 1.3).

3.3. LFA 02: Sedimentary Rocks below the No. 2 Seam

The lower 25-35m of this LFA are dominated by a quartzitic to slightly arkosic, medium- to coarse-grained sandstone facies, which has a sharp basal contact with LFA 01. Mica occurs in occasional beds of several centimeters thickness. In thin sections the sedimentary rocks appear mainly grain-supported with rare occurrences of interstitial mica and clay minerals. Sedimentary structures include horizontal bedding (a few centimeters to decimeters thick) and large scale planar cross-bedding (set thickness up to approximately 1m).

This facies is mostly referred to as a massive unit in older borehole logs, however, from recent drilling it has become apparent that medium- and coarse-grained sandstone beds alternate randomly. Grain sizes within the sandstones typically vary from approximately 0.1-1.0mm and display subtle upward-fining and upward-coarsening trends (Fig. 3.4). The grain size distribution indicates variable sorting in the basal portion of this facies; the amount of very fine material increases towards the middle portion where the sorting

Digitised by the Department of Library Services in support of open access to information, University of Pretoria, 2021.

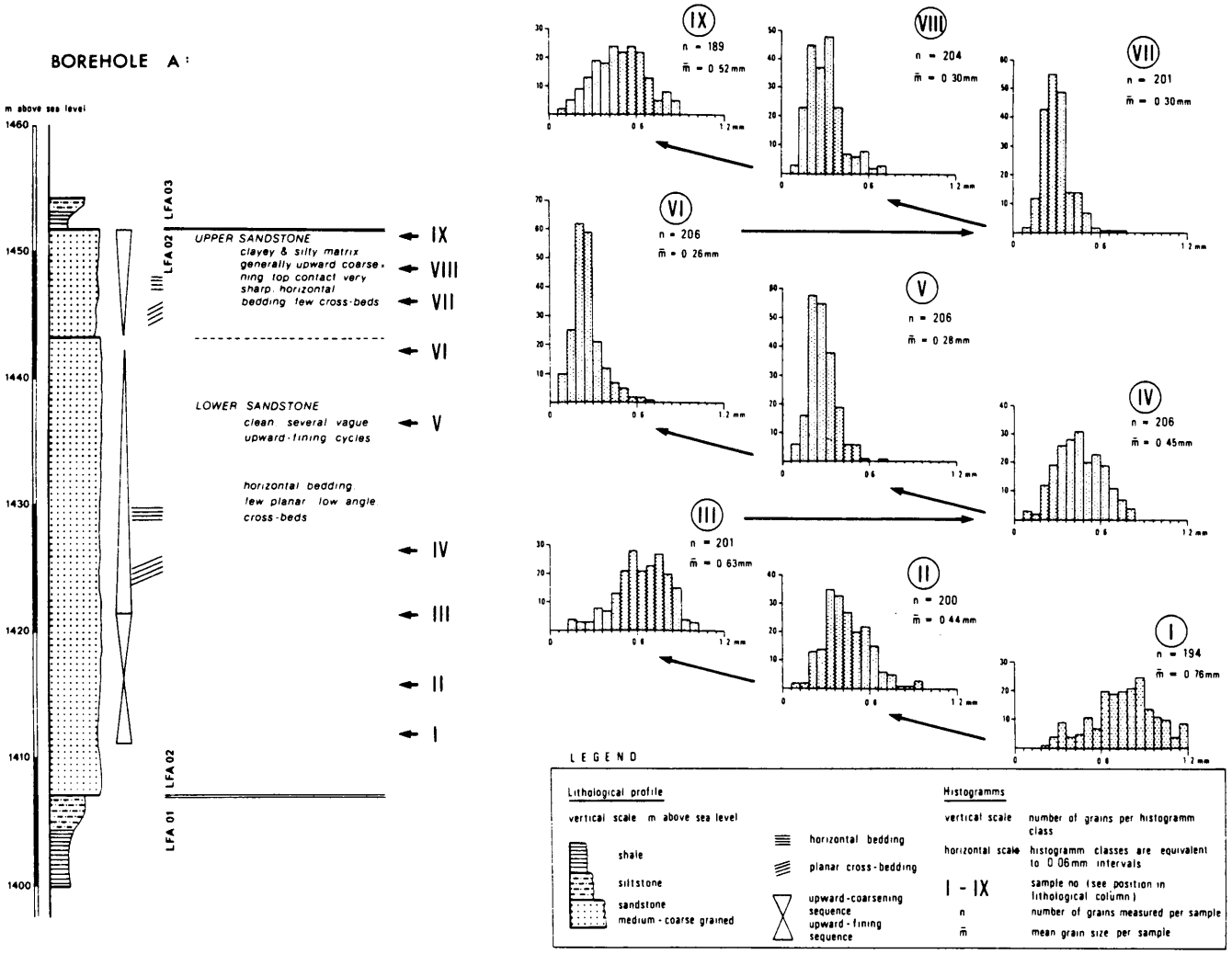
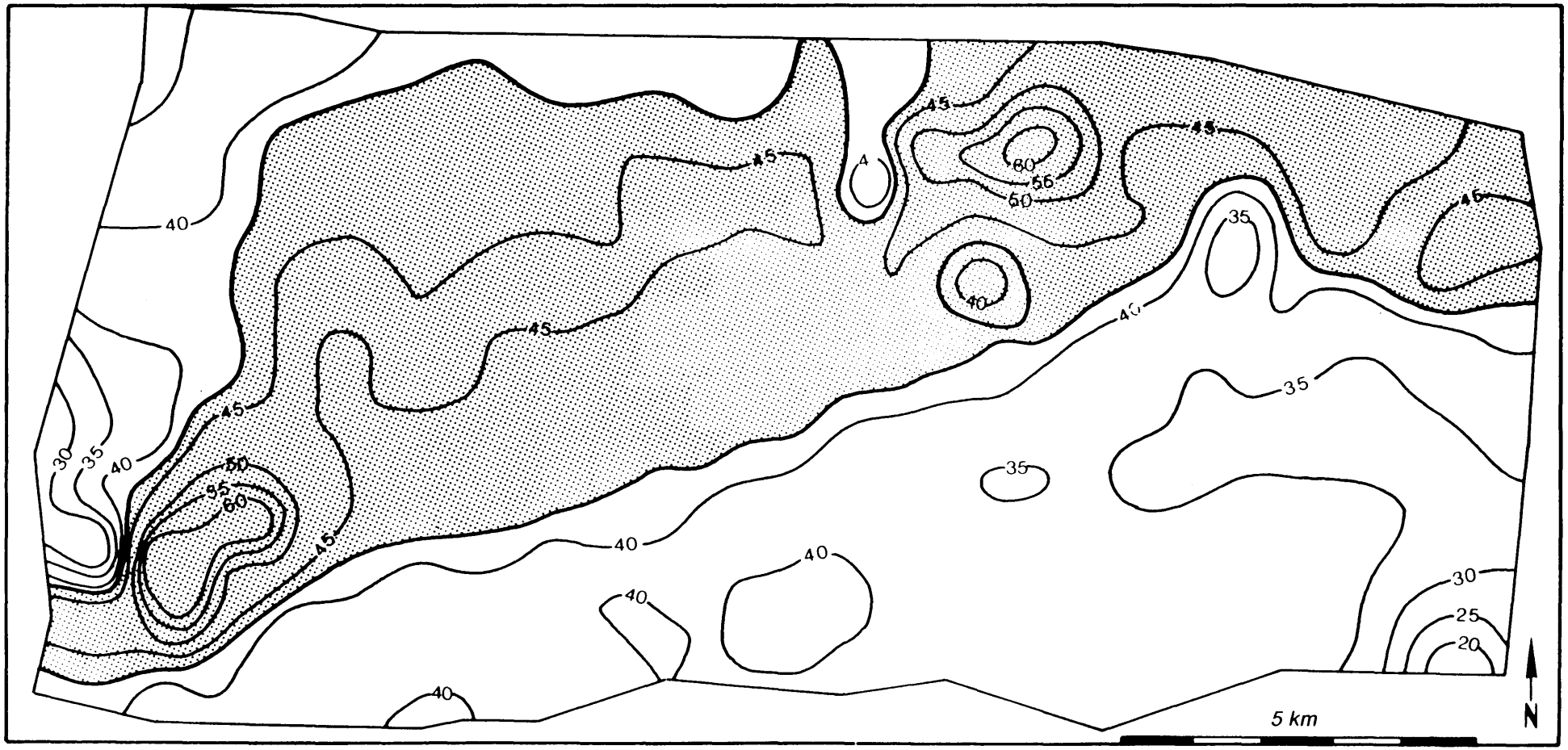


Fig. 3.4 Sample-profile from borehole **A** (see figure 2.1 for location) with lithologic description and grain size distribution histograms of LFA 02.

Digitised by the Department of Library Services in support of open access to information, University of Pretoria, 2021.



LEGEND

Thick elongated sandstone body with the outline along the 42,5 m isopach.

Map 2 Isopach map showing the geometry of LFA 02 (contour interval in meters).

Digitised by the Department of Library Services in support of open access to information, University of Pretoria, 2021.

becomes very good. Grain shapes are subangular to rounded throughout, with the exception of the basal portion where they are well rounded.

The upper 10-20m of this LFA contain a sandstone facies with a clayey and silty matrix and fine interbeds of siltstone. Mica and feldspar are generally more abundant in thin sections of this facies than in the sandstones below. In a few borehole cores plant debris and bioturbation occur at the top of this sequence. Grain sizes are medium to coarse, and locally gritty (about 0.3-0.5mm on average). The facies is generally upward-coarsening (Fig. 3.4), with the relative grain sorting decreasing towards the top and grains being poorly rounded to angular.

All lithological transitions between the different sandstones within LFA 02 are gradational and merely due to grain size variations. The top contact is either sharp or gradational over less than 10cm.

LFA 02 has an average thickness of 43m. The sediments are evenly spread, in a sheet-like manner, with the isopach contours trending east-west and southwest-northeast (Map 2). A zone of thicker accumulation of sand (>45m) is orientated east-northeast to west-southwest along the fault zone and in the northern portion of the study area. Some relatively thin occurrences (<35m) lie to the southeast and northwest of the elongated sandstone body. Low accumulations of about 20m occur in the southeastern corner and maxima of more than 65m fill a depression in the western pre-Karoo paleovalley, which remained after Dwyka sedimentation.

3.4. LFA 03: The No. 2 Coal Seam

LFA 03 correlates with the No. 2 coal seam in other areas of the Secunda Coalfield (Mr. B. HOSKING, 1985, pers. comm.), which becomes an economic seam in parts of the Highveld and Witbank Coalfields (WYBERGH, 1928; CAIRNCROSS, 1980).

This LFA comprises a black carbonaceous shale facies and an interlaminated shale and siltstone facies; siltstones and sandstones occur as coarse-grained interbeds in both these facies. The black carbonaceous shales commonly contain coal seams, that reach 15-30cm, rarely 170cm, in thickness. Pyrite is abundant as nodules and also occurs finely disseminated throughout these shales. The interlaminated shales and siltstones display soft sediment deformation structures in many places and bioturbation in their upper portions. Both facies alternate vertically and horizontally with each other.

The carbonaceous shale facies is more dominant in the basal half of LFA 03, and towards the top the silty facies and the sandy interbeds increase. This indicates a subtle upward-coarsening trend

Digitised by the Department of Library Services in support of open access to information, University of Pretoria, 2021.



LEGEND

Areas where LFA 03 is not developed.

Areas where coal occurs in LFA 03.

Zone of thick sandstone body in LFA 02.

Map 3 Isopach map showing the geometry of LFA 03 (the No. 2 coal seam) (contour interval in meters).

Digitised by the Department of Library Services in support of open access to information, University of Pretoria, 2021.

within the LFA; however, random interbedding of the two facies prevails throughout the sequence.

LFA 03 averages 4-5m in thickness, but is commonly unevenly distributed, depending on the distribution of the previous rock sequence (LFA 02). Maxima of up to 16m prevail in the eastern half of the study area where underlying sandstones are generally less than 40m thick (Map 3). Minima of less than 2m occur mostly where LFA 02 reaches more than 45m in thickness (Maps 2 and 3). In the southwestern reaches of the coalfield, near the fault zone, LFA 03 is absent. Instead, sandstones from LFA 02 are thicker here (>65m) and are laterally contiguous with LFA 03.

The thicker portions of LFA 03 are made up of more sandy and silty material. The thin portions comprise pure shales overlying depressions within LFA 02 sandstones (Maps 2 and 3). Most of the coal seamlets occur in these same areas, which are mostly situated southeast of the thick sandstone body (>45m) of LFA 02 (Map 3).

3.5. LFA 04: Sedimentary Rocks between the No. 2 Coal Seam and the Main Coal Zone

The facies association here is more complex than in the previous LFA's (Fig. 3.5). One facies comprises a medium- to coarse-grained sandstone, locally containing a silty to clayey matrix. Feldspar grains are sporadic; mica and pyrite are rare. Sedimentary structures include horizontal bedding (a few millimeters to centimeters thick) and low-angle, planar cross-bedding (set thickness mostly 3-5cm; inclination angles less than 10°).

The other facies comprises finely laminated siltstones and shales, with lesser fine- to medium-grained and rare coarse-grained sandstone interbeds (Fig. 3.6). Coal seamlets of up to 20cm thick and coalified plant debris are occasionally associated with black carbonaceous shales in this facies. There are abundant soft sediment deformation structures, particularly load casts and ball-and-pillow structures, and minor bioturbation (Fig. 3.6) in the second facies. Mica and pyrite are more common in the shale and siltstone facies than in the sandstone facies.

Several upward-coarsening and upward-fining sequences occur within LFA 04 (Fig. 3.5), but in general upward-fining trends are more common. The two facies alternate vertically in large scale units, up to several meters thick; within one facies alternations of rock types are in smaller units of a centimeter to decimeter range. The lateral extent of the two facies is limited, and thus areas exist where only the sandstone facies or only the shale and siltstone facies occur.

Digitised by the Department of Library Services in support of open access to information, University of Pretoria, 2021.

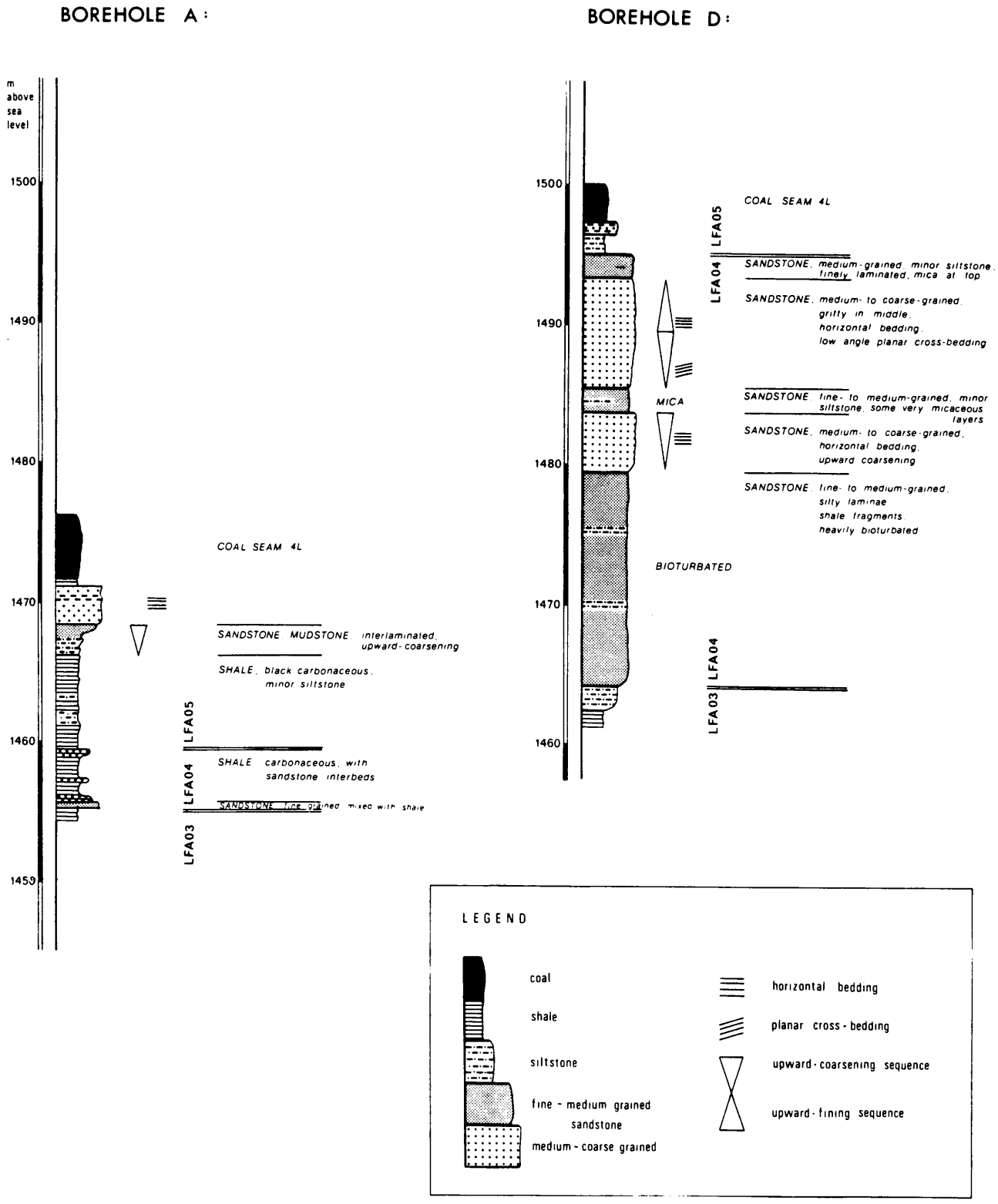


Fig. 3.5 Two sample-profiles from boreholes **A** and **D** (see figure 2.1 for location) displaying the variablity in lithology and thickness of LFA 04.

Digitised by the Department of Library Services in support of open access to information, University of Pretoria, 2021.

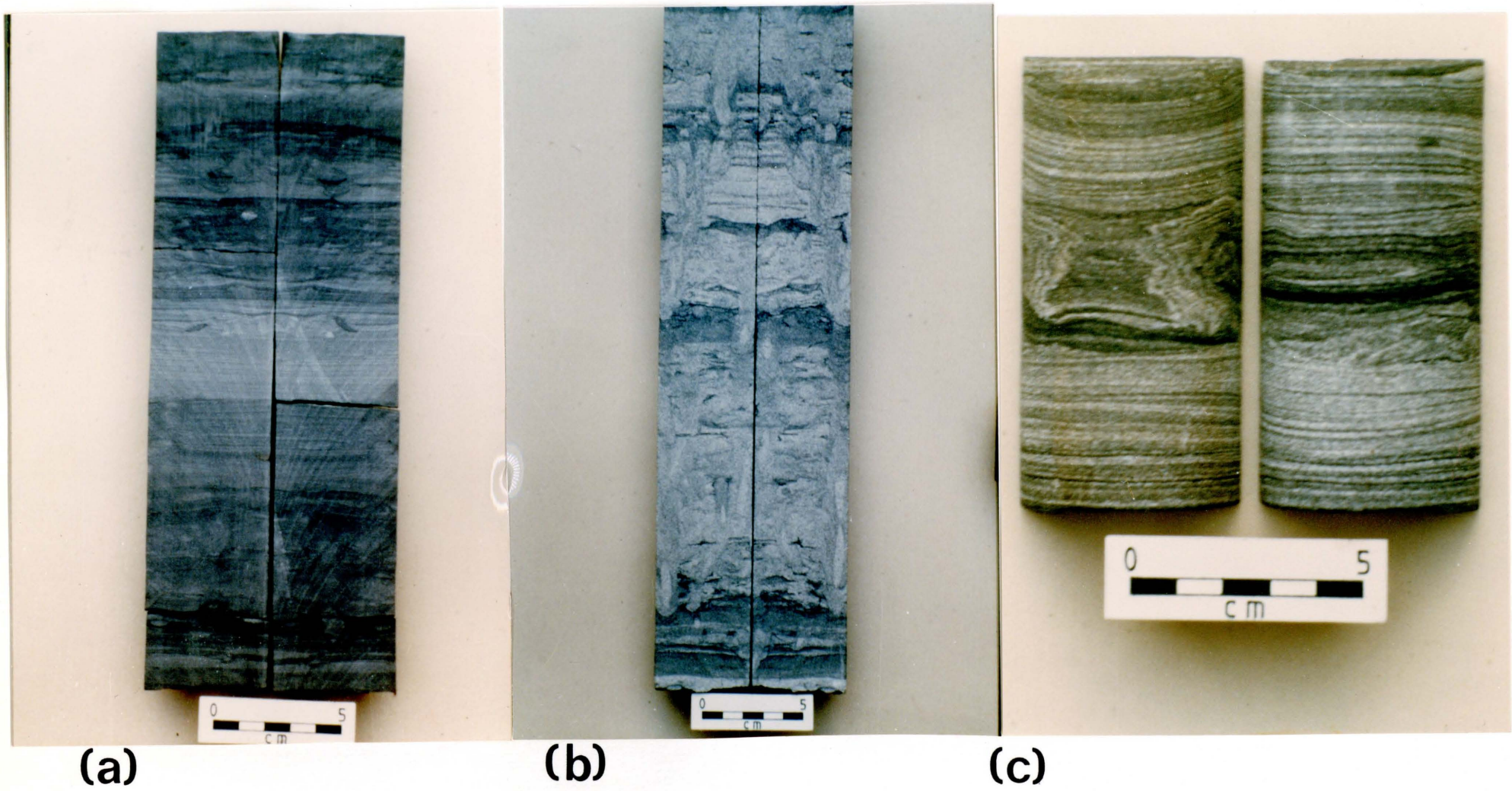


Fig. 3.6 Samples of (a) interlaminated shales and siltstone, (b) bioturbation and (c) soft sediment deformation structures within LFA 04.

Digitised by the Department of Library Services in support of open access to information, University of Pretoria, 2021.

The sediment package of LFA 04 is to a large extent evenly distributed over the study area with an average thickness of 25-30m. Values of up to 40m are reached over the southern parts of the western pre-Karoo paleovalley (Map 4.1). Here LFA 03 was thin to absent whereas LFA 02 developed a thick sequence (Maps 2 and 3). An elongated sediment body, up to 40m thick, stretches approximately north-south over the eastern pre-Karoo paleohigh. Thicknesses of less than 20m occur in a southwest-northeasterly orientation over the central pre-Karoo paleoridge, parallel to the fault zone and in an extensive area overlying the eastern pre-Karoo paleovalley. The preferred direction of the LFA 04 isopachs is southwest-northeast in the western and central parts of the study area and north-south in the eastern part.

3.5.1. Summary of LFA's 02 to 04

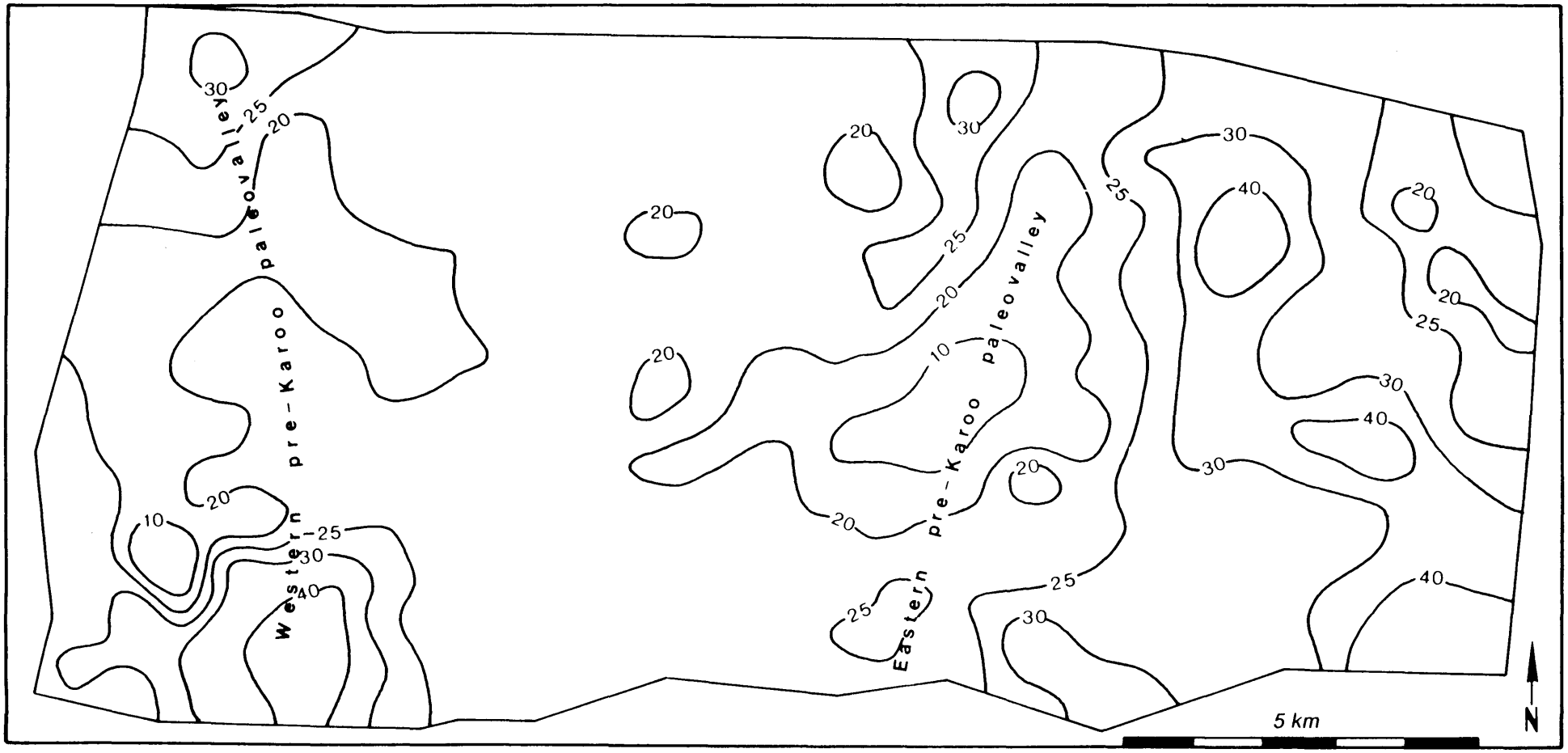
A remarkable feature of the sequence of LFA's 02 to 04 is that, as a whole, it spreads almost evenly in a sheet-like layer over the entire Twistdraai Coalfield. Both thinner and thicker accumulations do, however, occur over the eastern half of the study area (Map 4.2) and correlate well with the underlying pre-Karoo topography in that part.

The 70m isopach for the cumulative thickness of all three LFA's and zones thicker than 75m are generally parallel to the fault zone and to the main isopach trends of LFA's 02 and 04 (compare maps 2, 4.1 and 4.2). Northwest of the fault zone the cumulative sediment thickness drops to 65-67m and towards the southeast it increases to more than 70m.

The present-day top surface of LFA 04 is gently undulating and resembles a muted version of the topography of the pre-Karoo floor (Maps 4.3 and 0). The paleoslope of 2.31m/km is about the same as that of the post-Dwyka surface of 2.42m/km. The eastern paleovalley is still prominent, whereas the western paleovalley has largely become leveled out (Map 4.3).

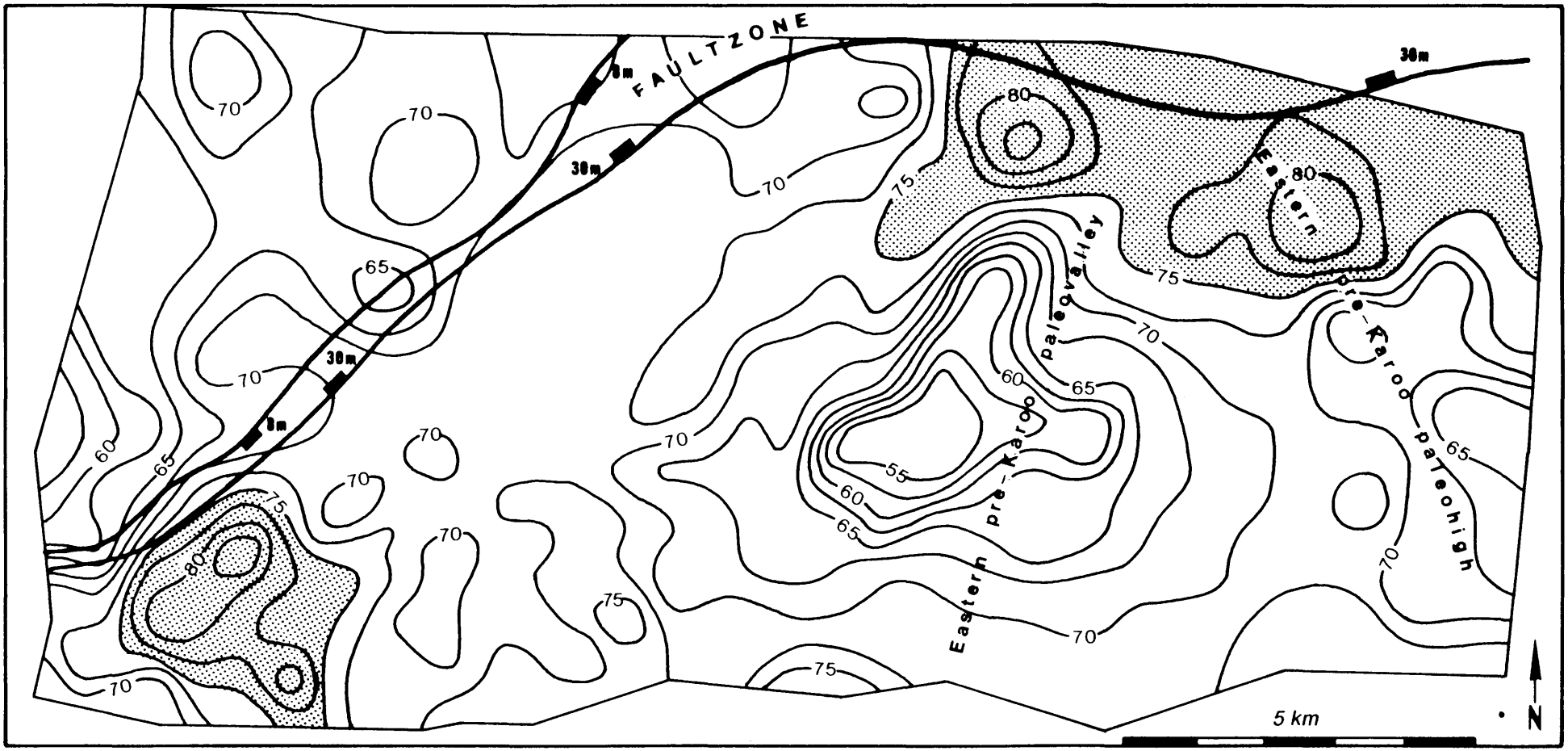
Paleohighs, overlying pre-Karoo paleohighs, exist in the west and stretch from the central northern to the eastern parts of the study area (Map 4.3). The contour lines generally trend east-west with north-south directions over the eastern pre-Karoo paleovalley.

Digitised by the Department of Library Services in support of open access to information, University of Pretoria, 2021.



Map 4.1 Isopach map showing the geometry of LFA 04 (contour interval in meters).

Digitised by the Department of Library Services in support of open access to information, University of Pretoria, 2021.

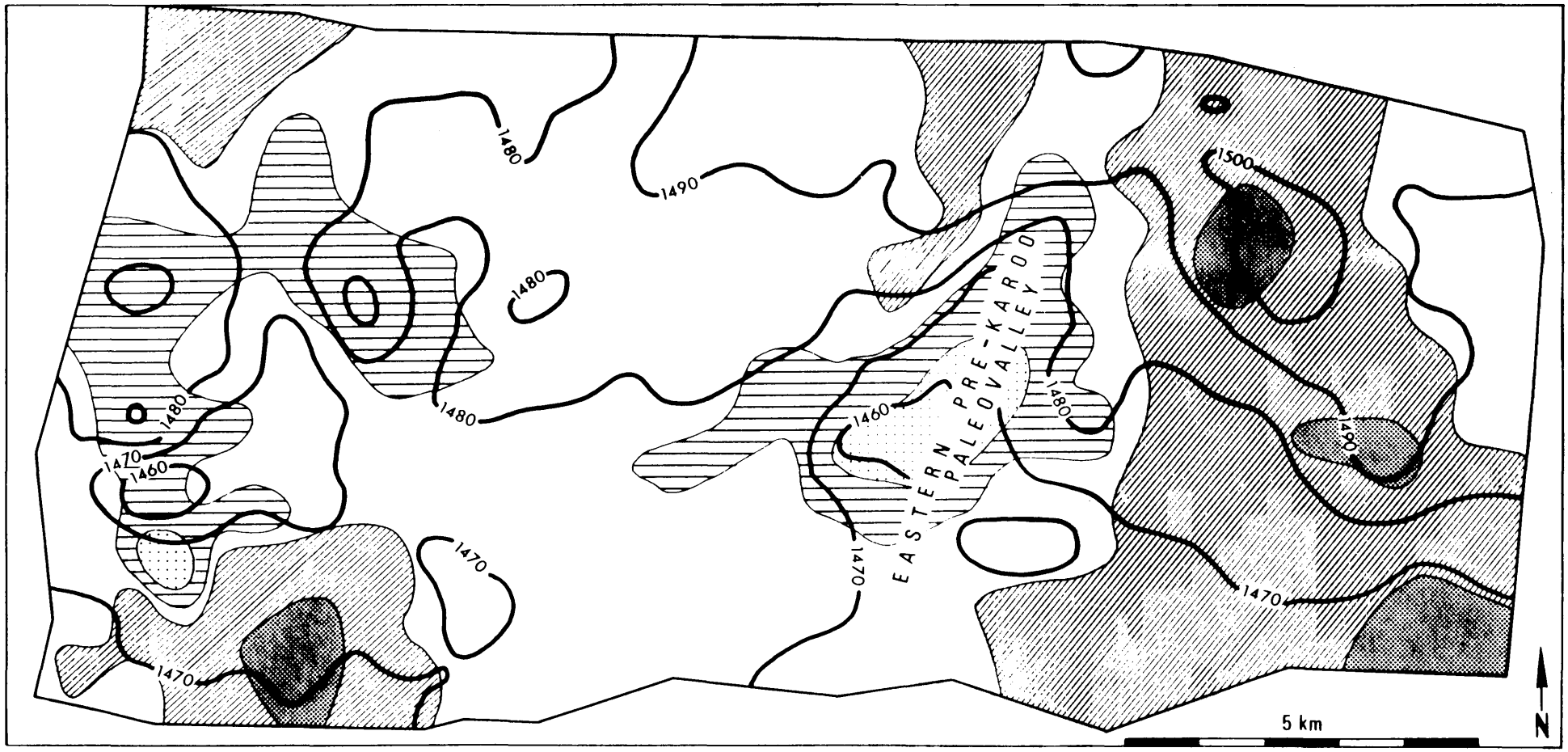


LEGEND

Areas where the cumulative thickness of LFA's 02 to 04 is greater than 75 m.

Map 4.2 Isopach map of cumulative thickness of LFA's 02 to 04 (contour interval in meters).

Digitised by the Department of Library Services in support of open access to information, University of Pretoria, 2021.



LEGEND

LFA 04 thicker than 40 m	LFA 04 thicker than 25 m	LFA 04 thinner than 20 m	LFA 04 thinner than 10 m

Map 4.3 Present-day topography at top contact of LFA 04 (contours in meters above sea level. corrected for dolerite sills in underlying LFA's).(Shadings

Digitised by the Department of Library Services in support of open access to information, University of Pretoria, 2021.

3.6. LFA 05: The Main Coal Zone

The main coal zone includes coal seams No. 3, No. 4L and No. 4U and their respective partings (Fig. 3.7). The No. 3 and No. 4U seams are commonly initiated by shales and siltstones in the floor rocks, whereas No. 4L largely developed on fine- to medium-grained sandstones. The partings between the seams are characterized by sandy and gritty material, with minor silty and shaly sedimentary rocks.

The total thickness of LFA 05 averages about 10-14m in most parts of the study area, however, a maximum thickness of up to 24m is recorded in region III above the eastern paleovalley (Map 5.1). For the purpose of more detailed description and the subsequent discussion of this LFA, the three seams and their partings will be referred to separately. However, as will become clear in the discussion, it is more appropriate to the development of the sedimentary model to group these sediments into one major LFA.

3.6.1. The No. 3 Coal Seam

The coal of No. 3 seam mainly consists of mixed lithotypes, clarain and duroclarain. There are only a few clastic lenses in the seam, which mostly incorporate silty and shaly material with minor amounts of sandstone. The coal commonly contains siderite and pyrite concretions and nodules, as well as calcite along joints and cracks.

Shales and siltstones commonly form the floor rocks of the coal seam (Map 5.2). The shales are commonly carbonaceous and contain minor coarse-grained sandstone interbeds, fine laminations and soft sediment deformation structures. Minerals include abundant mica and localized pyrite and siderite. This facies resembles the shales and siltstones within LFA 04.

The shales and siltstones underlying the coal mostly occupy depressions in the present-day elevation of the top of LFA 04 (Maps 4.3 and 5.2). Consequently, several deposits of up to 6m are situated north of the fault zone, as well as in an extensive area over the eastern pre-Karoo paleovalley. This facies thins out to 1m and less over large areas of the central pre-Karoo paleoridge and towards the eastern margin of the study area, above the underlying sedimentary rocks of LFA 04. Shales are normally concentrated in the thin deposits, whereas the amount of silty and sandy interbeds increases in the thicker deposits of this facies.

The coal of the No. 3 seam is restricted to the central and southern reaches of the Twistdraai Coalfield (Map 5.3). The average thickness is about 50-60cm; zones of relatively thick coal, up to 140cm, run from east to west in the southern parts and from north to south in the centre of the study area.

Digitised by the Department of Library Services in support of open access to information, University of Pretoria, 2021.

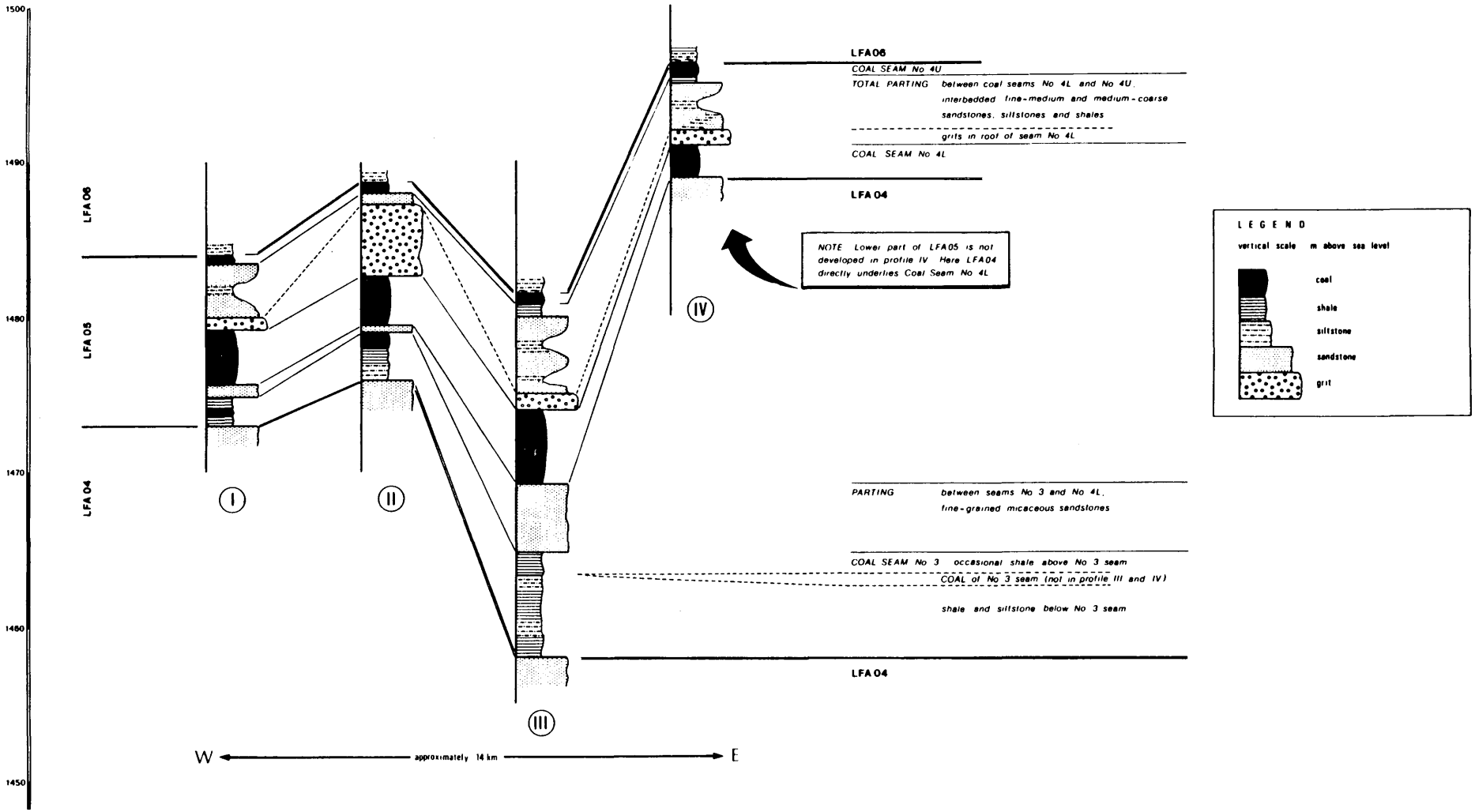
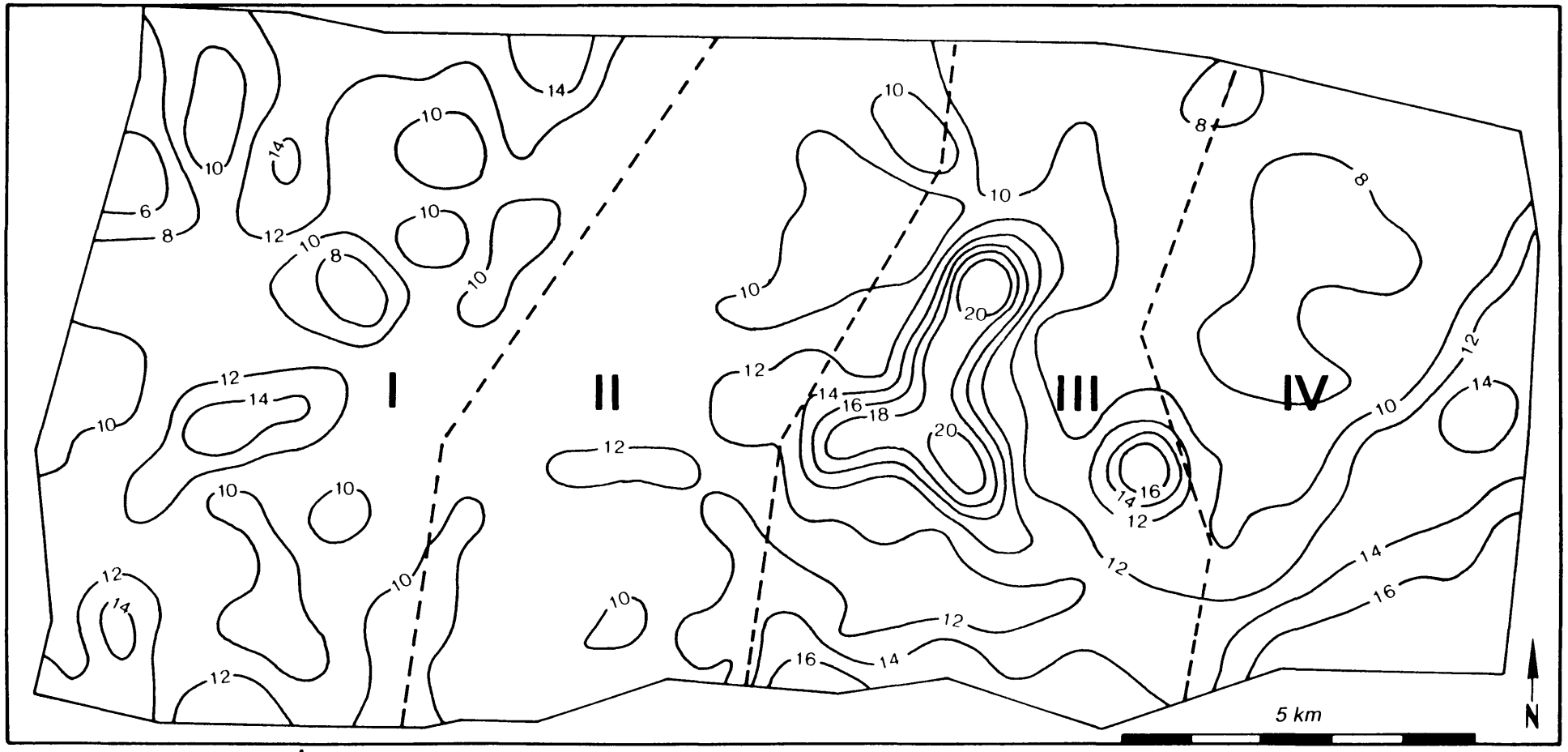


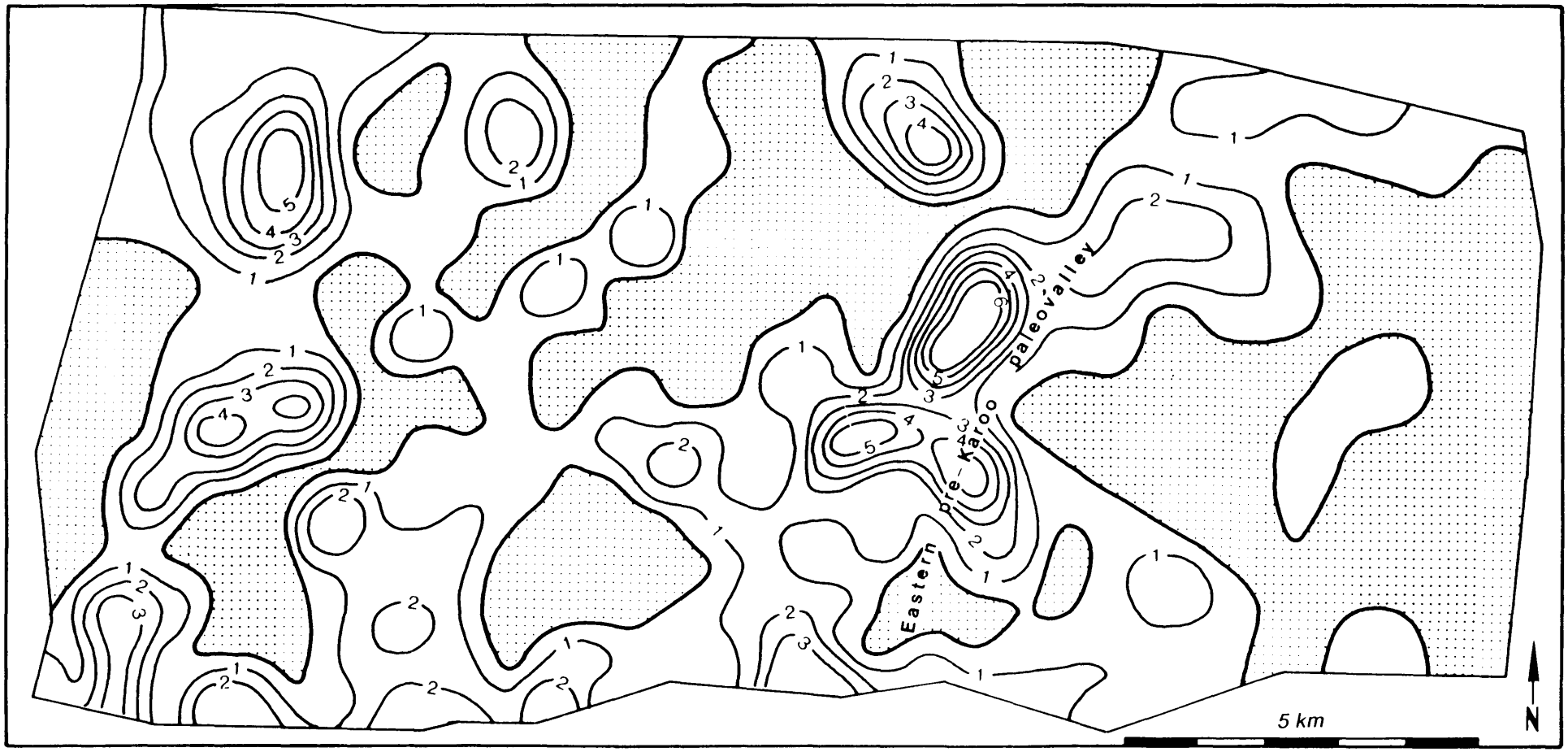
Fig. 3.7 Four type-profiles of LFA 05 (the main coal zone), each one being representative for a respective depositional region within the study area (see map 5.1)

Digitised by the Department of Library Services in support of open access to information, University of Pretoria, 2021.



Map 5.1 Isopach map showing the geometry of LFA 05 (the main coal zone) (contour interval in meters).

Digitised by the Department of Library Services in support of open access to information, University of Pretoria, 2021.

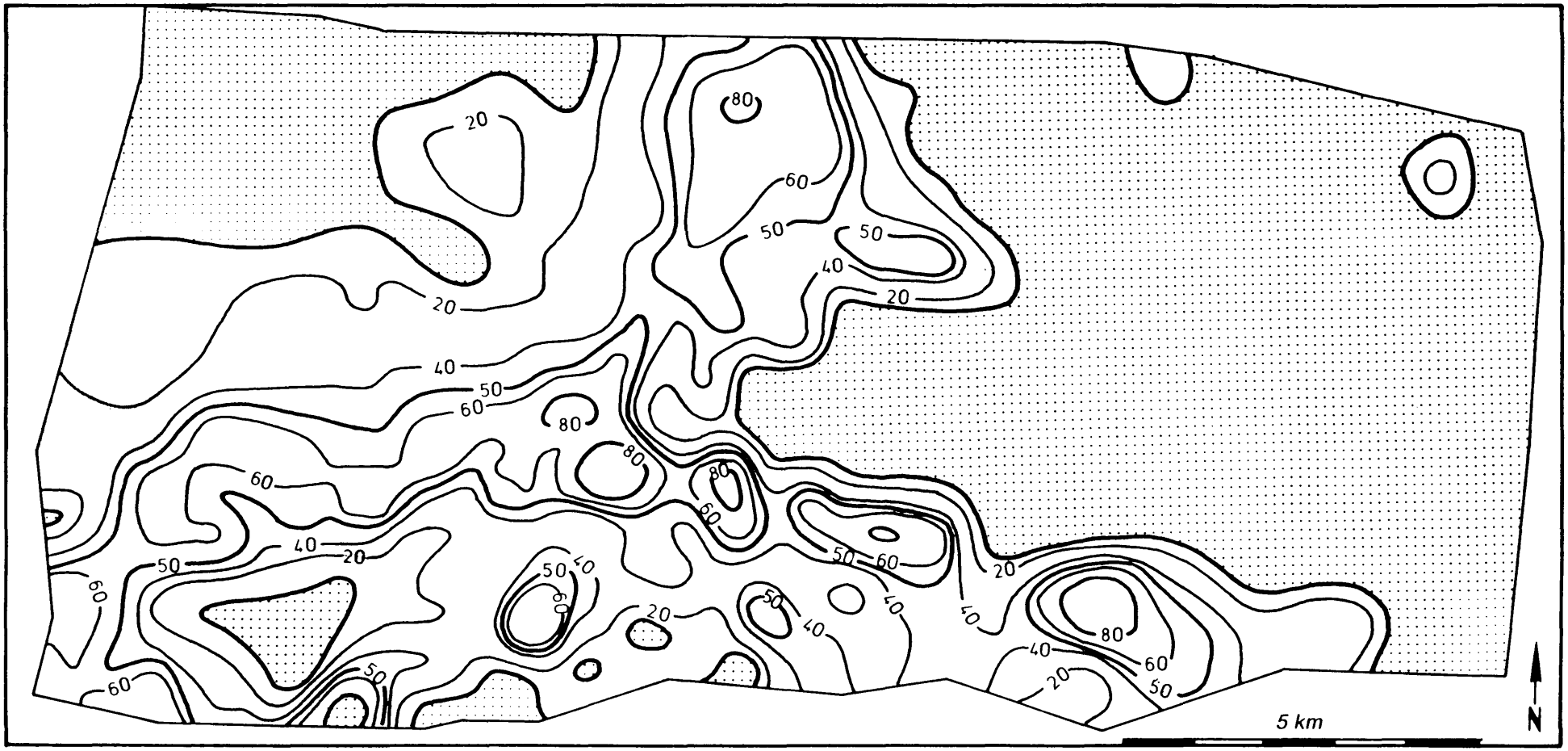


LEGEND

Areas where the floor rocks of the No. 3 coal seam comprise sandstones of LFA 04.

Map 5.2 Distritubion and isolith map of shales and siltstones (contour interval in meters) in the floor of the No. 3 coal seam.

Digitised by the Department of Library Services in support of open access to information, University of Pretoria, 2021.

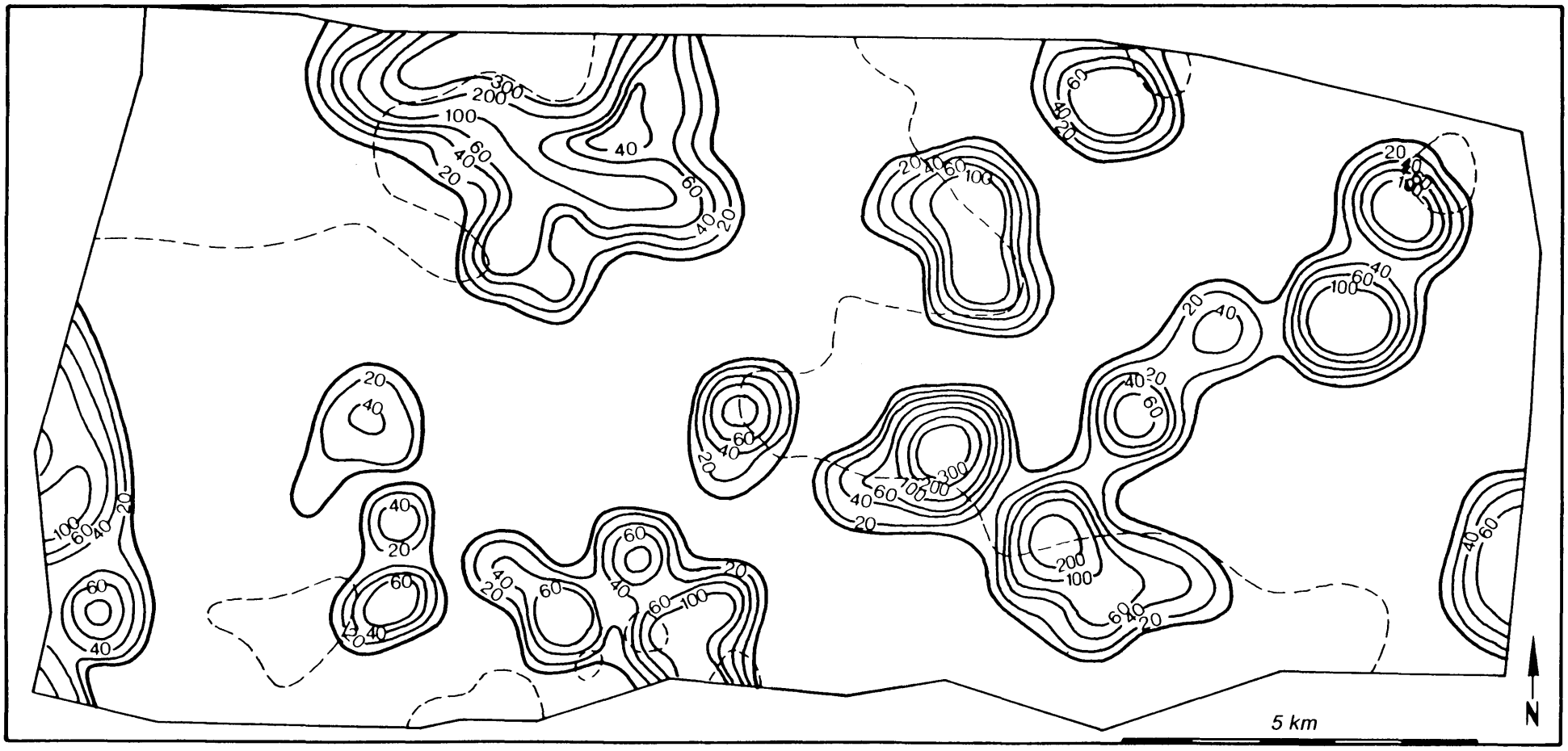


LEGEND

Areas where the No. 3 coal seam is not developed.

Map 5.3 Distribution and isopach map of the coal in the No. 3 seam (contour interval in centimeters).

Digitised by the Department of Library Services in support of open access to information, University of Pretoria, 2021.



Map 5.4 Distrubution and isolith map of shales which abut and overlie the No. 3 coal seam (contour in centimeters). The dotted line indicates the outline of the underlying No. 3 coal seam.

Digitised by the Department of Library Services in support of open access to information, University of Pretoria, 2021.

The seam thickness gradually decreases to zero across the fault zone to the northwest and also pinches out rapidly towards the east along the western flank of the eastern pre-Karoo paleovalley. Thus coal is absent in the northwest of the study area and only present in patches thinner than 10cm in the eastern half. Towards the south the seam becomes gradually thinner and is locally absent.

The underlying shale and siltstone facies, in some instances, passes laterally into and overlaps the No. 3 coal seam. This generally occurs along the margins of the coal seam, particularly south of the northeastern portion of the fault zone and over the eastern pre-Karoo paleovalley (Map 5.4).

Relating the coal thickness to floor rock lithology (Maps 5.2 and 5.3) reveals that maximum thicknesses of the coal concentrate above and alongside thin and intermediate shale deposits in the central, southwestern and southern portions of the study area. No coal occurs above the thick shales and siltstones overlying the eastern pre-Karoo paleovalley. Only towards the south is coal present over sandstones of LFA 04.

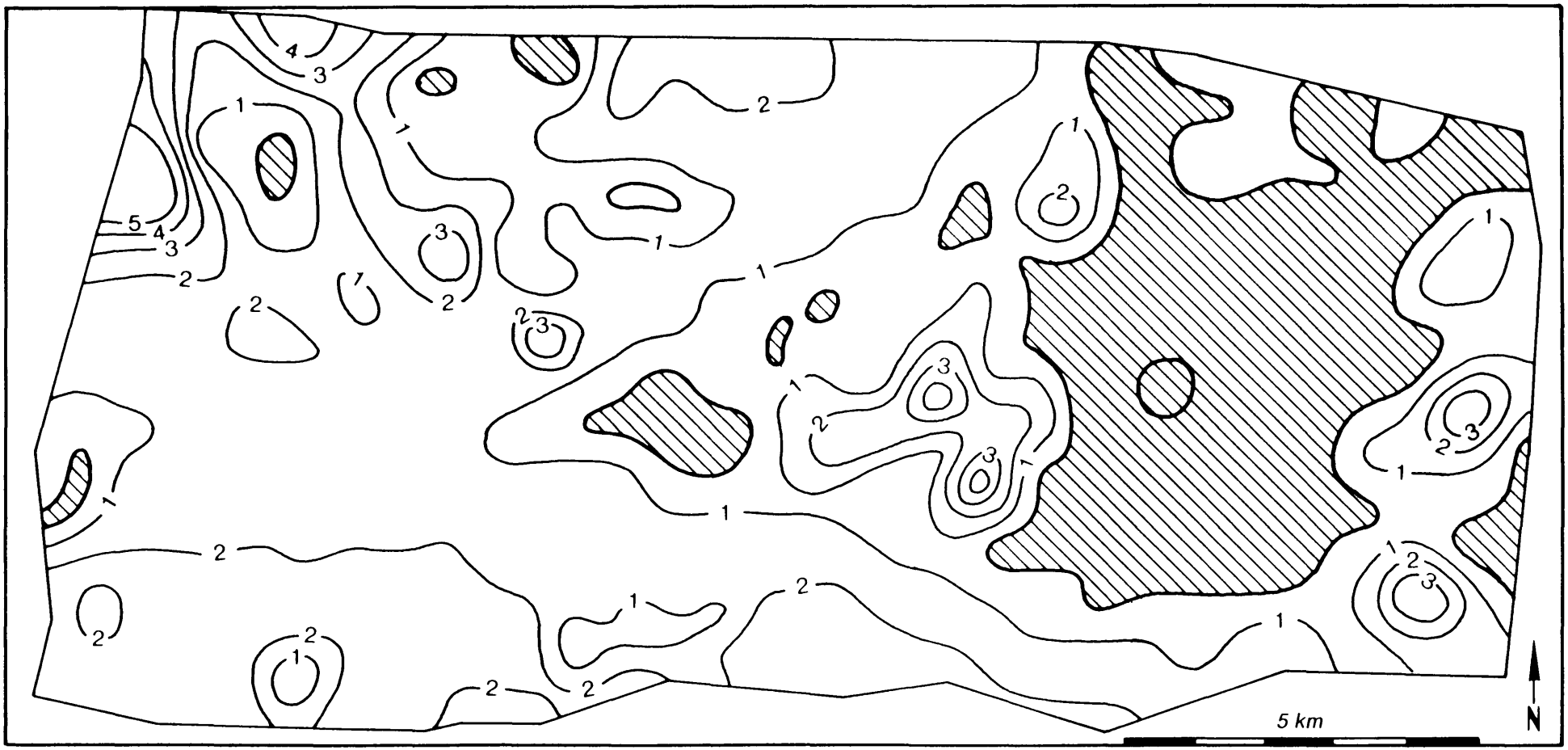
3.6.2. Parting between No. 3 and No. 4L Coal Seams

The sandstone parting between seams No. 3 and No. 4L is fine-grained, grey to brownish and rich in mica. Pyrite and siderite occur in rare concretions, generally in areas where No. 3 coal underlies the parting. Planar cross-bedding is common, with fewer trough cross-beds and horizontal stratification. The dimensions of all structures lie in a centimeter range.

In areas where No. 3 coal seam is not present this sandstone parting either lies above the shale and siltstone facies associated with No. 3 coal seam, or directly above the sandstone facies of LFA 04. The sandstone parting is distinguished from the latter by its generally finer grain size and its higher mica content.

The thickness distribution of the parting is irregular (Map 5.5). The sandstones have an average thickness of 1,5m and thin out to less than 1m, or wedge out entirely, above thick coals of the underlying No. 3 seam. A thicker sandstone parting, over 2m, is commonly found overlying areas where the No. 3 coal seam is thin or absent (Maps 5.3 and 5.5). This includes parts of the southern margin as well as the northwestern reaches of the coalfield, besides a few local occurrences. A maximum parting of approximately 3-4m is found above the eastern pre-Karoo paleovalley and in the northwestern corner of the study area. The eastern pre-Karoo paleohigh as well as the eastern margin of the coalfield remains mainly uncovered by this sandstone facies.

Digitised by the Department of Library Services in support of open access to information, University of Pretoria, 2021.



LEGEND

Areas where the sandstone parting is not developed.

Map 5.5 Distrubution and isolith map of the sandstone parting between No.3 and No. 4L coal seam (contour interval in meters).

Digitised by the Department of Library Services in support of open access to information, University of Pretoria, 2021.

3.6.3. The No. 4L Coal Seam

Coal seam No. 4L consists of mixed and dull coals, clarain and durain, with a few prominent bright coal bands of vitrain. Torbanites and torbanitic shales are present as sporadic lenses and beds; in other parts of the Secunda Coalfields, however, they reach considerable thickness and lateral extent (Mr. B. Hosking, 1985, pers. comm.). Pyrite concretions and calcite along joints and cracks occur throughout the No. 4L seam, siderite nodules form some distinct horizons.

In figure 3.8 detailed descriptions of the measured profiles of No. 4L coal seam in sections 59, 60, 61 and 62 of the mine are given (see Fig. 2.1 for locality of sections). In brief the profiles can be laterally correlated, and are vertically divided into four cycles, which correlate with the cycles distinguished micropetrographically in section 3.13. These cycles generally commence with predominantly durain bands in their basal portion and grade into clarain and vitrain bands towards the top. The basal cycle A, which is relatively thin in section 61, mainly contains durain bands and is mostly capped by a prominent vitrain band. Cycle B, the thickest one, often comprises an alteration of durain and clarain bands, with the latter increasing towards the top. In the centre of the coalfield (section 61) this cycle is often underlain by clastic rock lenses. Typically, cycle C commences with a prominent durain band which is capped by a laterally persistent vitrain layer. This vitrain is usually associated with shale and siltstone lenses at its basal and top contacts. It is less distinctive in section 61, where clarain dominates instead. The topmost cycle D is only fully developed in section 59 and comprises alternating durain and clarain bands with minor vitrain.

In sections 60 and 62 the seam is thinner (2.8m) than in section 59 (3.7m). However, in borehole B (Fig. 2.1 for location), situated in the vicinity of section 62, the seam reaches a similar thickness to that in section 59 (Fig. 3.8). In borehole E (Fig. 2.1), which lies just to the east of section 60, the seam is once again thinner. Seam profiles in section 61 have an inconsistent seam thickness, approximately 2.6m, and the lithotype bands are thinner and alternate more rapidly. Their cyclicity is thus not as noticeable as in the other mining sections. For further detail refer to the micropetrographic description of the seam profiles in section 3.13.

In principle, the seam consists of three major portions; the basal and top portions (cycles A and D) are inpersistently developed throughout the study area. The middle portion (cycles B and C) appears to be present in all parts of the coalfield. This distinction of three major seam sections is also indicated by the vertical distribution of in-seam clastic partings which mostly occur in the bottom and top parts of the No. 4L coal seam, and rarely in the middle. They comprise

Digitised by the Department of Library Services in support of open access to information, University of Pretoria, 2021.

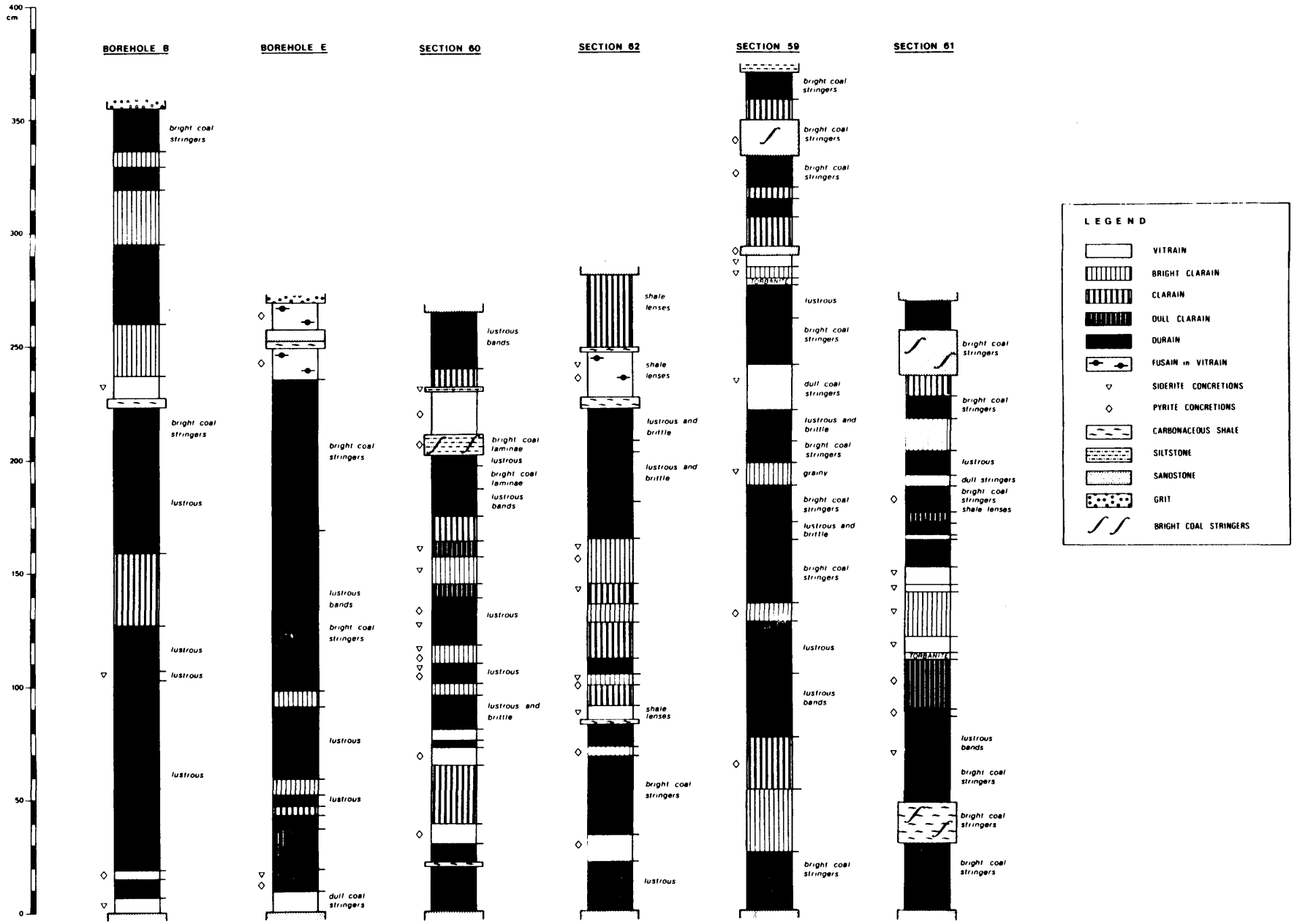


Fig. 3.8 Sample-profiles of macropetrographic seam sections of the No. 4L coal seam. A comparison of two drill core profiles with four profiles measured underground in the Twistdraai Mine (see figure 2.1 for localities of all profiles)

Digitised by the Department of Library Services in support of open access to information, University of Pretoria, 2021.

mainly medium-grained, locally cross-bedded sandstones and minor shales. In places these sandstones become particularly gritty within the top third of the seam.

The cumulative thickness of these clastic lenses within either the top or the basal portion of the seam may be up to 50cm, but generally remains in the range of 10-20cm (Maps 5.7 and 5.8). Single lenses seldom exceed 10m in lateral extent, but areas in which they occur are estimated to be up to several 100m in diameter as deduced from the borehole records.

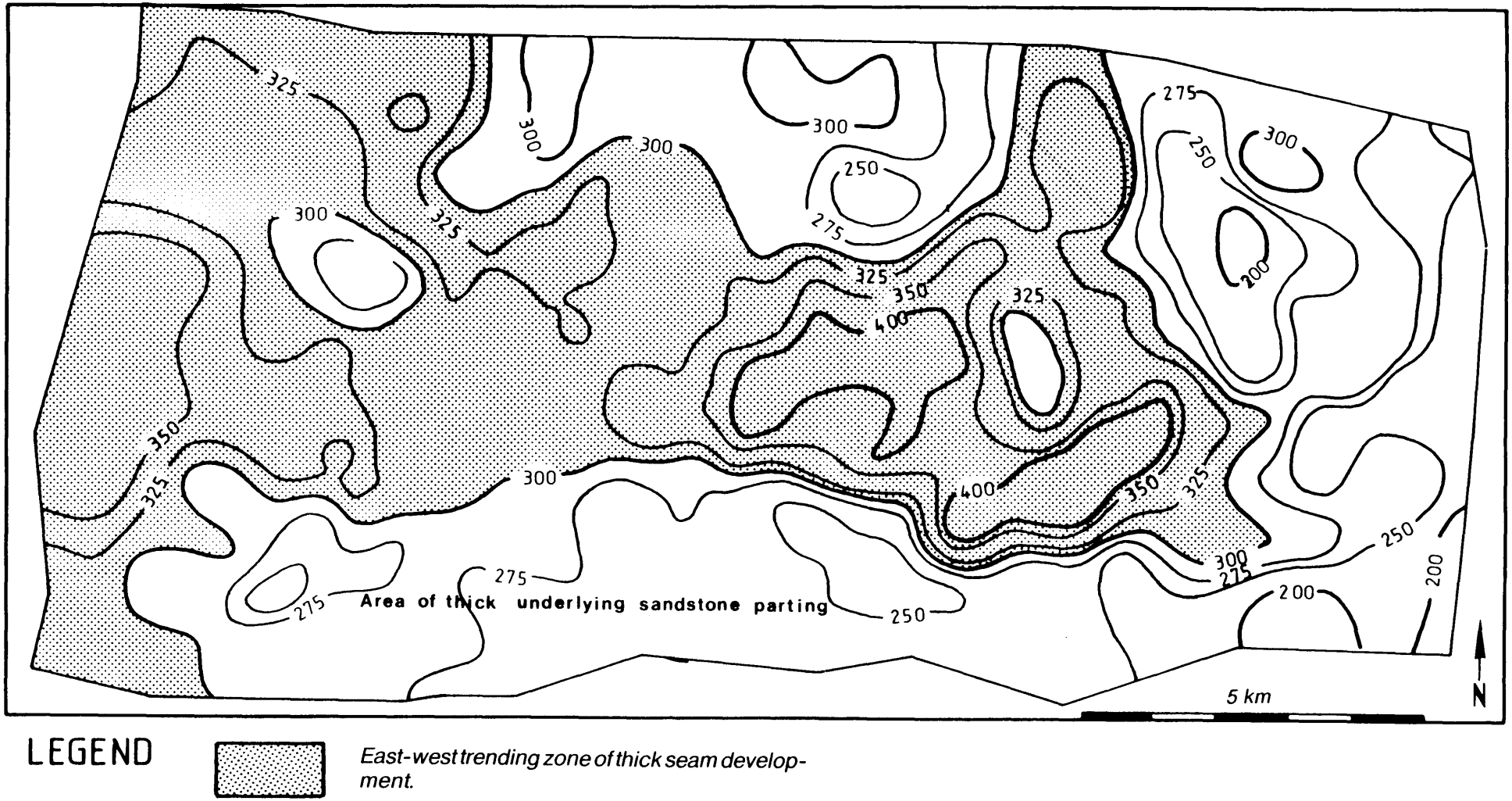
The No. 4L coal seam covers the entire Twistdraai Coalfield with an average thickness of 3.5m (Map 5.6). An east-west oriented zone of coal thicker than 3m extends from the western margin over the mine itself and gradually thins out towards the northern, southern, and eastern margins of the study area. Thinner coals, down to 2.5m, overlie relatively thick sandstone partings along the southern and northern margins (Maps 5.5 and 5.6). The thinnest coals, of less than 2m, are concentrated in the eastern part, where the underlying LFA 04 sandstones are thick. Coal accumulated to more than 4m over the eastern pre-Karoo paleovalley, where a thick sandstone parting over thick shales is developed underneath, but no coals of No. 3 seam occur (Map 5.6).

The No. 4L coal seam generally overlies the fine sandstones of the parting underneath; locally shale lies below the coal seam. However, in the eastern portions of the coalfield the shales of No. 3 seam and the sandstones of LFA 04 commonly form the floor rocks.

Clastic lenses present in the bottom of the seam are concentrated in the thick coals overlying the eastern pre-Karoo paleovalley (Maps 5.6 and 5.7). Towards the east they disappear abruptly with the thinning of the coals; towards the west they only occur very sporadically. These lenses are abundantly developed where they overlie the eastern margins of No. 3 coal seam (Map 5.7), which also coincides with a rather thin sandstone parting in between the two seams. In the course of recent mining operations this area is being approached from the southwest and a noticeable difference in floor conditions has become apparent. Whereas the floor of the seam elsewhere is relatively flat, it is undulating here (approximately 1-2m amplitude) and the number of in-seam lenses in the bottom part of the seam increases. Some of these lenses protrude into the seam from the sandstone parting below.

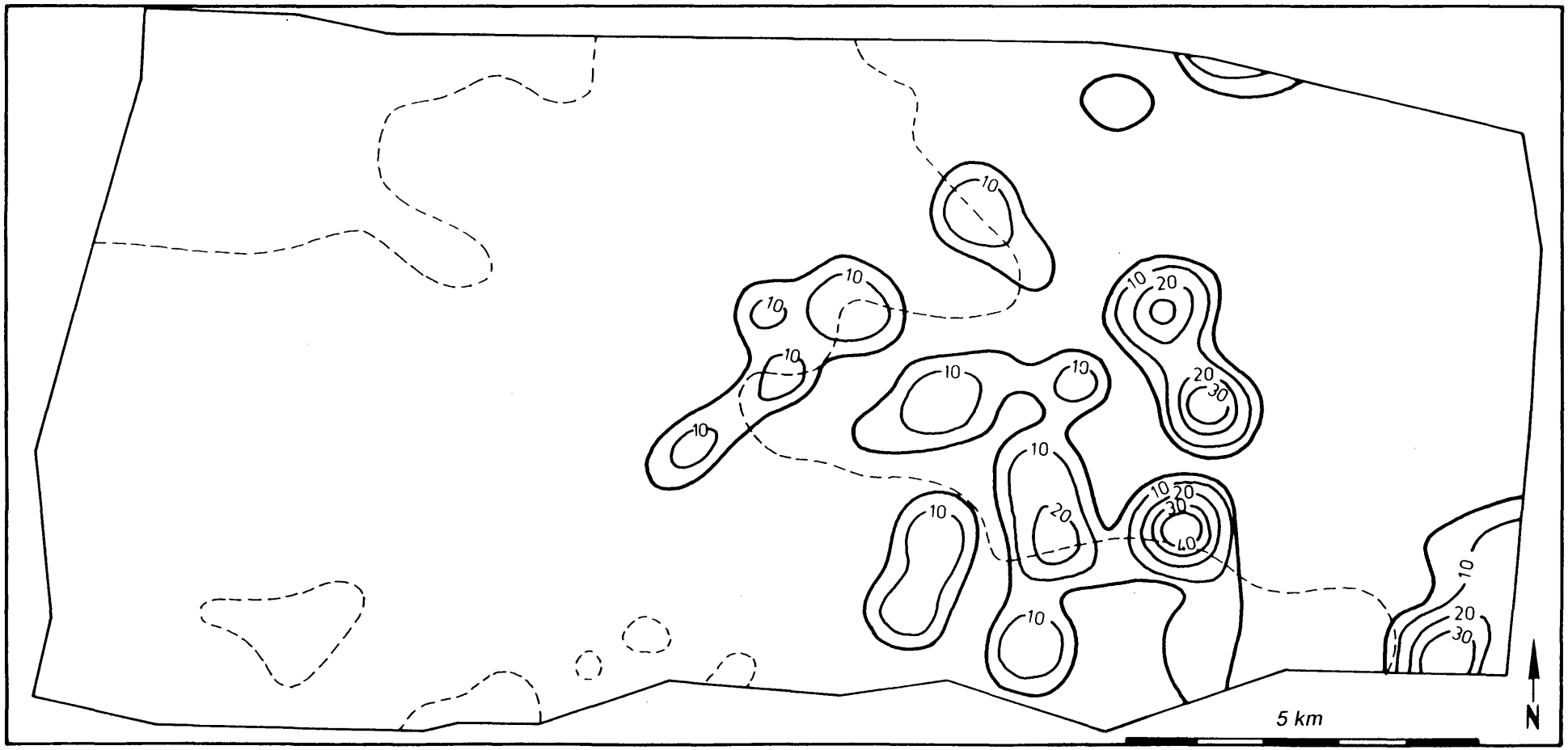
The clastics in the top of the No. 4L seam extend further to the east than those in the bottom (Maps 5.8 and 5.7). There are also occurrences of in-seam lenses which spread into the study area from the central northern regions.

Digitised by the Department of Library Services in support of open access to information, University of Pretoria, 2021.



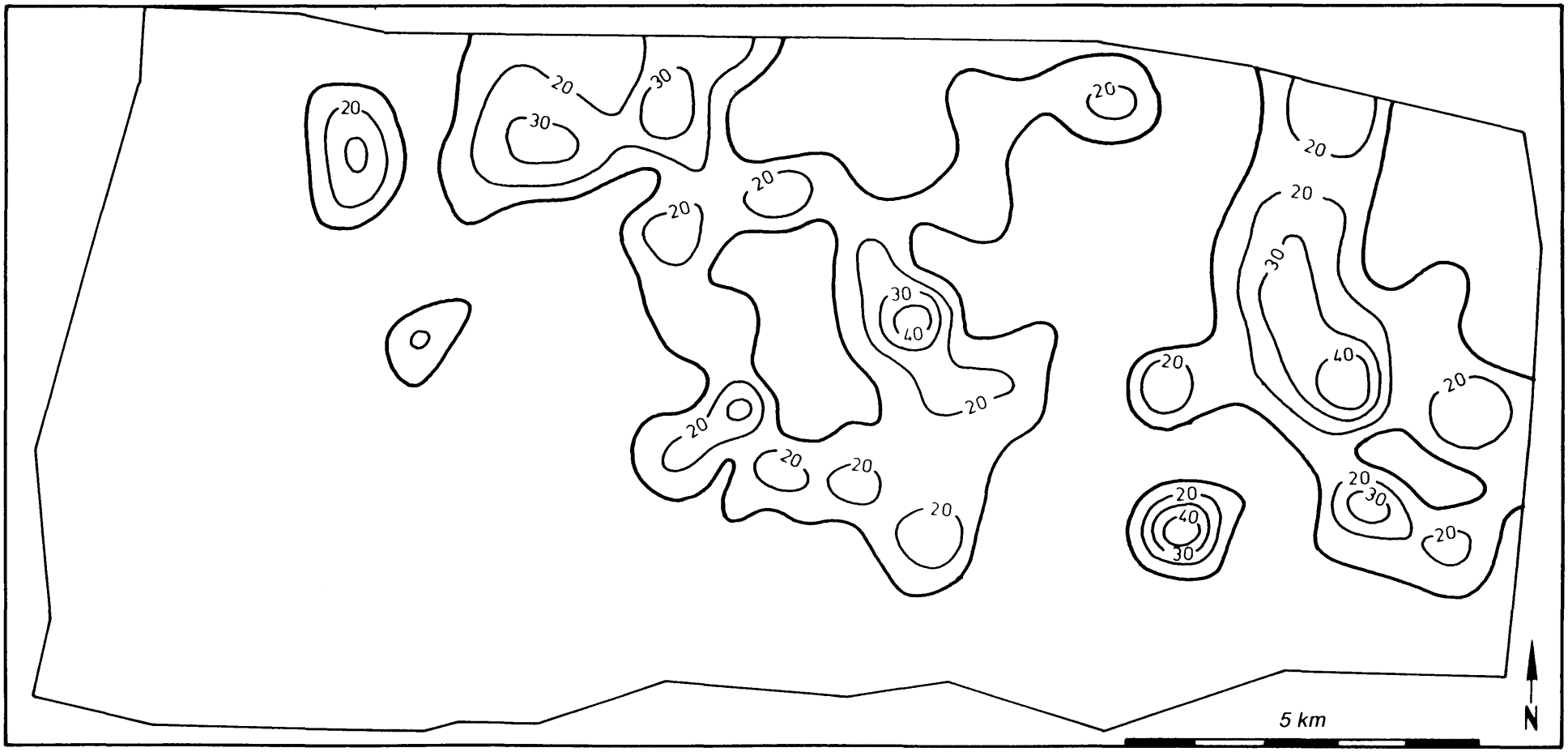
Map 5.6 Isopach map of the No. 4L coal seam (contour interval in centimeters).

Digitised by the Department of Library Services in support of open access to information, University of Pretoria, 2021.



Map 5.7 Distribution and isolith map of clastic lenses in the bottom one third of the No. 4L coal seam (contour interval in centimeters). The dotted line indicates the outline of the underlying No. 3 coal seam.

Digitised by the Department of Library Services in support of open access to information, University of Pretoria, 2021.



Map 5.8 Distribution and isolith map of clastic lenses in the top one third of the No. 4L coal seam (contour interval in centimeters).

Digitised by the Department of Library Services in support of open access to information, University of Pretoria, 2021.

3.6.4. Parting between No. 4L and No. 4U Coal Seams

An irregular succession of coarse-grained to gritty sandstones and gritstones, with medium- to fine-grained sandstones, siltstones, and shales, overlies the No. 4L seam. The sandstones and gritstones are generally quartz-rich and rarely arkosic, white to light grey in colour, and locally micaceous; pyrite and siderite occur as finely disseminated material or as concretions. Glauconite is rare, but, if it is present, forms a prominent glauconitic sandstone bed, up to 15cm thick, within 30cm of the base of the parting. The results of a detailed investigation of the glauconites are reported in section 3.11. The rocks are either massive or exhibit horizontal bedding and small scale, low-angle, planar cross-bedding. The dimensions of the structures range within centimeter scale and cross-strata inclinations are generally less than 10°.

The siltstone and shale facies is grey to black in colour and locally carbonaceous. In most cases these rocks are finely interlaminated, predominantly horizontally bedded, with lesser trough cross-laminae. Sandy lenses occur throughout these fine sedimentary rocks, and when sandstones overlie siltstones or shales, load casts can often be observed.

This entire facies association is intensively interbedded; laminae and lenses of coarse- to medium-grained sandstones commonly occur in the shales and siltstones, whereas the sandstones and gritstones may have a silty to shaly matrix. The alternation of these different facies ranges from a centimeter to a meter scale. Upward-fining and upward-coarsening sequences alternate rapidly, but generally the facies are randomly interbedded. However, the top portion is often upward-fining as it grades into the shales forming the floor rocks of the No. 4U coal seam.

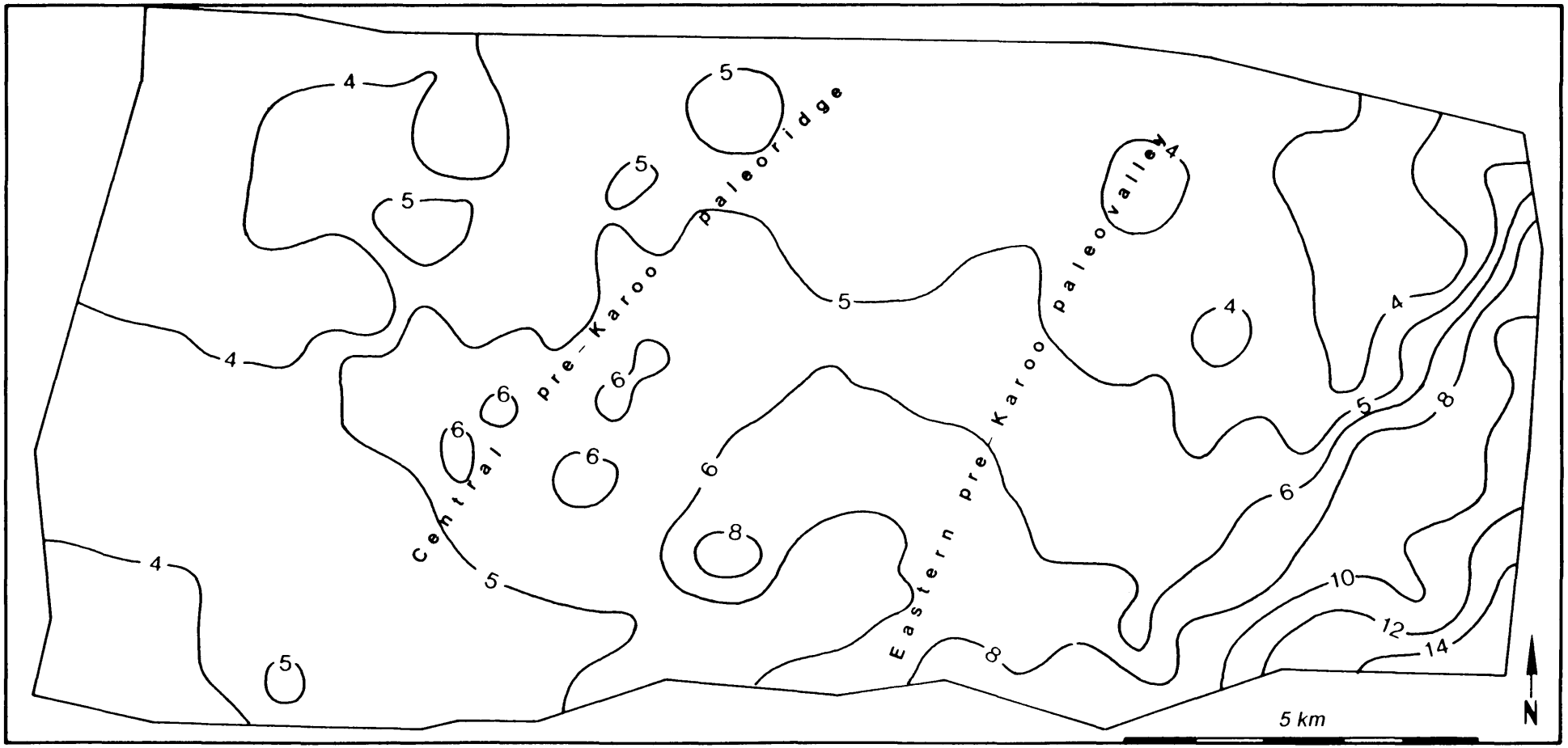
The average thickness of this sedimentary sequence is about 5m. Along the eastern margin of the study area the thickness ranges from less than 4m in the north to 14m in the south. It thins out rapidly northwestwards until it reaches a thickness of about 5m above the eastern paleovalley and the central pre-Karoo paleoridge (Map 5.9).

A detailed isopach map (Map 5.10) of the distribution of gritstones and gritty sandstones in the immediate roof rocks of seam No. 4L shows the following main occurrences of these sediment types:

* To the southeast of the fault zone these coarse rocks form narrow elongated bodies of up to 5m gritstone, that occupy a 3-4km wide zone which becomes broader towards the southwest.

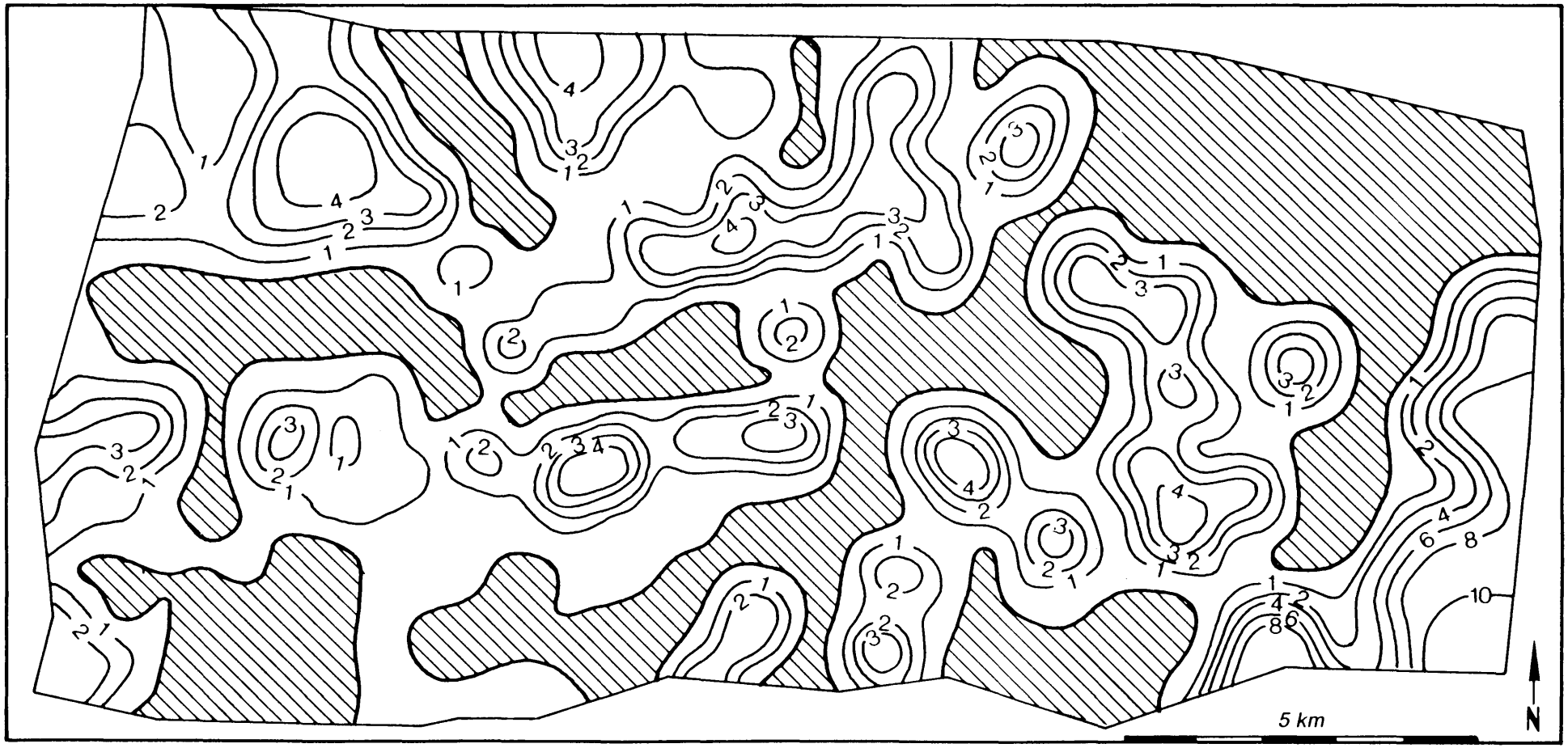
* Very thick gritstones occur along the eastern margin of the study area.

Digitised by the Department of Library Services in support of open access to information, University of Pretoria, 2021.



Map 5.9 Isopach map showing the geometry of the total parting between No. 4L and No. 4U coal seams (contour interval in meters).

Digitised by the Department of Library Services in support of open access to information, University of Pretoria, 2021.



LEGEND

Areas with no grits in the immediate roof rocks of the No. 4L coal seam.

Map 5.10 Distribution and isolith map of grits in the roof of the No. 4L coal seam (contour interval in meters).

Digitised by the Department of Library Services in support of open access to information, University of Pretoria, 2021.

The first occurrence coincides with an approximately 4km wide zone of slightly thinner coals in the No. 4L seam (Maps 5.6 and 5.10); this zone cuts in a southwest-northeasterly direction through the otherwise east-west striking thick coal described previously. Also here, near the southwestern end of the fault zone, elongated gritstone and coarse sandstone bodies can be mapped underground in the roof structures of the seam (Fig. 2.1, for location). They are considered to be channel-fills and show a highly braided pattern with a general north-south paleocurrent trend (Fig. 3.9). The average cross-section across these sandstone bodies comprises two main types. Type A shows a symmetrical profile with both channel margins developing slopes of 20-50° from the vertical, and the channel has an almost horizontal bottom surface. Type B is asymmetrical, with a steep flank to one side and a gently sloping flank to the other. Thus the lowest part of the channel is shifted to one side. The latter type of channel profile is more common and in most of these cases the western edge is steeper than the eastern one. Low sinuosity current ripples, observed in the interchannel areas, indicate a main flow direction from north to south (Fig. 3.9). Further paleocurrent indicators are fossilized plant stems that are embedded in the channels either parallel to the main current direction or perpendicular to it in ripple troughs.

The second occurrence of thick gritstones and coarse sandstones in the eastern half of the study area coincides with extremely thin coals of the No. 4L seam underneath and an extremely thick total parting between coal seams No. 4L and No. 4U (Maps 5.6, 5.9 and 5.10).

3.6.5. The No. 4U Coal Seam

Coal seam No. 4U is widely initiated by a shale and siltstone facies that mainly occupies the southern portions of the coalfield and averages 40-60cm in thickness (Map 5.11). Generally, thicker portions of up to 2m occur in the southwest and southeast of the study area; another thick shale deposit overlies the eastern pre-Karoo paleovalley and trends north-south at thicknesses of 1-1.5m. These shale occurrences pinch out towards the northwest and north against gritstone layers that accumulated along the fault zone as part of this parting. The thick shales in the southeast lie adjacent to or above the thick total parting underneath (compare Maps 5.11 and 5.9).

The coal seam itself averages 40-50cm in thickness, comprises mixed coals and occupies almost the entire coalfield (Map 5.12). In the southwest and southeast of the field area the coal is locally absent and instead shales and siltstones up to 3m thick are found. In the southwest and along the eastern margin sandstone and gritstone partings, from 10-160cm thick, split the seam. The thickness of the seam is variable with extremes of nil and 180cm. It is over 50cm thick

Digitised by the Department of Library Services in support of open access to information, University of Pretoria, 2021.

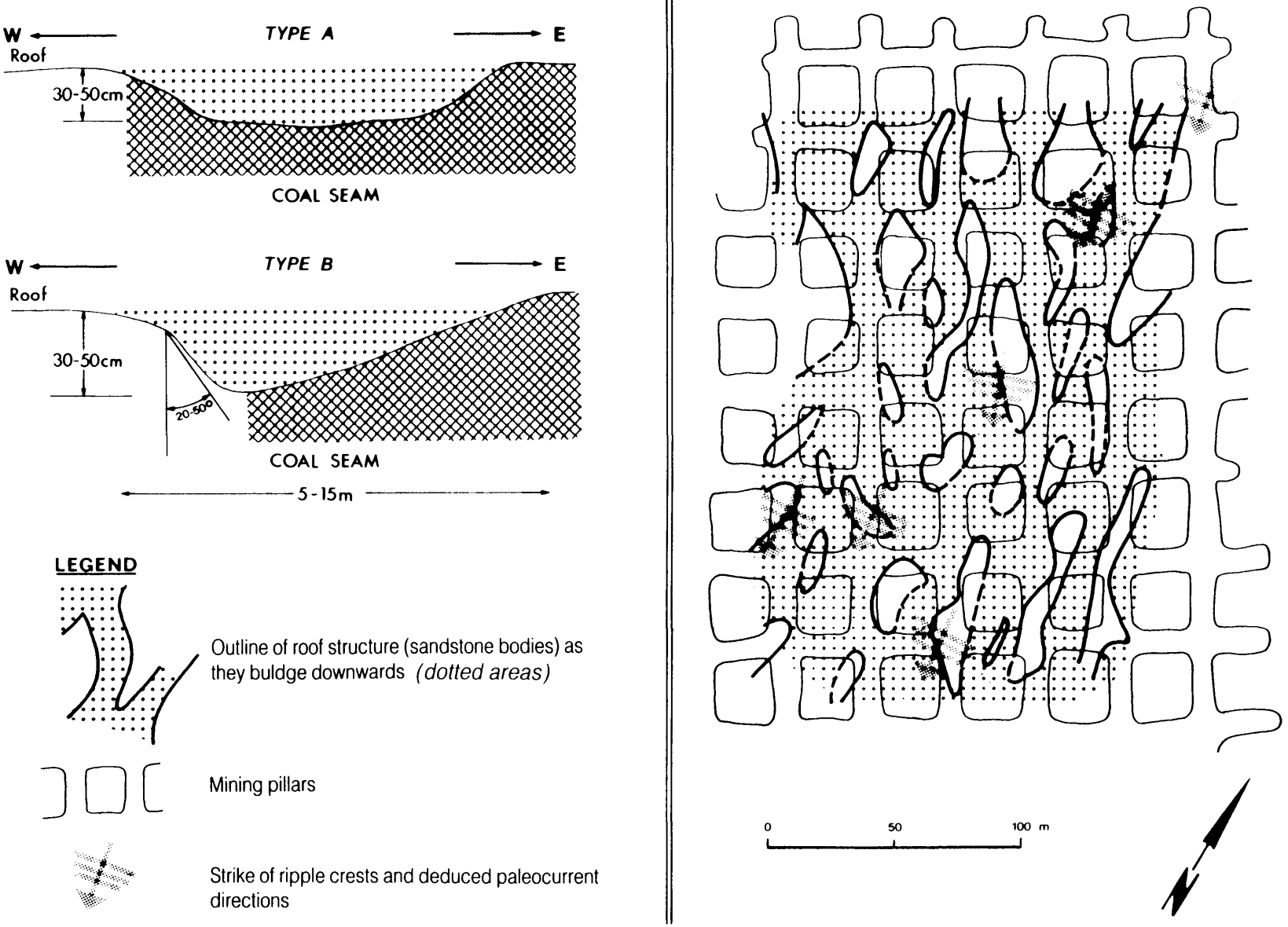
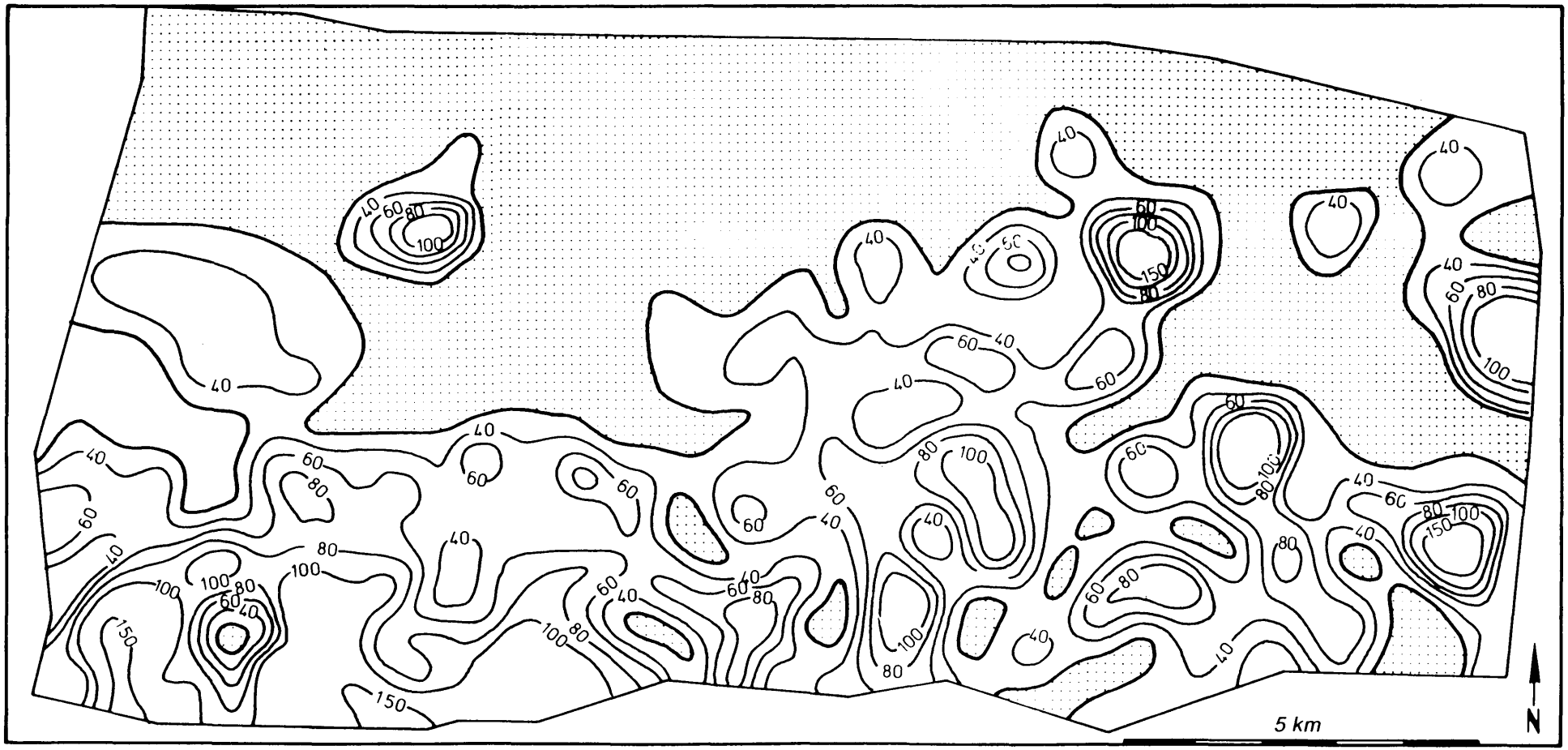


Fig. 3.9 Diagram illustrating roof structures of seam No. 4L in the southwestern corner of the mine (see figure 2.1 for locality). Plan (right) delineates the braided pattern of these structures. The two cross-sections illustrate the symmetrical (Type A) and asymmetrical (Type B) shapes of these sandstone bodies which protrude from the roof of the seam.

Digitised by the Department of Library Services in support of open access to information, University of Pretoria, 2021.



LEGEND

Areas where the floor rocks of No. 4U coal seam consist of sandstones and grits.

Map 5.11 Distribution and isolith map of shales in the floor of the No.4U coal seam (contour interval in centimeters).

Digitised by the Department of Library Services in support of open access to information, University of Pretoria, 2021.



LEGEND

Areas where shale developed in the place of coal

Map 5.12 Isopach map of the No. 4U coal seam (contour interval in centimeters).

Digitised by the Department of Library Services in support of open access to information, University of Pretoria, 2021.

along the western margin where it overlies a slightly thinner parting (Maps 5.9 and 5.12). In the eastern half of the study area the seam is generally thick (>50cm), especially over the pre-Karoo paleovalley, where it locally reaches 180cm. The thick coals of the No. 4U seam are mainly overlying and adjacent to major shales and siltstones in the floor, which in turn cap relatively thick partings underneath the seam (compare maps 5.9, 5.11 and 5.12).

3.6.6. Summary of LFA 05: The Main Coal Zone

As found with the foregoing LFA's, the most conspicuous characteristics of LFA 05 occur in the eastern half of the study area and in a narrow band along the fault zone. Maximum and minimum sediment thicknesses occur in the eastern half of the coalfield. This is not only valid for the cumulative thickness of the entire LFA 05, but also for single partings as well as coal seams therein:

* Coal seam No. 3 is widely absent here and, instead, underlying and contemporaneous shales and siltstones reach both maximum and minimum thicknesses in this region.

* The fine sandstone parting between No. 3 and No. 4L seams is thickly developed as well as absent in major parts of this half of the coalfield.

* No. 4L seam displays both its thickest and thinnest occurrences here, as well as the bulk of all in-seam clastic lenses.

* The parting between No. 4L and No. 4U seams is particularly thick and also grit-dominated along the eastern margin of the coalfield.

* The floor rocks of the No. 4U seam comprise abundant shaly and silty material here.

The western half of the study area appears to be characterized by more evenly distributed sediment thicknesses and lithologies. The fault zone is, however, an exception:

* Shales underneath No. 3 seam appear to be abundant northwest of the fault zone.

* It broadly forms the northwestern margin of the occurrence of coals in the No. 3 seam.

Digitised by the Department of Library Services in support of open access to information, University of Pretoria, 2021.

* In-seam partings in No. 4L coal seam occur in patches along the fault zone and contain gritty material.

* The roof rocks of No. 4L seam are especially gritty over and adjacent to the fault zone.

* In major parts of the fault zone the total parting between seams No. 4L and No. 4U remains predominantly gritty throughout and up into the immediate floor rocks of the No. 4U seam.

3.7. LFA 06: Sedimentary Rocks between No. 4U and No. 5 Coal Seams

The total succession of sedimentary rocks that separates the No. 5 coal seam from the main coal-bearing zone (LFA 05) is spread evenly, in a sheet-like manner, over the entire coalfield, with an average thickness of 38m. In parts its facies are comparable to those of previous LFA's, especially LFA's 02 and 04.

LFA 06 can be divided into a basal and an upper portion, which differ considerably from each other in their facies associations. The two portions are approximately equal in thickness.

The **BASAL PORTION** of LFA 06 is comparable to the sedimentary rocks of LFA 04, in that a sandstone facies as well as a siltstone and shale facies form the main components. Gritstones occur to a lesser extent just above the No. 4U seam.

The sandstones are medium- to coarse-grained and contain mica, pyrite and siderite in variable amounts; the latter two minerals occur as concretions and are also finely disseminated. Glauconite occurs sporadically just above the No. 4U seam. All internal structures are of a centimeter scale and include horizontal bedding, some trough cross-beds, and rare flaser beds and ripples marks. Coaly plant debris as well as black carbonaceous shale and mudstone clasts occur within the sandstones.

The siltstones and shales are mostly interlaminated, grey to black, partly carbonaceous, and bear interbeds and lenses of medium- to coarse-grained sandstones. Contacts with overlying sandstones are locally erosional and display slump structures (centimeter scale) and ball-and-pillow structures.

Similar to LFA 04, predominantly sandstone beds alternate with layers of siltstone and shale on a meter scale (Fig. 3.10). Generally there is no overall cyclicity of these two facies; however, the basal portion of LFA 06 often has one or two upward-coarsening sequences, that are followed by a number of upward-fining arrangements.

Digitised by the Department of Library Services in support of open access to information, University of Pretoria, 2021.

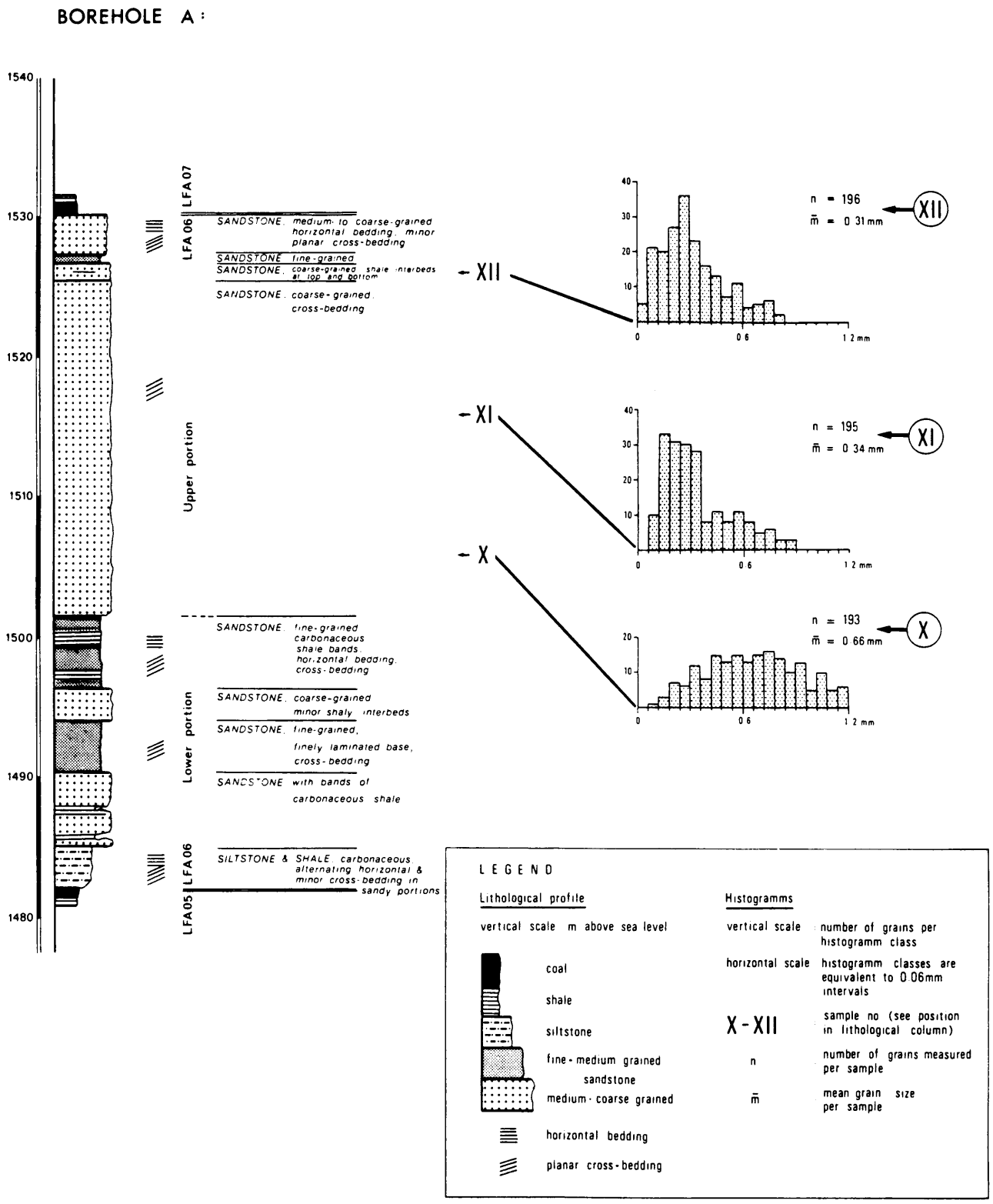


Fig. 3.10 Sample-profile from borehole **A** (see figure 2.1 for locality) with lithologic descriptions and grain size distriburion histograms in the upper portion of LFA 06.

Digitised by the Department of Library Services in support of open access to information, University of Pretoria, 2021.

The **UPPER PORTION** of LFA 06 resembles the sandstones of LFA 02 and is dominated by medium- to coarse-grained sandstones with gritstone interbeds. In comparison to LFA 02 the sandstones here display more feldspar in thin section. Mica and clay minerals account for most of the matrix in these rocks. Pyrite, siderite and glauconite are rare. The grain size distribution is more variable than in LFA 02 (Figs. 3.10 and 3.4), and the sediments are poorer sorted and upward-fining. Sedimentary structures include horizontal bedding (centimeter scale) and planar cross-bedding (set thicknesses greater than 30cm).

Siltstones and shales are rare throughout these sandstones, but locally form a layer of up to 6.5m thick. However, this layer is generally less than 1.5m in thickness, and it lies about 5-7m below the top of LFA 06. The shales are finely laminated and have minor soft sediment deformation structures and bioturbation. Locally they also include coal seams of up to 40cm thickness.

The **TOTAL THICKNESS** OF LFA 06 averages 36-38m in the western half of the study area (Map 6.1). The eastern portion has a 40-47m thick sedimentary package near the centre of the coalfield, which forms a southwest-northeast trending sedimentary body. LFA 06 is thinner in the southeastern corner (Map 6.1). The thickness distribution of LFA 06 in relation to foregoing layers is as follows:

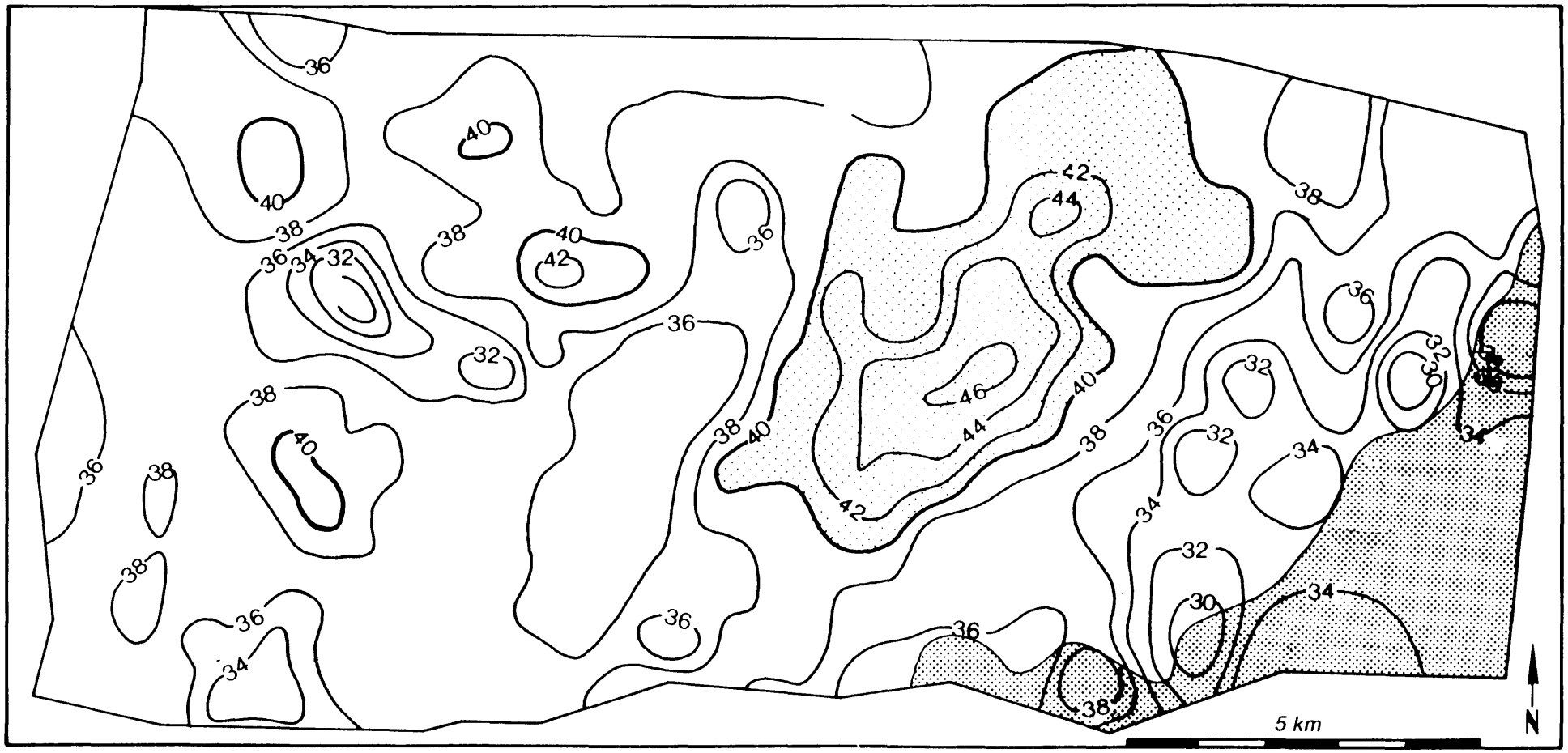
* It is generally thinner in the southeastern corner overlying an extremely thick development of the parting between seams No. 4L and No. 4U. This is also the area where this parting is dominated by coarse sandstones and gritstones. Furthermore LFA 06 is thin in the same regions where these two coal seams are thin.

* It is thickest over the northern part of the eastern pre-Karoo paleovalley, where the parting between seams No. 4L and No. 4U is thinner, with an average thickness of 5m. Here both seams, together with the sandstone parting between No. 3 and No. 4L seams and the shales underlying this parting (contemporaneous with the No. 3 seam), are thickly developed.

* In the western half of the study area LFA 06 is fairly evenly distributed, as are many of the facies of LFA 05.

The shales and siltstones in the upper portion of LFA 06 form a local occurrence which does not extend over the entire study area (Map 6.2). The coal seams therein mainly occur above the southern parts of the eastern pre-Karoo paleovalley and above the central pre-Karoo paleoridge. This means that these coal seamlets lie within close proximity (to the southeast and southwest) of the major accumulation of LFA 06 (Maps 6.1 and 6.2).

Digitised by the Department of Library Services in support of open access to information, University of Pretoria, 2021.



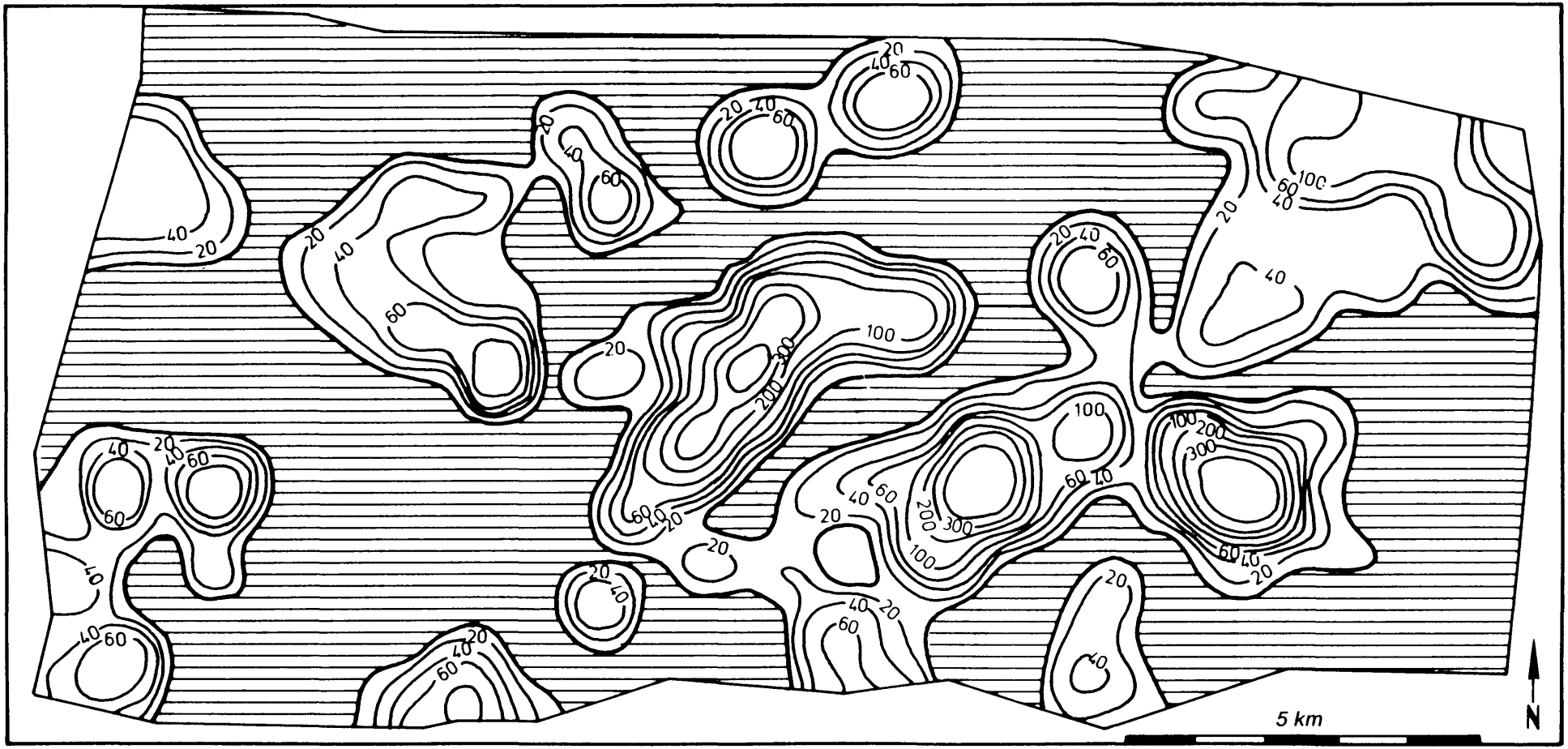
LEGEND

Area of thich sandstone deposits over eastern paleovalley.

Area of thick parting between seams No. 4L and No. 4U (more than 8m)

Map 6.1 Isopach map showing the geometry of LFA 06 (contour interval in meters).

Digitised by the Department of Library Services in support of open access to information, University of Pretoria, 2021.



LEGEND

Areas where the sandstone deposition in the upper portion of LFA 06 is continuous.

Map 6.2 Distribution and isolith map of the siltstone-shale-coal facies in the top portion of LFA 06 (contour interval in centimeters).

Digitised by the Department of Library Services in support of open access to information, University of Pretoria, 2021.

3.8. LFA 07: The No. 5 Coal Seam

Coal seam No. 5 comprises mixed and bright coals as well as torbanitic and black carbonaceous shales. The major macroscopically discernible mineral matter is pyrite, in the form of concretions and as finely disseminated material, and calcite along joints and cracks; siderite occurs in minor quantities. Medium- to coarse-grained sandstone and lesser shale splits become up to 120cm thick. The coals lie with a sharp contact over the preceding LFA 06 sandstones, which form major parts of the immediate floor rocks. Locally the coal may be replaced by carbonaceous shales. Generally 1-2m of black carbonaceous shale, which is often torbanitic in its basal 50cm, covers the coal seam. Thus a generalized profile for seam No. 5 can be established as follows:

* Coal with minor shale lenses, at the base.

* Mixed and bright coal in the top of the coal band.

* Torbanitic shale and eventually black carbonaceous shale above the coal band.

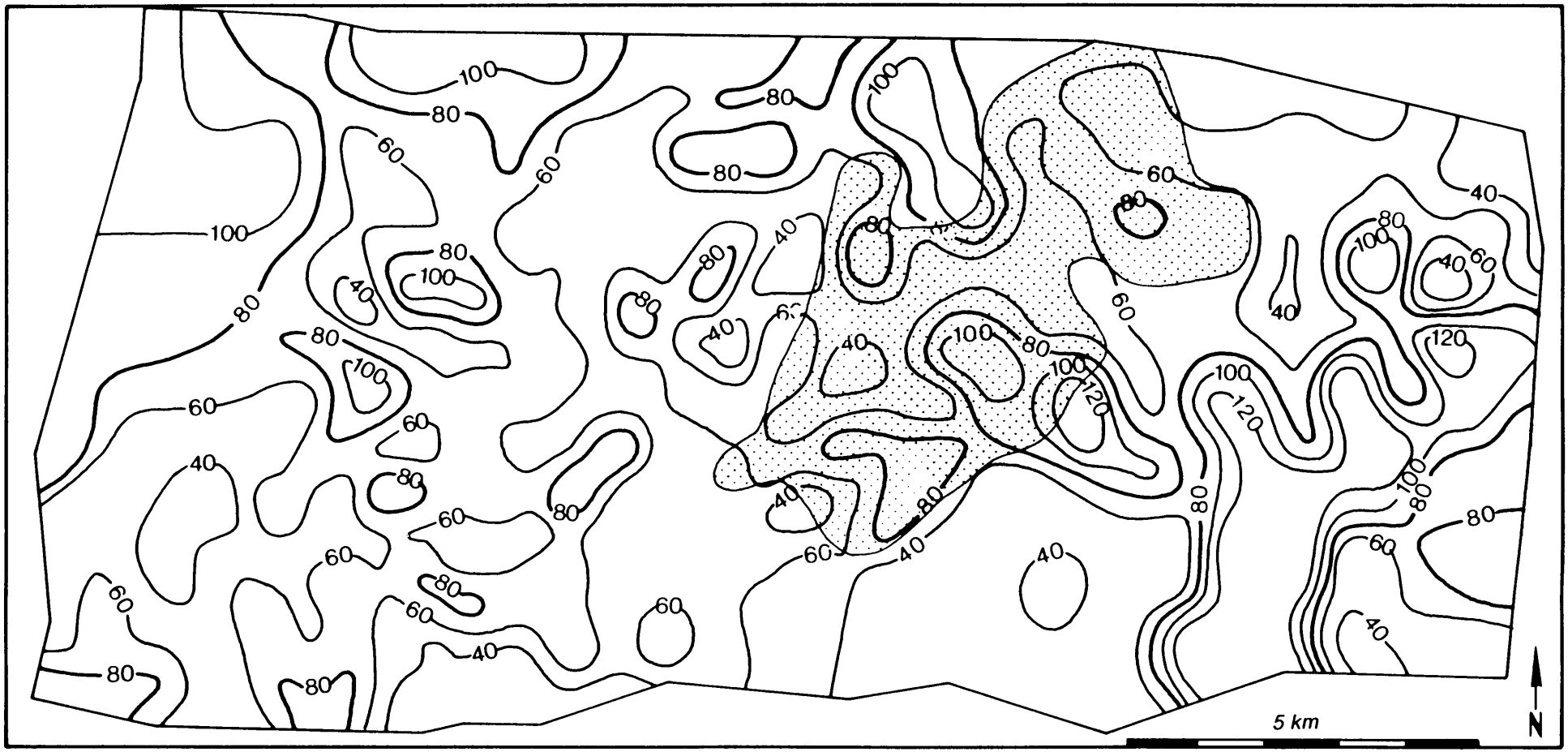
The coal seam is more or less evenly developed over the study area, averaging about 60-80cm in thickness (Map 7). Thick coal is mainly concentrated in the northwest and over extensive areas in the eastern half of the study area, particularly the southeast. These thick occurrences are generally adjacent to relatively thick sedimentary rocks of LFA 06 (Maps 6.1 and 7). The coal is thin in the southeastern-most part, and of average thickness above the central pre-Karoo paleoridge and the southwest-northeast trending thick zone of LFA 06.

3.9. LFA 08: Sedimentary Rocks above the No. 5 Coal Seam

The facies association here resembles LFA 04 and the basal portion of LFA 06. A medium- to coarse-grained sandstone facies alternates fairly regularly with a laminated siltstone and shale facies. Each facies has comparatively thick vertical sequences, up to several meters.

The sandstones are commonly micaceous, horizontally bedded as well as planar cross-bedded, and contain mudstone clasts and scattered coaly plant debris. Glauconite occurs just above the No. 5 seam, as well as found above No. 4L and No. 4U coal seams.

Digitised by the Department of Library Services in support of open access to information, University of Pretoria, 2021.



LEGEND

Principal area of thick sandstone deposits in LFA 06.

Map 7 Isopach map of LFA 07 (the No. 5 coal seam) (contour interval in centimeters).

Digitised by the Department of Library Services in support of open access to information, University of Pretoria, 2021.

The siltstone and shale facies exhibits pyrite and siderite. Ball-and-pillow structures and load casts are found near the interfaces with overlying sandstones. Bioturbation is locally developed.

LFA 08 forms the top of the Ecca sequence in the Twistdraai Coalfield and either outcrops at the present-day surface or underlies a major dolerite sill that often caps the sedimentary column in this region. As it is partly eroded, no isopach map of this LFA was compiled.

The lithological characteristics of the Karoo sedimentary sequence at Twistdraai are summarized in table 3.1.

Digitised by the Department of Library Services in support of open access to information, University of Pretoria, 2021.

Table 3.1: Detailed summarizing lithostratigraphic table of the sequence of lithofacies associations at the Twistdraai Mine.

LFA 08	SANDSTONE: medium- to coarse-grained , matrix-supported, micaceous in parts, rare glauconite, horizontal stratification and planar cross-bedding. SILTSTONE & SHALE: finely laminated, some pyrite and siderite, locally bioturbated.	distribution uncertain owing to overlying dolerite sills and erosion.
LFA 07	COAL SEAM No. 5: overlain by torbanitic and black carbonaceous shale.	even thickness distribution of 60-80cm, thick in northwest and over eastern half of study area.
LFA 06	UPPER PORTION: SANDSTONE: medium- to coarse-grained, slightly arkosic, silty and shaly matrix, grain sizes variable and poorly sorted, mica common, pyrite and siderite very rare, horizontal stratification and planar cross-bedding. SILTSTONE, SHALE & COAL: finely interlaminated, soft sediment deformation structures, bioturbated. LOWER PORTION: SANDSTONE: medium- to coarse-grained with gritstone, shaly laminae, coaly debris; mica, pyrite and siderite in variable amounts, glauconite very rare, horizontal bedding, trough cross-beds, ripple and flaser structures. SILTSTONE & SHALE: grey to black, finely interlaminated, coarse sandy interbeds, soft sediment deformation structures.	generally even thickness distribution of 36-38m, thinner over eastern margin of study area (locally less than 20m).
LFA 05	COAL SEAM No. 4U: mixed lithotypes, mainly shales in floor rocks of the southern parts of the study area. PARTING BETWEEN SEAMS No. 4L & No. 4U: poorly sorted and interlaminated: Gritstone: erosional effects on coal of the No. 4L seam; Sandstone: gritty and coarse-grained, quartzitic, locally micaceous; rare pyrite, siderite & glauconite; Siltstone & shale: grey to black, fine horizontal lamination and trough cross-bedding, load casts. COAL SEAM No. 4L: vitrain, clarain & durain bands; in-seam clastic lenses concentrated in top and bottom portion of seam in eastern half of study area. PARTING BETWEEN SEAMS No. 3 & No. 4L: sandstone, fine- to medium-grained, micaceous, rare pyrite and siderite, horizontal stratification and planar cross-bedding. COAL SEAM No. 3: mixed lithotypes, underlying shales are partly interlaminated with the coals. * coal mainly above thin and intermediate shales. Siltstone & shale: finely interlaminated. * mainly occupying depressions in previous topography.	average thickness 40-50cm, underlying shales are thickest over eastern paleovalley. average thickness generally less than 5m, up to 14m along eastern margin of study area. generally evenly distributed, average thickness 3.5m, thinning towards eastern margin of study area (less than 2m). mainly 1-2m thick, thicker over eastern paleovalley, thin to absent over eastern paleohigh and thick coals of the No. 3 seam. averages 50-60cm thickness, only in southern and cantral parts of study area.
LFA 04	SANDSTONE: medium- to coarse-grained, partly arkosic, silty to shaly matrix, rare mica and pyrite, horizontal bedding, low-angle planar cross-bedding. SILTSTONE & SHALE: finely interlaminated, sandstoen interbeds, occasional coaly debris and seamlets, abundant soft sediment deformation structures. * irregular lateral and vertical distribution of the two facies. *alternating upward-coarsening and upward-fining sequences.	TOP SURFACE AFTER LFA 04 DEPOSITION: eastern paleovalley and eastern paleohigh similar to the pre-Karoo surface reoccur. LFA 04: evently distributed, averages 20-25m thickness, thicker over western paleovalley where LFA 03 is not developed and LFA 02 is thick, more than 40m thick over eastern paleohigh, thinner than 20m over eastern paleovalley.
LFA 03	SILTSTONE: dark-grey to black, soft sediment deformation structures, bioturbated. SHALE: black carbonaceous, abundant pyrite, sporadic coal seamlets of 15-30cm thickness. * thicker portions appear more sandy and silty. * coal seamlets mainly to southeast of major sandstone body of LFA 02.	averages 4-5m thickness, depending on the distribution of LFA 02, maximum of 16m in eastern half where LFA 02 is thin, less than 2m where LFA 02 is thick.
LFA 02	SANDSTONE (UPPER PORTION): medium- to coarse-grained, partly gritty, rarely arkosic, clayey and silty matrix, fine siltstone interbeds, some mica-rich layers, grains poorly rounded, grain sorting decreases towards top, generally upward-coarsening. SANDSTONE (LOWER PORTION): medium- to coarse-grained, clean, grain supported, slightly arkosic, several mica-rich bands, grain sorting poor in bottom and improving towards top, subtle cyclicity due to grain size changes, large scale planar cross-bedding, horizontal bedding. * upper sandstone facies averages 10-15m. * lower sandstone facies averages 30m thickness.	evenly distributed, averages 43m thickness, maximum thickness over western pre-Karoo paleovalley, minimum in southeast of study area, major elongated body of sand stone along fault zone.
LFA 01	SHALE: black carbonaceous, sandy interbeds near top, coaly debris, dropstones, uncommonly bioturbated, ball-and-pillow structures. DIAMICTITE: massive and unstratified, blue-grey and red, fine- to medium-grained matrix. CONGLOMERATE & SANDSTONE: coarse-grained to gritty, matrix-supported. SHALE: blue and grey, varved layering, interbedded in diamictite and conglomerate facies.	POST-DWYKA SURFACE: less undulating and gentler north-south paleoslope than pre-Karoo surface. SHALE FACIES: evenly distributed, averaging 3-8m. DIAMICTITE FACIES: concentrated in pre-Karoo paleovalleys (up to 50m thick), thinning out and even absent over previous topographic highs.
PRE-KAROO ROCKS:	TRANSVAAL SEQUENCE. VENTERSDORP SUPERGROUP. WITWATERSRAND SUPERGROUP.	

Digitised by the Department of Library Services in support of open access to information, University of Pretoria, 2021.

3.10. Clay Minerals and Carbonates of the Karoo Sedimentary Rocks at the Twistdraai Coalfield

The qualitative XRD analyses of all the samples indicated that the following minerals are present in the sedimentary sequence of the Twistdraai Coalfield:

Quartz	(low 5-490)
Clay Minerals:	Kaolinite (1T 14-164)
	Illite (1Md 29-1596)
	Montmorillonite/Rectorite (25-781; 29-1495)
	Chlorite (16-351 or Prochlorite from an internal standard at the NICR)
Carbonates:	Siderite (29-696)
	Calcite (05-586)
	Dolomite (11-078)
	Ankerite (12-88)C
Micas:	Muscovite (1M 07-025; Vanadium-rich)
	Biotite (1M 02-045)
Feldspars	mainly Albite (low 09-466)
Pyrite	(06-710)

The numbers in brackets indicate the file number of the card catalogue of the JCPDS (Joint Committee of Powder Diffraction Standards) according to which the identification of the minerals was done.

Quartz and the clay minerals account for by far the largest proportion of each sample. In some sandstones with little matrix material, however, clay minerals are a minor component. The other minerals listed above generally make up small proportions of the samples; carbonates and mica predominate, but quantitative results will be given for the carbonates only, in order to compare these with the paleo-pH measurements. Feldspars and pyrite occur randomly in a few samples and are thus not quantified.

The quantitative XRD results of both boreholes B and C show a predominance of kaolinite in the clay mineral fraction of the samples. Illite only occurs in a small number of samples, but it is concentrated in certain horizons. Montmorillonite was only found sporadically and rarely accounted for more than 1% of any sample. Micas, pyrite and chlorite, especially prochlorite, occur randomly and rarely throughout the whole succession and were thus not quantified.

Generally there is a good correlation of clay minerals between the two boreholes, which is expressed by an overall average of 23% kaolinite in each borehole. Within LFA 01 there is an increase in kaolinite towards the top, to above 40% (Figs. 3.11 and 3.12). This is followed by a drastic decrease to nil in the basal few meters of LFA

Digitised by the Department of Library Services in support of open access to information, University of Pretoria, 2021.

02. Kaolinite is virtually absent throughout LFA 02 in borehole C, but shows some, even high, re-occurrences in the top of LFA 02 in borehole B.

In borehole C, the kaolinite content maintains constant values of about 30% from LFA 03 to LFA 08. Some odd samples reach considerably lower values particularly in the upper portion of LFA 06 (Fig. 3.11; Appendix 1). Extreme values of greater than 60% and even 70% occur below the No. 4L seam and within the parting between seams No. 4L and No. 4U (Fig. 3.11). This, however, is attributed to the occurrence of dickite in these samples (marked with * in Fig. 3.11), which is a monoclinic variety in the kaolinite group (MILLOT, 1970, p3). It has a very similar diffractogram to kaolinite, thus causing interferences and enhancement of the major kaolinite peaks (BRINDLEY and BROWN, 1980). Due to a lack of standard material containing dickite the quantification of kaolinite is not reliable in these samples and is most propably exaggerated. Dickite has been reported from Pennsylvanian coals by HONESS and WILLIAMS (1935) and from the Millstone Grit Formation (Namurian, Upper Carboniferous) in England by SMITHSON and BROWN (1954), where it fills the interstitial spaces of gritty sandstones.

In borehole B the kaolinite content is somewhat more erratic from LFA 04 on upwards (LFA 03 is not identified in this borehole). However, relatively low values again appear in the upper portion of LFA 06 and also in the sandstones above the No. 4U seam (Fig. 3.12; Appendix 1). A series of samples containing dickite again occurs below No. 4L and No. 3 coal seams.

The illite content of those samples, where this mineral occurs, averages 24% in borehole B and 37% in borehole C. Illite mainly occurs in LFA 02 where kaolinite is absent (Figs. 3.11 and 3.12). Towards the top of LFA 02 (borehole B) and in LFA 03 (borehole C), illite and kaolinite occurrences overlap. A minor amount of illite appears in LFA 01 of borehole C. There are rare occurrences throughout the rest of the sedimentary sequence, but too small to be quantified. A few prominent illite peaks occur in LFA 08 of borehole B (Fig. 3.12). Some peaks, especially within LFA 02, are enhanced by mica, leading to a possibly exaggerated illite content.

Amongst the carbonates a distinction is made between siderite on the one hand and dolomite and calcite on the other (Fig. 3.11 and 3.12). In the latter group calcite normally predominates. The siderite content averages 2% in borehole B and 1% in borehole C, while calcite and dolomite together are at 1% and below 1%, respectively. In parts of the sequence there is a good correlation between the two boreholes. Siderite predominates in LFA 01, especially in borehole B. Throughout LFA 02, in both boreholes, there is a predominance of calcite and dolomite with a decreasing trend towards the top.

Through LFA 03 and LFA 04 (borehole C) and from the top 15m of

Digitised by the Department of Library Services in support of open access to information, University of Pretoria, 2021.

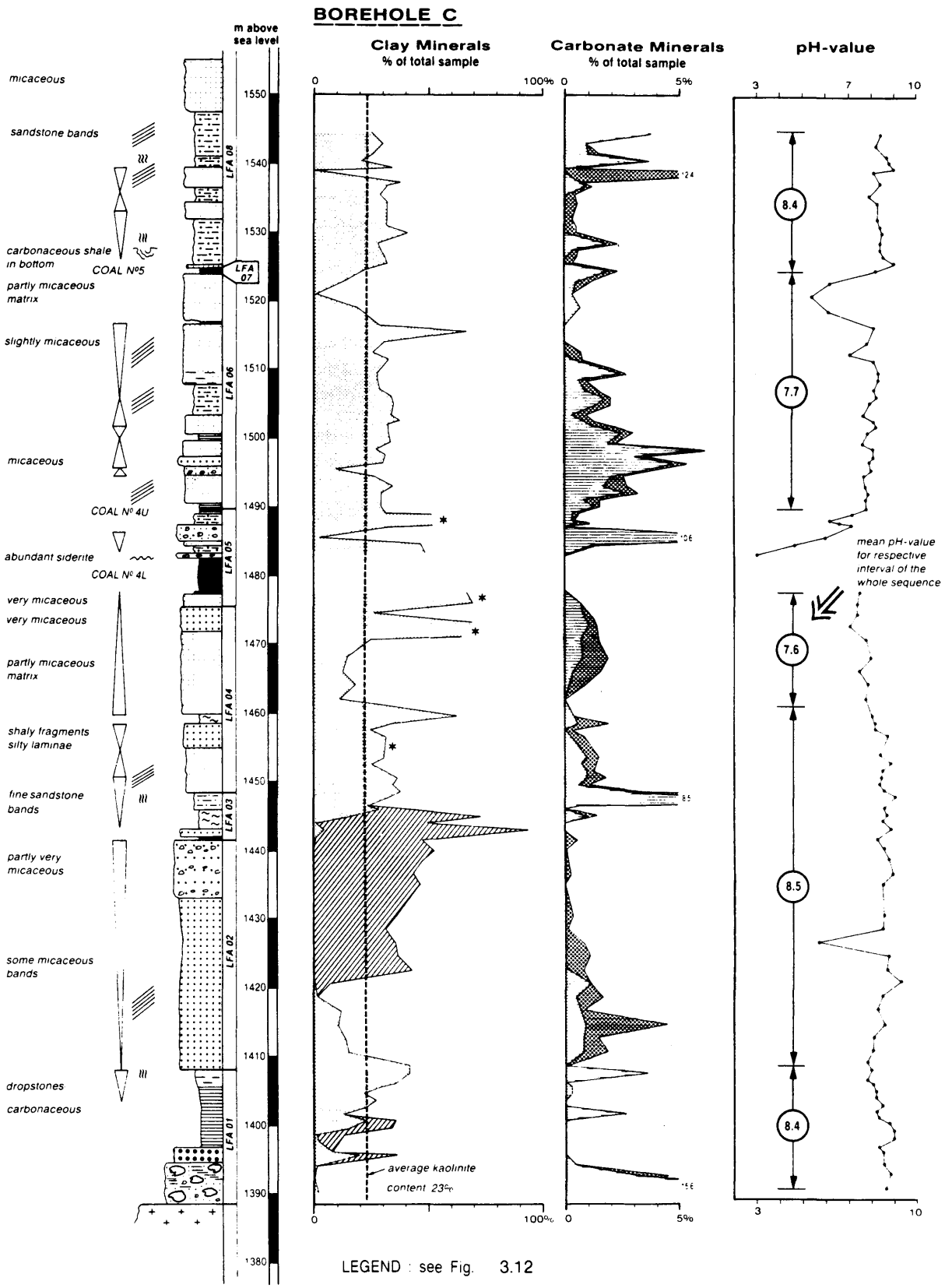


Fig. 3.11 Litostratigraphic columns of borehole **C** (see figure 2.1 for locality) with plotted XRD-results of quantitative clay mineral and carbonate analyses, also showing the results of the paleo-pH determination.

Digitised by the Department of Library Services in support of open access to information, University of Pretoria, 2021.

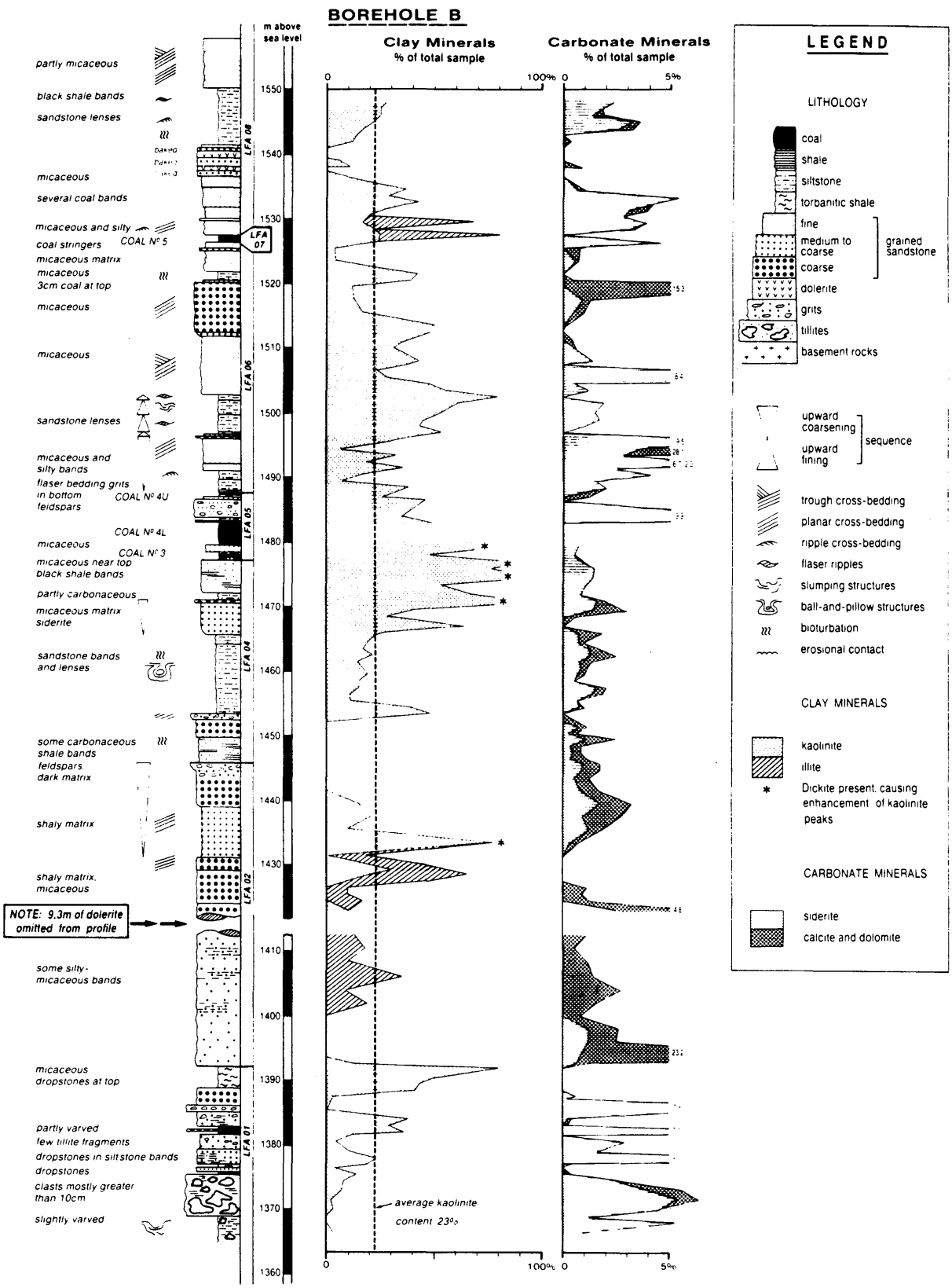


Fig. 3.12 Lithostratigraphic column of borehole **B** (see figure 2.1 for locality) with plotted XRD-results of quantitative clay mineral and carbonate analyses.

Digitised by the Department of Library Services in support of open access to information, University of Pretoria, 2021.

LFA 02 and through LFA 04 (borehole B), the samples maintain a fairly constant carbonate content. Both borehole profiles indicate extremely high siderite peaks in the parting between coal seams No. 4L and No. 4U and in the lower portion of LFA 06. From the upper portion of LFA 06 towards the top of the succession the siderite content decreases, with an occasional high peak above coal seam No. 5 in both boreholes. Calcite and dolomite generally remain insignificant in this portion of the sequence.

3.11. Results of Glauconite Petrography

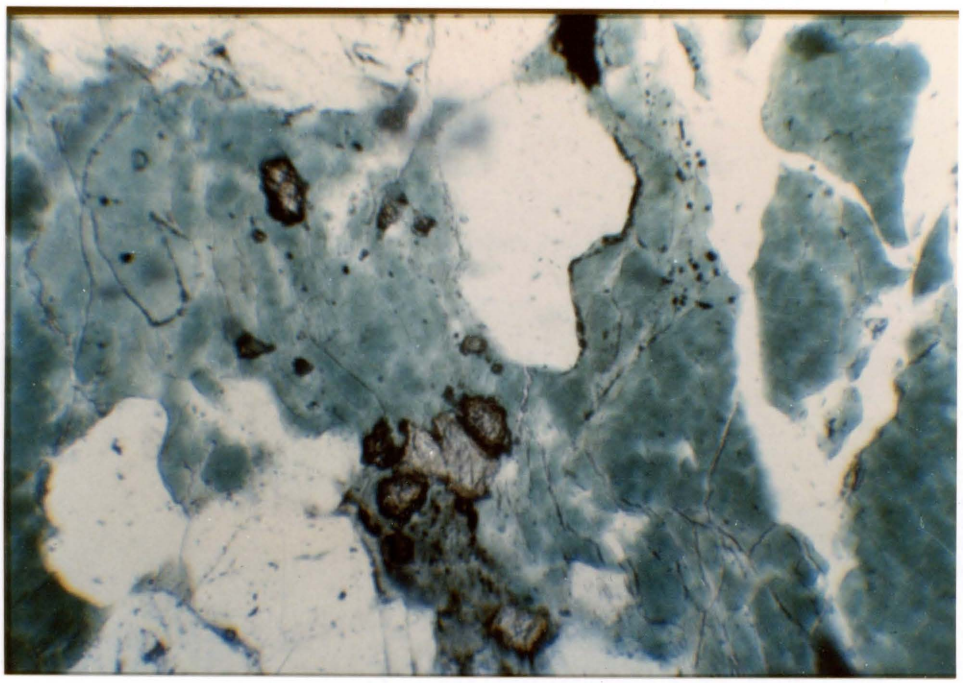
The glauconite is a green, earthy, granular material occurring as angular pellets of up to 3mm in diameter. It is normally found in distinct interbedded arenaceous and argillaceous horizons directly above the coal seams (samples A and B). Occasionally the glauconite is present in arenaceous rock sequences with mainly matrix-supported coarse sandstones and gritstones. In these cases it appears as green speckles, filling interstitial grain spaces in the host rock (samples D, C and E). The Greensand sample from Northern Germany, which was chosen for comparison, is a fine-grained sandstone which is highly impregnated by glauconite and thus appears blueish-green.

The glauconite of samples A to E normally fills pore spaces in between quartz and feldspar grains, thus having irregular shapes. It has a slight pleochroism from colourless or light-green to yellowish-green, is dark-green under crossed polarizers and is optically negative. The glauconite is generally flaky and massive and does not exhibit any cleavage; it rarely forms crypto-crystalline granular aggregates (Fig. 3.13a). Associated minerals are other clay minerals and siderite. Occasionally glauconite replaces biotite along edges and cleavage planes (also observed by GALLIHER, 1939) or may be completely pseudomorphous after mica, then showing a distinct cleavage (Figs. 3.13b and c). Glauconite rarely fills cell cavities of higher fossilized plants (Fig. 3.13d).

In the Cretaceous Greensand sample the glauconite is dark bottle-green, in crypto-crystalline aggregates, forming well-rounded grains amongst quartz and a very fine-grained carbonate (mainly sideritic) matrix. This glauconitic material also commonly fills foraminiferal tests (Fig. 3.13e).

X-ray diffractograms of the whole rock indicate quartz and siderite as major components and muscovite, biotite and feldspar as traces, besides the glauconite. In all the diffractograms the glauconite was identified by the 10, 4.8, 3.3, 2.6, 2.4, 2.27, 2.15 and 1.51Å peaks (Fig. 3.14); the last peak does not appear in the

Digitised by the Department of Library Services in support of open access to information, University of Pretoria, 2021.



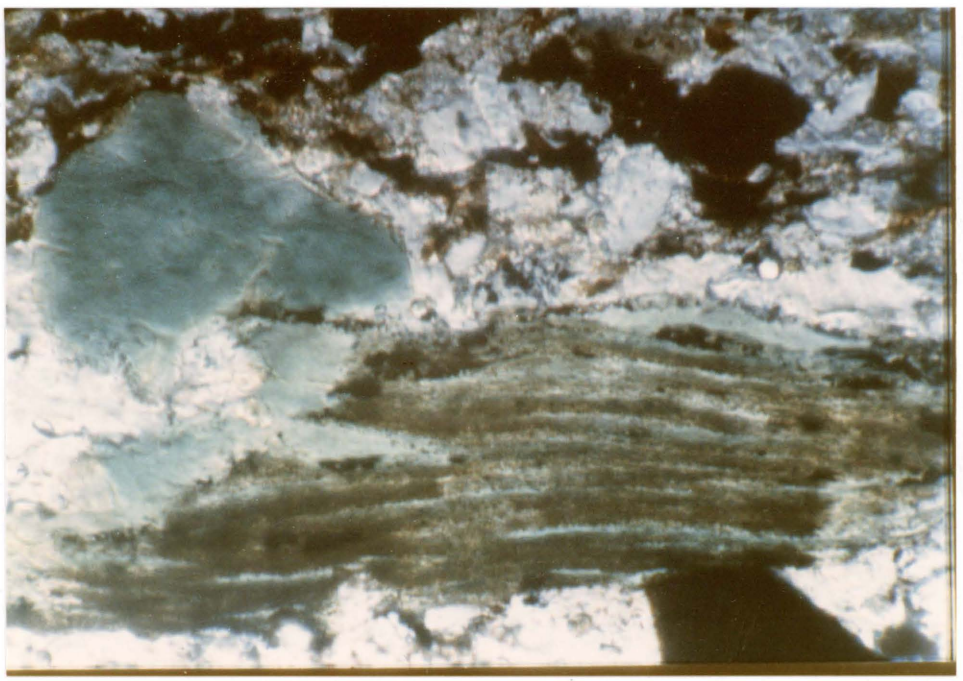
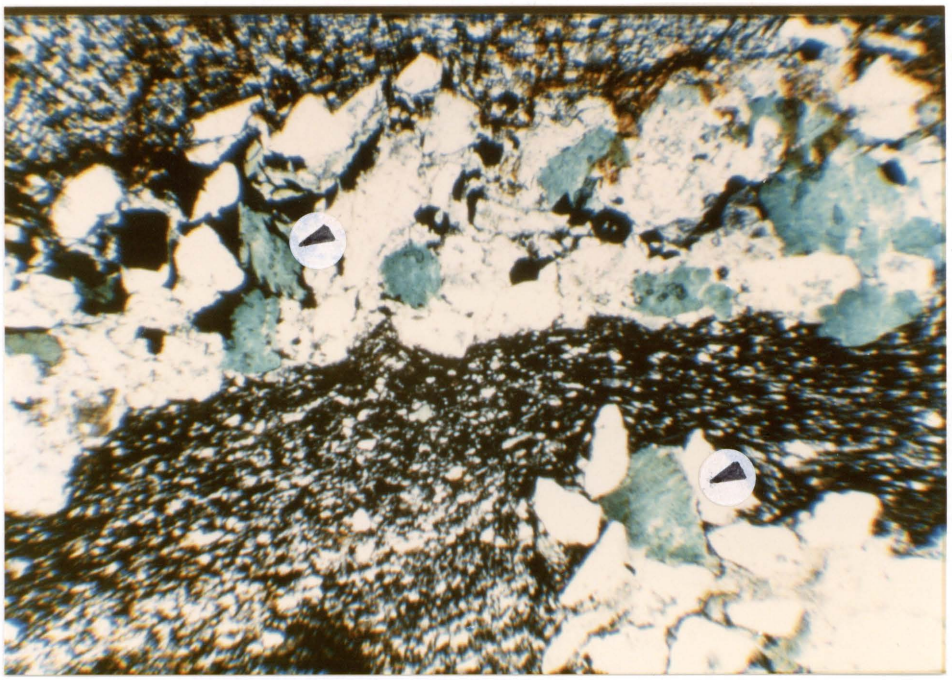


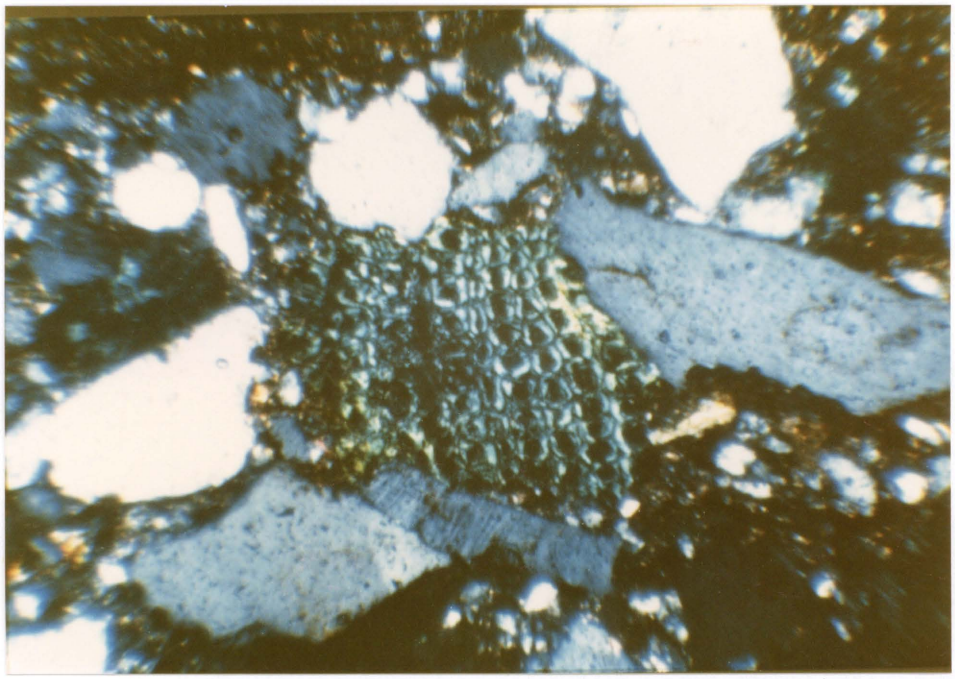
Fig. 3.13 Photomicrographs of (a) flaky massive glauconites filling interstitial grain spaces, (b) glauconite formation on edges and cleavages of an altered biotite, (c) glauconite as a pseudomorph after mica minerals (arrow), (d) glauconite filling cell cavities of higher plants and (e) glauconite as rounded grains and filling foraminiferal tests in Cretaceous sandstones, Germany.

Digitised by the Department of Library Services in support of open access to information, University of Pretoria, 2021.



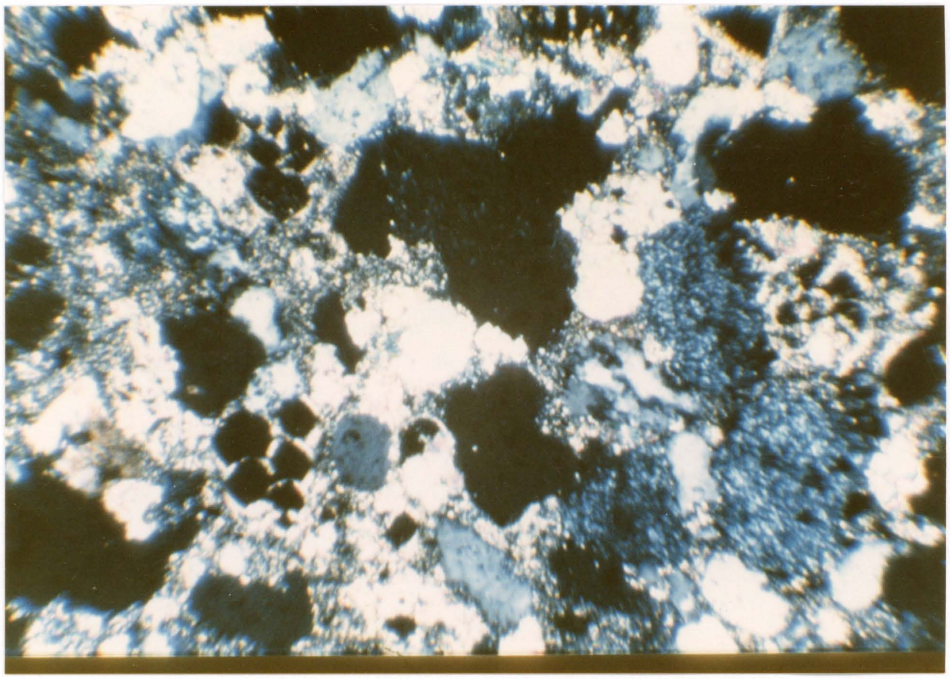
31µm

c



10µm

d



10µm

×Nicols

e

Digitised by the Department of Library Services in support of open access to information, University of Pretoria, 2021.

diffractograms shown here. The presence of the 4.8Å peak, the subdued nature of the 10Å peak and the asymmetrical shape of the three major peaks (10, 4.8 and 3.3Å) signify the 1Md (disordered) glauconite (BURST, 1958b, Fig. I, pattern 4). However, the broad peaks at 10.0Å and 10.4Å suggest some interlayering with illite-montmorillonite. This is supported by the diffractogram of the glycolated specimen (Fig. 3.14c), where the 10.4Å peak shifts to 10.6Å and the 4.8, 2.6 and 2.4Å peaks show a broadening to the low-angle side. After heating at 600°C the illite-montmorillonite structures apparently collapse and the main glauconite peaks become narrower and enhanced. The peak at 3.3Å is enhanced by quartz impurities. The 1.51Å peak indicates that the material is dioctahedral and it is thus essentially analogous to a glauconitic illite (PORRENGA, 1968).

The average chemical analyses per sample, are listed in table 3.2. From these a representative structural formula for all the samples can be calculated, based on 24(O and OH) per unit cell:

$$(K_{1.345}\ Ca_{0.02}\ Na_{0.043})\ (Al_{1.72}\ Fe^{2+}_{2.099}\ Mg_{0.709}\ Ti_{0.017})$$
$$(Si_{7.748}\ Al_{0.242})\ O_{20}\ (OH)_4$$

The composition of the glauconite filling plant cells compares well with this average formula, except that it is enriched in K_2O and FeO and depleted in octadedral Al. The glauconite from the marginally altered biotite grain of sample B is chemically similar to the average glauconite of all samples. The composition of the less altered part of the same grain resembles biotite analyses (DEER et al., 1970). Tetrahedral Al is much higher in typical biotites than in the one under consideration here, which is attributed to glauconitization along cleavage planes.

In general, there is a good correlation between Transvaal glauconites and marine as well as non-marine glauconites selected from the literature (Table 3.2). In all cases the total octahedral cations exceed the theoretical value of 4.0 per unit cell for a dioctahedral mica lattice, whereas the interlayer cations are less than 2.0; this is also pointed out by TYLER and BAILEY (1961). However, the rather high silica content and consequently low tetrahedral Al, compared to the marine glauconites found in the literature, is worth mentioning. Throughout all samples the Mg content is significantly constant. In a ternary diagram of FeO, K_2O and Al_2O_3, the analytical values cluster along the line of approximately 20% K_2O (Fig. 3.15), and fluctuations of the composition are mainly due to variations in the Al/Fe ratio. Samples A, B and D form a relatively Fe-rich group and partly overlap with the field of marine glauconites as defined by WEAVER and POLLARD (1973). Samples C and E are poor in Fe and comprise a field which is chemically closer to the illites (WEAVER and POLLARD, 1973). Undifferentiated glauconite, in terms of a marine or non-marine origin

Digitised by the Department of Library Services in support of open access to information, University of Pretoria, 2021.

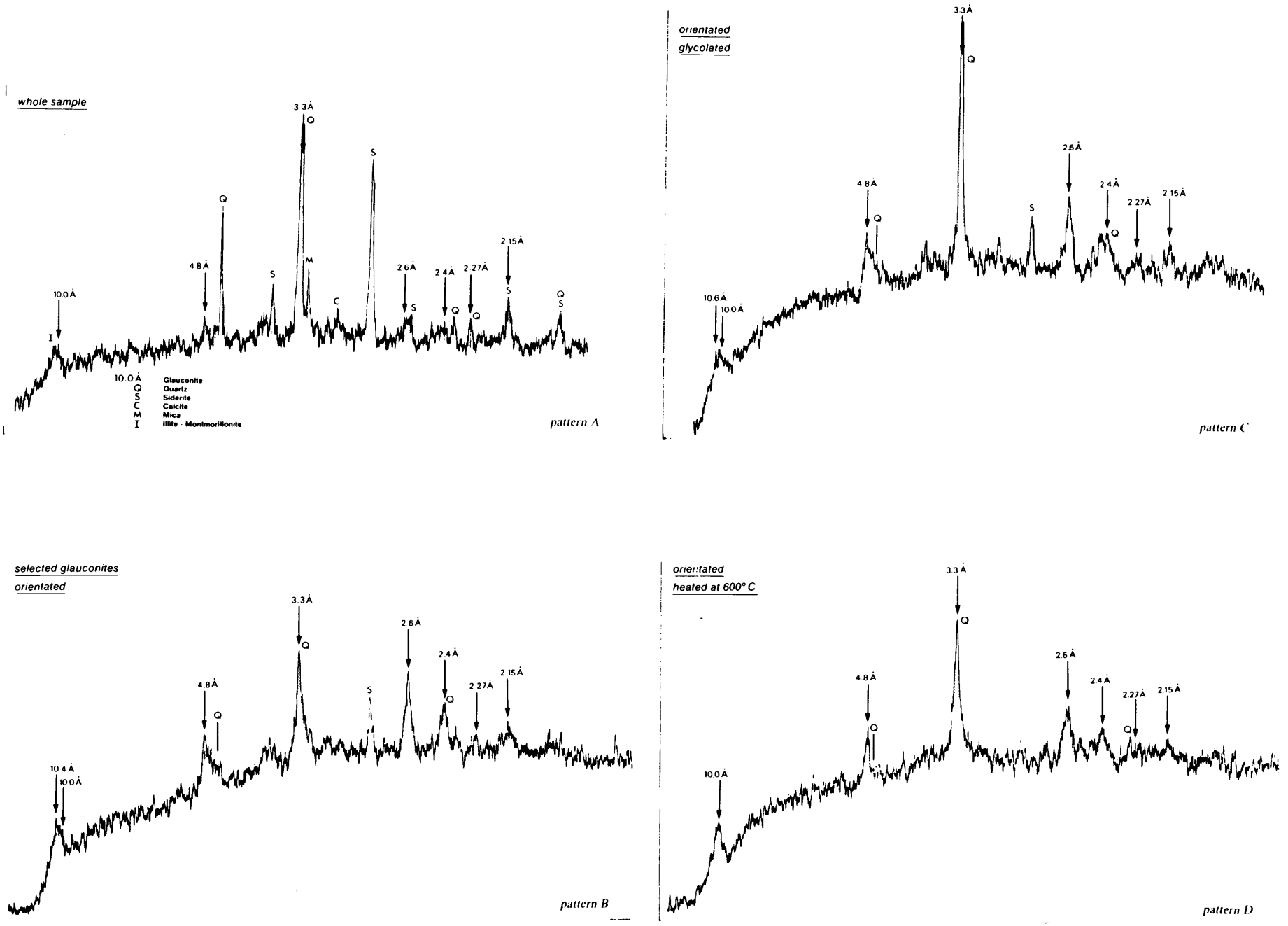


Fig. 3.14 X-ray diffractograms of glauconites from the Transvaal Coalfields. Pattern A: the diffractogram of the whole sample; Pattern B: selected orientated glauconite grains; Pattern C: orientated and glycolated glauconite grains; Pattern D: after heating of the orientated sample at 600°C

Digitised by the Department of Library Services in support of open access to information, University of Pretoria, 2021.

Table 3.2: Chemical analyses and ionic composition of various glauconites from the Transvaal Coalfields compared to analyses taken from the literature

Analyses of Transvaal glauconites (in weight %)

sample	A	B	C	D	E	average	I	II	III
SiO2	52.19	53.13	53.33	51.86	50.40	52.18	54.07	48.94	52.05
Al2O3	9.20	9.15	14.82	9.12	14.17	11.29	13.64	16.36	7.21
TiO2	0.11	0.13	0.15	0.05	0.10	0.11	0.12	3.40	0.09
Fe2O3									
FeO	18.84	20.14	13.37	18.43	13.62	16.88	16.04	14.21	21.91
MnO	0.01	0.01	0.01	0.01	0.02	0.01	0.03	0.01	0.00
MgO	3.54	3.58	2.73	3.52	2.63	3.20	3.76	3.98	3.73
CaO	0.12	0.08	0.16	0.12	0.18	0.13	0.37	0.37	0.07
Na2O	0.20	0.13	0.12	0.10	0.16	0.14	0.13	0.17	0.13
K2O	7.33	7.89	7.01	7.27	6.04	7.11	6.24	5.48	8.08
Cr2O3	0.03	0.02	0.02	0.01	0.02	0.02	0.03	0.02	0.01
H2O	8.43	5.74	8.28	9.51	12.66	8.92	5.57	7.06	6.72
total	100.00	100.00	100.00	100.00	100.00	100.00	100.00	100.00	100.00

number of ions on the basis of 22 O (* = 24 O)

tetrahedal								*	
Si	7.826	7.791	7.663	7.842	7.620	7.748	7.268	7.637	7.832
Al	0.174	0.209	0.337	0.158	0.380	0.252	0.732	0.363	0.168
octahedral									
Al	1.447	1.371	2.173	1.466	2.145	1.720	1.537	2.644	1.110
Ti	0.036	0.013	0.017	0.005	0.014	0.017	0.013	0.399	0.009
Fe3+									
Fe2+	2.359	2.466	1.606	2.336	1.726	2.099	1.891	1.856	2.758
Mn									
Mg	0.793	0.784	0.587	0.791	0.590	0.709	0.789	0.928	0.841
interlayer									
Ca	0.018	0.009	0.026	0.018	0.027	0.020	0.059	0.066	0.009
Na	0.054	0.035	0.035	0.036	0.055	0.043	0.034	0.056	0.036
K	1.405	1.480	1.278	1.400	1.163	1.345	1.119	1.088	1.556

I: glauconitic marginal zone of altered biotite grain
II: central zone of altered biotite grain; glauconitization already occurring along cleavage plains;
III: glauconitic filling of plant cell cavities
average: of all samples A - E

Analyses taken from literature (in weight %)

sample	1	2	2a	3	4	5	6	7	8	9
SiO2	49.22	49.29	36.83	49.53	49.92	51.28	41.6	49.03	54.18	46.90
Al2O3	9.15	3.17	16.54	14.59	14.59	4.43	11.0	17.93	14.20	6.20
TiO2		0.12	3.08			0.67	0.1	1.06	0.22	0.17
Fe2O3	17.95	21.72	4.81	14.48	14.48	22.30	16.1	13.11	12.11	21.45
FeO	3.43	3.19	18.47	3.39	3.39	7.07	0.7	1.31	2.03	3.16
MnO			0.09						0.03	0.02
MgO	3.58	3.85	7.87	3.35	3.35	3.85	4.8	2.79	4.01	4.20
CaO	0.64	0.74	0.53	0.39	0.39	0.11	0.9	0.39	0.68	0.70
Na2O	0.46	0.12	0.56	0.30	0.30	0.21	3.3	0.10	0.04	0.76
K2O	6.88	6.02	8.13	6.09	6.09	5.30	3.8	7.84	6.07	7.25
Cr2O3										
H2O	8.48	11.81	2.88	7.55	7.55	4.92	16.5	6.00	6.56	8.92
total	99.80	100.03	99.79	99.67	100.05	100.14	98.82	99.56	100.13	99.73

number of ions (* = as from literature)
(** = recalculated on the basis of 22 O)

tetrahedral	*	*	*	*	*	*	**	**	**	**
Si	7.30	7.63	5.66	7.13	7.13	7.43	6.77	6.87	7.46	7.16
Al	0.70	0.37	2.34	0.87	0.87	0.57	1.24	1.13	0.54	0.85
octahedral										
Al	0.89	0.21	0.66	1.55	1.55	0.27	0.88	1.90	1.77	0.27
Ti		0.01	0.36			0.08	0.01	1.14	0.03	0.02
Fe3+	2.02	2.53	0.55	1.58	1.58	2.34	1.97	1.38	1.26	2.64
Fe2+	0.41	0.41	2.40	0.41	0.42	0.87	0.10	0.15	0.23	0.40
Mn			0.01						0.00	0.00
Mg	0.78	0.89	1.78	0.72	0.72	0.83	1.16	0.58	0.83	0.95
interlayer										
Ca	0.13	0.12	0.09	0.01	0.01	0.02	0.16	0.06	0.10	0.12
Na	0.12	0.04	0.16	0.09	0.09	0.06	1.04	0.03	0.02	0.22
K	1.31	1.19	1.52	1.11	1.11	0.98	0.78	1.40	1.06	1.41

1: WEAVER and POLLARD, 1973: average of a suite of marine glauconites
2: DEER, HOWIE and ZUSSMAN, 1967: glauconite sandstone from New Zealand
2a: average of four biotite analyses
3: BURST, 1958a: suite of ordered marine glauconites
4: BURST, 1958a: suite of disordered marine glauconites
5: TYLER and BAILEY, 1961: average of a suite of marine glauconites
6: PARRY and REEVES, 1966: lacustrine glauconitic mica
7: KELLER, 1956: non-marine glauconitic mica from the Morrison Formation
8: PORRENGA, 1968: non-marine glauconitic illite, Oligocene, Belgium
9: DJADTSCHENKO and CHATUZEWA, 1957: alluvial and eluvial glauconites

Digitised by the Department of Library Services in support of open access to information, University of Pretoria, 2021.

(BURST, 1958a), is spread over the entire range from WEAVER and POLLARD's glauconites to illites. Analyses of non-marine glauconites (KELLER, 1966; PORRENGA, 1968) concentrate in and near the field of samples C and E; however, DJADTSCHENKO and CHATUZEWA's (1957) recent alluvial and eluvial continental glauconites chemically resemble WEAVER and POLLARD's marine glauconites. Marine glauconites, studied by TYLER and BAILEY (1961) and interpreted as of secondary origin, are extremely Fe-rich, which can partly be related to their proximity to an iron-ore body.

In all samples with the exception of two, the number of K^+ atoms per lattice unit falls into BURST's range of disordered glauconite, namely 0.8 to 1.4 atoms (BURST, 1958b, Fig. 2). This range of K^+ content also overlaps with illite. In this regard the chemical results correlate well with those of the XRD.

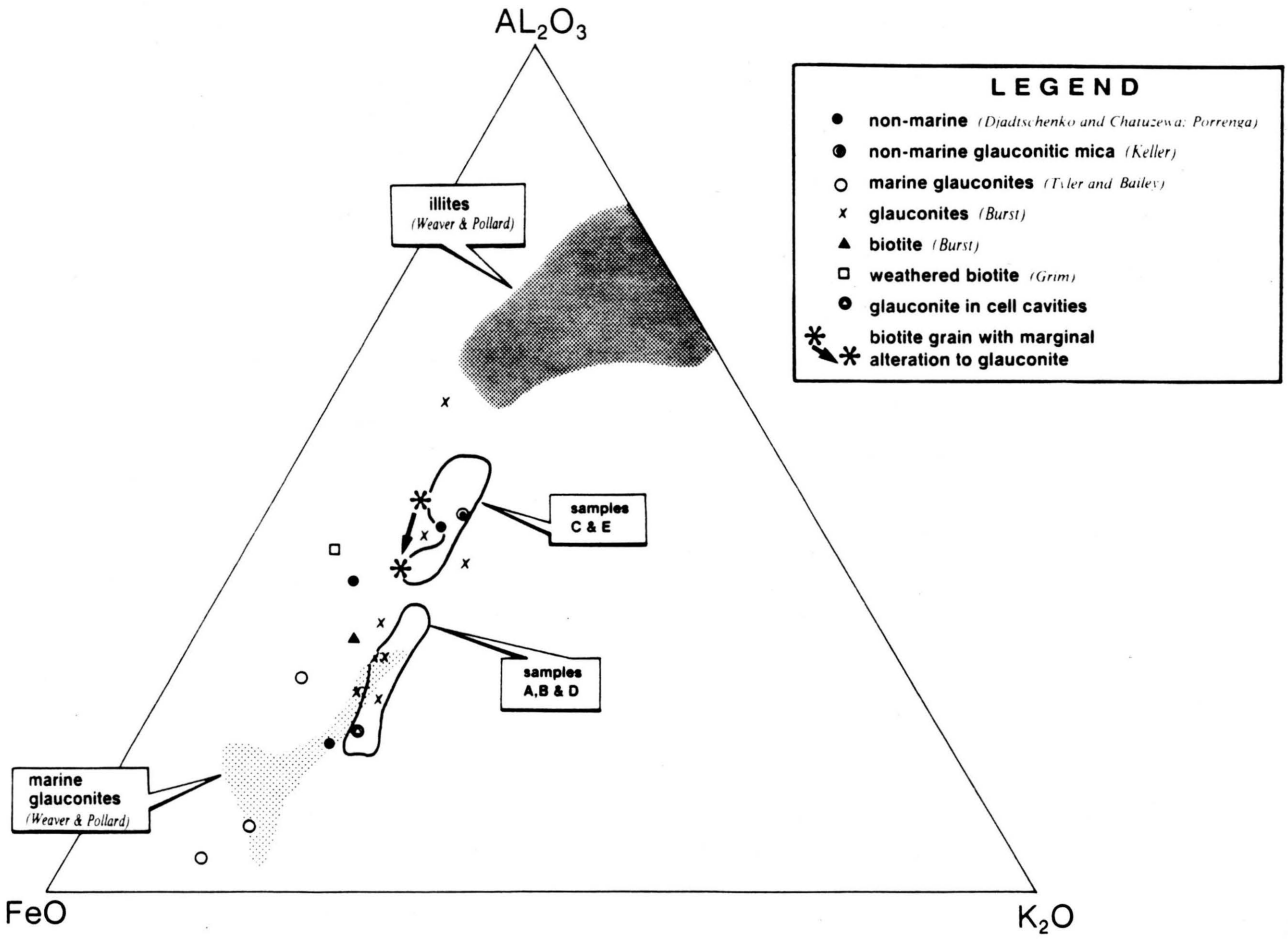


Fig. 3.15 Ternary diagram of FeO, K_2O and Al_2O_3 for glauconite analyses of this study, compared to results found in the literature.

Digitised by the Department of Library Services in support of open access to information, University of Pretoria, 2021.

3.12. Paleo-pH Results

Irrespective of lithology and porosity, the bulk of the measured values throughout the succession range from pH 7.2 to pH 9.4 (average pH 8.1) (Fig. 3.11; Appendix 2). They are generally higher from LFA 01 to the lower half of LFA 04 (average pH 8.4), with an exceptionally low value of pH 5.7. Paleo-pH values are lower below the coal zone and throughout most parts of LFA 06 (average pH 7.6 and pH 7.7, respectively), and high again above the No. 5 coal seam (average pH 8.4). Just above the coal seams pH values reach relative minima, as low as pH 3.1 above the No. 4L coal seam (Fig. 3.11).

Generally there is little correlation between pH values and clay mineral or carbonate contents; however, a few coinciding features can be outlined. In LFA 01 the pH values show a subtle upward decreasing trend, which coincides with an increasing kaolinite content. The slight change in pH at about the middle of LFA 04 coincides with a point in the sequence where the kaolinite content changes from very irregular to more even concentrations, and above which no illite occurs except for one sample in LFA 08. The only coinciding minima for ph value and kaolinite content in this sequence are in the upper portion of LFA 06, at about 1520m above sea level. The carbonates, especially calcite and dolomite, which are present in different concentrations throughout the sequence, do not show any correlation with the pH values.

3.13. Micropetrography of the No. 4L Coal Seam

The Twistdraai coals are rich in inertinite group macerals. Vitrinite is only abundant in samples taken from vitrain layers and exinite is a minor constituent throughout. The vitrinite mainly comprises telocollinite, collinite and to a lesser extent telenite, the cell cavities of which are mostly filled by either micrinite or clay minerals, rarely by pyrite. Oxidation rims on collinite are regular features in all vitrinite-poor samples.

The inertinite group macerals cover a wide range of low and high reflecting components. However, inertodetrinite is the most abundant maceral and is mainly concentrated in the durain bands and partly in the clarain bands. Inertodetrinite and semifusinite of varying reflectivity often form agglomerations together with clay minerals and quartz, but rarely with vitrinites and exinites (Fig. 3.16). Thus the major microlithotype of these coals is inertitic carbominerite and to a lesser extent vitrinertitic carbominerite.

The average maceral composition in sections 59, 60 and 61 of the

Digitised by the Department of Library Services in support of open access to information, University of Pretoria, 2021.

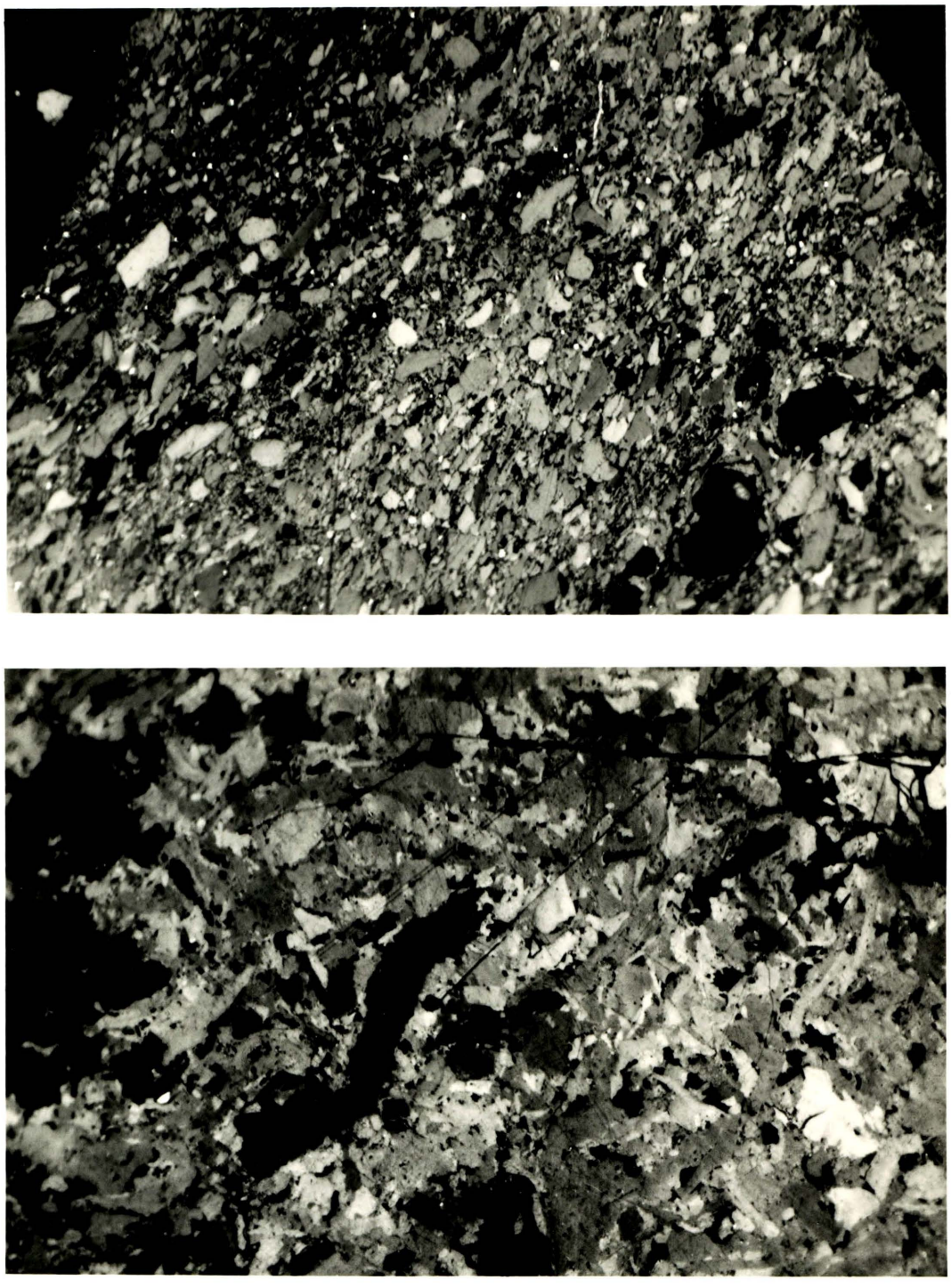


Fig. 3.16 Typical (a) fine-grained and (b) coarse-grained carbominerites, mainly comprising inertodetrinite and semifusinite of varying reflectivity, as well as minor occurrences of vitrinite. Oil immersion at 500 X magnification.

Digitised by the Department of Library Services in support of open access to information, University of Pretoria, 2021.

Table 3.3 Average maceral composition of the No. 4L coal seam in sections 59, 61 and 62. The complete set of results is given in appendix 3a and 3b.

section	62	59	61
collinite	19.0	23.7	31.5
low reflecting macrinite	5.5	2.6	2.3
high reflecting macrinite	0.8	0.3	0.3
vitrodetrinite	2.4	0.4	3.4
low reflecting inertodetrinite	32.0	32.0	23.3
high reflecting inertodetrinite	17.0	14.3	15.1
telinite	0.3	2.1	0.4
low reflecting semifusinite	16.1	16.4	16.4
high reflecting semifusinite	4.6	4.5	4.4
fusinite	0.5	1.3	0.3
micrinite and sclerotinite	0.7	0.8	0.9
exinite	1.1	1.6	1.7
total	100.0	100.0	100.0

No. 4L seam are very similar. However, the contents of collinite and low reflecting inertodetrinite indicate some fluctuation between the three sections, although the combined proportion of these two macerals exhibits consistent values in all three profiles (Table 3.3; Appendix 3). The macerals collinite and low reflecting inertodetrinite generally comprise the largest proportion in each profile (20-32% each); the high reflecting inertodetrinite and low reflecting semifusinite amount to about 16% each. Of the other macerals, the low reflecting macrinite, vitrodetrinite and high reflecting semifusinite constitute 2-4% each, whereas the remaining macerals comprise quantities around 1%.

By grouping all macerals, with the exception of exinite, sclerotinite and micrinite, into massive, detrital and cellular categories, it appears that detrital macerals dominate in most samples (Appendix 3A). In some cases the massive macerals become predominant, but rarely the cellular macerals. A larger group of samples (B in figure 3.17) contains more than 40% detrital macerals and about equal percentages of the other two categories. A smaller group of samples (A in figure 3.17) contains 60% and more of massive macerals, the remainder being dominated by detrital macerals.

A similar grouping of the same samples is formed on the basis of vitrinite, low reflecting inertinite and high reflecting inertinite (including sclerotinite) (Appendix 3B). Again, exinite and micrinite are excluded. In this case the low reflecting inertinite predominates in most samples, the high reflecting inertinite seldom exceeds 30% and the vitrinite only attains more than 60% in exceptional cases. Sample group B in figure 3.17 corresponds with sample group Z in figure 3.18 and contains more than 40% of low reflecting inertinite; vitrinite and high reflecting inertinite account for the rest in complementary

Digitised by the Department of Library Services in support of open access to information, University of Pretoria, 2021.

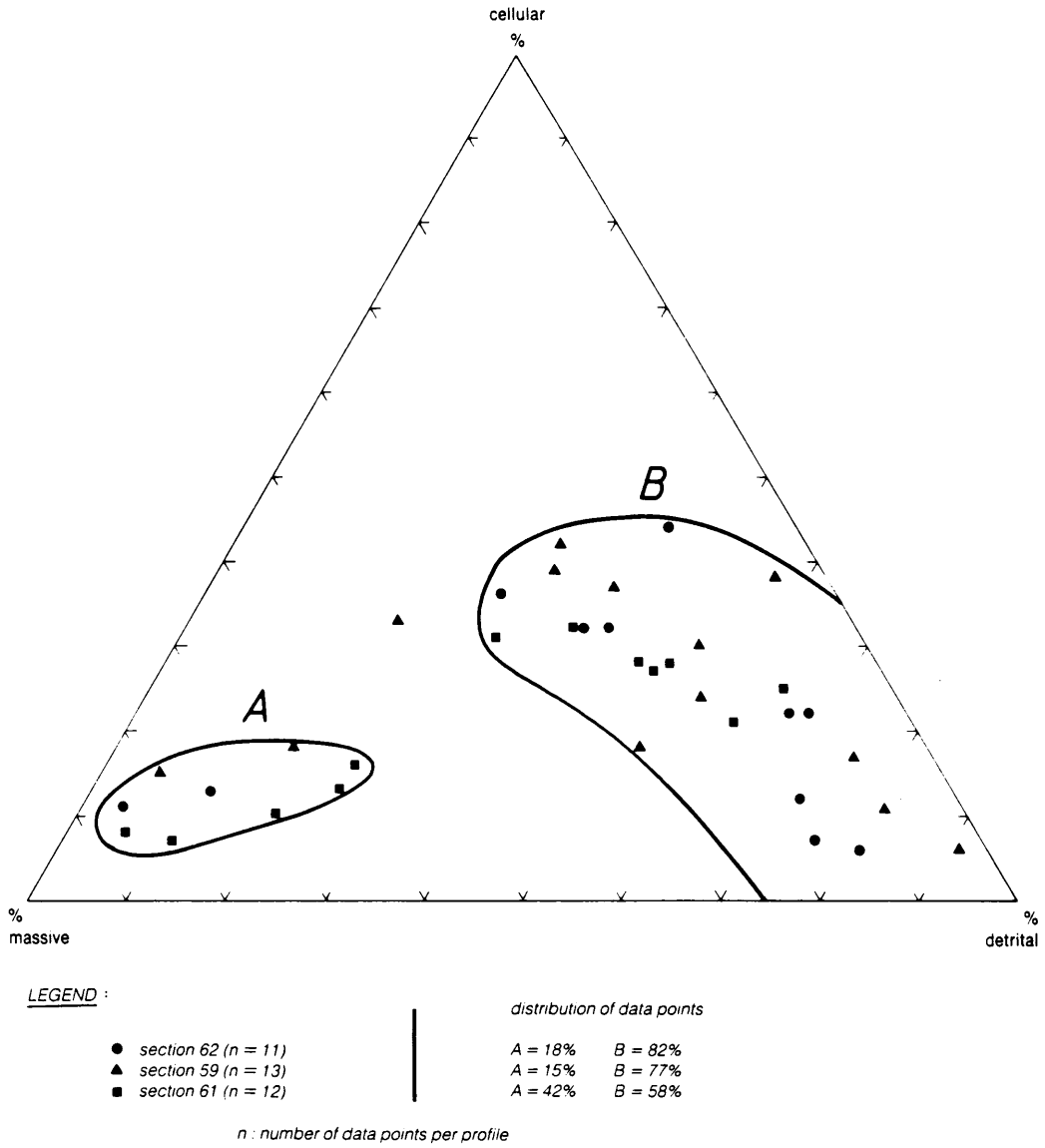


Fig. 3.17 Distribution of cellular, detrital and massive macerals in all samples of sections **59**, **61** and **62** (see figure 2.1 for location)

amounts. Sample groups X and Y in figure 3.18 correlate with group A in figure 3.17; they are characterized by more than 60% and 80% of vitrinite, respectively. The low reflecting inertinite generally accounts for the major part of the remaining macerals.

In profile, the microscopic composition of the coals in the three sections shows similar cyclic patterns to the macroscopic description. Four cycles can be distinguished on the basis of the ratio of vitrinite, low reflecting inertinite and high reflecting inertinite (Fig. 3.19), and also by the proportions of detrital, massive and cellular macerals (Fig. 3.20). A fifth cycle caps the seam in section 59.

The basal cycle, A, is relatively rich in vitrinite, but low reflecting inertinite predominates. The detrital material generally

Digitised by the Department of Library Services in support of open access to information, University of Pretoria, 2021.

predominates, but is exceptionally low in sample 183 of section 62, where the vitrinite is extremely high. There are more cellular structures in sections 59 and 61 than in 62 (Fig's 3.19 and 3.20).

Cycles B and C both have an upward-increasing vitrinite content in all three profiles; however, this is less prominent in cycle C of section 61. The proportion of high reflecting inertinite remains relatively constant throughout. The low reflecting inertinite is generally the major component in all samples, although it decreases drastically with extremely high vitrinite contents (e.g. sample 193 in figure 3.19). The amount of massive macerals is proportional to the vitrinite content, whereas the ratio of the detrital material varies apathetically. The percentage of cellular structures remains irregular, but can be proportional to the vitrinite content, as for instance in cycle B of section 59.

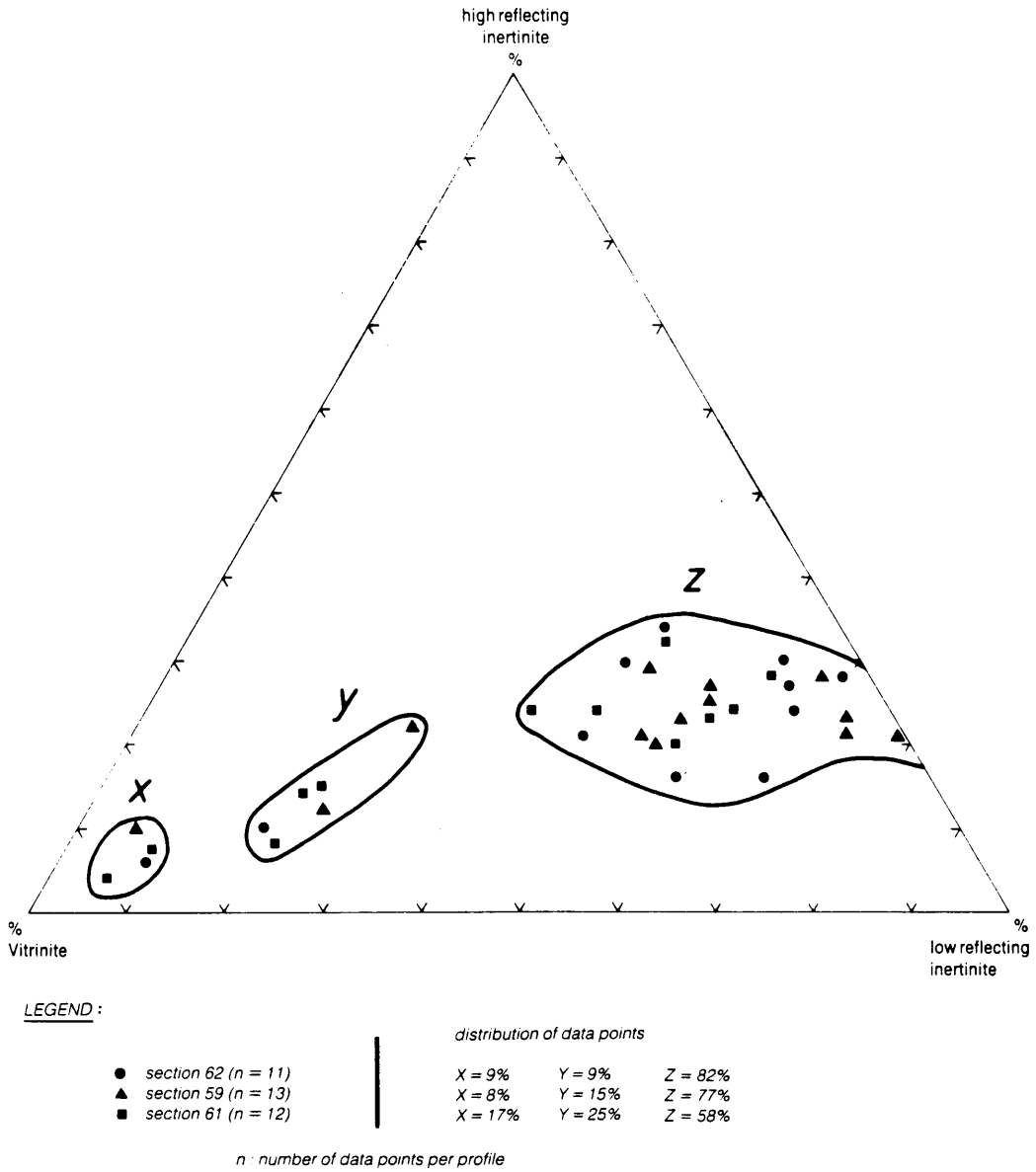


Fig. 3.18 Distribution of high and low reflecting inertinite and vitrinite in all samples of sections **59**, **61** and **62** (see figure 2.1 for location).

Digitised by the Department of Library Services in support of open access to information, University of Pretoria, 2021.

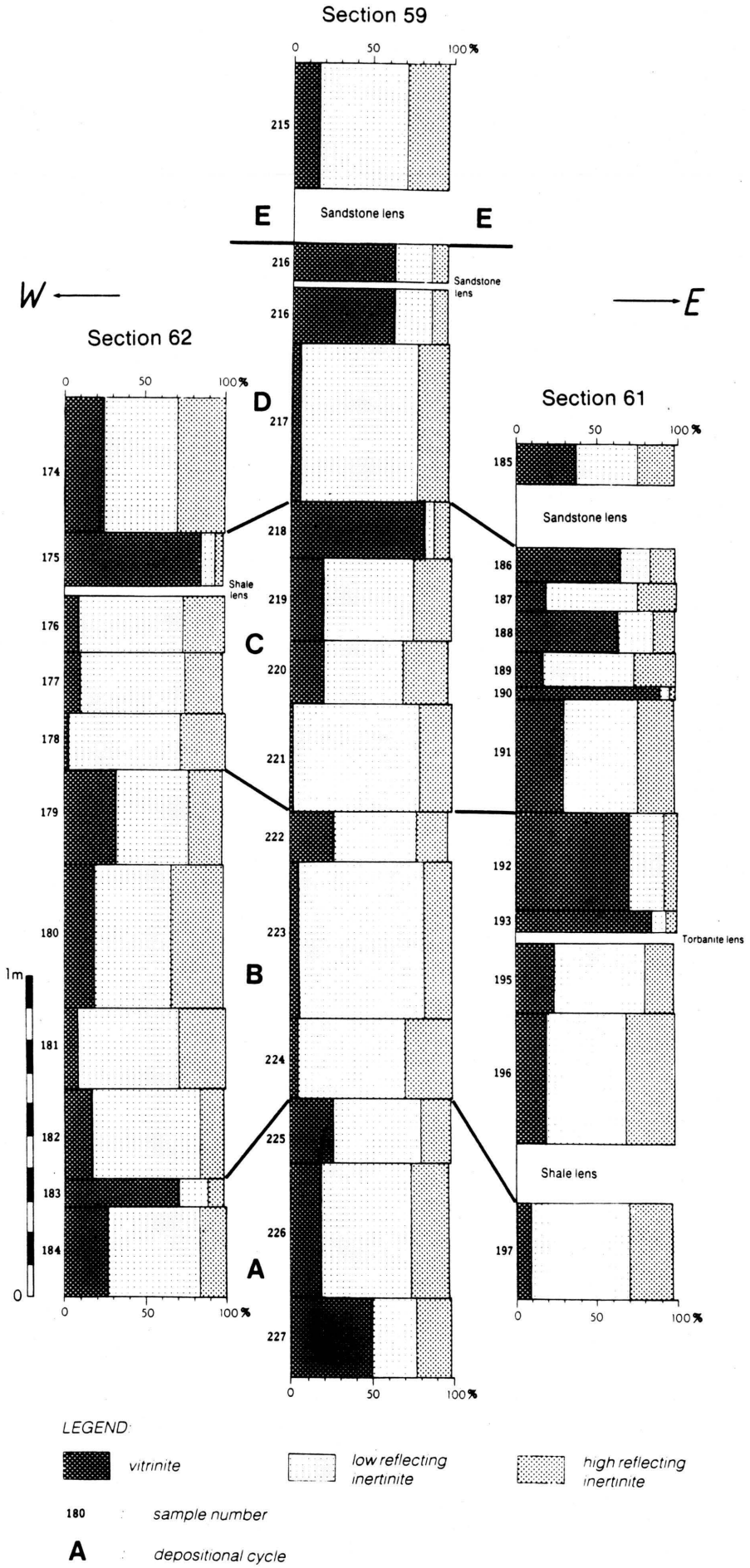


Fig. 3.19 Three representative profiles from sections **59**, **61**and **62** of the No. 4L coal seam showing the cyclicity of the relative distribution of vitrinite and low and high reflecting inertinite within the lithotype bands.

Digitised by the Department of Library Services in support of open access to information, University of Pretoria, 2021.

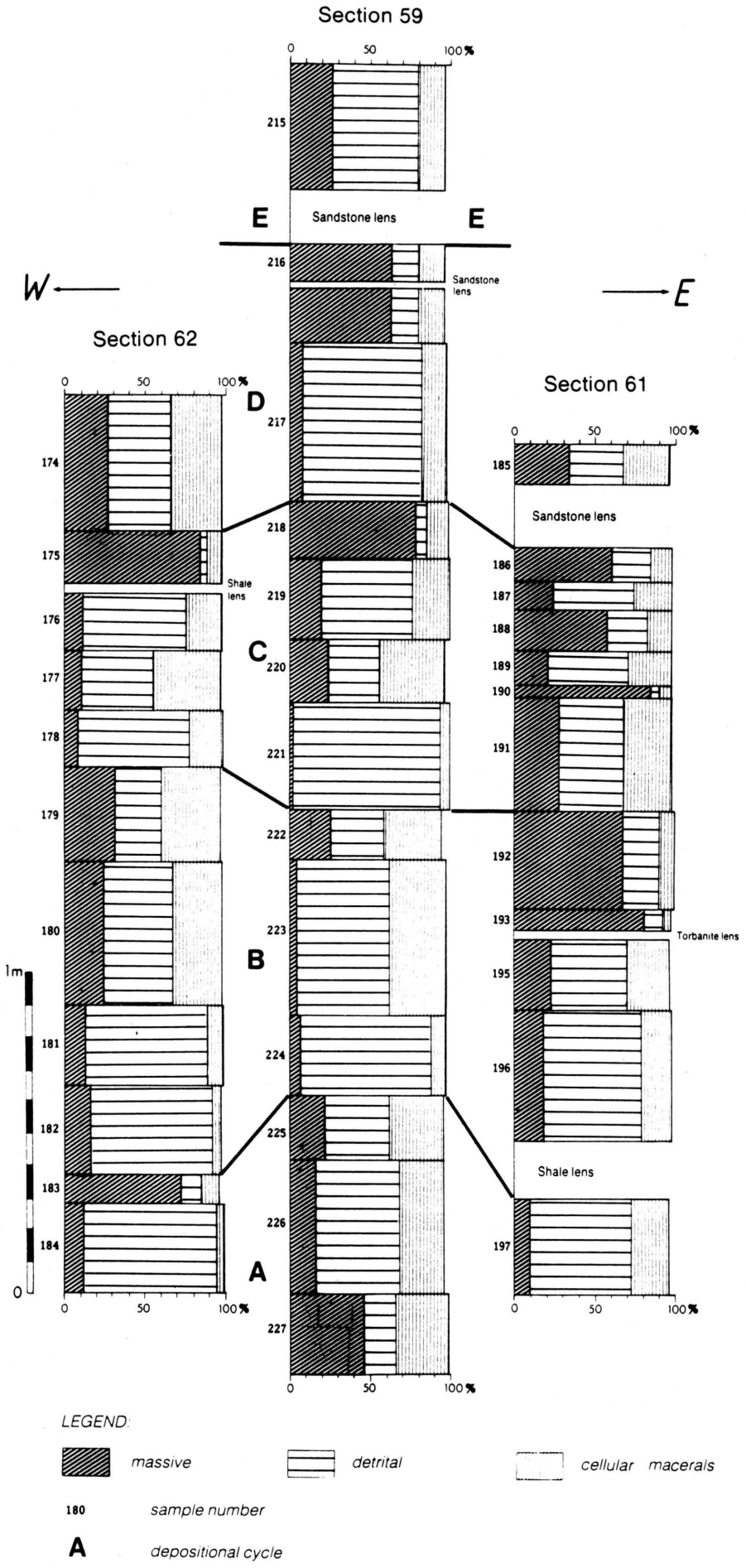


Fig. 3.20 Three representative profiles from section **59**, **61**and **62** of the No. 4L seam showing the cyclicity of the relative distribution of massive, detrital and cellular macerals within the lithotype bands.

Digitised by the Department of Library Services in support of open access to information, University of Pretoria, 2021.

Cycle D at the top is mainly developed in the profile of section 59 and is truncated in the other two sections. As in the two preceeding cycles, a vitrinite-rich band, which is poor in detrital macerals, terminates this cycle. The low reflecting inertinite is generally predominant and the high reflecting inertinite maintains a relatively constant percentage. The detrital and massive fractions are variable and are compensated for by each other, whereas the cellular category remains relatively constant throughout the cycle.

Cycle E is only present in section 59. It consists of a basal sandstone lens and an overlying coal band which is vitrinite-poor and rich in detrital material.

It is, therefore, obvious that there is a strong inverse relationship between the amount of detrital macerals and vitrinite. Generally, the low reflecting inertinite is most abundant, ranging between 60% and 80% (averaging 70%) of the total inertinites, except where the vitrinite exceeds 50%. In these cases the proportion of the low reflecting inertinites averages 60% and can fall to 35% (Appendix 3B).

Digitised by the Department of Library Services in support of open access to information, University of Pretoria, 2021.

4. MODEL OF DEPOSITIONAL PALEOENVIRONMENT

In the previous chapter lithofacies associations were established on the basis of their sedimentary characteristics and their facies inter-relationships. It was found that the LFA's and their succession were largely representative for the entire study area.

Subsequent interpretation of the lithofacies associations, in order to establish a model of the depositional paleoenvironment, necessitates recognizing the various processes that may have formed the facies. These are mainly depositional processes in the sense of REINECK and SINGH (1980, p5), in contrast to erosional processes. READING (1982, p10-11) distinguishes between normal and catastrophic sedimentary processes. The latter occur almost instantaneously and erratically, and usually have a much greater energy level than normal sedimentation. Examples of such processes are turbidites or avalanches. As a coal-forming environment, however, requires steady, long-lasting and balanced sedimentation (STACH et al., 1982, p9), normal processes in the sense of READING (1982) can be expected to predominate within such depositional settings. These normal processes include pelagic settling, organic growth, tidal and fluvial currents, as well as compaction and diagenesis. Consequently, in this study, it is considered that mainly normal depositional processes, and in exceptional cases normal erosional processes, formed the observed lithofacies associations.

It is the objective of this chapter to relate the characteristics of the LFA's to sedimentary processes and these in turn to a logical succession of paleoenvironments. The term 'Event' will be introduced here to represent the term 'LFA' of the previous chapter. An event (READING, 1982, p10-11) is the occurrence of a single sedimentary process or of several contemporaneous, interacting processes that together form a depositional environment, which in turn determines the lithofacies association of the subsequently preserved sediments. By using the term 'Event' in the following chapters, the LFA's will be looked at from a genetic point of view.

As the events are defined on the basis of the different LFA's and the genetic processes that comprised the depositional paleoenvironments, they can grossly be regarded as time-equivalent throughout the coalfield. However, temporal overlaps of two succeeding events do occur and will be pointed out. The initial Events 01 to 03 produced relatively uncomplicated paleoenvironmental conditions, whereas the subsequent Events 04 to 08 are believed to have formed highly complex associations of paleoenvironments (Fig. 4.1). These circumstances caused numerous lateral and vertical changes in the relevant LFA's.

Digitised by the Department of Library Services in support of open access to information, University of Pretoria, 2021.

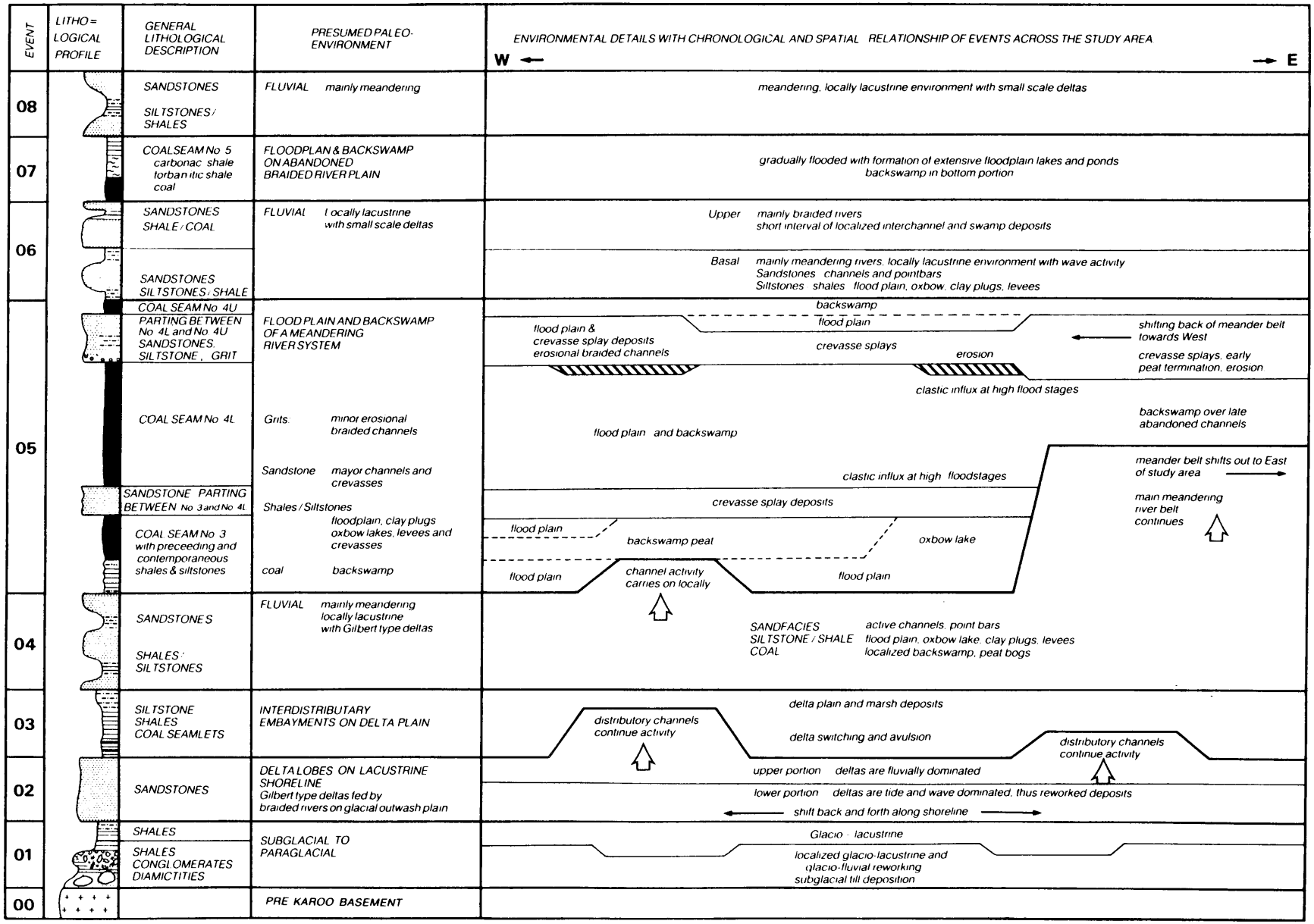


Fig. 4.1 Diagram of the chronological succession and spatial relationship of all eight events. The right hand part of the diagram shows an unscaled east-west section through the coalfield, with the spatial inter-relationships of the various processes that controlled the succession of events.

Digitised by the Department of Library Services in support of open access to information, University of Pretoria, 2021.

4.1. General Aspects of Coal-forming Environments

Coal deposits usually form in low-lying, flat areas with no or almost no water movement. Good conditions for the preservation of accumulating plant debris must include a constant water level at, or just above, the surface of the accumulating peat (STACH et al., 1982, p9). This requires a balance between rate of subsidence and peat growth. Furthermore, the low area where the coal swamp forms must be protected from any regular influx of oxygen-rich waters and clastic sediment. These basic conditions for peat formation and peat preservation are commonly met in either:

* back-barrier lagoon,
* deltaic,
* fluvial, or
* alluvial fan environments (GALLOWAY and HOBDAY, 1983, p255-290).

The back-barrier coal association typically comprises barrier sandstones which intercalate seawards with red and green calcareous shales and carbonate rocks containing a marine fossil fauna; landward they develop lagoonal shales characterized by extensive burrowing (HORNE et al., 1978, p2380). The main elements of a preserved barrier island environment are elongated, shore-parallel sand bodies (barriers), enclosed lagoonal sediments and filled inlet channels (GALLOWAY and HOBDAY, 1983, p124). Back-barrier coals have distinct shore-parallel distribution trends and the host rocks commonly exhibit upward-coarsening sequences of shales and siltstones. Coals are thin, discontinuous and have high sulphur contents (GALLOWAY and HOBDAY, 1983, p268).

The delta paleoenvironment is highly complex and normally reflects the interaction of fluvial and basinal processes. Coals cap upward-coarsening delta-front and interdistributary bay sequences. Rapid lateral changes of distributary channel sediments and interdistributary bay sediments are discernible. Peats usually accumulate in interdistributary and localized back-barrier bays and abandoned channels (GALLOWAY and HOBDAY, 1983, p266). Subsequent coal seams are laterally extensive, with variable trends and are commonly split by erratic crevasse splay sediments (FIELDING, 1985, p46).

The fluvial setting is less complex than the deltaic one and is dominated by coarse-grained channel deposits, with minor fine-grained channel-fill sediments, and adjacent argillaceous floodplain and backswamp deposits (READING, 1982, p15-60). Channel systems undergo frequent lateral shifts, thereby producing laterally extensive sheet-like deposits. Peat in this environment usually forms on the top of upward-fining fluvial cycles (GALLOWAY and HOBDAY, 1983, p280) and

Digitised by the Department of Library Services in support of open access to information, University of Pretoria, 2021.

commonly thickens away from the levees towards the backswamps. Elongated coal seams trend parallel to the channels and most splits occur in close proximity to the channel belt (FIELDING, 1985, p46).

The alluvial fan environment is part of an intermontane system and therefore comprises large amounts of conglomerate and pebbly sandstone in juxtaposition with coals and shales (HEWARD, 1978, p455). These rocks are often related to sporadic tectonic movement which produces strike-slip faulting and a subsequent erratic fan pattern (GALLOWAY and HOBDAY, 1983, p286).

The alluvial fan coal-forming environment can immediately be eliminated as a possible model for this study, as almost no conglomeratic sediments are found in the coalfield, except in LFA 01, where, however, no coal occurs. The back-barrier model is also an implausible interpretation, due to a lack of extensive burrowing, marine fossils and red- and green-coloured shales in the study area. In addition, no shore-parallel major sandstone bodies or related inlet features can be discerned in the Twistdraai sediments; such a shoreline trend should be roughly east-west near the northeastern margin of the Karoo Basin (TANKARD et al., 1982, p364). A thick LFA 02 sandstone body oriented northeast-southwest (Map 2) in the study area is most likely related to the fault zone.

The remaining two environmental settings are both defined by features which can be recognized in the sedimentary sequence of the Twistdraai Coalfield; it is possible that an interaction of both settings may have occurred. A predominance of fluvial processes is assumed, mainly due to the sheet like appearance of the sediment layers and LFA's. Based on these general conclusions the following model of the depositional paleoenvironment of the Twistdraai Coalfield is proposed.

4.2. Pre-Karoo Topography

The pre-Karoo Sequence topography (Map 0) is the result of erosion by glaciers during the Permo-Carboniferous glaciation of Gondwanaland. The main topographic features of north-south trending paleovalleys and paleoridges which are clearly recognizable in the study area (Map 0), coincide with the major directions of ice movement reported by DU TOIT (1954) and TANKARD et al. (1982) for the northeastern Karoo Basin.

Digitised by the Department of Library Services in support of open access to information, University of Pretoria, 2021.

4.3. Event 01

The coexistence of diamictites, conglomerates, coarse-grained sandstones and black shales in LFA 01 point to a complex paleoenvironmental association of various energy levels. These most likely reflect glacial, fluvial and lacustrine sedimentary processes, which generally interact within an overall glacial environment (REINECK and SINGH, 1980, p192).

This facies association can be assigned to the continental glacial setting characterized mainly by grounded ice sheets (EYLES and MIALL, 1984). Extensive ice caps developed on elevated regions and southward-flowing ice lobes eventually encroached on an extensive body of water, situated at a present-day latitude of about 30° south (VON BRUNN and STRATTEN, 1981). The diamictites, which are interpreted as subglacial tillite deposits, formed hummocks and ridges of debris oriented transversely to the general ice flow. Meltwater ponds were thus allowed to dam up and provide locally restricted proglacial lacustrine environments in close proximity to the ice sheet (EYLES and MIALL, 1984, p21). The blueish to greyish varved shales and mudstones at Twistdraai, as well as some coarser-grained fan deposits, are presumed to have been laid down in a similar setting.

The association of massive tillites, with crudely-interbedded coarse-grained, gritty, matrix-supported sandstones and conglomerates of glaciofluvial deposition, indicate a glacial outwash plain, characterized by braided channel systems (EYLES and MIALL, 1984, p19). These facies associations thus form a laterally variable assemblage of glacial, glaciofluvial and glaciolacustrine sediments, which VISSER (1986) ascribes to deposition from sediment gravity flows and glacial outwash. VON BRUNN and STRATTEN (1981) also suggest a complex glaciofluvial and glaciolacustrine paleoenvironment with braided streams for this depositional phase of the northern Karoo Basin sequence.

During the later stage of Event 01, a laterally more continuous paleoenvironmental setting was present over the coalfield. This is indicated by the presence of widespread, thick carbonaceous shales and siltstones, containing dropstones; such sediments commonly cover glacial lake bottoms (READING, 1982, p416). VISSER (1986) relates such sediments to debris rain processes and suspension settling in his studies on the central and northern Karoo Basin. Bioturbation, coal fragments and pyrite in the shales indicate quiescent, secluded water basins with marginal peat development and localized reducing conditions, such as observed by FOUCH and DEAN (1982) in recent northern temperate lakes. A periglacial lacustrine paleoenvironment, as defined by EYLES and MIALL (1984, p20), is inferred, and the fine-grained sediments presumably reflect deposition from suspension (EASTERBROOK, 1982, p8).

Digitised by the Department of Library Services in support of open access to information, University of Pretoria, 2021.

Lakes in a glacial paleoenvironment can commonly be of small extent and may follow the retreating glacier margins; thus lake and beach deposits may cover a large area (READING, 1982, p421). This seems unlikely for this study area, as the isopach map of these sediments (Map 1.2) shows an evenly distributed layer, indicating that former topographic irregularities were largely levelled after the tillite deposition and that conditions were set for a wide-open water body.

Towards the final phase of this event, sandstone and siltstone interbeds and soft sediment deformation structures in the shales at the top of LFA 01 probably indicate increasing fluvial activity and more rapid sedimentation (READING, 1982, p64). These are regarded to be precursors of Event 02.

4.4. Event 02

The occurrence of both upward-fining and upward-coarsening cycles in this LFA suggests an interaction of fluvial and deltaic activity (CADLE and HOBDAY, 1977; READING, 1982, p48&98). The large thickness, sheet-like form, the planar cross-bedding and variable grain sizes of this LFA imply lateral accretion, rapid sedimentation and fluctuating discharges, a combination which is typical of meltwater streams and glacially-related deltas (EASTERBROOK, 1982, p7). Similar, Gilbert-type deltas, as described by STANLEY and SURDAM (1978) from the northwestern United States, are reported by CAIRNCROSS and WINTER (1984) from the Rietspruit Colliery in the southern Witbank Coalfield. However, there they occur further up in the succession, between coal seams No. 4 and No. 5.

The uniform lateral distribution of LFA 02, the lack of elongated sandstone bodies and the maturity of the sandstones, suggest that active delta lobes were rapidly shifting along a shoreline that exceeded, at least, the boundaries of the study area. Fine particles in the sandstones were removed by the winnowing effects of basinal processes, such as tidal and wave reworking (REINECK and SINGH, 1980, p432; READING, 1982, p63); this is supported by the predominance of mature, quartz-rich sandstones in the study area.

In such a fluvial and deltaic paleoenvironment horizontal bedding can be related to high energy upper flow regime processes (REINECK and SINGH, 1980, p122); the planar cross-bedded sandstones most probably reflect fluvial, deltaic or basinal bar migration. STEYN (1976) finds flaser bedded sandstones (his facies 9) in the bottom of the sequence at the Davel Coalfield. Their position in the sedimentary column corresponds to the top of LFA 02 in this study, and their origin is

Digitised by the Department of Library Services in support of open access to information, University of Pretoria, 2021.

tidal (REINECK and SINGH, 1980, p112), in its widest sense of generally fluctuating water and energy levels, rather than a strictly lunar-controlled tidal effect. This suggests an extensive water-filled basin, or a number of larger lakes, rather than small lakes shifting with a retreating ice shield. The silty matrix and the bioturbation in the sandstones at the top of this succession, indicate decreasing energy levels, probably due to partial abandonment of the study area by the active distributaries. Plant debris was most likely imported from peripheral early swamps, lying beyond the study area boundaries.

For most of the time during Event 02 tidal and wave effects probably predominated over fluvial and deltaic processes. Towards the end of the event, river-dominated deltaic processes became prominent, as indicated by a final upward-coarsening cycle, characterized by poorler sorted sediments rich in fine-grained material.

MIALL (1984, p109) refered to the problem of identifying wave- and tide-dominated deltas and beach-fronts in ancient sedimentary rocks. A large sediment volume and a facies change to a landward fluvial sequence are often the only evidence of such deposits. This is the case in the present study as well. The abundance of coarse-grained sandstones and minor shales and siltstones in the top of LFA 02 points to sandy braided river deposition, capping the deltaic sequence. RUST (1978) and N.D. SMITH (1970) refer to similar lithological characteristics in braided river deposits. READING (1982, p103) emphasizes that, due to irregular discharge and high bedload proportions, braiding commonly occurs in delta distributary channels in a high altitude climate. A similar paleoclimate can be assumed to have prevailed during Event 02, following the subglacial and paraglacial period of Event 01. Analogous sediments are also described from recent proglacial environments in Alaska and Iceland by BOOTHROYD and NUMMEDAL (1978). CANT (1978) and N.D. SMITH (1970) present slope figures for braided rivers of 0.3m/km and 1-2m/km, respectively; these compare reasonably well with the paleoslope of 2.42m/km calculated for the beginning of Event 02.

The preceding glaciolacustrine paleoenvironment of Event 01 thus appears to have been succeeded by a phase of inter-related deltaic and fluviodeltaic complexes, still associated with an overall glaciolacustrine setting. Reworking of delta sediments by basinal processes took place on a large scale. Towards the close of Event 02, the depositional activity in the study area was controlled by the braided distributaries of these lacustrine deltas. The thick sandstone body along the fault zone and in the western pre-Karoo paleovalley probably reflects a major channel in this part of the deltaic system. Thinner LFA 02 sediments, such as in the southeast of map 2, suggest an early exclusion of that area from further channel deposition. During Event 02 the glacial influence diminished and is assumed to be of minor importance in the succeeding events.

Digitised by the Department of Library Services in support of open access to information, University of Pretoria, 2021.

4.5. Event 03

The association of dark grey siltstones, carbonaceous shales and coal in LFA 03 indicates an environment which, in fluvial systems, is commonly met on floodplains, in abandoned channels and in oxbow lakes. In deltaic systems similar associations are known to occur in interdistributary embayments, which are protected from basinal influences by barrier sands, and from channel influences by levees (READING, 1982, p38&125).

As the previous event appears to have been terminated by a fluvially-dominated deltaic system, LFA 03 is interpreted as an interdistributary bay paleoenvironment, with localized marsh deposits (Map 3.M). In this context, quiet water deposition from suspension (finely-laminated shales and siltstones), reducing conditions (pyrite) and burrowing organisms are characteristic of lacustrine environments in a delta setting (COLEMAN and PRIOR, 1982, p147). Soft sediment deformation structures are the result of crevassing into these secluded areas.

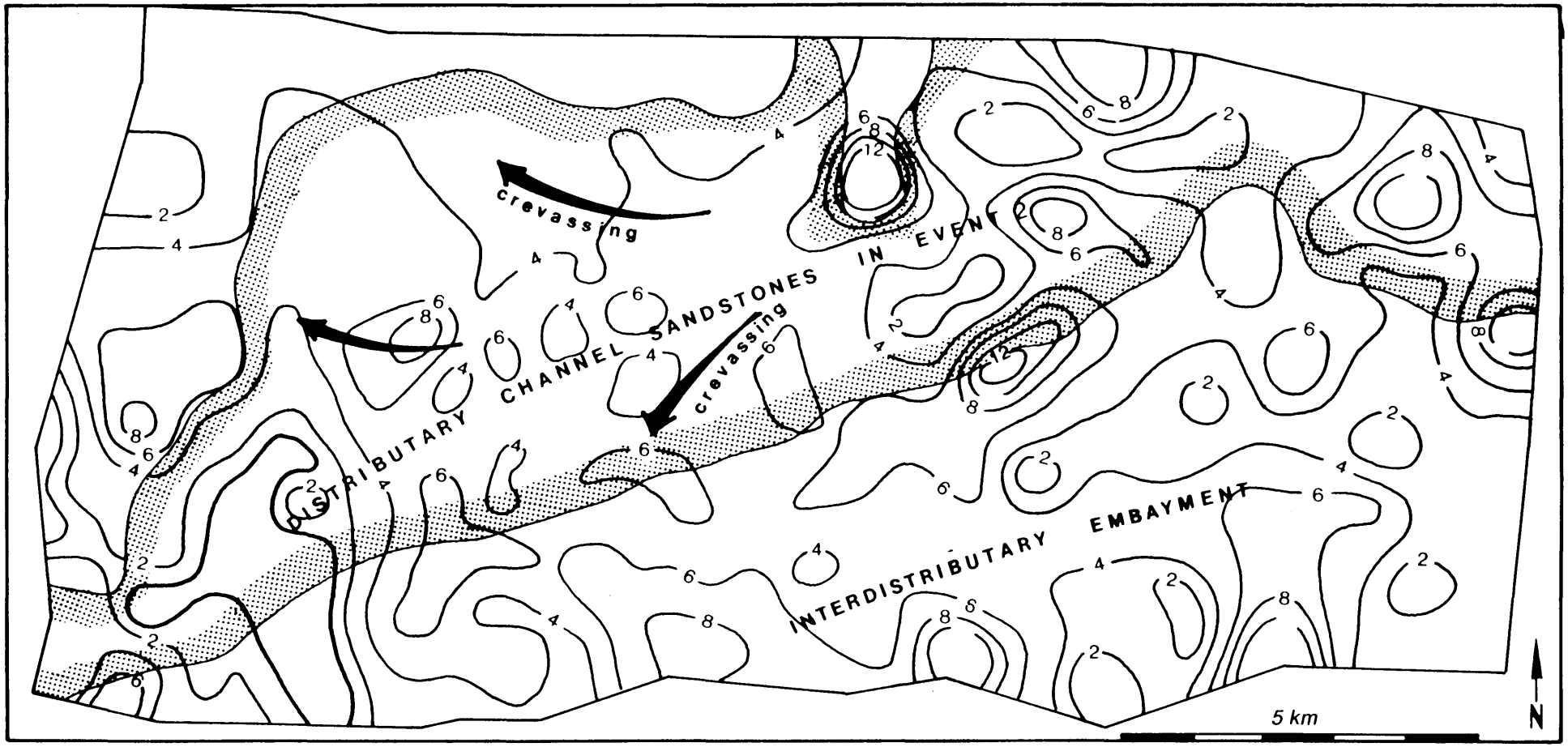
The initial stages of this event were largely contemporanous with LFA 02 channel sandstones, which were still being deposited along the fault zone (Map 3.M). In some cases the vertical transition from Event 02 to 03 was abrupt due to local channel shifting. An increase in silty and sandy interbeds towards the final stages of this third event, points to an increase in crevasse and channel activity, before the succeeding Event 04.

Siltstones and interlaminated sandstones and siltstones of LFA 03 occur to the northwest and especially to the southeast of the major channel sandstones of Event 02 (Map 3.M). They are indicators of crevasse activity adjacent to the channel zone. Further away from this channel area, shales and carbonaceous shales settled out from suspension within the interdistributary embayments. Analogous fining of sediments away from channels towards the interior of floodplains is commonly reported from recent and ancient overbank deposits (READING, 1982, p38-39; REINECK and SINGH, 1980, p298). Within the interdistributary embayments, in close proximity to the channel, water depth, water circulation and nutrient supply locally promoted plant growth and peat accumulation and preservation (Map 3.M).

4.6. Event 04

Quiet, shallow water conditions were prevalent during Event 03; inferred interdistributary bay and marsh paleoenvironments indicate that a low-lying, flat area with a gentle paleoslope had replaced the

Digitised by the Department of Library Services in support of open access to information, University of Pretoria, 2021.



LEGEND

outline of thick LFA 02 sandstones

Map 3.M Paleoenvironmental interpretation of Event 03. Thicknesses of LFA 03 (contour interval in meters) are shown superimposed over thick LFA 02 sandstone body.

Digitised by the Department of Library Services in support of open access to information, University of Pretoria, 2021.

more uneven paleotopography present after Event 01. There is no indicaton of a hiatus, or sudden subsidence of the depositional area which could have enabled another deltaic sequence to follow LFA 03. LFA 04 is, therefore, interpreted as having formed in a fluvial paleoenvironment which would be a plausible depositional setting to follow the preceding delta plain conditions (CANT, 1982, p118). Current velocity was most likely less than in the preceding events, as is supported by the generally finer sandstones and the many intercalations of siltstones and even shales within the arenites of LFA 04.

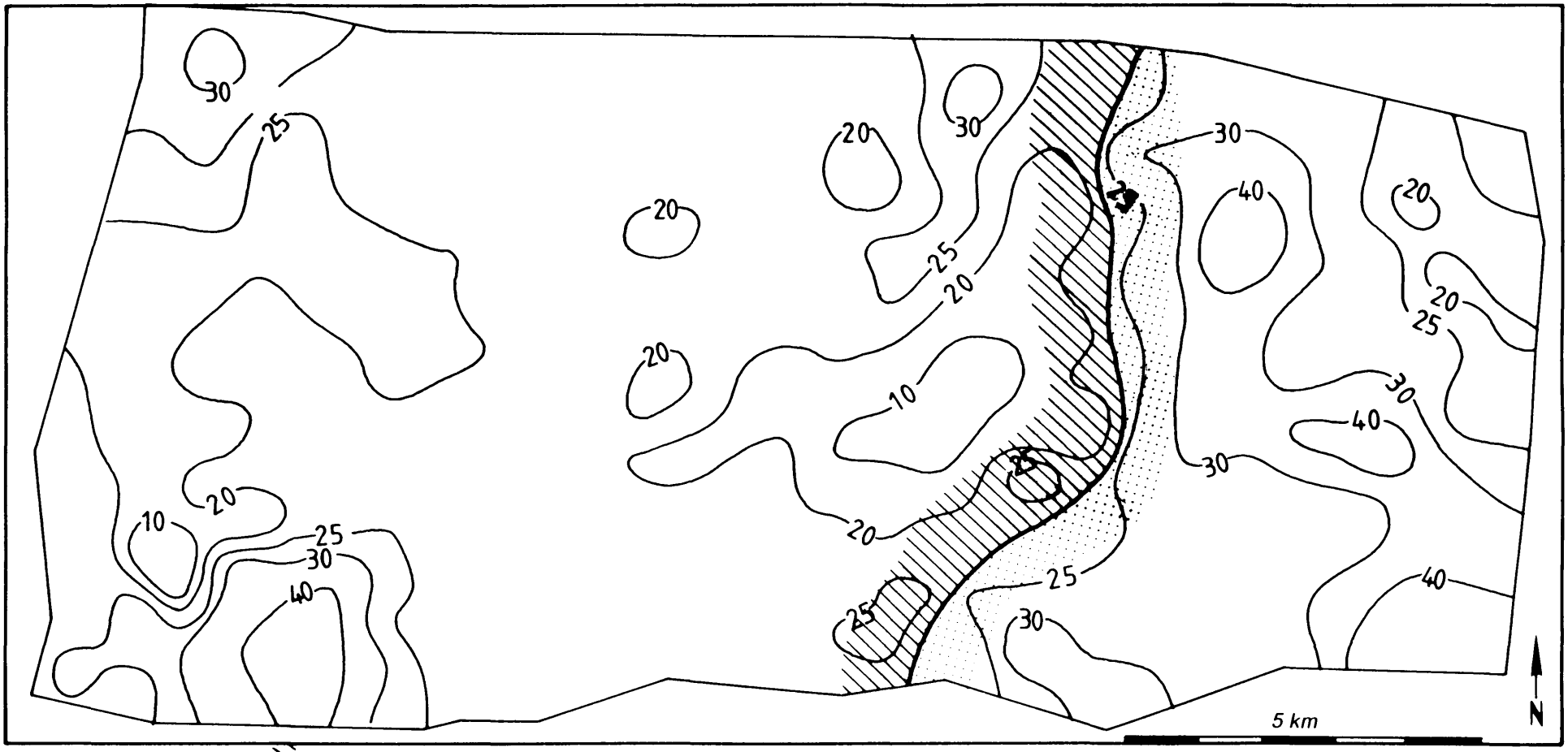
The combination of horizontal bedding and soft sediment deformation structures in the finer clastics, with cross-bedding in the coarser clastics, and bioturbation and coal seamlets, indicate a highly variable fluvial paleoenvironment, with localized lakes (READING, 1982, p53). Such a fluvial environment, where the main facies undergo rapid vertical and horizontal changes, is attributed to a meandering river system (JACKSON, 1978, p543), in which the partly cross-bedded, sandy sediment successions indicate channel and point bar deposits as well as crevasse splays. The finer siltstones and shales and their associated coal seamlets represent floodplain deposits and clay plugs from oxbow lakes and abandoned channels.

A meandering river system is a more plausible interpretation than a braided river system, as the proportion of suspended load clastics (clays and silt) is generally high (READING, 1982, p31; CANT, 1982, p119) in LFA 04. Braided river systems require a predominantly sandy succession. The lateral impersistence of the present facies further supports the existence of a meandering river belt, which normally shifts less laterally than a braided river (CANT, 1982, p119), thereby not promoting laterally extensive sedimentary bodies. The lower paleoslope, present after Event 03, would also have promoted a meandering river setting. However, internal braiding within the meanders cannot be ruled out (CAIRNCROSS, 1980).

This proposed meandering fluvial paleoenvironment generally appears to have persisted throughout the subsequent Event 05 as well. In Event 04 the overall paleoenvironment was still variable, with rapid lateral and vertical alternations of channel and crevasse deposits with floodplain and oxbow lake sediments. Towards the end of Event 04, channel and crevasse sandstone deposition became concentrated in the eastern portion of the study area. Thus, Event 04 sediments are thicker there than elsewhere in the coalfield (Map 4.1.M), as for instance over the eastern pre-Karoo paleovalley, where early channel cut-off occurred. In the western and central portions of the study area, floodplain and oxbow lake deposits of Event 05 were emplaced contemporaneously with the Event 04 channel sandstones in the east.

The present-day elevation of the paleotopography resulting after

Digitised by the Department of Library Services in support of open access to information, University of Pretoria, 2021.



LEGEND

Principal area of meandering river belt (east of line) and of floodplain deposition (west of line) at the transition from Event 04 to Event 05.

Map 4.1.M Paleoenvironmental interpretation of Event 04, based on thicknesses of LFA 04 (contour interval in meters).

Digitised by the Department of Library Services in support of open access to information, University of Pretoria, 2021.

deposition of LFA 04 shows re-occurrences of depressions above previously low-lying areas from earlier events and in the pre-Karoo paleosurface. Much of this can be attributed to differential compaction in these areas; initially they were regions where much fine-grained, highly compactible sediment accumulated, forming shales in LFA 01 and the whole of LFA 03. Furthermore, earlier channel abandonment over the eastern pre-Karoo paleovalley and continued sedimentation along the eastern margin of the study area enhanced the pre-existing topographic features.

4.6.1. Summary of Events 01 to 04

A number of different paleoenvironmental phases appear to have played a role in the development of a meandering river setting within the study area. Extensive, long-lasting floodplains within this setting later led to swamp development and the formation of major coal deposits.

* Initially, sediment type was determined by subglacial and proglacial conditions, with a high paleoslope and erratic meltwater discharge from glaciers. Sediment thickness was to a large extent controlled by an undulating paleotopography and irregularities were largely filled by glaciogene deposits. This phase (Event 01) was terminated by a glaciolacustrine setting.

* The next phase (Event 02) was characterized by a gently undulating paleotopography and by fluviodeltaic deposition, with basinal reworking processes along a lacustrine basin margin. This resulted in extensive sheet-like deposits which left behind an even paleotopographic surface with a low paleoslope, thus allowing the establishment of interdistributary bays and swamps on upper delta plains (Event 03).

* Event 04 was dominated by low energy meandering river systems and a gentle paleoslope; little water movement, restriction of the main channels to active channel belts and extensive floodplains in interdistributary areas produced favourable conditions for wide-spread, uniform peat growth and preservation during the succeeding Event 05, which formed the main coal zone.

* The fault zone in the western half of the study area is believed to have been active during Events 02 to 04. This is inferred from the isopach map of LFA 02 (Map 2) and from the cumulative isopach map of LFA's 02 to 04 (Map 4.2). Both maps show trends of contour lines parallel to the fault zone and thick sediment packages to

Digitised by the Department of Library Services in support of open access to information, University of Pretoria, 2021.

the southeast of it. This indicates that the western fault of the graben structure was active during this early sedimentation, and it probably led to a south-westerly oriented paleodrainage system. Since this trend can mainly be traced on the map for LFA 02, it is assumed that the fault zone was more active during this period and only sporadically so during later events.

4.7. Event 05: The Main Coal Zone

In section 4.6 it was pointed out that Events 04 and 05 were partially contemporaneous in the study area (Fig. 4.1), at least until the peat of seam No. 4L began to occupy the entire coalfield. Event 05 principally appears to have comprised a meandering river paleoenvironment. Internally these meanders were partially braided, as the roof rocks of seam No. 4L show. During Event 04 meander belts were present throughout the area at different times during the event; the main channel activity ceased in the western and central portions of the coalfield, especially over the fault zone, towards the end of that event. During Event 05 floodplain and backswamp conditions prevailed at certain times, and at other periods the paleoenvironment was characterized by channel influences.

JACKSON (1978, p543) points out that meandering river systems exhibit a wide range of lithological variety, both vertically and laterally. These lithologies include channel, point-bar and natural levee deposits, as well as clay plugs, floodplain and backswamp sediments. He further emphasizes, by means of recent examples, that meandering river deposits are not necessarily characterized by an upward-fining sequence only. FLORES (1983) gives a similar, detailed study of the complexity of the lithofacies associations of coal-rich Tertiary meandering fluvial deposits in the Northern Powder Basin, northwestern United States.

4.7.1. The No. 3 Coal Seam

This assemblage of shales, siltstones and coal points to a floodplain and backswamp paleoenvironment during the initial stages of Event 05. This is well illustrated in the western and especially the central portions of the study area, where shaly and silty floor rocks and subsequent thick peat of the No. 3 coal seam were formed. It is thought that the proposed backswamp paleoenvironment had few channel influences and therefore little influx of clastic material that could have formed in-seam lenses. A predominance of mixed coal lithotypes

Digitised by the Department of Library Services in support of open access to information, University of Pretoria, 2021.



LEGEND

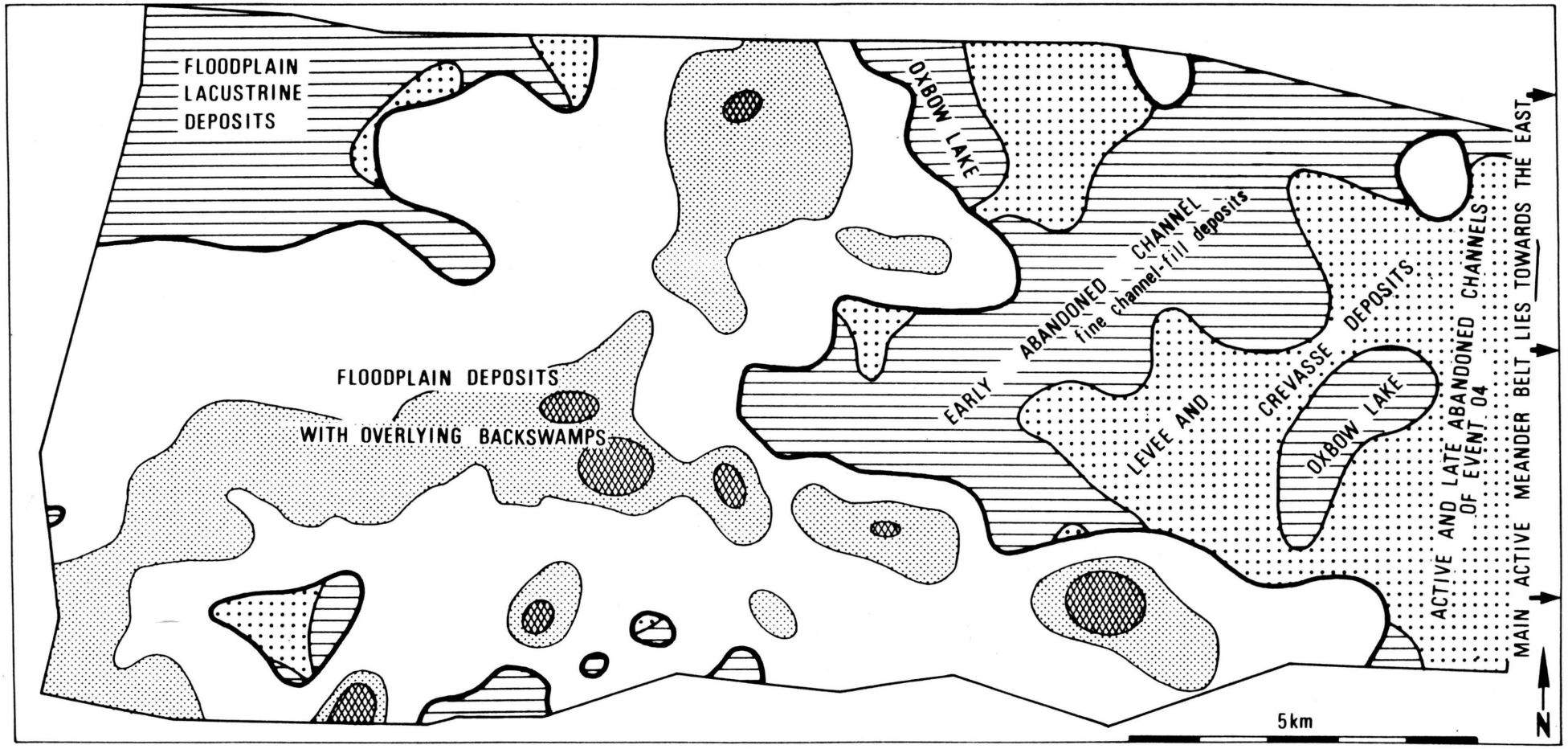
Principal area of oxbow-lake deposition.

Principal area of early floodplain deposition in ponds and lakes.

Sandstones of previous Event 04.

Map 5.2.M Paleoenvironmental interpretation of shales and siltstones in the floor of the No. 3 coal seam (contour interval of the shale and siltstone thicknesses given in meters).

Digitised by the Department of Library Services in support of open access to information, University of Pretoria, 2021.



LEGEND

thick sandstones of LFA 04, not covered by No 3 seam, and associated shales

shales before and contemporaneous with No 3 coal seam

coal (< 50 cm)

coal (50 - 80 cm)

coal (> 80 cm)

Map 5.3.M Paleoenvironmental interpretation of the coal of the No. 3 seam.

Digitised by the Department of Library Services in support of open access to information, University of Pretoria, 2021.

indicates relatively inferior peat preservation conditions, due to contact with oxygen-rich waters (STACH et al., 1982, p34). Pyrite and siderite are typically associated with coal deposits, due to the generally reducing conditions that their formation requires. Siderite, particularly, indicates a predominance of freshwater influx into the swamp (STACH et al., 1982, p164&193).

The northwestern part of the study area was initially characterized by deeper water lacustrine floodplain deposits. These were subsequently overgrown by a peat swamp that extended northwestwards across the fault zone.

In the eastern portion of the coalfield, meander belts were still active and deposited lithologies belonging to LFA 04, contemporaneous with LFA 05. However, subsequently this belt gradually moved eastwards, leaving abandoned channels and oxbow lakes behind. One such feature is marked by the thick shale and siltstone deposit laid down above the eastern pre-Karoo paleovalley (Map 5.2.M). These fine-grained channel-fills (clay plugs) were deposited before and contemporaneously with the peat of seam No. 3. At the same time the meander belt was still active along the eastern margin of the study area (Map 5.3.M); this is reflected in sandy interbeds and soft sediment deformation structures within the basal shales of LFA 05, due to deposition during overbank flood stages and crevasse events.

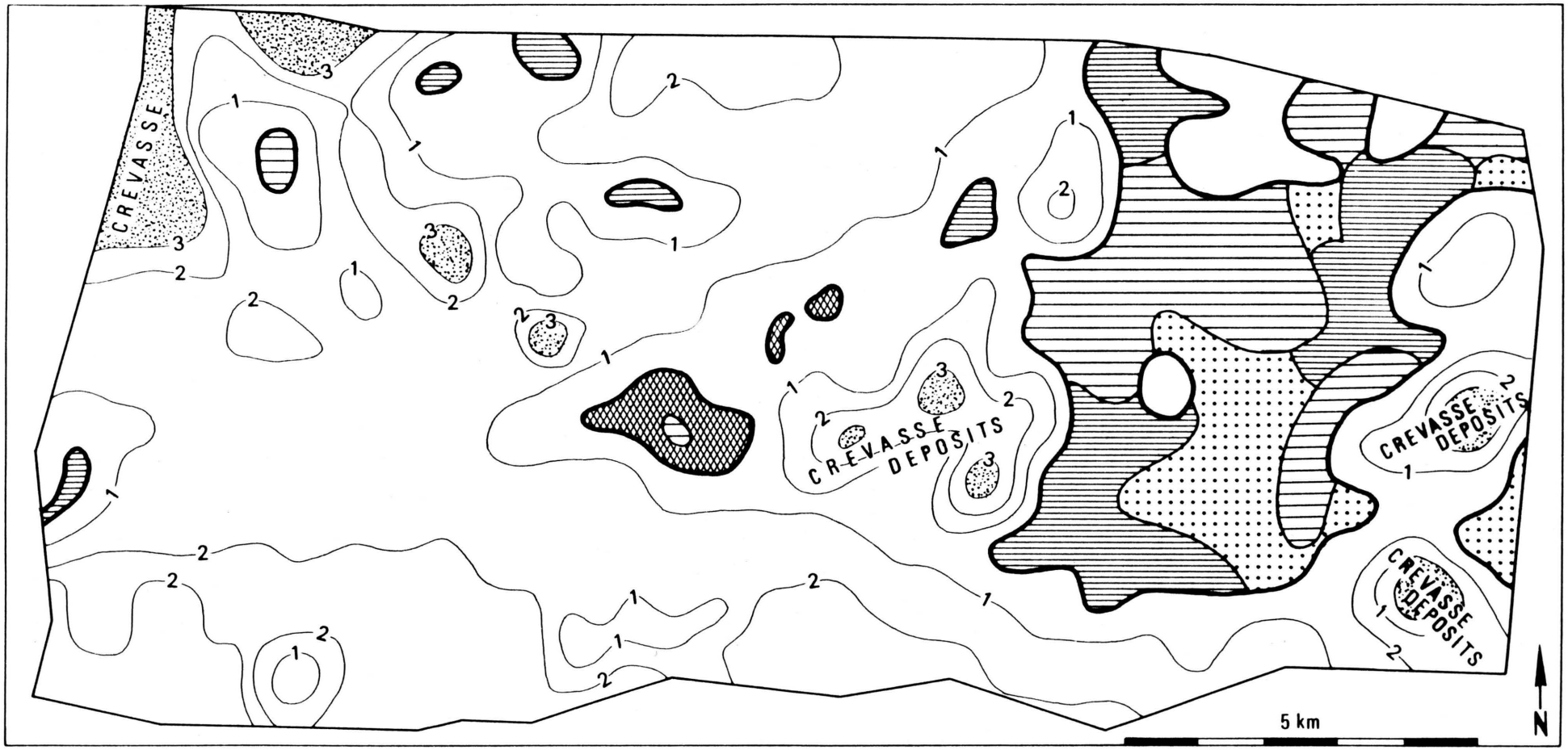
Local occurrences of shales and siltstones that abut and overlap the No. 3 coal seam indicate a gradual rise in the regional water level. In the northwest of the study area this can be attributed to localized reactivation of the fault zone; hence, deeper water terminated peat preservation. However, the main reasons appear to be an increase in channel activity, which subsequently produced the sandstone above the seam,

The rapid pinching out of seam No. 3 towards the east indicates the proximity of another persistent deep, open water body, which could have formed adjacent to the eastward migrating meander belt . It provided good plant growth and preservation conditions along its margin, but restricted plant growth towards the east of this.

4.7.2. Parting between No. 3 and No. 4L Coal Seams

Coal seam No. 3 is covered by a sandstone, separating it from seam No. 4L. In an overall fluvial paleoenvironment, such a widespread, fine-grained, cross-bedded sandstone parting covering backswamp and floodplain deposits, is usually the result of a major phase of crevassing, a common occurrence within meandering river systems. Trough cross-beds develop in these sandstones as a result of small scale channel systems on top of the crevasse deposits (COLEMAN, 1969; READING, 1982, p39&105) and horizontal lamination most likely

Digitised by the Department of Library Services in support of open access to information, University of Pretoria, 2021.



LEGEND

- thick parting > 3m
- shales before and contemporaneous with No. 3 seam
- outline of parting sandstones
- sandstones of LFA 04 not covered by parting
- shales overlapping No. 3 seam and LFA 04
- coal of No. 3 seam

Map 5.5.M Paleoenvironmental interpretation of the sandstone parting (contour interval in meters) between No. 3 and No. 4L coal seams. This map indicates the spatial coexistence of the last Event 04 sediments and the early sediments of Event 05. It thus gives the lateral distribution of all lithological units forming the immediate floor of coal seam No. 4L

Digitised by the Department of Library Services in support of open access to information, University of Pretoria, 2021.

results from overbank deposition. The abundance of mica within the sandstones suggests that basinal winnowing processes did not affect the deposits. Pyrite and siderite again give evidence of locally reducing conditions.

Crevasse sandstones were deposited from meander channel systems to the east and possibly also the west of the study area and filled up depressions in the floodplain with relatively thick deposits (Map 5.5.M), such as into the presumed oxbow lake over the eastern pre-Karoo paleovalley. Thick crevasse sandstone partings also occur along the southern margin of the coalfield where the underlying seam remained relatively thin (Map 5.5.M and figure 4.2).

4.7.3. The No. 4L Coal Seam

This paleoenvironment comprised long-lasting, fairly stable backswamp conditions over the entire study area, as indicated by a generally thick coal seam and by laterally persistent lithotype bands within the seam (STACH et al., 1982, p376), particularly the vitrain bands. Siderite and pyrite are commonly associated with coal, as found in previous events; in particular, laterally persistent siderite marker horizons within the seam give proof of very stable freshwater-dominated periods during this part of Event 05 (STACH et al., 1982, p164). In-seam clastic lenses include cross-bedded sandstones, deposited as crevasse splays, and silty and shaly sediments, which settled out from suspension into swamp lakes and ponds, these are all common features associated with nearby channel activity in a backswamp setting. Both processes are the result of over-bank sedimentation (READING, 1982, p38), which occurs at flood peak when current velocities are high and the concentration of suspended material is low. Therefore, individual clastic lenses are thin and not very extensive. The sporadic occurrence of torbanite and torbanitic shale in the seam is a further indication of the existence of open water bodies within the swamp (STACH et al., 1982, p264).

The development of the No. 4L coal seam throughout the eastern half of the study area can be divided into three phases, indicated by the macropetrographic seam profiles and particularly by the in-seam clastics. In the western half, the swamp appears to have had more uniform conditions throughout the period of peat growth.

* The first phase is marked by the presence of a meander belt in the eastern reaches of the study area. Channel, levee and crevasse deposits from LFA 04 directly underly the seam and are regarded to be contemporaneous with the early coal deposits from other parts of the study area (Fig. 4.1). Clastic lenses occur within the basal portion of the coal seam over and just to the

Digitised by the Department of Library Services in support of open access to information, University of Pretoria, 2021.

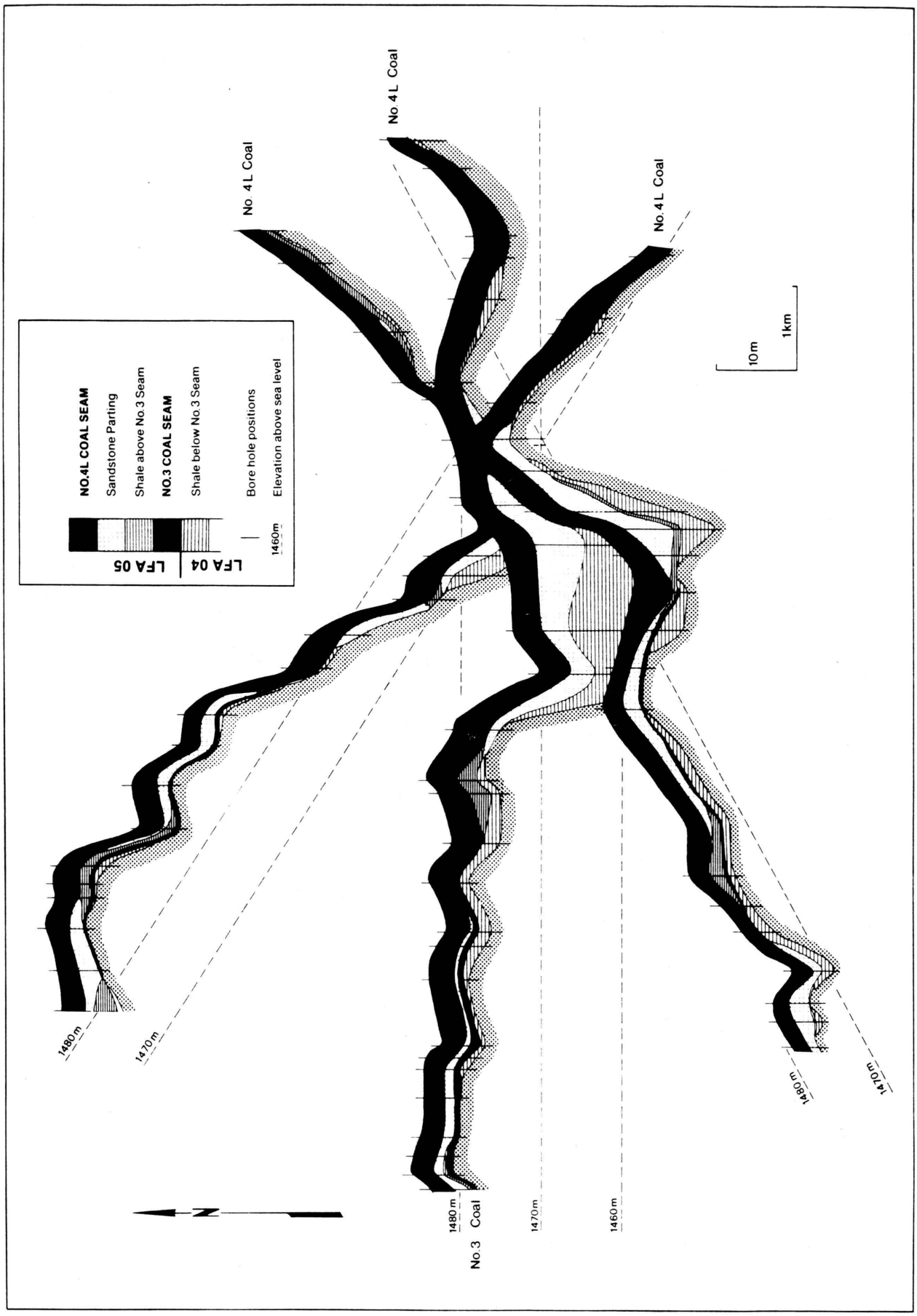


Fig. 4.2 Three fence diagrams through the eastern pre-Karoo paleovalley (see figure 2.1 for position of profiles).

Digitised by the Department of Library Services in support of open access to information, University of Pretoria, 2021.

west of these LFA 04 sediments. At this stage peat growth in the eastern half of the study area was probably sporadic and may not yet have begun in many parts.

* The second phase is almost uniformly developed over the entire coalfield. Clastic lenses are less common and the seam profiles show a higher vitrain content and relatively abundant clarain bands; both point to constant flooding under comparatively shallow water conditions (STACH et al., 1982, p376). This in turn indicates that the channel had moved farther towards the east, leaving widespread quiet water conditions, favourable for peat growth and preservation throughout most of the study area.

* The third phase very much resembles the first one. A repetition of abundant in-seam clastic lenses and a predominance of durain over clarain in the upper parts of the seam profiles indicate an increase in channel activity and a related rise in water level. This most likely reflects a shifting of the meander belt back towards the west, which is accompanied by an early termination of peat growth in the eastern half as compared to the western half of the study area. In this context the in-seam partings are seen as early precursors of the following parting between coal seams No. 4L and No. 4U.

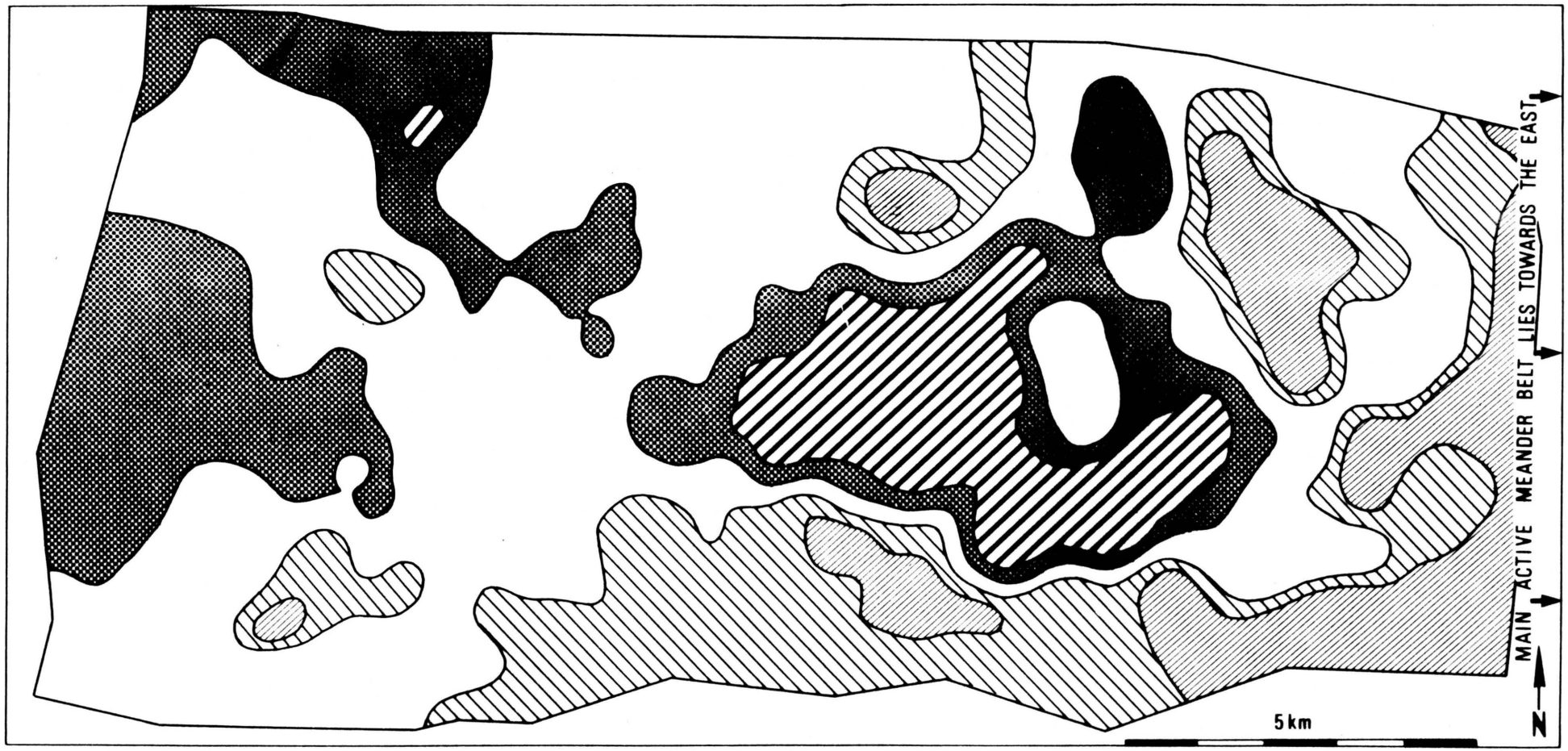
In the western and central portions of the Twistdraai region the seam thickness is fairly constant, due to little or no channel influence. Along the eastern margin of the study area, however, the seam is relatively thin, due to late commencement and early termination of peat growth, which in turn are both due to channel shifting (Map 5.6.M). An extremely thick development of coal, as found above the eastern pre-Karoo paleovalley, was probably due to the proximity of a channel which, due to frequent crevassing and flooding, provided ample nutrient supply to improve plant growth (STACH et al., 1982, p31).

The possibility that coal seams No. 3 and No. 4L merge along the eastern margin of seam No. 3 is unlikely, although the eastern margin of seam No. 3 and the 4m isopach of seam No. 4L match readily (Maps 5.3 and 5.6). The main reason is that the crevasse sandstone parting between seams No. 3 and No. 4L can be widely traced below seam No. 4L, into areas where seam No. 3 is not present underneath.

4.7.4. Parting between No. 4L and No. 4U Coal Seams

This assemblage of gritstones, sandstones, siltstones and shales, with structures including soft sediment deformation, horizontal

Digitised by the Department of Library Services in support of open access to information, University of Pretoria, 2021.



LEGEND

coal thicknesses

< 250 cm

250 - 275 cm

275 - 325 cm

325 - 350 cm

> 350 cm

Map 5.6.M Paleoenvironmental interpretation of the No. 4L coal seam.

Digitised by the Department of Library Services in support of open access to information, University of Pretoria, 2021.

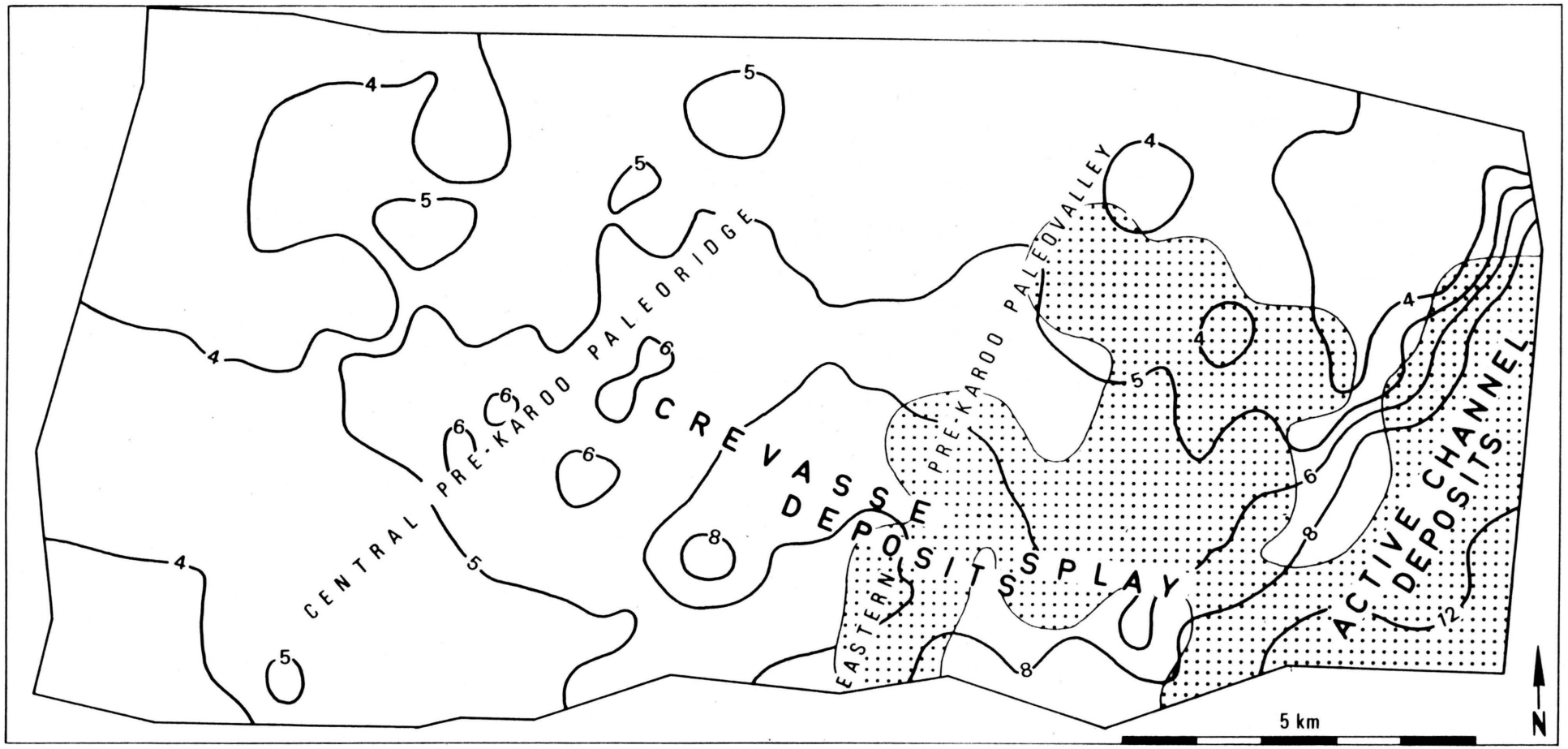
stratification and planar cross-bedding, has already been recognized in earlier depositional phases, especially LFA 04 and the lower portions of LFA 05. The random facies relationships reflect a complex interfingering of channel and rapid crevasse deposition with steady floodplain sedimentation during this phase of Event 05. However, the cross-bedded coarse sandstones and gritstones that account for major parts of this sedimentary package reflect deposition by stronger channel currents than in previous events. The upward fining of these sediments into the silty and shaly parts of the floor rocks of seam No. 4U is regarded as the result of gradual cessation of channel activity and the re-occupation of the study area by quiescent floodplain conditions.

These sandstone deposits reach maximum thicknesses along the eastern margin of the study area, with concomittant high contents of gritty material. This channel reactivation not only caused early termination of the preceding swamp phase (coal seam No. 4L), specifically along the eastern margin of the study area (Map 5.9.M), but probably also resulted in considerable erosion of the underlying peat of No. 4L seam.

Erosional activity is a common feature of high flood stages over a floodplain (READING, 1982, p38), due to lower sediment loads and higher water velocities. In the present study it is also regarded as a cause for a diminished seam thickness along the fault zone, where coarse sandstones and grits form the roof rocks of seam No. 4L (Map 5.10). Underground mapping of elongated sandstone bodies in the roof of the No. 4L seam near the southwestern end of the fault zone reveals a braided channel system with a north-south flow direction. As this evidence of braiding seems to be restricted to this portion of the mine, it is thought to have been a relatively short-lived localized episode, which did not greatly affect the meandering river model proposed. Braiding is generally favoured by a high discharge fluctuation and a coarse sediment load (WALKER and CANT, 1984, p79).

The coarse and gritty material in these parting sandstones points to channel erosion and rapid, high energy fluvial sedimentation above the coal seam, possibly related to channel switching. The braiding observed in the southwest of the study area may reflect temporary re-activation of the fault zone which increased the local gradient. Internal braiding within a generally meandering system can be proposed, because most of the braided channels have an asymmetrical cross section, which is typical for high sinuousity channels (READING, 1982, p33). Crevasse sandstones were also widely deposited over the underlying floodplain shales and siltstones. A major channel appears to have been present along the southeastern margin of the coalfield, which caused thick and extensive parting sandstone deposits here (Map 5.9.M).

Digitised by the Department of Library Services in support of open access to information, University of Pretoria, 2021.



LEGEND

areas of particularly gritty parting

Map 5.9.M Paleoenvironmental interpretation of the parting between No. 4L and No. 4U coal seams (contour interval in meters).

Digitised by the Department of Library Services in support of open access to information, University of Pretoria, 2021.

4.7.5. The No. 4U Coal Seam

This final period of Event 05 was characterized by floodplain and backswamp conditions in most parts of the study area, as indicated by wide-spread siltstones, shales and coals. The predominance of mixed coal lithotypes suggests a peat swamp with relatively deep water conditions, similar to coal seam No. 3; depths may have increased towards the channel system in the east, where, in places, shales and siltstones caused seam splitting and partly replaced the coal.

In the southern and central parts of the study area, where shales and siltstones form the floor rocks of seam No. 4U, floodplain deposition started early, contemporaneously with parting sandstone deposits in the east. Thickly developed shales and siltstones in the floor rocks (Map 5.11) probably outline oxbow lakes of a meandering river system, preceding the peat growth. The conditions for peat growth and preservation were most favourable in the southern and central portion of the study area where the thickest coal deposits are found (Map 5.12). This is attributed to early commencement of floodplain conditions in interchannel areas and subsequent peat growth alongside the oxbow lakes. Furthermore, thick coal is formed, as in seam No. 4L, over and in proximity to crevasse deposits and abandoned channels, where influx of nutrients supported peat growth.

Channel, levee and crevasse deposition, represented by thick, coarse to gritty as well as fine lithologies in the underlying parting, still prevailed in the east and along the fault zone. This new floodplain and backswamp paleoenvironment is related to another retreat of the active channel belt towards the east.

4.7.6. Summary of Event 05: The Main Coal Zone

The sedimentation of Event 05 was controlled by a meandering river channel belt and adjacent floodplain and backswamp setting. The dominant meander belt was situated along and east of the eastern margin of the coalfield, with, probably, a less prominent one towards the west of the study area. As a result of channel shifting, the floodplains and backswamps occupy either parts of the study area (No. 3 coal seam) or the entire area (No. 4L and No. 4U coal seams). Throughout the event the eastern part of the coalfield remained under the influence of the nearby channel, as is indicated by:

* a thick development of channel, levee and crevasse sediments belonging to LFA 04 in the east, contemporaneous in their upper parts with No. 3 coal seam;

* a total absence of backswamp conditions during the development of

Digitised by the Department of Library Services in support of open access to information, University of Pretoria, 2021.

seam No. 3 peat and, instead, thick, fine-grained channel-fill deposits in oxbow lakes within the eastern portion of the coalfield;

* abundant in-seam partings in No. 4L and No. 4U coal seams in this region, as a result of frequent crevassing and overbank deposition;

* thick and relatively coarse-grained parting sediments between seams No. 4L and No. 4U, which indicate a shift of the eastern channel belt back towards the west, accompanied by subsequent levee and crevasse deposition.

4.8. Event 06

The facies association of the basal portion of LFA 06, comprising partly micaceous sandstones containing pyrite and siderite and an interlaminated silty and shaly facies, compares well with LFA 04. Therefore, it is assumed that after Event 05 the study area was still characterized by a meandering river system, with the distinction that fluvial channel processes now became dominant over floodplain influences. This is supported by the widespread vertical and horizontal alternation of sandy and silty facies, as also found in previous events. The sedimentary structures in this part of LFA 06 support a similar model to that suggested for LFA 04. However, flaser-bedding and ripples in LFA 06 point to localized lacustrine conditions; short-lived currents flowing up the regional paleoslope, perhaps driven by wind, may have formed these structures (READING, 1982, p74; REINICK and SINGH, 1980, p112).

It is assumed that the pre-existing coal swamp gradually drowned and was succeeded by extensive lacustrine conditions, with some marginal swamp development which provided the coaly debris found in these sediments. Fluvial inwashes were initially uncommon, as shown by minor gritty sandstones in the immediate roof rocks of seam No. 4U, but increased later. COLEMAN and PRIOR (1982) refer to comparable examples of lacustrine environments that became increasingly dominated by subsequent fluvial processes.

The initial one or two upward-coarsening sequences in the basal portion of the LFA 06 succession probably reflect local crevasse deltas (FLORES, 1983), which rapidly filled inter-channel ponds and lakes. Crevasse deltas are proposed, in contrast to a major deltaic phase, as there is no evidence of a hiatus in deposition or a major increase in subsidence that could have allowed such major changes in

Digitised by the Department of Library Services in support of open access to information, University of Pretoria, 2021.

depositional conditions. Furthermore, the laterally restricted nature of these sandstones, and the fact that they commonly pass laterally into floodplain deposits (siltstone, shale and coaly fragments), implies crevasse deposition (COLEMAN, 1969; READING, 1982, p38). The succeeding upward-fining cycles in the basal portion of LFA 06 were probably formed by fluvial channel and abandoned channel sedimentation.

With higher discharge through the channels, sediments became coarser and more sandy in the upper portion of LFA 06; however, they are poorly sorted and contain more interstitial fine material than, for instance, the sandstones of LFA 02. This indicates a fluvial paleoenvironment with irregular dicharges (REINECK and SINGH, 1980, p311), rather than a deltaic setting with basinal reworking, as presumed for Event 02. Thin horizontal bedding and planar cross-bedding can be ascribed to upper flow regime plane bed deposition and bar migration, respectively (REINECK and SINGH, 1980, p122&109), both commonly found in fluvial settings. The previously assumed meandering river system was most probably succeeded by a braided river system in the later part of Event 06, which deposited a more evenly distributed sediment package. Braiding already appears to have played a role in the later stages of Event 02 and was also observed, on a small scale, in the roof of No. 4L seam. Subordinate braided tendencies may well have been present throughout many of the preceding fluvial paleoenvironments. The braided channels in Event 06 were sand-dominated, in the sense of RUST (1978, p608); the finer fractions presumably accumulated elsewhere, as separate, minor fine-grained deposits. In the present study these fine-grained sediments are represented by localized siltstone bands. COLEMAN (1969, p142-143) gives a recent analogue of a change from a meandering system to a braided river setting, due to a higher discharge and sediment load.

During the late stages of Event 06, braided channel activity lessened in the centre of the study area, allowing the establishment of local swampy interchannel conditions, indicated by the presence of shaly layers with coal seamlets (Map 6.2). They can be seen as precursors of the coal swamp which formed coal seam No. 5, but were covered by arenaceous sediments of another short series of crevasse splays and channel switching.

The distribution of LFA 06 sediments is generally dependent on sedimentation patterns within previous deposits. The relatively thick LFA 06 package generally tended to level previous paleotopographic features. This resulted in thin deposits along the eastern margin, covering thick crevasse and levee deposits of Event 05. On the other hand, LFA 06 is thick over the eastern pre-Karoo paleovalley where, due to thick shales and coals underneath, the sedimentary column had a higher compactibility than in other areas. Major channels appear to have existed where LFA 06 deposits are thick, particularly above the

Digitised by the Department of Library Services in support of open access to information, University of Pretoria, 2021.

eastern pre-Karoo paleovalley (Map 6.1). Floodplain and backswamp conditions, adjacent to these, formed the sporadic silt, mud and peat layers in the top of LFA 06.

4.9. Event 07

Coal seam No. 5 is commonly underlain by LFA 06 sandstones, with localized shales and siltstones. The paleoenvironmental change from Event 06 therefore seems to have been rapid. Channel switching and subsequent abandonment of the study area is the most probable explanation for this rapid change.

A backswamp paleoenvironment appears to have prevailed throughout the study area during Event 07; as the coal distribution is relatively even, comparable conditions are assumed to have started contemporaneously over the entire coalfield. In the beginning, overbank sedimentation still took place as indicated by localized in-seam lenses in the base of the seam. Later, relatively deeper water conditions dominated with influx of organic debris, to allow mixed coal lithotypes to develop. Water depth slowly increased throughout the area towards the onset of Event 08, as shown by a gradual transition into torbanitic and eventually carbonaceous shales, that were presumably deposited in extensive lakes and ponds (STACH et al., 1982, p264).

The eastern margin of the study area, however, remained under the influence of a channel (Map 7), as indicated by an increased occurrence of in-seam partings, similar to those in seam No. 4U. It is also believed that the fault zone was active during this event, resulting in a higher subsidence rate there, with another concentration of in-seam partings in this region.

4.10. Event 08

This lithofacies association appears to be a repetition of previous ones, such as LFA 06. The distribution of individual facies indicates an intercalation of channel and floodplain deposition within an overall fluvial paleoenvironment, as assumed for Events 04 to 06. The pre-existing lacustrine setting of Event 07 was thus covered by fluviolacustrine sediments of LFA 08, under conditions similar to those prevalent at the begining of Event 06. The fluvial activity appears to have become important only during the later stages of Event

Digitised by the Department of Library Services in support of open access to information, University of Pretoria, 2021.

08, as fine-grained floodplain and lacustrine deposits are relatively thick in the lower portions of LFA 08. The alternation of sand-dominated and silt-dominated horizons in the upper part of LFA 08 indicates an irregular movement of active channel belts with frequent abandonment of the channel loops, as occurred in the meander belts in Events 04 and 06.

4.11. Discussion of Possible Marine Influence in the Paleoenvironment

South African coalfields are believed to have been inundated by marine transgressions at certain horizons of the sedimentary column (CADLE, 1979; CAIRNCROSS, 1980; LE BLANC SMITH, 1980). The common occurrence of macroscopically-identified glauconite grains in these horizons is regarded as support for this postulate.

However, unlike other coalfields in the world, which in fact experienced marine transgressions, the South African coalfields and their coals lack any further indication of marine influences. These confirmatory factors should include:

* Marine fossil fauna within the coal seams and associated rocks (STACH et al., 1982);

* "Coal balls", which are mainly dolomitic carbonate concretions, and which are found to occur throughout the Katharina seam in Germany (TEICHMULLER, 1955) and in Pennsylvanian coals in the USA (MAMAY and YOCHELSON, 1962);

* The sulphur content of marine-influenced coals is generally higher than that of fresh water coals (CASAGRANDE et al., 1977). Values for the Lower Kittanning seam in Pennsylvania exceed 3% where the coal is overlain by marine strata and are less than 2% where they are overlain by fresh water sedimentary rocks (WILLIAMS and KEITH, 1963). South African coals typically contain less than 2% sulphur (NICR, 1985). See also the ultimate sulphur results in section 6.5.

In the following sections the results of the clay mineralogy, the glauconite investigation and the paleo-pH tests will be discussed in order to establish the possibility of marine transgression in the Twistdraai Coalfield sequence.

Digitised by the Department of Library Services in support of open access to information, University of Pretoria, 2021.

4.11.1. Clay Minerals and Carbonates

Clay minerals deposited as alluvium are inherited and tend to reflect the composition of the source rocks rather than the environment of deposition (MILLOT, 1970, p139). Thus, quite a variety of clay mineral assemblages can result from fluvial sedimentation. Another important factor influencing the clay mineral composition of ancient rocks is the neoformation of these minerals during sedimentation and diagenesis. The term "neoformation" refers to an accumulation of clay minerals by precipitation from solutions, either in surface waters or in pore waters (MILLOT, 1970, p323; GRIM, 1968, p562). Kaolinite develops under continental neoformation from soils and other weathering products. It cannot develop in sedimentary basins. During early diagenesis kaolinite formation is favoured by percolating acid waters in porous rocks. Illite and chlorite, however, are in most cases inherited and no certain neoformation of these minerals is known during sedimentation. During diagenesis, they may form from mica or even from kaolinite (MILLOT, 1970, p325).

GRIFFIN and INGRAM (1955) find a marked change in the kaolinite-illite-chlorite components of sediments deposited in the Neuse River estuary as the environment changes from freshwater to saline. Kaolinite is by far the dominant clay mineral introduced into the estuary by the river. With increasing salinity this component decreases due to an increasing illite and especially chlorite component. Similar adjustments to marine environments are also reported by POWERS (1957). An estuary environment, however, is problematical, as marine sediments might be transferred into the freshwater-dominated part of it by tidal and other marine currents (MILLOT, 1970, p141). This is, however, not the case in the Neuse River estuary, as there are no tidal influences and hardly any wind-driven counter-movements to the down stream fluvial current. It thus serves as an undisturbed example of freshwater transgressing into a saline setting (GRIFFIN and INGRAM, 1955).

Dickite, the second-most common mineral of the kaolinite group, is often regarded as a hydrothermal product (MILLOT, 1970, p3; WEAVER and POLLARD, 1973, p145). It is also believed to form as a secondary product, from recrystallization of aluminous muds weathered from microcline (SMITHSON and BROWN, 1954). Microcline is believed to be a constituent of the source rocks for the Twistdraai Coalfield (RYAN, 1968), and can also be recognized in some arkoses of the present sedimentary sequence. As the dickite occurrences in the present boreholes appear to be unrelated to the dolerite intrusives (Fig. 3.12), but are concentrated in coarse sandstones and close to the coal seams, they are regarded to have formed through secondary processes.

Summarizing the literature, it becomes apparent that illite and chlorite are typical marine clay minerals and that this environment is

Digitised by the Department of Library Services in support of open access to information, University of Pretoria, 2021.

fundamentally unfavourable for kaolinite (GRIM, 1968). Major occurrences of marine kaolinite are attributed to source rock composition and probable rapid sedimentation that led to its preservation. Any continental environment, whether lacustrine, fluvial or glacial, preserves clay mineral associations that reflect the source rock composition (GRIM, 1968; MILLOT, 1970).

Carbonates in sediments are not reliable paleoenvironmental indicators. Calcite and dolomite, where they only appear as interstitial material in clastic rocks, are mainly the product of diagenesis, where they precipitate from circulating pore solutions (BROWNLOW, 1979, p327-331). Certain elements may concentrate into segregations, such as layers, concretions or nodules, to form siderite and pyrite (BERNER, 1969; in BROWNLOW, 1979). Siderite, especially, is normally taken as a freshwater indicator in coal-forming environments. Its occurrence within and close to coal seams is possibly caused by relatively high pH-values, the influx of iron-bearing bicarbonate solutions [$(Fe(HCO_3)_2$] and rapid precipitation under reducing conditions (STACH et al., 1982, p193&293).

The results of the present study show a dominance of kaolinite in both borehole sequences. This, in a proposed fluvial setting, can be attributed to the freshwater environment and the composition of the parent material of these sediments. High peaks of kaolinite in portions of the sedimentary sequence close to the coal seams are partly due to the possible occurrence of dickite, which has also been observed together with kaolinite in Carboniferous sandstones in North Wales (SMITHSON and BROWN, 1954). However, a diagenetically controlled accumulation of kaolinite-group minerals might have occurred, while, due to compaction, acidic water was pressed out of the coal seams into the porous sediments in the floor and roof rocks. Humic acids could have caused a leaching of clay minerals, especially montmorillonite, thereby enriching kaolinite, as also reported from the Snuggedy Swamp, South Carolina (STAUB and COHEN, 1978).

The glacially-influenced portion of LFA 01 and LFA 02 shows a high variability in kaolinite content. The major but irregular occurrence of illite in parts of LFA 02, together with an absence of siderite in the same horizons, suggests a possible brackish to marine influence in the paleoenvironment. This would coincide with Event 02 being the only phase in the proposed depositional model to have developed under control of major basinal processes. On the other hand, in a still glacially-controlled environment, as is also presumed for Event 02, illite could generally be the dominant weathering product of either igneous or sedimentary source rocks. This would correspond with glacial deposits from Scandinavia and northern Canada, where illite dominates the clay mineral fraction (MILLOT, 1970, p136-137). This proposal is more consistent with the present model, as it also compares well with the recent example of Lake Michigan, USA, where the

Digitised by the Department of Library Services in support of open access to information, University of Pretoria, 2021.

predominance of illite in the lake deposits is a reflection of the clay mineral composition of the surrounding glacial tills (GRIM, 1968, p544).

The good correlation of some XRD clay mineral determinations in certain portions of the two borehole sequences investigated also aids the formulation of the paleoenvironment. Here, attention should be brought to the top 20m of LFA 02 in borehole B and to LFA 03 in borhole C (Figs. 3.11 and 3.12). Their correlation supports the previously proposed depositional setting during Events 02 and 03 in the study area (sections 4.4. and 4.5.). Event 02 is assumed to have lasted longer, thus developing thicker distributary channel deposits in the western portion of the study area, where borehole B lies. Contemporaneously, Event 03 had already formed an interdistributary floodplain environment in the central and eastern parts of the study area, where borehole C is situated (Figs. 2.1, 3.11 and 3.12). The corresponding XRD analyses support the contention that these two portions of the depositional sequence at the Twistdraai Mine were partly contemporaneous, with similar chemical depositional characteristics, but developing lateral facies variations.

4.11.2 Glauconite

Glauconite is generally regarded as a product of marine sedimentation and diagenesis, but its formation is still uncertain (BURST, 1958a and b; TYLER and BAILEY, 1961; McRAE, 1972). It is further assumed that it forms under various environmental conditions, thus occurring in a variety of chemical compositions and crystal structures, with no sharp boundaries between illites, glauconitic illites and glauconites (PORRENGA, 1968). Others also propose a non-marine origin for glauconite, based on the facies associations in which it is found, which are typically lacustrine or fluvial (KELLER, 1956; DJADTSCHENKO and CHATUZEWA, 1957; PARRY and REEVES, 1966; PORRENGA, 1968;).

According to BURST (1958a) there are three basic requirements for the formation of glauconite:

* a layered silicate lattice, which could be provided by a deteriorated, weathered mica lattice (also emphasized by GALLIHER, 1939);

* a sufficient supply of Fe and K as a weathering product, which is controlled by the environment. Their availability determines the Fe/Al ratio and the ordered and disordered character, in terms of K^+ content, of the developing glauconite;

Digitised by the Department of Library Services in support of open access to information, University of Pretoria, 2021.

* a favourable oxidation potential, which should be slightly reducing.

BURST (1958a) thus develops four possible processes of glauconite formation, which all commence with the accumulation of clayey material in pelletal form, thus providing the layered lattice structure. Fecal pellets and tests of foraminifera and other decaying organisms ensure the locally restricted reducing environment. The direct conversion of biotite to glauconite is possible, where at least the Fe is already abundantly present within the lattice, which is supported by GALLIHER's (1939) observations. The agglomeration of clay minerals is also considered a possible starting point for glauconite formation. Provided any one of these prerequisites exists, the final step to glauconitization would be the adjustment to the depositional environment, which means the fixation of Fe and K cations within the lattice structure to an extent determined by their availability in the environment.

Another process of glauconite formation, also discussed by BURST (1958a) and GRIM (1968, p541), is suggested by HADDING (1932), namely an impregnation of pore spaces and fossil fragments by colloidal solutions. This would be comparable to the formation of celadonite in basaltic rocks as described by HENDRICKS and ROSS (1941), who assume that both celadonite and glauconite pass through a gel state in their formation.

Generally, the marine environment is considered to be the only one to provide sufficient amounts of K and Fe for glauconite to form (CLOUD, 1955; BURST, 1958a). HENDRICKS and ROSS (1941) stress the neccessity of a critical Mg content in the environment, reflected in a constant percentage of this element in glauconite analyses. Further, they assume a reducing environment which is maintained by bacterial activity. However, DJADTSCHENKO and CHATUZEWA (1957), who found glauconite in alluvial sands and clays as well as in eluvial horizons of granites, envisage glauconite formation as a transformation from mainly feldspars and pyroxenes, via an intermediate stage of clay minerals, which then reacted with colloidal solutions of Fe-oxides and K-silicates.

The relatively low tetrahedral Al content of the glauconite from Twistdraai makes it comparable to the non-marine glauconite and alluvial glauconitic illite described by PORRENGA (1968) and DJADTSCHENKO and CHATUZEWA (1957). The TiO_2 content allows the conclusion, that if biotite is a precursor to glauconite, this element is rapidly removed from the lattice. TiO_2 becomes particularly conspicuous in the analysis of the marginally altered biotite grain. However, the non-marine glauconitic mica studied by KELLER (1956) has an exceptionally high TiO_2 value. The MgO content of the present specimens tends to resemble those of marine glauconites, according to

Digitised by the Department of Library Services in support of open access to information, University of Pretoria, 2021.

TYLER and BAILEY (1961), who found that non-marine glauconite generally contains more than 1.14 Mg-ions per unit cell. The same authors also find for the marine glauconite, that with an increase in total octahedral cations, the interlayer cations decrease (their figure 2). This trend cannot be followed in the analyses of the Transvaal samples. On the other hand, non-marine celadonite tends to have more octahedral cations at a given interlayer cation total than does marine glauconite. This would make the present glauconite more related to the non-marine celadonites, a term which has, however, been reserved for glauconite-like minerals that normally occur in cavities of basaltic rocks (HENDRICKS and ROSS, 1941).

It can be concluded that the present glauconite shows structural and chemical resemblances to both marine and non-marine glauconite and glauconitic illite or mica. On the basis of this, and taking an overall fluvial depositional environment into account, the glauconite of this study area is regarded to have formed under non-marine conditions. Its general occurrence as flaky agglomerates in pore spaces or as cell-fillings in coalified plant material suggests a predominant formation from weathered feldspars, mica and colloidal solutions, as has been concluded by HADDING (1932) and DJADTSCHENKO and CHATUZEWA (1957). In this case the Fe, Mg and K cations would have been provided by the precursor minerals, some of which are still found in the sediments, and also by the secondary clays which accumulated in pore spaces to form the flaky rounded, even crypto-crystalline agglomerations, as was described by BURST (1958a). Glauconite formation from altered biotites appears to be another, but less prominent process in the generation of the present samples, as is indicated by partly transformed biotites and by glauconite pseudomorphs after mica.

A locally reducing environment is readily provided in the proximity of decaying peat material. Reducing conditions in pore spaces of sandstones, deposited in an otherwise oxidizing environment, is most likely provided by humic acids and gels which formed during peatification (STACH et al., 1982, p228), and which were subsequently extruded from the peat, together with bacteria, due to compaction.

4.11.3. Paleo-pH Results

The paleo-pH-values reflect the considerable amounts of carbonates in the clastic sedimentary rocks at Twistdraai, which were also apparent in the XRD results. These relatively high pH values for clastic sediments (pH>7) are atypical of coal-forming environments (Stach et al., 1982, p31). Thus, these results can be attributed to diagenetic processes (BROWNLOW, 1979).

High compaction rates during early diagenesis resulted in the

Digitised by the Department of Library Services in support of open access to information, University of Pretoria, 2021.

expulsion of large amounts of acidic water from the peats. These caused unfavourable conditions for carbonate precipitation in the sediments overlying the coal seams, which is reflected by relatively low pH values.

pH value determination of sedimentary rocks is not a meaningful method to support paleoenvironmental studies of a variety of argillaceous and arenaceous rocks, and does not, in general, reflect the original pH of the waters in which sedimentation took place. The influence of diagenetic processes on the chemical properties of rocks is considered to be of great importance, especially for porous sedimentary rocks such as sandstones and siltstones. Nevertheless, the method seems applicable to flint clays, which are extremely dense and which therefore do not allow considerable ground water circulation during diagenesis.

4.12. Discussion of the Micropetrography of the Coals

Coal macerals can be divided into two major groups, which either represent well preserved, or more or less degraded plant material. The first group allows the recognition of original plant structures and comprises exinite, telinite, fusinite, semifusinite and fungal sclerotinite. The other macerals do not give indications of their botanical precursors and are regarded as products of degradation and humification (STACH et al., 1982, p223).

Vitrinite results from vitrinitization processes that take place under mainly anaerobic environmental conditions. Persistent water coverage and stagnant water are prerequisites so that fairly low pH values, which inhibit bacterial activity, and a low oxidizing potential can develop. These are unfavourable for plant decay. The formation of inertinite requires aerobic conditions, high bacterial activity and the chemical processes of fusinitization (STACH et al., 1982, p223-285; HARVEY and DILLON, 1985).

The generally persistent ratio of high to low reflecting inertinite in the present samples indicates a relatively constant oxidizing environment. The predominance of low reflecting inertinite, however, suggests that a large portion of initially partly vitrinitized plant remains has undergone further oxidation before being finally deposited in a reducing environment. This oxidation of vitrinitized material is also indicated by the sporadic oxidation rims of the vitrinite macerals. This is probably due to fluctuating water levels or to oxidation during transport of existing peat material. Therefore, one can assume that the original swamp environment allowed the preservation of considerable amounts of vitrinite, as represented

Digitised by the Department of Library Services in support of open access to information, University of Pretoria, 2021.

by some vitrinite-rich bands. At the same time, a certain fraction of the decaying plant material was fusinitized to form inertinite. During subsequent rafting of the original peat to its final depositional environment, many of the initially humified components underwent partial oxidation to form the low reflecting inertinites. This theory on their origin is further supported by the ratio of high to low reflecting inertinite, which only exceeds 1 in vitrinite-dominated coal bands; there the proportion of carbomineritic microlithotypes is low. It is thus concluded that these vitrain bands were formed under stable preservation conditions, not allowing rafting and subsequent oxidation and mixing of initially gelified macerals.

The predominance of detrital macerals over massive and cellular macerals in most samples indicates a generally hypautochthonous deposition of the peats at Twistdraai, rather than *in situ* oxidation due to water level fluctuations. The intimate mixing of the detrital macerals of different reflectivities with mineral matter, thus forming the various carbominerites, points to physical disintegration of the rafted peat before redeposition from suspension. The transportation of the peat presumably took place in active swamp channels, such as described by STACH *et al.* (1982, p19) from Florida and Siberia.

The fact that the relative amounts of detrital and vitrinitic macerals are inversely proportional supports these proposed depositional conditions for the peat (Figs. 3.16, 3.17, 3.18 and 3.19). Phases of favourable and quiescent preservation conditions alternated with periods of increased peat erosion, transportation, oxidation and redeposition. These irregularities are to be expected in an overall meandering river system, as proposed before, with crevassing activity and avulsion along the distributaries. Thus, the following depositional history of the main peat deposits is suggested, based on the micropetrography of the coals of the No. 4L seam:

* Cycle A (Fig. 3.19) is thin and laterally inconsistent; it formed in locally secluded depressions and was probably not developed in the eastern half of the study area. The generally low vitrinite content and medium to high content of detrital macerals suggest that most of these first coal bands are of hypautochthonous origin, especially as no seat earths were found.

* The lower portions of cycles B and C, which are characterized by low vitrinite contents and a high detrital fraction, formed under an increased influx of fresh water which transported peat into the area. This view is supported by the occurrence of in-seam clastic lenses in section 61 and further towards the eastern half of the study area, where cycle B is assumed to be the lowermost cycle. The eastern meandering river belt, proposed in the depositional model, would have been the source of these influxes.

Digitised by the Department of Library Services in support of open access to information, University of Pretoria, 2021.

In both cycles the influx of water with peat debris ceased towards the top, as indicated by increasing vitrinite and decreasing detrital fractions. Also, the ratio of high reflecting to low reflecting inertinite increases as the vitrinite content increases. The torbanitic lens in cycle B of section 61 implies localized, temporary deep water and anaerobic conditions (STACH et al., 1982, p264), which also provided good preservation conditions for the development of the overlying vitrinite-rich band.

* Cycle D again started after an influx of fresh water from the east, which is indicated by the sandstone lenses in sections 59 and 61, abundant detrital material and lower vitrinite content. Conditions were unstable so that cycle D is irregularly distributed. Reasons for this local truncation of the seam profile were discussed earlier (see sections 4.7.3. and 4.7.4.). In section 59 conditions became more stable and cycle D is terminated by a vitrain band. Once again a new influx of fresh water, accompanied by the deposition of sandstone, characterizes the beginning of cycle E in section 59. Towards the top of the cycle rapid deepening of the water resulted in siliciclastic sedimentation so that peat could no longer form.

A comparison of the macropetrographic seam profiles and the micropetrographic findings, shows a good correlation between the results of the two approaches. In both instances a similar cyclicity is found. Each corresponding macro- and micropetrographic cycle can be placed in the same principal environment on the basis of the coal petrography and the associated rock types.

4.13. Summary and Discussion of the Model

The Twistdraai Coalfield underwent a paleoenvironmental history ranging from a subglacial period to a fluvial setting in which the main coal-bearing strata were formed. It was mainly characterized by continental influences which produced fluvial, fluviodeltaic and lacustrine facies associations.

In brief, the study area went through the following sequential paleoenvironmental stages:

* Preliminary subglacial conditions which were followed by proglacial outwash plains with glaciofluvial and glaciolacustrine deposits (Event 01); these sediments caused the glacial paleotopography to be largely filled up.

Digitised by the Department of Library Services in support of open access to information, University of Pretoria, 2021.

* A lacustrine or shallow basinal paleoenvironment which was dominated by lacustrine or Gilbert-type deltas within a glacially controlled paleoclimatic setting. The deltas were initially extensively altered by basinal shoreline activity, namely wave and tidal processes. Later fluviodeltaic conditions with braided channels prevailed (Event 02).

* An alluvial plain dominated sedimentation for most of the time during Events 03 to 08. Throughout the main coal-forming period, meandering rivers characterized the paleoenvironment. Braided channels appeared towards the close of Event 06. A coexistence of channel, floodplain, backswamp and lacustrine settings, with localized crevasse deltas in the latter, resulted in a great variety of sediments, in both vertical and horizontal extents.

In general there is an apparent lack of lateral facies changes within the Twistdraai Sequence (Fig. 1.3, p. 5); this is probably related to the fact that borehole data only provide insight to vertical facies changes. However, for LFA's 04 to 06 and 08, for which a meandering fluvial deposition is proposed, lateral facies changes appear to be fairly common (Fig. 4.1, p 105).

The meandering fluvial setting is best documented by the distribution of coal seam No. 3 and associated deposits, and by the parting between seams No. 3 and No. 4L. STEYN (1976) postulates a similar meandering river model for the Davel Coalfield. He distinguishes between an upward-fining arkosic sandstone (active channel-fill) and thick carbonaceous shales (abandoned channel-fill), which are both overlain by coal. This compares favourably with the deposits of Event 05 in the Twistdraai area, and especially for seams No. 3 and No. 4L.

MCLEAN and JERZYKIEWICZ (1978, p441) point out, in their studies on coals related to alluvial environments, how peat accumulates in close proximity to fluvial channels, thus forming elongated seams parallel to the channels. Even on the small scale of this study, this feature can be seen in the distribution of the No. 3 seam. MCLEAN and JERZYKIEWICZ further emphasize the high complexity of the environmental setting that characterizes alluvial peat deposits. There is no evidence of large scale lacustrine delta accretion or lacustrine shoreline deposits in their study. This agrees with the study at Twistdraai, as the lacustrine and subsequent Gilbert-type delta phases are only known from the strata below the coal-bearing zone, towards the base of the succession.

The factors which controlled sedimentation at the Twistdraai Mine include the following:

* Gradual decrease in paleoslope, which was initially steep and

Digitised by the Department of Library Services in support of open access to information, University of Pretoria, 2021.

which was greatly influenced by the filling-up of the glacial valleys. Contemporary isostatic rebound is not regarded as very important by VON BRUNN and STRATTEN (1981), but is supported by HOBDAY (1978). It most probably affected the paleoslope in the study area, but was compensated for by the above-mentioned filling of the paleovalleys. For the Dwyka Formation, STRATTEN (1970) places a mildly positive and stable area where the present-day Highveld and southeastern Transvaal Coalfields lie. Hence, they were regions of slow to no subsidence during Dwyka sedimentation. Paleoslope mainly gives a regional control over paleocurrents and over the orientations of major paleotopographic depressions in the Karoo Basin. RYAN (1968) emphasized paleocurrent patterns in his study of the Ecca Group. According to his research the Twistdraai area is situated in a region of conjunctive southeasterly- and southwesterly-oriented paleocurrents. Thus both tendencies can be expected in the present study area. The southwesterly trend is confirmed in this investigation, especially along the fault zone (for example Event 02).

* The pre-Karoo Sequence paleotopography, which appears to be of major importance for sediment distribution in other South African coalfields (CAIRNCROSS, 1980; LE BLANC SMITH, 1980), only had an impact during early sedimentation in the Twistdraai Coalfield, especially for Event 01. Later, sediment distribution was the result of environmental changes or localized subsidence due to differential compaction of sediments of different composition.

* A braided stream system was present during the non-coal-bearing phases (Event 02 and upper portion of Event 06) and a meandering river system was dominant during major coal-bearing phases (Event 03 to basal portion of Event 06). Events 03 and 07 are an exception in that they encompass backswamp conditions immediately succeeding a braided river paleoenvironment. These two events can both be regarded as the initiators of quiescent periods, which formed under meandering river conditions. Thus lateral channel shifting is relatively high during non-coal-bearing events and relatively restricted during coal-bearing events. This causes laterally uniform sheet-like sedimentation during braided river periods and laterally variable facies associations during meandering river phases. N.D. SMITH (1970) attributes braided streams to rapid and extreme discharge fluctuations and easily erodible banks, with mainly arenaceous sediments, as found for the lithofacies associations formed during Event 02 and the upper portion of Event 06. Contrary to this, meandering rivers require a lower slope, cohesive bank material, as provided by mainly

Digitised by the Department of Library Services in support of open access to information, University of Pretoria, 2021.

argillaceous sediments and peat, and a relatively steady discharge (D.G. SMITH, 1976; READING, 1982, p31). The latter conditions were encountered from Event 03 to the basal portion of Event 06, and particularly during Event 05.

* On the local scale of the mine area itself, irregular water supply, periodic channel shifting and erosion directly controlled the sediment distribution and lithology.

* Synsedimentary fault movement is assumed to have partially controlled sediment thickness and distribution, as FLORES (1983) proposed. The graben-like faultzone presumably enhanced sediment accumulation at certain stages of the depositional history. It also partly influenced peat accumulation itself, as shown by the wedging out of coal seam No. 3. and an apparent erosion of seam No. 4L along the fault zone.

* On the basis of the clay mineralogy and glauconite petrography and chemistry, it is concluded that no marine inundation influenced the sedimentation of the Karoo Sequence at Twistdraai.

Apart from the regional geological factors named above, peat growth within a fluvial paleoenvironment, such as that proposed for Twistdraai, is mainly controlled by the following circumstances:

* **Peat is thickly developed**
(due to regular nutrient supply provided by frequently-occurring flood stages, and due to sufficient water coverage to allow the peat to be preserved),
  ** on the floodplains beyond natural levees and in close proximity and parallel to the channels;
  ** along the banks of open water bodies, such as ponds and oxbow lakes in the backswamps;
  ** on top of crevasse deposits.
  ** Peat will also be thickly developed due to a comparatively high compaction rate of thick, fine-grained sediments beneath the peat swamp.

* **Peat is thinly developed,**
  ** further back in the backswamp, away from channel influences, due to a smaller nutrient supply and lesser water coverage;
  ** above natural levees due to poor preservation conditions;
  ** above channels, due to relatively late commencement of peat growth compared to adjacent areas;
  ** where post-swamp erosional activity in any part of the coal swamp occurs.

Digitised by the Department of Library Services in support of open access to information, University of Pretoria, 2021.

* Peat growth in the Twistdraai area does not appear to have been significantly controlled by features in the pre-Karoo paleotopography, as suggested for other South African coalfields (CAIRNCROSS, 1980; LE BLANC SMITH, 1980), where pre-Karoo paleovalleys are assumed to have favoured peat accumulation. The coal distribution of seam No. 3 at Twistdraai shows, rather, a contrary situation, with thick coals over a pre-Karoo ridge. Other seams, such as No. 4L, have major coal occurrences in the eastern half of the study area due to differential compaction of underlying sediments. None of the seams at Twistdraai display any prominent features in the western half of the study area that can readily be related to characteristics in the western pre-Karoo paleotopography.

Previous studies on depositional paleoenvironments in South African coalfields (CADLE, 1979; CAIRNCROSS, 1980; LE BLANC SMITH, 1980) generally propose several deltaic cycles, at least for the basal portion of the coal-bearing Ecca sedimentary rocks. Some authors carry this interpretation through until after the coal-forming environments. HOBDAY (1978) and CAIRNCROSS (1980) consider major fluvial paleoenvironments as controlling factors over coal formation. Fluvial processes on an alluvial plain at times of major peat growth are proposed by HOBDAY (1978); other authors tend to place the peat swamps only on delta plains.

This study differs from most previously-established models for South African coalfields, in that basinal influences and even deltaic control (Event 02) over the sedimentation are proposed to have been of minor importance and to have stopped before the main coal development. They thus had no influence on coal distribution. Evidence for a fluvial paleoenvironment on an alluvial plain, as proposed here, has also been found in other South African coalfields (HOBDAY, 1978); however, no mention of specific fluvial conditions is made. The meandering fluvial setting, proposed for the Twistdraai area throughout most of the depositional phases and especially during peat accumulation, is different to other paleoenvironmental interpretations of South African coalfields, with the exception of the study of the Davel Coalfield (STEYN, 1976). The basis of this different conclusion lies mainly in the characteristics and sequence of the lithofacies associations in the study area. The lower LFA's compare favourably to various other studies that took climatically similar conditions into account (e.g. EASTERBROOK, 1982). Other authors (GALLOWAY and HOBDAY, 1983; FIELDING, 1985) compare various recent and ancient coal-forming environments, of which the fluvial settings and their deposits most closely resemble the sedimentary rocks at Twistdraai. A specifically meandering fluvial model is adopted after comparing the complex facies associations and coal distribution patterns with the work of JACKSON

Digitised by the Department of Library Services in support of open access to information, University of Pretoria, 2021.

(1978). He comes to the conclusion that a meandering river facies model displays various characteristics, such as upward-fining and upward-coarsening sequences, lateral variability of facies distributions and interfingering of floodplain and channel deposits; all these features occur in the study area.

The model proposed here for the Twistdraai Mine is not necessarily contradictory to other models for South African coalfields. Most of these investigations are concentrated on the Witbank Coalfield (CAIRNCROSS, 1980; LE BLANC SMITH, 1980), which lies to the north of the present study area, and on the northern Natal areas (CADLE and HOBDAY, 1977), which lie to the southeast. The mainly deltaic paleoenvironments suggested for the Witbank coals, specifically Gilbert-type lacustrine deltas (CAIRNCROSS and WINTER, 1984), appear plausible, as that basin was almost entirely surrounded by pre-Karoo basement rocks, including the Smithfield Ridge to the south (Fig. 1.1). This paleogeographic factor most probably placed the Witbank Basin in a unique and secluded situation as a major lacustrine basin. From there towards the south, into the main Karoo Basin it appears very likely that sedimentation and peat development took place on a very gentle paleoslope, further away from the source areas. By comparison with CAIRNCROSS' (1980) and LE BLANC SMITH's (1980) work, where the pre-Karoo floor appears to be still pronounced and of importance to sedimentation at least for the No. 2 coal seam, it becomes clear, that the initial pre-Karoo paleotopography at Twistdraai had a lesser impact on subsequent deposition. Paleocurrent analysis in the Ecca Group by RYAN (1968), of the area south of the Smithfield Ridge, indicates that source areas for the Secunda Coalfields lay mainly towards the north and northeast, in and beyond the Smithfield Ridge. This again seems to place the Witbank Coalfield into the secluded position of a major, probably lacustrine basin, which only had contact with the main Karoo Basin via a number of prominent streams across a wide foreland, on which both the Secunda and the Davel Coalfield developed.

As the northern margins of the Karoo Basin, and particularly the Highveld and southeastern Transvaal Coalfields, were characterized by continental sedimentation before (Dwyka Formation) and after (Beaufort Group) the coal-forming phases (HOBDAY, 1978), it appears unlikely that the Ecca Group in this part of the Karoo Basin was under the influence of any major open water or even marine paleoenvironment. This study suggests a paleoenvironment analagous to that which can be observed in present-day Siberia, Finnland and northern Canada. Here, extensive peat swamps in fluvial and lacustrine environments dominate large parts of the landscape, as, for instance, the muskeg in northern Canada (RADFORTH, 1969). These recent swamp and alluvial deposits in most cases succeed Quarternary glacial sediments (N.D. SMITH, 1975; D.G. SMITH, 1976).

Digitised by the Department of Library Services in support of open access to information, University of Pretoria, 2021.

5. THE EFFECT OF DEPOSITIONAL ENVIRONMENT ON COAL QUALITY PARAMETERS

The relationship of coal distribution and sedimentary environment has been discussed in sections 4.7.1 and 4.7.3 and thus does not need to be repeated. In this chapter it will be attempted to correlate coal quality parameters in the No. 4L seam and depositional features. Quality parameters that are of interest here and for which data were made available are ash content (a.d.), calorific value (d.a.f.) and volatile matter (d.a.f.).

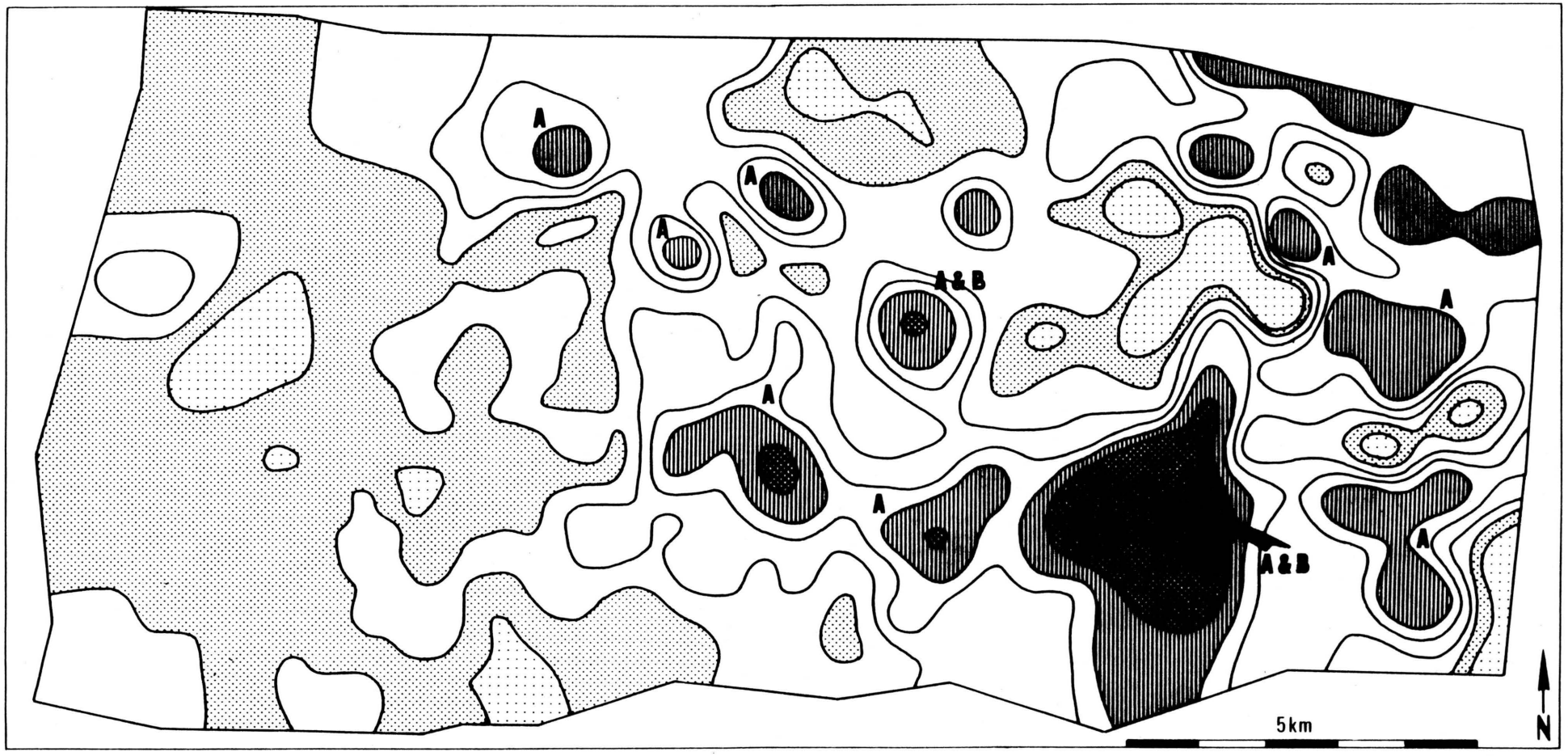
5.1. The Ash Content

The ash content of coal is generally considered a dilutent to the properties of the coal. This is especially evident in its performance in power station boilers or in coking ovens. Furthermore, an abundance of ash or of certain components therein can cause environmental problems in a coal processing plant or its surrounding areas. Ash in coal therefore decreases its quality and economic value. It is, thus, the aim in short- and long-term mine planning to delineate areas of high ash, or low coal quality, in order either to avoid their mining or to take certain beneficiation measures.

Ash, which originates from the inorganic mineral matter of coal, has various origins and pathways into the peat swamp. The greatest amount of the mineral matter is detrital and is either transported by water or, to a lesser extent, by wind. It either occurs as microscopically discernible grains within the organic matrix, as clastic lenses of centimeter to meter dimensions within the seam, or as major seam splits up to several tens of meters in dimension. Ash can also be inherited from the inorganic constituents of the decaying plants, which integrated nutrient elements from soils and solutions in the swamp waters into their cell structures. Chemical processes during sedimentation and diagenesis also contribute to the ash of coal. Mineral matter is then precipitated from solutions in the highly reactive acidic waters of a swamp (STACH et al., 1982, p30).

In most parts of the study area the ash content is about 20-26%(a.d.). It is conspicuous that the western half, away from the channel influences, has wide areas of less than 20% ash (a.d.), whereas the eastern half shows both extremes of less than 20% and more than 30% ash (Fig. 5.1). The high ash concentrations are mainly found along the margins of the underlying major crevasse deposits and correspond well with the occurrences of in-seam clastic lenses (compare figure 5.1 with maps 5.7 and 5.8). They also overlap with the

Digitised by the Department of Library Services in support of open access to information, University of Pretoria, 2021.



LEGEND

ash content (a.d.)

A = coresponds with in-seam clastic lenses in top of the seam (Map 5.8)

B = coresponds with in-seam clastic lenses in bottom of the seam (Map 5.7)

< 18%

18 - 20 %

20 - 26 %

contours at 22 and 24%

26 - 30 %

> 30%

Fig. 5.1 Distribution of the ash content **(a.d.)** in the coals in the No. 4L seam.

Digitised by the Department of Library Services in support of open access to information, University of Pretoria, 2021.

contours of the thickest coals of the seam. It is also noticeable that the highest ash concentrations do not occur on the far eastern margin of the study area, closest to the channel, but above the older levee and crevasse deposits (Map 5.3.M). This is attributed to the abandonment of channel activity and a subsequent encroaching of the peat from the west over these crevasse and levee deposits, during the growth of cycles B and C (sections 3.6.3 and 4.7.3) of the No. 4L coal in that part of the coalfield. This portion of the seam profile had significantly fewer clastic incursions (sections 3.6.3 and 4.7.3), which led to a lower ash content.

Above the abandoned channel which preceded the swamp in the northeast of the study area (Map 5.5.M), and where the seam is relatively thin, there is also a remarkably low ash content in the coals (Fig. 5.1). This correlates with a lack of crevassing into this area, which has few in-seam clastic lenses (Maps 5.7 and 5.8).

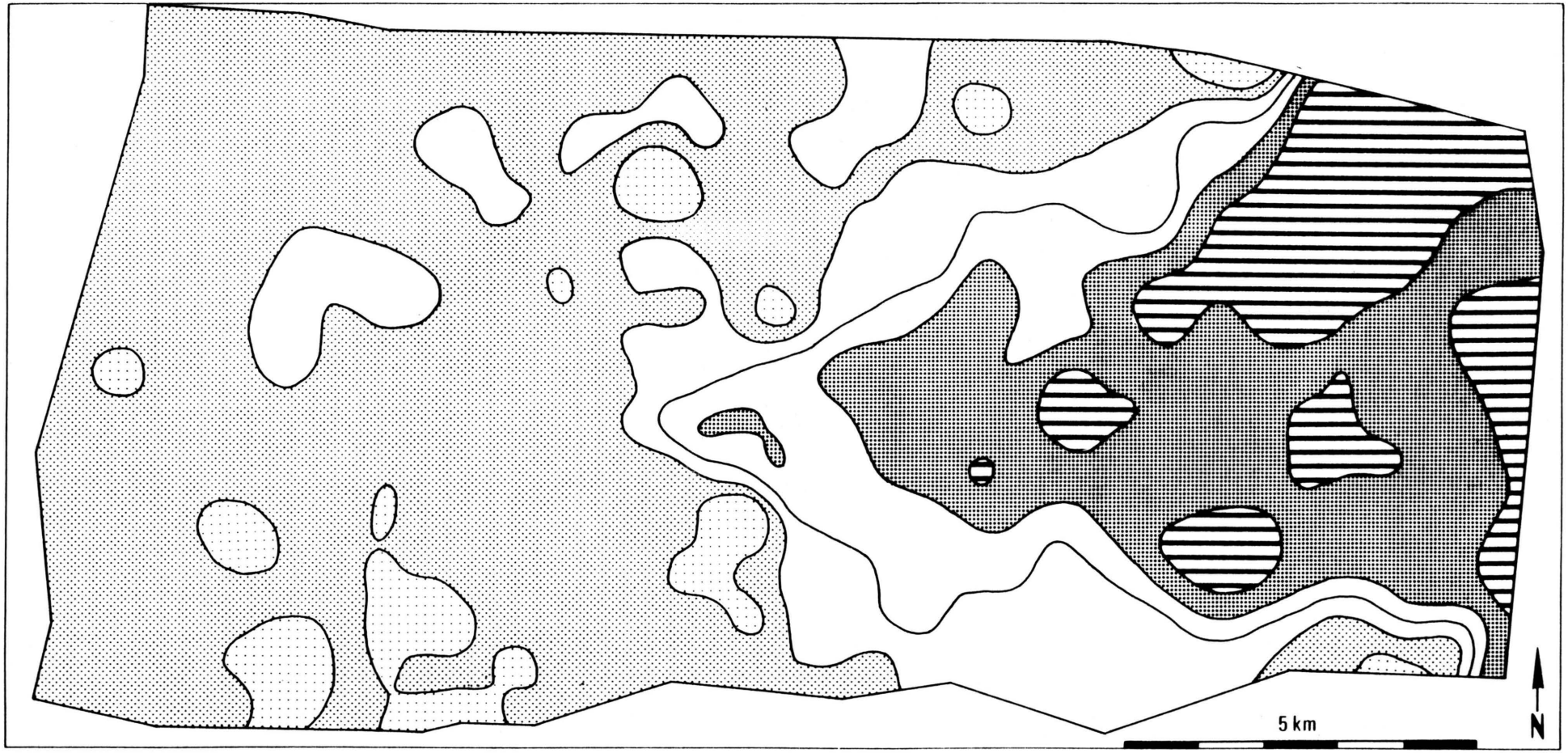
5.2. The Volatile Matter Content

The volatile matter content of a coal is of great importance in many technological applications. For the coking process it determines the degasification and swelling properties of the coal. In coal liquefaction and gasification it determines the yield of hydrocarbons. Finally, in a power plant combustion process it adds to the calorific value of the coals.

The volatile matter is usually taken as a rank parameter of coals and is therefore not directly related to primary sedimentology. However, as it is also dependent on the maceral composition of coals, it is in turn also the result of plant community and peat preservation (STACH et al., 1982, p88&219). Both the factors are controlled by depositional environment.

Volatile matter (d.a.f.) in the No. 4L seam is less than 32% in the western half of the study area; extremes of less than 30% are related to localized devolatilization by dolerite intrusions (Fig. 5.2). Values of more than 36% in the eastern half are associated with underlying crevasse, levee and channel deposits, which allowed a higher plant community to grow, due to more nutrient supply (HARVEY and DILLON, 1985) and more stable rooting ground. This would have resulted in the accumulation and preservation of more vitrinite macerals, on account of a higher water level, thus also providing better preservation conditions. The vitrinite group macerals have a higher volatile matter content compared to the inertinites (STACH et al., 1982, p88); the latter are the major component of the Twistdraai coals (section 3.13). An extremely high volatile matter content of

Digitised by the Department of Library Services in support of open access to information, University of Pretoria, 2021.



LEGEND

volatile matter content (d.a.f.)

< 30%

30 - 32 %

32 - 36 %
contour at 34%

36 - 38 %

> 38%

Digitised by the Department of Library Services in support of open access to information, University of Pretoria, 2021.

38%(d.a.f.) is found in the coals above the eastern abandoned channel, where deep water cover allowed mainly vitrodetrinitic and minor inertinitic material to be preserved. In such deep water depostitional areas of a swamp an increased accumulation of alginite could have lead to the formation of torbanite or other boghead coals. These exinite-rich coals usually have extraordinarily high amounts of volatile matter, due to abundant volatiles in the exinite group macerals (STACH et al., 1982, p177). An increased number of torbanite occurrences is reported from some parts of the eastern half of the study area (Mr. B. HOSKING, 1985, pers. comm.).

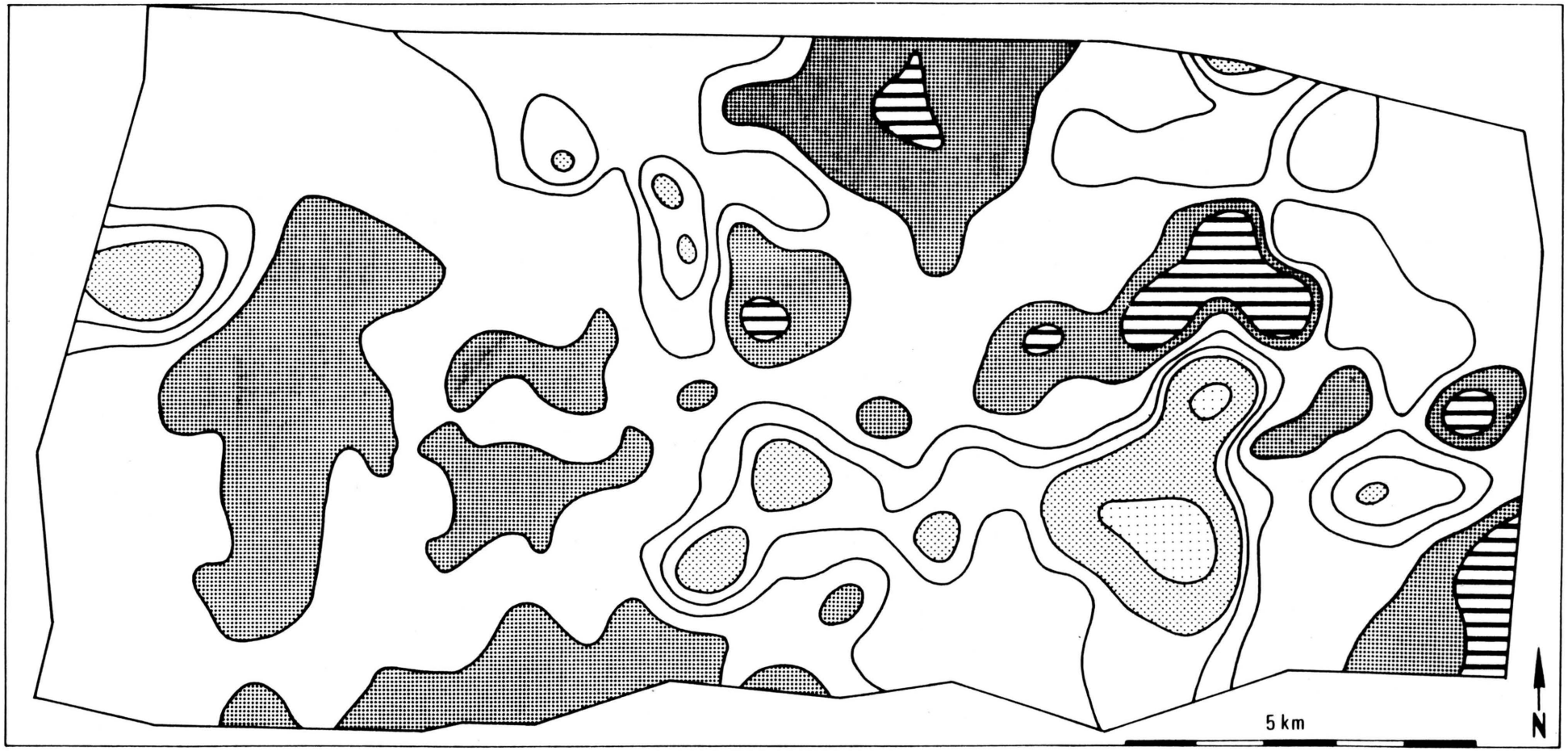
Some of the high-volatile coals (>36%) coincide with high ash coals (Figs. 5.1 and 5.2), due to the occurrences of in-seam clastic lenses. This does not necessarily imply the release of volatiles from ash (TEICHMULLER et al., 1979), because these would only be significant in carbonates and sulphides, and a precise ash composition is not known. However, the rapid burial and preservation of the vitrinite precursors in the peat, due to the crevassing (HORNE et al., 1978), might have resulted in a localized enhancement of the volatile matter content, which would then be related to the maceral composition.

5.3. The Calorific Value

The calorific value of coal is mainly controlled by the carbon and hydrogen content, which in turn is partly the result of maceral composition and mainly of rank (STACH et al., 1982, p467; SNYMAN et al., 1983). As the latter factor, particularly, does not, under normal circumstances, change very drastically over an area the size of Twistdraai, its effect on spatial changes in the calorific value will not be very significant. Therefore, components that diminish the calorific value, such as ash in the coal, will have a much greater effect. This can readily be seen from the distribution of the calorific values (a.d.) over the coalfield, which correlates inversely with the ash content (compare figures 5.1 and 5.3). However, maceral composition and its resulting volatile matter content also have a great influence on the calorific value of a coal.

In the eastern half of the study area extremes of less than 22MJ/kg (a.d.) and more than 25MJ/kg (a.d.) correspond to highs and lows of the ash concentration, respectively, and the contour lines of figures 5.1 and 5.3 show major common trends. However, in the northeastern corner and above the preceding crevasse splay deposits (over the eastern paleovalley) there are divergences where the calorific value appears to be relatively high in relation to the ash

Digitised by the Department of Library Services in support of open access to information, University of Pretoria, 2021.



LEGEND

calorific value (a.d.)

< 18 MJ/kg

18 - 22 MJ/kg

22 - 25 MJ/kg

contours at 23 and 24 MJ/kg

25 - 26 MJ/kg

> 26 MJ/kg

Fig. 5.3 Distribution of the calorific value **(a.d.)** of the coals in the No. 4L seam.

Digitised by the Department of Library Services in support of open access to information, University of Pretoria, 2021.

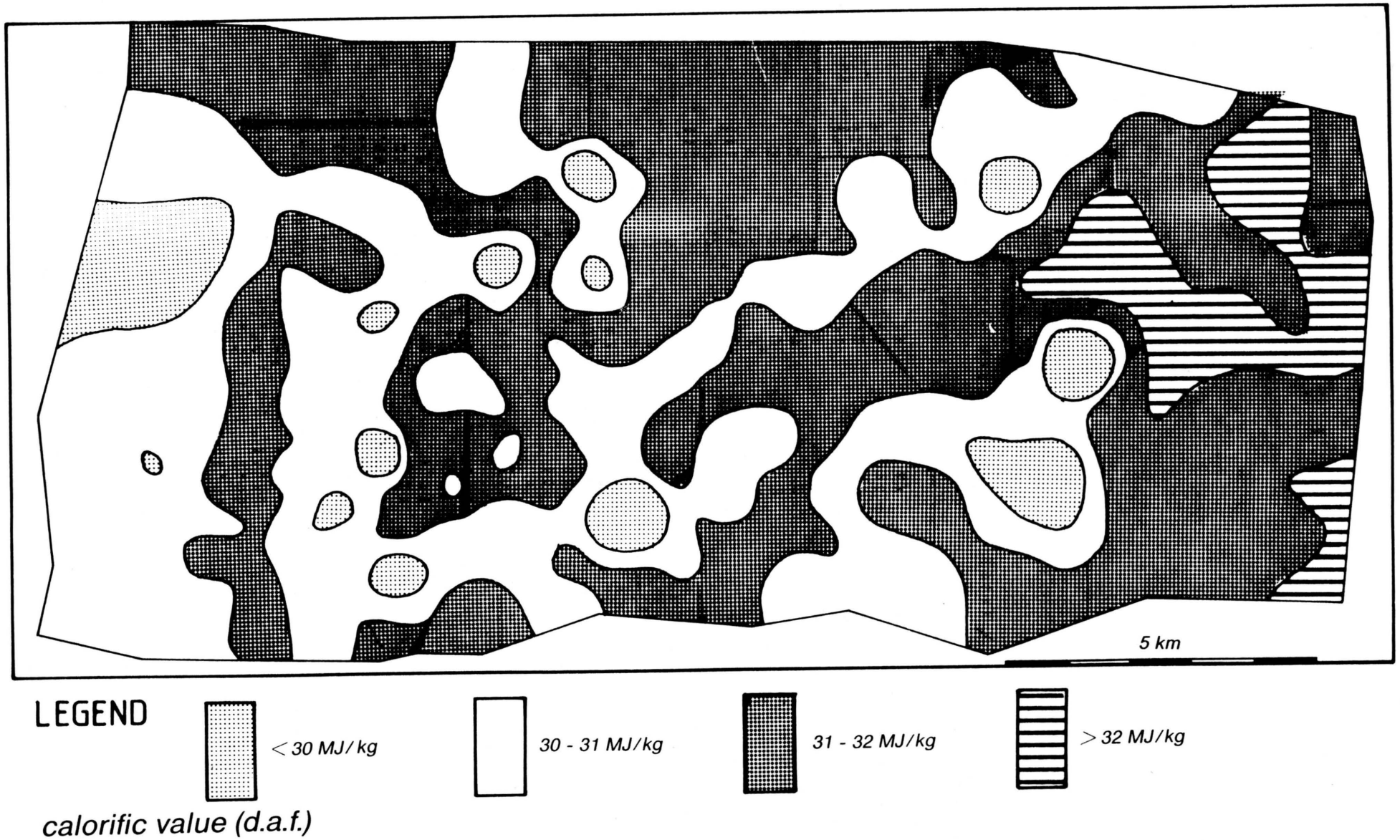


Fig. 5.4 Distribution of the calorific value **(d.a.f.)** of the coals in die No. 4L seam.

Digitised by the Department of Library Services in support of open access to information, University of Pretoria, 2021.

contents. This is attributed to extremely high volatile matter contents in these areas, which counteracted the ash content and improved the calorific value. In the western half the calorific value is constantly between 18-25MJ/kg (a.d.).

The calorific value (d.a.f.) generally lies in a narrower range, between 30MJ/kg and 32MJ/kg (Fig. 5.4) and is less variable over the coalfield. There are some trends in the eastern half of the study area that can be related to the volatile matter content and sedimentological features. Particular isoline trends of the calorific value (d.a.f.) run approximately parallel to abandoned paleochannels in the underlying sedimentary rocks (compare with maps 5.3.M and 5.5.M). In the western half of the study area the calorific value (d.a.f.) is less variable; very localized lows indicate values from one or two boreholes that intersected dolerite-affected parts of the seam. The two figures 5.3 and 5.4 of the calorific value (a.d.) and (d.a.f.), respectively, illustrate that in principle the calorific value is more diminished by the ash content of a coal than it is enhanced by the volatile matter.

Digitised by the Department of Library Services in support of open access to information, University of Pretoria, 2021.

6. THE EFFECT OF DOLERITE INTRUSIONS ON THE QUALITY OF COAL

In order to find an answer to the second key question of this study (section 1.3), emphasis will be placed on the thermometamorphic effect on the coals, rather than on the endometamorphism in the dolerites.

Initially, the petrographic and chemical characteristics of the unaffected coals will be discussed for each seam bench of the No. 4L coal seam. This will result in a representative seam profile for the present coalfield. Subsequently, the petrographic and chemical characteristics which resulted from the thermal influences will be outlined and related to sampling distance and original seam bench parameters of the unaffected coals.

6.1. Field Relations, Petrography and Chemistry of the Dolerites

In the study area two main dolerites can be distinguished. The one is a major sill of 20-30m thickness which occurs near the surface over the entire study area, about 80m above the uppermost coal seam. It does not intersect the seams and is therefore not discussed further in this study.

The other dolerite is an undulating anastomosing sill. In the extreme west of the study area it is more than 10m thick and occurs below the coal seams. Towards the east it bifurcates into various minor sheets of only a few meters in thickness, which intersect the coals in the western and central portions of the coalfield. No occurrences of dolerite sills in the coals are known from the eastern part of the study area.

Dolerite intrusions not in direct contact with coal are porphyritic in their central parts, with a green to dark green pyroxene-rich matrix and variable amounts of needle-shaped feldspar phenocrysts, up to 3cm in length. Chilled margins, up to 100cm wide on either side of the sills, are mostly microcrystalline.

At intersections with the coal seams the dolerite becomes microcrystalline, with few feldspar phenocrysts. The matrix is light grey to grey in colour and contains considerable amounts of carbonate, forming a so-called "white trap" (KISCH and TAYLOR, 1966). The contact planes of the dykes and the coal seams are even to very irregular with some apophyses into the coal; the latter are a few centimeters wide and up to several meters long. Such phenomena are also reported by KISCH and TAYLOR (1966) and ROBERTS (1987). Within approximately 0.5m of the contact calcite is concentrated on joint planes in both the coal and the dolerite. These joints may extend up to several meters

Digitised by the Department of Library Services in support of open access to information, University of Pretoria, 2021.

into the coal. Injections of coaly material into the sill and coaly fragments in the dolerite are common within this contact zone.

The dolerite dykes at sampling localities A, B, C and D (Fig. 2.2) are small compared to similar intrusions reported from other South African coalfields (WALKER and POLDERVAART, 1949; ROBERTS, 1987). They average 2.5-3m in thickness, cut sub-vertically through the seam (Fig. 6.1) and strike north-south. At other localities in the mine the dolerites cut obliquely through the seam and might even follow a path parallel to the seam, either within the coal bands or at the top or the bottom of the seam. The dolerites bifurcate and intrude the coal in a broad zone and are usually wider in the coal than in the floor and roof rocks (Fig. 6.1). This irregular bulging within the coal has been attributed to plasticity and shrinkage of the coals, due to the loss of large amounts of volatiles and moisture from low rank coals under thermal metamorphism (HAMILTON, 1983).

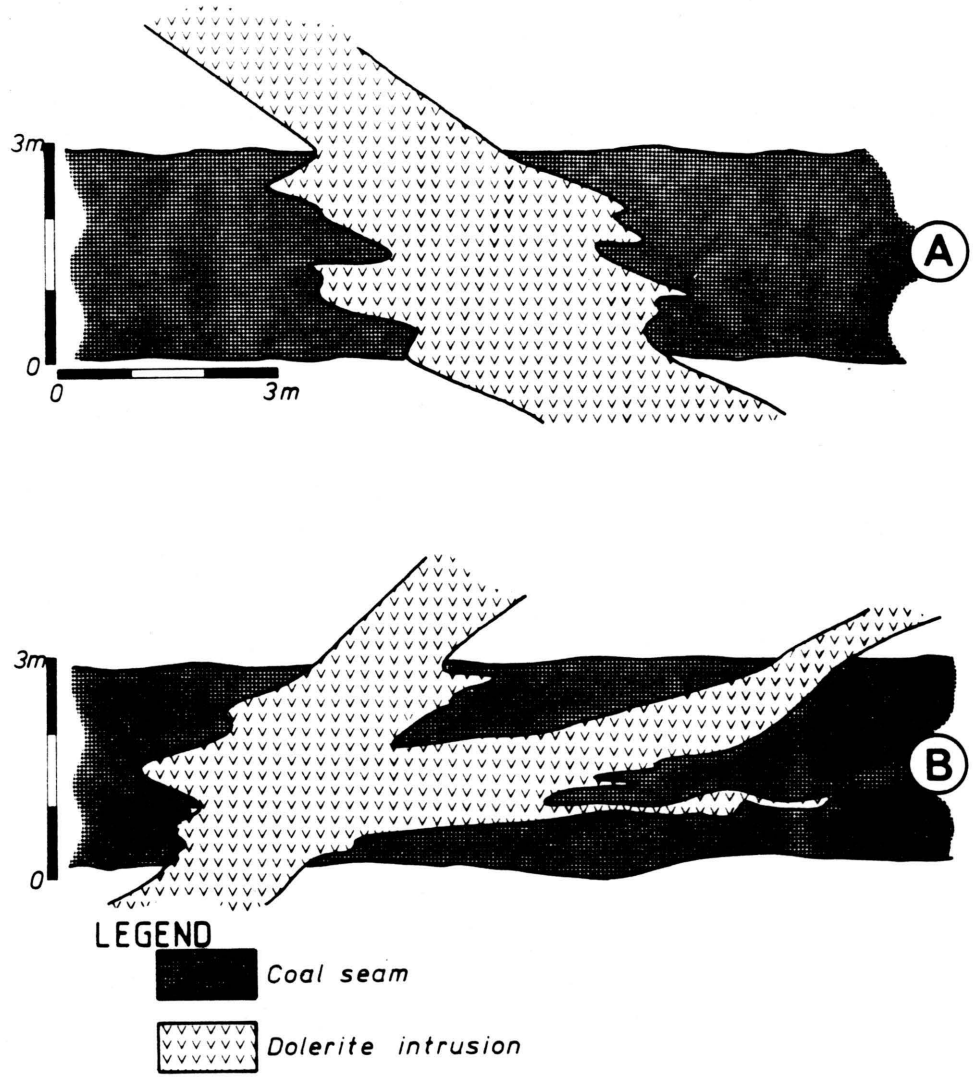


Fig. 6.1 Scematic cross-section illustrating how dolerite dykes intersect a coal seam, (A) either widening in the seam or (B) bifurcating.

Digitised by the Department of Library Services in support of open access to information, University of Pretoria, 2021.

Dolerite sampled from a borehole core about 100m above the coal seam shows no sign of endometamorphism by the coal. It mainly contains euhedral and glomeroporphyritic labradorite phenocrysts, in a matrix dominated by pyroxenes (mainly pigeonite, accessory augite), with variable amounts of opaque minerals (magnetite and ilmenite) and traces of quartz. Similar tholeiitic dolerites have also been described by WALKER and POLDERVAART (1949). One sample from the margin of such an unaffected dyke contains considerable amounts of kaolinite, which is regarded as a secondary product.

Dolerite of the "white trap" variety exhibits fewer of the larger feldspar phenocrysts than the unaffected dolerites, but numerous agglomerations of smaller feldspar needles. The degree of alteration varies from slight to complete. These altered dolerites consist almost solely of matrix material, comprising micro- to cryptocrystalline plagioclase, pyroxene, carbonate and accessory quartz. Siderite, determined from X-ray diffractograms, appears to be the most abundant carbonate mineral. The "white trap" is contaminated with slithers and specks of carbonaceous material, which include pyrolytic carbon and natural coke. These are especially abundant near the intrusive contacts.

In comparison to chemical analyses of other Karoo dolerites (WALKER and POLDERVAART, 1949) the present dolerites are enriched in Ti, Fe, Cu, Ni, V and Sc, but depleted in Si, Mg, K, Zr, Rb, Th, Cr and Ba (Table 6.1; full sets of analytical data are given in appendix 4). The Ti, Fe and Mg contents of the Twistdraai dolerites are comparable to dolerite pegmatites investigated by WALKER and POLDERVAART (1949). The high Fe content is attributed to the major occurrence of iron oxide minerals.

Most element concentrations are of the same order of magnitude in the unaltered dolerites and in the "white trap". Si and Na, however, are depleted in the coal-affected dolerites, whereas Fe, Ni and Ga are only marginally lower. On the other hand, Sr and Ba are considerably enriched; Rb, Cr and Sc are marginally increased.

In both the unaltered dolerites and the "white trap", certain elements show depletion and others enrichment tendencies from the core of a dyke to the margin (Table 6.1). This can largely be attributed to differential crystallization, as the margins were normally chilled. In the "white trap" these trends towards the contact with the coal are also partially due to chemical interaction with the seam and will be discussed later.

However, the average chemistry of the "white trap" at dyke margins and in the centres is largely similar, with the exception that Ca, and in most cases Mg also, are depleted towards the margin; this can also be observed in the unaltered dolerites. Cu, Zr, Cr, V and Ba are enriched and Sr is depleted towards the margin (Table 6.1). These changes are not taken to be significant, because fluctuations of these

Digitised by the Department of Library Services in support of open access to information, University of Pretoria, 2021.

Table 6.1 Geochemical analyses of unaltered dolerites and "white trap" dolerites in comparison with analyses of other Karoo dolerites (major elements in %, trace elements in ppm).

element	"white trap" centre	"white trap" margin	unaffected dolerites centre	unaffected dolerites margin	other Karoo dolerites (1)	other Karoo dolerites (2)	other Karoo dolerites (3)
SiO_2	36.52	34.90	48.05	41.57	54.4	50.9	52.52
TiO_2	1.83	2.15	2.09	2.56	1.09	1.0	2.56
Al_2O_3	13.81	13.07	13.30	15.57	15.1	15.2	11.26
Fe_2O_3	15.71*	16.51*	16.78*	18.52*	1.68		2.88
FeO	0.00	0.00	0.00	0.00	8.2	10.0 **	14.22
MnO	0.23	0.23	0.24	0.25	0.18	0.17	0.41
MgO	4.02	3.46	4.62	2.34	6.1	6.37	2.57
CaO	10.24	6.43	9.39	5.85	8.19	10.53	7.22
Na_2O	1.99	1.87	2.69	2.11	2.27	2.00	1.65
K_2O	0.35	0.46	0.38	0.30	1.2	0.52	1.34
P_2O_5	0.18	0.22	0.20	0.23	0.14	0.14	0.23
LOI	12.47	17.86	0.79	7.58	n.d.	n.d.	1.48
H2O	0.70	0.84	0.30	0.85	n.d.	1.73	1.37
TOTAL	98.09	98.07	98.89	98.07	98.55	98.56	99.71
Zn	155	143	133	149	164	71	
Cu	283	344	311	342	94	99	
Ni	73	68	75	84	45	112	
Co	40	49	42	61	40	84	
Ga	25	25	28	31	26	16	
Mo	0	0	0	0	n.d.	1	
Nb	4	6	7	7	n.d.	11	
Zr	112	133	123	132	210	84	
Y	32	37	38	37	40	33	
Sr	411	369	185	271	n.d.	260	
Rb	9	15	7	4	57	22	
U	2	2	0	3	n.d.	1	
Th	0	0	0	0	82	2	
Pb	11	7	8	11	10	2	
Cr	141	257	132	120	531	470	
V	439	511	402	521	324	463	
Ba	901	1017	143	224	469	104	
Sc	48	55	39	47	25	n.d.	

(1) from WALKER and POLDERVAART (1949)
(2) from ROBERTS (1987)
(3) dolerite pegmatite (WALKER and POLDERVAART, 1949)
n.d. not determined
* total iron expressed as Fe_2O_3
** total iron expressed as FeO

element concentrations are often very large (Appendix 4). It is thus assumed that the chemical interaction of coal and magma for most elements was more or less evenly effective throughout the "white trap". A larger amount of combustible carbonaceous matter and carbonates in the marginal portions of the intrusions probably causes the considerable increase in LOI within the marginal samples.

6.2. Petrographic Description of the Coals

Coal seam No. 4L is evenly thick (+/-3m) and has a persistently developed lithotype banding over the western half of the coalfield, where the depositional environment is assumed to have remained laterally stable (sections 4.12 and 4.13). Therefore, it is adequate to divide the seam profile into six seam benches (A-F) in order to simplify the correlation from one channel to another . These benches are represented by samples marked with the same letters (A-F) at each

Digitised by the Department of Library Services in support of open access to information, University of Pretoria, 2021.

sample channel (Fig. 2.3). It is thus sufficient to concentrate the macroscopic description on a representative profile of the six seam benches.

BENCH Z is an exceptional coal band, only present at the bottom of the channel at locality G (Fig. 2.3). It has no corresponding sample at other localities. This bench comprises 55cm of clarain and duroclarain in almost equal amounts. Some calcite occurs on joints and cracks in the bright coal bands.

BENCH A is commonly 80-100cm thick and occurs at the base of each channel. At locality G it lies above bench Z and is 80cm thick. Duroclarain and durain are the main lithotypes, but vary considerably in their relative proportions. The basal 20-30cm usually contains clarain and vitrain bands of less than 10mm thickness. In some channels the durain is lustrous in the top part. Concretions and nodules of siderite and pyrite are common and can reach 3-5cm in diameter. They are mostly concentrated in a prominent horizon in the middle of the bench.

BENCH B overlies A and generally represents approximately 50cm of the seam profile. It mainly comprises durain, which is lustrous in parts. Notably at localities D, E and H (Fig. 2.3) it incorporates a considerable amount of clarain. Pyrite and siderite are rare.

BENCH C is a 45-50cm thick layer above bench B. At all sampling localities it contains mainly lustrous durain, which is often brittle. Bright coal stringers (<3mm thick) occur locally in this band. Pyrite and siderite are rare. Where they are present they are concentrated in a 5-10cm wide horizon.

BENCH D is a very prominent vitrain-rich band of 20-30cm thickness and serves as a marker horizon at all the sampling localities. In profile G this band is poorly developed and appears as a clarain. Durain and torbanitic shale bands, up to 3cm in thickness, occur near the top and the base of the bench. Siderite nodules (<5mm in diameter) are abundant; pyrite concretions occur less often, and calcite commonly fills joints and cracks in the vitrain bands.

BENCH E averages 50cm in thickness, but it can be as thin as 35cm. In most cases it consists of durain, which occasionally has lustrous bands and a few bright coal stringers of less than 5mm thickness. At locality C, however, this sample contains mainly clarain, whereas at locality B only the topmost 5-10cm contains clarain. Mineral matter is rare, being predominantly associated with the clarain.

BENCH F varies between 40cm and 60cm in thickness. It has been distinguished at all localities except B, where it may possibly be included in the top 5-10cm of clarain in bench E. Sample F usually contains clarain and, in parts, vitrain. In some instances sandstone lenses up to 8cm thick are associated with this coal band, but they

Digitised by the Department of Library Services in support of open access to information, University of Pretoria, 2021.

have not been incorporated in the sample. Where sandstone lenses are present, the vitrain content of the bench is higher than in profiles where no clastic lenses occur. Pyrite concretions are common; siderite and calcite appear less often. At locality C, bench F contains mainly durain, with lustrous bands and bright coal stringers of less than 3mm thickness; these are mostly concentrated towards the top.

The width of the metamorphic aureole in the coal on either side of a dyke is generally +/-9m, but it can be as little as 4m, as at locality C. The transition from slightly burnt to completely unaffected coal is abrupt, or gradational over not more than 0.5m. The degree of visual burning of the coal decreases non-linearly from the dyke. Within about 1m of the contact the foliation and bedding planes of the coal are almost undistinguishable and the coal may be intensively drag-folded and brecciated, similar to features found by DAPPLES (1939) in thermally altered coals in Colorado. This deformation even affects the present coals at microscopic scale. Further away from the contact bright coal bands and stringers become visible, and eventually banding of lustrous and dull portions within the dull coal becomes discernible. Concomitantly the amount of fine-grained calcite on joint planes, especially in bright coal, decreases. Mechanical stress effects on the coal seam therefore decrease away from the intrusion; this is substantiated by fewer faults and slickensides and by wider spacing between the faults at greater distances from the dyke. Fault planes and slickensides generally dip away from the dyke and cause normal displacement of lithotype bands in the order of 10-30cm. Within about 50cm of the contact with the dyke the coal is very fractured and brittle.

6.2.1. Micropetrography of the Coals

Qualitative Results

A detailed description of the macerals in the unaltered coals has already been given in section 3.13. Here only their association with each other and with mineral impurities, as well as features due to the thermal metamorphism will be described.

In most samples a trimaceritic carbominerite predominates, with an intricate agglomeration of mainly low and high reflecting inertinites, some vitrinite and uncommon exinite. Other microlithotypes, such as clarite, durite and even vitrite occur rarely. In the vitrinite-rich coals, such as from bench D, the microlithotypes are more banded and mainly comprise vitrite, to a lesser extent bands of vitrinertite and trimacerite, but rarely clarite and durite.

Visible mineral matter predominantly comprises clay minerals and

Digitised by the Department of Library Services in support of open access to information, University of Pretoria, 2021.

quartz, which are enriched in the carbominerites. Clay minerals also occur in cell cavities of telinite or are interlayered with vitrinite. Siderite and pyrite are either finely dispersed or form framboidal agglomerations; they sporadically fill cell cavities in telinite and semifusinite. Carbonates, other than siderite, seldom fill cell cavities, but mostly joints and cracks in vitrinite. Closer to the dykes the amount of these carbonates increases.

Micrinite occurs in minor amounts in almost every sample. Strongly affected coals (closer than 4m to a dyke) rarely show micrinite. It is mostly associated with vitrinite, occasionally being finely dispersed, but generally filling cell cavities. Some semifusinite also hosts micrinite between cell fragments.

Exinite normally disappears within 4m of a dyke. It is reported to be the maceral group least resistent to thermal alteration (CRELLING and DUTCHER, 1968). In most seam benches, however, its reflectance already increases at more than 4m from the intrusion. In particular cutinite and resinite show an increase in reflectance at a greater distance than sporinite.

Apart from micrinite and exinite, vitrinite is also strongly affected by thermal metamorphism. Low reflecting inertinite alters to a lesser extent, but develops diffuse contours, a feature that corresponds to observations on fusinite and semifusinite by CRELLING and DUTCHER (1968).

Vitrinite devolatilizes and exhibits an increase in reflectivity at lower metamorphic grades (i.e. further away from the dyke) than low reflecting inertinite. Some unaltered coals appear partially affected, as they contain vitrinite of variable reflectance, some even resembling low reflecting inertinite. This makes the distinction of these two maceral groups rather difficult. In these cases, differentiation mainly relies on habit, association with types of inertinite and occasional devolatilization vesicles. Vitrinite and low reflecting inertinite appear to be more difficult to distinguish in thermally-altered coals than in gradually coalified coals of similar rank. Vitrinite-rich coals, especially from bench D, within 4m of the dyke, show a greater resemblance of vitrinite to low reflecting inertinite, and more coke-formation than the other coals. Occasionally, vitrinites with a slightly increased reflectance may already exhibit devolatilization vesicles.

Coke, which in this study is taken as any thermally-altered maceral containing devolatilization vesicles of any size, is mostly derived from vitrinite. It is thus more abundant in originally vitrinite-rich coal bands. Low reflecting inertinite, though reactive in technological coking processes (STEYN and SMITH, 1977), normally increases in reflectance but seldom develops pores during natural coke-formation of the present coals. Both mosaic textures and flow structures occur in the coke, especially in the samples at the

Digitised by the Department of Library Services in support of open access to information, University of Pretoria, 2021.

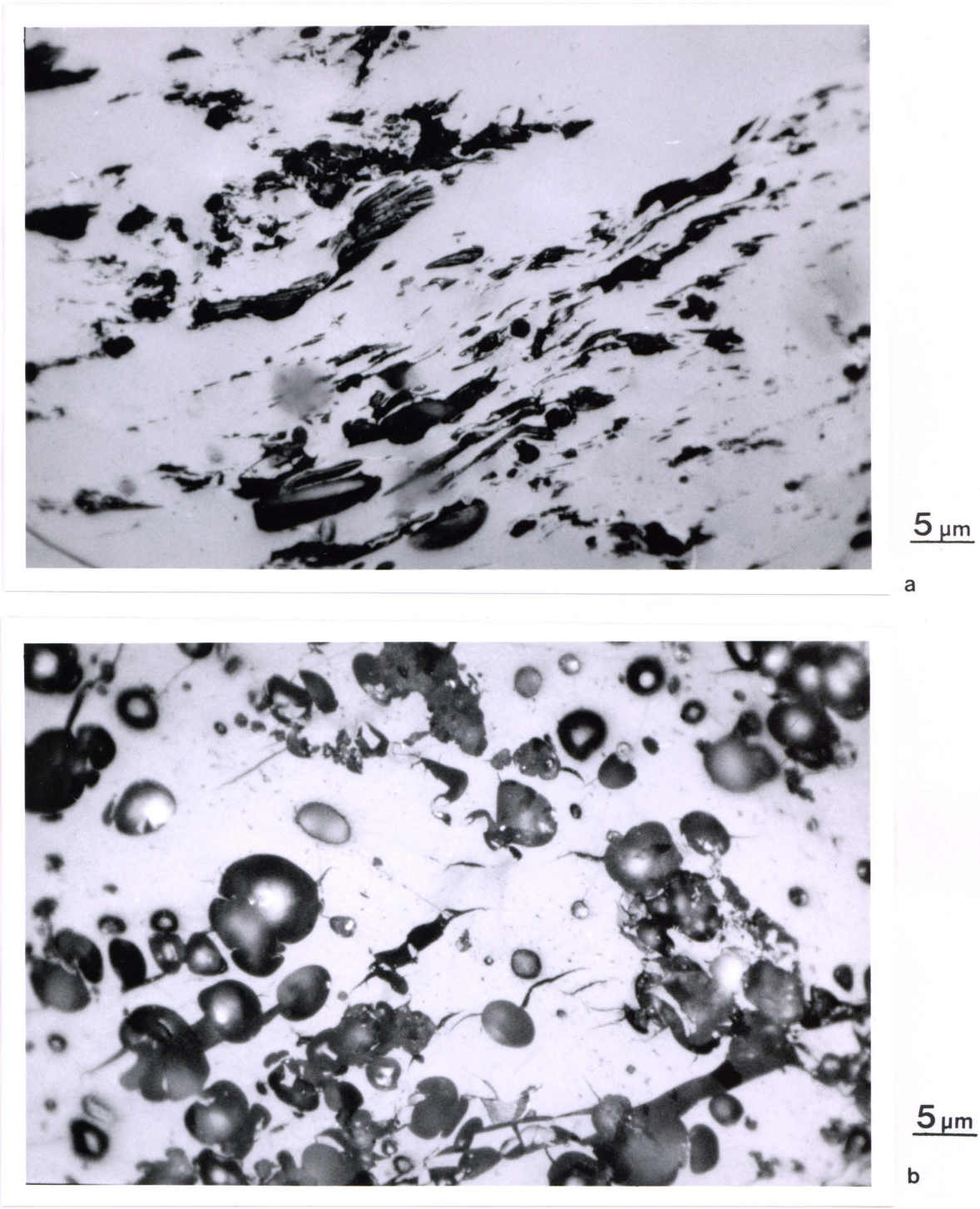


Fig. 6.2 Photomicrographs of coke from the contact (a) and from 4 m distance (b). The coke on the contact has compressed vesicles while coke from 4 m distance has open uncompressed vesicles. Both photomicrographs at 200 X magnification under oil immersion.

Digitised by the Department of Library Services in support of open access to information, University of Pretoria, 2021.

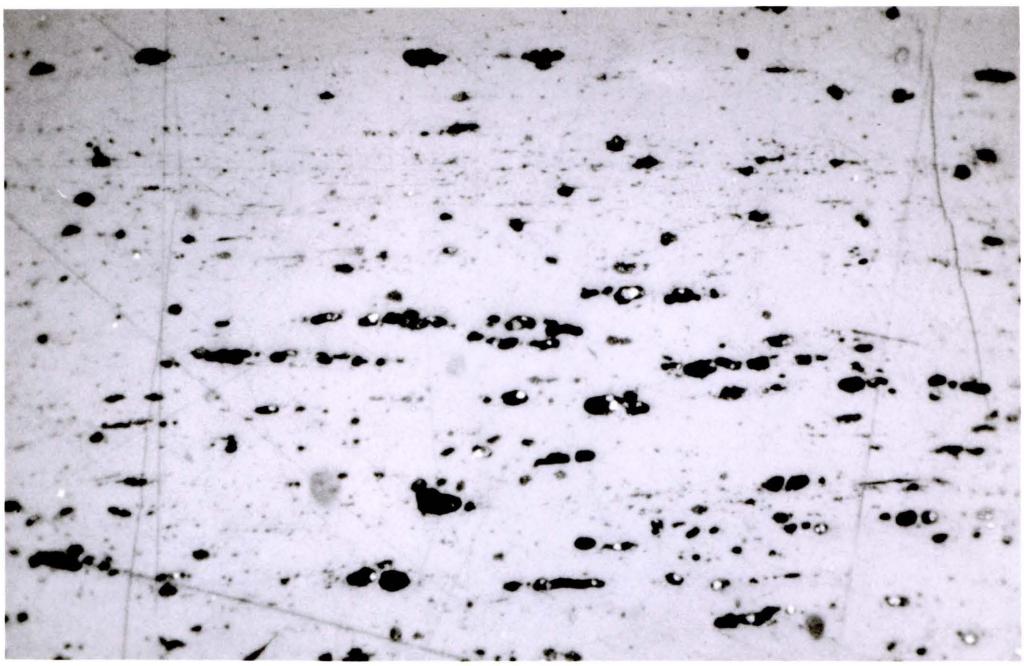


Fig. 6.3 Photomicrograph of devolatilization vesicles aligned in a "pearl string" manner, presumably along former bedding planes.

contact. Vesicles in the natural coke become larger with decreasing sampling distance from the intrusion. The vitrinite-rich coal bands tend to develop coke with large vesicles. However, vesicular coke predominates at a greater distance (2-4m) from the dykes and occurs less commonly in samples taken directly from the contact (Fig. 6.2). During early stages of devolatilization the vesicles often become aligned, in a "pearl-string" manner, along what appear to be former bedding planes (Fig. 6.3). They may already occur near the outer margin of the contact aureole. The devolatilization pores are generally vacant and not filled by secondary mineralization.

Quantitative Results

All the maceral analyses are given in appendix 5. The maceral composition of unaffected or only slightly affected samples (more than 10m from a dyke) is very consistent. Vitrinite generally ranges from 28% to 33%, low reflecting inertinite from 50% to 53%, high reflecting inertinite is fairly constant at about 14%, micrinite is below 1% and exinite between 1% and 2% (Table 6.2). Locality G is exceptional, mainly due to a lower vitrinite content and a consequently increased proportion of low reflecting inertinite.

Most conspicuously, bench D shows the highest vitrinite content (up to 70%), which is associated with the lowest percentages of low

Digitised by the Department of Library Services in support of open access to information, University of Pretoria, 2021.

Table 6.2 Average maceral composition of each seam bench, sorted by sampling localities. For localities **B**, **C** and **D** the average petrographic composition for cindered and for unaltered coals is given seperately.

LOCALITY B unaffected coals

bench	V %	LI %	HI %	M %	E %	
E	24.1	59.7	13.5	0.5	2.2	
D	70.6	19.3	9.1	0.1	0.9	
C	11.6	75.2	12.2	0.1	0.9	
B	22.8	56.3	19.2	0.2	1.2	
A	25.2	54.6	18.8	0.6	0.8	
average	30.9	53.0	14.6	0.3	1.2	total: 100.0%

LOCALITY B thermally-affected coals

bench	V %	LI %	HI %	M %	E %	C %	
E	9.3	69.9	9.0	0.0	0.0	11.9	
D	17.9	25.0	6.3	0.0	0.0	51.0	
C	1.0	81.8	11.1	0.0	0.0	6.1	
B	2.8	63.8	13.8	0.4	0.0	19.4	
A	7.9	67.5	9.0	0.3	0.0	15.4	
average	7.8	61.6	9.8	0.1	0.0	20.8	total: 100.1%

LOCALITY D unaffected coals

bench	V %	LI %	HI %	M %	E %	
F	52.4	35.6	9.5	0.2	2.3	
E	20.2	62.1	15.7	0.3	1.7	
D	65.8	25.3	7.8	0.0	1.0	
C	8.4	77.5	13.2	0.1	0.7	
B	17.4	65.8	15.5	0.6	0.6	
A	24.9	54.5	18.5	0.6	1.5	
average	31.5	53.5	13.4	0.3	1.3	total: 100.0%

LOCALITY D thermally-affected coals

bench	V %	LI %	HI %	M %	E %	C %	
F	43.1	41.6	11.9	0.1	0.1	3.1	
E	17.2	62.2	14.9	0.0	0.1	5.7	
D	43.8	30.1	6.2	0.0	0.1	19.7	
C	5.5	73.9	18.1	0.6	0.0	1.9	
B	10.7	67.7	16.3	0.7	0.1	4.5	
A	15.4	66.8	15.4	0.4	0.0	2.1	
average	22.6	57.0	13.8	0.3	0.1	6.2	total: 100.0%

LOCALITY C unaffected coals

bench	V %	LI %	HI %	M %	E %	
F	17.6	61.7	18.1	0.2	2.5	
E	37.3	44.2	15.6	0.1	2.8	
D	69.4	19.7	9.1	0.0	1.7	
C	6.4	78.5	13.7	0.3	1.0	
B	12.6	69.2	16.3	1.2	1.8	
A	27.3	54.2	15.8	0.7	2.0	
average	28.4	54.6	14.8	0.4	2.0	total: 100.2%

LOCALITY C thermally-affected coals

bench	V %	LI %	HI %	M %	E %	C %	
F	10.6	64.3	10.6	0.0	0.0	14.5	
E	8.2	69.9	7.7	0.0	0.0	14.3	
D	35.0	35.1	10.0	0.0	0.0	19.9	
C	4.0	78.6	16.2	0.5	0.2	0.5	
B	7.0	72.7	16.7	0.0	1.0	2.7	
A	20.8	55.0	21.5	0.9	1.4	0.6	
average	14.3	62.6	13.8	0.2	0.4	8.8	total: 100.1%

LOCALITIES E-F-H

bench	V %	LI %	HI %	M %	E %	
F	39.7	43.7	13.7	0.3	2.6	
E	21.0	63.3	12.8	0.7	2.1	
D	70.2	19.8	8.3	0.1	1.5	
C	16.6	70.0	12.0	0.4	1.0	
B	24.9	55.7	17.5	0.9	0.9	
A	26.9	50.5	19.8	0.5	1.6	
average	33.2	50.5	14.0	0.5	1.6	total: 99.8%

LOCALITY G

bench	V %	LI %	HI %	M %	E %	
F	19.0	66.8	11.8	0.3	2.3	
E	8.3	76.0	12.3	0.5	2.5	
D	23.0	65.5	9.5	0.0	2.0	
C	7.8	75.3	15.3	0.0	1.8	
B	16.8	67.8	13.0	0.5	2.0	
A	18.8	65.8	10.5	1.8	3.0	
Z	33.5	51.3	12.5	0.8	1.8	
average	18.2	66.9	12.1	0.6	2.2	total: 100.0%

V=vitrinite; LI=low reflecting inertinite; HI=high reflecting inertinite; M=micrinite; E=exinite; C=coke;

and high reflecting inertinites (about 20% and 9%, respectively). Lithotype bands B and C generally have the lowest vitrinite contents, with C normally less than B, accompanied by the highest percentages of low reflecting inertinite (Fig. 6.4). High reflecting inertinite appears to be the least variable group of macerals in all seam benches (samples A to F) (see also section 3.13). Lithotype bands A, E and F contain intermediate amounts of vitrinite, with F normally having the highest, up to 50 % (Table 6.2).

Micrinite maintains very low values, especially in benches C and D. This is notable for bench D, in view of the fact that in the present coals micrinite is normally associated with vitrinite. Bench B often contains the highest amounts of micrinite (up to 1.2%).

At sampling locality G the proportions of both vitrinite and low

Digitised by the Department of Library Services in support of open access to information, University of Pretoria, 2021.

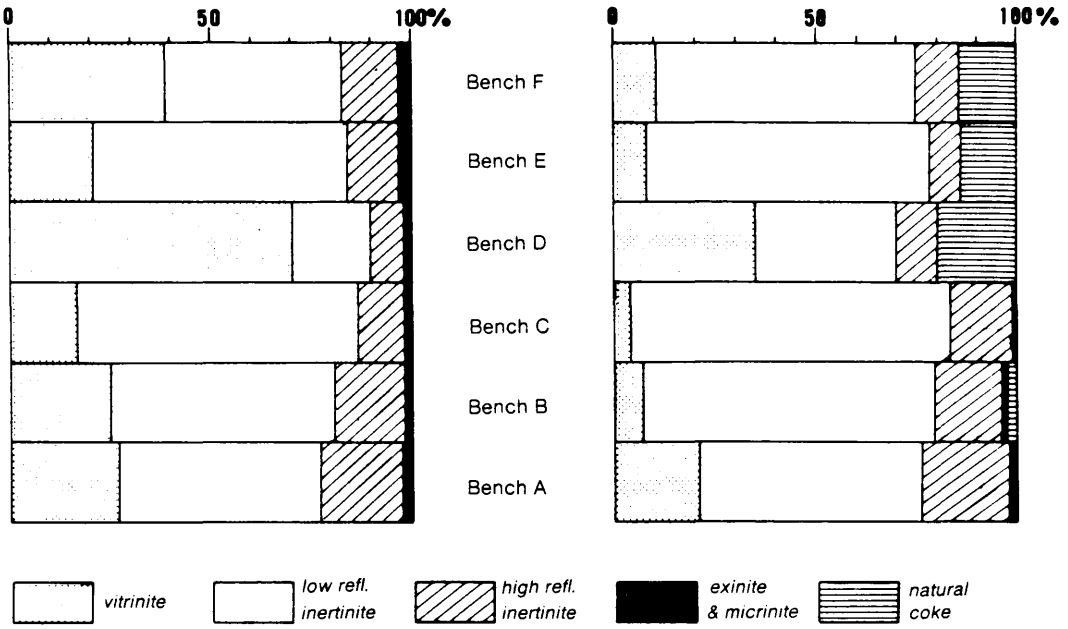


Fig. 6.4 Average maceral composition of unaltered coals (left) and of thermally metamorphosed coals (right) at sampling locality **C**.

reflecting inertinite from any one coal bench relative to another is comparable to those of the other channels. The petrographic results thus support the macroscopic correlation of the lithotype bands at locality G with those at other localities and also the introduction of an additional sample, Z, at the bottom of channel G.

Although the overall maceral composition of coal is not generally dependent on rank (STACH et al., 1982), some significant changes occur with increasing grade of thermal metamorphism. Most obvious is the sharp decline in vitrinite content, together with the appearance of coke particles. The sum of vitrinite and coke approximates the original vitrinite percentage in the unaffected coals of a respective seam bench, which indicates that most of the natural coke is derived from vitrinite. However, some low reflecting inertinite might also form coke and some vitrinite may only increase reflectivity, thus resembling low reflecting inertinite. This in turn will lead to misidentifications, and subsequently to a slight increase in determinations of low reflecting inertinites, in the thermally-altered coals. High reflecting inertinite contents show insignificant changes, which lie within the limits of experimental error.

Therefore, most changes in maceral composition of thermally metamorphosed coals as compared to their unaltered counterparts of the same lithotype band, are due to subjective errors and to the formation of natural coke from vitrinite. Decreases in micrinite and exinite contents, however, are absolute changes caused by their partial thermal alteration (CRELLING and DUTCHER, 1968; STACH et al., 1982). Exinite is the first maceral group to disappear, due to its increasing resemblance to vitrinite and inertinite during thermal and regional (normal) coalification (STACH et al., 1982). It will, therefore,

Digitised by the Department of Library Services in support of open access to information, University of Pretoria, 2021.

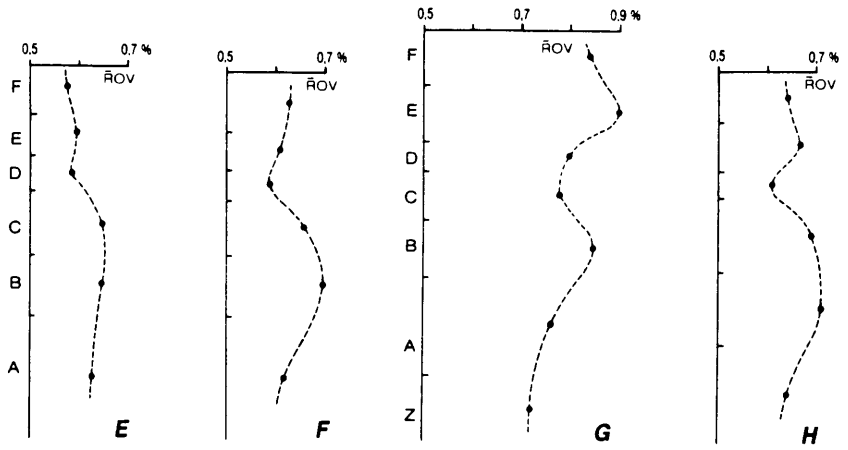
become unrecognizable by ordinary microscopic techniques. Both micrinite and exinite can thus be expected to increase determinations of low reflecting inertinite, and to a minor extent also those of high reflecting inertinite.

Generally, the thermal alteration of the maceral composition due to the formation of natural coke is most pronounced at locality B and least noticeable at D (Table 6.2). This change shows similar tendencies in each lithotype bench (Appendix 5).

6.3. Vitrinite Reflectivity

The average rank of the thermally-unaffected coal at Twistdraai is 0.67% $\bar{R}$OV, as determined from channels E-F-H and B32, C36 and D32, which are situated far away from dolerite intrusions (Table 6.3). This places the coal in the rank of high volatile bituminous B coals, or the "Flammkohlen".

In the unaltered coals the $\bar{R}$OV of samples from one channel normally varies over two V-classes, from V5 to V7 and in exceptional cases over three V-classes, up to V8 (Table 6.3; Fig. 6.5). The means of samples B and C are between one half and one V-class higher than those of the other samples in the same channel; sample D has the lowest mean random reflectivity in each respective channel. In general, coals of the lower three benches have a reflectance of



LEGEND

---•--- *mean R̄OV per sample*

A — F *seam benches*

Fig. 6.5 V-class distribution of samples of unaffected coals from channels **E**, **F**, **G** and **H**.

Digitised by the Department of Library Services in support of open access to information, University of Pretoria, 2021.

Table 6.3 Mean vitrinite reflectivity (%ROV) per bench and per channel.

bench / channel	Z	A	B	C	D	E	F	average per channel random ROV	average per channel max ROV
B 0		5.37	5.57	5.64	5.58	5.30			5.49
B 2		2.68	3.51	2.95	2.72	2.41			2.85
B 4		1.99	2.03	2.00	1.77	1.82			1.92
B 8		1.17	1.10	1.07	0.85	0.78		0.99	
B10		0.82	0.84	0.82	0.67	0.65		0.76	
B16		0.63	0.64	0.68	0.53	0.57		0.61	
B32		0.67	0.73	0.69	0.59	0.58		0.65	
C 0		4.84	4.79	4.60	5.00	4.89	4.99		4.85
C 2		1.29	1.84	2.23	2.48	2.76	2.97		2.26
C 4		0.89	0.97	1.31	1.08	2.24	1.46		1.33
C 8		0.76	0.83	0.87	0.67	0.75	0.76	0.77	
C20		0.80	0.78	0.86	0.70	0.71	0.74	0.77	
C36		0.79	0.78	0.84	0.71	0.77	0.77	0.78	
D 0		5.75	6.53	5.79	5.75	5.60	3.95		5.56
D 2		2.23	2.58	3.62	2.53	2.36	1.77		2.52
D 4		1.06	1.00	1.02	0.90	0.87	0.76	0.94	
D 8		1.32	1.41	1.36	1.38	0.83	1.10		1.23
D10		0.73	1.06	0.92	0.93	0.77	0.69	0.85	
D16		0.70	0.75	0.75	0.64	0.77	0.70	0.72	
D32		0.65	0.68	0.76	0.61	0.65	0.62	0.66	
E		0.63	0.65	0.65	0.59	0.60	0.58	0.61	
F		0.62	0.70	0.66	0.59	0.61	0.63	0.64	
G	0.72	0.76	0.85	0.78	0.80	0.90	0.84	0.81	
H		0.64	0.71	0.69	0.61	0.67	0.64	0.66	

approximately half a V-class higher than those in the top benches; this is especially noticeable in channels B32, C36 and D32 (Fig's. 6.6, 6.7 and 6.8).

Within a single sample of the unaffected coals the reflectogram usually spans three V-classes and rarely four. In the latter case one of the extreme classes (lower or upper) is then normally represented by only 5% of the measurements. Reflectograms of bench D samples often occupy only two V-classes. This is attributed to their relatively high vitrinite content, thus allowing a sufficiently large number of vitrinite grains with no impurities to be measured (Appendix 6).

As in the petrographic analysis, samples from locality G are exceptional in that the reflectivity profile shows the highest values amongst the unaffected coals, with 0.81% $\overline{R}OV$. The coals in the top benches of channel G also tend to have a higher rank than those in the lower benches (Fig. 6.5).

Up to about 8m towards the dolerite dykes the average rank per channel first increases slightly to 1-1.2% $\overline{R}OV$. Closer to the contact, a rapid increase in rank finally results in reflectivities of above 5.5% $\overline{R}OV_{max}$ (localities B and D), giving these cindered coals characteristics of anthracitic and meta-anthracitic coals (Fig. 6.6 and 6.8). Similar reflectivity increases at intrusions into low rank coals are reported by KHORASANI (1983).

Digitised by the Department of Library Services in support of open access to information, University of Pretoria, 2021.

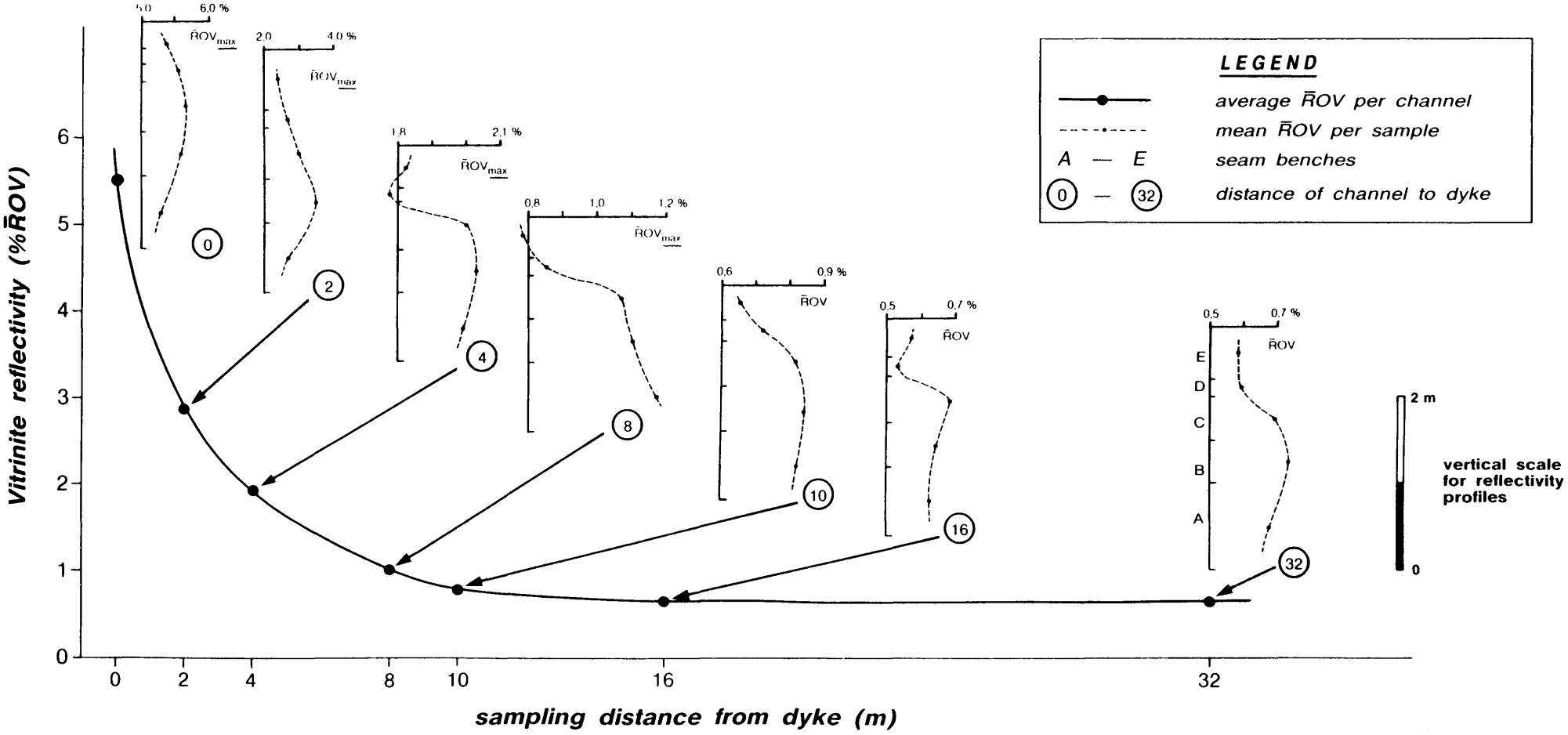


Fig. 6.6 Diagram illustrating the increase in average vitrinite reflectivity per channel at sampling locality **B**. Inset diagrams show reflectivity profiles of each channel.

Digitised by the Department of Library Services in support of open access to information, University of Pretoria, 2021.

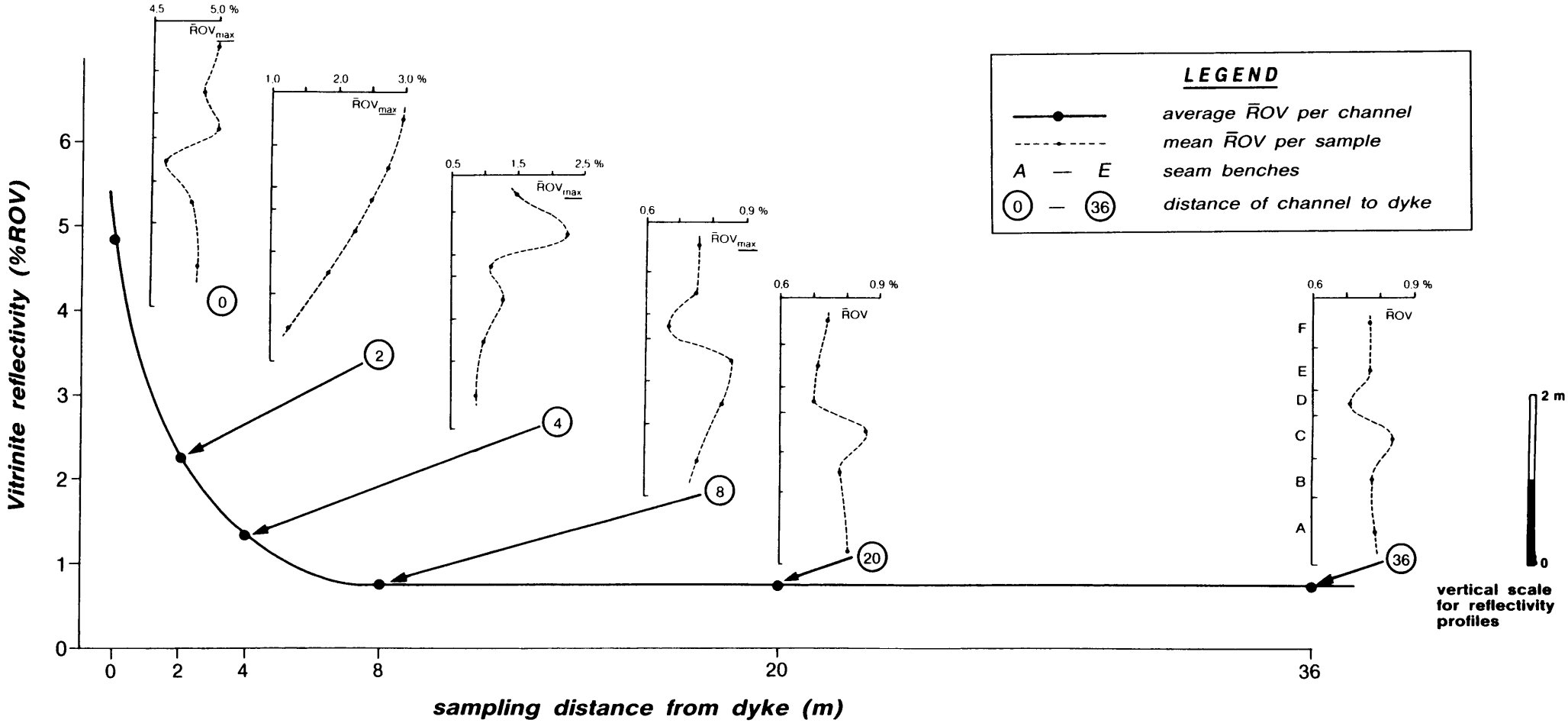


Fig. 6.7 Diagram illustrating the increase in average vitrinite reflectivity per channel at sampling locality **C**. Inset diagrams show reflectivity profiles of each channel.

Digitised by the Department of Library Services in support of open access to information, University of Pretoria, 2021.

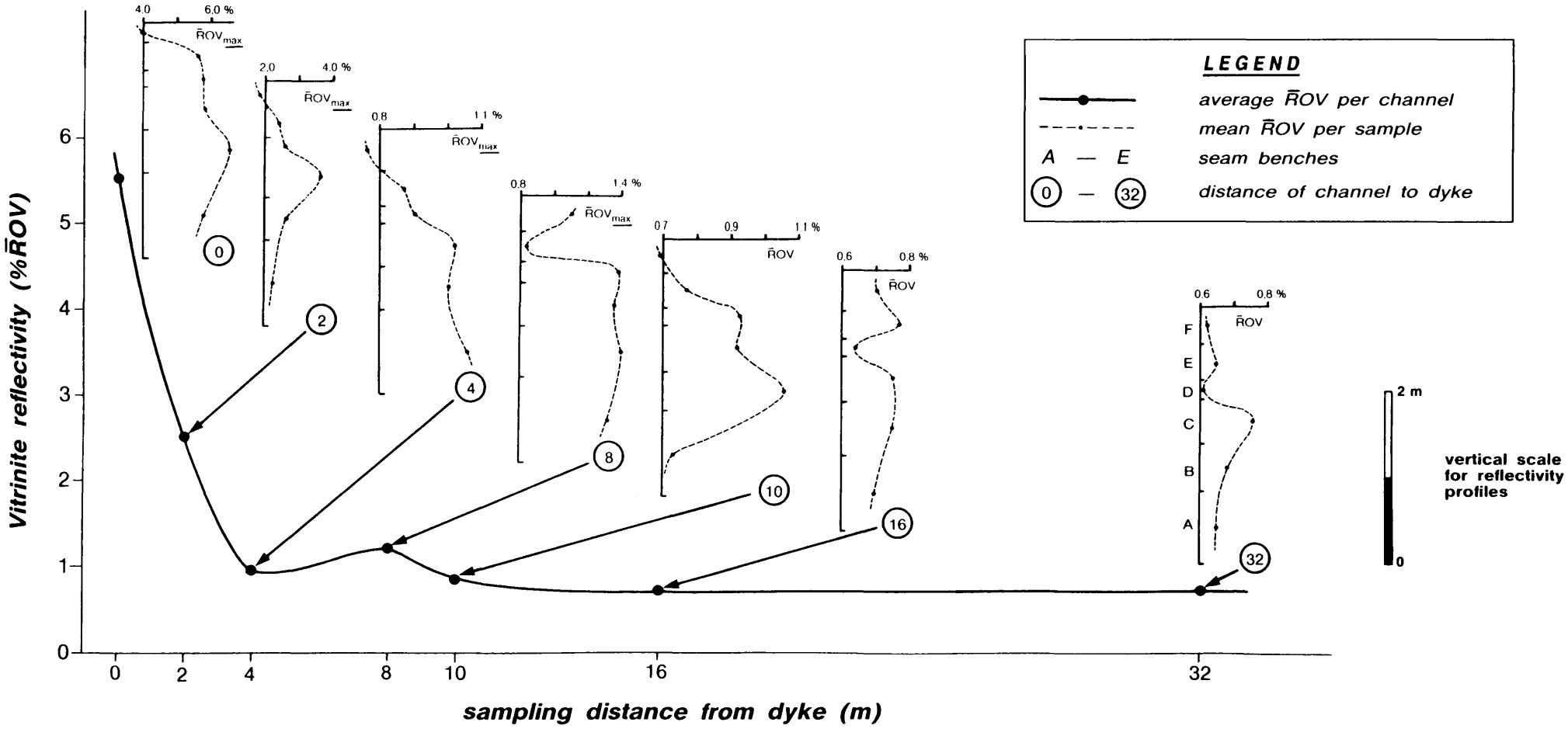


Fig. 6.8 Diagram illustrating the increase in average vitrinite reflectivity per channel at sampling locality **D**. Inset diagrams show reflectivity profiles of each channel.

Digitised by the Department of Library Services in support of open access to information, University of Pretoria, 2021.

At locality C the rapid increase in reflectivity occurs at a shorter distance from the contact than at locality B, reaching a maximum of 4.85% $\overline{R}OV_{max}$ on the contact. This is in agreement with the observation that the metamorphic aureole is narrower at locality C than at locality B (section 6.1). At locality D the rank increase is not as continuous as at the others, being interrupted by a minimum of 0.94 % $\overline{R}OV_{max}$ at the 4m channel (Fig. 6.8).

Differences in rank of one or more V-classes at localities E, F and H occur amongst the samples of one channel. Close to the intrusions, the coal from the basal benches is normally of higher rank than those from the top ones. These rank differences become continously larger towards the dyke, until they reach eight V-classes between top and bottom in the 2m channel at locality B (Fig. 6.6). Reflectivity profiles at locality D exhibit similar trends, but are irregular, especially in the 2m and 10m channels, where the coal in the top and the bottom benches has a relatively low rank. The highest reflectances are in benches B, C and D (Fig. 6.8). At locality C higher reflecting vitrinite occurs in the bottom benches of channels C36, C20 and C8, but in channels C4 and C2 the situation is reversed and the upper seam layers become higher reflecting with a range of up to ten V-classes (Fig. 6.7).

At the dyke/coal contact all seam benches generally appear to be of fairly similar rank, especially at locality C. At locality B the reflectivity profile is symmetrical from top to bottom, with the central portion (bench C) being of the highest rank. However, at locality D there is still a definite decrease in rank towards the top of the 0m channel, especially for seam bench F (Fig. 6.8).

With increasing rank the reflectograms of each sample can become as wide as ten V-classes, or even more. They may also become bimodal, as for channel C4 (Fig. 6.9), which lies just at the margin of the metamorphic aureole. Towards the top of the seam in this channel, however, the aureole is more intense (2.24% and 1.46% $\overline{R}OV_{max}$ for benches E and F, respectively) and its lateral extent probably increases to about 10m from the dyke (Fig. 6.7). In channel C4, samples C and F are clearly bimodal and sample B is skewed towards the higher V-classes. The reflectograms of samples A, D and E have a normal distribution, with a high mean for E. With the exception of E, the samples in channel C4 have their lower distribution peaks on the reflectograms between 0.9% and 1.3% $\overline{R}OV_{max}$; the higher peaks for samples C and F are at about 1.5% $\overline{R}OV_{max}$. The $\overline{R}OV_{max}$ of normal distribution for sample E corresponds with the $\overline{R}OV_{max}$ of a third, minor reflectogram peak in sample F. It is also noteworthy that the coal of bench D is almost as low reflecting as in bench A , in spite of the fact that benches C and E consist of coals of a higher rank.

In some samples close to a dyke the vitrinites may already show some devolatilization pores in spite of a relatively low $\overline{R}OV_{max}$ (such

Digitised by the Department of Library Services in support of open access to information, University of Pretoria, 2021.

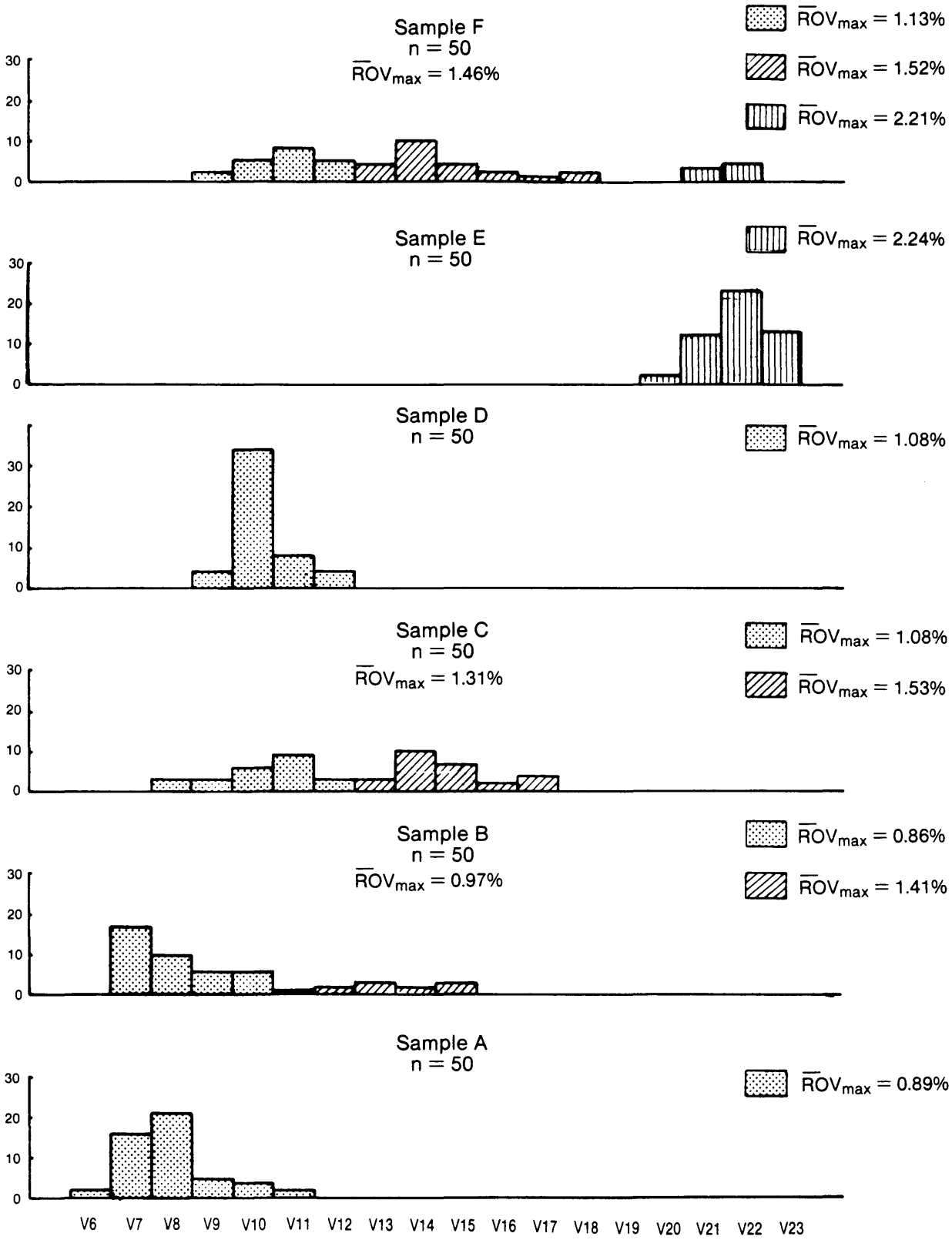


Fig. 6.9 Reflectograms of each sample form channel **C4**, which illustrates the wide range and bimodal distribution of reflectivity values in the samples of this channel, due to partial metamorphism.

Digitised by the Department of Library Services in support of open access to information, University of Pretoria, 2021.

as C2A with 1.29%). In comparison to the strongly devolatilized coal on the dyke contacts, this vitrinite has small pores, which only occupy a minor proportion of the observed surface.

6.4. Proximate Analyses

To prevent repetition, not all the results of the proximate analyses will be dicussed in detail and only general trends will be outlined. Results from selected channels or samples will be emphasized in order to highlight certain metamorphic effects of the dolerites at different localities and to demonstrate the inter-relationships of chemical parameters. The fixed carbon content will not be dealt with as it is determined by difference; thus only the other values of the proximate analyses are used for the characterization of the coal. All the analytical results are listed in appendix 7.

MOISTURE content generally ranges from 4.5% to 6.0% in coals that are unaffected by dykes (localities E-F-G-H). Although moisture is largely dependent on rank (STACH et al., 1982, p40), there is a noticeable correlation in this study between the moisture content and the type of the coal. Seam benches A, B and C tend to have noticeably higher amounts of moisture, whereas the moisture content of D normally lies at the lower end of the range (Fig. 6.10). This is attributed to the higher microporosity of inertinite compared to that of vitrinite, so that the inertinite-rich coals have a higher moisture absorption capacity than the vitrinite-rich coals. Lithotype bands E and F are intermediate in both maceral composition and moisture content.

These trends are consistent up to the outer limit of the contact aureole around dykes: 10m at locality B, 8m at locality C and 16m at locality D. These limits correspond to major changes in the ROV. Inside the aureole towards the dyke, the moisture content is largely dependent on the rank of the coal and is inversely related to the vitrinite reflectivity. On the dolerite/coal contact the moisture content ranges from 2-4%, with the greatest variation at locality C. A close correspondence between %ROV and moisture in individual seam benches is noticeable (Figs. 6.6, 6.7, 6.8 and 6.10); for instance benches A and B of channel C4 are considerably higher in moisture than E and F, owing to a marked increase in rank in the two top benches of this channel (section 6.3). Similarly, benches A, E and F of channel D10 are higher in moisture and lower in rank than the other three samples of the same channel.

In some instances, especially at localities C and D, there is a pronounced increase in moisture content from the 2m channel to the

Digitised by the Department of Library Services in support of open access to information, University of Pretoria, 2021.

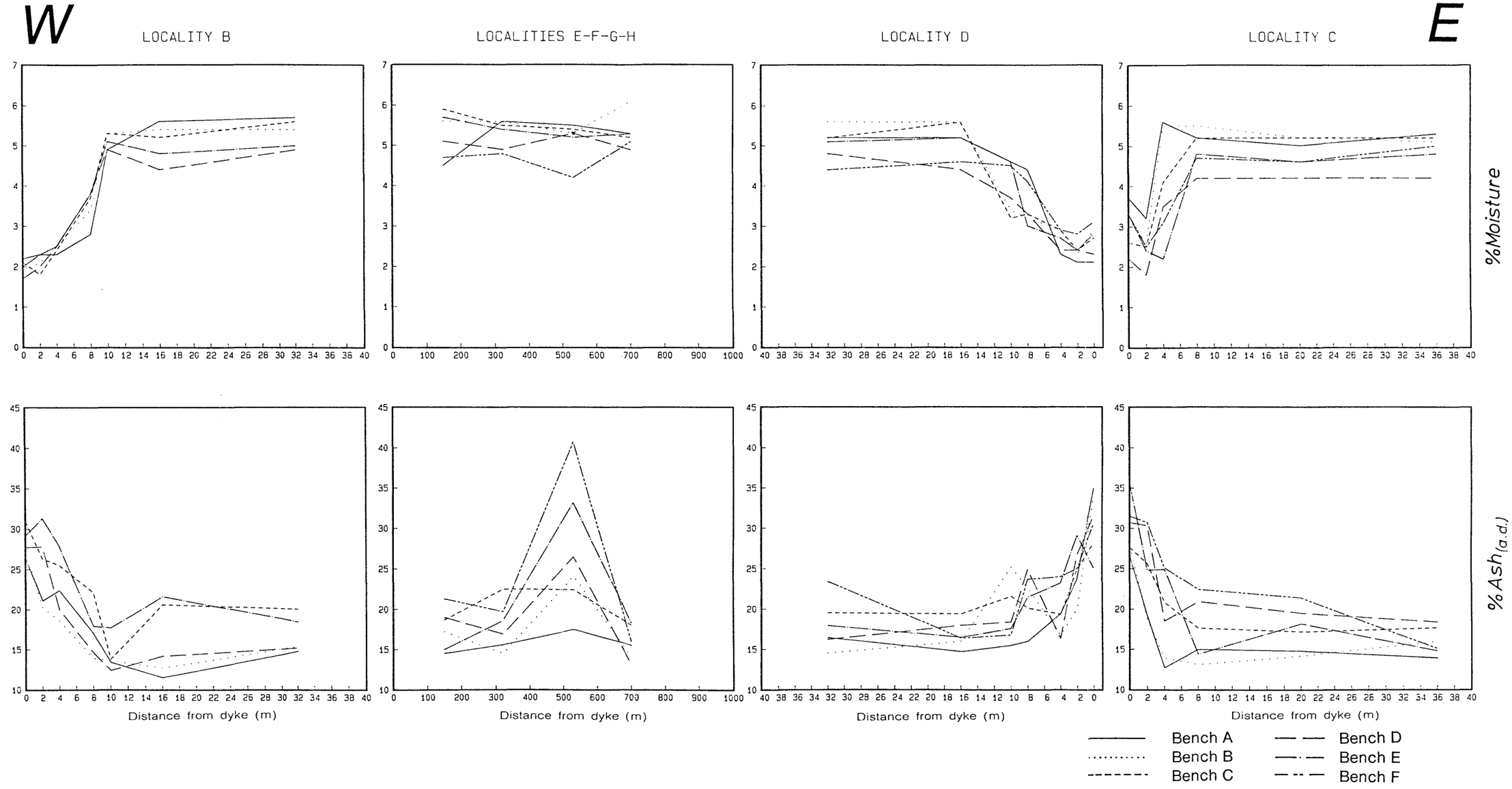


Fig. 6.10 Moisture and ash (a.d.) contents of unaffected and of metamorphosed coals in an east-west cross-section through all sampling localities (compare figures 2.2 and 2.3 for localities).

Digitised by the Department of Library Services in support of open access to information, University of Pretoria, 2021.

0m channel. This is, on the one hand, attributed to an increase in porosity due to natural coke-formation, and on the other hand, to an increased porosity in anthracitic coals (STACH et al., 1982, p41&46).

The **ASH** content generally ranges from 13% to 23%(a.d.) in the unaffected coals. However, at locality G, the ash content of all the benches is considerably higher (17-40%) than that of the corresponding seam benches elsewhere (Fig. 6.10). Apart from that, a slight regional trend of lower ash content from west to east can be recognized in benches B, D and F. In the other seam layers the ash content increases slightly in the same direction, or remains constant. The ash values of the seam benches generally maintain their relative values within the same channel. Samples A and B tend to contain the least ash, whereas C often exhibits the highest values. In the case of the latter the high ash content is related to a predominance of low reflecting inertinite and its deposition as detrital material (section 4.12).

The high ash content of the D-bench in most channels is due to the common occurrence of torbanite and torbanitic shale lenses within this lithotype band. Benches E and F contain variable amounts of ash, which depend on the occurrence of clastic lenses and the localized gradual transition to roof material.

In the proximity of dolerites the general ash trends noted above persist up to the margin of the aureole as defined by the rank parameters. Then there is an increase in ash of up to 25-35%(a.d.) at the contacts. As with the moisture content, the ash shows the smallest variation at locality B. The changes in ash content in a single lithotype band are generally more continuous at the other localities. That of benches E and F is the most erratic.

The **CARBON DIOXIDE** content, derived from carbonate minerals in the coal, normally ranges from 0% to 5%. In most channels benches A, B and C tend to have higher amounts of CO_2 than D, E and especially F. This is even more pronounced in channel samples of cindered coal (Fig. 6.11). At localities B and C, CO_2 content has a narrower range than at locality D. In this latter case there is an increase to about 16% CO_2, from approximately 8m away, towards the contact. The range of CO_2 content becomes wider towards the dykes and may increase drastically, especially in benches A, B and C; benches E and F contain relatively little CO_2 and sample D is intermediate and variable.

The **VOLATILE MATTER** content is consistently erroneously high, due to the CO_2 contamination. Although this is relatively unimportant in samples that are not affected by dolerites, CO_2 was determined on all samples and the volatile matter content was corrected according to formula (1) in section 2.7.5, to obtain comparable results for all coals. The effect of CO_2 on the volatile matter (d.a.f.) is

Digitised by the Department of Library Services in support of open access to information, University of Pretoria, 2021.

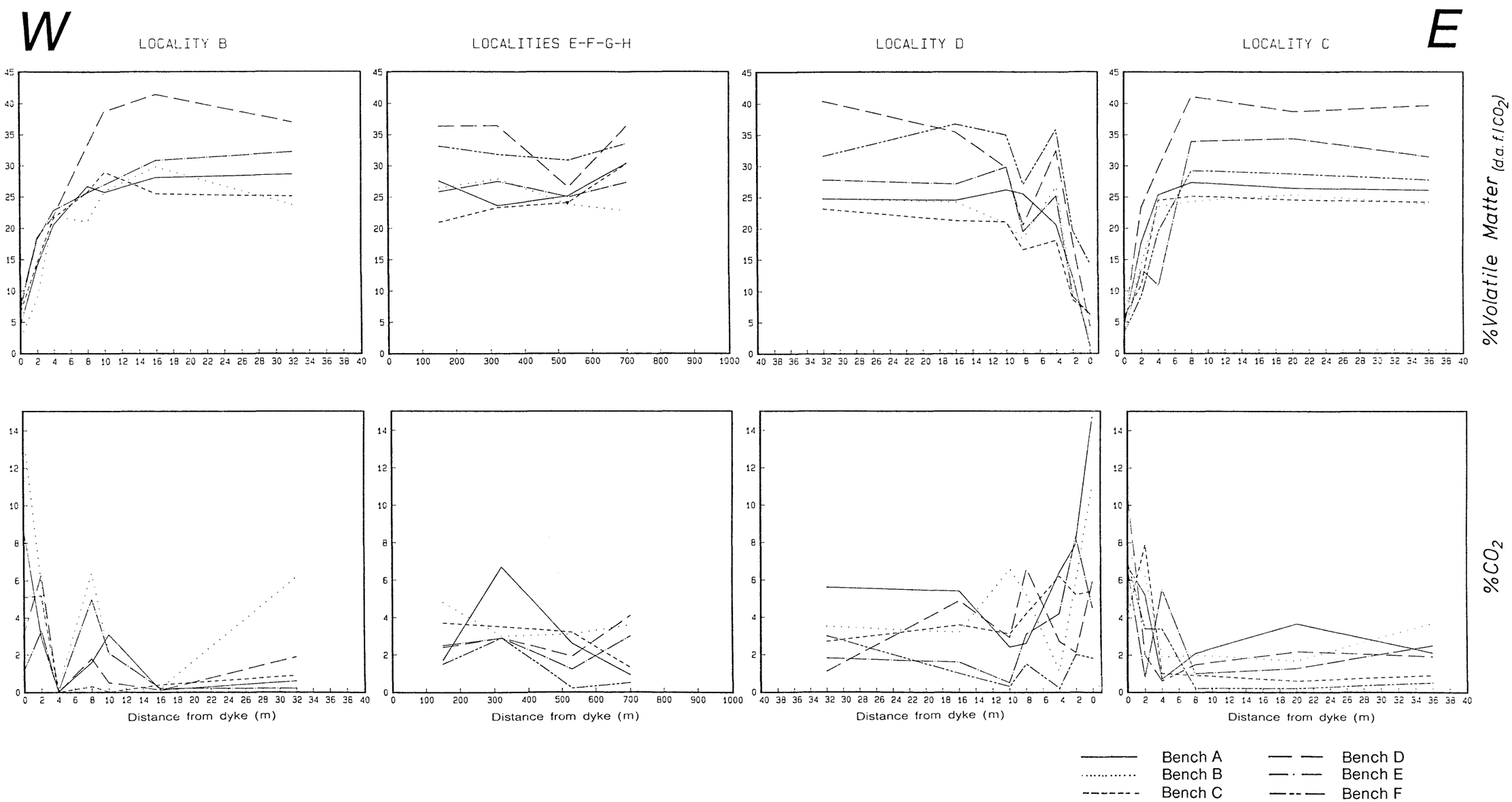


Fig. 6.11 Volatile matter (d.a.f. / CO_2) and CO_2 contents of unaffected and of metamorphosed coals in an east-west cross-section through all sampling localities (compare figures 2.2 and 2.3 for localities).

Digitised by the Department of Library Services in support of open access to information, University of Pretoria, 2021.

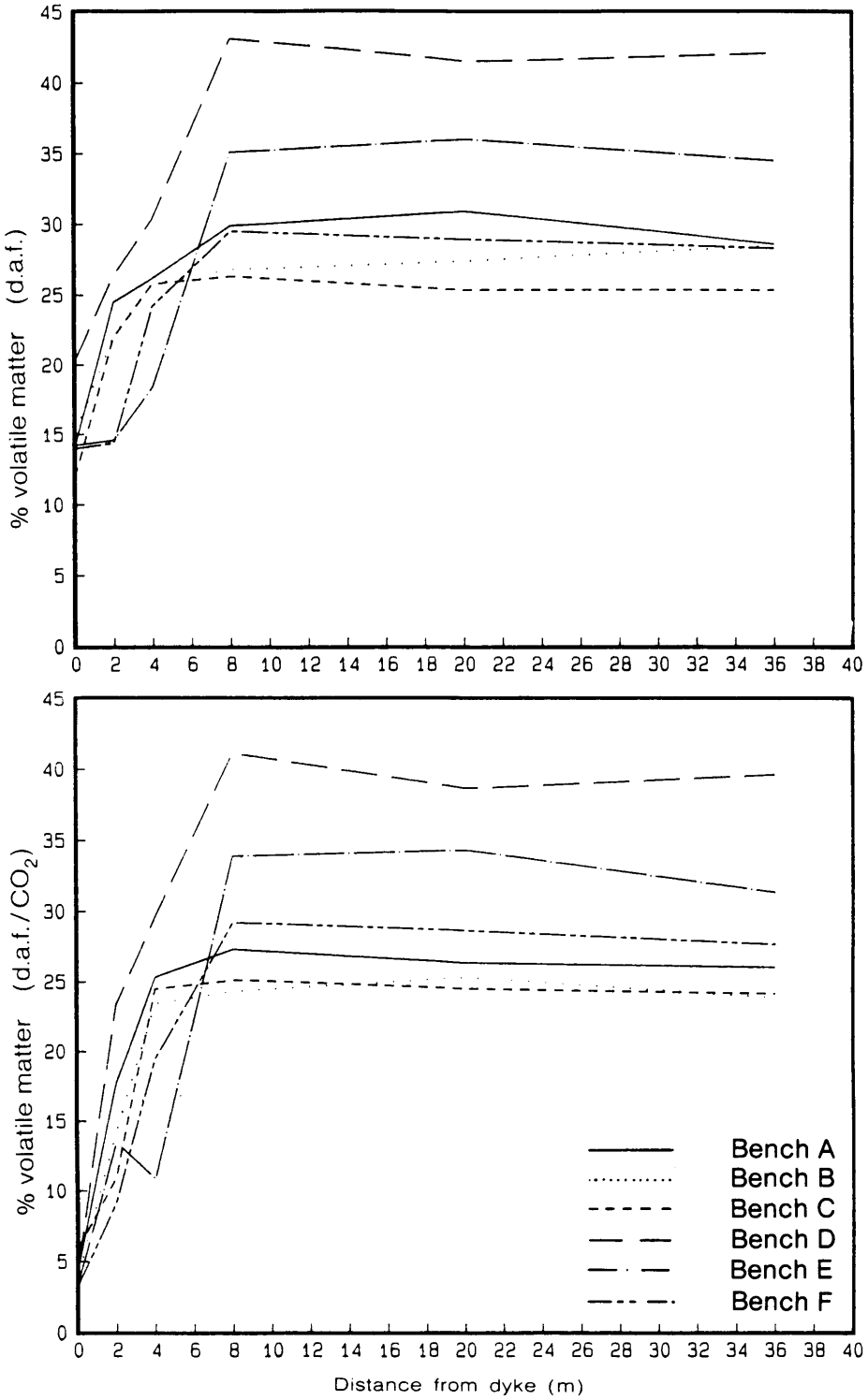


Fig. 6.12 A comparison of the volatile matter (d.a.f.) content without correction for CO_2 (upper diagram) and with the correction (lower diagram) for unaffected and metamorphosed coals at locality **C**.

Digitised by the Department of Library Services in support of open access to information, University of Pretoria, 2021.

demonstrated in figure 6.12, with sampling locality C as an example. After correction for CO_2 the volatile matter content in the cindered coals decreases considerably. Therefore, only CO_2-corrected volatile matter (d.a.f.) will be discussed.

In general the volatile matter content varies from about 20% to more than 40% in unaltered coals, depending on the maceral composition (Fig. 6.11). The volatile matter content is also affected to a lesser extent by the reflectivity. Differences in volatile matter content due to grade, and more specifically due to clay mineral content, are not considered important for the present coals, in view of the correction for CO_2.

Coals from benches A, B and C always have volatile matter contents in the lower range, generally between 20% and 27%, whereas the D-sample in all channels generally contains the highest amounts of volatile matter (approx. 40%). Benches E and F normally contain intermediate amounts. The extremely high values of the vitrinite-rich coals in bench D are attributed to the fact that the vitrinite group macerals generally contain more volatile matter than the inertinites, in coals of the same rank (SNYMAN et al., 1983). In a corresponding trend, the D-samples mostly contain the lowest reflecting coals of each channel, whereas the lower benches tend to have higher reflectances in the reflectivity profiles (Figs. 6.6, 6.7 and 6.8). The intermediate volatile matter content of benches E and F corresponds to marginally lower reflectance values in these coals, although their maceral composition is comparable to those of A and B.

These trends persist up to the margin of the aureole of the intrusions at channels B10, C8 and D16. Closer to the dykes the volatile matter content of all seam layers decreases drastically, to below 10% at the contact. The relative values of the benches, from any one channel to the next, are generally persistent (Fig. 6.11). Samples E and F in channel C4 are exceptional in being considerably lower in volatiles than the other samples of the same channel. This correlates with the patterns of reflectance and moisture. The vitrinite-rich bench D shows the strongest relative and absolute decrease in volatile matter and also at a greater distance from the dolerite contact. The reflectivity and volatile matter content of the vitrinite thus approaches those of inertinite, especially of low reflecting inertinite. This corresponds with the findings of VAN KREVELEN (1961, p267) regarding the coking properties of macerals, namely that vitrinite has a higher devolatilization rate than micrinite and other inertinite.

In channel D4 volatile matter content is anomalously high compared to channel D8, for all samples with the exception of A (Fig. 6.11). This concurs with the reflectance profiles of these two channels (Fig. 6.8). VAN VUUREN and QUASS (1982) reported a similar enrichment of volatile matter at a certain distance from an intrusion,

Digitised by the Department of Library Services in support of open access to information, University of Pretoria, 2021.

probably due to the entrapment of tars and volatiles which were distilled off closer to the contact.

6.5. Ultimate Analyses

The results of ultimate analyses (C, H, N and S) will be dealt with in a similar, generalized way as were the proximate analyses. Because the values depend on coal type and rank, they will be discussed in terms of maceral composition and $\overline{R}OV$; cross-references will be made to the proximate analyses. The oxygen content, which is determined by difference, is not very meaningful, particularly as a result of the variable sulphur content. All results are listed in appendicies 8 and 9.

The **CARBON** content is influenced by the presence of carbonate minerals in the coal. Calculation of the carbon content (d.a.f.) should therefore take the CO_2 content into account (section 2.7.5). The effect of this correction is demonstrated in figure 6.13, which shows that the C-content generally increases in all samples; in addition, the relative changes from uncorrected to corrected %C (d.a.f.) are more pronounced in the cindered coals.

In table 6.4 the %C (d.a.f.), the CO_2-corrected %C (d.a.f.) according to BS1016 and according to the extended formula (section 2.7.5), are compared with the carbon content of normally coalified coal at the respective reflectances (TEICHMÜLLER, 1971). The percentage carbon according to the BS1016 correction is always lower than the percentage carbon according to TEICHMÜLLER (1971), but the percentage carbon, corrected according to formula (3), is generally within TEICHMÜLLER's range. A slightly lower carbon content in contact

Table 6.4 Five selected sample analyses, showing the effect of different methods of correction of % carbon (d.a.f.) for CO_2. In the last column a comparison is given for % carbon (d.a.f.) of coals of the same rank, but through normal coalification (after TEICHMÜLLER, 1971).

sample No.	ROV %	%ash& moist	%CO_2	%C(ad)	%C(daf)	%C(daf)* CO_2 corr	%C(daf)** CO_2 corr	%C(daf)*** range
B0A	5.37	28.5	8.6	63.66	89.03	85.75	93.82	91-94.5
B2E	2.41	33.6	3.3	54.92	82.71	81.35	84.13	89-93
C0A	4.84	30.2	6.7	61.50	88.11	85.49	91.63	91-94.5
D2A	2.23	25.8	7.9	63.46	85.53	82.61	89.71	88.5-92.5
D2C	3.62	27.3	5.2	62.86	86.46	84.51	89.15	91-94

* CO_2 correction after BS1016
** CO_2 correction after formula (3) (section 2.7.5)
*** range of carbon content at respective rank (after TEICHMÜLLER, 1971)

Digitised by the Department of Library Services in support of open access to information, University of Pretoria, 2021.

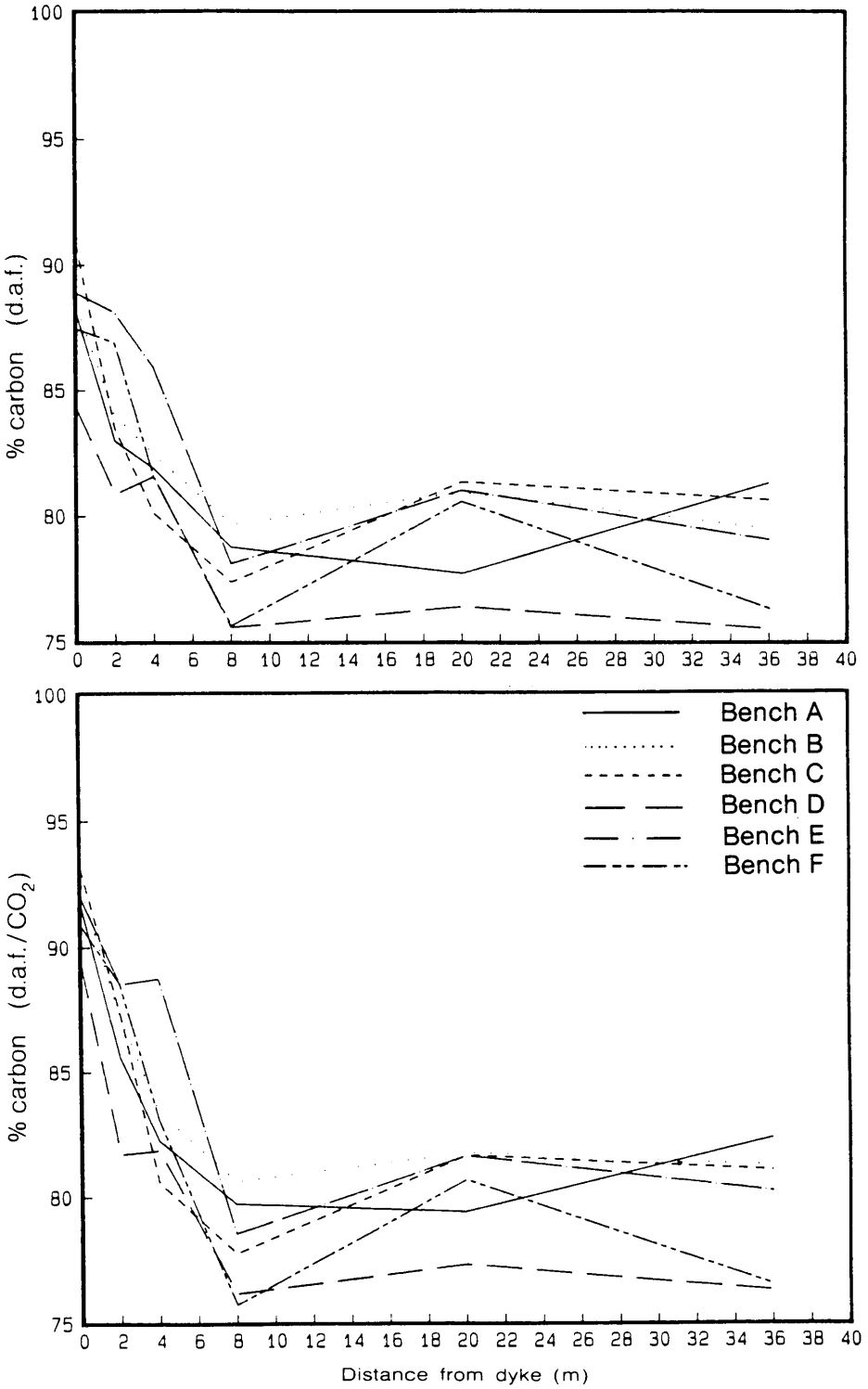


Fig. 6.13 A comparison of the carbon (d.a.f.) content without correction for CO_2 (upper diagram) and with the correction (lower diagram) for unaffected and metamorphosed coals at locality **C**.

Digitised by the Department of Library Services in support of open access to information, University of Pretoria, 2021.

metamorphic coals compared with regionally metamorphosed coals of the same rank is acceptable according to TEICHMÜLLER (1973) and was probably caused by slight oxidation after coke-formation was completed. It is therefore apparent that the correction by formula (3) is more significant for high CO_2 contents in high rank coals. For the sake of uniformity, all carbon values were corrected according to the extended formula (3) and only the results of this correction will be discussed (the full set of corrected results is given in appendix 9).

In the unaffected coals of channels E, F, G, H, B32, C36 and D32 the carbon content (d.a.f./CO_2) ranges from 76% to 84%. In these channels the carbon content seems to be largely controlled by the maceral composition of coal bands (Fig. 6.14). The inertinite-rich coals of benches A, and especially of B and C, tend to have higher carbon values than the vitrinite-dominated coals of bench D. The top part of the seam (benches E and F) shows the greatest variation from one channel to the next. These results concur with those of VAN KREVELEN (1961, p323), in that the inertinite group macerals have a higher carbon content than the vitrinite in coals of the same rank.

The trends are once again largely continuous up to the outer limit of the metamorphic aureole. However, the carbon content (d.a.f./CO_2) generally lies above 80% at locality B and below 82% at locality C. Towards the contact the carbon content increases rapidly to 93-94% (locality B), 89-93% (locality C) and to 86-92% (locality D) (Fig. 6.14). In accordance with the $\overline{R}OV_{max}$ and volatile matter content, samples E and F of channels C2 and C4 have a higher percentage carbon than the other coal bands in these channels. At localilty D, samples D, E and F of channels D2, D4 and D8 are conspicuously low in carbon (Fig. 6.14); this corresponds to the reflectance profiles of these channels (Fig. 6.8). Similar relations exist for the top benches of the seam in channels B2 and B4.

The **HYDROGEN** content varies between 3.5% and 5.0% (d.a.f.) in the unaffected coals, and is more consistent than the carbon content (Fig. 6.14). The lower seam portion (benches A, B and C) generally contains between 3.5% and 4.1% hydrogen, while the D-samples lie between 4.5% and 5.0% (d.a.f.); the top seam portion (samples E and F) contains variable amounts of hydrogen, which are mostly intermediate. This corresponds with the fact that vitrinite, and thus vitrinite-rich coals, tend to have a higher H-content than others of the same rank (TISSOT and WELTE, 1978, p213; BOUSKA, 1981, p150).

Within the metamorphic aureole the H-content decreases to about 2% on the coal/dolerite contact itself (Fig. 6.14). Similar, and even lower H contents, were found by DUTCHER et al. (1966) in coals with an initial hydrogen percentage of about 5.0%. These general trends again correspond with the results of the carbon and volatile matter analyses and $\overline{R}OV_{max}$ measurements, and also with results obtained on German

Digitised by the Department of Library Services in support of open access to information, University of Pretoria, 2021.

W

LOCALITY B

LOCALITIES E-F-G-H

LOCALITY D

LOCALITY C

E

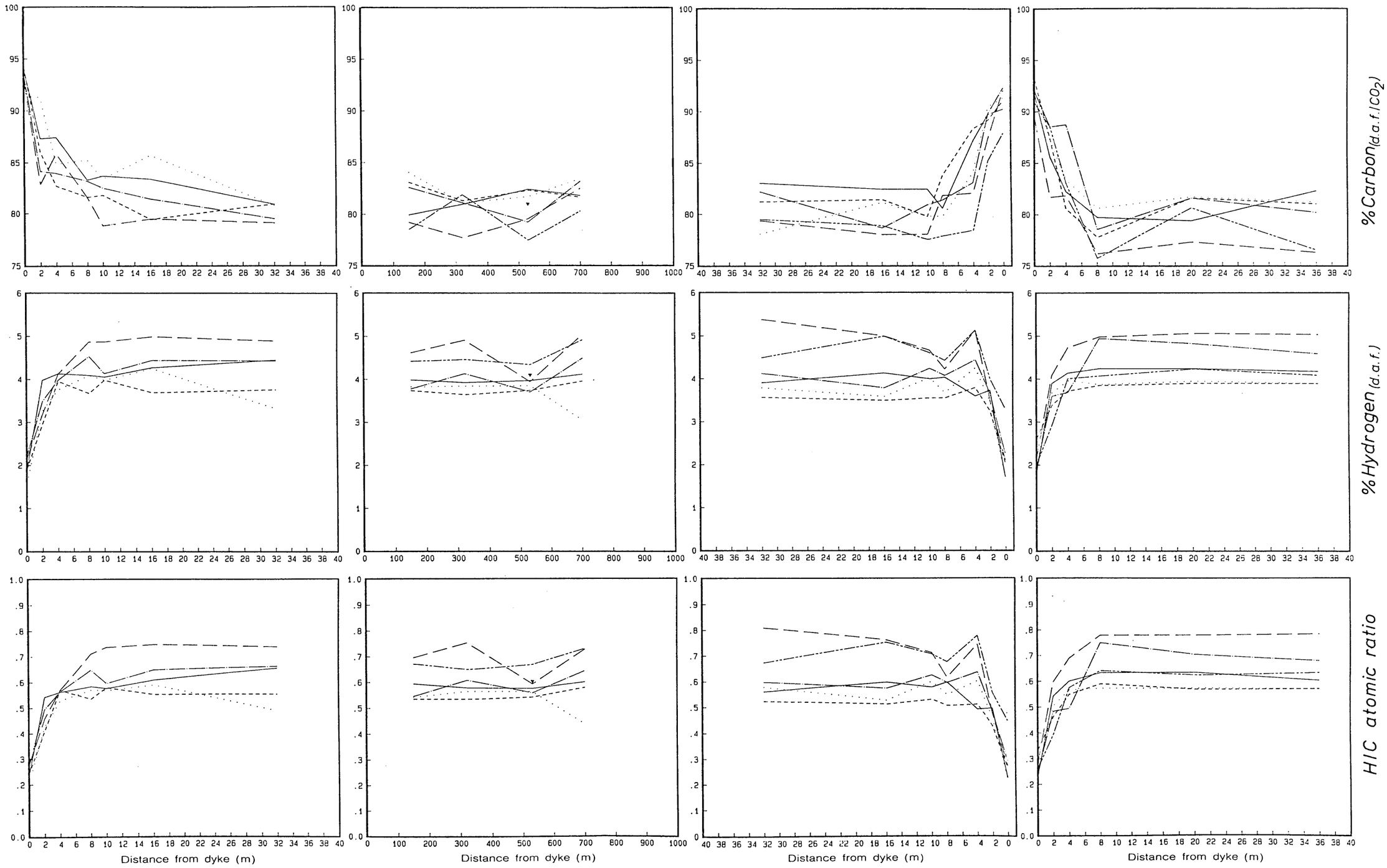


Fig. 6.14 Carbon (d.a.f. / CO_2) and hydrogen contents and H / C atomic ratio of unaffected and of metamorphosed coals in an east-west cross-section through all sampling localities (compare figures 2.2 and 2.3 for localities).

Digitised by the Department of Library Services in support of open access to information, University of Pretoria, 2021.

coals (TEICHMÜLLER, 1973). Detailed features, such as the increased rank of samples E and F in channels C2 and C4, and a lower rank of all samples in channel D4 compared to D8, are also reflected in the H content. Figure 6.14 also relates the H/C atomic ratio to the sampling distance. The dependence of both H and C on petrographic composition and rank is again clearly apparent. In the unaffected coals the vitrinite-rich coals have a considerably higher H/C ratio, which matches well with the diagram of VAN KREVELEN (1961, p123, Fig. VI,8). The variation in H/C ratios is large in low-rank coals, but as the rank increases it diminishes and becomes less dependent on petrographic composition. For the high ranking coals, the anthracites and meta-anthracites, it is noticeable that dehydrogenation and demethanation are the dominating chemical processes which take place in this stage of coalification, thus resulting in a steep decline in the H/C ratio.

The **NITROGEN** content of the present coals shows a similar pattern to hydrogen. The nitrogen content ranges from about 1.8% to 2.2% (d.a.f.) in unaffected coals. Similar to the hydrogen trends, benches A, B and C generally contain less nitrogen than benches E, F and, especially, D. Only at locality D do the results show a wider spread and are they laterally less persistent throughout a single seam band (Fig. 6.15).

Close to the dolerite intrusions the nitrogen content drops to between about 1.0% and 1.4% (d.a.f.) and the variation shows trends similar to the hydrogen and volatile matter contents, for example in samples E and F of channels C2 and C4. At locality D, channel D10 shows major discrepancies in hydrogen and nitrogen contents, especially for samples A, D, E and F. Channel D8 appears to have a similar increase in N-content to that displayed for hydrogen and volatile matter by D4.

As the **SULPHUR** determination on the present coals only comprises total sulphur, the results are very dependent on the sporadic occurrence of pyrite and to a lesser extent of other sulphide minerals in the individual samples. The results, therefore, are not very meaningful and correlations with other analytical results are not possible.

The sulphur content of the Twistdraai coals is highly variable in different lithotype bands, but generally remains below 2% (d.a.f.) (Fig. 6.15). There seems to be no preferential pyrite formation in particular seam benches, but in benches D and F the sulphur content may increase to about 5%, which corresponds to sporadic occurrences of large pyrite concretions in those individual samples.

Digitised by the Department of Library Services in support of open access to information, University of Pretoria, 2021.

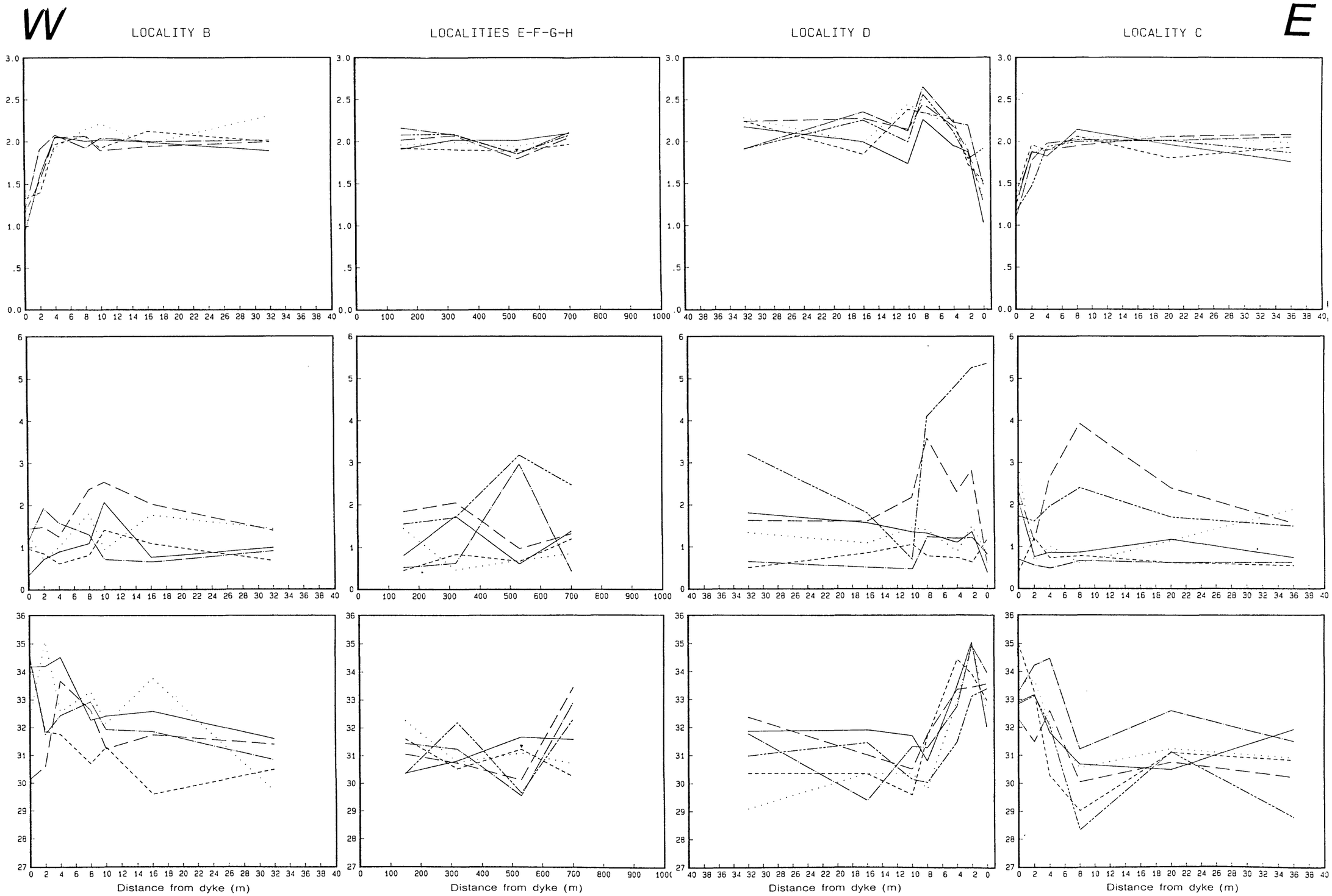


Fig. 6.15 Nitrogen (d.a.f.) and sulphur (d.a.f.) contents and calorific value (MJ / kg) (d.a.f.) of unaffected and of metmorphosed coals in an east-west cross-section through all sampling localities (compare figures 2.2 and 2.3 for localities).

Digitised by the Department of Library Services in support of open access to information, University of Pretoria, 2021.

6.5.1. Calorific Value on the Basis of Carbon and Hydrogen Content

The calorific values of the present coals were derived from the ultimate hydrogen and carbon contents (after CO_2 correction) and range between 28MJ/kg and 34MJ/kg (d.a.f.). Consequently, the calorific value shows similar trends in a particular seam bench, and from one bench to another, to the analytical values on which they are based. Thus, the calorific values of the unaffected coals are also closely related to their petrographic composition, except for minor deviations due to variations in ash and moisture contents.

In the cindered coals the calorific value is mainly dependent on rank (Fig. 6.15), which causes an increase to about 36-37MJ/kg (d.a.f.) in the meta-anthracitic coals. As the calorific value is only calculated from the ultimate analyses, it only refers to the organic constituents in the coal. The detrimental effect of ash, and specifically of large amounts of carbonates, such as in the cindered coals, must be taken into account when considering the raw coal. Then one would expect a decrease in calorific value in the heat-affected coals on the basis of an analytical determination. This was indicated by locally low calorific values in the western half of the study area (section 5.3; figures 5.3 and 5.4).

6.6. Inorganic Geochemistry of the Coals

In the preceding sections the coals studied were divided into unaffected coals and thermally-affected coals, on the basis of rank and proximate and ultimate analyses. In order to tie the geochemical results in with this basic distinction, the characteristic major and trace element concentrations of the unaffected coals of Twistdraai will first be established. Emphasis will be placed on the correlation of inorganic geochemistry with petrography and proximate analyses, the association of major and trace elements and on significant changes in these parameters from one seam bench to another. With this as basis, thermo-metamorphically related variations will then be outlined.

The major and especially the trace elements in coal may be either organically or inorganically bound. The latter elements can be present in different mineral phases of allogenic, authigenic or epigenic origin. Therefore, their relative ratios within a single seam are subject to variation. Due to this, much about the mode of occurrence of certain elements in coal is still unknown (VALKOVIC, 1983). In order to identify all the mineral phases present in coal, it would be necessary to conduct detailed microprobe studies; however, this is not

Digitised by the Department of Library Services in support of open access to information, University of Pretoria, 2021.

an objective of the present study.

The elemental concentrations are reported on a whole-coal basis, although they mainly contribute to the inorganic portion of the coals. As such their proportions are very dependent on the total ash content itself. Thus trends or variations in certain element proportions that may merely be due to corresponding trends in the ash content, may lead to erroneous conclusions. In order to correct for this influence, the elemental proportions can be recalculated either to an ash compostion for each individual sample, or by applying an ash correction factor to each element analysis in every single sample. This ash correction factor would be based on an average ash content throughout the whole of the unaffected coal seam. A correction of each individual sample in terms of element concentrations, relative to an overall average of the whole seam, will be more significant than an absolute change determined on the basis of ash composition alone.

The average ash content of the unaffected coals (all samples taken at distances greater than 16m from the contact) is 18.08% (a.d.); this is taken as a nominal value by which the ash values of each individual sample were divided. The resulting "ash factor" was subsequently applied to every element analysis of the respective sample in the following way:

$$Z_{corr} = Z_{det} \; / \; ashfac$$

Z_{corr} : corrected element concentration, either in % or ppm.
Z_{det} : element concentration as determined, either in % or in ppm.

ashfac : "ash factor" = ash of sample/18.08%

The effect of this correction is illustrated in figure 6.16. It becomes especially important in the evaluation of dolerite effects on the trace and major element concentrations in the thermally metamorphosed coals, in which the amount of ash increases considerably. In the following sections only the corrected element concentrations will be discussed. A table of both uncorrected and corrected concentration values can be found in the appendices 10-13.

Generally there is little correlation (Pearson coefficients above +/-0.7) between proximate analyses and petrography on the one hand, and major or trace elements on the other, if all the analyses of the unaffected coals are combined in one correlation matrix (Appendix 14 and 15). This is partly due to the fact that these elements can occur in different mineral phases or in organic components. However, in correlation matrices for the separate lithotype bands, significant

Digitised by the Department of Library Services in support of open access to information, University of Pretoria, 2021.

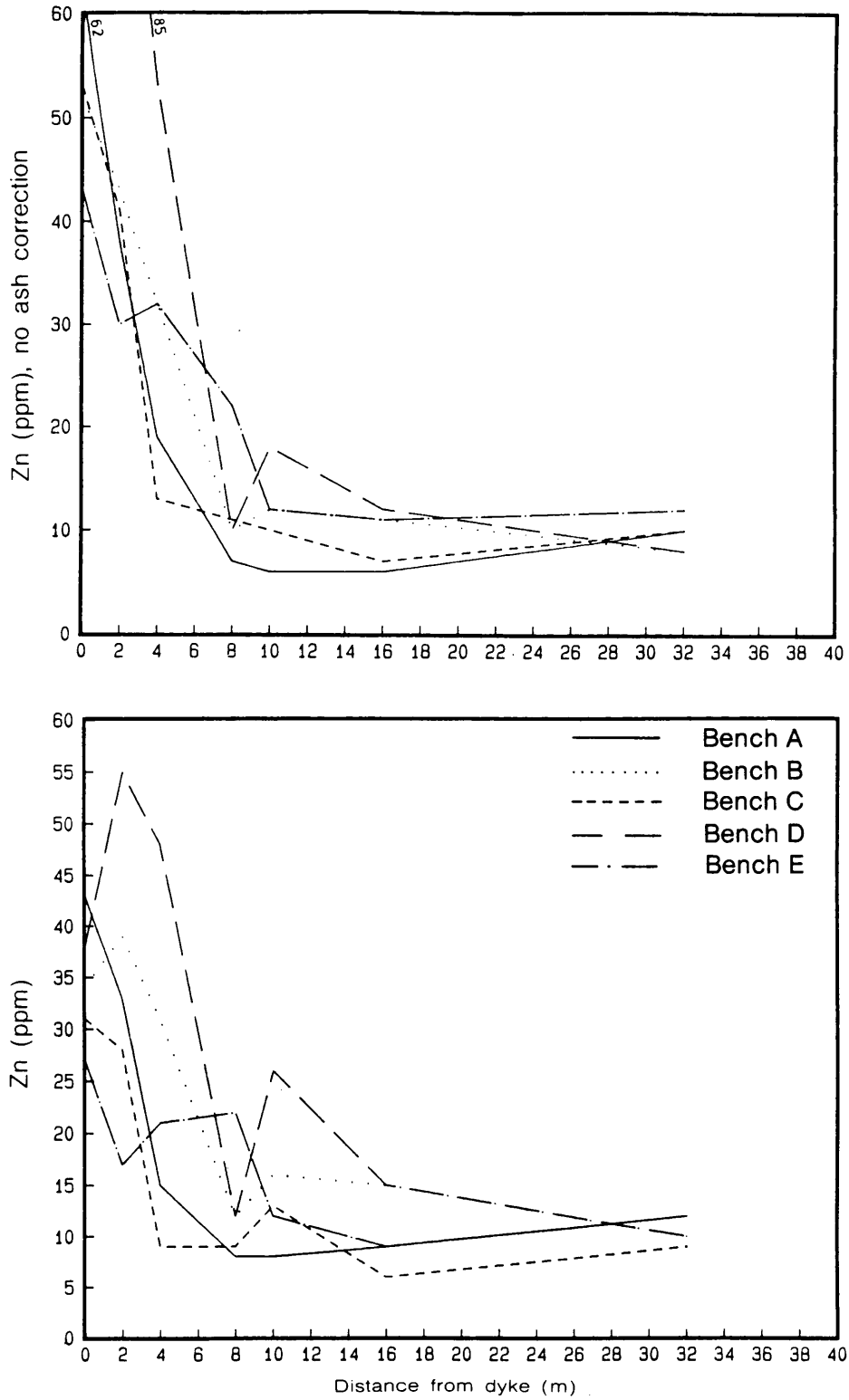


Fig. 6.16 Diagrams illustrating the effect of the "ash-factor" correction on element concentrations (locality **B**). Note that for both elements concentrations increase, where the ash content of that specific sample is below average (18.08 % a.d.).

Fig. **6.16b** overleaf

Digitised by the Department of Library Services in support of open access to information, University of Pretoria, 2021.

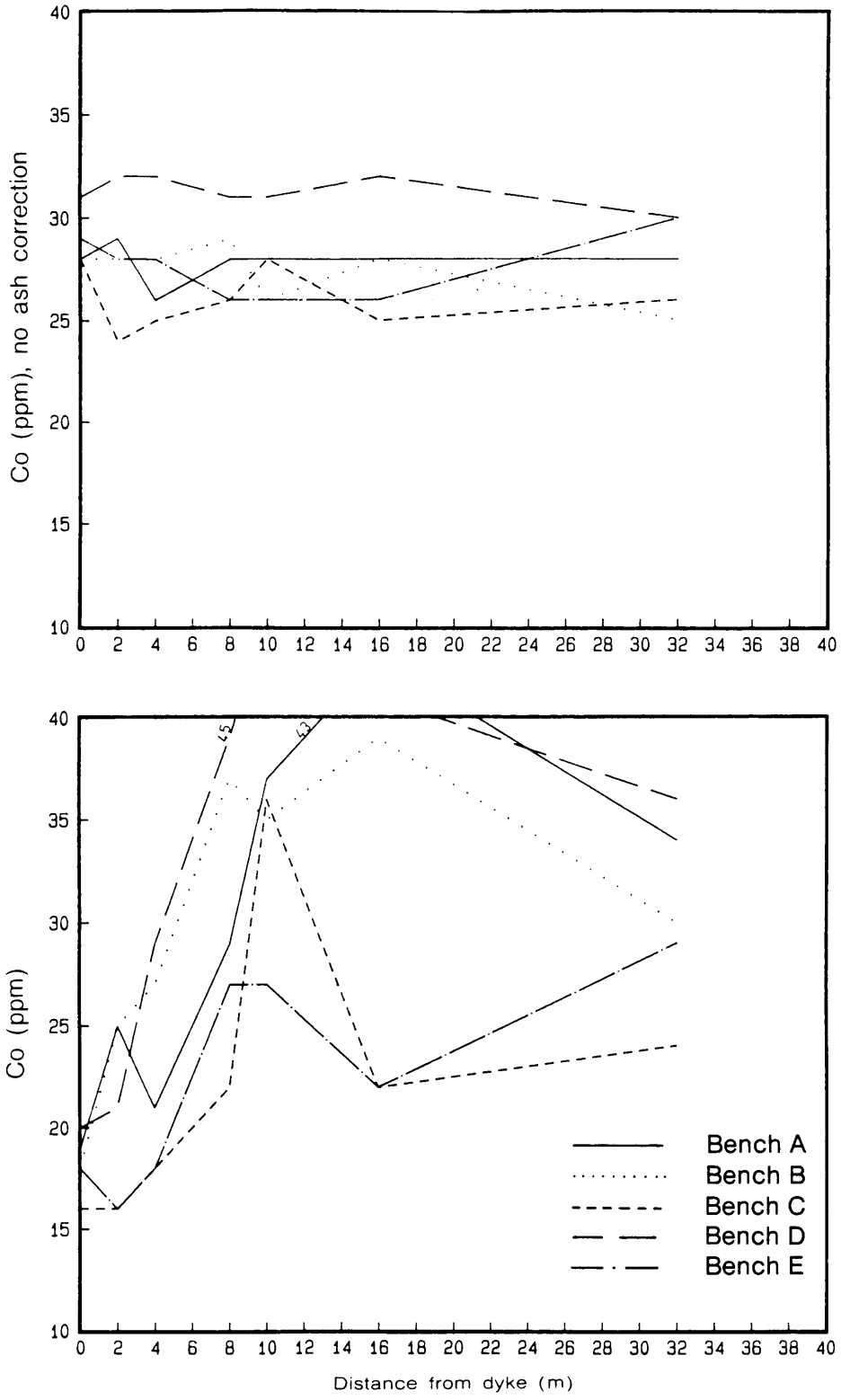


Fig. 6.16 b

Digitised by the Department of Library Services in support of open access to information, University of Pretoria, 2021.

relationships become apparent amongst major and trace elements, but there is still little proportionality between element concentrations and coal type (Appendices 14-23). This is shown by element concentrations that reach similar values in adjacent lithotype bands of very differing type (Fig. 6.17).

6.6.1. Regional Trends in Element Distribution

The major and trace element concentrations are laterally and vertically highly variable throughout the No. 4L seam (Fig. 6.17; Appendices 11 and 13). The average results for the unaffected coals, however, generally compare well with values of similar analyses given for Orange Free State coals (SARM 20) and for Natal coals (ROBERTS, 1987). At Twistdraai the coals are depleted in SiO_2, Al_2O_3, TiO_2 and

Table 6.5 Average inorganic geochemical results of Twistdraai coals compared to results of other South African coals.

element	Twistdraai %	Secunda(1) %	Sasolburg(2) %	Klipriver(3) %
SiO_2	7.69	11.05	17.66	3.74
TiO_2	0.27	0.32	0.63	0.11
Al_2O_3	4.98	6.16	11.27	2.35
Fe_2O_3	0.00	1.00	1.17	5.89
FeO	0.85	n.d.	n.d.	n.d.
MnO	0.02	n.d.	n.d.	0.00
MgO	0.61	0.55	0.43	0.04
CaO	2.04	1.70	1.87	0.70
Na_2O	0.03	0.13	0.27	0.13
K_2O	0.13	0.16	0.14	0.09
P_2O_5	0.24	0.28	0.14	0.05
	ppm		ppm	ppm
Zn	10		17	9
Cu	1		18	3
Ni	15		25	72
Co	30		8	82
Ga	10		16	8
Mo	3		80	5
Nb	8		16	tr
Zr	141		180	93
Y	16		29	17
Sr	1025		330	318
Rb	6		10	tr
U	1		4	tr
Th	7		18	tr
Pb	0		26	tr
Cr	28		67	60
V	35		47	118
Ba	747		372	79
Sc	2		10	n.d.
Cl	233		n.d.	n.d.
F	1374		n.d.	n.d.

(1) average results from annual report by NICR (1985)
(2) certified values from SARM 20
(3) average values after ROBERTS (1987)
n.d. not determined
tr traces

Digitised by the Department of Library Services in support of open access to information, University of Pretoria, 2021.

Na_2O, with respect to the average for Secunda and Sasolburg coals (Table 6.5). Ni, Co, Mo, Zr, Pb, Cr and V are depleted and Sr and Ba are generally enriched in these coals, compared to the others noted above. As XRF analysis does not distinguish between Fe^{2+} and Fe^{3+}, and because most iron in coal is present as FeO in sulphides or carbonates, all iron values referred to are given as FeO.

Co, Ga, Nb, Y, Sr, V and F are erratic from one lithotype band to the next and cover a wide range of concentrations within each channel profile (Fig. 6.17). Cu, Pb, U, Mo, Sc and to a certain extent Th as well, have extremely low concentrations, with only sporadic occurrences above detection limits. Zn, Ni, Zr, Rb, Cr, Ba and Cl are generally evenly distributed across the seam, but have some erratic values in various seam benches.

The regional variation of element concentrations is generally not very significant at the investigated localities, except for locality G, where SiO_2 and TiO_2 and to a lesser extent Na_2O, are enriched as the ash content rises. A depletion of FeO, and to a lesser extent of MgO and CaO as well, compared to the adjacent localities occurs at locality G. P_2O_5 is extremely depleted in this channel (Fig. 6.19b). Of the trace elements at locality G, Zn, Ni, Co, Ga, Sr, Ba, Cl and F are depleted, while Rb and Cr are slightly enriched relative to the adjacent channels E, F and H (Figs. 6.18 to 6.20). The anomalous trend of channel G, first recognized on the basis of other parameters, is thus also reflected in the major and trace element content. The other element concentrations can be regarded as laterally persistent in the individual seam benches. Ni and Mo are enriched in the unaffected coals at locality D; Co and Nb are depleted at localities C and D, respectively. There is no Cu in the unaffected coals of localities G, H and D.

6.6.2. Element Distribution in Unaltered Coals

The grade of a coal is mainly determined during the depositional stage of coal formation when clastic (allogenic) minerals are washed into the coal swamps. These minerals predominantly comprise quartz and clay minerals, hence the SiO_2, Al_2O_3 and K_2O contents of a coal are indicative of the degree of influx of clastic minerals (BOUSKA, 1981). Another major group of minerals in coal are authigenic and form during deposition and diagenesis. They include carbonates, sulphides and phosphates, which will be reflected by the concentrations of CaO, MgO, FeO and P_2O_5 (BOUSKA, 1981).

On this basis, seam benches C, E and F are highly contaminated by clastic minerals, with F containing more quartz and E more kaolinite, while bench C may contain a higher percentage of illite than E, on account of the higher K_2O content (Fig. 6.17). In general, kaolinite

Digitised by the Department of Library Services in support of open access to information, University of Pretoria, 2021.

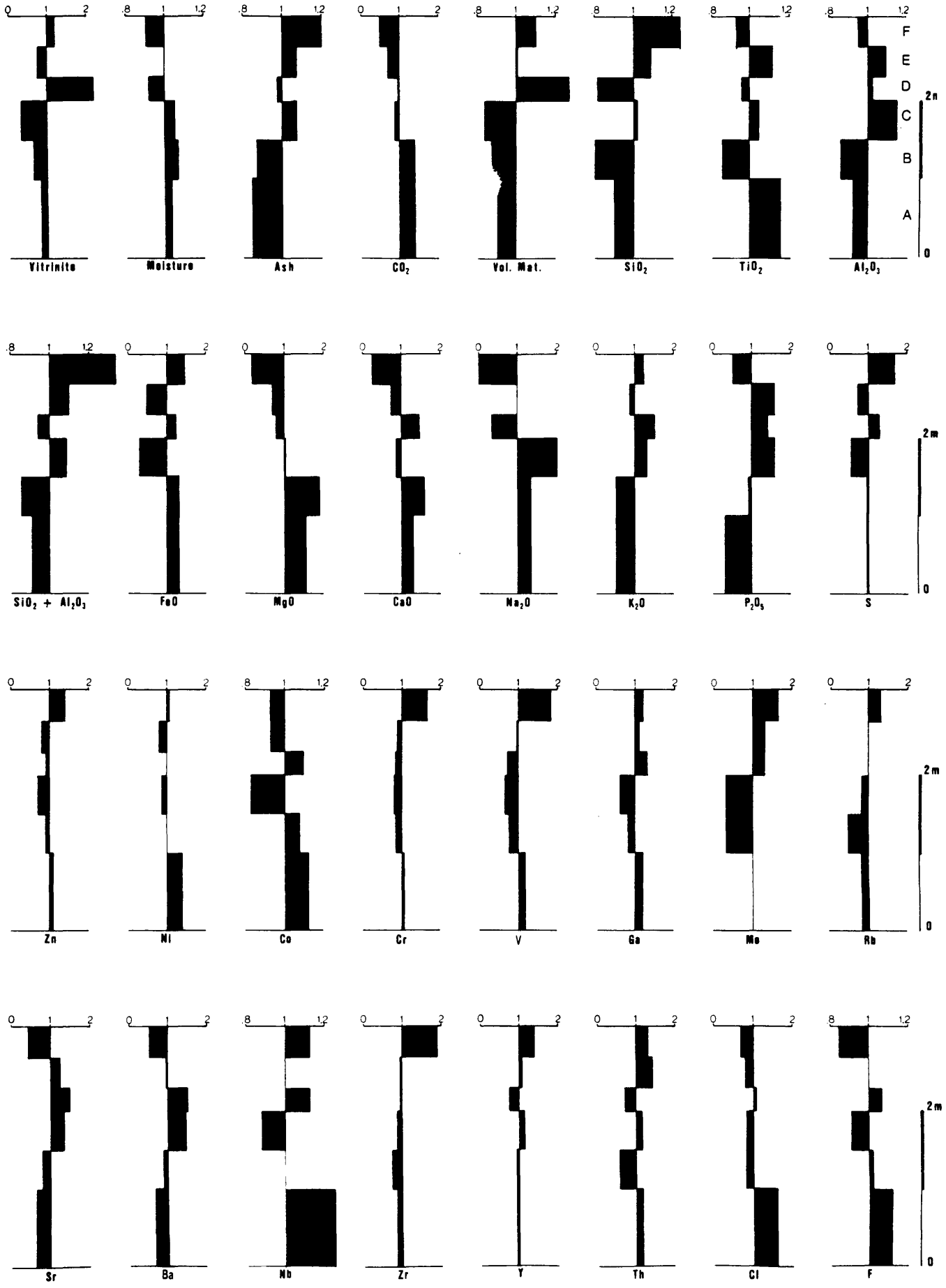


Fig. 6.17 Vitrinite content, proximate analyses and element concentrations of the individual seam benches (A - F) relative to a normative average value of each parameter of all unaffected coals (>16 m sampling distance from intrusion). The normative value is given as "1". The scale for depletion and enrichment ratios is from 0 to 2 or from 0.8 to 1.2.

Digitised by the Department of Library Services in support of open access to information, University of Pretoria, 2021.

predominates throughout the seam profile, which is indicated by higher Al_2O_3 values (appendix 10) and confirmed by XRD analyses (Table 6.6). Benches A, B and particularly D are relatively poor in clastic quartz and kaolinite, but bench D seems to be enriched in illite, which may be of diagenetic (authigenic) origin as it is normally associated with vitrinite (SNYMAN et al., 1983). The relatively low content of SiO_2, Al_2O_3 and K_2O of seam benches A and B, and hence the low content of clastic minerals, may also be ascribed to very low energy conditions conducive to the formation of vitrinite. Na_2O shows an inverse relation to all these elements (Fig. 6.17) but no significant correlation coefficient is evident (Appendix 21).

On the other hand, CaO and MgO are mainly accommodated in carbonate minerals and are therefore in sympathetic relationship with the CO_2 content, which has an inverse trend to the ash content and the allogenic elements. The ratio of dolomite to calcite generally seems to be constant, except for seam benches C and D, where either dolomite or calcite predominate (Fig 6.17).

FeO is associated with the carbonates to a lesser extent (siderite and ankerite), and shows a particular correspondence with macroscopically identified siderite occurrences in benches A, C and D. CaO, MgO and FeO may therefore be considered indicative of lithophile elements preferentially accomodated in authigenic minerals.

A portion of the iron is, however, bound as authigenic sulphide, as indicated by a high positive correlation between iron and sulphur (Table 6.7) and also other typical chalcophile elements. The iron is irregularly distributed and its concentration is mainly related to the erratic occurrence of pyrite. In figure 6.17 iron ratios show inverse trends with Al_2O_3 and to a lesser extent with Na_2O, K_2O and P_2O_5. This is also expressed in some high, negative correlation coefficients for iron with these elements (Table 6.7). P_2O_5 is the most inconsistent major element throughout all lithotype bands (Fig. 6.19b) and is particularly enriched in benches C, D and E.

It appears that the change in ash composition from bottom to top of the coal seam and the amount of ash itself are largely dependent on the influx of detrital silicates. The decreasing amount of carbonate

Table 6.6 XRD analyses of clay minerals on some selected coal samples, in percentage of the whole coal (analysed by NICR).

sample No.	illite %	kaolinite %
C 0 C	16.0	--
C 2 C	12.0	0.5
C 4 C	0.5	10.5
C 8 C	--	14.0
C20 C	--	11.7
C36 C	--	14.6

Digitised by the Department of Library Services in support of open access to information, University of Pretoria, 2021.

(calcite, dolomite and siderite) from bottom to top of the seam is, therefore, due to a relatively stronger influx of clastics, particularly quartz, towards the top of the seam. An absolute increase in epigenic carbonates from bottom to top of the seam is considered to have had a minor influence on the ash composition. The correlation coefficients amongst the major elements are generally better in the bottom benches of the seam (A, B and C) than in the top (Appendix 21).

Elements of allogenic affinity mainly include TiO_2, K_2O and, to a lesser extent, Zr, Y and Th. The remarkably good correlations of SiO_2 and TiO_2 in each coal band (Fig. 6.17; Table 6.7) allow the assumption that rutile is present in quartz as sagenite, or that allogenic titanium minerals are associated with allogenic quartz (BOUSKA, 1981, p153). Bench F shows the highest lateral variation of all the seam bands in SiO_2 and TiO_2 content (Fig. 6.18a).

K_2O only has good positive correlations with Al_2O_3 in benches D and F, which again points to their association in illite (Table 6.7). Zr and Th, which have good correlations with SiO_2 and TiO_2 in some lower seam benches (Table 6.7), may be present in zircon and thorite.

Table 6.7 Some selected correlation coefficients that are referred to in the text. Correlation coefficients are given separately for each seam bench. The complete set of correlation matrices is listed in appendices **19** to **23.**

Sample	A	B	C	D	E	F
FeO/Al_2O_3	-0.75577	-0.55725	-0.49595	-0.51297	-0.18464	0.43718
FeO/Na_2O	-0.51707	-0.39280	-0.63986	-0.58490	-0.06230	0.13030
FeO/K_2O	-0.42021	-0.23778	-0.68615	-0.16533	0.29317	-0.02508
FeO/P_2O_5	-0.28576	0.49000	-0.56087	0.50193	-0.35280	0.58679
FeO/SO_3	0.93701	0.97201	0.83011	0.67097	0.98357	0.01435
SiO_2/TiO_2	0.74350	0.95304	0.80074	0.71060	0.83048	0.74575
K_2O/Al_2O_3	0.26955	0.03898	0.51840	0.87432	0.04520	0.71734
TiO_2/CaO	-0.73751	-0.86905	-0.77852	-0.48939	-0.46509	0.12022
SiO_2/Zr	0.78288	0.00699	-0.32960	-0.38406	-0.37342	-0.02688
SiO_2/Th	0.80076	0.72664	0.48801	0.42234	0.39002	-0.40419
TiO_2/Zr	0.84681	0.16035	-0.31743	0.07317	0.05813	0.55896
TiO_2/Th	0.81289	0.61737	0.17081	0.58788	0.71460	0.21462
SiO_2/Cr	0.46443	0.70665	0.03568	0.42600	-0.03137	0.54594
SiO_2/V	0.27493	0.49874	0.31987	0.17757	0.06965	0.20509
Al_2O_3/Cr	0.43376	0.71224	-0.55993	-0.21223	0.05716	0.77512
Al_2O_3/V	-0.01116	0.48520	0.13376	0.02185	-0.31660	0.44278
Ca/Ba	0.06373	-0.02166	0.20717	-0.26099	0.51294	0.54324
Ca/Sr	0.43826	0.64151	0.65493	-0.07879	0.53492	0.58522
Mg/Ba	-0.24518	0.34664	0.13887	-0.46477	0.23358	0.57140
Mg/Sr	0.16236	0.76469	0.54701	-0.42477	0.29513	0.54349
P_2O_5/Ba	0.54237	0.53195	0.70029	0.69177	0.98589	0.23564
P_2O_5/Sr	0.63809	0.89460	0.92522	0.75616	0.94108	0.41812
Zn/Ni	-0.18573	0.12995	-0.28211	0.08604	0.47211	-0.10847
Co/Ni	0.76834	0.59609	0.71796	0.54947	0.73540	0.83391
Ash/Co	-0.93246	-0.95690	-0.79529	-0.90982	-0.85101	-0.73890
Ash/F	-0.78293	-0.73306	-0.70468	-0.89674	-0.81878	-0.81100

Digitised by the Department of Library Services in support of open access to information, University of Pretoria, 2021.

Y, which has a strong positive correlation with Zr through all seam benches, may be accounted for by traces of various Y-silicates (e.g. yttrialite, rowlandite) or phosphates (e.g. xenotime). Nb is inversely proportional to Y (Figs. 6.17 and 6.18).

Correlations of allogenic elements with SiO_2 and Al_2O_3 are only good in certain seam benches (Appendix 22). Cr and V have poor correlations (Table 6.7), probably due to a variable number of mineral phases in which they may occur and to their preferential association with the organic matter (BOUSKA, 1981). V, specifically, may be present in muscovite; a V-rich variety was found in the XRD analyses of the host rocks in section 3.10. Rb occurs rarely, hence showing little correlation with any other element (Fig. 6.18d).

Elements of lithophile authigenic affinity will mainly be associated with carbonates and phosphates, and generally comprise TiO_2, Sr, Ba and, to a lesser extent, Fe, Cl and F (Fig. 6.19). In the lower seam benches (A to C), however, TiO_2 and CaO have a strong negative correlation which emphasizes the stronger affinity of TiO_2 to other allogenic elements rather than to lithophile authigenic elements in these coals (Table 6.7).

Conspicuously, Sr and Ba are depleted in benches A, B and F but are enriched in the others, which allows the assumption that they are associated with P_2O_5 rather than with Ca- or Mg-carbonates. This is supported by the correlation coefficients (Table 6.7). It is thus suggested that Sr and Ba, in seam benches C, D and E, occur in goyazite and goerceixite. Goyazite was detected by XRD analyses of the small series of samples listed in table 6.6. VALKOVIC (1983, p72) reports similar mineral associations and ROBERTS (1987) found these minerals through microprobe analyses in coals from Natal. The occurrence of Ba and Sr in feldspars or in carbonates is generally assumed to be rare in the present coals. However, witherite and strontianite might be accessory minerals in bench D, due to the relative abundance of the relevant elements there; P_2O_5 is slightly depleted (Figs. 6.17 and 6.19b).

Cl and F show authigenic affinities, mainly on account of their decreasing abundance from bottom to top of the seam (Fig. 6.19c), which resembles the trends for CaO and MgO. However, as XRF results for Cl and F are not reliable, due to a lack of standardization, the correlation coefficients are poor and the present values for these two elements can only be taken as approximations. Fe as an authigenic element has already been attributed to siderite and ankerite.

Elements of chalcophile affinity are Fe, Ni, Cu, Co, Zn, Ga and Mo (Figs. 6.18e and 6.20). Fe in the chalcophile community mainly accounts for the occurrence of sulphides, which have already been discussed. Trace elements Ga and Mo are rare in most samples and below detection limits of the XRF spectrometer in seam benches B and C.

Zn and Ni are typically enriched in benches A and F, but depleted

Digitised by the Department of Library Services in support of open access to information, University of Pretoria, 2021.

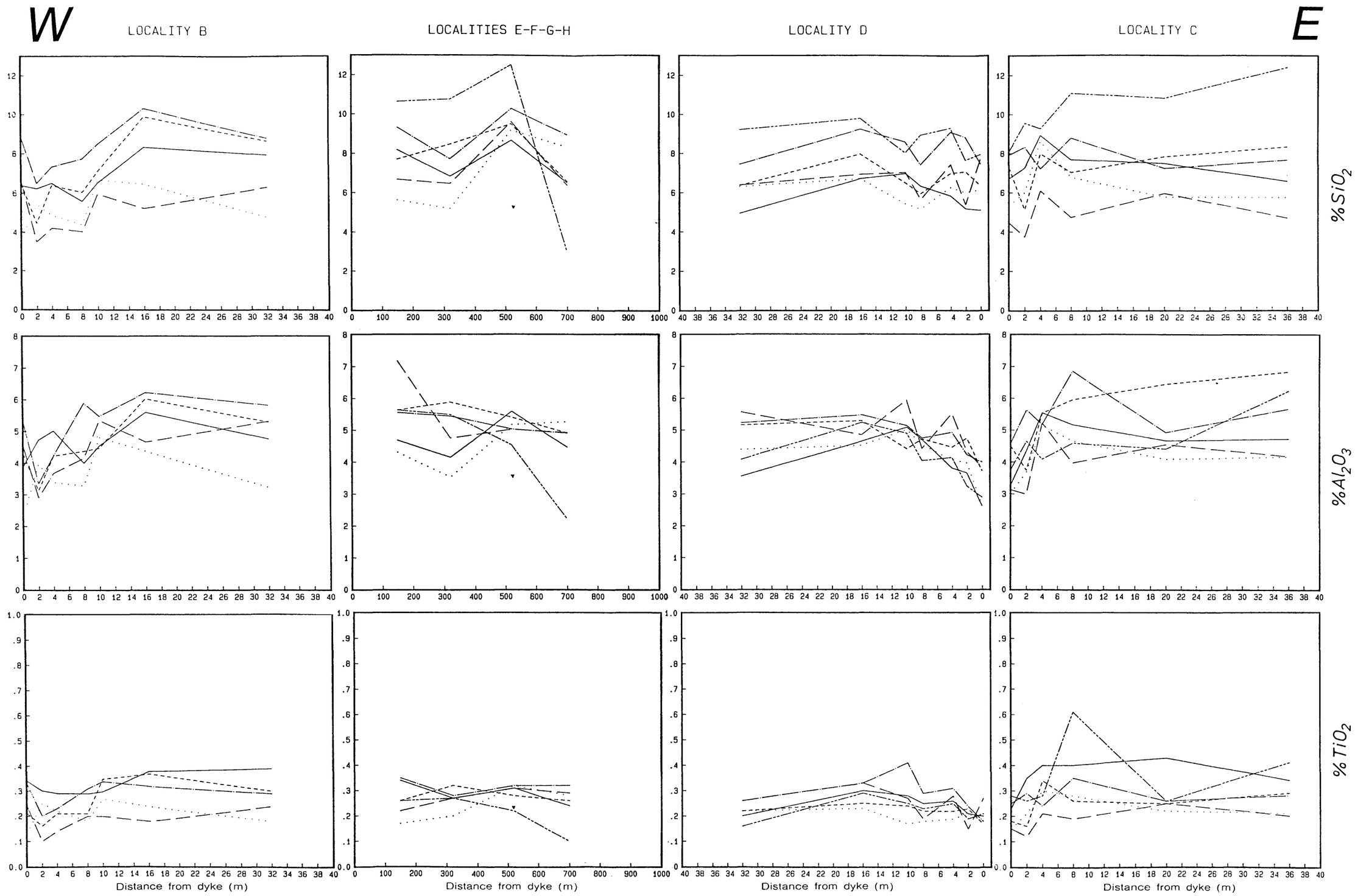


Fig. 6.18 Concentrations of mainly allogenic elements of unaffected and of metamorphosed coals in an east-west cross-section through all sampling localities (compare figures 2.2 and 2.3 for localities).

(a) % SiO_2; % Al_2O_3; % TiO_2
(b) % $SiO_2 + Al_2O_3$; % K_2O; Th (ppm)
(c) Zr (ppm); Y (ppm); Nb (ppm)
(d) Cr (ppm); V (ppm); Rb (ppm)
(e) % Na_2O; % FeO

Digitised by the Department of Library Services in support of open access to information, University of Pretoria, 2021.

W

LOCALITY B

LOCALITIES E-F-G-H

LOCALITY D

LOCALITY C

E

$\%SiO_2 + Al_2O_3$

$\%K_2O$

$Th_{(ppm)}$

Distance from dyke (m)

Distance from dyke (m)

Distance from dyke (m)

Distance from dyke (m)

Bench A
Bench B
Bench C
Bench D
Bench E
Bench F

Fig. 6.18 b

Digitised by the Department of Library Services in support of open access to information, University of Pretoria, 2021.

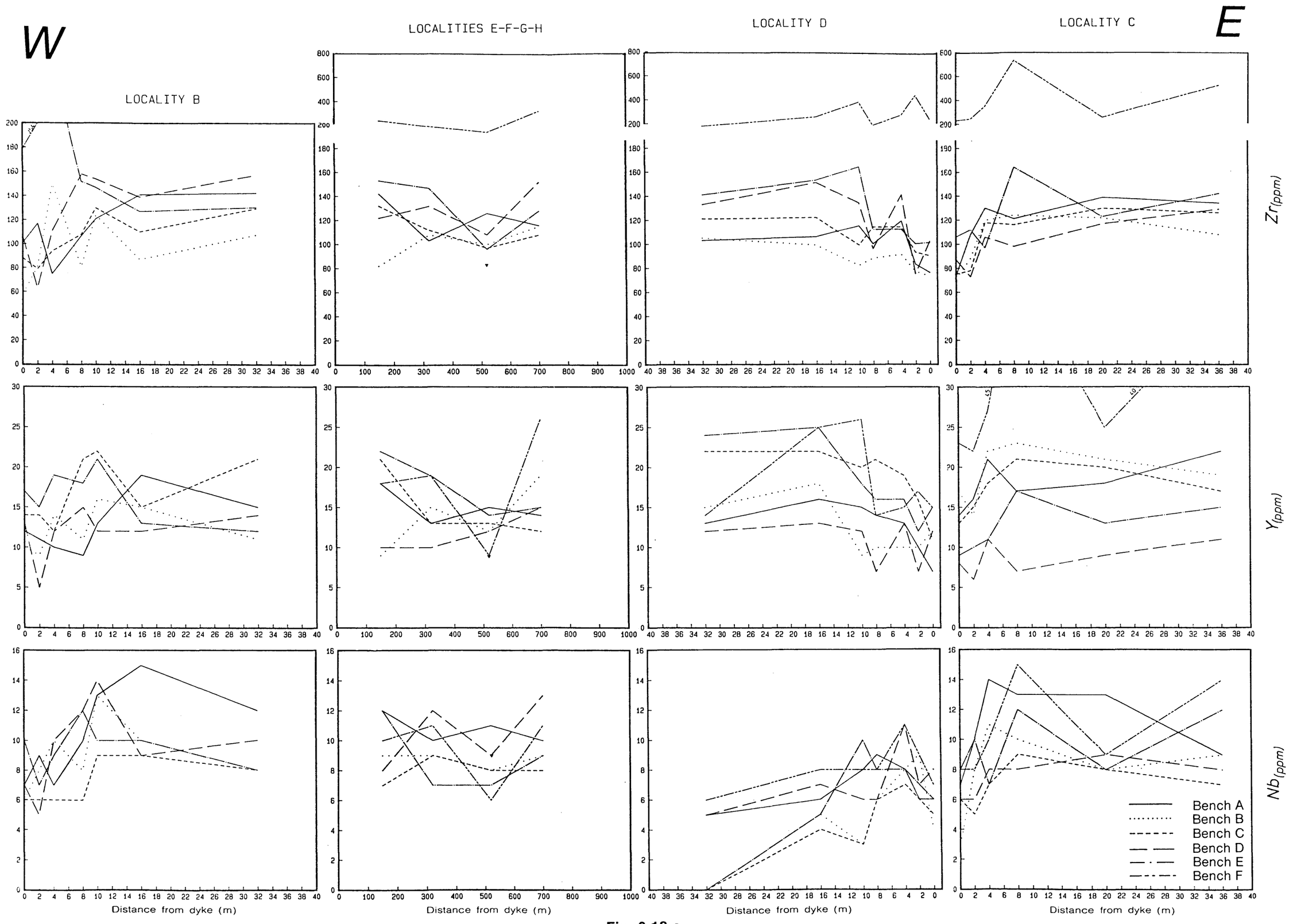


Fig. 6.18 c

Digitised by the Department of Library Services in support of open access to information, University of Pretoria, 2021.

W

LOCALITY B

LOCALITIES E-F-G-H

LOCALITY D

LOCALITY C

E

Cr(ppm)

V(ppm)

Rb(ppm)

Distance from dyke (m)

Distance from dyke (m)

Distance from dyke (m)

Distance from dyke (m)

Bench A
Bench B
Bench C
Bench D
Bench E
Bench F

Fig. 6.18 d

Digitised by the Department of Library Services in support of open access to information, University of Pretoria, 2021.

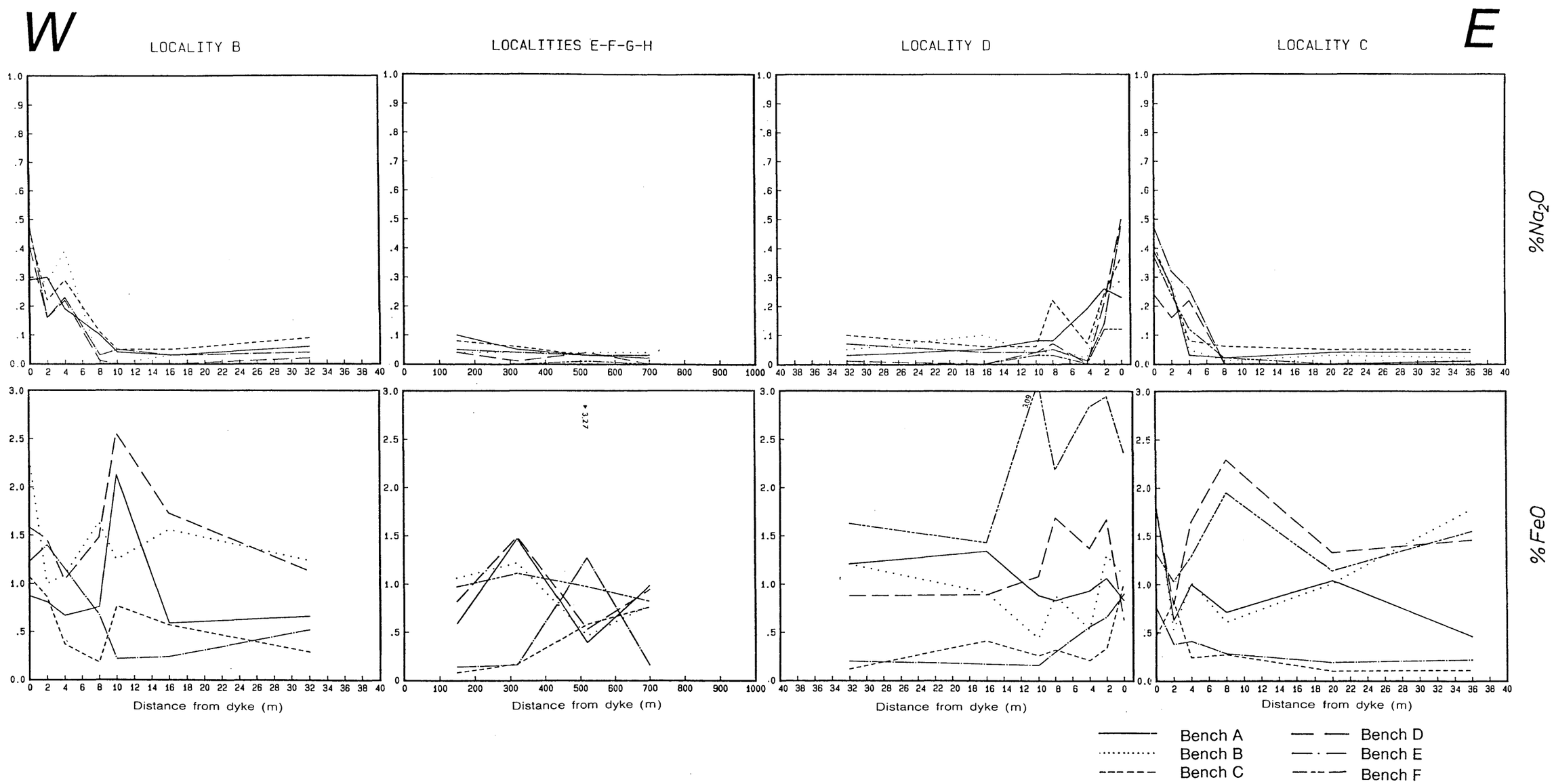


Fig. 6.18 e

Digitised by the Department of Library Services in support of open access to information, University of Pretoria, 2021.

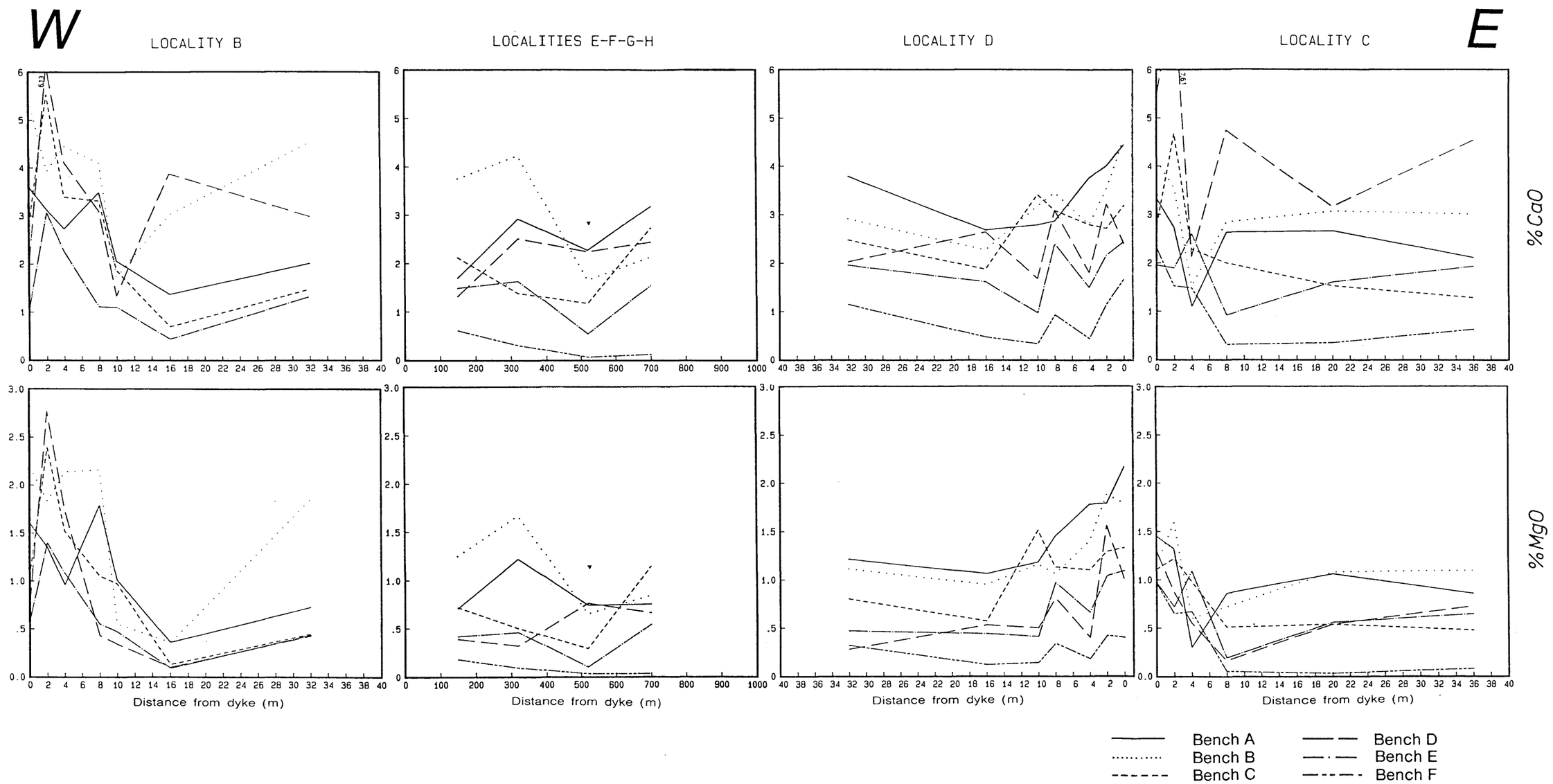


Fig. 6.19 Concentrations of mainly lithophile authigenic elements of unaffected and of metamorphosed coals in an east-west cross-section through all sampling localities (compare figures 2.2 and 2.3 for localities).
(a) % CaO; MgO
(b) % P_2O_5; Sr (ppm); Ba (ppm)
(c) Cl (ppm); F (ppm)

Digitised by the Department of Library Services in support of open access to information, University of Pretoria, 2021.

W

LOCALITY B

LOCALITIES E-F-G-H

LOCALITY D

LOCALITY C

E

$\%P_2O_5$

$Sr_{(ppm)}$

$Ba_{(ppm)}$

Distance from dyke (m)

Distance from dyke (m)

Distance from dyke (m)

Distance from dyke (m)

Bench A
Bench B
Bench C
Bench D
Bench E
Bench F

Fig. 6.19 b

Digitised by the Department of Library Services in support of open access to information, University of Pretoria, 2021.

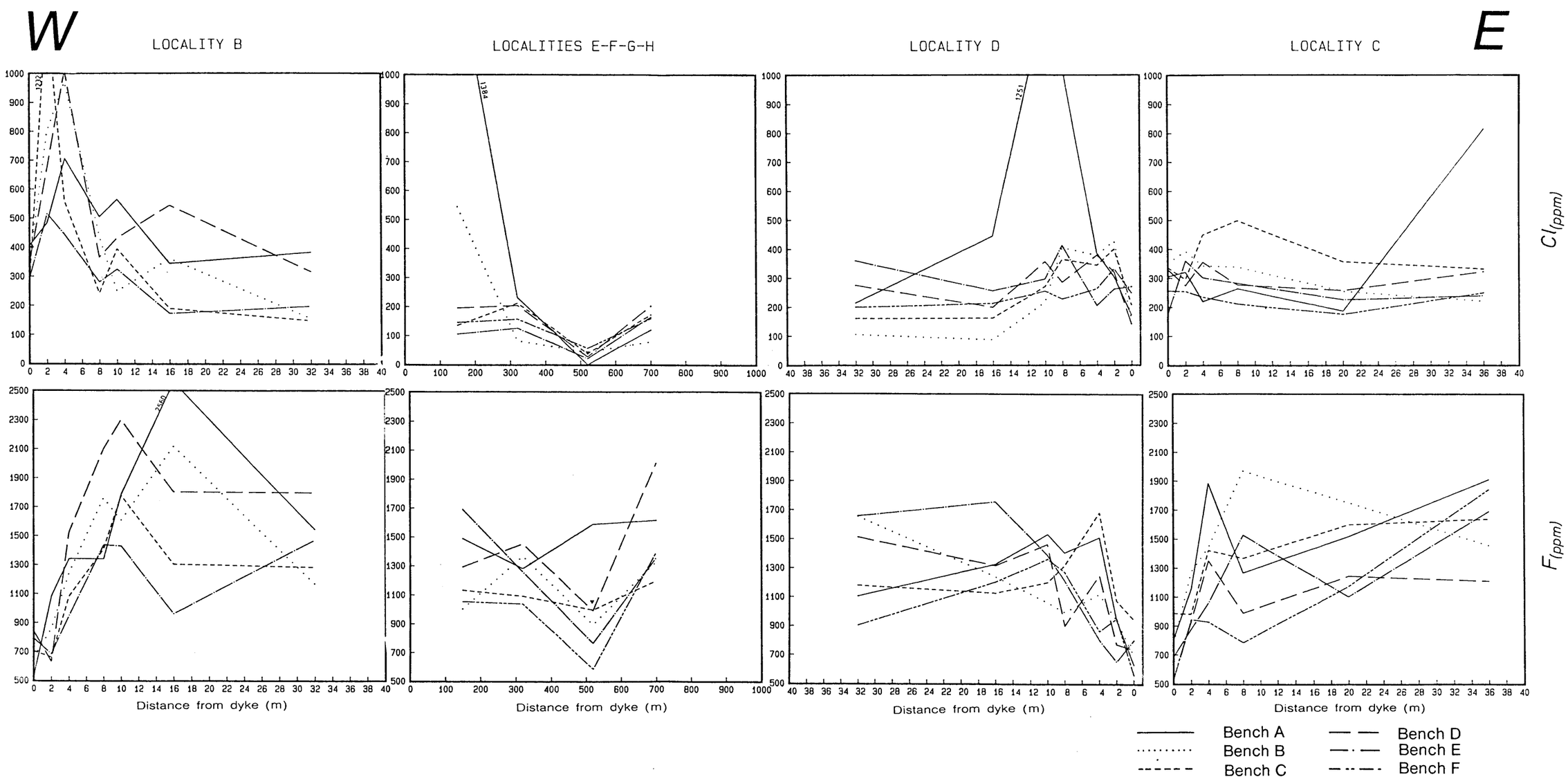


Fig. 6.19 c

Digitised by the Department of Library Services in support of open access to information, University of Pretoria, 2021.

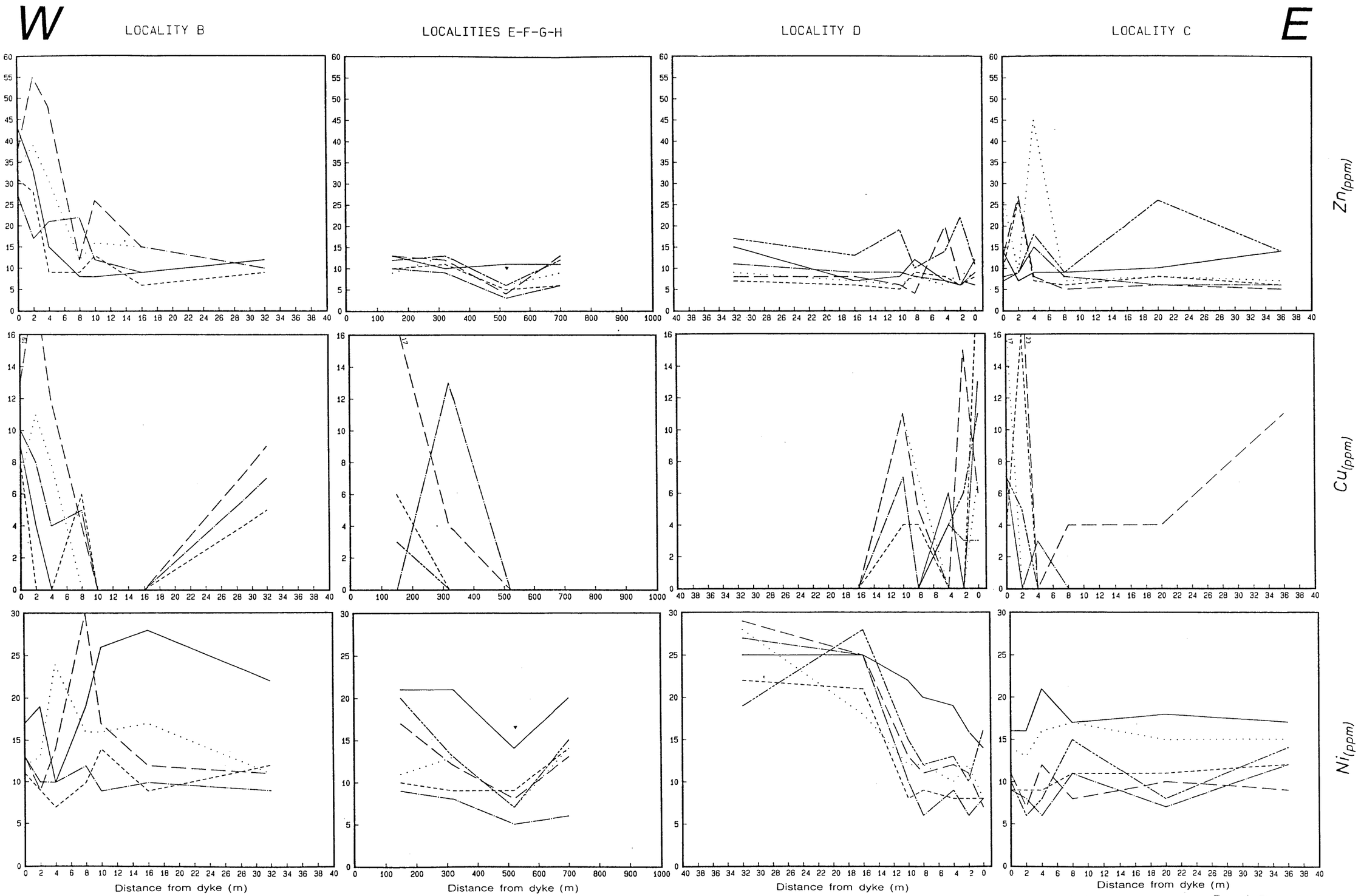


Fig. 6.20 Concentrations of mainly chalcophile authigenic elements of unaffected and of metamorphosed coals in an east-west cross-section through all sampling localities (compare figures 2.2 and 2.3 for localities).

(a) Zn (ppm); Cu (ppm); Ni (ppm)

(b) Co (ppm); Ga (ppm); Mo (ppm)

Digitised by the Department of Library Services in support of open access to information, University of Pretoria, 2021.

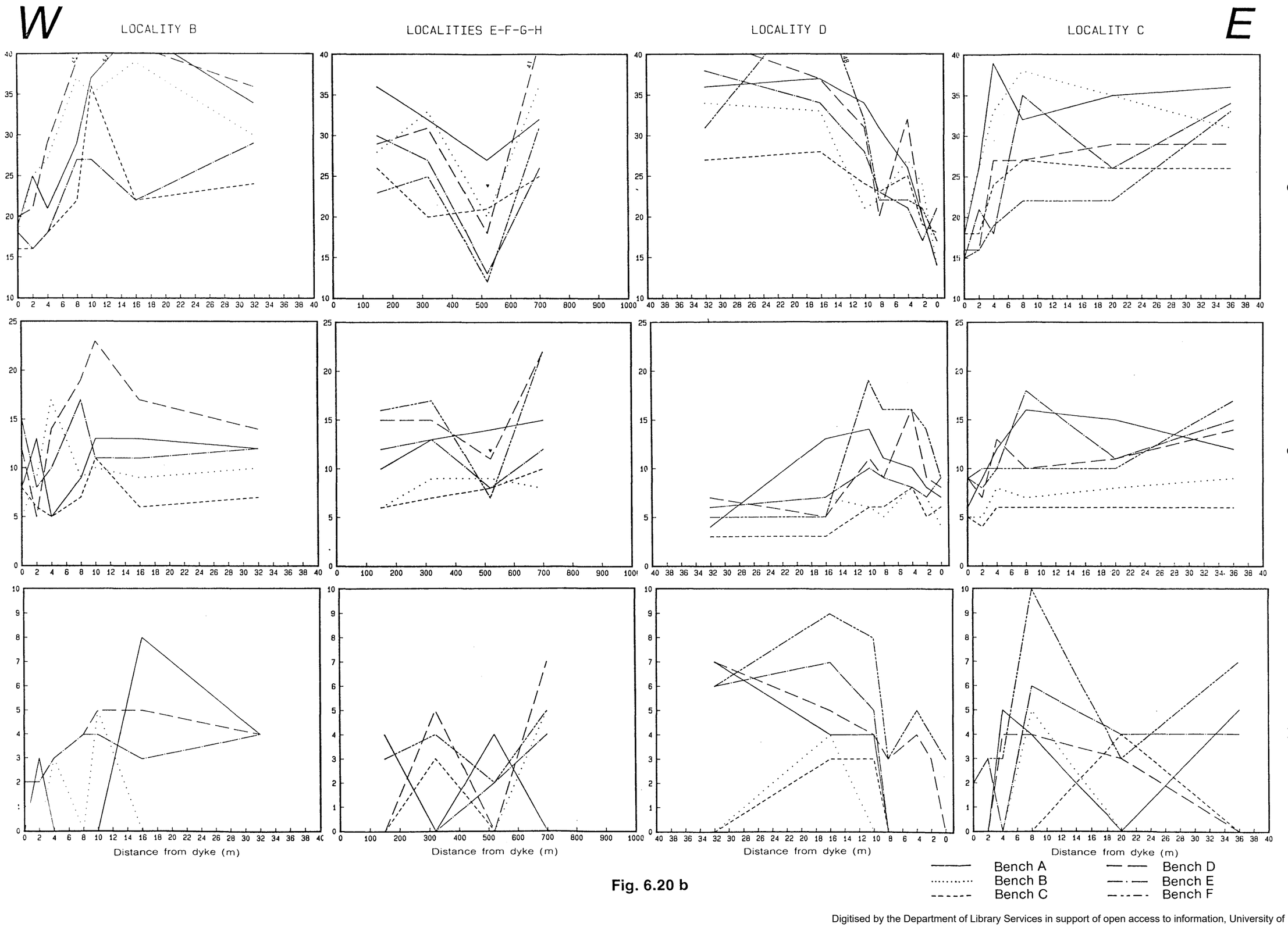


Fig. 6.20 b

Digitised by the Department of Library Services in support of open access to information, University of Pretoria, 2021.

in the others, with a minimum in bench C. Their interrelations, however, are poor, as expressed in the low correlation coefficients (Figs. 6.17 and 6.20a; Table 6.7). Co follows these trends to a limited extent, but has some good correlations with Ni (Table 6.7). This group of elements has poor correlations with the major elements (Appendix 22); the reason probably lies in the occurrence of these elements in various mineral associations, as well as relatively high organic affinities of Ni and Co (ZUBOVIC et al., 1960).

Elements with organic affinity are Ga, Mo, Ni, Co, Cu, V, Cr and, partially, TiO_2, K_2O and P_2O_5 (OTTE, 1953; ZUBOVIC et al., 1960). The latter three elements are, however, dominantly associated with inorganic components of the present coals, so that their occurrence in organic bonds is of minor importance.

There is little correlation of major and trace elements with the petrography or with most of the proximate results of the coals (Appendices 19 and 20), except for correlations with CO_2 and ash. An association of particular trace elements with low-ash coal, preferentially vitrinite-rich seam benches, may suggest an organic affinity, unless these trace elements are distinctly correlated with allogenic and lithophile or chalcophile authigenic major elements.

Most enrichments of trace elements can be directly related to major element concentrations in these coal benches. However, of the trace elements with organic affinity listed above, Ga, Mo, Co and Cu are present in such low concentrations, that their partial association in organic bonds may well have such an impact that correlations to certain mineral phases cannot be drawn.

Gumz et al. (1958, p76&77) found similarly poor relations between petrography and trace element concentrations. Enrichment or depletion of certain elements, however, does exist in individual seam benches or groups of benches. Exceptionally, Co and F show a strong negative correlation with the ash content (Table 6.7). This indicates a high affinity of these elements with the organic material of the present coals and concurs with trends reported by BOUSKA (1981) and VALKOVIC (1983).

6.6.3. Element Distribution in Thermally-affected Coals

Most concentration changes take place within the metamorphic aureole, as defined by rank parameters and other proximate and ultimate analyses. Changes are normally expressed in a more erratic concentration distribution of the elements within both channels and lithotype benches (Figs. 6.18 to 6.20). Trends indicate depletion as well as enrichment of certain elements with an increasing degree of thermal metamorphism. Certain trace elements follow trends and correlations that are similar to those of major elements, with which

Digitised by the Department of Library Services in support of open access to information, University of Pretoria, 2021.

they are normally associated. Many trace elements, however, experience a depletion, either for a complete channel succession or for single horizons only.

SiO_2 and TiO_2 show very similar changes for each seam band near all three dolerite intrusions. The concentrations generally remain consistent within the metamorphic aureole; however, some slight depletion can be observed for individual seam benches, especially at localities B and D (Fig. 6.18a). KUNSTMANN and GASS (1957) found by laboratory test that the TiO_2 content of a coal remains constant on ashing or carbonization. It is thus concluded that TiO_2 is not volatile, but that depletion is only apparent, due to the marked increase in calcite and dolomite contents near the contact.

Al_2O_3 is the only major element that shows a considerable depletion in the cindered coals, from about 5-6% down to 3-4% (Fig. 6.18a), which is probably complimentary to the enrichment of CaO and MgO (Fig 6.19a). At locality B this trend is slightly subdued, due to a certain amount of enrichment in some seam horizons, from 2m distance to the dolerite contact.

Na_2O and K_2O are enriched, and therefore inversely related to AL_2O_3 within the aureole, which might be ascribed to intensified illitization of the clay minerals in the thermally-altered coals (Table 6.6). Similar observations, of increasing illite crystallinity and an absence of kaolinite in shaly matter in a seam near an intrusive/coal contact, were made in sedimentary rocks and coals of the Bramsche Massiv in Germany (TEICHMÜLLER et al., 1979).

Of the trace elements with allogenic affinity, Y, Zr, Nb and Th generally occur in erratic concentrations, but have slight depletion tendencies. Rb is enriched and has a good correlation with K_2O and Na_2O near the dykes (Fig. 6.18).

Of the authigenic elements, MgO and CaO show significant increases within the burnt coals and towards the dyke/coal contacts (Fig. 6.19a). In the case of MgO and CaO this corresponds with the macroscopically observed carbonate enrichment.

Although P_2O_5 concentrations vary considerably throughout the seam, enrichment trends can be outlined at all three dolerite localities. Particularly seam benches C and D show enrichment from 8m to 2m distance from the dyke contact. Sr and Ba both follow the enrichment trends of P_2O_5 (Fig. 6.19b), especially at approxiamtely 4-8m from the dyke, after having been depleted at the outer margin of the contact aureole.

FeO, of which the concentration also varies greatly, does not seem to be depleted or enriched as the dyke contact is approached. Increasing concentration trends in the top lithotype band at locality D and in some seam layers at other localities can be considered exceptions.

Of those elements with relatively high organic affinity, only Ni,

Digitised by the Department of Library Services in support of open access to information, University of Pretoria, 2021.

Co and F show distinct depletion towards the dykes. Cu becomes enriched in cindered coals, which is remarkable, because it is almost absent in the unaltered coals. Ga and Mo are variable to slightly depleted; so is V, while Cr is enriched.

At sampling locality D the 4m-channel shows distinct discontinuities in the enrichment and depletion trends of some element concentrations. SiO_2 and TiO_2 are slightly enriched, while FeO, MgO, CaO, Na_2O, K_2O and Rb show distinct depletion trends. Most other trace element trends exhibit a maximum value at channel D4 (Figs. 6.18 to 6.20).

In comparison to trace element analyses from the dolerite dykes, Cr and Ba are enriched in both the "white trap" and the cindered coals. Sr is enriched in the "white trap", but depleted along its margins and in the altered coals (compare table 6.1 with figures 6.18d and 6.19b).

6.7. Discussion of Dolerite Occurrences

Mode of Occurrence

The occurrence of dolerite intrusions in the coal measures is restricted to the western half of the sudy area. On the one hand, they seem to be related to the presence of a southwest-northeast trending fault zone in this part of the coalfield. The intrusions, therefore, partially follow the weakened area of the fault zone, which was already active during sedimentation (section 4.6.1). On the other hand, the dolerites mainly intrude the more argillaceous sedimentary sequences typical of the western half of the study area. In the east, arenaceous units deposited adjacent to the presumed paleochannel belt prevail.

WALKER and POLDERVAART (1949) report a preferred occurrence of dolerite sills concordant to the bedding planes of interlaminated sandstone and siltstone/shale units. A bifurcation of the intrusives appears more likely where silty and shaly layers dominate, because they are less competent. This bifurcation also seems to be concentrated in the upper portions of the sedimentary sequence, where overburden pressure is less (LEAMAN, 1975). It therefore appears that the mechanism of intrusion in the study area was comparable to the one suggested by LEAMAN (1975) for Tasmanian dolerites. It is mainly ascribed to wedging by the magma, which then intruded less resistant layers. A collapsing of the magma chamber, as proposed by HAMILTON (1983), appears less likely in this area, mainly due to a lack of basalt overburden.

Digitised by the Department of Library Services in support of open access to information, University of Pretoria, 2021.

Width of Contact Aureole

From a literature study it became apparent that the width of a contact aureole in a coal seam can be very variable. TEICHMÜLLER (1973) describes an aureole of approximately 0.8m width adjacent to a 0.7m wide dyke. Similar 1:1 correlations are reported by BLIGNAUT (1952). However, CLEGG (1955) finds no correlation between these two parameters and ROBERTS (1987) reports ratios ranging from about 3:1 to 0.5:1.

In this study the metamorphic aureole is found to be irregular in width, but tends to be about three times as wide as the investigated dykes. This is related to a generally higher ash content of the original coals, which averages about 18% (up to 23% in bench C), while the coals investigated by BLIGNAUT (1952), CLEGG (1955), TEICHMÜLLER (1973) and ROBERTS (1987) generally contain about 10% ash. It is assumed that the ash content of the present coals, mainly consisting of silicates, provided these coals with a higher heat conductivity than coals with a lower ash content. This could allow the metamorphic front to penetrate further into the coal seam. More detail on this aspect and on the possible influence of coal type on the amount of metamorphism will be discussed with the results of the rank determinations.

Other factors, such as magma temperature and cooling rate during either a single or multiple intrusive pulse through one dyke, will also have an impact on the grade of metamorphism. These aspects have been dealt with by DAPPLES (1939), KISCH and TAYLOR (1966), JÜNTGEN et al. (1973) and ROBERTS (1987) and will not be discussed further, because this study concentrates on a relatively limited number of dykes, with little variation in geometrical configuration and petrographic composition.

6.8. Discussion of Coal Petrography, Reflectivity and Chemistry

The combination of petrographic, proximate and ultimate analyses allows a clear distinction of individual seam benches to be made. Reflectivity, and volatile matter, carbon and hydrogen contents provide the best correlation parameters. In the unaffected coals the analytical results on a dry-ash-free basis are closely related to the maceral composition of the seam benches. In the cindered coals the analytical results are more dependent on rank and substantiate the conclusions of BOUSKA (1981, p102) in this regard. The width of the metamorphic aureole, as reflected by analytical results, agrees closely with the macroscopically defined aureole.

Digitised by the Department of Library Services in support of open access to information, University of Pretoria, 2021.

Micropetrography of the Coals

The major petrographic changes in the coals on thermal alteration are the disappearance of the exinite group macerals and micrinite, as well as the formation of natural coke. A more rapid increase in the reflectivity of exinite compared to vitrinite also results in their apparent disappearance during normal coalification (VAN KREVELEN, 1961). This phenomenon in regard to contact metamorphism has been related to temperatures of about 425°C (TEICHMÜLLER, 1973), which in this study must have been effective up to about 5m from the dyke contacts.

According to CRELLING and DUTCHER (1968) micrinite and sclerotinite are the most resistent macerals to thermal alteration. In the case of sclerotinite this cannot be determined at Twistdraai, because there are too few particles of this maceral in the present coals. Micrinite, however, shows a more sensitive reaction to heat than vitrinite, but is less reactive than, for instance, exinite.

The formation of coke with mosaic and flow structures and devolatilization vescicles indicates temperatures of about 400°C and that the coals had reached stages of plasticity (CRELLING and DUTCHER, 1968; STACH et al., 1982). This would relate to the reactions of coking coals in the technological coking process. However, the maximum temperature in the seam might have been as low as 320°C, which would have been sufficient, if a longer period of heating is taken into account (JÜNTGEN et al., 1973). Coke at 0m distance has a mosaic texture and is less vesicular than coke at greater distance. The reason, therefore, probably lies in the compaction of the plastic coal during emplacement of the intrusion (CRELLING and DUTCHER, 1968), which compressed already developed vesicles and gave the partially plastic maceral grains an irregular orientation. The latter formed the mosaic structure with undulating reflectivity of the cokes.

Slow heating rates at greater distances from a contact where limited plasticity occurred, could explain a lesser development of vesicles (JÜNTGEN et al., 1973). The first-formed vesicles in the slightly heat-affected coals are orientated in a 'pearl-string' arrangement, which probably occured along relatively weak bedding planes of the maceral components.

Rank Parameters

In most channels there is a reflectivity gradient, with values decreasing from bottom to top of the seam. This gradient is enhanced with decreasing sampling distance from the dyke contact and generally indicates a heat source from below. Inversion of this gradient, such as in channel C2 and to a lesser extent in channel G, may indicate a stronger heat source from above the seam. In both these cases this can possibly be related to a downward deflection of generally undulating dolerite sheets.

Digitised by the Department of Library Services in support of open access to information, University of Pretoria, 2021.

Similar phenomena were observed in some Natal coalfields where the rank of a complete seam was increased to the anthracite stage (Mr. M.C.J. VAN VUUREN, 1987, pers. comm.). It can be explained by the development of a steep temperature gradient through the sedimentary succession and, more specifically, through the coal seams.

As the distance between the seam and underlying intrusive sheet gradually decreases, before the dyke eventually cuts through the coal, the temperature gradient increases and enhances the rank difference between top and bottom of the seam.

These reflectivity variations, specifically in the unaffected coals, cannot be correlated with rank parameters from proximate and ultimate analyses. The latter are largely dependent on maceral composition, which was shown to be very variable from one seam bench to another.

Reflectograms for $\overline{R}OV_{max}$ become wider as the mean $\overline{R}OV_{max}$ of the coals increases. This could have been caused by different reactivities of vitrinite and low reflecting inertinite to thermal influences, which would allow the vitrinites to react more quickly. Thus, a subjective error distinguishing thermally-affected vitrinite from normally coalified low reflecting inertinite may influence the statistics, at least in some of the lesser metamorphosed coals.

Coals from benches B and C of a particular channel often have a slightly higher reflectivity than coals from the other seam layers. This is generally attributed to a relatively high proportion of detrital macerals in these coals, which also include vitrodetrinite. This maceral is, however, slightly higher-reflecting than telocollinite, which is normally measured, but which is not present in sufficient quantity in these two specific seam benches.

For coals within the contact aureole the relatively high reflectivity in benches B and C, especially if compared to bench D, is attributed to an irregular advance of the thermo-metamorphic front through the different seam layers. This, in turn, will be controlled by the high ash and inertinite content of benches B and C. As discussed earlier, the ash most probably increases the heat conductivity of the coal, thus allowing thermal alteration to project into more distant parts of the seam. Additionally, inertinite-rich coals are less reactive to heat than vitrinite-rich coals, such as in bench D. As the physico-chemical reactions on normal coalification and thermal alteration are largely endothermic, a reactive vitrinite-rich coal would absorb more heat, while an inertinite-rich coal, which hardly reacts, will conduct the heat. Thus the same amount of initial heat from the dolerite intrusion affects inertinite-rich coals over greater distances than vitrinite-rich coals.

This phenomenon of irregular advance of the thermo-metamorphic front is especially obvious in channel C4, where the topmost layers have a considerably higher rank than the lower ones. This may,

Digitised by the Department of Library Services in support of open access to information, University of Pretoria, 2021.

however, also be attributed to a possible deflection of the dyke to an inclined or subhorizontal sheet a short distance above the seam. This is also supported by an inverted rank gradient in channel C2.

Bimodal reflectograms in benches B, C and F, as well as a relatively low reflectance in bench D, are again related to an irregular advance of the metamorphism. In this case the margin of the contact aureole lies at the sampled channel, due to which parts of the benches were sampled on either side of this margin. Thus, coals of different reflectivity were sampled from one bench.

As pointed out, there is a discontinuity in reflectance increase from channels D8 to D4. This is accompanied by a higher volatile matter content, higher hydrogen and lower carbon percentage in all the samples of channel D4 compared to those of D8. These may be caused by the migration and accumulation of tarry matter away from the contact to the position of channel D4, similar to the findings of VAN VUUREN and QUASS (1982) on thermally-affected coals from other fields in South Africa. A migration of tar away from an intrusive is also indicated by SANYAL (1965), who found tarry matter in unaltered portions of coals near an intrusive.

Other authors have observed similar accumulations of tarry matter at a certain distance from a dyke (KISCH and TAYLOR, 1966; TEICHMÜLLER, 1973); they explain this as a migration of tarry matter, released from slightly affected coals, towards the intrusion and into parts of the seam that had an already enlarged pore volume due to earlier devolatilization and coke-formation. This process of migration towards the intrusion appears more likely to have taken place in the present coals, because it is very probable that the volatiles, released near the contact, were assimilated by the magma, or might have migrated into the overlying sedimentary rocks along the dyke.

This apparent reversal in rank is also indicated by the proximate and ultimate analyses and can perhaps be called a "retrograde" coalification. Although the $\bar{R}OV$ generally refers to a physical property of the vitrinite macerals, it is also dependent on the chemical composition of the vitrinte, namely the degree of aromaticity. The reflectivity can specifically be decreased by the microscopical impregnation of the vitrinite by tar (STACH et al., 1982, p435). CRELLING and DUTCHER (1968) found an increase in volatile matter (d.a.f.) towards the contact of an intrusion, which, however, did not influence the reflectivity. The explanation here is that the volatiles were either reabsorbed after having migrated from other parts of the seam, or were never released. The latter assumption appears highly unlikely, as a loss of volatiles is one of the early reactions when a coal is heated.

The present study does not enable a comparison of the thermal effects on coals of initially different rank. However, KHORASANI (1983) has shown similar rank increases of low rank coals on thermal

Digitised by the Department of Library Services in support of open access to information, University of Pretoria, 2021.

metamorphism from less than 1%$\overline{R}OV$ to 5.6%$\overline{R}OV_{max}$. These values strongly resemble those obtained in the present study. Medium rank coals are affected to a rank of 9% to 12%$\overline{R}OV_{max}$ (KHORASANI, 1983; TEICHMÜLLER, 1973).

Proximate Analyses

The results of the proximate analyses have largely been discussed in section 6.4 and, specifically, the volatile matter content (d.a.f.) has been related to the $\overline{R}OV$ in the preceding paragraphs. The CO_2 content, however, deserves a little more attention here.

The enrichment of carbonates in the coals towards the dyke contact is often regarded as epigenetic (TEICHMÜLLER, 1973), the carbonates having precipitated from percolating groundwater in the pores and shrinkage cracks of the cinder (VAN VUUREN and QUASS, 1982). In this context it seems important to note that the Ca content in the marginal portions of the dyke is about 40% lower than in the central portion. This would support the proposal of precipitation from groundwater, where the relevant carbonates had first been dissolved from the marginal parts of the dyke. This mechanism probably accounts for most of the carbonate occurrences in the cindered coals, rather than a metasomatic interaction between intrusive and coal as suggested by KISCH and TAYLOR (1966) and by PIETZNER (1973).

Inorganic Constituents of Unaltered Coals

Few elements have good correlation coefficients or exhibit trends of association in certain mineral phases. Most element concentrations are variable and have little or no correlation with each other; this indicates their occurrence in several mineral phases, which can have different associations from one seam bench to another.

Chalcophile elements should, to a certain extent, correlate with vitrinite, due to the anaerobic conditions that would promote their formation, if they were formed syngenetically. As, however, these mineral phases also form during diagenesis, where the conditions become more homogeneous throughout a coal seam, a relationship between initial deposition and preservation conditions and occurrencs of chalcophile elements will become overprinted. For this reason, most probably, there is little correlation between Fe, Ni, Cu, Co, Zn, Mo and vitrinite.

On account of changing element concentrations through the seam benches, a change in ash composition can be assumed, thus indicating variable genetic conditions for the seam as a whole. Initially, during deposition of benches A, B and C, conditions were fairly confined. The influx of clastic material was low and possibly characterized by a small variance of mineral phases, as indicated by better correlation coefficients in these lower benches. Later, during the deposition of benches D, E and F, influx of clastics increased and became dominated

Digitised by the Department of Library Services in support of open access to information, University of Pretoria, 2021.

by quartz and associated minerals. Clay minerals are assumed to have been equally important throughout deposition and are dominated by kaolinite. In certain seam benches illite might prevail, which, however, can also form diagenetically. The observed decrease in clay mineral content is probably only relative, due to an increase in quartz and related minerals. The variability of the mineral spectrum apparently increases towards the top of the seam, which accounts for poorer correlation coefficients in these horizons.

Most of the authigenic elements and minerals certainly accumulated and formed during diagenetic processes. Carbonates comprise the important minerals thus formed. Siderite possibly formed at a relatively early stage of diagenesis and was dependent on the supply of FeO, which might still have differed from seam bench to seam bench at that early stage of diagenesis. As a result siderite only formed in certain horizons of some seam benches.

During later diagenesis, when conditions were more homogeneous throughout the seam, the formation of calcite and dolomite predominated. The decreasing content of carbonates towards the top is related to a generally higher vitrinite content in the uppermost benches, where the pH values might still have been too low for more carbonate crystallization.

Other authigenic minerals such as pyrite and, more specifically, phosphate were largely dependent on the available elements from sediment influxes, and on specific preservation and diagenetic conditions. Hence, they accumulated in certain horizons of the seam only. Most elements, particularly trace elements, show erratic and relatively high concentrations in seam benches E and F. This is largely attributed to major influxes of clastics during the final phases of deposition. Enrichment of certain elements from groundwater during diagenesis probably added to these high concentrations.

It is noticeable at locality G that most allogenic elements are markedly enriched, while some authigenic elements are depleted, especially P_2O_5, Ba and Sr. This, together with similar divergences in petrographic, proximate and ultimate results, allows the assumption that the coals of channel G were deposited under conditions different to those for the adjacent coals. It was probably a deeper water environment, which accounts for a higher ash and inertinite content. Energy level and oxidation potential are also assumed to have been higher than in the surrounding swamps. This led to the deposition of more allogenic minerals and a lesser formation of authigenic material. The latter indicates that some authigenic minerals, particularly phosphates, form during early stages of the swamp phase.

Inorganic Constituents of the Thermally-altered Coals

Metasomatic alterations of the country rocks associated with the intrusions are generally very limited throughout the Karoo Sequence

Digitised by the Department of Library Services in support of open access to information, University of Pretoria, 2021.

(WALKER and POLDERVAART, 1949). Similar limited interactions of inorganic constituents of both dolerites and coals are noted in the present study.

Most allogenic major and trace elements show little depletion or enrichment, although their concentrations become somewhat irregular within the contact aureole. Depletion tendencies, in particular, are not related to absolute changes but to relative changes, due to an absolute increase in authigenic elements. They include, in particular, CaO and MgO. The relations generally concur with findings by LEUTWEIN and RÖSSLER (in: GUMZ et al., 1958, p158), that the chemistry of coke ashes does not differ considerably from that of coal ashes. Distinct depletion tendencies of Ni, Co, Ga, Mo and V, which have organic affinities, were also found by LEUTWEIN and RÖSSLER, who attributed them to the volatile character of these elements.

An increase of element concentrations is mainly associated with the authigenic material, particularly the lithophile components associated with MgO, CaO and P_2O_5. These increases are largely attributed to precipitation from groundwater.

The only endometamorphic effect of the coals on the dykes, in terms of inorganic constituents, appears to be a drastic enrichment of Sr and Ba in the dolerites, as well as a general increase in carbonates. This can be attributed to the inherent abundance of Sr and Ba in these coals. It is assumed that during the intrusion of the magma these elements were largely dissolved from the coals, and migrated towards the intrusion, to be assimilated in the magma. However, the magma might have become saturated in Sr and Ba, so that the remaining portion of these elements accumulated at the contact, where it might have crystallized as phosphates and carbonates. As a result, the dolerites of Twistdraai are considerably enriched in Sr and Ba compared to other Karoo dolerites, not only in the "white trap", but also in the apparently unaltered portions.

Digitised by the Department of Library Services in support of open access to information, University of Pretoria, 2021.

7. SUMMARY AND CONCLUSIONS

Two major factors influencing the quality of South African coals were investigated at the Twistdraai Coalfield. These are the depositional environment, in which the peat swamps formed, and the intrusion of dolerite sills and dykes, which partially metamorphosed the coals. An attempt will be made here to evaluate these factors and also to compare their importance.

On the scale of a single mine, which in this case extends over 180km^2, variations of the depositional conditions of the coals can be observed over a few square kilometers. This causes some of the coal properties to change over these relatively small lateral intervals as well.

Coal distribution was controlled by fluvial channel and floodplain depositional and erosional processes, as well as by subsidence due to differential compaction. Coal parameters (ash, volatile matter and calorific value) show significant correspondence with depositional features. Major changes in coal distribution and quality parameters, and thus in the economic value of the seam, can be expected in the vicinity of major active and abandoned channels, whereas floodplain settings produced coal seams of laterally persistent thickness and quality.

A relatively consistent run-off-mine quality can be expected from floodplain-dominated areas. This would enable production planning for a longer period in advance. Complications, however, may arise from unstable roof conditions. These are mainly caused by the weak bedding plane contacts which commonly exist in the finely laminated siltsone and shale units. These lithologies are a common feature in the roof rocks of floodplain-deposited coals. "Swelling clays" (e.g. montmorillonite) might play a major role in weakening the roof rock material. Although the present clay mineralogical study (section 3.1) did not indicate considerable amounts of these clay minerals, a more detailed investigation of the immediate roof rocks in this respect might be advisable.

In proximity to the distributary channels the thickness and quality of the coal seam were found to be very variable. Many square kilometers of the seam were contaminated by in-seam clastic splits in the top and bottom of the seam. This will certainly drastically decrease the grade of the coals in these areas, if the seam were to be mined as a whole. Selective mining of the seam portion with the least impurities would enable production of an approximately constant grade of coal. However, the remaining portions of the seam would still have to be extracted separately, in order to ensure safe roof conditions. This factor will necessitate a regular review of the production planning on a shorter term basis, as such areas of in-seam splits are irregularly distributed and depend directly on crevassing activities

Digitised by the Department of Library Services in support of open access to information, University of Pretoria, 2021.

of the paleochannels.

The coal type, in general has a more regional variation from paleofloodplain to paleochannel settings. It will, however, affect short-term planning in areas where the coal seam overlies oxbow lake deposits directly adjacent to channel deposits. These can cause considerable variations in volatile matter content, which is petrographically controlled and not due to rank variations. A fluctuation in volatile matter will influence the gasification properties of these coals.

The short-term production planning and geological activity at the Twistdraai Colliery is at present mainly directed towards the location of dolerite intrusions and the extent of their impact on the coals. Every aspect of coal mining is involved, from coal quality to mine production and roof safety.

The metamorphic effects of the dolerite dykes on the coal quality parameters are similar to observations made at analogous occurrences around the world. The intrusion forms a distinctly visible metamorphic aureole in which all petrographic and chemical alterations to the coal occur at variable degrees. Only the rank parameters, and specifically the $\overline{R}OV$, tend to show more widespread alterations.

Therefore, with regard to the objectives of this part of the study, it can be concluded that with proximate and ultimate analyses, as well as inorganic geochemistry, limited predictions of the locality of dolerite intrusions can be made. A direct link between coal parameters and dolerite petrography, chemistry and thickness, could not be established, because the variability of these parameters is very limited within the Twistdraai Coalfield.

$\overline{R}OV$ might prove to be a more significant parameter in order to predict dolerite localities. With a detailed sampling over the entire coalfield and determination of $\overline{R}OV$ at the top and bottom of the seam, one might be able to establish a rank gradient which is typical for the seam. This gradient could either be expressed as $\%\overline{R}OV/m$ coal thickness or, more simply, as a reflectance difference between top and bottom layers of the seam. Deviations from this gradient, and even inversions thereof, might indicate the proximity of an intrusion and its position below or above the seam. These gradients should be contoured in order to establish their relationship to known intrusions.

Future work with regard to predicting dolerite intrusions should, therfore, mainly focus on rank parameters. Although the investigated samples of the dyke and the "white trap" proved to be fairly uniform, a more detailed petrographic and chemical analysis of the dolerites themselves, as recovered from boreholes, might assist in the correlation of the dykes and sills.

In evaluating the importance of the one geological factor (depositional conditions) over the other (dolerite intrusions) with

Digitised by the Department of Library Services in support of open access to information, University of Pretoria, 2021.

regard to the quality and the mineability of a coalfield, one can conclude that both are important, but from different viewpoints.

The depositional conditions are of importance during coal-formation and thus determine type and grade of the coals on a regional scale. To establish a depositional model and to correlate it with the coal parameters will always be of assistance in the evaluation of a prospective field. This model can be continuously developed and improved, from early exploration stages through to feasibility studies and even during the production stages of the mine. The depositional model, in conjunction with the relevant coal parameters, thus helps in the evaluation and delineation of a prospective coalfield and in the long term development of a mine.

In relation to this, the influence of the dolerite sills appears to be of minor significance. Although they directly affect only minor portions of the total volume of available coal the dolerites can be detrimental to the feasibility of an entire coalfield. Their major influence is on the method of mining, thereby the costs involved in the development of a mine or a particular mining section. This factor thus affects the short-term planning of extraction methods for a mine.

The western half of the Twistdraai Coalfield, which lies in the floodplain-dominated portion of the paleoenvironment, exhibits most of the dolerite occurrences within the No. 4L coal seam. Hence, the advantageous paleoenvironmental setting of the main coal seam at Twistdraai is spoilt by the effect of the contact metamorphism.

Digitised by the Department of Library Services in support of open access to information, University of Pretoria, 2021.

REFERENCES

BENNETS, K.P. (1965); The Flint Clay Deposits of the Area Between Pretoria and Belfast, Transvaal, Bull. Geol. Surv. S. Afr., **45**, p 79.

BLIGNAUT, J.J.G. (1952); Field Relationships of the Dolerite Intrusions in the Natal Coalfields; Trans. Geol. Soc. S.Afr., **55**, pp 19-31.

BLIGNAUT, J.J.G. and FURTER, F.J.J. (1952); The Northern Natal Coalfield - The Utrecht-Newcastle Area; Dept. of Mines, Coal Surv., **Mem. 2**, p 228.

BOOTHROYD, J.C. and NUMMEDAL, D. (1978); Proglacial Braided Outwash: A Model for Humid Alluvial-Fan Deposits; in MIALL, A.D., Fluvial Sedimentology, Can. Soc. Pet. Geol., Alberta, pp 413-429.

BOUSKA, V. (1981); Geochemistry of Coal; Elsevier, Amsterdam, p 284.

BREDELL, J.H. (1983); Refractory Clays in the Transvaal: Exploration, Genesis and Property Interrelationships, Ph.D. Thesis, Univ. of Pretoria, p 174.

BRINDLEY, G.W. and BROWN, G. (1980); Crystal Structures of Clay Minerals and their X-ray Identification; Min. Soc., London, p 495.

BROWNLOW, A.H. (1979); Geochemistry; Prentice Hall, p 498.

BURGER, A.J. and COERTZE, F.J. (1971); Radiometric Age Measurements on Rocks from Southern Africa to the End of 1971; Bull. Geol. Surv. S.Afr., **58**, p 45.

BURST, J.F. (1958a); Mineral Heterogeneity in "Glauconite" Pellets; Am. Min., **43**, pp 481-497.

_____, (1958b); Glauconite Pellets: Their Mineral Nature and Application to Stratigraphic Interpretations; Am. Ass. Petrol. Geol. Bull., **42**, pp 310-327.

CADLE, A.B. (1979); Depositional Models from the Middle Ecca and Their Influence on Coal Accumulation in the Eastern Transvaal, Geocongress 79 Abstracts, Part 2, 18th Congr. Geol. Soc. S.Afr., pp 77-78.

CADLE, A.B. and HOBDAY, D.K. (1977); A Subsurface Investigation of the Middle Ecca and Lower Beaufort in Northern Natal and the Southeastern Transvaal; Trans. Geol. Soc. S.Afr., **80**, pp 111-115.

CAIRNCROSS, B. (1979); Depositional Framework and Control of Coal Distribution and Quality, van Dykes Drift Area, Northern Karoo Basin; M.Sc. Thesis, University of Natal, Pietermaritzburg, p 89.

_____, (1980); Anastomosing River Deposits: Paleoenvironmental Control on Coal Quality and Distribution, Northern Karoo Basin; Trans. Geol. Soc. S.Afr., **83**, pp 327-332.

CAIRNCROSS, B. and WINTER, M.F. (1984); High Constructive Lobate Deltas in the Lower Permian Vryheid Formation, Rietspruit, South Africa; Trans. Geol. Soc. S.Afr., **87**, pp 101-109.

CANT, D.J. (1978); Development of a Facies Model for Sandy Braided River Sedimentation; Comparison of the South Saskatchewan River and the Battery Point Formation; in MIALL, A.D., Fluvial Sedimentology, Can. Soc. Pet. Geol., Alberta, pp 627-639.

Digitised by the Department of Library Services in support of open access to information, University of Pretoria, 2021.

_____ (1982); Fluvial Facies Models and Their Application; in SCHOLLE, P.A. and SPEARING, D., Sandstone Depositional Environments, AAPG Publication, Tulsa, Oklahoma, pp 115-137.

CASAGRANDE, D.J.; SIEFERT, K.; BERSCHINSKI, C. and SUTTON, N. (1977); Sulfur in Peat-forming Systems of the Okefenokee Swamp and Florida Everglades: Origin of Sulfur in Coal; Geochim. Cosmochim. Acta, **41**, pp 161-167.

CHATTERJEE, P.K. and POOLEY, F.D. (1977); An Examination of some Trace Elements in South Wales Coals; Aust. Inst. Min. Metall., **Proc. 263**, pp 19-30.

CLEGG, K.E. (1955); Metamorphism of Coal by Peridotite Dikes in Southern Illinois; Ill. State Geol. Surv., **Report 178**, pp 18.

CLOUD, P.E. (1955); Physical Limits of Glauconite Formation; Am. Ass. Petrol. Geol. Bull., **39**, pp 484-492.

COLEMAN, J.M. (1969); Brahmaputra River: Channel Processes and Sedimentation; Sedim. Geol., **3**, pp 129-239.

COLEMAN, J.M. and PRIOR, D.B. (1982); Deltaic Environments; in SCHOLLE, P.A. and SPEARING, D., Sandstone Depositional Environments, Am. Ass. Petrol. Geol. Publication, Tulsa, Oklahoma, pp 139-178.

CRELLING, J.C. and DUTCHER, R.R. (1968); A Petrographic Study of a Thermally Altered Coal from the Pugatoire River Valley of Colorado; Geol. Soc. Am. Bull., **79 (10)**, pp 1375-1386.

DAPPLES, E.C. (1939); Coal Metamorphism in the Anthracite - Crested Butte Quadrangles, Colorado; Econ. Geol., **34**, pp 369-398.

DEER, W.A.; HOWIE, R.A. and ZUSSMAN, J. (1970); An Introduction to the Rock-forming Minerals; Longmans, London, p 528.

DEPARTMENT OF MINERAL AND ENERGY AFFAIRS (1985); Draft White Paper on the Energy Policy of the Republic of South Africa, no page numbers.

DJADTSCHENKO, M.G. and CHATUZEWA, A.A. (1957); Die Bildung von Glauconiten unter kontinentalen Bedingungen; Geologie, **6**, pp 217- 220.

DUTCHER, R.R.; CAMPBELL, D.L. and THORNTON, C.P. (1966); Coal Metamorphism and Igneous Intrusives in Colorado; Am. Chem. Soc., Adv. Chem. Ser., **65**, pp 708-723.

DU TOIT, A.L. (1954); Geology of South Africa, 3rd ed., Oliver&Boyd, Edinburgh, p 611.

EASTERBROOK, D.J. (1982); Glacial Sediments; in SCHOLLE, P.A. and SPEARING, D., Sandstone Depositional Environments, AAPG Publication, Tulsa, Oklahoma, pp 1-10.

EYLES, N. and MIALL, A.D. (1984); Glacial Facies; in WALKER, R.G., Facies Models, 2nd ed., Geol. Ass. Can., pp 15-38.

FALCON, R.M.S. (1977); Coal in South Africa - Part 1, The Quality of South African Coals in relation to its Uses and World Energy Resources, Minerals Sci. Eng., 9, pp 198-219.

FIELDING, C.R. (1985); Coal Depositional Models and the Distinction Between Alluvial and Delta Plain Environments, Sedim. Geol., **42**, pp 41-48.

Digitised by the Department of Library Services in support of open access to information, University of Pretoria, 2021.

FLORES, R.M. (1983); Basin Facies Analysis of Coal-Rich Tertiary Fluvial Deposits, Northern Powder Basin, Montana and Wyoming; in COLLINSON, J.D. and LEWIN, J., Modern and Ancient Fluvial Systems, Int. Ass. Sed., Spec. Publ. No. 6, pp 501-515.

FOUCH, T.D. and DEAN, W.E. (1982); Lacustrine and Associated Clastic Depositional Environments; in SCHOLLE, P.A. and SPEARING, D., Sandstone Depositional Environments, Am. Ass. Petrol. Geol. Publication, Tulsa, Oklahoma, pp 87-114.

GALLIHER, E.W. (1939); Biotite-Glauconite Transformation and associated minerals; in P.D. Trask: Recent Marine Sediments; Am. Ass. Petrol. Geol. Publ., Tulsa, Oklahoma, pp 513-515.

GALLOWAY, W.E. and HOBDAY, D.K. (1983); Terrigenous Clastic Depositional Systems, Applications to Petroleum, Coal and Uranium Exploration, Springer Verlag, New York, p 423.

GLUSKOTTER, H.J.; RUCH, R.R.; MILLER, W.G.; CAHILL, R.A.; DREHER, G.B. and KUHN, J.K. (1977); Trace Elements in Coal: Occurrence and Distribution; Ill. State Geol. Surv., **C 499**, p 154.

GRAHAM, K.W.T.; VAN ZIJL, J.S.V. and HALES, A.L. (1962); Palaeomagnetic Evidence Regarding the Relative Ages of the Stormberg Lavas and the Karoo Dolerites; Trans. Geol. Soc. S. Afr., **65/2**, pp 47-54.

GRIFFIN, G.M. and INGRAM, R.L. (1955); Clay Minerals of the Neuse River Estuary; J. Sed. Petr., **25**, pp 194-200.

GRIM, R.E. (1968); Clay Mineralogy, 2nd ed., Mc Craw-Hill, London, p 596.

GUMZ, W.; KIRSCH, H. and MACKOWSKY, M-TH. (1958); Schlackenkunde, Untersuchungen über die Minerale im Brennstoff und ihre Auswirkungen im Kesselbetrieb; Springer Verlag, Berlin, p 422.

HADDING, A. (1932); The Pre-Quartenary Rocks of Sweden, IV, Glauconite and Glauconite Rocks; Medd. Lunds. Geol.-Mineral. Inst., **51**.

HAGELSKAMP, H.H.B. (1983); Aspekte der Exploration und Petrographie der Kohlen des Waterbergfeldes im Nordwesten von Transvaal, Dipl. Arbeit, RWTH Aachen, p 128.

HAMILTON, L.H. (1983); Mechanisms of Magma Intrusion into Coal Seams; paper presented at the 4th Int. Coal Expl. Symp., 15.-20. May, Sydney, Australia, no page numbers.

HARVEY, R.D. and DILLON, J.W. (1985); Maceral Distribution in Illinois Coals and Their Paleoenvironmental Implications; Int. J. Coal Geol., Elsevier, Amsterdam, 5, pp 141-165.

HENDRICKS, S.B. and ROSS, C.S. (1941); Chemical Composition and Genesis of Glauconite and Celadonite; Am. Min., **26/12**, pp 683- 708.

HEWARD, A.P. (1978); Alluvial Fan and Lacustrine Sediments from Stephanian A and B (La Magdalena, Cinera-Matallana, and Sobero Coalfields), Northern Spain, Sedimentology, **25**, pp 451-488.

HOBDAY, D.K. (1973); Middle Ecca Deltaic Deposits in the Muden Tugela Ferry Area of Natal; Trans. Geol. Soc. S. Afr., **76**, pp 309-318.

Digitised by the Department of Library Services in support of open access to information, University of Pretoria, 2021.

_____, (1978); Fluvial Deposits of the Ecca and Beaufort Groups in the Eastern Karoo Basin, South Africa; in MIALL, A.D., Fluvial Sedimentology, Can. Soc. Pet. Geol., Alberta, pp 413-429.

HOBDAY, D.K.; TAVERNER-SMITH, R.; MATHEW, D. (1975); Markov Analyses and the Recognition of Palaeoenvironments in the Ecca Group near Vryheid, Natal; Trans. Geol. Soc. S. Afr., **78**, pp 75-82.

HONESS, A.P. and WILLIAMS, F.J. (1935); Dickite from Pennsylvania, Am. Min., **20**, pp 462-466.

HORNE, J.C.; FERME, J.C.; CARUCCIO, F.T. and BAGANZ, B.P. (1978); Depositional Models in Coal Exploration and Mine Planning in Appalachian Regions, Am. Ass. Petrol. Geol. Bull., **62/12**, pp 2379-2411.

ICCP (1971); Handbook for Coal Petrography; 2nd. ed., Int. Com. Coal Petr., Paris, Centr Nat. Rech. Scient.

JACKSON, R.G. (1978); Preliminary Evolution of Lithofacies Models for Meandering Alluvial Streams; in MIALL, A.D., Fluvial Sedimentology, Can. Soc. Pet. Geol., Alberta, pp 543-576.

JÜNTGEN, H.; VAN HEEK, K.-H. and FEISTER, P.P. (1973); Physikalisch-chemische Untersuchungen an Naturkoks und Rückschlüsse auf die Temperatur/Zeit-Bedingungen bei seiner Entstehung; Geol. Mittl., Aachen, **12**, pp 301-318.

KARR, C. (1978); Analytical Methods for Coal and Coal Products; Academic Press, New York, p 580.

KELLER, W.D. (1956); Glauconitic Mica in the Morrison Formation in Colorado; in: Clays and Clay Minerals, 5th international conference 1956, pp 120-128.

KHORASANI, G.K. (1983); Thermally Metamorphosed Coal from Eastern Australia; paper presented at the 4th Int. Coal Expl. Symp., 15.-20. May, Sydney, Australia, no page numbers.

KISCH, H.J. and TAYLOR, G.H. (1966); Metamorphism and Alteration near an Intrusive-Coal Contact; Econ. Geol., **61/2**, pp 343-361.

KUNSTMANN, F.H. and GASS, S.B. (1957); The Occurrence of Titanium in South African Coals; Jour. S. Afr. Inst. Mining Metall., pp 165-170.

LEAMAN, D.E. (1975); Form, Mechanism and Control of Dolerite Intrusions Near Hobart, Tasmania; J. Geol. Soc. Austr., **22**, pp 175-186.

LE BLANC SMITH, G. (1980); Genetic Stratigraphy and Paleoenvironmental Controls on Coal Distribution in the Witbank Basin Coalfield; Ph.D. Thesis (unpubl.), Univ. Wits., Johannesburg, p 242.

LE BLANC SMITH, G. and ERIKSSON, K.A. (1979); A Fluvioglacial and Glaciolacustrine Deltaic Depositional Model for Permo-Carboniferous Coals of the North-Eastern Karoo Basin, S.A.; Palaeogegr. Palaeoclim. Palaeoecol., **27**, pp 67-84.

LE ROUX, J.P. (1985); Die Eienskappe en Korrelasie van Steenkoollae in die Witbank-Bethal-Breyten Gebied, MSc. Thesis, Univ. of Pretoria, p 203.

MAMAY, S.H. and YOCHELSON, E.L. (1962); Occurrence and Significance of Marine Animal Remains in American Coal Balls; U.S. Geol. Surv. Prof. Pap **354-I**, Washington D.C., pp 193-224.

Digitised by the Department of Library Services in support of open access to information, University of Pretoria, 2021.

McDOUGALL, I. (1963); Potassium-Argon Measurements on Dolerites from Antarctica and South Africa; J. Geophys. Res., **68/5**, pp 1535-1545.

McLEAN, J.R. and JERZYKIEWICZ (1978); Cyclicity, Tectonics and Coal: Some Aspects of Fluvial Sedimentology in the Brazean-Paskapoo Formations, Coal Valley Area, Alberta, Canada; in MIALL, A.D., Fluvial Sedimentology, Can. Soc. Pet. Geol., Alberta, pp 441-468.

McRAE, S.G. (1972); Glauconite, Earth Science Review, **8**, pp 397-440.

MEHLISS, A.T.M. (1985); Operating and Developing Coal Mines in the Republic of South Africa, Minerals Bureau, Department of Mineral and Energy Affairs, Directory 2/85, p 57.

MIALL, A.D. (1984); Deltas; in WALKER, R.G., Facies Models, 2nd ed., Geol. Ass. Can., pp 105-118.

MILLOT, G. (1970); Geology of Clays, Springer, Berlin, p 429.

MOORE, L.R. (1968); Some Sediments Closely Associated with Coal Seams; in MURCHISON, D.G. and WESTOLL, T.S., Coal and Coal-Bearing Strata, Oliver and Boyd, Edinburgh, pp 105-123.

NICHOLLS, G.D. (1968), The Geochemistry of Coal Bearing Strata; in MURCHISON, D. and WESTOLL, T.S.; Coal and Coal-Bearing Strata; Elsevier, New York, pp 269-307.

NICR (Nat. Inst. for Coal Res.) (1985); Annual Report 1984/85; CSIR Spec. Rep. Coal 5, Pretoria, p 52.

NORRISH, K. and CHAPPEL, B.W. (1977); X-ray Fluorescence Spectrography; in ZUSSMANN, J.; Physical Methods in Determinative Mineralogy; Academic Press, New York, pp 161-214.

OTTE, M.U. (1953); Spurenelemente in einigen deutschen Steinkohlen; Chemie der Erde, Jena, **16**, pp 239-294.

PARRY, W.T. and REEVES, C.C. (1966); Lacustrine Glauconitic Mica from Pluvial Lake Mound, Lynn and Terry Countries, Texas; Am. Min., **51**, pp 229-235.

PIETZNER, H. (1973); Mikrosondenuntersuchungen an Carbonat-Einschlüssen im Naturkoks des Flözes Präsident/Helene der Zeche Friedrich-Heinrich bei Kamp-Lintfort (Linker Niederrhein); Geol. Mittl., Aachen, **12**, pp 255-276.

PLUMSTEAD, E.P. (1957); The Permo-Carboniferous Coal Measures of the Transvaal, South Africa - An Example of Contrasting Stratigraphy in the Southern and Northern Hemisphere, C.r. 4. Congr. int. Strat. Geol. Carbonifere, Maastricht, **2**, pp 545-550.

PORRENGA, D.H. (1968); Non-marine Glauconitic Illite in the Lower Oligocene of Aardeburg, Belgium; Clay Min., **7**, pp 421-430.

POWERS, M.C. (1957); Adjustment of Land Derived Clays to the Marine Environment; J. Sed. Petr., **27**, pp 355-372.

PRYOR, W.A. and GLASS, H.D. (1961); Cretaceous-Tertiary Clay Mineralogy of the Upper Mississippi Embayment; J. Sed. Petr., **31**, pp 38-51.

RADFORTH, N.W. (1969); Environmental and Structural Differentials in Peatland Development; in DAPPLES, E.C. and HOPKINS, M.E., Environments of Coal Deposition, Geol. Soc. Am., Spec. Paper 114, pp 87-104.

Digitised by the Department of Library Services in support of open access to information, University of Pretoria, 2021.

READING, H.G. (1982); Sedimentary Environments and Facies; Blackwell Scientific Publications, Oxford-London, p 569.

REINECK, H.E. and SINGH, I.B. (1980); Depositional Sedimentary Environments, Springer Verlag, New York, p 439.

ROBERTS, J.R. de R. (1987); The Effect of Dolerite Dykes on Coal Seams of the Klip River Coalfield, North Natal; MSc. thesis, Univ. Natal, Durban, p 411.

RUST, B.R. (1978); Depositional Models for Braided Alluvium; in MIALL, A.D., Fluvial Sedimentology, Can. Soc. Pet. Geol., Alberta, pp 605-626.

RYAN, P.J. (1968); Stratigraphy of the Ecca Series and Lowermost Beaufort Beds (Permian) in the Karoo Basin of South Africa, Ph.D. Thesis (unpubl.), Univ. Wits., Johannesburg, p 210.

SACS (SOUTH AFRICAN COMMITTEE FOR STRATIGRAPHY) (1980); Stratigraphy of South Africa Part I, compiled by L.E. KENT; Lithostratigraphy of the Republic of South Africa, SWA/Namibia, and the Republic of Bophuthatswana, Transkei and Venda: Handbook Geol. Surv. S. Afr., 8, p 690.

SAMPSON, R.J. (1975); SURFACE II Graphics System, Kansas Geol. Surv., Op. Res. Sec., p 240.

SANYAL, S.P. (1965); Nature of a Thin Vein of Solidified Tarry Matter Formed During Natural Carbonization of Coal from Victoria West Collieries, Raniganj Coalfield, India; Fuel, London, **44**, pp 333-338.

SHRIVASTAVA, B.B.P.; MUKHERJEE, T.K. and TRIPATHI, B. (1983); Geological Location of Igneous Intrusions in Coal Beds, The 'Pest' of Permian Coal Measures in India; paper presented at the 4th Int. Coal Expl. Symp., 15.-20. May, Sydney, Australia, no page numbers.

SIEPKER, E.H. (1986); Genetiese Stratigrafie en Sedimentologie van die Opeenvolging Karoo in die Westelike en Noeerdelike Deel van die Waterbergsteenkoolveld; M.Sc. Thesis, Rand Afrikaanse Universiteit, Johannesburg, p 177.

SMITH, D.G. (1976); Effect of Vegetation of Lateral Migration of Anastomosed Channels of a Glacial Meltwater River; Geol. Soc. Am. Bull., **87**, pp 857-860.

SMITH, N.D. (1970); The Braided Stream Depositional Environment: Comparison of the Platte River with some Silurian Clastic Rocks, North Central Appalachians; Geol. Soc. Am. Bull., **81**, pp 2993-3014.

_____, (1975); Sedimentary Environments and Late Quarternary History of a "Low Energy" Mountain Delta; Can. Jour. Earth Sci., **12**, pp 2004-2013.

SMITHSON, F. and BROWN, G. (1954); The Petrography of Dickite Sandstones in North Wales and Northern England; Geol. Mag., **41**, 3, pp 177-188.

SNYMAN, C.P. (1961); Die Petrographie südafrikanischer Gondwanakohlen - Ein Vergleich zwischen Gondwana und euramerischen Kohlen, Dissertation, Rheinische Friedrich-Wilhelms Universität, Bonn, p 103.

SNYMAN, C.P.; VAN VUUREN, M.C.J. and BARNARD, J.M. (1983); Chemical and Physical Characteristics of South African Coals and a Suggested Classification System, NICR, Pretoria, p 63.

Digitised by the Department of Library Services in support of open access to information, University of Pretoria, 2021.

STACH, E.; MACKOWSKY, M-Th.; TEICHMÜLLER, M.; TAYLOR, G.H.; CHANDRA, D. and TEICHMÜLLER, R. (1982); Stach's Textbook of Coal Petrology; 3rd ed., Gebr. Borntraeger, Berlin, p 535.

STANISTREET, I.G.; LE BLANC SMITH, G.; CADLE, A.B. (1980); Trace Fossils as Sedimentological and Paleoenvironmental Indices in the Ecca Group (Lower Permian) of the Transvaal; Trans. Geol. Soc. S. Afr., **83**, pp 333-344.

STANLEY, K.O. and SURDAM, R.C . (1978); Sedimentation on the Front of Eocene Gilbert-Type Deltas, Washakie Basin, Wyoming; J. Sed. Petr., **48/2**, pp 557-573.

STAUB, J.R. and COHEN, A.D. (1978); Kaolinite-Enrichment Beneath Coals: A Modern Analog, Snuggedy Swamp, South Carolina; J. Sed. Petr., **48**, pp 203-210.

_____, (1979); The Snuggedy Swamp of South Carolina: A Back-Barrier Coal-Forming Environment; J. Sed. Petr., **49**, pp 133-144.

STEYN, J.D.G. and SMITH, W. (1977); Coal Petrography in the Evaluation of South African Coals, Coal, Gold and Base Minerals, Johannesburg, **9.**

STEYN, P.P.A. (1976); Die Sedimentologie van die Davelsteenkoolveld in die Oos-Transvaal met spesiale Verwysings na die Vryheid Formasie van die Karoo Supergroep; M.Sc. Thesis, RAU, Johannesburg, p 88.

_____, (1983); In-Seam longhole Drilling - An Effective Tool, paper presented at the 4th Int. Coal Expl. Symposium, 15.-20. May, Sydney, Australia, no page numbers.

STRATTEN, T. (1970); Tectonic Framework of Sedimentation During the Dwyka Period in South Africa; Proc. 2nd Int. Gondwana Symposium, IUGS, S.Afr., pp 483-490.

TANKARD, A.J.; JACKSON, M.P.A.; ERIKSSON, K.A.; HOBDAY, D.K.; HUNTER, D.R. and MINTER, W.E.L. (1982); Crustal Evolution of South Africa - 3.8 Billion Years of Earth History; Springer Verlag, New York, p 523.

TAVERNER-SMITH, R. and MASON, T.R. (1985); The Vryheid Formation (Middle Ecca) at the Tugela Ferry: A Postscript to Earlier Work, S. Afr. Jour. Sci., **81**, pp 275-279.

TEICHMÜLLER, M. (1955); Anzeichen mariner Beeinflussung bei der Kohle aus Flöz Katharina der Zeche Friedrich-Heinrich; N. Jb. Geol. Palaont. Ml., pp 193-201.

_____ (1971); Anwendung kohlenpetrographischer Methoden bei der Erdöl und Erdgas Prospektion; Erdöl und Kohle, **24**, pp 69-76.

_____ (1973); Zur Petrographie und Genese von Naturkoksen im Flöz Präsident/Helene der Zeche Friedrich Heinrich bei Kamp-Lintfort (linker Niederrhein); Geol. Mitt., Aachen, **12/9**, pp 219-254.

TEICHMÜLLER, M.; TEICHMÜLLER, R. and WEBER, K. (1979); Inkohlung und Illit-Kristallinität, Vergleichende Untersuchungen im Mesozoikum und Paläozoikum von Westfalen; Fortschr. Geol. Rheinl. und Westf. **27**, pp 201-276.

TISSOT, B.P. and WELTE, D.H. (1978); Petroleum Formation and Occurrence, Springer Verlag, Berlin, p 538.

Digitised by the Department of Library Services in support of open access to information, University of Pretoria, 2021.

TRUSWELL, J.F. (1977); The Geological Evolution of South Africa, 2nd. ed., Purnell, Johannesburg, p 218.

TYLER, S.A. and BAILEY, S.W. (1961); Secondary Glauconite in the Biwabic Iron Formation of Minnesota; Econ. Geol., **56**, pp 1033-1044.

VALKOVIC, V. (1983); Trace Elements in Coal; CRC Press, Florida, Vol. I, p210, Vol II, p 281.

VAN KREVELEN, D.W. (1961); Coal, Typology - Chemistry - Physics - Constitution; Elsevier, Amsterdam, p 514.

VAN VUUREN, C.J. (1983); A Basin Analysis of the Northern Facies of the Ecca Group; Ph.D. Thesis, University of the Orange Free State, p 249.

VAN VUUREN, M.C.J. and QUASS, F.W. (1982); What Happens to Coal when a Dyke Intrudes?; Coal, Gold and Base Minerals, Johannesburg, **30**, pp 143-146.

VAN ZYL, C. (1982); Rapid Preparation of Robust Pressed Powder Briquetts Containing a Styrene and Wax Mixture as Binder; X-ray Spectrometry, **11**, 1, pp 29-31.

VISSER, D.J.L. (1984); Geological Map of the Republics of South Africa, Transkei, Bophuthatswana, Venda and Ciskei, and the Kingdoms of Lesotho and Swaziland, scale 1:1.000.000, Government Printer, Pretoria

VISSER, J.N.J. (1986); Lateral Lithofacies Relationships in the Glacigene Dwyka Formation in the Western and Central Parts of the Karoo Basin; Trans. Geol. Soc. S.Afr., **89/3**, pp 373-384.

VON BRUNN, V. and STRATTEN, T. (1981); Late Paleozoic Tillites of the Karoo Basin of South Africa; in HAMBREY, M.J. and HARLAND, W.B., Earth's Pre-Pleistocene Glacial Record, Cambr. Univ. Press, London, p 1004.

WALKER, F. and POLDERVAART, A. (1949); Karoo Dolerites of the Union of South Africa; Geol. Soc. Am. Bull., **60**, pp 591-706.

WALKER, R.G. and CANT, D.J. (1984); Sandy Fluvial Systems; in WALKER, R.G., Facies Models, 2nd ed., Geol. Ass. Can., pp 71-89.

WEAVER, C.E. and POLLARD, L.D. (1973); The Chemistry of Clay Minerals; Series: Developments in Sedimentology, No. 15; Elsevier, Amsterdam, p 213.

WHATELEY, M.K.G. (1980); Deltaic and Fluvial Deposits of the Eccca Group, Nongoma Graben, Northern-Zululand; Trans. Geol. Soc. S. Afr., **83**, pp 345-351.

WHITEHURST, D.D.; MITCHELL, T.O. and FARCASIU, M. (1980); Coal Liquefaction - The Chemistry and Technology of Thermal Processes; Academic Press, New York, p 378.

WILLIAMS, E.G. and KEITH, M.L. (1963); Relationship between Sulfur in Coals and the Occurrence of Marine Roof Beds; Econ. Geol., **58**, pp 720-729.

WILLIS, J.P. and HART, R,J, (1985); Trace Element Analysis of Coals by INAA and XRFS; J. Trace and Microprobe Techniques, **3(1&2)**, pp 109-127.

WYBERGH, W.J. (1928); The Coal Resources of the Union of South Africa, Vol 3, Geol. Surv. of S. Afr., **Mem. 19**, p 181.

Digitised by the Department of Library Services in support of open access to information, University of Pretoria, 2021.

ZUBOVIC, P.; STADNICHENKO, T. and SCHEFFEY, N.B. (1960); The Association of Minor Elements with Organic and Inorganic Phases of Coal; Prof. Paper 400-B, U.S. Geol. Surv., Reston, Va., pp B84-B87.

BS 1016, (1956); British Standard Methods for the Analyses and Testing of Coal and Coke, Part 16, Reporting of Results.

NBS 1632a (1978); National Bureau of Standards Certificate and Analysis; Standard Reference Material 1632a, Trace Elements in Coal (Bituminous).

SARM 19; South African Reference Material, Certificate of Analysis, Coal (O.F.S.).

SARM 20; South African Reference Material, Certificate of Analysis, Coal (Sasolburg).

Digitised by the Department of Library Services in support of open access to information, University of Pretoria, 2021.

A P P E N D I X

Digitised by the Department of Library Services in support of open access to information, University of Pretoria, 2021.

LIST OF APPENDICES

APPENDIX 1A: Quantitative clay mineral and carbonate analyses of all samples of borehole **B.** 228

APPENDIX 1B: Quantitative clay mineral and carbonate analyses of all samples of borehole **C.** 228

APPENDIX 2 : Complete set of paleo-pH results of borehole **C.** Samples 329 to 347 were measured in triplicate, once after the solution had rested for 10min (1) and once after 24h (2). 231

APPENDIX 3A: Distribution of massive, cellular and detrital macerals in sections 59, 61 and 62. 232

APPENDIX 3B: Distribution of maceral groups in sections 59, 61 and 62. Inertinite is subdivided into low and high reflecting categories. 232

APPENDIX 4 : XRF results of major and trace element concentrations of unaffected dolerites and "white trap" material. Samples indicated with **"*"** are taken from the marginal zone of the respective dyke. Total iron is expressed as Fe_2O_3. 233

APPENDIX 5 : Maceral analyses of all unaffected and heat-affected coals. Maceral analyses was not carried out on samples at 0m sampling distance from the dyke, for reasons explained in the text. 234

APPENDIX 6 : V-class distribution of all samples of unaffected and thermally-affected coals. Figures indicate the number of measurements per v-class. On most samples 20 points werer measured, in exceptional cases 50 points. 236

APPENDIX 7 : Proximate analyses of thermally-affected coals on an air-dry basis (left) and on a dry-ash-free basis (right). 238

APPENDIX 8 : Ultimate analyses of thermally-affected coals on an air-dry basis (left) and on a dry-ash-free basis (right). 240

APPENDIX 9 : Ultimate and proximate analyses, with inferred calorific value and H/C and O/C atomic ratios, of thermally-affected coals after correction for CO_2 content. 242

APPENDIX 10: Major element concentrations on a whole coal air-dry basis **without** ash factor correction. 244

APPENDIX 11: Major element concentrations on a whole coal air-dry basis **with** ash factor correction. 246

APPENDIX 12: Trace element concentrations on a whole coal air-dry basis **without** ash factor correction. 248

Digitised by the Department of Library Services in support of open access to information, University of Pretoria, 2021.

APPENDIX 13: Trace element concentrations on a whole coal air-dry basis **with** ash factor correction. 250

APPENDIX 14: Pearson correlation matrix for petrographic and proximate analyses vs. major element concentrations of all samples of unaffected coals (59 samples). 252

APPENDIX 15: Pearson correlation matrix for petrographic and proximate analyses vs. trace element concentrations of all samples of unaffected coals (59 samples). 252

APPENDIX 16: Pearson correlation matrix for major element vs. major element concentrations of all samples of unaffected coals (59 samples). 253

APPENDIX 17: Pearson correlation matrix for major element vs. trace element concentrations of all samples of unaffected coals (59 samples). 253

APPENDIX 18: Pearson correlation matrix for trace element vs. trace element concentrations of all samples of unaffected coals (59 samples). 254

APPENDIX 19: Pearson correlation matrix for petrographic and proximate analyses vs. major element concentrations of all samples of unaffected coals (59 samples). Matrices are given separately for each seam bench **A** to **F.** Sample **GZ** is incorporated in the matrix for bench **A.** 255

APPENDIX 20: Pearson correlation matrix for petrographic and proximate analyses vs. trace element concentrations of all samples of unaffected coals (59 samples). Matrices are given separately for each seam bench **A** to **F.** Sample **GZ** is incorporated in the matrix for bench **A.** 258

APPENDIX 21: Pearson correlation matrix for major element vs. major element concentrations of all samples of unaffected coals (59 samples). Matrices are given separately for each seam bench **A** to **F.** Sample **GZ** is incorporated in the matrix for bench **A.** 261

APPENDIX 22: Pearson correlation matrix for major element vs. trace element concentrations of all samples of unaffected coals (59 samples). Matrices are given separately for each seam bench **A** to **F.** Sample **GZ** is incorporated in the matrix for bench **A.** 264

APPENDIX 23: Pearson correlation matrix for trace element vs. trace element concentrations of all samples of unaffected coals (59 samples). Matrices are given separately for each seam bench **A** to **F.** Sample **GZ** is incorporated in the matrix for bench **A.** 267

Digitised by the Department of Library Services in support of open access to information, University of Pretoria, 2021.

APPENDIX 1A: Quantitative clay mineral and carbonate analyses of all samples of borehole **B.**

sample No.	elev. (m aSL)	Kaol. %	Ill. %	Mont. %	Sid. %	Calc. %	Dolo. %
34	1548.0	28.2	0.0	0.0	2.3	0.0	0.0
35	1547.0	25.0	0.0	0.0	1.8	0.0	0.0
36	1546.0	24.7	0.0	0.0	1.3	0.6	0.0
37	1545.0	22.4	0.0	0.0	3.2	0.3	0.0
38	1544.0	17.3	0.0	0.0	2.6	0.6	0.0
39	1543.0	13.5	0.0	0.0	0.0	0.0	0.0
40	1542.0	11.6	0.0	0.0	0.0	0.4	0.0
41	1541.0	0.2	0.0	0.0	0.0	0.0	0.0
42	1539.0	6.4	0.0	0.0	0.0	0.0	0.0
43	1538.0	11.0	0.0	0.0	0.0	0.9	0.0
44	1536.5	9.9	0.0	0.0	0.0	0.0	0.0
45	1534.5	37.1	0.0	0.0	0.7	0.0	0.3
46	1533.5	28.7	0.0	0.0	5.4	0.0	0.0
47	1532.5	42.7	0.0	0.0	4.2	0.0	0.0
48	1531.5	28.2	0.0	0.0	3.1	0.2	0.6
49	1530.5	20.0	0.0	0.0	2.8	0.0	0.0
50	1529.5	16.8	51.3	0.0	3.9	0.0	0.0
51	1528.5	22.0	0.0	0.0	3.0	0.2	0.0
52	1527.5	25.2	54.5	0.0	0.0	0.0	0.0
53	1526.5	23.6	0.0	0.0	4.5	0.0	0.0
54	1525.5	4.3	0.0	0.0	0.0	0.0	0.8
55	1523.5	4.8	0.0	0.0	0.6	0.0	0.1
56	1521.5	42.3	0.0	0.0	0.0	0.0	0.0
57	1520.5	39.3	0.0	0.0	0.0	0.5	0.0
58	1519.5	11.5	0.0	0.0	0.0	12.3	3.3
59	1517.5	12.5	0.0	0.0	0.9	0.0	0.4
60	1515.5	17.3	0.0	0.0	0.5	0.0	0.5
61	1513.5	50.1	0.0	0.0	0.0	0.1	0.0
62	1512.5	48.4	0.0	0.0	0.0	0.0	0.0
63	1511.0	34.7	0.0	0.0	0.0	0.0	0.5
64	1510.0	30.5	0.0	0.0	0.6	0.0	0.0
65	1508.0	43.4	0.0	0.0	1.4	0.0	0.0
66	1507.5	37.7	0.0	0.0	0.0	0.0	0.0
67	1506.5	22.5	0.0	0.0	5.5	1.0	0.0
68	1505.5	28.2	0.0	0.0	8.4	0.0	0.0
69	1504.5	46.8	0.0	0.0	0.5	0.2	0.0
70	1503.5	54.5	0.0	0.0	1.2	0.0	0.0
71	1502.5	78.9	0.0	0.0	0.0	0.0	0.0
72	1501.5	50.5	0.0	0.0	1.9	0.0	0.0
73	1500.0	42.5	0.0	0.0	1.5	0.0	0.0
74	1499.0	44.8	0.0	0.0	1.7	0.0	0.0
75	1498.0	42.7	0.0	0.0	1.0	0.0	0.0
76	1497.0	52.8	0.0	0.0	0.0	0.0	0.0
77	1496.5	41.4	0.0	0.0	4.7	0.0	0.0
78	1495.5	26.0	0.0	0.0	9.5	0.4	0.0
79	1494.5	6.3	0.0	0.0	3.5	6.0	18.1
80	1493.5	32.1	0.0	0.0	2.8	0.2	0.0
81	1492.5	18.1	0.0	0.0	6.7	0.0	2.3
82	1491.5	35.1	0.0	0.0	2.5	0.0	0.0
83	1490.3	16.7	0.0	0.0	4.1	0.0	0.1
84	1489.5	7.1	0.0	0.0	1.5	0.0	0.0
85	1488.5	38.3	0.0	0.0	2.0	0.0	0.0

APPENDIX 1B: Quantitative claymineral and carbonate analyses of all samples of borehole **C.**

sample No.	elev. (m aSL)	Kaol. %	Ill. %	Mont. %	Sid. %	Calc. %	Dolo. %
235	1544.5	24.8	0.0	0.0	3.7	0.0	0.0
236	1543.0	29.7	0.0	0.0	0.9	0.0	0.0
237	1541.5	26.3	0.0	0.0	1.0	0.5	0.0
238	1540.5	20.7	0.0	0.0	3.6	0.0	0.0
239	1539.5	33.5	0.0	0.0	0.0	0.4	0.0
240	1539.0	1.4	0.0	0.0	0.0	12.4	0.4
241	1537.0	38.1	0.0	0.0	0.0	0.0	1.0
242	1536.5	32.0	0.0	0.0	0.9	0.3	0.0
243	1535.5	29.2	0.0	0.0	0.0	0.4	0.0
244	1534.5	32.3	0.0	0.0	0.0	0.5	0.0
245	1532.0	32.1	0.0	0.0	0.0	0.3	0.0
246	1531.0	31.7	0.0	0.0	0.0	0.5	0.0
247	1530.0	41.1	0.0	0.0	0.0	0.5	0.0
248	1528.5	32.6	0.0	0.0	0.2	0.4	0.0
249	1528.5	23.1	0.0	0.0	1.8	0.5	0.0
250	1527.5	29.0	0.0	0.0	0.4	0.2	0.0
251	1526.5	30.8	0.0	0.0	0.0	0.5	0.0
252	1525.5	31.5	0.0	0.0	0.0	0.3	0.0
253	1524.5	21.8	0.0	0.0	1.9	0.4	0.0
254	1523.0	14.1	0.0	0.0	0.5	0.0	0.6
255	1521.0	0.8	0.0	0.0	0.3	0.0	0.0
256	1519.0	19.0	0.0	0.0	0.7	0.0	0.0
257	1516.5	29.3	0.0	0.0	0.0	0.0	0.0
258	1515.5	67.9	0.0	0.0	0.0	0.0	0.0
259	1514.0	31.4	0.0	0.0	0.1	0.0	0.0
260	1512.5	25.6	0.0	0.0	0.0	0.7	0.0
261	1511.5	32.6	0.0	0.0	0.3	0.5	0.0
262	1509.5	27.5	0.0	0.0	2.4	0.3	0.0
263	1508.5	28.1	0.0	0.0	0.6	0.3	0.0
264	1507.0	28.6	0.0	0.0	0.9	0.5	0.0
265	1506.0	33.9	0.0	0.0	1.7	0.3	0.0
266	1505.0	34.8	0.0	0.0	1.4	0.6	0.0
267	1503.5	34.0	0.0	0.0	0.3	0.6	0.0
268	1502.5	37.7	0.0	0.0	0.9	0.4	0.0
269	1502.0	33.1	0.0	0.0	1.2	0.6	0.0
270	1501.0	33.4	0.0	0.0	2.5	0.5	0.0
271	1499.5	33.4	0.0	0.0	1.9	0.4	0.0
272	1498.5	27.7	0.0	0.0	5.6	0.4	0.0
273	1497.5	32.3	0.0	0.0	3.0	0.3	0.0
274	1496.5	30.6	0.0	0.0	4.7	0.6	0.0
275	1495.5	10.3	0.0	0.0	3.7	0.0	0.2
276	1494.5	26.6	0.0	0.0	2.0	0.5	0.0
277	1493.0	35.0	0.0	0.0	1.7	1.0	0.0
278	1492.0	28.9	0.0	0.0	2.6	0.6	0.0
279	1491.0	29.7	0.0	0.0	0.8	0.7	0.0
280	1490.0	30.3	0.0	0.0	1.3	0.2	0.0
281	1489.0	32.4	0.0	0.0	0.3	0.3	0.0
282	1488.0	80.9	0.0	0.0	0.3	0.0	0.0
283	1487.5	87.2	0.0	0.0	0.5	0.0	0.6
284	1487.0	32.7	0.0	0.0	0.0	0.0	0.0
285	1485.5	3.0	0.0	0.0	10.6	0.0	0.2
286	1484.5	47.3	0.0	0.0	1.3	0.0	0.2

Digitised by the Department of Library Services in support of open access to information, University of Pretoria, 2021.

APPENDIX 1A: continued

sample No.	elev. (m aSL)	Kaol. %	Ill. %	Mont. %	Sid. %	Calc. %	Dolo. %
86	1487.0	24.7	0.0	0.0	0.0	0.0	1.1
87	1486.5	45.8	0.0	0.0	0.0	0.0	0.0
88	1484.0	33.6	0.0	0.0	9.9	0.0	0.6
89	1483.0	48.8	0.0	0.0	0.0	0.0	0.2
90	1479.5	96.1	0.0	0.0	0.7	0.0	0.0
91	1478.0	47.6	0.0	0.0	0.5	0.0	0.0
92	1477.5	98.3	0.0	0.0	0.6	0.0	0.2
93	1476.0	76.0	0.0	0.0	1.4	0.0	0.0
94	1474.5	98.0	0.0	0.0	1.3	0.0	0.0
95	1473.5	53.3	0.0	0.0	1.0	0.0	0.0
96	1472.0	67.9	0.0	0.0	0.8	0.0	0.0
97	1471.0	90.7	0.0	0.0	1.6	0.0	0.3
98	1469.5	40.2	0.0	0.0	1.3	0.8	0.9
99	1468.5	28.1	0.0	0.0	0.0	0.0	0.5
100	1467.0	64.4	0.0	0.0	0.0	0.0	0.0
101	1466.0	25.7	0.0	0.0	0.7	0.0	1.2
102	1465.5	22.0	0.0	0.0	0.7	0.0	0.8
103	1464.5	18.6	0.0	0.0	0.7	0.0	0.2
104	1463.5	16.7	0.0	0.0	1.2	0.0	0.5
105	1462.5	21.0	0.0	0.0	1.2	0.0	1.3
106	1461.5	14.0	0.0	0.0	0.7	0.0	0.6
107	1460.5	17.3	0.0	0.0	0.8	0.0	0.3
108	1459.5	19.1	0.0	0.0	0.6	0.0	0.4
109	1458.5	15.0	0.0	0.0	0.5	0.0	0.0
110	1457.5	15.3	0.0	0.0	1.5	0.0	0.5
111	1456.5	11.3	0.0	0.0	1.3	0.0	0.5
112	1455.5	11.3	0.0	0.0	0.6	0.0	0.0
113	1454.5	39.8	0.0	0.0	0.7	0.3	0.0
114	1453.5	48.3	0.0	0.0	0.0	0.0	0.0
115	1452.5	0.0	0.0	0.0	0.0	0.0	0.7
116	1451.5	0.0	0.0	0.0	0.7	0.0	0.4
117	1450.5	0.0	0.0	0.0	0.2	0.0	0.4
118	1449.5	0.0	0.0	0.0	1.0	0.5	0.9
119	1448.5	0.0	0.0	0.0	0.3	0.0	0.5
120	1447.5	0.0	0.0	0.0	0.4	0.2	0.2
121	1446.5	0.0	0.0	0.0	0.3	0.0	0.7
122	1445.5	0.0	0.0	0.0	0.9	0.1	0.7
123	1444.5	0.0	0.0	0.0	0.8	0.3	0.6
124	1443.5	0.0	0.0	0.0	0.5	0.2	0.5
125	1441.5	0.0	0.0	0.0	0.8	0.0	0.9
126	1439.5	15.0	0.0	0.0	1.7	0.0	1.5
127	1437.5	21.2	0.0	0.0	0.9	0.5	1.3
128	1435.5	9.6	0.0	0.0	1.2	0.2	0.4
129	1433.5	76.5	0.0	0.0	0.3	0.0	0.4
130	1431.5	0.0	18.1	0.0	0.0	0.0	0.0
131	1429.0	30.0	28.0	0.0	0.0	0.0	0.0
132	1428.5	20.0	44.8	0.0	0.1	0.0	0.0
133	1427.5	9.4	40.0	0.0	0.0	0.0	0.0
134	1426.5	0.0	9.5	0.0	0.0	1.1	0.0
135	1425.5	0.0	10.3	0.0	0.0	0.9	0.0
136	1424.5	0.0	16.5	0.0	0.0	0.6	0.6
137	1423.0	10.1	0.0	0.0	2.4	2.8	2.0
138	1412.5	0.0	12.7	0.0	0.0	0.6	0.5

APPENDIX 1B: continued

sample No.	elev. (m aSL)	Kaol. %	Ill. %	Mont. %	Sid. %	Calc. %	Dolo. %
287	1483.0	48.5	0.0	0.0	0.1	0.0	0.0
288	1477.5	67.3	0.0	0.0	0.1	0.0	0.0
289	1476.0	69.5	0.0	0.0	0.7	0.0	0.0
290	1474.5	26.5	0.0	0.0	0.8	0.3	0.0
291	1472.5	83.4	0.0	0.0	1.1	0.3	0.0
292	1470.5	24.8	0.0	0.0	0.7	0.0	0.8
293	1468.0	15.4	0.0	0.0	0.8	0.0	1.1
294	1466.0	13.1	0.0	0.0	0.4	0.1	1.1
295	1464.0	19.0	0.0	0.0	0.2	0.0	0.7
296	1462.0	12.1	0.0	0.0	1.1	0.1	0.7
297	1459.5	62.8	18.5	0.0	0.0	0.0	0.0
298	1458.5	36.1	0.0	0.0	0.0	0.4	0.0
299	1457.5	24.7	0.0	0.0	0.6	0.4	1.0
300	1456.5	32.0	0.0	0.0	0.0	0.3	0.0
301	1455.0	95.0	0.0	0.0	0.0	0.0	0.0
302	1453.5	31.2	0.0	0.0	0.3	0.6	0.0
303	1452.5	25.7	0.0	0.0	1.0	0.5	0.0
304	1451.5	31.8	0.0	0.0	0.7	0.7	0.0
305	1450.5	36.9	0.0	0.0	1.0	0.3	0.0
306	1449.5	34.7	0.0	0.0	1.0	0.8	0.0
307	1448.5	38.0	0.0	0.0	0.6	0.5	0.0
308	1447.5	31.9	0.0	0.0	3.0	0.4	0.0
309	1446.5	23.6	0.0	0.0	8.5	2.2	0.0
310	1446.0	28.6	0.0	0.0	0.7	0.0	0.0
311	1445.0	17.1	56.2	0.0	0.0	0.0	0.0
312	1444.0	1.3	49.0	0.0	1.0	0.5	0.0
313	1443.0	4.8	88.6	0.0	0.0	0.0	0.0
314	1441.5	0.6	46.5	0.0	0.0	0.0	0.0
315	1440.0	0.0	52.5	0.0	0.0	0.4	0.2
316	1438.5	0.0	48.0	0.0	0.0	0.1	0.0
317	1436.5	0.0	43.6	0.0	0.0	0.0	0.2
318	1435.0	0.0	46.6	0.0	0.0	0.3	0.0
319	1433.0	0.0	43.0	0.0	0.0	0.0	0.0
320	1430.5	0.0	36.6	0.0	0.0	0.0	0.4
321	1428.5	0.0	31.7	0.0	0.0	0.2	0.0
322	1426.5	0.0	35.5	0.0	0.0	0.6	0.3
323	1424.5	0.0	37.2	0.0	0.0	1.1	0.0
324	1422.5	0.0	43.4	0.0	0.0	0.8	0.0
325	1420.5	0.0	6.7	0.0	1.1	0.0	0.0
326	1418.5	1.5	0.0	0.0	0.5	0.0	1.2
327	1416.5	12.3	0.0	0.0	0.7	0.0	0.2
328	1414.5	10.5	0.0	0.0	0.9	0.2	3.4
329	1412.5	13.6	0.0	0.0	0.8	0.1	0.6
330	1410.5	14.7	0.0	0.0	0.8	0.4	0.7
331	1408.5	42.4	0.0	0.0	0.0	0.2	0.0
332	1407.5	41.5	0.0	0.0	3.6	0.0	0.0
333	1406.0	36.2	0.0	0.0	0.0	0.1	0.0
334	1405.5	29.9	0.0	0.0	0.3	0.0	0.0
335	1404.5	21.5	0.0	0.0	0.3	0.0	0.0
336	1403.5	25.6	0.0	0.0	0.0	0.0	0.0
337	1402.5	22.9	0.0	0.0	0.0	0.0	0.0
338	1401.5	12.7	0.0	0.0	2.7	0.0	0.0
339	1400.5	23.3	12.7	0.0	0.0	0.0	0.0

Digitised by the Department of Library Services in support of open access to information, University of Pretoria, 2021.

APPENDIX 1A: continued

sample No.	elev. (m aSL)	Kaol. %	Ill. %	Mont. %	Sid. %	Calc. %	Dolo. %
139	1410.5	0.0	18.4	0.0	0.0	0.5	0.0
140	1408.5	0.0	9.9	0.0	0.0	0.7	0.4
141	1406.0	0.0	35.2	0.0	0.0	0.5	0.9
142	1404.0	0.0	8.8	0.0	0.0	2.7	0.0
143	1402.0	0.0	19.4	0.0	0.0	0.7	0.9
144	1400.0	0.0	0.0	0.0	0.0	0.3	0.5
145	1398.0	0.0	0.0	0.0	1.2	0.4	1.0
146	1396.0	0.0	0.0	0.0	1.2	0.5	0.8
147	1393.5	0.0	0.0	0.0	0.7	22.4	0.8
148	1392.5	12.5	0.0	0.0	0.6	0.2	0.5
149	1392.0	80.0	0.0	0.0	0.0	0.0	0.0
150	1390.5	50.0	0.0	0.0	0.0	0.0	0.0
151	1389.5	42.9	0.0	0.0	0.0	0.0	0.0
152	1388.5	40.7	0.0	0.0	0.6	0.0	0.0
153	1387.5	2.7	0.0	0.0	0.2	0.0	0.0
154	1385.5	0.0	0.0	0.0	7.8	0.0	0.0
155	1384.0	37.7	0.0	0.0	0.2	0.0	0.2
156	1383.0	28.8	0.0	0.0	0.0	0.2	0.0
157	1382.0	36.2	0.0	0.0	7.1	0.0	0.0
158	1381.5	12.2	0.0	0.0	0.0	0.0	0.0
159	1380.5	3.9	0.0	0.0	3.9	0.0	0.0
160	1379.0	11.2	0.0	0.0	1.6	0.0	0.0
161	1378.0	23.2	0.0	0.0	6.1	0.0	0.4
162	1377.0	18.5	0.0	0.0	0.0	0.2	0.2
163	1376.5	3.8	0.0	0.0	0.0	0.0	0.0
164	1375.5	14.0	0.0	0.0	0.0	0.0	0.4
165	1374.5	7.9	0.0	0.0	2.2	0.0	0.0
166	1373.0	7.3	0.0	0.0	4.0	0.3	1.3
167	1371.5	2.1	0.0	0.0	5.3	0.0	1.1
168	1370.0	3.3	0.0	0.0	4.5	0.0	0.0
169	1369.0	0.1	0.0	0.0	1.2	0.0	0.0
170	1367.5	0.0	0.0	0.0	5.2	0.0	0.0
171	1366.5	2.5	0.0	0.0	0.9	0.0	0.3

Digitised by the Department of Library Services in support of open access to information, University of Pretoria, 2021.

APPENDIX 1B: continued

sample No.	elev. (m aSL)	Kaol. %	Ill. %	Mont. %	Sid. %	Calc. %	Dolo. %
340	1399.5	15.7	17.8	0.0	0.0	0.0	0.0
341	1398.5	1.3	11.7	0.0	0.0	0.0	0.0
342	1397.5	2.0	9.1	0.0	0.0	0.0	0.0
343	1396.0	8.0	0.0	0.0	0.0	0.1	0.0
344	1395.5	19.8	16.4	0.0	0.0	0.0	0.0
345	1394.0	1.0	0.0	0.0	0.5	0.0	0.0
346	1392.5	0.0	0.0	0.0	3.2	1.3	0.0
347	1390.0	2.1	0.0	0.0	15.6	0.3	0.0

Digitised by the Department of Library Services in support of open access to information, University of Pretoria, 2021.

APPENDIX 2: Complete set of paleo-pH results of borehole **C.** Samples 329 to 347 were measured in triplicate, once after the solution had rested for 10min (1) and once after 24h (2).

sample No.	elev. (m. a. SL)	pH	sample No.	elev. (m. a. SL)	pH		
235	1544.5	8.4	290	1474.5	7.5		
236	1543.0	8.5	291	1472.5	7.2		
237	1541.5	8.3	292	1470.5	7.9		
238	1540.5	8.8	293	1468.0	8.1		
239	1539.5	8.9	294	1466.0	7.6		
240	1539.0	9.1	295	1464.0	8.0		
241	1537.0	8.2	296	1462.0	7.9		
242	1536.5	8.5	297	1459.5	8.2		
243	1535.5	8.3	298	1458.5	8.3		
244	1534.5	8.0	299	1457.5	8.3		
245	1532.0	8.4	300	1456.5	8.9		
246	1531.0	8.4	301	1455.0	8.5		
247	1530.0	8.5	302	1453.5	9.0		
248	1528.5	8.6	303	1452.5	8.6		
249	1528.5	8.5	304	1451.5	8.6		
250	1527.5	8.5	305	1450.5	8.6		
251	1526.5	8.7	306	1449.5	8.5		
252	1525.5	9.1	307	1448.5	8.7		
253	1524.5	8.4	308	1447.5	9.2		
254	1523.0	6.3	309	1446.5	8.8		
255	1521.0	5.5	310	1446.0	8.7		
256	1519.0	6.2	311	1445.0	8.8		
257	1516.5	8.2	312	1444.0	8.6		
258	1515.5	7.9	313	1443.0	9.0		
259	1514.0	7.1	314	1441.5	8.4		
260	1512.5	8.2	315	1440.0	8.7		
261	1511.5	8.4	316	1438.5	8.9		
262	1509.5	8.4	317	1436.5	9.0		
263	1508.5	8.2	318	1435.0	8.6		
264	1507.0	8.3	319	1433.0	8.7		
265	1506.0	8.0	320	1430.5	8.6		
266	1505.0	7.7	321	1428.5	5.8		
267	1503.5	8.2	322	1426.5	8.9		
268	1502.5	8.3	323	1424.5	8.8		
269	1502.0	7.9	324	1422.5	9.4		
270	1501.0	7.7	325	1420.5	8.6		
271	1499.5	8.2	326	1418.5	8.4		
272	1498.5	8.2	327	1416.5	8.7		
273	1497.5	8.0	328	1414.5	8.2		
274	1496.5	8.1				(1)	(2)
275	1495.5	7.8	329	1412.5	8.2	8.9	8.7
276	1494.5	7.9	330	1410.5	7.9	8.9	8.3
277	1493.0	8.0	331	1408.5	8.1	8.3	8.5
278	1492.0	7.9	332	1407.5	7.9	8.6	8.4
279	1491.0	7.9	333	1406.0	8.2	8.4	8.4
280	1490.0	7.3	334	1405.5	8.3	8.6	8.6
281	1489.0	6.3	335	1404.5	8.3	8.9	8.6
282	1488.0	6.7	336	1403.5	8.6	8.7	8.8
283	1487.5	7.3	337	1402.5	8.3	9.4	9.1
284	1487.0	6.1	338	1401.5	8.4	9.0	8.6
285	1485.5	4.8	339	1400.5	8.9	8.7	8.6
286	1484.5	3.1	340	1399.5	9.1	8.8	8.5
287	1483.0	7.9	341	1398.5	9.1	9.6	9.6
288	1477.5	7.6	342	1397.5	8.4	9.5	9.3
289	1476.0	7.5	343	1396.0	8.6	8.7	8.7
			344	1395.5	8.6	9.1	9.0
			345	1394.0	8.9	9.1	9.0
			346	1392.5	8.7	9.7	9.5
			347	1390.0	9.5	9.6	9.6

Digitised by the Department of Library Services in support of open access to information, University of Pretoria, 2021.

APPENDIX 3A: Distribution of massive, cellular and detrital macerals in sections 59, 61 and 62.

	sample No.	massive macerals %	detrital macerals %	cellular macerals %	other macerals %
section 62	174	27.2	39.2	32.1	1.5
	175	84.8	3.6	10.3	1.3
	176	12.1	65.3	21.5	1.1
	177	12.4	41.6	43.7	2.3
	178	9.3	68.2	21.5	1.0
	179	32.3	28.7	35.7	3.3
	180	24.0	42.7	31.0	2.3
	181	15.4	71.6	11.8	1.2
	182	15.8	75.4	6.5	2.3
	183	73.3	11.5	11.3	3.9
	184	13.1	81.1	5.5	0.3
section 59	215	28.2	51.6	17.1	3.1
	216	63.5	16.6	17.0	2.9
	217	8.2	73.1	16.2	2.5
	218	78.7	5.7	14.3	1.3
	219	20.2	55.9	23.4	0.5
	220	23.6	31.1	41.7	3.6
	221	2.8	91.7	5.5	0.0
	222	25.8	32.8	37.1	4.3
	223	4.6	56.5	37.1	1.8
	224	7.4	79.7	10.8	2.1
	225	21.0	40.3	36.0	2.7
	226	16.0	51.1	29.1	3.8
	227	45.1	20.6	32.6	1.7
section 61	185	36.1	30.6	30.3	3.0
	186	60.1	24.3	13.8	1.8
	187	22.1	49.6	26.8	1.5
	188	58.0	25.0	15.0	2.0
	189	20.3	49.8	27.5	2.4
	190	85.2	5.3	7.4	2.1
	191	27.3	38.5	31.6	2.6
	192	69.1	20.4	9.6	0.9
	194	81.5	10.6	6.1	1.8
	195	22.2	47.3	26.2	4.3
	196	17.1	60.3	20.1	2.5
	197	9.3	63.1	23.3	4.3

APPENDIX 3B: Distribution of maceral groups in sections 59, 61 and 62. Inertinite is subdivided into low and high reflecting categories.

	sample No	vitrinite %	inertinite low refl. %	inertinite high refl. %	proportion of low refl. in total inertinites %	exinite %
section 62	174	23.6	45.6	30.3	60.1	0.5
	175	84.8	8.5	5.4	61.2	1.3
	176	8.9	64.3	26.2	71.0	0.6
	177	9.4	65.4	23.4	73.6	1.8
	178	3.0	69.1	27.4	71.6	0.5
	179	32.3	45.4	20.0	57.6	2.3
	180	17.5	47.6	33.4	58.8	1.5
	181	7.4	62.6	29.4	68.0	0.6
	182	16.5	66.8	15.4	81.3	1.3
	183	70.6	18.1	9.6	65.3	1.7
	184	25.8	57.9	16.0	78.3	0.3
section 59	215	15.9	55.3	26.2	67.9	2.8
	216	63.7	22.7	10.9	67.6	2.7
	217	5.6	72.6	20.0	78.4	1.8
	218	83.8	5.3	9.6	35.4	1.3
	219	21.0	55.1	23.4	70.2	0.5
	220	20.8	48.8	28.1	63.5	2.3
	221	1.0	77.7	21.3	78.5	0.0
	222	26.4	51.0	20.1	71.7	2.5
	223	4.5	71.8	23.2	75.6	0.5
	224	4.1	67.3	27.9	70.7	0.7
	225	25.8	53.8	19.2	73.7	1.2
	226	17.6	55.6	24.3	69.6	2.5
	227	49.9	27.3	21.1	56.4	1.7
section 61	185	36.3	38.1	23.1	62.3	2.5
	186	64.3	19.2	15.2	55.8	1.3
	187	18.6	57.4	23.0	71.4	1.0
	188	62.7	21.5	14.3	60.1	1.5
	189	16.7	58.3	24.1	70.8	0.9
	190	88.5	5.8	3.9	59.8	1.8
	191	29.2	45.1	23.4	65.8	2.3
	192	70.0	21.6	7.6	74.0	0.8
	194	84.3	8.8	6.4	57.9	0.5
	195	23.3	55.6	19.3	74.2	1.8
	196	18.3	48.9	31.8	60.6	1.0
	197	9.1	60.5	27.4	68.8	3.0

Digitised by the Department of Library Services in support of open access to information, University of Pretoria, 2021.

APPENDIX 4: XRF results of major and trace element concentrations of unaffected dolerites and "white trap" material. Samples indicated with "*" are taken from the marginal zone of the respective dyke. Total iron is expressed as Fe_2O_3.

sample No.	DA-1 *	DA-2	DA-3 *	DB-1 *	DB-2	DB-3 *	DB-4 *	DC-1 *	DC-2	DC-3 *	DD-1 *	DD-2	DD-3 *	85516 *	85514	85513	85510 *
SiO_2	32.94	37.73	32.70	37.79	33.46	39.35	32.76	39.73	30.62	28.90	35.06	44.25	32.69	39.73	48.40	47.69	43.41
TiO_2	2.12	2.20	2.23	2.20	1.72	2.80	2.24	2.00	1.45	1.22	2.38	1.96	2.23	2.14	2.12	2.06	2.37
Al_2O_3	13.95	14.43	14.11	11.93	16.01	15.57	14.46	13.31	11.49	9.49	12.82	13.30	13.40	14.71	12.95	13.64	16.43
Fe_2O_3	15.38	14.18	17.18	16.14	14.82	15.41	17.23	15.26	17.11	16.16	19.27	16.71	17.31	19.21	17.19	16.37	17.82
FeO	0.00	0.00	0.00	0.00	0.00	0.00	0.00	0.00	0.00	0.00	0.00	0.00	0.00	0.00	0.00	0.00	0.00
MnO	0.22	0.18	0.24	0.23	0.21	0.20	0.23	0.20	0.29	0.22	0.27	0.25	0.27	0.38	0.25	0.22	0.12
MgO	3.93	2.54	4.29	3.33	3.70	2.80	4.39	2.92	5.21	3.28	3.44	4.61	3.67	2.51	4.81	4.42	2.16
CaO	8.32	11.57	7.36	6.87	9.65	2.38	5.93	7.47	10.35	3.56	6.60	9.38	8.85	6.24	9.23	9.55	5.45
Na_2O	1.76	1.91	1.87	1.89	1.94	2.24	1.68	1.94	1.61	1.30	2.13	2.50	1.87	2.11	2.62	2.76	2.10
K_2O	0.42	0.48	0.47	0.45	0.40	0.56	0.57	0.38	0.16	0.39	0.49	0.35	0.54	0.35	0.38	0.37	0.25
P_2O_5	0.19	0.21	0.18	0.28	0.20	0.27	0.22	0.17	0.08	0.24	0.18	0.18	0.23	0.23	0.23	0.16	0.22
H_2O	0.77	0.51	0.71	0.54	0.82	0.68	0.55	1.15	1.20	2.01	0.45	0.25	0.39	1.26	0.26	0.33	0.43
LOI	17.46	12.87	15.96	16.35	14.94	15.56	18.68	14.62	17.47	31.63	15.27	4.60	16.05	8.19	0.16	1.41	6.96
CO_2	n.d.	n.d.	n.d.	n.d.	n.d.	n.d.	n.d.	n.d.	n.d.	n.d.	n.d.	n.d.	n.d.	n.d.	n.d.	n.d.	n.d.
TOTAL	97.46	98.81	97.30	98.00	97.87	97.82	98.94	99.15	97.04	98.40	98.36	98.34	97.50	97.06	98.60	98.98	97.72
Zn	149	270	162	130	127	195	152	125	95	75	155	127	146	141	141	124	157
Cu	335	346	359	335	270	472	349	325	204	174	392	311	358	332	348	274	351
Ni	67	62	73	64	81	82	67	67	71	52	69	79	71	82	75	74	86
Co	47	21	55	48	52	64	41	51	40	31	53	47	50	65	43	40	56
Ga	29	24	29	23	32	25	27	23	21	16	26	21	29	30	28	27	31
Mo	0	0	0	0	0	0	0	0	0	0	0	0	0	0	0	0	0
Nb	8	5	4	8	4	7	5	7	0	6	6	7	5	7	6	8	6
Zr	125	134	136	138	102	163	132	125	94	104	141	116	165	129	129	117	134
Y	37	37	37	37	28	41	41	33	25	25	44	35	40	40	38	38	34
Sr	384	503	345	489	386	165	275	404	485	340	441	268	477	308	176	193	233
Rb	15	17	14	12	11	23	13	11	0	18	15	9	16	7	8	5	0
U	6	0	0	0	0	0	0	5	6	4	0	0	0	5	0	0	0
Th	0	0	0	0	0	0	0	0	0	0	0	0	0	0	0	0	0
Pb	8	11	8	8	11	6	8	5	13	7	11	10	6	9	5	10	13
Cr	169	150	873	135	147	146	159	133	141	433	121	127	144	130	148	115	109
V	509	494	565	495	446	635	547	448	418	346	538	397	519	527	406	397	514
Ba	819	737	1045	1043	1083	974	1068	761	1376	1820	890	408	736	263	148	137	184
Sc	56	68	59	61	40	63	54	55	42	33	69	40	48	49	44	33	44

Digitised by the Department of Library Services in support of open access to information, University of Pretoria, 2021.

APPENDIX 5: Maceral analyses of all unaffected and heat-affected coals. Maceral analyses was not carried out on samples at 0m sampling distance from the dyke, for reasons explained in the text.

sample No.	Vitr. %	Inert/1 %	Inert/h %	Micr. %	Exin. %	Coke %	Total %
b 0 a							
b 0 b							
b 0 c							
b 0 d							
b 0 e							
b 2 a	5.25	61.00	10.50	0.25	0.00	23.00	100.00
b 2 b	1.50	48.25	16.50	0.25	0.00	33.50	100.00
b 2 c	1.25	77.50	10.75	0.00	0.00	10.50	100.00
b 2 d	9.75	26.50	7.75	0.00	0.00	56.00	100.00
b 2 e	13.75	60.75	7.75	0.00	0.00	17.75	100.00
b 4 a	10.50	74.00	7.50	0.25	0.00	7.75	100.00
b 4 b	4.00	79.25	11.00	0.50	0.00	5.25	100.00
b 4 c	0.75	86.00	11.50	0.00	0.00	1.75	100.00
b 4 d	26.00	23.25	4.75	0.00	0.00	46.00	100.00
b 4 e	4.75	79.00	10.25	0.00	0.00	6.00	100.00
b 8 a	26.75	58.75	14.25	0.00	0.25	0.00	100.00
b 8 b	28.00	51.00	20.25	0.50	0.25	0.00	100.00
b 8 c	9.50	77.75	12.75	0.00	0.00	0.00	100.00
b 8 d	83.55	10.47	5.98	0.00	0.00	0.00	100.00
b 8 e	33.25	53.25	11.50	0.50	1.50	0.00	100.00
b 10 a	28.25	54.00	15.25	1.00	1.50	0.00	100.00
b 10 b	21.50	62.50	14.00	0.00	1.75	0.25	100.00
b 10 c	22.00	64.75	11.75	0.50	1.00	0.00	100.00
b 10 d	69.88	18.07	10.60	0.00	1.45	0.00	100.00
b 10 e	16.75	70.25	10.25	0.25	2.50	0.00	100.00
b 16 a	22.50	51.00	24.50	0.75	1.25	0.00	100.00
b 16 b	22.38	47.92	28.71	0.00	0.99	0.00	100.00
b 16 c	7.56	75.85	15.85	0.00	0.74	0.00	100.00
b 16 d	70.32	17.52	10.96	0.00	0.96	0.24	100.00
b 16 e	24.25	52.75	19.25	0.50	3.25	0.00	100.00
b 32 a	23.19	54.83	21.26	0.48	0.24	0.00	100.00
b 32 b	19.44	63.89	14.12	0.46	1.86	0.23	100.00
b 32 c	7.46	82.59	8.46	0.00	1.49	0.00	100.00
b 32 d	58.75	31.25	8.75	0.25	1.00	0.00	100.00
b 32 e	22.28	62.38	12.87	0.74	1.73	0.00	100.00
c 0 a							
c 0 b							
c 0 c							
c 0 d							
c 0 e							
c 0 f							
c 2 a	25.84	51.67	21.05	0.48	0.00	0.96	100.00
c 2 b	3.38	72.95	18.36	0.00	0.00	5.31	100.00
c 2 c	0.50	77.00	20.50	1.00	0.00	1.00	100.00
c 2 d	4.48	43.28	12.44	0.00	0.00	39.80	100.00
c 2 e	10.91	65.45	8.64	0.00	0.00	15.00	100.00
c 2 f	9.00	59.50	12.00	0.00	0.00	19.50	100.00
c 4 a	15.50	58.25	22.00	1.25	2.75	0.25	100.00
c 4 b	10.60	72.53	14.94	0.00	1.93	0.00	100.00
c 4 c	7.57	80.14	11.82	0.00	0.47	0.00	100.00
c 4 d	65.45	27.01	7.54	0.00	0.00	0.00	100.00
c 4 e	5.50	74.25	6.75	0.00	0.00	13.50	100.00
c 4 f	12.25	69.00	9.25	0.00	0.00	9.50	100.00
c 8 a	31.50	53.50	12.25	1.25	1.50	0.00	100.00
c 8 b	8.85	70.10	18.66	0.48	1.91	0.00	100.00
c 8 c	8.93	79.90	10.42	0.00	0.75	0.00	100.00
c 8 d	60.50	27.00	8.75	0.00	3.75	0.00	100.00
c 8 e	41.30	39.91	15.31	0.00	2.78	0.70	100.00
c 8 f	19.25	62.25	15.75	0.25	2.00	0.50	100.00
c 20 a	33.41	49.52	13.94	0.48	2.65	0.00	100.00
c 20 b	12.50	69.00	14.00	2.75	1.75	0.00	100.00
c 20 c	4.33	74.76	18.75	0.96	1.20	0.00	100.00
c 20 d	71.19	16.43	11.43	0.00	0.95	0.00	100.00
c 20 e	35.99	43.96	17.87	0.00	2.18	0.00	100.00
c 20 f	16.54	61.23	20.25	0.25	1.73	0.00	100.00
c 36 a	16.95	59.43	21.24	0.48	1.91	0.00	100.01
c 36 b	13.00	68.50	16.25	0.50	1.75	0.00	100.00
c 36 c	6.03	80.74	12.07	0.00	1.16	0.00	100.00
c 36 d	76.50	15.75	7.25	0.00	0.50	0.00	100.00
c 36 e	34.62	48.80	12.97	0.24	3.37	0.00	100.00
c 36 f	16.95	61.50	17.92	0.00	3.63	0.00	100.00
d 0 a							
d 0 b							
d 0 c							
d 0 d							
d 0 e							
d 0 f							

Digitised by the Department of Library Services in support of open access to information, University of Pretoria, 2021.

APPENDIX 5: continued

sample No.	Vitr. %	Inert/l %	Inert/h %	Micr. %	Exin. %	Coke %	Total %
d 2 a	14.50	69.50	11.50	0.50	0.00	4.00	100.00
d 2 b	7.00	77.00	7.50	0.00	0.00	8.50	100.00
d 2 c	2.80	75.70	17.76	0.47	0.00	3.27	100.00
d 2 d	20.50	36.50	4.00	0.00	0.00	39.00	100.00
d 2 e	12.35	62.96	13.58	0.00	0.00	11.11	100.00
d 2 f	25.00	51.50	17.50	0.00	0.00	6.00	100.00
d 4 a	16.25	64.00	19.25	0.25	0.00	0.25	100.00
d 4 b	14.39	58.31	25.06	1.49	0.25	0.50	100.00
d 4 c	8.25	72.00	18.50	0.75	0.00	0.50	100.00
d 4 d	67.07	23.73	8.47	0.00	0.25	0.48	100.00
d 4 e	21.99	61.34	16.20	0.00	0.24	0.23	100.00
d 4 f	61.25	31.75	6.25	0.25	0.25	0.25	100.00
d 8 a	16.48	60.00	23.52	0.00	0.00	0.00	100.00
d 8 b	12.50	63.70	23.32	0.48	0.00	0.00	100.00
d 8 c	8.68	72.95	18.12	0.25	0.00	0.00	100.00
d 8 d	54.00	37.25	8.75	0.00	0.00	0.00	100.00
d 8 e	20.75	58.25	19.50	0.50	1.00	0.00	100.00
d 8 f	56.50	38.25	5.00	0.00	0.25	0.00	100.00
d 10 a	27.50	54.50	15.75	0.50	1.75	0.00	100.00
d 10 b	17.50	67.50	14.25	0.50	0.25	0.00	100.00
d 10 c	7.75	78.00	14.00	0.00	0.25	0.00	100.00
d 10 d	60.66	28.79	9.89	0.00	0.66	0.00	100.00
d 10 e	21.25	64.50	13.00	0.00	1.25	0.00	100.00
d 10 f	43.17	40.00	13.17	0.49	3.17	0.00	100.00
d 16 a	26.49	58.54	11.90	0.96	2.11	0.00	100.00
d 16 b	15.98	70.94	11.62	0.49	0.97	0.00	100.00
d 16 c	7.13	83.61	7.60	0.24	1.43	0.00	100.01
d 16 d	72.50	18.75	5.75	0.00	2.50	0.50	100.00
d 16 e	21.25	62.00	14.75	0.25	1.75	0.00	100.00
d 16 f	58.09	26.42	12.76	0.23	2.50	0.00	100.00
d 32 a	29.25	45.00	22.75	1.00	2.00	0.00	100.00
d 32 b	23.50	61.25	13.00	1.00	1.25	0.00	100.00
d 32 c	10.00	75.50	13.25	0.00	1.25	0.00	100.00
d 32 d	76.00	16.25	7.00	0.00	0.75	0.00	100.00
d 32 e	17.43	63.68	15.50	0.48	2.91	0.00	100.00
d 32 f	52.00	37.75	7.00	0.00	3.25	0.00	100.00
ea	22.00	54.50	20.50	0.50	2.50	0.00	100.00
eb	27.00	54.75	16.50	0.75	1.00	0.00	100.00
ec	9.25	78.00	11.75	0.25	0.75	0.00	100.00
ed	67.50	23.50	6.25	0.25	2.50	0.00	100.00
ee	16.25	68.00	14.00	0.50	1.25	0.00	100.00
ef	39.50	43.75	14.25	0.00	2.50	0.00	100.00
fa	27.25	47.50	23.00	0.25	2.00	0.00	100.00
fb	29.50	51.50	17.00	1.00	1.00	0.00	100.00
fc	15.00	73.75	10.50	0.25	0.50	0.00	100.00
fd	65.75	21.00	12.00	0.00	1.25	0.00	100.00
fe	25.25	59.75	12.75	1.00	1.25	0.00	100.00
ff	41.75	40.75	15.25	0.25	2.00	0.00	100.00
gz	33.50	51.25	12.75	0.75	1.75	0.00	100.00
ga	18.75	65.75	10.75	1.75	3.00	0.00	100.00
gb	16.75	67.75	13.00	0.50	2.00	0.00	100.00
gc	7.75	75.25	15.25	0.00	1.75	0.00	100.00
gd	23.00	65.50	9.50	0.00	2.00	0.00	100.00
ge	8.25	76.00	12.75	0.50	2.50	0.00	100.00
gf	19.00	66.75	11.75	0.25	2.25	0.00	100.00
ha	31.50	49.50	16.25	0.75	2.00	0.00	100.00
hb	18.25	60.75	19.25	1.00	0.75	0.00	100.00
hc	25.50	58.25	13.75	0.75	1.75	0.00	100.00
hd	77.25	15.00	7.00	0.00	0.75	0.00	100.00
he	21.50	62.25	12.00	0.50	3.75	0.00	100.00
hf	37.75	46.50	11.75	0.75	3.25	0.00	100.00

Digitised by the Department of Library Services in support of open access to information, University of Pretoria, 2021.

APPENDIX 6: V-class distribution of all samples of unaffected and thermally-affected coals. Figures indicate the number of measurements per v-class. On most samples 20 points were measured, in exceptional cases 50 points.

sample No.	V34 35	V36 37	V38 39	V40 41	V42 43	V44 45	V46 47	V48 49	V50 51	V52 53	V54 55	V56 57	V58 59	V60 61	V62 63	V64 65	V66 67	V68 69	V70 71	V72 73	V74 75
b 0 a								1	5	5	4	5									
b 0 b									2	6	6	3	0	1	0	2					
b 0 c									2	4	4	4	2	2	1	0	1				
b 0 d									6	2	2	5	1	1	3						
b 0 e									3	3	5	3	2	3							
c 0 a				1	2	4	3	2	3	3	2										
c 0 b				1	4	3	5	6	3	2	2										
c 0 c		1	2	4	1	3	2	2	1	2	2										
c 0 d		1	3	3	2	3	6	4	11	4	6	3	3	2							
c 0 e	1	0	1	0	1	2	4	4	3	2	0	2	0	1							
c 0 f				2	3	3	3	3	5												
d 0 a										1	3	4	4	4	2	2					
d 0 b													4	4	2	1	1	5	0	2	1
d 0 c									2	3	3	1	5	1	4	1					
d 0 d									1	4	3	2	6	2	2						
d 0 e										5	8	3	1	2	1						
d 0 f		7	5	6	3																

sample No.	V10	V11	V12	V13	V14	V15	V16	V17	V18	V19	V20	V21	V22	V23	V24	V25	V26	V27	V28	V29	V30	V31	V32	V33	V34	V35	V36
b 2 a												1	1	3	4	2	0	1	3	1	0	2	1	0	1		
b 2 b																								4	5	7	4
b 2 c																			1	2	5	8	3	0	1		
b 2 d																	9	9	2								
b 2 e												1	4	4	6	4	1										
c 2 a	1	12	19	5	12	1																					
c 2 b							9	15	7	12	6	1															
c 2 c								1	4	9	4	3	8	6	3	9	3										
c 2 d												2	1	8	17	14	8										
c 2 e																1	12	22	12	2	1						
c 2 f																		9	13	10	7	5	1	3	2		
d 2 a					1	0	0	1	2	2	0	0	2	6	2	4											
d 2 b														3	6	2	3	3	3								
d 2 c																1	3	6	4	5	2	0	3	1			
d 2 d														2	5	8	5										
d 2 e									2	2	0	3	3	3	3	4	1	4									
d 2 f					3	1	6	3	6	3	3																

sample No.	V4	V5	V6	V7	V8	V9	V10	V11	V12	V13	V14	V15	V16	V17	V18	V19	V20	V21	V22	V23
b 4 a															7	5	2	5	1	
b 4 b															4	5	4	5	2	
b 4 c															1	10	7	2		
b 4 d													4	9	7					
b 4 e														8	10	2				
c 4 a			2	16	21	5	4	2												
c 4 b				17	10	6	6	1	2	3	2	3								
c 4 c					3	3	6	9	3	3	10	7	2	4						
c 4 d						4	34	8	4											
c 4 e																	2	12	23	13
c 4 f						2	5	8	5	4	10	4	2	1	2	0	0	3	4	
d 4 a					2	5	5	6	2											
d 4 b						13	6	1												
d 4 c					2	8	5	5												
d 4 d				3	13	5														
d 4 e				5	7	7	1													
d 4 f			3	13	3	1														
b 8 a						2	3	5	9	1										
b 8 b						2	10	5	3											
b 8 c						3	11	5	1											
b 8 d				4	13	3														
b 8 e			3	9	8															
c 8 a			5	10	4	1														
c 8 b				7	10	3														
c 8 c				5	6	9														
c 8 d			17	3																
c 8 e			5	11	4															
c 8 f			3	13	7															
d 8 a								5	5	4	4	2								
d 8 b								1	1	8	7	2	1							
d 8 c									6	7	6	1								
d 8 d										15	4	1								
d 8 e			5	8	3	5														
d 8 f						3	6	9	2											
b 10 a			1	8	7	4														
b 10 b				3	16	1														
b 10 c				9	9	2														
b 10 d		2	13	5																
b 10 e		3	14	3																

Digitised by the Department of Library Services in support of open access to information, University of Pretoria, 2021.

APPENDIX 6: continu

	V4	V5	V6	V7	V8	V9	V10	V11	V12	V13	V14	V15	V16	V17	V18	V19	V20	V21	V22	V23
d 10 a		1	7	9	2	1														
d 10 b						3	12	5												
d 10 c			12	3	0	0	2	10	4											
d 10 d					8	8	4													
d 10 e			3	11	6															
d 10 f		1	11	8																
b 16 a	3	4	9	3	1															
b 16 b		9	6	3	2															
b 16 c		2	11	6	1															
b 16 d	5	14	1																	
b 16 e	5	8	6	1																
d 16 a		1	10	7	2															
d 16 b		1	3	11	5															
d 16 c			8	6	5	1														
d 16 d		5	12	3																
d 16 e		1	4	7	7	1														
d 16 f			11	9																
c 20 a			1	11	5	3														
c 20 b			2	11	7															
c 20 c				6	7	6	1													
c 20 d			11	9																
c 20 e			11	7	2															
c 20 f			7	9	4															
b 32 a		3	10	7																
b 32 b			6	13	1															
b 32 c		3	9	6	2															
b 32 d	1	11	8																	
b 32 e	1	13	5	1																
d 32 a		5	11	4																
d 32 b		1	13	6																
d 32 c			5	8	7															
d 32 d	1	7	12																	
d 32 e		4	12	4																
d 32 f		6	14																	
c 36 a			1	13	4	2														
c 36 b			2	11	6	1														
c 36 c			1	7	7	4	1													
c 36 d			12	5	3															
c 36 e			3	11	6															
c 36 f			3	10	7															
ea		9	7	3	1															
eb		4	13	3																
ec		5	11	4																
ed		13	6	1																
ee		13	4	3																
ef	1	14	4	1																
fa	1	7	9	3																
fb		1	9	10																
fc		5	9	5	1															
fd		12	8																	
fe	1	9	8	2																
ff		6	12	2																
gz			9	8	3															
ga			3	13	4															
gb				3	14	3														
gc			3	10	5	2														
gd				11	9															
ge					10	10														
gf			1	11	8															
ha		6	11	3																
hb		1	8	10	1															
hc		4	5	10	1															
hd		10	8	2																
he		5	7	8																
hf		5	12	3																

Digitised by the Department of Library Services in support of open access to information, University of Pretoria, 2021.

APPENDIX 7: Proximate analyses of thermally-affected coals on and air-dry basis (left) and on a dry-ash-free basis (right).

sample No.	thickn. (cm)	Moist. %	Ash %	V.M. %	F.C. %	CO2 %	V.M. %
b 0 a	85	2.2	26.3	12.0	59.5	8.6	16.8
b 0 b	50	1.9	27.4	15.6	54.6	13.9	22.1
b 0 c	52	2.1	30.9	9.6	57.4	5.1	14.3
b 0 d	22	1.7	27.7	8.3	62.3	3.2	11.8
b 0 e	55	2.0	29.2	6.7	62.1	1.2	9.7
b 2 a	80	2.3	21.1	13.7	62.9	2.9	17.9
b 2 b	52	2.1	20.2	12.9	64.8	5.9	16.6
b 2 c	58	1.8	26.3	15.7	56.2	5.2	21.8
b 2 d	20	2.0	27.8	19.3	50.9	6.3	27.5
b 2 e	70	2.3	31.3	15.4	51.0	3.3	23.2
b 4 a	80	2.3	22.4	15.5	59.8	0.0	20.6
b 4 b	50	2.5	18.6	17.5	61.4	0.2	22.2
b 4 c	56	2.4	25.5	15.6	56.5	0.0	21.6
b 4 d	16	2.5	20.0	17.0	60.5	0.0	21.9
b 4 e	47	2.5	27.9	15.9	53.7	0.0	22.8
b 8 a	80	2.8	17.0	23.0	57.2	1.6	28.7
b 8 b	50	3.4	13.9	23.8	58.9	6.4	28.8
b 8 c	50	3.7	22.1	19.4	54.8	0.3	26.1
b 8 d	22	3.8	14.6	28.9	52.7	1.8	35.4
b 8 e	50	3.8	17.9	25.1	53.2	5.0	32.1
b 10 a	80	4.9	13.4	24.1	57.6	3.1	29.5
b 10 b	50	5.3	13.6	23.1	58.0	2.1	28.5
b 10 c	58	5.3	13.8	23.4	57.5	0.0	28.9
b 10 d	21	4.9	12.4	32.5	50.2	0.5	39.3
b 10 e	35	5.1	17.7	22.9	54.3	2.1	29.7
b 16 a	80	5.6	11.5	23.4	59.5	0.1	28.2
b 16 b	50	5.4	12.7	24.6	57.3	0.2	30.0
b 16 c	55	5.2	20.6	19.3	54.9	0.4	26.0
b 16 d	23	4.4	14.2	33.8	47.6	0.1	41.5
b 16 e	42	4.8	21.6	22.9	50.7	0.2	31.1
b 32 a	102	5.7	14.8	23.4	56.1	0.6	29.4
b 32 b	50	5.4	15.4	25.0	54.2	6.2	31.6
b 32 c	48	5.6	20.0	19.6	54.8	0.9	26.3
b 32 d	18	4.9	15.2	31.4	48.5	1.9	39.3
b 32 e	57	5.0	18.4	24.9	51.7	0.2	32.5
c 0 a	100	3.7	26.5	10.0	59.8	6.7	14.3
c 0 b	50	3.2	27.8	10.4	58.6	7.5	15.1
c 0 c	60	2.6	27.6	8.4	61.4	4.2	12.0
c 0 d	30	2.2	30.7	13.6	53.5	10.5	20.3
c 0 e	50	3.3	35.5	8.7	52.5	6.5	14.2
c 0 f	50	3.3	31.5	9.1	56.1	6.9	14.0
c 2 a	80	3.2	19.1	19.0	58.7	5.2	24.5
c 2 b	50	2.6	18.7	17.4	61.3	6.2	22.1
c 2 c	50	2.5	25.6	15.8	56.1	7.9	22.0
c 2 d	30	1.8	30.3	17.9	50.0	2.0	26.4
c 2 e	52	2.4	24.8	10.6	62.2	0.8	14.6
c 2 f	60	2.5	30.7	9.6	57.2	3.4	14.4
c 4 a	80	5.6	12.7	21.4	60.3	0.7	26.2
c 4 b	50	5.5	13.9	20.8	59.8	1.9	25.8
c 4 c	50	4.1	20.8	19.4	55.7	1.0	25.8
c 4 d	30	3.5	18.5	23.7	54.3	0.6	30.4
c 4 e	53	2.2	24.9	13.4	59.1	5.5	18.4
c 4 f	40	3.1	25.1	17.4	54.4	3.4	24.2
c 8 a	85	5.2	15.0	23.9	55.9	2.1	29.9
c 8 b	50	5.5	13.1	21.8	59.6	2.0	26.8
c 8 c	50	5.2	17.6	20.3	56.9	0.9	26.3
c 8 d	30	4.2	20.9	32.3	42.6	1.5	43.1
c 8 e	50	4.8	14.4	28.4	52.4	1.0	35.1
c 8 f	60	4.7	22.4	21.5	51.4	0.2	29.5
c 20 a	85	5.0	14.8	24.8	55.4	3.7	30.9
c 20 b	47	5.2	14.2	22.1	58.5	1.7	27.4
c 20 c	48	5.2	17.2	19.6	58.0	0.6	25.3
c 20 d	31	4.2	19.5	31.7	44.6	2.2	41.5
c 20 e	48	4.6	18.2	27.8	49.4	1.3	36.0
c 20 f	57	4.6	21.4	21.4	52.6	0.2	28.9
c 36 a	82	5.3	13.9	23.1	57.7	2.1	28.6
c 36 b	45	5.1	16.0	22.5	56.4	3.7	28.5
c 36 c	48	5.2	17.7	19.5	57.6	0.9	25.3
c 36 d	30	4.2	18.4	32.6	44.8	1.9	42.1
c 36 e	50	4.8	14.8	27.7	52.7	2.5	34.5
c 36 f	60	5.0	15.1	22.6	57.3	0.5	28.3
d 0 a	100	2.1	34.9	15.4	47.6	14.7	24.4
d 0 b	50	2.9	33.9	12.5	50.7	11.0	19.8
d 0 c	50	2.7	28.1	9.8	59.4	5.4	14.2
d 0 d	23	2.3	31.5	8.8	57.4	5.9	13.3
d 0 e	30	2.8	25.1	9.0	63.1	4.5	12.5
d 0 f	23	3.1	30.5	11.4	55.0	1.8	17.2

Digitised by the Department of Library Services in support of open access to information, University of Pretoria, 2021.

APPENDIX 7: continued

sample No.	thickn. (cm)	Moist. %	Ash %	V.M. %	F.C. %	CO2 %	V.M. %
d 2 a	100	2.1	23.7	17.0	57.2	7.9	22.9
d 2 b	50	2.3	20.0	13.6	64.1	5.9	17.5
d 2 c	50	2.4	24.9	11.4	61.3	5.2	15.7
d 2 d	18	2.4	26.7	14.8	56.1	2.1	20.9
d 2 e	34	2.4	29.1	14.5	54.0	8.3	21.2
d 2 f	34	2.8	25.0	16.2	56.0	2.0	22.4
d 4 a	100	2.3	19.4	22.5	55.8	6.4	28.7
d 4 b	50	2.9	16.7	22.6	57.8	1.1	28.1
d 4 c	53	2.9	19.3	20.3	57.5	6.2	26.1
d 4 d	20	2.4	16.3	29.1	52.2	2.7	35.8
d 4 e	43	2.7	23.2	22.9	51.2	4.2	30.9
d 4 f	45	2.9	24.0	26.4	46.7	0.2	36.1
d 8 a	100	4.4	16.0	22.9	56.7	2.6	28.8
d 8 b	60	3.2	22.6	18.8	56.0	5.2	25.3
d 8 c	50	3.3	20.1	16.9	59.7	4.2	22.1
d 8 d	25	3.3	24.9	21.3	50.5	6.6	29.7
d 8 e	35	3.0	21.5	17.8	57.7	3.1	23.6
d 8 f	43	4.1	23.7	21.0	51.2	1.5	29.1
d 10 a	100	4.6	15.5	23.3	56.6	2.4	29.2
d 10 b	45	3.4	25.2	21.4	50.0	6.6	30.0
d 10 c	55	3.2	21.6	18.9	56.3	3.1	25.1
d 10 d	22	3.7	18.4	26.0	51.9	2.9	33.4
d 10 e	38	4.6	17.6	23.7	54.1	0.5	30.5
d 10 f	40	4.5	16.8	27.8	50.9	0.3	35.3
d 16 a	87	5.2	14.7	25.0	55.1	5.4	31.2
d 16 b	63	5.6	16.0	22.2	56.2	3.2	28.3
d 16 c	53	5.6	19.4	19.5	55.5	3.6	26.0
d 16 d	21	4.4	18.0	32.4	45.2	4.9	41.8
d 16 e	33	5.2	16.5	22.8	55.5	1.6	29.1
d 16 f	48	4.6	16.4	30.0	49.0	1.0	38.0
d 32 a	85	5.2	16.4	25.0	53.4	5.6	31.9
d 32 b	55	5.6	14.5	23.3	56.6	3.5	29.2
d 32 c	53	5.2	19.5	20.1	55.2	2.7	26.7
d 32 d	23	4.8	16.2	33.0	46.0	1.1	41.8
d 32 e	40	5.1	17.9	23.2	53.8	1.8	30.1
d 32 f	43	4.4	23.4	25.8	46.4	3.0	35.7
ea	100	4.5	14.5	24.0	57.0	1.7	29.6
eb	50	5.6	17.2	25.2	52.0	4.8	32.6
ec	55	5.9	18.7	19.5	55.9	3.7	25.9
ed	28	5.1	19.0	30.0	45.9	2.4	39.5
ee	35	5.7	15.0	23.0	56.3	2.5	29.0
ef	37	4.7	21.3	26.0	48.0	1.5	35.1
fa	100	5.6	15.6	25.3	53.5	6.7	32.1
fb	50	5.6	14.5	25.3	54.6	3.0	31.7
fc	45	5.5	22.5	20.3	51.7	3.5	28.2
fd	24	4.9	16.9	31.4	46.8	2.9	40.2
fe	30	5.4	18.6	23.8	52.2	2.9	31.3
ff	50	4.8	19.7	26.9	48.6	2.9	35.6
gz	55	5.3	19.7	24.5	50.5	6.7	32.7
ga	80	5.5	17.5	22.0	55.0	2.6	28.6
gb	45	5.3	24.1	19.9	50.7	3.1	28.2
gc	40	5.4	22.4	20.6	51.6	3.2	28.5
gd	25	5.3	26.5	20.0	48.2	1.9	29.3
ge	45	5.2	33.2	16.6	45.0	1.2	26.9
gf	45	4.2	40.7	17.2	37.9	0.2	31.2
ha	83	5.3	15.5	25.0	54.2	0.9	31.6
hb	60	6.1	14.0	21.8	58.1	3.6	27.3
hc	60	5.2	18.0	24.6	52.2	1.3	32.0
hd	23	4.9	13.1	33.9	48.1	4.1	41.3
he	40	5.3	18.3	23.9	52.5	3.0	31.3
hf	40	5.1	16.0	27.0	51.9	0.5	34.2

Digitised by the Department of Library Services in support of open access to information, University of Pretoria, 2021.

APPENDIX 8: Ultimate analyses of thermally-affected coals on an air-dry basis (left) and on a dry-ash-free basis (right).

sample No.	C %	H %	N %	S %	O %	C %	H %	N %	S %	O %
b 0 a	63.66	1.35	0.67	0.24	5.58	89.03	1.89	0.94	0.34	7.80
b 0 b	59.44	1.12	0.71	0.91	8.52	84.07	1.58	1.00	1.29	12.05
b 0 c	61.26	1.28	0.89	0.64	2.93	91.43	1.91	1.33	0.96	4.37
b 0 d	64.38	1.52	0.82	1.02	2.86	91.19	2.15	1.16	1.44	4.05
b 0 e	63.79	1.53	0.82	0.80	1.86	92.72	2.22	1.19	1.16	2.70
b 2 a	65.73	3.05	1.23	0.55	6.04	85.81	3.98	1.61	0.72	7.89
b 2 b	68.33	2.54	1.17	0.55	5.11	87.94	3.27	1.51	0.71	6.58
b 2 c	60.04	2.13	1.01	0.61	8.11	83.50	2.96	1.40	0.85	11.28
b 2 d	56.22	2.24	1.09	1.04	9.61	80.09	3.19	1.55	1.48	13.69
b 2 e	54.92	2.32	1.27	1.28	6.61	82.71	3.49	1.91	1.93	9.95
b 4 a	65.85	3.11	1.55	0.68	4.11	87.45	4.13	2.06	0.90	5.46
b 4 b	66.87	2.97	1.52	0.80	6.74	84.75	3.76	1.93	1.01	8.54
b 4 c	59.60	2.85	1.42	0.44	7.79	82.66	3.95	1.97	0.61	10.80
b 4 d	66.54	3.19	1.59	0.97	5.21	85.86	4.12	2.05	1.25	6.72
b 4 e	58.41	2.77	1.45	1.10	5.87	83.92	3.98	2.08	1.58	8.43
b 8 a	66.13	3.28	1.61	0.88	8.30	82.46	4.09	2.01	1.10	10.35
b 8 b	67.73	3.38	1.78	1.50	8.31	81.90	4.09	2.15	1.81	10.05
b 8 c	60.41	2.72	1.54	0.61	8.92	81.42	3.67	2.08	0.82	12.02
b 8 d	65.80	3.97	1.69	1.94	8.20	80.64	4.87	2.07	2.38	10.05
b 8 e	63.20	3.55	1.51	1.02	9.02	80.72	4.53	1.93	1.30	11.52
b 10 a	67.07	3.31	1.66	1.69	7.97	82.09	4.05	2.03	2.07	9.76
b 10 b	66.74	3.23	1.80	0.77	8.56	82.29	3.98	2.22	0.95	10.55
b 10 c	66.13	3.22	1.56	1.14	8.85	81.74	3.98	1.93	1.41	10.94
b 10 d	64.98	4.03	1.57	2.11	10.01	78.57	4.87	1.90	2.55	12.10
b 10 e	62.89	3.19	1.58	0.55	8.99	81.46	4.13	2.05	0.71	11.65
b 16 a	69.01	3.54	1.66	0.63	8.06	83.24	4.27	2.00	0.76	9.72
b 16 b	70.07	3.48	1.62	1.45	5.28	85.56	4.25	1.98	1.77	6.45
b 16 c	58.77	2.74	1.58	0.81	10.30	79.20	3.69	2.13	1.09	13.88
b 16 d	64.61	4.06	1.59	1.65	9.49	79.37	4.99	1.95	2.03	11.66
b 16 e	59.81	3.27	1.48	0.48	8.56	81.26	4.44	2.01	0.65	11.63
b 32 a	64.03	3.54	1.50	0.79	9.64	80.54	4.45	1.89	0.99	12.13
b 32 b	61.65	2.63	1.83	1.13	11.96	77.84	3.32	2.31	1.43	15.10
b 32 c	59.87	2.80	1.49	0.50	9.74	80.47	3.76	2.00	0.67	13.09
b 32 d	62.48	3.91	1.60	1.11	10.80	78.20	4.89	2.00	1.39	13.52
b 32 e	60.78	3.39	1.55	0.70	10.18	79.35	4.43	2.02	0.91	13.29
c 0 a	61.50	1.26	0.87	1.45	4.72	88.11	1.81	1.25	2.08	6.76
c 0 b	61.05	1.36	0.84	2.01	3.74	88.48	1.97	1.22	2.91	5.42
c 0 c	63.42	1.82	0.96	0.28	3.32	90.86	2.61	1.38	0.40	4.76
c 0 d	56.55	1.44	0.88	1.55	6.68	84.28	2.15	1.31	2.31	9.96
c 0 e	54.41	1.18	0.67	0.42	4.52	88.91	1.93	1.09	0.69	7.39
c 0 f	57.05	1.31	0.76	1.13	4.95	87.50	2.01	1.17	1.73	7.59
c 2 a	64.46	3.03	1.46	0.58	8.17	82.96	3.90	1.88	0.75	10.51
c 2 b	66.10	2.90	1.50	0.50	7.70	83.99	3.68	1.91	0.64	9.78
c 2 c	60.01	2.44	1.41	0.87	7.17	83.46	3.39	1.96	1.21	9.97
c 2 d	54.91	2.78	1.26	0.77	8.18	80.87	4.09	1.86	1.13	12.05
c 2 e	64.16	2.62	1.29	0.40	4.33	88.13	3.60	1.77	0.55	5.95
c 2 f	58.06	1.96	0.98	1.07	4.73	86.92	2.93	1.47	1.60	7.08
c 4 a	66.90	3.38	1.49	0.70	9.23	81.88	4.14	1.82	0.86	11.30
c 4 b	66.45	3.19	1.51	0.82	8.63	82.44	3.96	1.87	1.02	10.71
c 4 c	60.17	2.79	1.42	0.55	10.17	80.12	3.72	1.89	0.73	13.54
c 4 d	63.63	3.69	1.48	2.06	7.14	81.58	4.73	1.90	2.64	9.15
c 4 e	62.64	2.69	1.44	0.35	5.78	85.93	3.69	1.98	0.48	7.93
c 4 f	58.55	2.88	1.39	1.41	7.57	81.55	4.01	1.94	1.96	10.54
c 8 a	62.85	3.38	1.71	0.69	11.17	78.76	4.24	2.14	0.86	14.00
c 8 b	64.86	3.15	1.67	0.49	11.23	79.68	3.87	2.05	0.60	13.80
c 8 c	59.74	2.97	1.59	0.60	12.30	77.38	3.85	2.06	0.78	15.93
c 8 d	56.61	3.73	1.46	2.94	10.16	75.58	4.98	1.95	3.93	13.56
c 8 e	63.11	3.99	1.63	0.53	11.54	78.11	4.94	2.02	0.66	14.28
c 8 f	55.15	2.97	1.46	1.75	11.57	75.65	4.07	2.00	2.40	15.87
c 20 a	62.32	3.40	1.57	0.94	11.97	77.71	4.24	1.96	1.17	14.93
c 20 b	65.23	3.18	1.66	0.92	9.61	80.93	3.95	2.06	1.14	11.92
c 20 c	63.12	3.03	1.40	0.47	9.58	81.34	3.90	1.80	0.61	12.35
c 20 d	58.30	3.86	1.57	1.82	10.75	76.41	5.06	2.06	2.39	14.09
c 20 e	62.54	3.72	1.55	0.47	8.92	81.01	4.82	2.01	0.61	11.55
c 20 f	59.62	3.13	1.49	1.26	8.50	80.57	4.23	2.01	1.70	11.49
c 36 a	65.68	3.37	1.41	0.59	9.75	81.29	4.17	1.75	0.73	12.07
c 36 b	62.72	3.07	1.56	1.48	10.07	79.49	3.89	1.98	1.88	12.76
c 36 c	62.16	3.00	1.49	0.42	10.03	80.62	3.89	1.93	0.54	13.01
c 36 d	58.44	3.89	1.61	1.20	12.26	75.50	5.03	2.08	1.55	15.84
c 36 e	63.55	3.68	1.65	0.50	11.02	79.04	4.58	2.05	0.62	13.71
c 36 f	60.97	3.26	1.49	1.18	13.00	76.31	4.08	1.86	1.48	16.27
d 0 a	52.49	1.08	0.65	0.24	8.54	83.32	1.71	1.03	0.38	13.56
d 0 b	54.36	1.08	0.83	0.49	6.44	86.01	1.71	1.31	0.78	10.19
d 0 c	61.06	1.41	1.05	0.82	4.86	88.24	2.04	1.52	1.18	7.02
d 0 d	58.91	1.39	0.84	0.37	4.69	88.99	2.10	1.27	0.56	7.08
d 0 e	64.74	1.63	1.07	0.59	4.07	89.79	2.26	1.48	0.82	5.64
d 0 f	57.79	2.19	1.27	3.56	1.59	87.03	3.30	1.91	5.36	2.39

Digitised by the Department of Library Services in support of open access to information, University of Pretoria, 2021.

APPENDIX 8: continued

sample No.	C %	H %	N %	S %	O %	C %	H %	N %	S %	O %
d 2 a	63.46	2.77	1.39	1.00	5.58	85.53	3.73	1.87	1.35	7.52
d 2 b	67.74	2.69	1.49	1.16	4.62	87.18	3.46	1.92	1.49	5.95
d 2 c	62.86	2.33	1.25	0.45	5.81	86.46	3.20	1.72	0.62	7.99
d 2 d	61.22	2.47	1.34	2.00	3.87	86.35	3.48	1.89	2.82	5.46
d 2 e	58.66	2.49	1.50	0.83	5.02	85.64	3.64	2.19	1.21	7.33
d 2 f	60.85	2.87	1.29	3.80	3.39	84.28	3.98	1.79	5.26	4.70
d 4 a	65.63	2.81	1.53	0.85	7.48	83.82	3.59	1.95	1.09	9.55
d 4 b	67.13	3.42	1.76	0.71	7.38	83.50	4.25	2.19	0.88	9.18
d 4 c	66.16	2.95	1.76	0.57	6.36	85.04	3.79	2.26	0.73	8.17
d 4 d	65.65	4.17	1.77	1.87	7.84	80.75	5.13	2.18	2.30	9.64
d 4 e	60.12	3.29	1.65	0.88	8.16	81.13	4.44	2.23	1.19	11.01
d 4 f	57.28	3.75	1.55	3.55	6.97	78.36	5.13	2.12	4.86	9.53
d 8 a	63.16	3.21	1.80	1.04	10.39	79.35	4.03	2.26	1.31	13.05
d 8 b	57.53	2.72	1.74	1.03	11.18	77.53	3.67	2.35	1.39	15.07
d 8 c	62.62	2.72	1.79	0.59	8.88	81.75	3.55	2.34	0.77	11.59
d 8 d	56.67	3.03	1.76	2.57	7.77	78.93	4.22	2.45	3.58	10.82
d 8 e	60.38	3.07	2.00	0.93	9.12	79.97	4.07	2.65	1.23	12.08
d 8 f	55.79	3.19	1.85	2.96	8.41	77.27	4.42	2.56	4.10	11.65
d 10 a	64.94	3.19	1.38	1.07	9.32	81.28	3.99	1.73	1.34	11.66
d 10 b	55.01	2.87	1.74	1.03	10.75	77.04	4.02	2.44	1.44	15.06
d 10 c	58.96	2.67	1.79	0.79	10.99	78.40	3.55	2.38	1.05	14.61
d 10 d	59.82	3.63	1.67	1.69	11.09	76.79	4.66	2.14	2.17	14.24
d 10 e	62.77	3.30	1.65	0.36	9.72	80.68	4.24	2.12	0.46	12.49
d 10 f	60.91	3.62	1.57	0.54	12.06	77.40	4.60	1.99	0.69	15.32
d 16 a	63.92	3.31	1.59	1.25	10.03	79.80	4.13	1.99	1.56	12.52
d 16 b	62.45	2.81	1.55	0.85	10.74	79.66	3.58	1.98	1.08	13.70
d 16 c	59.84	2.62	1.38	0.64	10.52	79.79	3.49	1.84	0.85	14.03
d 16 d	58.90	3.87	1.76	1.24	11.83	75.90	4.99	2.27	1.60	15.24
d 16 e	61.03	2.96	1.84	0.39	12.08	77.94	3.78	2.35	0.50	15.43
d 16 f	61.96	3.94	1.78	1.42	9.90	78.43	4.99	2.25	1.80	12.53
d 32 a	62.97	3.06	1.70	1.41	9.26	80.32	3.90	2.17	1.80	11.81
d 32 b	61.15	3.02	1.82	1.06	12.85	76.53	3.78	2.28	1.33	16.08
d 32 c	60.23	2.68	1.69	0.38	10.32	79.99	3.56	2.24	0.50	13.71
d 32 d	62.30	4.25	1.77	1.28	9.40	78.86	5.38	2.24	1.62	11.90
d 32 e	62.63	3.17	1.47	0.49	9.24	81.34	4.12	1.91	0.64	12.00
d 32 f	56.49	3.24	1.38	2.31	8.78	78.24	4.49	1.91	3.20	12.16
ea	64.11	3.22	1.55	0.66	11.46	79.15	3.98	1.91	0.81	14.15
eb	63.08	2.95	1.51	1.11	8.55	81.71	3.82	1.96	1.44	11.08
ec	61.35	2.81	1.45	0.34	9.45	81.37	3.73	1.92	0.45	12.53
ed	59.33	3.51	1.53	1.40	10.13	78.17	4.62	2.02	1.84	13.35
ee	64.55	3.00	1.71	0.41	9.63	81.40	3.78	2.16	0.52	12.14
ef	57.65	3.27	1.54	1.15	10.39	77.91	4.42	2.08	1.55	14.04
fa	61.35	3.09	1.59	1.36	11.41	77.86	3.92	2.02	1.73	14.48
fb	63.68	3.07	1.59	1.17	10.39	79.70	3.84	1.99	1.46	13.00
fc	57.44	2.62	1.37	0.60	9.97	79.78	3.64	1.90	0.83	13.85
fd	59.77	3.84	1.62	1.60	11.37	76.43	4.91	2.07	2.05	14.54
fe	60.63	3.14	1.58	0.47	10.18	79.78	4.13	2.08	0.62	13.39
ff	60.83	3.37	1.58	1.28	8.44	80.57	4.46	2.09	1.70	11.18
gz	58.73	3.08	1.40	1.91	9.88	78.31	4.11	1.87	2.55	13.17
ga	62.53	3.06	1.55	0.46	9.40	81.21	3.97	2.01	0.60	12.21
gb	56.73	2.72	1.37	0.49	9.29	80.35	3.85	1.94	0.69	13.16
gc	58.41	2.70	1.36	0.48	9.25	80.90	3.74	1.88	0.66	12.81
gd	53.74	2.69	1.22	0.66	9.89	78.80	3.94	1.79	0.97	14.50
ge	48.54	2.28	1.14	1.83	7.81	78.80	3.70	1.85	2.97	12.68
gf	42.63	2.39	1.02	1.75	7.31	77.37	4.34	1.85	3.18	13.27
ha	64.44	3.26	1.66	1.09	8.75	81.36	4.12	2.10	1.38	11.05
hb	65.26	2.44	1.65	0.68	9.87	81.68	3.05	2.07	0.85	12.35
hc	62.23	3.04	1.51	0.92	9.10	81.03	3.96	1.97	1.20	11.85
hd	66.00	4.13	1.68	1.08	9.11	80.49	5.04	2.05	1.32	11.11
he	62.47	3.43	1.61	0.33	8.56	81.77	4.49	2.11	0.43	11.20
hf	63.17	3.88	1.64	1.95	8.26	80.06	4.92	2.08	2.47	10.47

Digitised by the Department of Library Services in support of open access to information, University of Pretoria, 2021.

APPENDIX 9: Ultimate and proximate analyses, with inferred calorific value and H/C and O/C atomic ratios, of thermally-affected coals after correction for CO_2 content.

sample No.	C %	H %	N %	S %	O %	V.M. %	CV/HC MJ/kg	H/C atomic	O/C atomic
b 0 a	93.82	1.89	0.94	0.34	3.02	4.76	34.17	0.240	0.024
b 0 b	91.41	1.58	1.00	1.29	4.71	2.40	32.43	0.206	0.039
b 0 c	94.16	1.91	1.33	0.96	1.65	6.72	34.38	0.242	0.013
b 0 d	92.93	2.15	1.16	1.44	2.31	7.22	34.14	0.276	0.019
b 0 e	93.36	2.22	1.19	1.16	2.06	7.99	34.48	0.284	0.017
b 2 a	87.31	3.98	1.61	0.72	6.39	14.10	34.20	0.543	0.055
b 2 b	91.25	3.27	1.51	0.71	3.27	9.01	35.09	0.427	0.027
b 2 c	86.00	2.96	1.40	0.85	8.78	14.60	31.86	0.410	0.077
b 2 d	82.86	3.19	1.55	1.48	10.92	18.52	30.60	0.459	0.099
b 2 e	84.13	3.49	1.91	1.93	8.54	18.22	31.76	0.495	0.076
b 4 a	87.45	4.13	2.06	0.90	5.46	20.58	34.52	0.563	0.047
b 4 b	84.85	3.76	1.93	1.01	8.44	21.93	32.57	0.529	0.075
b 4 c	82.66	3.95	1.97	0.61	10.80	21.64	31.75	0.570	0.098
b 4 d	85.86	4.12	2.05	1.25	6.72	21.94	33.67	0.571	0.059
b 4 e	83.92	3.98	2.08	1.58	8.43	22.84	32.44	0.565	0.075
b 8 a	83.24	4.09	2.01	1.10	9.56	26.68	32.27	0.585	0.086
b 8 b	85.24	4.09	2.15	1.81	6.71	21.04	33.30	0.571	0.059
b 8 c	81.55	3.67	2.08	0.82	11.89	25.74	30.70	0.536	0.109
b 8 d	81.50	4.87	2.07	2.38	9.18	33.21	32.63	0.711	0.085
b 8 e	83.13	4.53	1.93	1.30	9.11	25.67	32.93	0.650	0.082
b 10 a	83.65	4.05	2.03	2.07	8.20	25.70	32.42	0.577	0.074
b 10 b	83.34	3.98	2.22	0.95	9.51	25.89	32.14	0.569	0.086
b 10 c	81.74	3.98	1.93	1.41	10.94	28.92	31.31	0.580	0.100
b 10 d	78.80	4.87	1.90	2.55	11.88	38.69	31.24	0.737	0.113
b 10 e	82.45	4.13	2.05	0.71	10.66	26.94	31.93	0.597	0.097
b 16 a	83.30	4.27	2.00	0.76	9.67	28.11	32.59	0.611	0.087
b 16 b	85.66	4.25	1.98	1.77	6.34	29.79	33.78	0.591	0.056
b 16 c	79.38	3.69	2.13	1.09	13.71	25.47	29.61	0.554	0.130
b 16 d	79.42	4.99	1.95	2.03	11.61	41.40	31.75	0.748	0.110
b 16 e	81.35	4.44	2.01	0.65	11.54	30.84	31.86	0.651	0.107
b 32 a	80.82	4.45	1.89	0.99	11.85	28.68	31.60	0.657	0.110
b 32 b	80.71	3.32	2.31	1.43	12.23	23.74	29.70	0.490	0.114
b 32 c	80.87	3.76	2.00	0.67	12.69	25.13	30.50	0.555	0.118
b 32 d	79.05	4.89	2.00	1.39	12.66	36.92	31.40	0.738	0.120
b 32 e	79.43	4.43	2.02	0.91	13.20	32.25	30.84	0.664	0.125
c 0 a	91.63	1.81	1.25	2.08	3.24	4.73	32.90	0.235	0.027
c 0 b	92.44	1.97	1.22	2.91	1.45	4.20	33.59	0.254	0.012
c 0 c	93.13	2.61	1.38	0.40	2.49	6.02	34.98	0.334	0.020
c 0 d	89.39	2.15	1.31	2.31	4.84	4.62	32.29	0.286	0.041
c 0 e	91.98	1.93	1.09	0.69	4.31	3.59	33.28	0.250	0.035
c 0 f	90.88	2.01	1.17	1.73	4.21	3.37	32.84	0.263	0.035
c 2 a	85.58	3.90	1.88	0.75	7.89	17.76	33.17	0.543	0.069
c 2 b	87.25	3.68	1.91	0.64	6.53	14.23	33.69	0.503	0.056
c 2 c	87.37	3.39	1.96	1.21	6.07	10.99	33.27	0.463	0.052
c 2 d	81.70	4.09	1.86	1.13	11.22	23.42	31.48	0.597	0.103
c 2 e	88.54	3.60	1.77	0.55	5.54	13.46	34.22	0.484	0.047
c 2 f	88.54	2.93	1.47	1.60	5.46	9.28	33.13	0.395	0.046
c 4 a	82.23	4.14	1.82	0.86	10.96	25.34	31.82	0.600	0.100
c 4 b	83.38	3.96	1.87	1.02	9.77	23.45	32.13	0.566	0.088
c 4 c	80.56	3.72	1.89	0.73	13.10	24.50	30.27	0.549	0.122
c 4 d	81.86	4.73	1.90	2.64	8.87	29.62	32.60	0.689	0.081
c 4 e	88.75	3.69	1.98	0.48	5.11	10.84	34.47	0.495	0.043
c 4 f	83.08	4.01	1.94	1.96	9.01	19.50	32.06	0.575	0.081
c 8 a	79.71	4.24	2.14	0.86	13.04	27.32	30.68	0.633	0.123
c 8 b	80.62	3.87	2.05	0.60	12.85	24.32	30.55	0.572	0.120
c 8 c	77.77	3.85	2.06	0.78	15.55	25.13	29.03	0.589	0.150
c 8 d	76.18	4.98	1.95	3.93	12.97	41.12	30.05	0.779	0.128
c 8 e	78.55	4.94	2.02	0.66	13.83	33.91	31.22	0.749	0.132
c 8 f	75.73	4.07	2.00	2.40	15.79	29.22	28.34	0.641	0.157
c 20 a	79.38	4.24	1.96	1.17	13.25	26.31	30.51	0.636	0.125
c 20 b	81.74	3.95	2.06	1.14	11.11	25.31	31.26	0.575	0.102
c 20 c	81.62	3.90	1.80	0.61	12.07	24.48	31.12	0.570	0.111
c 20 d	77.32	5.06	2.06	2.39	13.18	38.66	30.78	0.780	0.128
c 20 e	81.61	4.82	2.01	0.61	10.95	34.33	32.61	0.704	0.101
c 20 f	80.66	4.23	2.01	1.70	11.40	28.65	31.15	0.625	0.106
c 36 a	82.31	4.17	1.75	0.73	11.05	25.99	31.92	0.604	0.101
c 36 b	81.22	3.89	1.98	1.88	11.04	23.83	30.89	0.571	0.102
c 36 c	81.03	3.89	1.93	0.54	12.60	24.12	30.80	0.572	0.117
c 36 d	76.28	5.03	2.08	1.55	15.06	39.66	30.18	0.785	0.148
c 36 e	80.20	4.58	2.05	0.62	12.55	31.34	31.48	0.680	0.117
c 36 f	76.52	4.08	1.86	1.48	16.06	27.66	28.76	0.635	0.158
d 0 a	90.21	1.71	1.03	0.38	6.66	1.11	32.01	0.226	0.055
d 0 b	91.30	1.71	1.31	0.78	4.90	2.37	32.57	0.223	0.040
d 0 c	91.02	2.04	1.52	1.18	4.24	6.36	32.96	0.267	0.035
d 0 d	91.98	2.10	1.27	0.56	4.09	4.38	33.56	0.272	0.033
d 0 e	92.24	2.26	1.48	0.82	3.20	6.24	33.96	0.292	0.026
d 0 f	87.87	3.30	1.91	5.36	1.55	14.46	33.38	0.447	0.013

Digitised by the Department of Library Services in support of open access to information, University of Pretoria, 2021.

APPENDIX 9: continued

sample No.	C %	H %	N %	S %	O %	V.M. %	CV/HC MJ/kg	H/C atomic	O/C atomic
d 2 a	89.71	3.73	1.87	1.35	3.34	12.26	35.04	0.496	0.028
d 2 b	90.44	3.46	1.92	1.49	2.68	9.91	34.98	0.456	0.022
d 2 c	89.15	3.20	1.72	0.62	5.31	8.53	33.89	0.428	0.045
d 2 d	87.37	3.48	1.89	2.82	4.43	17.91	33.43	0.475	0.038
d 2 e	89.78	3.64	2.19	1.21	3.18	9.05	34.92	0.482	0.027
d 2 f	85.23	3.98	1.79	5.26	3.75	19.67	33.11	0.556	0.033
d 4 a	87.17	3.59	1.95	1.09	6.21	20.56	33.49	0.491	0.053
d 4 b	84.05	4.25	2.19	0.88	8.63	26.74	32.95	0.603	0.077
d 4 c	88.34	3.79	2.26	0.73	4.87	18.12	34.43	0.511	0.041
d 4 d	82.06	5.13	2.18	2.30	8.33	32.47	33.35	0.745	0.076
d 4 e	83.08	4.44	2.23	1.19	9.07	25.24	32.75	0.637	0.082
d 4 f	78.44	5.13	2.12	4.86	9.45	35.84	31.47	0.779	0.090
d 8 a	80.55	4.03	2.26	1.31	11.85	25.50	30.78	0.597	0.110
d 8 b	79.77	3.67	2.35	1.39	12.83	18.33	29.78	0.548	0.121
d 8 c	83.77	3.55	2.34	0.77	9.57	16.58	31.67	0.505	0.086
d 8 d	81.82	4.22	2.45	3.58	7.93	20.47	31.74	0.615	0.073
d 8 e	81.38	4.07	2.65	1.23	10.68	19.47	31.26	0.595	0.099
d 8 f	77.87	4.42	2.56	4.10	11.05	27.01	30.02	0.676	0.107
d 10 a	82.44	3.99	1.73	1.34	10.51	26.16	31.69	0.577	0.096
d 10 b	79.79	4.02	2.44	1.44	12.31	20.73	30.36	0.600	0.116
d 10 c	79.75	3.55	2.38	1.05	13.27	21.01	29.58	0.530	0.125
d 10 d	78.04	4.66	2.14	2.17	12.99	29.65	30.50	0.712	0.125
d 10 e	80.91	4.24	2.12	0.46	12.26	29.82	31.31	0.625	0.114
d 10 f	77.52	4.60	1.99	0.69	15.20	34.94	30.13	0.707	0.147
d 16 a	82.41	4.13	1.99	1.56	9.91	24.47	31.91	0.597	0.090
d 16 b	81.14	3.58	1.98	1.08	12.22	24.23	30.35	0.526	0.113
d 16 c	81.41	3.49	1.84	0.85	12.41	21.20	30.34	0.511	0.114
d 16 d	78.00	4.99	2.27	1.60	13.15	35.44	31.01	0.762	0.127
d 16 e	78.64	3.78	2.35	0.50	14.73	27.08	29.38	0.573	0.141
d 16 f	78.87	4.99	2.25	1.80	12.09	36.71	31.46	0.753	0.115
d 32 a	83.02	3.90	2.17	1.80	9.11	24.74	31.85	0.560	0.082
d 32 b	78.07	3.78	2.28	1.33	14.55	24.78	29.08	0.577	0.140
d 32 c	81.20	3.56	2.24	0.50	12.49	23.11	30.34	0.522	0.115
d 32 d	79.35	5.38	2.24	1.62	11.41	40.38	32.35	0.808	0.108
d 32 e	82.18	4.12	1.91	0.64	11.16	27.79	31.76	0.597	0.102
d 32 f	79.49	4.49	1.91	3.20	10.91	31.58	30.97	0.673	0.103
ea	79.93	3.98	1.91	0.81	13.36	27.53	30.37	0.593	0.125
eb	84.05	3.82	1.96	1.44	8.74	26.42	32.25	0.542	0.078
ec	83.10	3.73	1.92	0.45	10.80	20.95	31.60	0.534	0.098
ed	79.21	4.62	2.02	1.84	12.31	36.36	31.05	0.696	0.117
ee	82.60	3.78	2.16	0.52	10.94	25.85	31.44	0.546	0.099
ef	78.53	4.42	2.08	1.55	13.42	33.11	30.36	0.671	0.128
fa	80.96	3.92	2.02	1.73	11.38	23.60	30.81	0.577	0.105
fb	81.11	3.84	1.99	1.46	11.60	27.91	30.76	0.564	0.107
fc	81.30	3.64	1.90	0.83	12.33	23.33	30.52	0.533	0.114
fd	77.67	4.91	2.07	2.05	13.30	36.45	30.72	0.753	0.129
fe	81.09	4.13	2.08	0.62	12.08	27.50	31.22	0.607	0.112
ff	81.90	4.46	2.09	1.70	9.85	31.79	32.18	0.649	0.090
gz	81.32	4.11	1.87	2.55	10.16	23.73	31.30	0.602	0.094
ga	82.43	3.97	2.01	0.60	10.99	25.19	31.66	0.574	0.100
gb	81.69	3.85	1.94	0.69	11.83	23.80	31.08	0.562	0.109
gc	82.32	3.74	1.88	0.66	11.39	24.10	31.22	0.541	0.104
gd	79.55	3.94	1.79	0.97	13.75	26.54	30.11	0.591	0.130
ge	79.22	3.70	1.85	2.97	12.26	25.00	29.55	0.557	0.116
gf	77.42	4.34	1.85	3.18	13.21	30.85	29.65	0.668	0.128
ha	81.79	4.12	2.10	1.38	10.62	30.43	31.56	0.600	0.097
hb	83.45	3.05	2.07	0.85	10.58	22.78	30.69	0.436	0.095
hc	81.63	3.96	1.97	1.20	11.25	30.34	31.22	0.578	0.103
hd	82.51	5.04	2.05	1.32	9.09	36.34	33.43	0.727	0.083
he	83.19	4.49	2.11	0.43	9.78	27.36	32.89	0.643	0.088
hf	80.29	4.92	2.08	2.47	10.24	33.59	32.09	0.730	0.096

Digitised by the Department of Library Services in support of open access to information, University of Pretoria, 2021.

APPENDIX 10: Major element concentrations on a whole coal air-dry basis **without** ash factor correction

sample No.	SiO_2 %	TiO_2 %	Al_2O_3 %	FeO %	MnO %	MgO %	CaO %	Na_2O %	K_2O %	P_2O_5 %	LOI %	H_2O^- %	TOTAL %
b 0 a	9.27	0.49	5.66	1.27	0.05	2.33	5.21	0.42	0.33	0.07	71.59	3.00	99.72
b 0 b	5.53	0.20	3.50	3.47	0.07	3.32	8.25	0.46	0.18	0.26	70.85	2.77	98.89
b 0 c	11.10	0.36	7.32	1.82	0.04	1.79	4.83	0.78	0.52	1.12	67.46	2.64	99.81
b 0 d	10.10	0.37	6.94	2.42	0.03	1.16	3.09	0.63	0.48	0.56	71.69	2.00	99.49
b 0 e	14.25	0.53	8.55	2.00	0.02	0.95	1.71	0.77	0.55	0.38	67.87	2.51	100.13
b 2 a	7.26	0.35	5.52	0.94	0.04	1.57	3.64	0.35	0.37	0.13	75.26	3.74	99.19
b 2 b	6.04	0.28	4.43	1.12	0.03	2.04	4.38	0.31	0.23	0.04	75.12	5.01	99.05
b 2 c	6.48	0.24	4.56	1.26	0.04	3.47	8.06	0.32	0.27	0.86	70.95	2.40	98.94
b 2 d	5.36	0.16	4.47	2.24	0.03	4.26	9.42	0.24	0.29	0.24	69.79	1.95	98.47
b 2 e	11.23	0.35	5.80	2.42	0.04	2.43	5.31	0.28	0.44	0.44	65.58	3.16	97.51
b 4 a	8.07	0.36	6.22	0.83	0.04	1.19	3.38	0.23	0.47	0.25	74.42	3.00	98.48
b 4 b	5.00	0.23	3.49	1.13	0.04	2.20	4.58	0.40	0.21	0.02	78.12	2.94	98.38
b 4 c	9.01	0.29	5.97	0.53	0.03	2.14	4.78	0.41	0.44	0.71	72.70	2.10	99.13
b 4 d	4.65	0.15	4.07	1.15	0.03	1.92	4.55	0.24	0.29	0.94	78.25	1.74	98.00
b 4 e	11.33	0.35	6.53	1.80	0.03	1.67	3.49	0.36	0.51	0.21	70.30	1.79	98.40
b 8 a	5.25	0.27	3.76	0.71	0.04	1.68	3.28	0.09	0.22	0.04	79.96	3.35	98.67
b 8 b	3.37	0.14	2.52	1.26	0.03	1.66	3.15	0.00	0.12	0.08	81.80	4.07	98.23
b 8 c	7.39	0.26	5.35	0.22	0.03	1.28	4.04	0.14	0.30	1.54	74.03	4.23	98.83
b 8 d	3.24	0.16	3.36	1.19	0.01	0.35	2.50	0.01	0.12	0.93	82.88	3.56	98.32
b 8 e	7.68	0.31	5.83	0.67	0.01	0.54	1.10	0.03	0.19	0.25	78.71	4.20	99.55
b 10 a	4.85	0.22	3.37	1.58	0.02	0.75	1.53	0.03	0.05	0.03	82.27	4.14	98.86
b 10 b	5.04	0.20	3.62	0.94	0.01	0.41	1.30	0.00	0.12	0.49	81.59	5.82	99.55
b 10 c	5.44	0.27	3.42	0.59	0.02	0.74	1.43	0.04	0.07	0.02	81.61	5.36	99.03
b 10 d	4.09	0.14	3.67	1.76	0.01	0.23	0.92	0.00	0.12	0.44	84.33	3.87	99.59
b 10 e	8.33	0.33	5.36	0.22	0.01	0.46	1.08	0.05	0.20	0.29	78.15	4.94	99.44
b 16 a	5.32	0.24	3.57	0.38	0.02	0.23	0.87	0.02	0.04	0.04	84.30	4.60	99.64
b 16 b	4.53	0.17	3.08	1.09	0.03	0.25	2.13	0.02	0.03	0.02	83.39	4.22	98.97
b 16 c	11.30	0.42	6.87	0.64	0.02	0.15	0.80	0.06	0.16	0.13	75.21	4.43	100.21
b 16 d	4.08	0.14	3.67	1.36	0.01	0.08	3.05	0.00	0.12	0.57	82.10	3.47	98.67
b 16 e	12.36	0.38	7.44	0.29	0.01	0.11	0.52	0.04	0.12	0.10	75.09	3.95	100.43
b 32 a	6.48	0.32	3.90	0.54	0.02	0.60	1.65	0.05	0.05	0.04	80.34	5.59	99.59
b 32 b	4.02	0.15	2.75	1.06	0.03	1.58	3.86	0.03	0.04	0.32	79.53	5.46	98.84
b 32 c	9.55	0.33	5.85	0.31	0.02	0.50	1.64	0.10	0.13	0.62	75.59	5.17	99.82
b 32 d	5.27	0.20	4.47	0.95	0.01	0.36	2.51	0.02	0.16	0.57	79.12	5.32	98.97
b 32 e	8.94	0.30	5.92	0.53	0.02	0.45	1.35	0.04	0.13	0.31	76.58	5.14	99.73
c 0 a	9.83	0.33	4.81	2.64	0.05	2.13	4.86	0.57	0.29	0.03	69.49	4.28	99.34
c 0 b	8.16	0.23	4.64	2.84	0.04	1.78	6.32	0.50	0.32	0.67	69.40	3.90	98.83
c 0 c	11.10	0.27	6.87	0.71	0.04	1.69	4.24	0.63	0.67	0.20	70.23	2.86	99.54
c 0 d	7.58	0.26	5.31	3.04	0.05	2.20	9.34	0.40	0.40	0.51	67.48	2.31	98.93
c 0 e	15.55	0.49	9.02	1.48	0.03	1.90	3.82	0.92	0.75	0.14	61.77	4.21	100.12
c 0 f	14.12	0.48	6.56	2.30	0.03	1.67	4.00	0.64	0.44	0.12	65.45	3.74	99.59
c 2 a	7.68	0.37	4.61	0.67	0.02	1.39	2.88	0.28	0.34	0.02	78.24	2.92	99.44
c 2 b	6.22	0.22	3.80	0.55	0.02	1.64	3.67	0.30	0.31	0.02	79.69	2.83	99.28
c 2 c	7.26	0.22	5.30	1.18	0.03	1.73	6.62	0.37	0.45	0.71	72.69	2.29	98.88
c 2 d	6.29	0.20	5.01	1.32	0.04	1.46	0.75	0.26	0.38	0.91	68.86	1.58	99.09
c 2 e	11.43	0.40	7.73	0.52	0.02	0.99	2.59	0.44	0.41	0.11	72.40	2.91	99.98
c 2 f	16.21	0.44	7.90	1.75	0.03	1.10	2.58	0.41	0.37	0.11	66.10	2.79	99.83
c 4 a	6.27	0.28	3.90	0.70	0.01	0.21	0.77	0.02	0.08	0.01	82.44	5.19	99.90
c 4 b	6.64	0.23	3.96	0.78	0.01	0.46	1.17	0.04	0.11	0.13	80.99	5.29	99.83
c 4 c	9.19	0.39	6.37	0.28	0.02	1.13	2.62	0.09	0.39	0.18	75.35	3.63	99.66
c 4 d	6.23	0.21	5.35	1.69	0.01	0.56	2.18	0.23	0.33	0.40	79.24	2.64	99.09
c 4 e	9.94	0.33	7.13	0.56	0.04	1.50	3.58	0.36	0.46	0.27	73.12	2.48	99.79
c 4 f	12.87	0.39	5.68	1.79	0.02	0.93	2.06	0.16	0.30	0.15	72.40	2.69	99.48
c 8 a	6.37	0.33	4.29	0.59	0.02	0.71	2.18	0.02	0.10	0.01	80.66	4.12	99.41
c 8 b	4.91	0.20	3.38	0.44	0.02	0.52	2.06	0.01	0.02	0.17	82.49	5.22	99.47
c 8 c	6.84	0.25	5.80	0.26	0.02	0.50	1.94	0.06	0.22	0.44	78.44	4.59	99.38
c 8 d	5.48	0.22	4.59	2.65	0.01	0.19	5.48	0.00	0.16	0.19	75.82	3.20	98.01
c 8 e	7.00	0.28	5.46	0.22	0.01	0.15	0.73	0.00	0.11	0.10	81.53	4.26	99.87
c 8 f	13.71	0.75	5.69	2.42	0.01	0.06	0.38	0.03	0.16	0.10	72.89	4.11	100.36
c 20 a	6.14	0.35	3.82	0.85	0.02	0.87	2.18	0.03	0.07	0.01	80.73	4.30	99.39
c 20 b	4.54	0.17	3.21	0.79	0.02	0.85	2.41	0.02	0.06	0.36	82.01	4.87	99.33
c 20 c	7.46	0.24	6.14	0.10	0.01	0.51	1.45	0.05	0.25	0.28	78.81	4.62	99.94
c 20 d	6.44	0.27	4.91	1.44	0.01	0.58	3.41	0.00	0.18	0.16	78.50	2.83	98.75
c 20 e	7.30	0.26	4.96	0.19	0.02	0.56	1.61	0.00	0.12	0.16	79.90	4.50	99.60
c 20 f	12.81	0.31	5.22	1.34	0.01	0.04	0.42	0.00	0.19	0.19	76.27	3.75	100.59
c 36 a	5.05	0.26	3.64	0.35	0.02	0.66	1.62	0.03	0.06	0.03	82.45	5.28	99.46
c 36 b	5.09	0.19	3.69	1.58	0.02	0.97	2.66	0.02	0.07	0.45	79.53	4.55	98.84
c 36 c	8.15	0.28	6.70	0.11	0.01	0.47	1.25	0.05	0.20	0.18	77.54	4.95	99.91
c 36 d	4.79	0.20	4.25	1.48	0.01	0.74	4.63	0.01	0.18	0.51	78.26	3.28	98.35
c 36 e	6.26	0.23	4.65	0.18	0.02	0.53	1.58	0.01	0.11	0.11	81.62	4.36	99.68
c 36 f	10.36	0.34	5.21	1.30	0.01	0.07	0.53	0.01	0.12	0.20	77.97	4.33	100.48
d 0 a	9.82	0.38	5.05	1.61	0.06	4.18	8.60	0.44	0.43	0.34	62.84	4.91	98.70
d 0 b	11.52	0.33	4.93	2.04	0.05	3.34	8.56	0.54	0.39	0.74	63.14	4.40	100.01
d 0 c	9.87	0.26	5.80	1.57	0.04	2.06	4.97	0.57	0.47	0.44	69.12	4.01	99.21
d 0 d	13.50	0.47	6.71	1.10	0.04	1.76	4.20	0.87	0.49	0.20	66.42	3.84	99.64
d 0 e	10.39	0.25	5.56	1.25	0.04	1.52	3.40	0.66	0.44	0.21	71.25	4.64	99.64
d 0 f	13.42	0.35	4.88	4.00	0.02	0.68	2.82	0.20	0.39	0.10	65.75	4.29	96.94

Digitised by the Department of Library Services in support of open access to information, University of Pretoria, 2021.

APPENDIX 10: continued

sample No.	SiO_2 %	TiO_2 %	Al_2O_3 %	FeO %	MnO %	MgO %	CaO %	Na_2O %	K_2O %	P_2O_5 %	LOI %	H_2O^- %	TOTAL %
d 2 a	6.78	0.28	4.79	1.38	0.03	2.35	5.27	0.34	0.38	0.39	73.70	2.85	98.57
d 2 b	6.61	0.23	4.39	1.43	0.03	2.08	3.92	0.26	0.35	0.06	76.53	3.07	98.98
d 2 c	9.72	0.31	6.54	0.46	0.03	1.78	3.74	0.33	0.52	0.63	72.30	3.04	99.43
d 2 d	7.95	0.22	6.38	2.47	0.02	2.30	4.77	0.31	0.46	0.24	70.75	2.69	98.59
d 2 e	14.22	0.39	6.81	1.07	0.03	1.67	3.49	0.23	0.55	0.34	67.26	3.59	99.69
d 2 f	10.59	0.26	4.48	4.08	0.02	0.58	1.61	0.16	0.45	0.31	73.41	2.59	98.58
d 4 a	6.24	0.28	4.08	1.00	0.03	1.91	4.05	0.20	0.29	0.26	78.40	1.95	98.71
d 4 b	5.78	0.18	3.75	0.49	0.03	1.29	2.59	0.02	0.20	0.08	81.13	3.30	98.86
d 4 c	7.45	0.24	4.76	0.22	0.02	1.17	2.99	0.08	0.31	0.88	77.63	3.43	99.20
d 4 d	6.70	0.25	4.99	1.24	0.01	0.36	1.63	0.00	0.22	0.17	81.96	1.75	99.30
d 4 e	11.66	0.40	6.32	0.72	0.02	0.85	1.92	0.01	0.31	0.26	74.19	3.17	99.85
d 4 f	12.34	0.33	5.50	3.78	0.01	0.24	0.59	0.00	0.31	0.09	74.93	2.10	100.25
d 8 a	5.59	0.22	4.16	0.73	0.02	1.28	2.54	0.07	0.14	0.03	79.73	4.43	98.96
d 8 b	6.44	0.22	5.67	1.10	0.03	1.32	4.32	0.06	0.59	0.49	74.50	3.54	98.30
d 8 c	6.60	0.24	5.25	0.36	0.02	1.26	3.44	0.25	0.36	0.86	77.09	3.44	99.19
d 8 d	7.71	0.26	6.04	2.30	0.02	1.11	4.22	0.09	0.54	0.28	72.80	2.55	97.94
d 8 e	8.81	0.35	5.65	0.36	0.03	1.15	2.85	0.06	0.43	0.59	77.27	1.72	99.29
d 8 f	11.71	0.30	5.29	2.87	0.02	0.45	1.22	0.04	0.37	0.09	75.05	2.59	100.03
d 10 a	5.97	0.24	4.36	0.76	0.02	1.01	2.39	0.07	0.11	0.04	81.44	3.16	99.59
d 10 b	7.54	0.23	6.99	0.62	0.03	1.61	4.43	0.04	0.72	0.48	72.26	3.64	98.61
d 10 c	7.74	0.29	5.27	0.31	0.03	1.80	4.09	0.07	0.28	0.68	75.30	3.39	99.27
d 10 d	7.14	0.27	6.06	1.10	0.02	0.51	1.71	0.04	0.35	0.26	78.70	2.91	99.08
d 10 e	8.35	0.40	5.00	0.16	0.01	0.40	0.94	0.04	0.18	0.12	79.63	4.86	100.11
d 10 f	7.45	0.23	4.55	2.87	0.01	0.13	0.31	0.03	0.15	0.13	80.56	3.82	100.26
d 16 a	5.45	0.24	3.78	1.09	0.02	0.86	2.18	0.04	0.04	0.02	80.88	4.53	99.14
d 16 b	5.93	0.20	4.00	0.80	0.02	0.84	2.01	0.09	0.03	0.13	79.20	6.06	99.32
d 16 c	8.54	0.27	5.69	0.44	0.02	0.61	2.01	0.06	0.15	0.41	76.08	5.36	99.66
d 16 d	6.89	0.33	4.83	0.89	0.01	0.53	2.63	0.00	0.16	0.21	78.48	3.97	98.95
d 16 e	8.42	0.30	5.00	0.16	0.02	0.40	1.47	0.04	0.09	0.44	78.25	5.28	99.89
d 16 f	8.87	0.26	4.75	1.30	0.01	0.11	0.43	0.00	0.16	0.07	79.60	4.51	100.09
d 32 a	4.48	0.18	3.22	1.10	0.03	1.10	3.44	0.03	0.05	0.17	79.79	5.12	98.73
d 32 b	5.06	0.18	3.52	0.97	0.02	0.89	2.33	0.04	0.04	0.04	80.33	5.83	99.26
d 32 c	6.87	0.24	5.57	0.13	0.02	0.86	2.66	0.11	0.22	1.11	75.46	6.07	99.34
d 32 d	5.73	0.23	4.99	0.78	0.01	0.25	1.81	0.01	0.21	0.18	80.62	4.52	99.35
d 32 e	7.38	0.26	5.18	0.20	0.02	0.47	1.93	0.07	0.14	1.15	77.03	5.59	99.44
d 32 f	11.94	0.21	5.28	2.11	0.01	0.41	1.47	0.00	0.20	0.15	73.24	4.74	99.78
ea	6.57	0.27	3.76	0.47	0.02	0.57	1.36	0.08	0.06	0.07	80.72	5.87	99.84
eb	5.36	0.16	4.10	1.01	0.03	1.19	3.57	0.04	0.09	0.14	78.17	5.54	99.42
ec	7.97	0.27	5.83	0.08	0.02	0.74	2.19	0.08	0.21	0.77	75.58	5.92	99.68
ed	7.02	0.23	7.55	0.86	0.01	0.41	1.39	0.04	0.60	0.53	75.69	4.87	99.22
ee	7.74	0.29	4.61	0.12	0.02	0.35	1.24	0.04	0.10	0.27	79.42	5.91	100.12
ef	12.53	0.31	6.65	1.14	0.01	0.21	0.72	0.00	0.34	0.14	73.95	4.56	100.58
fa	5.89	0.23	3.58	1.27	0.03	1.05	2.52	0.04	0.08	0.02	79.15	5.34	99.22
fb	4.16	0.16	2.83	0.98	0.03	1.34	3.39	0.03	0.07	0.23	79.60	6.27	99.11
fc	10.54	0.40	7.33	0.22	0.02	0.62	1.72	0.08	0.34	0.21	72.40	5.62	99.52
fd	6.04	0.25	4.45	1.39	0.01	0.30	2.35	0.01	0.20	0.13	79.54	4.61	99.30
fe	7.94	0.29	5.61	0.16	0.02	0.47	1.68	0.04	0.16	0.87	76.47	5.67	99.40
ff	11.73	0.29	5.99	1.21	0.01	0.10	0.33	0.00	0.25	0.08	75.83	4.62	100.46
gz	5.83	0.25	3.88	3.56	0.03	1.31	3.14	0.00	0.05	0.03	75.43	4.93	98.46
ga	8.40	0.30	5.42	0.38	0.02	0.72	2.20	0.03	0.09	0.14	76.96	5.04	99.72
gb	12.26	0.43	6.90	0.61	0.01	0.87	2.20	0.05	0.14	0.02	71.82	4.69	100.02
gc	11.80	0.35	6.70	0.71	0.02	0.36	1.45	0.04	0.14	0.02	73.69	4.58	99.88
gd	14.11	0.46	7.37	0.77	0.03	1.12	3.28	0.06	0.13	0.02	67.68	5.32	100.39
ge	18.92	0.59	9.26	2.33	0.02	0.19	0.99	0.06	0.26	0.03	62.90	5.02	100.61
gf	28.24	0.49	10.23	2.18	0.01	0.06	0.13	0.03	0.47	0.03	56.11	3.76	101.80
ha	5.59	0.21	3.83	0.84	0.02	0.64	2.73	0.02	0.08	0.08	79.32	5.43	98.80
hb	6.46	0.22	4.08	0.60	0.02	0.65	1.65	0.03	0.04	0.02	80.00	5.82	99.61
hc	6.54	0.26	4.90	0.76	0.03	1.13	2.72	0.03	0.15	0.14	77.76	4.66	99.10
hd	4.63	0.21	3.57	0.68	0.01	0.48	1.77	0.00	0.10	0.05	82.71	4.88	99.10
he	9.08	0.32	4.97	0.16	0.02	0.55	1.56	0.03	0.07	0.12	76.99	5.05	98.94
hf	2.65	0.09	1.96	0.72	0.00	0.03	0.11	0.00	0.03	0.04	89.86	4.55	100.05

Digitised by the Department of Library Services in support of open access to information, University of Pretoria, 2021.

APPENDIX II: Major element concentrations on a whole coal air-dry basis with ash factor correction.

sample No.	SiO_2 %	TiO_2 %	Al_2O_3 %	FeO %	MnO %	MgO %	CaO %	Na_2O %	K_2O %	P_2O_5 %
b 0 a	6.37	0.34	3.89	0.87	0.03	1.60	3.58	0.29	0.23	0.05
b 0 b	3.65	0.13	2.31	2.29	0.05	2.19	5.44	0.30	0.12	0.17
b 0 c	6.49	0.21	4.28	1.06	0.02	1.05	2.83	0.46	0.30	0.66
b 0 d	6.59	0.24	4.53	1.58	0.02	0.76	2.02	0.41	0.31	0.37
b 0 e	8.82	0.33	5.29	1.24	0.01	0.59	1.06	0.48	0.34	0.24
b 2 a	6.22	0.30	4.73	0.81	0.03	1.35	3.12	0.30	0.32	0.11
b 2 b	5.41	0.25	3.97	1.00	0.03	1.83	3.92	0.28	0.21	0.04
b 2 c	4.45	0.16	3.13	0.87	0.03	2.39	5.54	0.22	0.19	0.59
b 2 d	3.49	0.10	2.91	1.46	0.02	2.77	6.13	0.16	0.19	0.16
b 2 e	6.49	0.20	3.35	1.40	0.02	1.40	3.07	0.16	0.25	0.25
b 4 a	6.51	0.29	5.02	0.67	0.03	0.96	2.73	0.19	0.38	0.20
b 4 b	4.86	0.22	3.39	1.10	0.04	2.14	4.45	0.39	0.20	0.02
b 4 c	6.39	0.21	4.23	0.38	0.02	1.52	3.39	0.29	0.31	0.50
b 4 d	4.20	0.14	3.68	1.04	0.03	1.74	4.11	0.22	0.26	0.85
b 4 e	7.34	0.23	4.23	1.17	0.02	1.08	2.26	0.23	0.33	0.14
b 8 a	5.58	0.29	4.00	0.76	0.04	1.79	3.49	0.10	0.23	0.04
b 8 b	4.38	0.18	3.28	1.64	0.04	2.16	4.10	0.00	0.16	0.10
b 8 c	6.05	0.21	4.38	0.18	0.02	1.05	3.31	0.11	0.25	1.26
b 8 d	4.01	0.20	4.16	1.47	0.01	0.43	3.10	0.01	0.15	1.15
b 8 e	7.76	0.31	5.89	0.68	0.01	0.55	1.11	0.03	0.19	0.25
b 10 a	6.54	0.30	4.55	2.13	0.03	1.01	2.06	0.04	0.07	0.04
b 10 b	6.70	0.27	4.81	1.25	0.01	0.55	1.73	0.00	0.16	0.65
b 10 c	7.13	0.35	4.48	0.77	0.03	0.97	1.87	0.05	0.09	0.03
b 10 d	5.96	0.20	5.35	2.57	0.01	0.34	1.34	0.00	0.17	0.64
b 10 e	8.51	0.34	5.48	0.22	0.01	0.47	1.10	0.05	0.20	0.30
b 16 a	8.36	0.38	5.61	0.60	0.03	0.36	1.37	0.03	0.06	0.06
b 16 b	6.45	0.24	4.38	1.55	0.04	0.36	3.03	0.03	0.04	0.03
b 16 c	9.92	0.37	6.03	0.56	0.02	0.13	0.70	0.05	0.14	0.11
b 16 d	5.19	0.18	4.67	1.73	0.01	0.10	3.88	0.00	0.15	0.73
b 16 e	10.35	0.32	6.23	0.24	0.01	0.09	0.44	0.03	0.10	0.08
b 32 a	7.92	0.39	4.76	0.66	0.02	0.73	2.02	0.06	0.06	0.05
b 32 b	4.72	0.18	3.23	1.24	0.04	1.85	4.53	0.04	0.05	0.38
b 32 c	8.63	0.30	5.29	0.28	0.02	0.45	1.48	0.09	0.12	0.56
b 32 d	6.27	0.24	5.32	1.13	0.01	0.43	2.99	0.02	0.19	0.68
b 32 e	8.78	0.29	5.82	0.52	0.02	0.44	1.33	0.04	0.13	0.30
c 0 a	6.71	0.23	3.28	1.80	0.03	1.45	3.32	0.39	0.20	0.02
c 0 b	5.31	0.15	3.02	1.85	0.03	1.16	4.11	0.33	0.21	0.44
c 0 c	7.27	0.18	4.50	0.47	0.03	1.11	2.78	0.41	0.44	0.13
c 0 d	4.46	0.15	3.13	1.79	0.03	1.30	5.50	0.24	0.24	0.30
c 0 e	7.92	0.25	4.59	0.75	0.02	0.97	1.95	0.47	0.38	0.07
c 0 f	8.10	0.28	3.77	1.32	0.02	0.96	2.30	0.37	0.25	0.07
c 2 a	7.27	0.35	4.36	0.63	0.02	1.32	2.73	0.27	0.32	0.02
c 2 b	6.01	0.21	3.67	0.53	0.02	1.59	3.55	0.29	0.30	0.02
c 2 c	5.13	0.16	3.74	0.83	0.02	1.22	4.68	0.26	0.32	0.50
c 2 d	3.75	0.12	2.99	0.79	0.02	0.87	0.45	0.16	0.23	0.54
c 2 e	8.33	0.29	5.64	0.38	0.01	0.72	1.89	0.32	0.30	0.08
c 2 f	9.55	0.26	4.65	1.03	0.02	0.65	1.52	0.24	0.22	0.06
c 4 a	8.93	0.40	5.55	1.00	0.01	0.30	1.10	0.03	0.11	0.01
c 4 b	8.64	0.30	5.15	1.01	0.01	0.60	1.52	0.05	0.14	0.17
c 4 c	7.99	0.34	5.54	0.24	0.02	0.98	2.28	0.08	0.34	0.16
c 4 d	6.09	0.21	5.23	1.65	0.01	0.55	2.13	0.22	0.32	0.39
c 4 e	7.22	0.24	5.18	0.41	0.03	1.09	2.60	0.26	0.33	0.20
c 4 f	9.27	0.28	4.09	1.29	0.01	0.67	1.48	0.12	0.22	0.11
c 8 a	7.68	0.40	5.17	0.71	0.02	0.86	2.63	0.02	0.12	0.01
c 8 b	6.78	0.28	4.66	0.61	0.03	0.72	2.84	0.01	0.03	0.23
c 8 c	7.03	0.26	5.96	0.27	0.02	0.51	1.99	0.06	0.23	0.45
c 8 d	4.74	0.19	3.97	2.29	0.01	0.16	4.74	0.00	0.14	0.16
c 8 e	8.79	0.35	6.86	0.28	0.01	0.19	0.92	0.00	0.14	0.13
c 8 f	11.07	0.61	4.59	1.95	0.01	0.05	0.31	0.02	0.13	0.08
c 20 a	7.50	0.43	4.67	1.04	0.02	1.06	2.66	0.04	0.09	0.01
c 20 b	5.78	0.22	4.09	1.01	0.03	1.08	3.07	0.03	0.08	0.46
c 20 c	7.84	0.25	6.45	0.11	0.01	0.54	1.52	0.05	0.26	0.29
c 20 d	5.97	0.25	4.55	1.34	0.01	0.54	3.16	0.00	0.17	0.15
c 20 e	7.25	0.26	4.93	0.19	0.02	0.56	1.60	0.00	0.12	0.16
c 20 f	10.82	0.26	4.41	1.13	0.01	0.03	0.35	0.00	0.16	0.16
c 36 a	6.57	0.34	4.73	0.46	0.03	0.86	2.11	0.04	0.08	0.04
c 36 b	5.75	0.21	4.17	1.79	0.02	1.10	3.01	0.02	0.08	0.51
c 36 c	8.32	0.29	6.84	0.11	0.01	0.48	1.28	0.05	0.20	0.18
c 36 d	4.71	0.20	4.18	1.45	0.01	0.73	4.55	0.01	0.18	0.50
c 36 e	7.65	0.28	5.68	0.22	0.02	0.65	1.93	0.01	0.13	0.13
c 36 f	12.40	0.41	6.24	1.56	0.01	0.08	0.63	0.01	0.14	0.24
d 0 a	5.09	0.20	2.62	0.83	0.03	2.17	4.46	0.23	0.22	0.18
d 0 b	6.14	0.18	2.63	1.09	0.03	1.78	4.57	0.29	0.21	0.39
d 0 c	6.35	0.17	3.73	1.01	0.03	1.33	3.20	0.37	0.30	0.28
d 0 d	7.75	0.27	3.85	0.63	0.02	1.01	2.41	0.50	0.28	0.11
d 0 e	7.48	0.18	4.00	0.90	0.03	1.09	2.45	0.48	0.32	0.15
d 0 f	7.96	0.21	2.89	2.37	0.01	0.40	1.67	0.12	0.23	0.06

Digitised by the Department of Library Services in support of open access to information, University of Pretoria, 2021.

APPENDIX 11: continued

sample No.	SiO2 %	TiO_2 %	Al_2O_3 %	FeO %	MnO %	MgO %	CaO %	Na_2O %	K_2O %	P_2O_5 %
d 2 a	5.17	0.21	3.65	1.05	0.02	1.79	4.02	0.26	0.29	0.30
d 2 b	5.98	0.21	3.97	1.29	0.03	1.88	3.54	0.24	0.32	0.05
d 2 c	7.06	0.23	4.75	0.33	0.02	1.29	2.72	0.24	0.38	0.46
d 2 d	5.38	0.15	4.32	1.67	0.01	1.56	3.23	0.21	0.31	0.16
d 2 e	8.83	0.24	4.23	0.66	0.02	1.04	2.17	0.14	0.34	0.21
d 2 f	7.66	0.19	3.24	2.95	0.01	0.42	1.16	0.12	0.33	0.22
d 4 a	5.82	0.26	3.80	0.93	0.03	1.78	3.77	0.19	0.27	0.24
d 4 b	6.26	0.19	4.06	0.53	0.03	1.40	2.80	0.02	0.22	0.09
d 4 c	6.98	0.22	4.46	0.21	0.02	1.10	2.80	0.07	0.29	0.82
d 4 d	7.43	0.28	5.53	1.38	0.01	0.40	1.81	0.00	0.24	0.19
d 4 e	9.09	0.31	4.93	0.56	0.02	0.66	1.50	0.01	0.24	0.20
d 4 f	9.30	0.25	4.14	2.85	0.01	0.18	0.44	0.00	0.23	0.07
d 8 a	6.32	0.25	4.70	0.82	0.02	1.45	2.87	0.08	0.16	0.03
d 8 b	5.15	0.18	4.54	0.88	0.02	1.06	3.46	0.05	0.47	0.39
d 8 c	5.94	0.22	4.72	0.32	0.02	1.13	3.09	0.22	0.32	0.77
d 8 d	5.60	0.19	4.39	1.67	0.01	0.81	3.06	0.07	0.39	0.20
d 8 e	7.41	0.29	4.75	0.30	0.03	0.97	2.40	0.05	0.36	0.50
d 8 f	8.93	0.23	4.04	2.19	0.02	0.34	0.93	0.03	0.28	0.07
d 10 a	6.96	0.28	5.09	0.89	0.02	1.18	2.79	0.08	0.13	0.05
d 10 b	5.41	0.17	5.02	0.44	0.02	1.16	3.18	0.03	0.52	0.34
d 10 c	6.48	0.24	4.41	0.26	0.03	1.51	3.42	0.06	0.23	0.57
d 10 d	7.02	0.27	5.95	1.08	0.02	0.50	1.68	0.04	0.34	0.26
d 10 e	8.58	0.41	5.14	0.16	0.01	0.41	0.97	0.04	0.18	0.12
d 10 f	8.02	0.25	4.90	3.09	0.01	0.14	0.33	0.03	0.16	0.14
d 16 a	6.70	0.30	4.65	1.34	0.02	1.06	2.68	0.05	0.05	0.02
d 16 b	6.70	0.23	4.52	0.90	0.02	0.95	2.27	0.10	0.03	0.15
d 16 c	7.96	0.25	5.30	0.41	0.02	0.57	1.87	0.06	0.14	0.38
d 16 d	6.92	0.33	4.85	0.89	0.01	0.53	2.64	0.00	0.16	0.21
d 16 e	9.23	0.33	5.48	0.18	0.02	0.44	1.61	0.04	0.10	0.48
d 16 f	9.78	0.29	5.24	1.43	0.01	0.12	0.47	0.00	0.18	0.08
d 32 a	4.94	0.20	3.55	1.21	0.03	1.21	3.79	0.03	0.06	0.19
d 32 b	6.31	0.22	4.39	1.21	0.02	1.11	2.91	0.05	0.05	0.05
d 32 c	6.37	0.22	5.16	0.12	0.02	0.80	2.47	0.10	0.20	1.03
d 32 d	6.39	0.26	5.57	0.87	0.01	0.28	2.02	0.01	0.23	0.20
d 32 e	7.45	0.26	5.23	0.20	0.02	0.47	1.95	0.07	0.14	1.16
d 32 f	9.23	0.16	4.08	1.63	0.01	0.32	1.14	0.00	0.15	0.12
ea	8.19	0.34	4.69	0.59	0.02	0.71	1.70	0.10	0.07	0.09
eb	5.63	0.17	4.31	1.06	0.03	1.25	3.75	0.04	0.09	0.15
ec	7.71	0.26	5.64	0.08	0.02	0.72	2.12	0.08	0.20	0.74
ed	6.68	0.22	7.18	0.82	0.01	0.39	1.32	0.04	0.57	0.50
ee	9.33	0.35	5.56	0.14	0.02	0.42	1.49	0.05	0.12	0.33
ef	10.64	0.26	5.64	0.97	0.01	0.18	0.61	0.00	0.29	0.12
fa	6.83	0.27	4.15	1.47	0.03	1.22	2.92	0.05	0.09	0.02
fb	5.19	0.20	3.53	1.22	0.04	1.67	4.23	0.04	0.09	0.29
fc	8.47	0.32	5.89	0.18	0.02	0.50	1.38	0.06	0.27	0.17
fd	6.46	0.27	4.76	1.49	0.01	0.32	2.51	0.01	0.21	0.14
fe	7.72	0.28	5.45	0.16	0.02	0.46	1.63	0.04	0.16	0.85
ff	10.77	0.27	5.50	1.11	0.01	0.09	0.30	0.00	0.23	0.07
gz	5.35	0.23	3.56	3.27	0.03	1.20	2.88	0.00	0.05	0.03
ga	8.68	0.31	5.60	0.39	0.02	0.74	2.27	0.03	0.09	0.14
gb	9.20	0.32	5.18	0.46	0.01	0.65	1.65	0.04	0.11	0.02
gc	9.52	0.28	5.41	0.57	0.02	0.29	1.17	0.03	0.11	0.02
gd	9.63	0.31	5.03	0.53	0.02	0.76	2.24	0.04	0.09	0.01
ge	10.30	0.32	5.04	1.27	0.01	0.10	0.54	0.03	0.14	0.02
gf	12.54	0.22	4.54	0.97	0.00	0.03	0.06	0.01	0.21	0.01
ha	6.52	0.24	4.47	0.98	0.02	0.75	3.18	0.02	0.09	0.09
hb	8.34	0.28	5.27	0.77	0.03	0.84	2.13	0.04	0.05	0.03
hc	6.57	0.26	4.92	0.76	0.03	1.14	2.73	0.03	0.15	0.14
hd	6.39	0.29	4.93	0.94	0.01	0.66	2.44	0.00	0.14	0.07
he	8.97	0.32	4.91	0.16	0.02	0.54	1.54	0.03	0.07	0.12
hf	2.99	0.10	2.21	0.81	0.00	0.03	0.12	0.00	0.03	0.05

Digitised by the Department of Library Services in support of open access to information, University of Pretoria, 2021.

APPENDIX 12: Trace element concentrations on a whole coal air-dry basis **without** ash factor correction

sample No.	Zn ppm	Cu ppm	Ni ppm	Co ppm	Ga ppm	Mo ppm	Nb ppm	Zr ppm	Y ppm	Sr ppm	Rb ppm	U ppm	Th ppm	Pb ppm	Cr ppm	V ppm	Ba ppm	Sc ppm	Cl ppm	F ppm
b 0 a	62	13	25	28	12	0	11	148	17	502	18	0	11	5	49	49	1156	20	590	776
b 0 b	52	11	18	28	7	0	8	88	16	850	13	0	4	5	36	20	881	11	530	1002
b 0 c	53	14	19	28	14	0	10	150	24	1898	25	0	10	4	48	48	2068	13	504	1204
b 0 d	59	19	19	31	18	4	11	162	19	1346	19	4	11	0	52	85	1817	0	540	1286
b 0 e	43	16	22	29	24	4	17	289	28	1320	26	0	17	4	77	70	1777	16	476	1278
b 2 a	38	5	22	29	16	4	11	137	13	670	20	0	11	12	37	60	1114	13	565	1264
b 2 b	43	12	14	28	10	0	8	90	10	335	18	0	5	0	24	13	559	0	894	958
b 2 c	41	0	13	24	8	0	8	115	20	1309	18	0	4	0	41	52	1259	10	1792	961
b 2 d	85	29	14	32	8	4	8	97	8	760	13	0	4	0	36	18	851	16	1037	970
b 2 e	30	14	18	28	14	4	12	347	25	1261	22	0	11	4	68	43	2639	10	893	1184
b 4 a	19	0	12	26	6	0	8	92	12	439	14	0	4	4	30	48	1361	12	875	1661
b 4 b	32	8	25	28	18	4	11	155	14	1591	20	0	12	10	19	14	457	0	1000	1278
b 4 c	13	0	10	25	7	0	8	132	17	1458	23	0	10	0	14	0	1657	0	788	1524
b 4 d	53	13	16	32	16	4	11	122	13	1763	13	0	0	0	18	25	1762	0	1120	1686
b 4 e	32	6	16	28	16	5	13	391	30	744	23	0	14	0	62	82	4278	30	685	1460
b 8 a	7	0	18	28	8	0	10	101	8	583	13	0	6	0	30	25	755	0	475	1260
b 8 b	10	0	12	29	7	0	6	62	8	395	10	0	0	0	30	0	386	0	336	1354
b 8 c	11	7	12	26	8	0	7	132	25	2291	13	0	7	0	38	0	2206	0	298	1720
b 8 d	10	4	24	31	16	4	10	127	12	1828	6	4	4	0	22	22	1454	0	295	1696
b 8 e	22	5	12	26	17	4	12	150	18	1033	6	4	13	0	29	59	890	0	278	1422
b 10 a	6	0	19	28	10	0	10	90	10	413	5	0	7	0	31	24	251	0	419	1324
b 10 b	12	0	12	26	7	4	10	94	12	359	5	0	7	0	22	24	262	0	187	1207
b 10 c	10	0	11	28	8	0	7	100	17	797	6	0	5	0	30	10	708	0	301	1357
b 10 d	18	0	12	31	16	4	10	106	8	852	5	0	5	0	28	17	864	0	296	1578
b 10 e	12	0	8	26	11	4	10	144	20	907	6	0	11	0	29	19	772	0	318	1399
b 16 a	6	0	18	28	8	5	10	90	12	190	6	0	7	0	19	20	215	0	220	1628
b 16 b	11	0	12	28	6	0	7	61	11	139	0	0	0	0	13	19	157	0	254	1488
b 16 c	7	0	11	25	7	0	11	125	17	445	6	0	11	0	19	40	716	0	216	1486
b 16 d	12	0	10	32	13	4	7	109	10	1398	0	0	0	0	16	17	904	0	428	1417
b 16 e	11	0	12	26	13	4	12	151	16	713	7	0	12	0	11	19	562	0	206	1151
b 32 a	10	0	18	28	10	4	10	116	12	721	4	0	8	0	26	26	527	0	314	1265
b 32 b	8	0	10	25	8	0	7	91	10	1248	5	0	0	0	14	12	662	0	133	995
b 32 c	10	6	13	26	7	0	8	143	23	1895	5	0	8	0	22	23	1621	0	163	1420
b 32 d	8	7	10	30	12	4	8	132	12	1980	5	4	5	0	11	30	1432	0	266	1512
b 32 e	12	7	10	30	12	4	8	132	12	1980	5	4	5	0	40	48	716	0	202	1498
c 0 a	20	10	23	26	8	0	10	108	20	560	18	0	10	0	46	35	1466	20	446	1188
c 0 b	41	26	22	29	8	0	5	109	26	1600	16	0	6	0	7	37	1808	14	541	1199
c 0 c	16	6	14	28	7	0	8	115	20	872	30	0	10	0	35	46	2096	0	514	1505
c 0 d	23	40	18	28	16	0	10	148	13	1502	16	0	4	0	34	32	2063	0	559	907
c 0 e	14	0	17	29	17	4	16	209	17	547	32	4	17	0	29	35	1855	0	350	1349
c 0 f	13	12	17	26	16	4	14	398	40	436	24	0	10	0	84	178	1243	14	446	940
c 2 a	7	0	17	28	10	0	11	114	17	535	22	0	8	0	28	47	1307	13	340	1223
c 2 b	10	0	13	26	5	0	8	91	14	544	20	0	5	0	19	26	935	0	407	1316
c 2 c	37	23	13	25	6	0	7	110	22	1556	22	0	5	16	12	10	1579	0	418	1387
c 2 d	46	35	12	28	12	0	11	122	11	2305	16	0	4	6	29	16	1571	23	460	1565
c 2 e	12	0	11	29	13	4	13	154	14	476	20	0	13	0	38	42	1226	0	493	1205
c 2 f	16	8	11	28	14	5	14	412	37	370	20	0	8	0	84	126	1127	36	432	1602
c 4 a	6	0	14	28	8	4	10	91	14	106	7	0	8	0	29	18	259	0	154	1324
c 4 b	35	0	12	25	6	0	8	92	17	367	6	0	5	0	22	25	437	0	263	1109
c 4 c	8	0	11	28	7	0	8	136	20	911	13	0	8	0	31	26	1176	18	516	1634
c 4 d	8	0	12	28	13	4	8	108	11	992	11	0	4	0	11	8	1390	0	364	1382
c 4 e	20	4	8	25	14	0	10	133	16	832	24	0	10	0	23	66	1486	13	414	1459
c 4 f	25	0	11	26	14	5	13	487	37	356	18	0	8	0	76	203	877	0	325	1288
c 8 a	7	0	14	26	13	4	11	101	14	170	10	0	10	0	36	23	499	16	218	1050
c 8 b	5	0	12	28	5	4	7	90	17	576	0	0	0	0	19	23	894	0	245	1428
c 8 c	6	0	11	26	6	0	8	113	20	988	5	0	8	0	35	7	1241	0	485	1331
c 8 d	6	5	10	31	12	5	10	113	8	1361	6	0	5	0	32	29	768	0	319	1144
c 8 e	6	0	8	28	14	5	10	131	13	504	6	4	12	0	23	43	431	0	224	1217
c 8 f	11	0	18	28	12	12	18	905	55	233	7	0	12	0	132	92	332	18	260	952
c 20 a	8	0	14	29	12	0	11	114	14	534	7	0	8	0	25	42	428	0	152	1243
c 20 b	6	0	12	28	6	0	6	96	17	1184	0	0	5	0	20	31	614	0	199	1378
c 20 c	7	0	11	25	6	4	7	124	19	1612	6	0	10	0	0	35	1081	0	338	1523
c 20 d	6	5	11	31	12	4	10	126	10	1039	6	0	4	0	17	7	814	14	277	1342
c 20 e	6	0	7	26	11	4	8	124	13	900	5	0	7	0	22	42	607	0	227	1110
c 20 f	31	0	10	26	12	4	11	305	30	452	11	0	10	0	64	90	412	14	208	1390
c 36 a	11	0	13	28	10	4	7	103	17	590	5	0	7	0	31	28	366	0	628	1471
c 36 b	6	0	13	28	8	0	8	96	17	1014	4	0	5	0	25	42	866	0	194	1290
c 36 c	6	0	12	25	6	0	7	124	17	1247	4	0	10	0	20	8	1639	0	324	1607
c 36 d	5	11	10	30	14	0	8	131	11	1810	6	0	6	0	24	29	1000	0	328	1234
c 36 e	5	0	10	28	12	4	10	116	12	568	5	0	8	0	23	34	398	0	196	1386
c 36 f	12	0	12	28	14	6	12	439	34	390	6	0	8	0	60	92	298	10	208	1541
d 0 a	24	25	26	28	13	0	11	146	13	2736	22	0	7	0	55	28	2256	19	331	1217
d 0 b	16	13	16	26	7	0	8	136	22	1926	18	0	6	0	41	46	2454	0	294	1297
d 0 c	12	29	13	28	10	0	8	139	17	2395	23	0	7	0	42	10	2020	10	322	1465
d 0 d	10	11	12	25	13	0	13	178	20	2466	24	0	11	0	44	41	1499	0	246	1278
d 0 e	12	4	11	29	12	0	8	140	20	797	22	0	11	0	77	37	1291	16	374	1112
d 0 f	18	18	28	29	16	5	12	406	25	877	24	0	11	0	143	62	11496	0	419	943

Digitised by the Department of Library Services in support of open access to information, University of Pretoria, 2021.

APPENDIX 12: continu

sample No.	Zn ppm	Cu ppm	Ni ppm	Co ppm	Ga ppm	Mo ppm	Nb ppm	Zr ppm	Y ppm	Sr ppm	Rb ppm	U ppm	Th ppm	Pb ppm	Cr ppm	V ppm	Ba ppm	Sc ppm	Cl ppm	F ppm
d 2 a	8	0	20	26	11	0	8	109	13	960	23	0	6	0	18	29	1019	16	398	1232
d 2 b	10	0	13	26	7	0	10	85	11	409	23	0	5	0	29	16	650	0	474	1039
d 2 c	8	0	11	26	7	0	8	128	22	1064	30	0	7	0	37	34	1633	11	551	1478
d 2 d	11	22	16	30	13	5	10	110	11	660	22	0	4	0	35	13	1162	0	474	1136
d 2 e	10	5	10	28	12	0	11	161	19	688	29	0	10	0	53	50	1520	0	422	1049
d 2 f	30	8	14	29	19	6	12	606	24	816	24	0	10	0	118	202	5813	0	458	1315
d 4 a	7	6	20	28	11	0	8	127	14	1943	19	0	5	0	22	29	1055	0	414	1622
d 4 b	6	0	10	25	7	0	7	84	10	503	18	0	0	0	22	22	535	0	349	1033
d 4 c	8	0	8	26	8	0	7	121	20	1334	17	0	7	0	26	40	1654	17	367	1798
d 4 d	18	0	11	29	14	4	10	127	12	920	7	0	7	0	35	28	942	0	342	1128
d 4 e	10	5	12	26	11	0	11	144	20	724	12	0	12	0	16	26	1050	16	263	1030
d 4 f	19	5	17	29	22	6	14	362	20	1018	13	0	11	0	67	88	595	0	349	1146
d 8 a	11	0	18	28	10	0	8	89	12	425	8	0	6	0	17	20	388	0	924	1243
d 8 b	10	8	16	28	6	0	7	110	12	1962	16	4	6	0	24	11	1990	0	505	1242
d 8 c	10	5	10	25	7	0	7	127	23	1745	17	0	8	0	11	37	2327	0	404	1465
d 8 d	6	7	14	28	12	4	8	131	10	1506	17	0	5	0	20	54	1862	0	389	1231
d 8 e	10	0	7	28	11	0	10	133	19	712	25	0	7	0	17	20	1640	12	490	1441
d 8 f	13	0	16	29	20	4	11	242	18	414	19	0	7	0	35	80	808	0	298	1666
d 10 a	7	0	19	29	12	4	7	98	13	640	6	0	8	0	28	17	314	0	1073	1314
d 10 b	8	16	17	29	8	0	4	114	13	2360	14	4	5	0	25	26	2153	0	302	1478
d 10 c	6	5	10	29	7	4	4	119	24	1100	13	4	8	0	37	41	1680	19	323	1434
d 10 d	6	11	13	31	11	4	6	137	12	1805	8	5	6	0	20	19	1402	0	362	1490
d 10 e	8	7	10	28	10	5	10	160	18	718	7	5	14	0	30	40	668	10	288	1351
d 10 f	18	0	14	30	18	7	7	352	24	568	6	4	10	0	29	62	422	0	236	1266
d 16 a	6	0	20	30	11	4	5	86	13	415	5	0	7	0	14	25	254	0	361	1078
d 16 b	6	0	16	29	6	4	5	88	16	516	0	0	6	0	18	12	1056	0	77	1097
d 16 c	6	0	23	30	4	4	5	131	24	1548	6	4	10	0	26	23	1282	0	173	1208
d 16 d	8	0	25	37	5	5	7	150	13	1762	6	5	6	0	35	36	992	0	197	1309
d 16 e	8	0	23	31	6	6	5	139	23	1139	6	5	13	0	17	49	664	0	233	1604
d 16 f	12	0	25	43	5	8	7	230	23	470	7	5	12	0	49	73	460	11	192	1091
d 32 a	13	0	23	32	4	6	5	94	12	1048	0	4	6	0	18	14	506	0	194	1002
d 32 b	7	0	23	28	5	0	0	84	12	599	0	0	4	0	12	8	523	10	85	1328
d 32 c	7	0	24	29	4	0	0	131	24	3187	5	5	7	0	30	23	1961	0	174	1272
d 32 d	7	0	26	37	6	6	5	119	11	1246	7	5	7	0	14	20	979	0	246	1356
d 32 e	11	0	26	37	6	6	0	139	24	3355	5	7	8	0	16	31	1554	0	356	1643
d 32 f	22	0	25	40	6	8	7	232	18	706	8	4	7	0	35	53	558	0	259	1170
ea	11	0	17	29	8	4	10	114	14	491	4	0	8	0	31	61	274	0	1110	1194
eb	8	0	11	26	6	0	8	78	8	552	4	0	4	0	29	16	314	0	518	954
ec	11	6	11	26	6	0	7	137	22	2129	5	0	8	0	24	40	1171	0	140	1171
ed	13	18	18	30	16	0	8	128	11	3419	8	4	4	0	22	26	2326	0	206	1358
ee	8	0	7	25	10	4	10	127	18	740	5	0	10	0	31	22	506	0	88	1403
ef	14	4	24	28	19	4	12	281	22	786	11	0	8	0	54	53	562	10	172	1241
fa	8	0	18	28	11	0	8	89	11	526	5	0	5	0	19	37	320	0	199	1105
fb	11	0	11	26	7	0	7	86	12	890	0	0	0	0	12	16	522	0	66	1096
fc	13	0	11	25	8	4	11	139	17	1268	7	4	8	0	34	19	1216	0	264	1356
fd	11	4	11	29	14	5	11	124	10	1048	7	0	5	0	26	44	870	0	191	1357
fe	10	13	8	28	13	0	7	151	19	2440	6	4	8	0	32	0	1290	11	130	1295
ff	14	0	14	28	18	5	12	206	20	422	10	0	10	4	55	68	509	0	172	1129
gz	11	0	18	26	13	0	10	90	10	271	4	0	7	0	31	60	220	0	48	1156
ga	11	0	13	26	13	4	11	122	14	756	6	0	10	0	34	36	1028	11	0	1536
gb	8	0	10	26	12	0	11	133	16	223	10	0	11	0	52	55	468	12	58	1189
gc	6	0	11	26	10	0	10	120	16	180	8	0	10	0	49	34	427	0	47	1231
gd	6	0	12	26	16	0	13	158	18	148	11	0	10	0	47	42	472	13	40	1450
ge	6	0	8	24	16	4	13	176	26	151	17	0	17	4	60	82	666	17	38	1402
gf	14	0	16	28	16	4	13	318	20	128	22	0	11	5	73	86	469	10	126	1315
ha	10	0	17	28	13	0	8	100	12	668	5	0	7	0	29	36	563	11	103	1385
hb	7	0	11	28	6	4	7	89	14	378	5	0	6	0	25	35	514	10	61	1027
hc	6	0	14	25	10	0	8	108	12	1157	6	0	5	0	26	10	518	0	172	1190
hd	10	0	10	30	16	5	10	110	11	464	6	0	4	0	25	7	499	0	146	1457
he	6	0	6	26	12	4	10	130	16	546	5	0	12	0	12	42	398	0	166	1373
hf	11	0	13	28	19	5	10	281	23	454	6	0	10	0	25	50	258	0	140	1234

Digitised by the Department of Library Services in support of open access to information, University of Pretoria, 2021.

APPENDIX 13: Trace element concentrations on a whole coal air-dry basis with ash factor correction.

sample No.	Zn ppm	Cu ppm	Ni ppm	Co ppm	Ga ppm	Mo ppm	Nb ppm	Zr ppm	Y ppm	Sr ppm	Rb ppm	U ppm	Th ppm	Pb ppm	Cr ppm	V ppm	Ba ppm	Sc ppm	Cl ppm	F ppm
b 0 a	43	9	17	19	8	0	7	101	12	345	12	0	7	3	34	34	794	14	406	534
b 0 b	34	7	12	18	5	0	6	58	10	561	9	0	2	3	24	13	581	7	350	661
b 0 c	31	8	11	16	8	0	6	88	14	1111	15	0	6	2	28	28	1210	8	295	704
b 0 d	38	13	13	20	12	2	7	106	13	879	13	2	7	0	34	56	1186	0	352	840
b 0 e	27	10	13	18	15	2	10	179	17	817	16	0	10	2	48	43	1100	10	295	791
b 2 a	33	4	19	25	13	3	9	117	11	574	17	0	9	10	32	51	954	11	484	1083
b 2 b	39	11	13	25	9	0	8	81	9	300	16	0	4	0	21	12	501	0	800	857
b 2 c	28	0	9	16	6	0	6	79	14	900	12	0	2	0	28	35	865	7	1232	661
b 2 d	55	19	9	21	5	2	5	63	5	494	9	0	2	0	23	12	553	10	674	631
b 2 e	17	8	10	16	8	2	7	200	15	729	12	0	6	2	40	25	1524	6	516	684
b 4 a	15	0	10	21	5	0	7	75	10	354	12	0	3	3	24	39	1098	10	706	1341
b 4 b	31	8	24	27	17	3	10	150	14	1547	20	0	12	9	19	14	444	0	972	1242
b 4 c	9	0	7	18	5	0	6	94	12	1034	16	0	7	0	10	0	1175	0	559	1081
b 4 d	48	12	14	29	14	3	10	111	12	1594	12	0	0	0	16	23	1592	0	1012	1524
b 4 e	21	4	10	18	10	3	9	254	19	482	15	0	9	0	40	53	2772	19	444	946
b 8 a	8	0	19	29	9	0	10	107	9	620	14	0	6	0	32	27	803	0	505	1340
b 8 b	12	0	16	37	9	0	8	81	11	514	12	0	0	0	39	0	503	0	437	1761
b 8 c	9	6	10	22	7	0	6	108	21	1874	11	0	6	0	31	0	1804	0	243	1407
b 8 d	12	4	30	39	19	4	12	158	15	2263	7	4	4	0	27	27	1801	0	366	2100
b 8 e	22	5	12	27	17	4	12	152	18	1044	6	4	13	0	29	59	899	0	281	1436
b 10 a	8	0	26	37	13	0	13	121	13	557	6	0	10	0	42	32	338	0	565	1786
b 10 b	16	0	16	35	10	5	13	124	16	477	6	0	10	0	29	32	348	0	249	1605
b 10 c	13	0	14	36	11	0	9	130	22	1044	8	0	6	0	39	13	928	0	395	1778
b 10 d	26	0	17	45	23	5	14	154	12	1242	7	0	7	0	40	24	1260	0	432	2301
b 10 e	12	0	9	27	11	4	10	147	21	927	6	0	11	0	29	20	788	0	325	1429
b 16 a	9	0	28	43	13	8	15	141	19	298	9	0	11	0	30	32	338	0	345	2560
b 16 b	15	0	17	39	9	0	10	87	15	198	0	0	0	0	19	27	224	0	362	2118
b 16 c	6	0	9	22	6	0	9	110	15	391	5	0	9	0	17	35	629	0	190	1304
b 16 d	15	0	12	41	17	5	9	139	12	1780	0	0	0	0	20	21	1150	0	545	1804
b 16 e	9	0	10	22	11	3	10	127	13	597	6	0	10	0	9	16	470	0	173	963
b 32 a	12	0	22	34	12	4	12	142	15	881	4	0	10	0	32	32	644	0	384	1545
b 32 b	10	0	11	30	10	0	8	107	11	1465	6	0	0	0	17	14	778	0	156	1168
b 32 c	9	5	12	24	7	0	8	129	21	1713	4	0	8	0	20	21	1466	0	148	1283
b 32 d	10	9	11	36	14	4	10	157	14	2355	6	4	6	0	13	36	1703	0	317	1798
b 32 e	12	7	9	29	12	4	8	130	12	1946	5	4	5	0	39	47	704	0	198	1472
c 0 a	14	7	16	18	6	0	7	74	14	382	12	0	7	0	31	24	1000	14	305	811
c 0 b	27	17	14	19	5	0	3	71	17	1040	10	0	4	0	5	24	1176	9	352	780
c 0 c	10	4	9	18	5	0	6	75	13	571	20	0	6	0	23	30	1373	0	336	986
c 0 d	13	23	11	16	9	0	6	87	8	885	9	0	2	0	20	19	1215	0	329	534
c 0 e	7	0	9	15	9	2	8	106	9	279	17	2	9	0	15	18	945	0	178	687
c 0 f	8	7	10	15	9	2	8	229	23	250	14	0	6	0	48	102	714	8	256	539
c 2 a	7	0	16	26	9	0	10	108	16	507	20	0	8	0	26	44	1237	12	321	1157
c 2 b	9	0	13	26	5	0	8	88	14	526	20	0	5	0	19	26	904	0	393	1273
c 2 c	26	16	9	18	4	0	5	78	15	1099	15	0	3	11	8	7	1115	0	295	980
c 2 d	27	21	7	16	7	0	6	73	6	1376	9	0	2	4	17	9	937	14	274	934
c 2 e	9	0	8	21	10	3	10	112	10	347	15	0	10	0	28	31	894	0	360	878
c 2 f	9	5	6	16	8	3	8	242	22	218	12	0	5	0	49	74	664	21	254	943
c 4 a	9	0	21	39	12	5	14	130	21	150	10	0	12	0	41	26	369	0	219	1884
c 4 b	45	0	16	33	8	0	11	120	22	478	8	0	6	0	28	33	568	0	342	1442
c 4 c	7	0	9	24	6	0	7	118	18	792	11	0	7	0	27	23	1022	16	449	1421
c 4 d	8	0	12	27	13	4	8	106	11	970	11	0	4	0	11	8	1358	0	355	1351
c 4 e	15	3	6	18	10	0	7	97	11	604	17	0	7	0	17	48	1079	10	301	1060
c 4 f	18	0	8	19	10	3	10	351	27	257	13	0	6	0	54	146	632	0	234	927
c 8 a	9	0	17	32	16	4	13	121	17	205	12	0	12	0	43	27	602	19	263	1266
c 8 b	7	0	17	38	7	5	10	124	23	795	0	0	0	0	26	31	1234	0	338	1971
c 8 c	6	0	11	27	6	0	9	116	21	1015	5	0	9	0	36	7	1275	0	498	1367
c 8 d	5	4	8	27	10	4	8	98	7	1177	5	0	4	0	28	25	664	0	276	989
c 8 e	8	0	11	35	18	6	12	164	17	633	8	5	15	0	29	54	541	0	282	1528
c 8 f	9	0	15	22	10	10	15	730	45	188	6	0	10	0	107	75	268	15	210	768
c 20 a	10	0	18	35	15	0	13	139	18	652	9	0	10	0	31	51	523	0	186	1519
c 20 b	8	0	15	35	8	0	8	122	21	1508	0	0	6	0	26	40	782	0	254	1754
c 20 c	8	0	11	26	6	4	8	130	20	1694	6	0	10	0	0	37	1137	0	356	1601
c 20 d	6	4	10	29	11	3	9	117	9	964	6	0	3	0	16	7	754	13	257	1244
c 20 e	6	0	7	26	11	4	8	123	13	894	5	0	7	0	21	42	603	0	225	1103
c 20 f	26	0	8	22	10	3	9	258	25	382	9	0	8	0	54	76	348	12	175	1174
c 36 a	14	0	17	36	12	5	9	134	22	768	6	0	9	0	41	36	476	0	816	1914
c 36 b	7	0	15	31	9	0	9	108	19	1146	4	0	5	0	28	47	979	0	220	1458
c 36 c	6	0	12	26	6	0	7	126	17	1274	4	0	10	0	21	9	1674	0	331	1641
c 36 d	5	11	9	29	14	0	8	129	11	1778	6	0	6	0	24	28	982	0	322	1212
c 36 e	6	0	12	34	15	4	12	142	15	693	6	0	10	0	28	41	487	0	239	1693
c 36 f	14	0	14	33	17	7	14	526	40	467	7	0	10	0	72	111	356	11	249	1845
d 0 a	12	13	14	14	7	0	6	76	7	1417	11	0	4	0	29	14	1169	10	172	630
d 0 b	8	7	8	14	4	0	4	72	12	1027	10	0	3	0	22	24	1309	0	157	692
d 0 c	8	19	8	18	6	0	5	90	11	1541	15	0	5	0	27	6	1299	6	207	943
d 0 d	6	6	7	14	8	0	8	102	12	1415	14	0	6	0	25	23	860	0	141	734
d 0 e	9	3	8	21	9	0	6	101	15	574	16	0	8	0	55	27	930	11	270	801
d 0 f	11	11	16	17	9	3	7	240	15	520	14	0	6	0	85	37	6815	0	248	559

Digitised by the Department of Library Services in support of open access to information, University of Pretoria, 2021.

APPENDIX 13: continued

sample No.	Zn ppm	Cu ppm	Ni ppm	Co ppm	Ga ppm	Mo ppm	Nb ppm	Zr ppm	Y ppm	Sr ppm	Rb ppm	U ppm	Th ppm	Pb ppm	Cr ppm	V ppm	Ba ppm	Sc ppm	Cl ppm	F ppm
d 2 a	6	0	16	20	8	0	6	83	10	732	17	0	5	0	14	22	777	12	304	940
d 2 b	9	0	12	24	7	0	9	77	10	370	21	0	4	0	26	14	588	0	428	939
d 2 c	6	0	8	19	5	0	6	93	16	773	22	0	5	0	27	24	1186	8	400	1073
d 2 d	7	15	11	20	9	3	7	75	7	447	15	0	2	0	24	9	787	0	321	770
d 2 e	6	3	6	17	7	0	7	100	12	427	18	0	6	0	33	31	945	0	262	652
d 2 f	22	6	10	21	14	4	9	438	17	590	17	0	7	0	85	146	4204	0	332	951
d 4 a	7	6	19	26	10	0	8	119	13	1811	18	0	4	0	20	27	983	0	386	1512
d 4 b	6	0	10	27	8	0	8	91	10	544	19	0	0	0	23	23	579	0	378	1119
d 4 c	8	0	8	25	8	0	7	114	19	1250	16	0	7	0	25	37	1549	16	344	1684
d 4 d	20	0	12	32	16	4	11	141	13	1021	8	0	8	0	39	31	1045	0	379	1251
d 4 e	7	4	9	21	8	0	8	112	16	564	9	0	9	0	12	21	818	12	205	802
d 4 f	14	4	13	22	16	5	11	273	15	767	10	0	8	0	51	66	448	0	263	863
d 8 a	12	0	20	31	11	0	9	100	14	480	9	0	7	0	19	23	438	0	1044	1405
d 8 b	8	7	12	22	5	0	6	88	10	1570	12	3	5	0	19	9	1592	0	404	994
d 8 c	9	4	9	23	6	0	6	114	21	1569	15	0	8	0	10	33	2093	0	364	1318
d 8 d	4	5	10	20	9	3	6	95	7	1094	12	0	3	0	15	39	1352	0	282	894
d 8 e	8	0	6	23	9	0	8	112	16	598	21	0	6	0	14	17	1379	10	412	1212
d 8 f	10	0	12	22	16	3	8	185	14	316	15	0	5	0	27	61	616	0	227	1271
d 10 a	8	0	22	34	14	4	8	115	15	746	7	0	10	0	32	20	367	0	1251	1533
d 10 b	6	11	12	21	6	0	3	82	9	1693	10	3	3	0	18	19	1545	0	217	1061
d 10 c	5	4	8	24	6	3	3	99	20	921	11	3	7	0	31	34	1406	16	270	1200
d 10 d	6	11	13	31	11	4	6	134	12	1773	8	5	6	0	20	19	1377	0	356	1464
d 10 e	9	7	10	28	10	5	10	164	18	737	7	5	15	0	31	41	687	10	296	1388
d 10 f	19	0	15	32	19	8	8	378	26	611	6	4	10	0	31	67	455	0	254	1362
d 16 a	7	0	25	37	13	4	6	106	16	511	6	0	9	0	18	31	313	0	444	1325
d 16 b	7	0	18	33	7	4	5	99	18	583	0	0	7	0	20	14	1193	0	87	1239
d 16 c	6	0	21	28	3	3	4	122	22	1443	6	3	9	0	25	21	1194	0	161	1126
d 16 d	8	0	25	37	5	5	7	151	13	1769	6	5	6	0	35	36	997	0	198	1315
d 16 e	9	0	25	34	7	7	5	153	25	1248	7	5	14	0	18	54	727	0	255	1758
d 16 f	13	0	28	48	5	9	8	254	25	519	8	5	13	0	54	81	507	12	212	1203
d 32 a	15	0	25	36	4	7	5	103	13	1155	0	4	7	0	20	16	558	0	214	1105
d 32 b	9	0	28	34	6	0	0	105	15	747	0	0	4	0	15	10	652	12	106	1656
d 32 c	7	0	22	27	3	0	0	121	22	2955	4	4	7	0	28	21	1818	0	161	1179
d 32 d	8	0	29	42	7	7	5	133	12	1390	8	5	8	0	16	23	1093	0	275	1513
d 32 e	11	0	27	38	6	6	0	141	24	3389	5	7	8	0	16	32	1570	0	360	1659
d 32 f	17	0	19	31	5	6	6	179	14	545	6	3	6	0	27	41	431	0	200	904
ea	13	0	21	36	10	4	12	142	18	612	4	0	10	0	39	76	341	0	1384	1489
eb	9	0	11	28	6	0	9	82	9	580	4	0	4	0	30	16	330	0	545	1003
ec	10	6	10	26	6	0	7	132	21	2058	5	0	8	0	23	38	1132	0	136	1132
ed	13	17	17	29	15	0	8	122	10	3253	8	3	3	0	21	25	2213	0	196	1293
ee	10	0	9	30	12	4	12	153	22	892	6	0	12	0	38	26	610	0	106	1691
ef	12	3	20	23	16	3	10	238	18	667	9	0	7	0	46	45	477	8	146	1053
fa	10	0	21	32	13	0	10	103	13	609	6	0	6	0	22	43	371	0	231	1281
fb	13	0	13	33	9	0	9	108	15	1110	0	0	0	0	15	19	651	0	82	1366
fc	11	0	9	20	7	3	9	112	13	1019	6	3	7	0	27	15	977	0	212	1090
fd	12	4	12	31	15	5	12	132	10	1121	8	0	5	0	28	48	931	0	204	1452
fe	9	13	8	27	13	0	7	147	19	2371	6	3	8	0	31	0	1254	10	126	1259
ff	13	0	13	25	17	4	11	189	19	388	9	0	9	3	51	63	467	0	157	1036
gz	10	0	17	24	12	0	9	83	9	249	3	0	7	0	29	55	202	0	44	1061
ga	11	0	14	27	14	4	11	126	15	781	6	0	10	0	35	37	1062	11	0	1587
gb	6	0	7	20	9	0	8	100	12	167	7	0	8	0	39	41	351	9	43	892
gc	5	0	9	21	8	0	8	97	13	145	7	0	8	0	40	27	345	0	38	994
gd	4	0	8	18	11	0	9	108	12	101	7	0	7	0	32	29	322	9	27	989
ge	3	0	5	13	8	2	7	96	14	82	9	0	9	2	33	44	363	9	21	763
gf	6	0	7	12	7	2	6	141	9	57	10	0	5	2	33	38	208	4	56	584
ha	11	0	20	32	15	0	10	116	14	780	6	0	8	0	34	42	656	13	120	1615
hb	9	0	14	36	8	5	9	115	19	488	6	0	8	0	33	45	663	12	79	1327
hc	6	0	14	25	10	0	8	108	12	1162	6	0	5	0	27	10	521	0	172	1196
hd	13	0	13	41	22	7	13	152	15	641	8	0	5	0	35	10	689	0	202	2011
he	6	0	6	26	12	4	9	128	15	539	5	0	12	0	12	41	394	0	164	1356
hf	12	0	15	31	22	5	11	317	26	513	7	0	11	0	28	57	292	0	159	1394

Digitised by the Department of Library Services in support of open access to information, University of Pretoria, 2021.

APPENDIX 14: Pearson correlation matrix for petrographic and proximate analyses *vs.* major element concentrations of all samples of unaffected coals (59samples).

	Moist	Ash	CO_2	VM	Vitr.	ROV
SiO_2	-0.10383	0.53885	-0.37893	-0.15453	-0.33538	0.22609
	0.4339	0.0001	0.0031	0.2425	0.0094	0.0851
TiO_2	0.14446	-0.04786	-0.17560	-0.19497	-0.23217	0.16283
	0.2750	0.7188	0.1834	0.1389	0.0768	0.2179
Al_2O_3	0.05029	0.10098	-0.35685	-0.00050	-0.12193	0.01753
	0.7053	0.4467	0.0055	0.9970	0.3576	0.8952
FeO	-0.25349	-0.04967	0.30840	0.22943	0.39554	-0.10053
	0.0527	0.7087	0.0175	0.0805	0.0019	0.4487
MnO	0.60603	-0.43003	0.38670	-0.49729	-0.38055	0.00869
	0.0001	0.0007	0.0025	0.0001	0.0029	0.9479
MgO	0.42171	-0.36147	0.67612	-0.41989	-0.15462	0.15657
	0.0009	0.0049	0.0001	0.0009	0.2423	0.2363
CaO	0.13300	-0.45254	0.48764	0.02576	0.25010	-0.10110
	0.3153	0.0003	0.0001	0.8465	0.0561	0.4461
Na_2O	0.57403	-0.09060	0.09528	-0.63187	-0.59779	0.13944
	0.0001	0.4950	0.4729	0.0001	0.0001	0.2922
K_2O	-0.30979	0.28451	-0.17945	0.37454	0.34149	-0.15611
	0.0170	0.0290	0.1739	0.0035	0.0081	0.2377
P_2O_5	0.01456	-0.11588	-0.04828	0.02479	-0.01077	-0.17248
	0.9128	0.3821	0.7165	0.8522	0.9355	0.1915

Digitised by the Department of Library Services in support of open access to information, University of Pretoria, 2021.

APPENDIX 15: Pearson correlation matrix for petrographic and proximate analyses *vs.* trace element concentrations of all samples of unaffected coals (59samples).

	Moist	Ash	CO_2	VM	Vitr.	ROV
Zn	-0.13507	-0.27904	-0.10038	0.19017	0.17879	-0.41489
	0.3077	0.0323	0.4494	0.1491	0.1755	0.0011
Cu	-0.10455	0.02707	-0.05301	0.33450	0.34082	-0.32307
	0.4307	0.8387	0.6901	0.0096	0.0083	0.0126
Ni	0.04911	-0.43299	0.15005	0.03218	0.17263	-0.21406
	0.7119	0.0006	0.2566	0.8088	0.1911	0.1035
Co	-0.02482	-0.80115	0.06083	0.32398	0.42538	-0.38851
	0.8520	0.0001	0.6472	0.0123	0.0008	0.0024
Ga	-0.18684	-0.25674	-0.10014	0.44146	0.40867	-0.32561
	0.1565	0.0497	0.4505	0.0005	0.0013	0.0119
Mo	-0.26746	-0.22550	-0.19122	0.36912	0.32753	-0.24597
	0.0406	0.0859	0.1468	0.0040	0.0113	0.0604
Nb	-0.03794	-0.24936	-0.15352	0.20367	0.15970	-0.16762
	0.7754	0.0568	0.2457	0.1218	0.2270	0.2044
Zr	-0.27102	-0.07310	-0.33782	0.22671	0.09754	-0.05034
	0.0379	0.5822	0.0089	0.0842	0.4624	0.7050
Y	0.15730	-0.26636	-0.27500	-0.25182	-0.35383	0.17665
	0.2341	0.0414	0.0350	0.0543	0.0060	0.1808
Sr	-0.01959	-0.19185	-0.00135	0.16074	0.16445	-0.26556
	0.8829	0.1455	0.9919	0.2239	0.2133	0.0421
Rb	-0.27693	0.39366	-0.14697	0.21735	0.17176	0.09978
	0.0337	0.0020	0.2667	0.0982	0.1933	0.4521
U	-0.16308	-0.00278	0.02963	0.20375	0.23498	-0.23362
	0.2172	0.9833	0.8237	0.1217	0.0732	0.0749
Th	0.11157	0.00807	-0.20465	-0.23720	-0.30312	0.23348
	0.4002	0.9516	0.1200	0.0705	0.0196	0.0751
Pb	-0.20342	0.55632	-0.09813	0.03750	-0.04412	0.19961
	0.1223	0.0001	0.4597	0.7780	0.7400	0.1296
Cr	-0.14057	0.10780	-0.10985	0.02716	-0.01546	0.09038
	0.2883	0.4164	0.4075	0.8382	0.9075	0.4960
V	-0.24835	0.00493	-0.19983	0.04400	-0.04069	0.13815
	0.0579	0.9704	0.1292	0.7407	0.7596	0.2967
Ba	0.06592	-0.13134	-0.04224	0.09641	0.12361	-0.11497
	0.6199	0.3214	0.7508	0.4676	0.3510	0.3859
Sc	-0.03038	0.20738	-0.16054	0.00734	-0.01838	0.20671
	0.8193	0.1150	0.2245	0.9560	0.8901	0.1162
Cl	-0.22895	-0.36446	-0.13034	0.12758	0.07622	-0.18302
	0.0811	0.0045	0.3251	0.3356	0.5661	0.1653
F	0.15850	-0.74099	-0.25650	0.13692	0.08649	-0.19627
	0.2305	0.0001	0.0499	0.3011	0.5148	0.1363

Digitised by the Department of Library Services in support of open access to information, University of Pretoria, 2021.

APPENDIX 16: Pearson correlation matrix for major element vs. major element concentrations of all samples of unaffected coals (59 samples).

	SiO_2	TiO_2	Al_2O_3	FeO	MnO	MgO	CaO	Na_2O	K_2O	P_2O_5	S
SiO_2	1.00000	0.56368	0.56941	-0.27848	-0.34471	-0.58170	-0.75794	-0.01597	0.20174	-0.22597	-0.10246
	0.0000	0.0001	0.0001	0.0327	0.0075	0.0001	0.0001	0.9044	0.1255	0.0853	0.4400
TiO_2	0.56368	1.00000	0.53047	-0.32822	0.00159	-0.20831	-0.34315	0.19911	-0.06673	-0.24336	-0.44814
	0.0001	0.0000	0.0001	0.0112	0.9905	0.1134	0.0078	0.1306	0.6155	0.0633	0.0004
Al_2O_3	0.56941	0.53047	1.00000	-0.52905	-0.28601	-0.46188	-0.46731	0.19262	0.58946	0.14722	-0.48062
	0.0001	0.0001	0.0000	0.0001	0.0281	0.0002	0.0002	0.1438	0.0001	0.2658	0.0001
FeO	-0.27848	-0.32822	-0.52905	1.00000	0.06774	0.19395	0.34567	-0.48293	-0.14528	-0.23386	0.76769
	0.0327	0.0112	0.0001	0.0000	0.6102	0.1410	0.0073	0.0001	0.2723	0.0746	0.0001
MnO	-0.34471	0.00159	-0.28601	0.06774	1.00000	0.72705	0.55095	0.34713	-0.48253	-0.00066	-0.29487
	0.0075	0.9905	0.0281	0.6102	0.0000	0.0001	0.0001	0.0071	0.0001	0.9960	0.0234
MgO	-0.58170	-0.20831	-0.46188	0.19395	0.72705	1.00000	0.76828	0.30659	-0.39463	0.00933	-0.13513
	0.0001	0.1134	0.0002	0.1410	0.0001	0.0000	0.0001	0.0182	0.0020	0.9441	0.3075
CaO	-0.75794	-0.34315	-0.46731	0.34567	0.55095	0.76828	1.00000	0.07108	-0.28389	0.21911	0.01000
	0.0001	0.0078	0.0002	0.0073	0.0001	0.0001	0.0000	0.5927	0.0293	0.0954	0.9401
Na_2O	-0.01597	0.19911	0.19262	-0.48293	0.34713	0.30659	0.07108	1.00000	-0.11463	0.31915	-0.55108
	0.9044	0.1306	0.1438	0.0001	0.0071	0.0182	0.5927	0.0000	0.3873	0.0137	0.0001
K_2O	0.20174	-0.06673	0.58946	-0.14528	-0.48253	-0.39463	-0.28389	-0.11463	1.00000	0.27667	0.10540
	0.1255	0.6155	0.0001	0.2723	0.0001	0.0020	0.0293	0.3873	0.0000	0.0339	0.4269
P_2O_5	-0.22597	-0.24336	0.14722	-0.23386	-0.00066	0.00933	0.21911	0.31915	0.27667	1.00000	-0.26258
	0.0853	0.0633	0.2658	0.0746	0.9960	0.9441	0.0954	0.0137	0.0339	0.0000	0.0445
S	-0.10246	-0.44814	-0.48062	0.76769	-0.29487	-0.13513	0.01000	-0.55108	0.10540	-0.26258	1.00000
	0.4400	0.0004	0.0001	0.0001	0.0234	0.3075	0.9401	0.0001	0.4269	0.0445	0.0000

APPENDIX 17: Pearson correlation matrix for major element vs. trace element concentrations of all samples of unaffected coals (59 samples)

	SiO_2	TiO_2	Al_2O_3	FeO	MnO	MgO	CaO	Na_2O	K_2O	P_2O_5
Zn	0.02032	-0.11261	-0.17088	0.26606	0.00508	-0.14941	-0.07850	-0.20969	0.07226	0.00768
	0.8786	0.3958	0.1957	0.0417	0.9696	0.2587	0.5545	0.1109	0.5865	0.9540
Cu	-0.13391	-0.13921	0.27670	-0.04802	-0.19615	-0.12418	0.05997	0.01880	0.57671	0.43484
	0.3119	0.2930	0.0339	0.7180	0.1365	0.3487	0.6519	0.8876	0.0001	0.0006
Ni	-0.22367	0.02318	-0.11059	0.15892	0.14925	0.15512	0.13367	0.12235	-0.10797	0.03750
	0.0886	0.8617	0.4044	0.2293	0.2592	0.2408	0.3128	0.3559	0.4156	0.7780
Co	-0.43776	0.00210	-0.15369	0.19024	0.21109	0.16158	0.36028	-0.07434	-0.20939	0.11736
	0.0005	0.9874	0.2452	0.1490	0.1085	0.2215	0.0051	0.5758	0.1115	0.3760
Ga	-0.11398	0.06685	-0.08465	0.19988	-0.22996	-0.16102	-0.03296	-0.44563	0.03380	-0.17850
	0.3900	0.6149	0.5239	0.1291	0.0798	0.2231	0.8043	0.0004	0.7994	0.1762
Mo	0.16483	0.19038	0.09985	-0.04330	-0.29119	-0.39514	-0.29345	-0.28674	-0.02985	-0.09060
	0.2122	0.1487	0.4518	0.7447	0.0253	0.0020	0.0241	0.0277	0.8224	0.4950
Nb	0.13242	0.38944	0.04791	0.13303	-0.00652	-0.13841	-0.10872	-0.33739	-0.08112	-0.44421
	0.3174	0.0023	0.7186	0.3152	0.9609	0.2958	0.4124	0.0090	0.5414	0.0004
Zr	0.35121	0.15016	0.08226	0.09091	-0.43180	-0.46389	-0.46008	-0.33303	0.11269	-0.00463
	0.0064	0.2563	0.5357	0.4935	0.0006	0.0002	0.0002	0.0100	0.3954	0.9723
Y	0.28925	0.26532	0.14489	-0.20567	-0.09066	-0.25922	-0.39180	0.16227	-0.10626	0.24674
	0.0263	0.0423	0.2735	0.1181	0.4947	0.0474	0.0021	0.2195	0.4231	0.0596
Sr	-0.34709	-0.23154	0.24663	-0.27178	-0.03432	0.07311	0.25404	0.29974	0.47827	0.87891
	0.0071	0.0776	0.0597	0.0373	0.7964	0.5821	0.0522	0.0211	0.0001	0.0001
Rb	0.50527	0.33799	0.32238	-0.15136	-0.50725	-0.46866	-0.55526	-0.33846	0.39902	-0.22064
	0.0001	0.0088	0.0128	0.2525	0.0001	0.0002	0.0001	0.0087	0.0017	0.0931
U	-0.03172	-0.05855	0.17777	-0.15546	-0.12421	-0.16223	-0.05584	0.05629	0.29537	0.49149
	0.8115	0.6596	0.1780	0.2397	0.3486	0.2196	0.6744	0.6720	0.0231	0.0001
Th	0.45725	0.55357	0.34123	-0.43554	-0.27742	-0.36377	-0.59532	0.12943	-0.10719	-0.14977
	0.0003	0.0001	0.0082	0.0006	0.0334	0.0046	0.0001	0.3285	0.4190	0.2575
Pb	0.40387	-0.00615	0.03066	0.10127	-0.28584	-0.29976	-0.36117	-0.18672	0.17184	-0.17402
	0.0015	0.9631	0.8177	0.4453	0.0282	0.0211	0.0049	0.1568	0.1931	0.1874
Cr	0.48452	0.31848	0.06801	0.15320	-0.19344	-0.29330	-0.39299	-0.27081	0.02761	-0.24544
	0.0001	0.0140	0.6088	0.2467	0.1421	0.0242	0.0021	0.0380	0.8356	0.0610
V	0.41430	0.27009	-0.00381	0.25296	-0.24585	-0.32997	-0.42390	-0.26456	-0.03506	-0.20315
	0.0011	0.0386	0.9771	0.0532	0.0605	0.0107	0.0008	0.0429	0.7921	0.1228
Ba	-0.24731	-0.16554	0.41052	-0.30434	-0.16248	-0.01686	0.15153	0.36203	0.54505	0.73671
	0.0590	0.2102	0.0012	0.0191	0.2189	0.8991	0.2519	0.0048	0.0001	0.0001
Sc	0.33985	0.10754	0.05397	0.09984	-0.19842	-0.16636	-0.17012	-0.22789	-0.02221	-0.19347
	0.0085	0.4175	0.6847	0.4518	0.1319	0.2079	0.1977	0.0826	0.8674	0.1420
Cl	-0.17604	0.11309	-0.01960	-0.03465	0.09085	0.03692	0.13153	0.22741	-0.08011	0.03607
	0.1823	0.3938	0.8829	0.7945	0.4938	0.7813	0.3207	0.0832	0.5464	0.7862
F	-0.24413	0.25918	0.12432	-0.06466	0.22617	0.00348	0.19779	0.01322	-0.18669	0.12230
	0.0624	0.0475	0.3482	0.6266	0.0850	0.9792	0.1332	0.9209	0.1568	0.3561

Digitised by the Department of Library Services in support of open access to information, University of Pretoria, 2021.

APPENDIX 18: Pearson correlation matrix for trace element vs. trace element concentrations of all samples of unaffected coals (59samples).

	Zn	Cu	Ni	Co	Ga	Mo	Nb	Zr	Y	Sr	Rb	U
Zn	1.00000	0.00961	0.18239	0.32327	0.22406	0.32420	0.21693	0.41819	0.28673	0.01281	-0.04241	0.10641
	0.0000	0.9424	0.1668	0.0125	0.0880	0.0122	0.0989	0.0010	0.0277	0.9233	0.7498	0.4224
Cu	0.00961	1.00000	-0.20766	-0.06836	0.21654	-0.22482	-0.01607	-0.02157	-0.16739	0.58497	0.12415	0.20277
	0.9424	0.0000	0.1145	0.6069	0.0995	0.0869	0.9038	0.8712	0.2051	0.0001	0.3489	0.1235
Ni	0.18239	-0.20766	1.00000	0.67842	-0.19913	0.39257	-0.29212	0.05740	0.22067	0.14394	-0.13176	0.47399
	0.1668	0.1145	0.0000	0.0001	0.1305	0.0021	0.0248	0.6659	0.0931	0.2768	0.3198	0.0001
Co	0.32327	-0.06836	0.67842	1.00000	0.13183	0.53063	0.08986	0.13635	0.23508	0.18871	-0.25970	0.31692
	0.0125	0.6069	0.0001	0.0000	0.3196	0.0001	0.4985	0.3031	0.0731	0.1523	0.0470	0.0145
Ga	0.22406	0.21654	-0.19913	0.13183	1.00000	0.13169	0.67576	0.36450	0.02416	-0.14575	0.29913	-0.38303
	0.0880	0.0995	0.1305	0.3196	0.0000	0.3201	0.0001	0.0045	0.8559	0.2707	0.0214	0.0028
Mo	0.32420	-0.22482	0.39257	0.53063	0.13169	1.00000	0.13849	0.44054	0.34012	-0.07234	0.22991	0.39621
	0.0122	0.0869	0.0021	0.0001	0.3201	0.0000	0.2955	0.0005	0.0084	0.5861	0.0798	0.0019
Nb	0.21693	-0.01607	-0.29212	0.08986	0.67576	0.13849	1.00000	0.30418	0.03867	-0.43875	0.30378	-0.52331
	0.0989	0.9038	0.0248	0.4985	0.0001	0.2955	0.0000	0.0192	0.7712	0.0005	0.0193	0.0001
Zr	0.41819	-0.02157	0.05740	0.13635	0.36450	0.44054	0.30418	1.00000	0.72523	-0.09600	0.32153	0.04699
	0.0010	0.8712	0.6659	0.3031	0.0045	0.0005	0.0192	0.0000	0.0001	0.4695	0.0130	0.7238
Y	0.28673	-0.16739	0.22067	0.23508	0.02416	0.34012	0.03867	0.72523	1.00000	0.05862	0.08177	0.11630
	0.0277	0.2051	0.0931	0.0731	0.8559	0.0084	0.7712	0.0001	0.0000	0.6592	0.5381	0.3804
Sr	0.01281	0.58497	0.14394	0.18871	-0.14575	-0.07234	-0.43875	-0.09600	0.05862	1.00000	-0.16684	0.58468
	0.9233	0.0001	0.2768	0.1523	0.2707	0.5861	0.0005	0.4695	0.6592	0.0000	0.2066	0.0001
Rb	-0.04241	0.12415	-0.13176	-0.25970	0.29913	0.22991	0.30378	0.32153	0.08177	-0.16684	1.00000	0.05272
	0.7498	0.3489	0.3198	0.0470	0.0214	0.0798	0.0193	0.0130	0.5381	0.2066	0.0000	0.6917
U	0.10641	0.20277	0.47399	0.31692	-0.38303	0.39621	-0.52331	0.04699	0.11630	0.58468	0.05272	1.00000
	0.4224	0.1235	0.0001	0.0145	0.0028	0.0019	0.0001	0.7238	0.3804	0.0001	0.6917	0.0000
Th	-0.13590	-0.20655	0.15111	-0.02110	-0.01004	0.39656	0.13930	0.31227	0.51788	-0.20908	0.40309	0.10317
	0.3047	0.1165	0.2533	0.8740	0.9398	0.0019	0.2927	0.0160	0.0001	0.1120	0.0015	0.4368
Pb	-0.09819	-0.08777	-0.21474	-0.38918	0.06219	0.00084	-0.00092	0.02555	-0.06999	-0.24404	0.33488	-0.12071
	0.4594	0.5086	0.1024	0.0023	0.6399	0.9950	0.9945	0.8477	0.5984	0.0625	0.0095	0.3625
Cr	0.35044	-0.09906	-0.02864	-0.03607	0.26800	0.20437	0.37110	0.61273	0.42308	-0.34006	0.40811	-0.07814
	0.0065	0.4554	0.8295	0.7862	0.0401	0.1205	0.0038	0.0001	0.0008	0.0084	0.0013	0.5564
V	0.35589	-0.17455	0.07181	0.07797	0.22354	0.33368	0.35630	0.67129	0.53772	-0.29844	0.33822	-0.02817
	0.0057	0.1861	0.5889	0.5572	0.0888	0.0098	0.0056	0.0001	0.0001	0.0217	0.0088	0.8322
Ba	-0.09043	0.53309	0.08196	0.10102	-0.18425	-0.10674	-0.39315	-0.14642	0.03362	0.86241	-0.14460	0.44734
	0.4958	0.0001	0.5372	0.4465	0.1624	0.4210	0.0021	0.2685	0.8004	0.0001	0.2745	0.0004
Sc	0.08766	0.01276	-0.06601	-0.13810	0.05056	0.00159	0.00013	0.29289	0.16645	-0.26523	0.22098	-0.10599
	0.5091	0.9236	0.6194	0.2969	0.7037	0.9904	0.9992	0.0244	0.2077	0.0423	0.0926	0.4243
Cl	0.22946	-0.04405	0.24053	0.40207	0.03914	0.21888	0.15635	0.01694	0.08795	0.07666	-0.16525	-0.00324
	0.0804	0.7405	0.0665	0.0016	0.7685	0.0958	0.2370	0.8987	0.5077	0.5639	0.2110	0.9806
F	0.22398	-0.04527	0.34491	0.69348	0.32033	0.33090	0.32591	0.15212	0.33710	0.14079	-0.19278	0.00249
	0.0881	0.7335	0.0075	0.0001	0.0134	0.0105	0.0118	0.2501	0.0090	0.2875	0.1435	0.9851

Digitised by the Department of Library Services in support of open access to information, University of Pretoria, 2021.

APPENDIX 19: Pearson correlation matrix for petrographic and proximate analyses vs. major element concentrations of all unaffected coals. Matrices are given separately for each seam bench **A** to **F**. Sample **GZ** is incorporated in the matrix for bench **A**.

B E N C H A

	Moist	Ash	CO_2	VM	Vitr.	ROV
SiO_2	0.04919	-0.47796	-0.65662	0.40866	-0.56333	0.02844
	0.8858	0.1370	0.0282	0.2121	0.0711	0.9339
TiO_2	-0.02799	-0.61310	-0.55378	0.35154	-0.33354	0.34637
	0.9349	0.0449	0.0771	0.2891	0.3162	0.2967
Al_2O_3	0.19456	-0.56801	-0.70940	0.41117	-0.65074	0.15912
	0.5665	0.0683	0.0145	0.2090	0.0301	0.6403
FeO	0.01220	0.68254	0.72807	-0.52071	0.69623	-0.01395
	0.9716	0.0207	0.0111	0.1005	0.0173	0.9675
MnO	0.31083	0.03008	0.37218	-0.44293	0.00184	-0.14081
	0.3522	0.9300	0.2597	0.1725	0.9957	0.6796
MgO	-0.11877	0.62279	0.92568	-0.74071	0.56478	0.18044
	0.7280	0.0407	0.0001	0.0091	0.0703	0.5955
CaO	-0.00225	0.57677	0.65894	-0.35409	0.66507	-0.03019
	0.9948	0.0632	0.0274	0.2854	0.0256	0.9298
Na_2O	-0.48954	-0.44564	-0.26564	0.18782	-0.42347	-0.26566
	0.1264	0.1695	0.4298	0.5802	0.1944	0.4298
K_2O	0.00325	-0.04357	-0.17482	0.18069	-0.08276	0.23101
	0.9924	0.8988	0.6072	0.5950	0.8089	0.4943
P_2O_5	-0.09142	0.20028	-0.12016	0.09141	-0.17329	-0.23565
	0.7892	0.5549	0.7249	0.7892	0.6104	0.4855
LOI	-0.03694	-0.97497	-0.53633	0.41658	-0.38804	-0.13835
	0.9141	0.0001	0.0890	0.2025	0.2383	0.6850

B E N C H B

	Moist	Ash	CO_2	VM	Vitr.	ROV
SiO_2	0.29524	0.55139	-0.25423	-0.35129	-0.28526	0.41550
	0.4076	0.0985	0.4784	0.3196	0.4243	0.2324
TiO_2	0.14697	0.49082	-0.39028	-0.28349	-0.36826	0.51351
	0.6854	0.1497	0.2649	0.4274	0.2951	0.1290
Al_2O_3	0.36152	0.38970	-0.29712	-0.30907	-0.27691	0.22893
	0.3047	0.2656	0.4045	0.3849	0.4386	0.5246
FeO	-0.39433	-0.58504	-0.10850	0.40554	0.07884	-0.40654
	0.2595	0.0756	0.7654	0.2449	0.8286	0.2437
MnO	0.18399	-0.69394	-0.04015	0.56809	0.47013	-0.63900
	0.6109	0.0260	0.9123	0.0867	0.1703	0.0467
MgO	-0.00395	-0.14413	0.71877	-0.15686	0.30476	-0.06291
	0.9914	0.6912	0.0192	0.6652	0.3919	0.8629
CaO	-0.13487	-0.42608	0.38257	0.38219	0.51257	-0.46526
	0.7103	0.2195	0.2752	0.2757	0.1298	0.1754
Na_2O	0.35326	0.06536	0.11185	-0.19730	-0.00830	0.01502
	0.3167	0.8576	0.7584	0.5848	0.9818	0.9672
K_2O	-0.36622	0.63833	0.08683	-0.00219	0.08633	0.44325
	0.2980	0.0470	0.8115	0.9952	0.8126	0.1995
P_2O_5	-0.59556	-0.20343	0.22493	-0.13088	-0.36968	0.30408
	0.0693	0.5730	0.5321	0.7186	0.2931	0.3930
LOI	0.07753	-0.96995	-0.36680	0.44047	0.06121	-0.62094
	0.8314	0.0001	0.2971	0.2026	0.8666	0.0554

Digitised by the Department of Library Services in support of open access to information, University of Pretoria, 2021.

APPENDIX 19: continued

B E N C H C

	Moist	Ash	CO_2	VM	Vitr.	ROV
SiO_2	0.08722	0.55542	-0.15588	-0.13508	-0.47352	-0.05453
	0.8107	0.0955	0.6672	0.7098	0.1669	0.8811
TiO_2	-0.06376	0.46749	-0.35041	0.18529	-0.06103	-0.38279
	0.8611	0.1731	0.3209	0.6083	0.8670	0.2749
Al_2O_3	-0.26354	-0.26206	-0.40088	-0.19431	-0.53302	0.51129
	0.4619	0.4645	0.2509	0.5906	0.1126	0.1309
FeO	-0.25451	0.23398	-0.14524	0.65657	0.52531	-0.25346
	0.4779	0.5153	0.6889	0.0392	0.1189	0.4798
MnO	0.15982	0.28851	0.26778	0.44551	0.80345	-0.72362
	0.6592	0.4188	0.4545	0.1969	0.0051	0.0180
MgO	-0.00651	-0.50069	0.16219	0.33164	0.70604	-0.12643
	0.9858	0.1405	0.6544	0.3492	0.0225	0.7278
CaO	0.09322	-0.42916	0.29420	0.16725	0.59259	-0.14807
	0.7979	0.2158	0.4093	0.6442	0.0710	0.6831
Na_2O	0.38490	-0.03345	0.18867	-0.49769	-0.28169	-0.24169
	0.2721	0.9269	0.6017	0.1433	0.4304	0.5011
K_2O	-0.08900	-0.20880	0.07615	-0.23289	-0.01578	0.17808
	0.8069	0.5626	0.8344	0.5173	0.9655	0.6226
P_2O_5	0.31689	-0.23052	0.27173	-0.43639	-0.15263	-0.13648
	0.3723	0.5217	0.4476	0.2074	0.6738	0.7070
LOI	-0.37958	-0.95432	-0.60055	0.33896	-0.04577	0.54133
	0.2793	0.0001	0.0664	0.3380	0.9001	0.1061

B E N C H D

	Moist	Ash	CO_2	VM	Vitr.	ROV
SiO_2	0.73118	0.72093	0.21809	-0.93525	-0.84580	0.54110
	0.0163	0.0186	0.5450	0.0001	0.0020	0.1063
TiO_2	0.34441	0.33434	0.72852	-0.66283	-0.33573	0.40153
	0.3298	0.3450	0.0169	0.0367	0.3429	0.2501
Al_2O_3	0.60122	0.06062	-0.02034	-0.11680	-0.07189	-0.28831
	0.0660	0.8679	0.9555	0.7479	0.8436	0.4192
FeO	-0.65725	-0.50070	-0.36573	0.70136	0.48102	-0.44162
	0.0389	0.1405	0.2987	0.0238	0.1593	0.2013
MnO	0.53947	0.82802	-0.11208	-0.87484	-0.93686	0.72991
	0.1075	0.0031	0.7579	0.0009	0.0001	0.0166
MgO	0.06943	0.52245	0.46995	-0.58398	-0.33198	0.82737
	0.8488	0.1213	0.1705	0.0763	0.3487	0.0031
CaO	-0.75656	-0.19970	-0.29568	0.42848	0.24212	0.07352
	0.0113	0.5802	0.4069	0.2167	0.5003	0.8400
Na_2O	0.75099	0.64180	-0.18094	-0.62997	-0.69942	0.33345
	0.0123	0.0455	0.6169	0.0509	0.0244	0.3464
K_2O	0.27057	-0.03231	-0.02405	0.16367	0.21594	-0.34841
	0.4496	0.9294	0.9474	0.6514	0.5490	0.3238
P_2O_5	-0.26113	-0.40816	-0.51365	0.53075	0.24092	-0.54023
	0.4662	0.2416	0.1289	0.1145	0.5025	0.1069
LOI	-0.48934	-0.96036	0.03185	0.84977	0.87780	-0.76413
	0.1512	0.0001	0.9304	0.0019	0.0008	0.0101

Digitised by the Department of Library Services in support of open access to information, University of Pretoria, 2021.

APPENDIX 19: continued

B E N C H E

	Moist	Ash	CO_2	VM	Vitr.	ROV
SiO_2	0.26564	0.55727	-0.39638	-0.43786	-0.62947	0.11544
	0.4582	0.0942	0.2568	0.2057	0.0512	0.7508
TiO_2	0.59353	0.14809	0.03441	-0.59123	-0.54317	0.04312
	0.0705	0.6831	0.9248	0.0718	0.1047	0.9058
Al_2O_3	-0.12900	-0.22161	-0.45820	0.24114	0.12552	-0.50630
	0.7225	0.5383	0.1829	0.5021	0.7297	0.1354
FeO	-0.00864	0.90923	-0.38403	-0.28585	-0.58396	0.61425
	0.9811	0.0003	0.2733	0.4233	0.0763	0.0588
MnO	0.17854	-0.81415	0.52782	0.17514	0.41239	-0.26025
	0.6217	0.0041	0.1169	0.6284	0.2363	0.4677
MgO	-0.06657	-0.76779	0.57113	0.33032	0.61448	-0.08516
	0.8550	0.0095	0.0846	0.3512	0.0587	0.8151
CaO	0.08021	-0.76235	0.60706	0.12863	0.43042	-0.09245
	0.8257	0.0104	0.0627	0.7232	0.2144	0.7995
Na_2O	0.62307	-0.06571	0.06250	-0.59071	-0.67098	-0.34647
	0.0543	0.8569	0.8638	0.0722	0.0337	0.3267
K_2O	0.05216	0.18811	-0.00085	-0.03422	-0.06305	0.07300
	0.8862	0.6028	0.9981	0.9252	0.8626	0.8412
P_2O_5	0.29247	-0.31103	0.26280	-0.23489	-0.13022	-0.30512
	0.4122	0.3817	0.4632	0.5136	0.7199	0.3913
LOI	-0.14393	-0.97652	0.30544	0.48388	0.72520	-0.48847
	0.6916	0.0001	0.3908	0.1565	0.0176	0.1520

B E N C H F

	Moist	Ash	CO_2	VM	Vitr.	ROV
SiO_2	-0.50002	0.40531	0.00193	-0.45853	-0.37792	0.48282
	0.2070	0.3192	0.9964	0.2532	0.3560	0.2256
TiO_2	0.13759	-0.22347	-0.16130	-0.38461	-0.32997	0.36413
	0.7453	0.5947	0.7028	0.3468	0.4247	0.3752
Al_2O_3	-0.07986	-0.06739	0.15234	-0.23059	-0.10822	0.13836
	0.8509	0.8740	0.7188	0.5827	0.7987	0.7439
FeO	-0.13846	-0.27177	0.34052	-0.16819	0.24585	0.07071
	0.7437	0.5150	0.4092	0.6905	0.5573	0.8679
MnO	0.05206	-0.49595	0.47019	-0.10327	0.26085	-0.34943
	0.9026	0.2113	0.2397	0.8077	0.5326	0.3962
MgO	-0.28517	-0.09175	0.74839	0.20271	0.62713	-0.57587
	0.4936	0.8289	0.0327	0.6302	0.0961	0.1352
CaO	-0.13319	-0.27260	0.58757	-0.07110	0.40736	-0.42019
	0.7532	0.5136	0.1256	0.8671	0.3165	0.3000
Na_2O	-0.15617	0.46214	-0.47019	-0.53796	-0.65907	0.80369
	0.7119	0.2490	0.2397	0.1690	0.0755	0.0162
K_2O	-0.45730	0.34318	0.30748	0.05188	0.06118	-0.11046
	0.2546	0.4053	0.4588	0.9029	0.8856	0.7946
P_2O_5	0.37346	-0.53115	-0.06847	-0.59380	-0.32026	0.02722
	0.3621	0.1755	0.8720	0.1207	0.4393	0.9490
LOI	0.84326	-0.91497	0.02759	0.26743	0.32532	-0.52550
	0.0085	0.0014	0.9483	0.5220	0.4317	0.1811

Digitised by the Department of Library Services in support of open access to information, University of Pretoria, 2021.

APPENDIX 20: Pearson correlation matrix for petrographic and proximate analyses vs. trace element concentrationsof all unaffected coals. Matrices are given separately for each seam bench **A** to **F**. Sample **GZ** is incorporated in the matrix for bench **A**.

B E N C H A

	Moist	Ash	CO_2	VM	Vitr.	ROV
Zn	-0.23171	0.08024	-0.16724	0.13183	-0.27319	0.00533
	0.4930	0.8146	0.6231	0.6992	0.4163	0.9876
Cu	0.00000	0.00000	0.00000	0.00000	0.00000	0.00000
	1.0000	1.0000	1.0000	1.0000	1.0000	1.0000
Ni	0.08411	-0.59034	-0.10026	0.18034	0.06924	-0.66589
	0.8058	0.0559	0.7693	0.5957	0.8397	0.0253
Co	-0.10035	-0.93246	-0.43183	0.35689	-0.27760	-0.27822
	0.7691	0.0001	0.1847	0.2813	0.4085	0.4074
Ga	0.23521	-0.12368	-0.26995	0.26143	0.02477	0.31364
	0.4863	0.7171	0.4221	0.4374	0.9424	0.3476
Mo	0.08485	-0.50395	-0.36978	0.10004	-0.61031	-0.16803
	0.8041	0.1140	0.2630	0.7698	0.0461	0.6214
Nb	0.09338	-0.44464	-0.63999	0.51651	-0.19795	-0.01722
	0.7848	0.1706	0.0339	0.1038	0.5596	0.9599
Zr	-0.12963	-0.71735	-0.83225	0.63367	-0.54918	0.12388
	0.7040	0.0130	0.0015	0.0363	0.0802	0.7167
Y	-0.21389	-0.80626	-0.59747	0.34873	-0.62511	0.29597
	0.5277	0.0027	0.0522	0.2932	0.0397	0.3769
Sr	-0.00552	0.04754	-0.09646	0.14753	-0.13606	0.01430
	0.9871	0.8896	0.7778	0.6651	0.6900	0.9667
Rb	0.15417	-0.55294	-0.37630	0.26369	-0.12031	0.27451
	0.6508	0.0777	0.2540	0.4333	0.7246	0.4140
U	-0.08973	0.16643	0.31192	-0.22784	0.19791	-0.20776
	0.7930	0.6248	0.3504	0.5004	0.5597	0.5399
Th	-0.11490	-0.57529	-0.76614	0.51805	-0.49218	0.24665
	0.7366	0.0641	0.0060	0.1026	0.1241	0.4647
Pb	0.00000	0.00000	0.00000	0.00000	0.00000	0.00000
	1.0000	1.0000	1.0000	1.0000	1.0000	1.0000
Cr	-0.23492	-0.14764	-0.67673	0.51832	-0.48107	0.31880
	0.4868	0.6649	0.0222	0.1024	0.1341	0.3393
V	-0.64592	0.13726	-0.04299	0.09126	0.10121	0.00669
	0.0318	0.6873	0.9001	0.7896	0.7672	0.9844
Ba	0.27199	0.16011	-0.35354	0.23991	-0.32118	0.27907
	0.4185	0.6382	0.2862	0.4774	0.3355	0.4060
Sc	0.14763	0.25098	-0.32011	0.39698	-0.01992	0.02347
	0.6649	0.4566	0.3372	0.2267	0.9536	0.9454
Cl	-0.64006	-0.45579	-0.31416	0.20325	-0.48983	-0.15618
	0.0339	0.1589	0.3468	0.5489	0.1262	0.6465
F	0.25264	-0.78293	-0.76495	0.54070	-0.52122	-0.01700
	0.4536	0.0044	0.0061	0.0859	0.1001	0.9604

Digitised by the Department of Library Services in support of open access to information, University of Pretoria, 2021.

B E N C H B

	Moist	Ash	CO_2	VM	Vitr.	ROV
Zn	0.17447	-0.61088	-0.37890	0.83072	0.63899	-0.73576
	0.6298	0.0606	0.2802	0.0029	0.0467	0.0153
Cu	0.00000	0.00000	0.00000	0.00000	0.00000	0.00000
	1.0000	1.0000	1.0000	1.0000	1.0000	1.0000
Ni	0.15463	-0.55474	-0.24162	0.09112	0.07254	-0.40650
	0.6697	0.0960	0.5012	0.8023	0.8422	0.2437
Co	0.28762	-0.95690	-0.46506	0.39011	0.06899	-0.60406
	0.4203	0.0001	0.1756	0.2651	0.8498	0.0644
Ga	-0.37267	0.07288	-0.03531	0.03424	-0.23271	0.36557
	0.2889	0.8414	0.9229	0.9252	0.5176	0.2989
Mo	0.72261	-0.16076	0.03976	-0.43990	-0.23538	0.00626
	0.0182	0.6573	0.9132	0.2033	0.5127	0.9863
Nb	-0.12734	0.02858	-0.13105	0.27399	-0.02775	0.03763
	0.7259	0.9375	0.7182	0.4437	0.9393	0.9178
Zr	-0.01550	-0.19745	0.02765	-0.50126	-0.49619	0.48426
	0.9661	0.5845	0.9396	0.1400	0.1447	0.1561
Y	-0.02644	-0.42764	-0.48112	-0.19530	-0.60737	0.26878
	0.9422	0.2177	0.1592	0.5887	0.0626	0.4527
Sr	-0.35561	-0.35091	0.34498	-0.17683	-0.19847	0.15418
	0.3132	0.3201	0.3289	0.6250	0.5825	0.6706
Rb	0.08891	0.58563	0.58845	-0.60229	-0.20855	0.39029
	0.8070	0.0753	0.0735	0.0654	0.5631	0.2648
U	0.00000	0.00000	0.00000	0.00000	0.00000	0.00000
	1.0000	1.0000	1.0000	1.0000	1.0000	1.0000
Th	0.16204	0.46542	-0.01500	-0.67634	-0.59595	0.58106
	0.6547	0.1753	0.9672	0.0318	0.0690	0.0781
Pb	0.00000	0.00000	0.00000	0.00000	0.00000	0.00000
	1.0000	1.0000	1.0000	1.0000	1.0000	1.0000
Cr	-0.00863	0.66049	0.03013	-0.43369	-0.40837	0.52512
	0.9811	0.0376	0.9341	0.2105	0.2414	0.1191
V	-0.20352	0.20940	-0.30491	-0.30037	-0.62471	0.55175
	0.5728	0.5615	0.3916	0.3991	0.0535	0.0982
Ba	-0.06623	-0.20295	0.26315	-0.52875	-0.51000	0.35287
	0.8558	0.5739	0.4626	0.1161	0.1321	0.3172
Sc	0.51032	0.23236	0.05400	-0.46077	-0.00697	0.10782
	0.1318	0.5183	0.8822	0.1802	0.9848	0.7669
Cl	-0.18997	-0.20296	-0.07332	0.50046	0.24502	-0.53124
	0.5991	0.5739	0.8405	0.1407	0.4951	0.1141
F	-0.16615	-0.73306	-0.73090	0.54908	-0.05393	-0.40455
	0.6464	0.0159	0.0163	0.1002	0.8824	0.2462

Digitised by the Department of Library Services in support of open access to information, University of Pretoria, 2021.

APPENDIX 20:

BENCH C

	Moist	Ash	CO_2	VM	Vitr.	ROV
Zn	0.56389	0.13271	0.26455	-0.32291	0.04822	-0.47261
	0.0895	0.7148	0.4601	0.3628	0.8948	0.1678
Cu	0.77841	-0.08848	0.13251	-0.27479	-0.13047	-0.47978
	0.0080	0.8080	0.7152	0.4423	0.7194	0.1605
Ni	-0.10357	-0.27572	0.23462	-0.18052	0.04022	0.18234
	0.7759	0.4407	0.5141	0.6177	0.9122	0.6141
Co	0.03389	-0.79529	-0.01812	-0.22345	-0.17266	0.36399
	0.9260	0.0060	0.9604	0.5349	0.6334	0.3011
Ga	-0.10812	0.09832	-0.27213	0.74089	0.59320	-0.23727
	0.7662	0.7870	0.4469	0.0142	0.0707	0.5092
Mo	0.02778	-0.05572	0.14359	-0.27841	-0.18390	0.28459
	0.9393	0.8785	0.6923	0.4360	0.6110	0.4255
Nb	0.06525	0.18104	-0.34134	0.37709	0.12374	-0.21456
	0.8579	0.6167	0.3344	0.2827	0.7334	0.5517
Zr	0.33191	-0.64197	-0.14340	-0.41458	-0.42387	0.15383
	0.3488	0.0454	0.6927	0.2336	0.2222	0.6713
Y	0.35747	-0.41078	0.10195	-0.60982	-0.57187	0.18607
	0.3105	0.2383	0.7793	0.0612	0.0841	0.6068
Sr	0.15022	-0.47749	0.13782	-0.30844	-0.06621	0.05855
	0.6787	0.1628	0.7042	0.3859	0.8558	0.8724
Rb	0.04282	0.33782	0.35567	0.10093	0.23857	0.03113
	0.9065	0.3397	0.3131	0.7815	0.5068	0.9320
U	0.02778	0.28601	0.55950	-0.42073	0.06869	-0.08262
	0.9393	0.4231	0.0926	0.2260	0.8505	0.8205
Th	-0.02977	-0.23086	-0.27484	-0.49575	-0.90474	0.59419
	0.9349	0.5211	0.4422	0.1451	0.0003	0.0701
Pb	0.00000	0.00000	0.00000	0.00000	0.00000	0.00000
	1.0000	1.0000	1.0000	1.0000	1.0000	1.0000
Cr	0.20553	0.61958	0.61930	-0.03640	0.35608	-0.32162
	0.5689	0.0561	0.0562	0.9205	0.3126	0.3648
V	0.27691	0.00057	0.00972	-0.38038	-0.51420	-0.03998
	0.4386	0.9988	0.9787	0.2782	0.1284	0.9127
Ba	0.03719	-0.39484	-0.05008	-0.42112	-0.39087	0.28460
	0.9188	0.2588	0.8907	0.2255	0.2641	0.4255
Sc	0.00000	0.00000	0.00000	0.00000	0.00000	0.00000
	1.0000	1.0000	1.0000	1.0000	1.0000	1.0000
Cl	-0.44423	-0.62588	-0.55428	0.08018	-0.21766	0.53547
	0.1984	0.0529	0.0964	0.8257	0.5458	0.1107
F	-0.48431	-0.70468	-0.76152	0.16554	-0.37449	0.63160
	0.1561	0.0229	0.0105	0.6476	0.2863	0.0501

Digitised by the Department of Library Services in support of open access to information, University of Pretoria, 2021.

continued

	BENCH D					
	Moist	Ash	CO_2	VM	Vitr.	ROV
Zn	0.15770	-0.70977	-0.03967	0.39255	0.38503	-0.89903
	0.6635	0.0215	0.9134	0.2618	0.2719	0.0004
Cu	0.07026	0.05634	-0.08234	0.13727	0.11708	-0.08424
	0.8471	0.8771	0.8211	0.7053	0.7474	0.8170
Ni	-0.01478	-0.24547	0.20656	0.26283	0.40552	-0.32814
	0.9677	0.4942	0.5669	0.4632	0.2450	0.3546
Co	-0.28920	-0.90982	0.01584	0.70703	0.73046	-0.78078
	0.4177	0.0003	0.9654	0.0222	0.0164	0.0077
Ga	0.18284	-0.43112	-0.07649	0.12037	0.12512	-0.33239
	0.6131	0.2135	0.8337	0.7405	0.7306	0.3480
Mo	-0.10069	-0.72638	0.17122	0.40834	0.48323	-0.58147
	0.7820	0.0174	0.6362	0.2414	0.1571	0.0779
Nb	0.23789	-0.25640	0.29648	-0.19575	-0.08255	-0.13490
	0.5081	0.4746	0.4055	0.5878	0.8206	0.7102
Zr	-0.14993	-0.79578	0.34874	0.36601	0.48301	-0.62280
	0.6793	0.0059	0.3233	0.2983	0.1573	0.0544
Y	0.23455	-0.40651	0.28287	-0.13406	-0.01076	-0.18591
	0.5142	0.2437	0.4284	0.7120	0.9765	0.6071
Sr	-0.08522	-0.31407	-0.11093	0.43858	0.37927	-0.55420
	0.8149	0.3768	0.7603	0.2048	0.2797	0.0964
Rb	0.50113	0.23002	0.51157	-0.37203	-0.06681	0.29957
	0.1401	0.5226	0.1307	0.2898	0.8545	0.4004
U	0.10604	-0.15908	0.17867	0.11902	0.18334	-0.28093
	0.7706	0.6607	0.6214	0.7433	0.6122	0.4317
Th	0.32376	0.29232	0.29167	-0.39255	-0.24066	0.47203
	0.3615	0.4124	0.4135	0.2618	0.5030	0.1684
Pb	0.00000	0.00000	0.00000	0.00000	0.00000	0.00000
	1.0000	1.0000	1.0000	1.0000	1.0000	1.0000
Cr	0.19542	0.20147	0.70181	-0.54731	-0.18088	0.28712
	0.5885	0.5767	0.0237	0.1015	0.6170	0.4212
V	0.26626	0.11743	0.13611	-0.23426	-0.25492	-0.10888
	0.4571	0.7466	0.7077	0.5148	0.4772	0.7646
Ba	0.12597	-0.32326	-0.14240	0.36322	0.29320	-0.59683
	0.7288	0.3622	0.6947	0.3022	0.4110	0.0685
Sc	-0.08064	0.64503	-0.09837	-0.38963	-0.46262	0.68397
	0.8247	0.0440	0.7869	0.2657	0.1782	0.0292
Cl	-0.59364	-0.66808	-0.55045	0.83459	0.54765	-0.64554
	0.0704	0.0347	0.0992	0.0027	0.1013	0.0438
F	0.00370	-0.89674	-0.01371	0.46823	0.45724	-0.75247
	0.9919	0.0004	0.9700	0.1723	0.1840	0.0120

Digitised by the Department of Library Services in support of open access to information, University of Pretoria, 2021.

APPENDIX 20:

B E N C H E

	Moist	Ash	CO_2	VM	Vitr.	ROV
Zn	0.19663	-0.56210	-0.21370	0.12497	-0.01725	-0.78669
	0.5861	0.0908	0.5533	0.7309	0.9623	0.0069
Cu	0.23082	-0.06819	0.11529	0.03742	0.09243	-0.39620
	0.5211	0.8515	0.7511	0.9183	0.7995	0.2570
Ni	-0.00794	-0.35156	-0.02475	-0.14097	-0.08600	0.01850
	0.9826	0.3192	0.9459	0.6977	0.8133	0.9596
Co	0.02476	-0.85101	0.29136	0.15701	0.33853	-0.31249
	0.9459	0.0018	0.4141	0.6649	0.3387	0.3794
Ga	-0.06891	-0.36645	0.29524	0.39048	0.57415	-0.30977
	0.8500	0.2976	0.4076	0.2646	0.0826	0.3837
Mo	-0.13813	-0.42072	-0.13325	0.07252	0.01442	0.09065
	0.7035	0.2260	0.7136	0.8422	0.9685	0.8033
Nb	0.01166	-0.15131	0.10967	0.20276	0.31662	-0.10906
	0.9745	0.6765	0.7630	0.5743	0.3728	0.7642
Zr	0.35362	-0.87105	0.43133	-0.05972	0.26863	-0.46984
	0.3162	0.0010	0.2133	0.8698	0.4530	0.1706
Y	0.55789	-0.37004	0.41592	-0.57120	-0.30653	-0.00776
	0.0938	0.2926	0.2319	0.0846	0.3890	0.9830
Sr	0.11257	-0.35418	0.06071	0.02054	-0.01535	-0.44208
	0.7568	0.3153	0.8677	0.9551	0.9664	0.2008
Rb	0.21948	0.73114	-0.09622	-0.57368	-0.55288	0.72752
	0.5424	0.0163	0.7915	0.0829	0.0974	0.0171
U	0.10484	-0.22743	-0.10647	-0.11454	-0.19675	-0.17042
	0.7732	0.5274	0.7697	0.7527	0.5859	0.6378
Th	0.42819	-0.18841	0.42789	-0.54965	-0.19571	0.23056
	0.2170	0.6022	0.2174	0.0998	0.5879	0.5216
Pb	0.09738	0.92903	-0.17939	-0.45299	-0.61698	0.72402
	0.7890	0.0001	0.6200	0.1886	0.0574	0.0179
Cr	0.37039	0.07348	0.03649	-0.11797	-0.19881	0.05833
	0.2921	0.8401	0.9203	0.7455	0.5819	0.8728
V	-0.26586	0.05668	-0.23798	0.12788	-0.04275	0.55503
	0.4578	0.8764	0.5079	0.7248	0.9067	0.0958
Ba	0.17378	-0.27553	0.18125	-0.11289	-0.05558	-0.33375
	0.6311	0.4410	0.6163	0.7562	0.8788	0.3459
Sc	0.31638	0.62484	0.19358	-0.45144	-0.35102	0.32159
	0.3731	0.0534	0.5921	0.1903	0.3200	0.3649
Cl	-0.41614	-0.60051	-0.05111	0.40937	0.41749	-0.20869
	0.2316	0.0664	0.8885	0.2401	0.2300	0.5629
F	0.28081	-0.81878	0.38648	-0.06040	0.15451	-0.21264
	0.4319	0.0038	0.2699	0.8684	0.6700	0.5553

Digitised by the Department of Library Services in support of open access to information, University of Pretoria, 2021.

continued

B E N C H F

	Moist	Ash	CO_2	VM	Vitr.	ROV
Zn	0.09524	-0.40036	0.01475	-0.36843	-0.13654	-0.12502
	0.8225	0.3257	0.9724	0.3692	0.7471	0.7680
Cu	0.03408	-0.02214	0.09674	0.19361	0.10747	-0.50326
	0.9361	0.9585	0.8197	0.6460	0.8000	0.2036
Ni	0.12712	-0.51889	0.33352	0.75946	0.84653	-0.52383
	0.7642	0.1876	0.4195	0.0288	0.0080	0.1827
Co	0.37364	-0.73890	0.13262	0.52465	0.63869	-0.26701
	0.3619	0.0362	0.7542	0.1819	0.0883	0.5226
Ga	0.86394	-0.46045	-0.09775	-0.14897	-0.23927	-0.31813
	0.0057	0.2509	0.8179	0.7248	0.5682	0.4425
Mo	0.30166	-0.63655	0.12271	0.37432	0.53708	-0.09609
	0.4678	0.0897	0.7722	0.3610	0.1699	0.8209
Nb	0.89850	-0.67563	-0.15877	-0.31365	-0.30289	-0.10695
	0.0024	0.0659	0.7073	0.4493	0.4659	0.8010
Zr	0.72761	-0.62457	-0.39242	-0.38416	-0.35472	0.17262
	0.0408	0.0978	0.3363	0.3474	0.3886	0.6827
Y	0.77066	-0.76275	-0.35400	-0.28377	-0.25073	0.11208
	0.0252	0.0277	0.3896	0.4958	0.5492	0.7916
Sr	0.50908	-0.77958	0.36108	0.34124	0.55018	-0.80964
	0.1976	0.0225	0.3795	0.4081	0.1577	0.0149
Rb	-0.38203	0.56620	-0.29576	-0.03331	-0.38041	0.34588
	0.3503	0.1434	0.4769	0.9376	0.3526	0.4013
U	-0.30009	-0.19673	0.27105	0.63244	0.75783	-0.13429
	0.4702	0.6405	0.5161	0.0924	0.0294	0.7512
Th	0.65453	-0.77571	-0.17823	0.44814	0.34244	-0.12120
	0.0782	0.0237	0.6728	0.2655	0.4064	0.7750
Pb	-0.23333	0.46493	0.31153	-0.06922	-0.09448	0.16342
	0.5781	0.2457	0.4526	0.8706	0.8239	0.6990
Cr	0.36146	-0.45213	-0.22326	-0.35352	-0.32130	0.26506
	0.3790	0.2607	0.5951	0.3903	0.4377	0.5258
V	0.55107	-0.62586	-0.33384	-0.31775	-0.27389	0.31087
	0.1569	0.0969	0.4190	0.4431	0.5116	0.4536
Ba	0.13396	-0.57368	0.63306	0.46000	0.71782	-0.67652
	0.7518	0.1370	0.0920	0.2514	0.0450	0.0654
Sc	0.00655	-0.21872	-0.56103	-0.13650	-0.29054	0.38718
	0.9877	0.6028	0.1480	0.7472	0.4851	0.3433
Cl	0.51655	-0.84192	0.16970	-0.07566	0.24290	-0.23361
	0.1900	0.0087	0.6879	0.8587	0.5622	0.5777
F	0.84239	-0.81100	-0.26731	-0.24338	-0.17768	-0.02214
	0.0087	0.0146	0.5222	0.5614	0.6738	0.9585

Digitised by the Department of Library Services in support of open access to information, University of Pretoria, 2021.

APPENDIX 21: Pearson correlattion matrix for major element vs. major element concentrations of all unaffected coals. Matrices are given separately for each seam bench **A** to **F**. Sample **GZ** is incorporated in the matrix of bench **A**.

B E N C H A

	SiO_2	TiO_2	Al_2O_3	FeO	MnO	MgO	CaO	Na_2O	K_2O	P_2O_5	S
SiO_2	1.00000	0.74350	0.90072	-0.66535	-0.50686	-0.74170	-0.80707	0.48759	0.30847	-0.10793	-0.81640
	0.0000	0.0087	0.0002	0.0255	0.1116	0.0090	0.0027	0.1282	0.3560	0.7521	0.0022
TiO_2	0.74350	1.00000	0.66791	-0.52190	-0.36736	-0.51055	-0.73751	0.42671	0.15462	-0.45736	-0.67356
	0.0087	0.0000	0.0247	0.0996	0.2664	0.1086	0.0096	0.1906	0.6499	0.1572	0.0231
Al_2O_3	0.90072	0.66791	1.00000	-0.72577	-0.37975	-0.81932	-0.76679	0.23075	0.26955	-0.04527	-0.86587
	0.0002	0.0247	0.0000	0.0115	0.2493	0.0020	0.0059	0.4948	0.4228	0.8949	0.0006
FeO	-0.66535	-0.52190	-0.72577	1.00000	0.36694	0.64745	0.47366	-0.51707	-0.42021	-0.28576	0.93701
	0.0255	0.0996	0.0115	0.0000	0.2670	0.0313	0.1411	0.1034	0.1982	0.3943	0.0001
MnO	-0.50686	-0.36736	-0.37975	0.36694	1.00000	0.24538	0.14662	-0.40996	-0.21990	0.01238	0.37726
	0.1116	0.2664	0.2493	0.2670	0.0000	0.4671	0.6671	0.2105	0.5159	0.9712	0.2527
MgO	-0.74170	-0.51055	-0.81932	0.64745	0.24538	1.00000	0.78639	-0.21700	-0.04845	-0.10678	0.76980
	0.0090	0.1086	0.0020	0.0313	0.4671	0.0000	0.0041	0.5216	0.8875	0.7547	0.0056
CaO	-0.80707	-0.73751	-0.76679	0.47366	0.14662	0.78639	1.00000	-0.44928	0.07384	0.29172	0.70479
	0.0027	0.0096	0.0059	0.1411	0.6671	0.0041	0.0000	0.1657	0.8292	0.3841	0.0154
Na_2O	0.48759	0.42671	0.23075	-0.51707	-0.40996	-0.21700	-0.44928	1.00000	0.04293	-0.05394	-0.48051
	0.1282	0.1906	0.4948	0.1034	0.2105	0.5216	0.1657	0.0000	0.9003	0.8748	0.1346
K_2O	0.30847	0.15462	0.26955	-0.42021	-0.21990	-0.04845	0.07384	0.04293	1.00000	0.02723	-0.38897
	0.3560	0.6499	0.4228	0.1982	0.5159	0.8875	0.8292	0.9003	0.0000	0.9367	0.2371
P_2O_5	-0.10793	-0.45736	-0.04527	-0.28576	0.01238	-0.10678	0.29172	-0.05394	0.02723	1.00000	-0.13716
	0.7521	0.1572	0.8949	0.3943	0.9712	0.7547	0.3841	0.8748	0.9367	0.0000	0.6876
S	-0.81640	-0.67356	-0.86587	0.93701	0.37726	0.76980	0.70479	-0.48051	-0.38897	-0.13716	1.00000
	0.0022	0.0231	0.0006	0.0001	0.2527	0.0056	0.0154	0.1346	0.2371	0.6876	0.0000

B E N C H B

	SiO_2	TiO_2	Al_2O_3	FeO	MnO	MgO	CaO	Na_2O	K_2O	P_2O_5	S
SiO_2	1.00000	0.95304	0.93115	-0.68096	-0.61808	-0.70708	-0.90725	0.13153	0.13088	-0.66822	-0.72911
	0.0000	0.0001	0.0001	0.0302	0.0568	0.0222	0.0003	0.7172	0.7186	0.0347	0.0167
TiO_2	0.95304	1.00000	0.81703	-0.59519	-0.54053	-0.69949	-0.86905	0.04454	0.12319	-0.55147	-0.67437
	0.0001	0.0000	0.0039	0.0695	0.1067	0.0244	0.0011	0.9028	0.7346	0.0984	0.0325
Al_2O_3	0.93115	0.81703	1.00000	-0.55725	-0.62905	-0.78942	-0.92525	0.14498	0.03898	-0.67078	-0.60311
	0.0001	0.0039	0.0000	0.0942	0.0514	0.0066	0.0001	0.6894	0.9149	0.0337	0.0649
FeO	-0.68096	-0.59519	-0.55725	1.00000	0.40716	0.16258	0.52111	-0.39280	-0.23778	0.49000	0.97201
	0.0302	0.0695	0.0942	0.0000	0.2429	0.6536	0.1224	0.2615	0.5083	0.1505	0.0001
MnO	-0.61808	-0.54053	-0.62905	0.40716	1.00000	0.38856	0.75568	-0.26861	-0.27031	0.20722	0.45966
	0.0568	0.1067	0.0514	0.2429	0.0000	0.2671	0.0115	0.4530	0.4500	0.5657	0.1814
MgO	-0.70708	-0.69949	-0.78942	0.16258	0.38856	1.00000	0.79698	-0.01026	0.13416	0.57568	0.19531
	0.0222	0.0244	0.0066	0.6536	0.2671	0.0000	0.0058	0.9776	0.7118	0.0816	0.5887
CaO	-0.90725	-0.86905	-0.92525	0.52111	0.75568	0.79698	1.00000	-0.26794	0.02334	0.51601	0.60860
	0.0003	0.0011	0.0001	0.1224	0.0115	0.0058	0.0000	0.4542	0.9490	0.1268	0.0619
Na_2O	0.13153	0.04454	0.14498	-0.39280	-0.26861	-0.01026	-0.26794	1.00000	-0.49089	-0.32105	-0.38057
	0.7172	0.9028	0.6894	0.2615	0.4530	0.9776	0.4542	0.0000	0.1497	0.3657	0.2780
K_2O	0.13088	0.12319	0.03898	-0.23778	-0.27031	0.13416	0.02334	-0.49089	1.00000	0.21063	-0.15200
	0.7186	0.7346	0.9149	0.5083	0.4500	0.7118	0.9490	0.1497	0.0000	0.5592	0.6751
P_2O_5	-0.66822	-0.55147	-0.67078	0.49000	0.20722	0.57568	0.51601	-0.32105	0.21063	1.00000	0.44074
	0.0347	0.0984	0.0337	0.1505	0.5657	0.0816	0.1268	0.3657	0.5592	0.0000	0.2023
S	-0.72911	-0.67437	-0.60311	0.97201	0.45966	0.19531	0.60860	-0.38057	-0.15200	0.44074	1.00000
	0.0167	0.0325	0.0649	0.0001	0.1814	0.5887	0.0619	0.2780	0.6751	0.2023	0.0000

Digitised by the Department of Library Services in support of open access to information, University of Pretoria, 2021.

APPENDIX 21: continued

BENCH C

	SiO_2	TiO_2	Al_2O_3	FeO	MnO	MgO	CaO	Na_2O	K_2O	P_2O_5	S
SiO_2	1.00000	0.80074	0.37551	0.19652	-0.25421	-0.93129	-0.94322	-0.31723	-0.31346	-0.58274	0.12582
	0.0000	0.0054	0.2849	0.5863	0.4785	0.0001	0.0001	0.3718	0.3778	0.0771	0.7291
TiO_2	0.80074	1.00000	0.33929	0.26524	0.00000	-0.68134	-0.77852	-0.25399	-0.14856	-0.56411	0.45014
	0.0054	0.0000	0.3375	0.4589	1.0000	0.0300	0.0080	0.4789	0.6821	0.0894	0.1918
Al_2O_3	0.37551	0.33929	1.00000	-0.49595	-0.86243	-0.47972	-0.60923	-0.19552	0.51840	-0.32965	-0.28982
	0.2849	0.3375	0.0000	0.1449	0.0013	0.1606	0.0615	0.5883	0.1248	0.3523	0.4166
FeO	0.19652	0.26524	-0.49595	1.00000	0.69288	0.05398	0.01490	-0.63986	-0.68615	-0.56087	0.83011
	0.5863	0.4589	0.1449	0.0000	0.0263	0.8823	0.9674	0.0463	0.0285	0.0917	0.0030
MnO	-0.25421	0.00000	-0.86243	0.69288	1.00000	0.47868	0.50343	-0.08305	-0.45736	0.01945	0.61761
	0.4785	1.0000	0.0013	0.0263	0.0000	0.1616	0.1380	0.8196	0.1838	0.9575	0.0571
MgO	-0.93129	-0.68134	-0.47972	0.05398	0.47868	1.00000	0.96290	0.09297	0.17283	0.36946	0.08895
	0.0001	0.0300	0.1606	0.8823	0.1616	0.0000	0.0001	0.7984	0.6330	0.2934	0.8069
CaO	-0.94322	-0.77852	-0.60923	0.01490	0.50343	0.96290	1.00000	0.25429	0.07802	0.54726	-0.01974
	0.0001	0.0080	0.0615	0.9674	0.1380	0.0001	0.0000	0.4783	0.8304	0.1016	0.9568
Na_2O	-0.31723	-0.25399	-0.19552	-0.63986	-0.08305	0.09297	0.25429	1.00000	0.15135	0.91040	-0.54789
	0.3718	0.4789	0.5883	0.0463	0.8196	0.7984	0.4783	0.0000	0.6764	0.0003	0.1011
K_2O	-0.31346	-0.14856	0.51840	-0.68615	-0.45736	0.17283	0.07802	0.15135	1.00000	0.13734	-0.31107
	0.3778	0.6821	0.1248	0.0285	0.1838	0.6330	0.8304	0.6764	0.0000	0.7052	0.3816
P_2O_5	-0.58274	-0.56411	-0.32965	-0.56087	0.01945	0.36946	0.54726	0.91040	0.13734	1.00000	-0.57361
	0.0771	0.0894	0.3523	0.0917	0.9575	0.2934	0.1016	0.0003	0.7052	0.0000	0.0830
S	0.12582	0.45014	-0.28982	0.83011	0.61761	0.08895	-0.01974	-0.54789	-0.31107	-0.57361	1.00000
	0.7291	0.1918	0.4166	0.0030	0.0571	0.8069	0.9568	0.1011	0.3816	0.0830	0.0000

BENCH D

	SiO_2	TiO_2	Al_2O_3	FeO	MnO	MgO	CaO	Na_2O	K_2O	P_2O_5	S
SiO_2	1.00000	0.71060	0.25645	-0.79440	0.85483	0.37139	-0.62005	0.61768	-0.10844	-0.58657	-0.56468
	0.0000	0.0213	0.4745	0.0060	0.0016	0.2907	0.0558	0.0570	0.7656	0.0747	0.0890
TiO_2	0.71060	1.00000	-0.06182	-0.66784	0.40741	0.44909	-0.48939	0.02242	-0.32941	-0.80016	-0.43296
	0.0213	0.0000	0.8653	0.0348	0.2426	0.1929	0.1511	0.9510	0.3526	0.0054	0.2114
Al_2O_3	0.25645	-0.06182	1.00000	-0.51297	-0.03148	-0.25524	-0.78840	0.65562	0.87432	0.15604	-0.05713
	0.4745	0.8653	0.0000	0.1295	0.9312	0.4766	0.0067	0.0396	0.0009	0.6669	0.8754
FeO	-0.79440	-0.66784	-0.51297	1.00000	-0.55481	-0.46359	0.73261	-0.58490	-0.16533	0.50193	0.67097
	0.0060	0.0348	0.1295	0.0000	0.0960	0.1772	0.0160	0.0757	0.6481	0.1393	0.0337
MnO	0.85483	0.40741	-0.03148	-0.55481	1.00000	0.47688	-0.20270	0.60541	-0.31528	-0.41741	-0.60093
	0.0016	0.2426	0.9312	0.0960	0.0000	0.1634	0.5744	0.0636	0.3749	0.2301	0.0662
MgO	0.37139	0.44909	-0.25524	-0.46359	0.47688	1.00000	0.08171	0.21131	-0.28332	-0.48604	-0.55927
	0.2907	0.1929	0.4766	0.1772	0.1634	0.0000	0.8225	0.5578	0.4276	0.1544	0.0928
CaO	-0.62005	-0.48939	-0.78840	0.73261	-0.20270	0.08171	1.00000	-0.51801	-0.52739	0.42625	0.17203
	0.0558	0.1511	0.0067	0.0160	0.5744	0.8225	0.0000	0.1251	0.1172	0.2193	0.6346
Na_2O	0.61768	0.02242	0.65562	-0.58490	0.60541	0.21131	-0.51801	1.00000	0.49349	0.02535	-0.43766
	0.0570	0.9510	0.0396	0.0757	0.0636	0.5578	0.1251	0.0000	0.1472	0.9446	0.2059
K_2O	-0.10844	-0.32941	0.87432	-0.16533	-0.31528	-0.28332	-0.52739	0.49349	1.00000	0.29695	0.26600
	0.7656	0.3526	0.0009	0.6481	0.3749	0.4276	0.1172	0.1472	0.0000	0.4047	0.4576
P_2O_5	-0.58657	-0.80016	0.15604	0.50193	-0.41741	-0.48604	0.42625	0.02535	0.29695	1.00000	0.18964
	0.0747	0.0054	0.6669	0.1393	0.2301	0.1544	0.2193	0.9446	0.4047	0.0000	0.5998
S	-0.56468	-0.43296	-0.05713	0.67097	-0.60093	-0.55927	0.17203	-0.43766	0.26600	0.18964	1.00000
	0.0890	0.2114	0.8754	0.0337	0.0662	0.0928	0.6346	0.2059	0.4576	0.5998	0.0000

Digitised by the Department of Library Services in support of open access to information, University of Pretoria, 2021.

APPENDIX 21: continued

B E N C H E

	SiO_2	TiO_2	Al_2O_3	FeO	MnO	MgO	CaO	Na_2O	K_2O	P_2O_5	S
SiO_2	1.00000	0.83048	0.32121	0.49450	-0.74762	-0.82509	-0.84798	0.11571	-0.37616	-0.51755	0.46711
	0.0000	0.0029	0.3655	0.1462	0.0129	0.0033	0.0019	0.7503	0.2840	0.1255	0.1735
TiO_2	0.83048	1.00000	0.20838	0.14490	-0.32227	-0.45153	-0.46509	0.17558	-0.49061	-0.42069	0.14002
	0.0029	0.0000	0.5634	0.6896	0.3638	0.1902	0.1756	0.6275	0.1499	0.2260	0.6996
Al_2O_3	0.32121	0.20838	1.00000	-0.18464	-0.25355	-0.30921	-0.29818	0.12290	0.04520	-0.06812	-0.24668
	0.3655	0.5634	0.0000	0.6096	0.4797	0.3846	0.4027	0.7352	0.9013	0.8517	0.4920
FeO	0.49450	0.14490	-0.18464	1.00000	-0.64586	-0.60644	-0.61848	-0.06230	0.29317	-0.35280	0.98357
	0.1462	0.6896	0.6096	0.0000	0.0437	0.0631	0.0566	0.8642	0.4110	0.3174	0.0001
MnO	-0.74762	-0.32227	-0.25355	-0.64586	1.00000	0.92491	0.93220	0.10783	0.02060	0.44382	-0.67074
	0.0129	0.3638	0.4797	0.0437	0.0000	0.0001	0.0001	0.7668	0.9550	0.1988	0.0338
MgO	-0.82509	-0.45153	-0.30921	-0.60644	0.92491	1.00000	0.93353	-0.18213	-0.02533	0.24827	-0.62012
	0.0033	0.1902	0.3846	0.0631	0.0001	0.0000	0.0001	0.6146	0.9446	0.4892	0.0558
CaO	-0.84798	-0.46509	-0.29818	-0.61848	0.93220	0.93353	1.00000	0.11698	0.13033	0.54542	-0.60549
	0.0019	0.1756	0.4027	0.0566	0.0001	0.0001	0.0000	0.7476	0.7197	0.1030	0.0636
Na_2O	0.11571	0.17558	0.12290	-0.06230	0.10783	-0.18213	0.11698	1.00000	0.19106	0.72445	-0.06219
	0.7503	0.6275	0.7352	0.8642	0.7668	0.6146	0.7476	0.0000	0.5970	0.0178	0.8645
K_2O	-0.37616	-0.49061	0.04520	0.29317	0.02060	-0.02533	0.13033	0.19106	1.00000	0.47991	0.34055
	0.2840	0.1499	0.9013	0.4110	0.9550	0.9446	0.7197	0.5970	0.0000	0.1604	0.3356
P_2O_5	-0.51755	-0.42069	-0.06812	-0.35280	0.44382	0.24827	0.54542	0.72445	0.47991	1.00000	-0.30791
	0.1255	0.2260	0.8517	0.3174	0.1988	0.4892	0.1030	0.0178	0.1604	0.0000	0.3868
S	0.46711	0.14002	-0.24668	0.98357	-0.67074	-0.62012	-0.60549	-0.06219	0.34055	-0.30791	1.00000
	0.1735	0.6996	0.4920	0.0001	0.0338	0.0558	0.0636	0.8645	0.3356	0.3868	0.0000

B E N C H F

	SiO_2	TiO_2	Al_2O_3	FeO	MnO	MgO	CaO	Na_2O	K_2O	P_2O_5	S
SiO_2	1.00000	0.74575	0.84092	0.37032	0.43647	0.04064	0.15612	0.52709	0.71096	0.32640	-0.20347
	0.0000	0.0337	0.0089	0.3665	0.2796	0.9239	0.7120	0.1795	0.0480	0.4301	0.6289
TiO_2	0.74575	1.00000	0.90449	0.45655	0.57893	-0.14646	0.12022	0.46147	0.40015	0.66211	-0.68140
	0.0337	0.0000	0.0020	0.2555	0.1327	0.7293	0.7768	0.2497	0.3260	0.0737	0.0628
Al_2O_3	0.84092	0.90449	1.00000	0.43718	0.67229	0.13105	0.26713	0.32562	0.71734	0.49366	-0.57906
	0.0089	0.0020	0.0000	0.2787	0.0678	0.7571	0.5225	0.4312	0.0452	0.2138	0.1325
FeO	0.37032	0.45655	0.43718	1.00000	0.63619	0.58215	0.78183	0.13030	-0.02508	0.58679	-0.01435
	0.3665	0.2555	0.2787	0.0000	0.0899	0.1300	0.0219	0.7584	0.9530	0.1262	0.9731
MnO	0.43647	0.57893	0.67229	0.63619	1.00000	0.49519	0.66433	-0.33333	0.43568	0.66005	-0.59382
	0.2796	0.1327	0.0678	0.0899	0.0000	0.2121	0.0724	0.4198	0.2806	0.0749	0.1206
MgO	0.04064	-0.14646	0.13105	0.58215	0.49519	1.00000	0.91480	-0.34044	0.24083	0.16476	0.26389
	0.9239	0.7293	0.7571	0.1300	0.2121	0.0000	0.0014	0.4093	0.5656	0.6966	0.5277
CaO	0.15612	0.12022	0.26713	0.78183	0.66433	0.91480	1.00000	-0.20648	0.12280	0.53271	0.06218
	0.7120	0.7768	0.5225	0.0219	0.0724	0.0014	0.0000	0.6237	0.7721	0.1740	0.8837
Na_2O	0.52709	0.46147	0.32562	0.13030	-0.33333	-0.34044	-0.20648	1.00000	0.01013	0.16231	0.16782
	0.1795	0.2497	0.4312	0.7584	0.4198	0.4093	0.6237	0.0000	0.9810	0.7010	0.6912
K_2O	0.71096	0.40015	0.71734	-0.02508	0.43568	0.24083	0.12280	0.01013	1.00000	-0.04177	-0.26696
	0.0480	0.3260	0.0452	0.9530	0.2806	0.5656	0.7721	0.9810	0.0000	0.9218	0.5227
P_2O_5	0.32640	0.66211	0.49366	0.58679	0.66005	0.16476	0.53271	0.16231	-0.04177	1.00000	-0.55664
	0.4301	0.0737	0.2138	0.1262	0.0749	0.6966	0.1740	0.7010	0.9218	0.0000	0.1519
S	-0.20347	-0.68140	-0.57906	-0.01435	-0.59382	0.26389	0.06218	0.16782	-0.26696	-0.55664	1.00000
	0.6289	0.0628	0.1325	0.9731	0.1206	0.5277	0.8837	0.6912	0.5227	0.1519	0.0000

Digitised by the Department of Library Services in support of open access to information, University of Pretoria, 2021.

APPENDIX 22: Pearson correlation matrix for major element vs. trace element concentrations of all unaffected coals. Matrices are given separately for each seam bench A to F. Sample GZ is incorporated in the matrix for bench A.

B E N C H A

	SiO_2	TiO2	Al_2O_3	FeO	MnO	MgO	CaO	Na_2O	K_2O	P_2O_5
Zn	-0.23273	-0.18698	-0.27642	-0.28856	0.21190	0.03661	0.15487	0.18615	0.15215	0.60517
	0.4910	0.5820	0.4106	0.3895	0.5316	0.9149	0.6493	0.5837	0.6552	0.0485
Cu	0.00000	0.00000	0.00000	0.00000	0.00000	0.00000	0.00000	0.00000	0.00000	0.00000
	1.0000	1.0000	1.0000	1.0000	1.0000	1.0000	1.0000	1.0000	1.0000	1.0000
Ni	-0.06584	0.00181	-0.00913	-0.10167	0.20137	-0.20470	-0.06910	0.19176	-0.54296	0.05650
	0.8475	0.9958	0.9787	0.7661	0.5527	0.5460	0.8400	0.5722	0.0843	0.8690
Co	0.24935	0.44492	0.35718	-0.56176	0.07174	-0.45124	-0.38426	0.40966	-0.17279	-0.04030
	0.4596	0.1703	0.2809	0.0721	0.8340	0.1636	0.2433	0.2108	0.6114	0.9064
Ga	0.49752	0.44716	0.52277	-0.06899	-0.40548	-0.29428	-0.33881	-0.14282	0.45031	-0.63437
	0.1194	0.1679	0.0990	0.8403	0.2160	0.3797	0.3081	0.6753	0.1646	0.0360
Mo	0.18327	0.13052	0.36582	-0.50317	0.23999	-0.47826	-0.37298	0.18570	-0.42596	0.48311
	0.5896	0.7021	0.2686	0.1146	0.4772	0.1367	0.2586	0.5846	0.1915	0.1322
Nb	0.78126	0.73828	0.65095	-0.35102	-0.19035	-0.69438	-0.74209	0.19875	0.30086	-0.29447
	0.0045	0.0095	0.0301	0.2898	0.5750	0.0177	0.0089	0.5580	0.3686	0.3794
Zr	0.78288	0.84681	0.73340	-0.83169	-0.40294	-0.74113	-0.73456	0.55869	0.28164	-0.03488
	0.0044	0.0010	0.0102	0.0015	0.2192	0.0091	0.0100	0.0740	0.4014	0.9189
Y	0.50752	0.69071	0.63303	-0.76159	-0.11838	-0.54777	-0.62699	0.44892	0.23398	-0.16171
	0.1110	0.0186	0.0366	0.0065	0.7288	0.0811	0.0390	0.1660	0.4886	0.6348
Sr	-0.17370	-0.17871	-0.16962	-0.45754	-0.17671	0.16236	0.43826	0.16797	0.28799	0.63809
	0.6095	0.5991	0.6181	0.1571	0.6032	0.6334	0.1776	0.6215	0.3905	0.0346
Rb	0.60923	0.67516	0.69842	-0.33563	-0.20919	-0.45133	-0.51057	-0.00553	0.42609	-0.57158
	0.0466	0.0226	0.0168	0.3129	0.5370	0.1635	0.1085	0.9871	0.1913	0.0662
U	-0.57830	-0.51152	-0.51313	0.04843	0.34641	0.37643	0.61044	-0.14201	-0.23578	0.72388
	0.0624	0.1078	0.1065	0.3876	0.2967	0.2538	0.0461	0.6770	0.4852	0.0118
Th	0.80076	0.81289	0.83715	-0.63945	-0.48925	-0.79347	-0.79539	0.34766	-0.02391	-0.05049
	0.0031	0.0024	0.0013	0.0341	0.1267	0.0036	0.0034	0.2948	0.9444	0.8828
Pb	0.00000	0.00000	0.00000	0.00000	0.00000	0.00000	0.00000	0.00000	0.00000	0.00000
	1.0000	1.0000	1.0000	1.0000	1.0000	1.0000	1.0000	1.0000	1.0000	1.0000
Cr	0.46443	0.40998	0.43376	-0.42555	-0.21694	-0.56960	-0.56774	0.20465	0.39350	0.00542
	0.1501	0.2105	0.1826	0.1919	0.5217	0.0674	0.0685	0.5461	0.2312	0.9874
V	0.27493	0.20515	-0.01116	0.17274	-0.28114	-0.05796	-0.33204	0.41092	0.18432	-0.32922
	0.4132	0.5451	0.9740	0.6115	0.4023	0.8656	0.3185	0.2093	0.5875	0.3228
Ba	0.37268	0.06456	0.43216	-0.54331	-0.44428	-0.24518	0.06373	-0.09287	0.54348	0.54237
	0.2590	0.8504	0.1844	0.0841	0.1710	0.4674	0.8523	0.7859	0.0840	0.0848
Sc	0.18670	-0.26983	0.29606	-0.23252	-0.42852	-0.27864	0.18059	-0.31548	0.53846	0.39964
	0.5825	0.4223	0.3767	0.4914	0.1885	0.4067	0.5951	0.3446	0.0875	0.2233
Cl	0.25807	0.29672	0.12875	-0.38422	-0.11650	-0.28320	-0.51719	0.31957	-0.11775	-0.06704
	0.4436	0.3756	0.7060	0.2433	0.7330	0.3987	0.1033	0.0020	0.7302	0.8447
F	0.59595	0.57253	0.78202	-0.59563	0.08916	-0.85993	-0.73092	0.03390	0.12245	-0.10996
	0.0530	0.0657	0.0045	0.0532	0.7943	0.0007	0.0106	0.9212	0.7198	0.7476

B E N C H B

	SiO_2	TiO2	Al_2O_3	FeO	MnO	MgO	CaO	Na_2O	K_2O	P_2O_5
Zn	-0.38153	-0.28411	-0.39794	0.45108	0.83264	0.02728	0.51763	-0.25587	-0.27433	-0.15611
	0.2766	0.4263	0.2548	0.1907	0.0028	0.9404	0.1254	0.4755	0.4431	0.6667
Cu	0.00000	0.00000	0.00000	0.00000	0.00000	0.00000	0.00000	0.00000	0.00000	0.00000
	1.0000	1.0000	1.0000	1.0000	1.0000	1.0000	1.0000	1.0000	1.0000	1.0000
Ni	-0.17512	-0.16874	-0.00732	0.34365	-0.08059	-0.12112	-0.06839	0.26848	-0.59074	-0.15972
	0.6285	0.6412	0.9840	0.3309	0.8248	0.7389	0.8511	0.4532	0.0721	0.6594
Co	-0.32705	-0.25239	-0.16499	0.48363	0.57334	-0.12342	0.17368	0.00295	-0.69169	0.03911
	0.3563	0.4817	0.6488	0.1567	0.0831	0.7341	0.6313	0.9935	0.0267	0.9146
Ga	-0.05582	0.16764	-0.32246	0.20122	0.32974	0.13318	0.20701	-0.42364	0.13273	0.36600
	0.8783	0.6434	0.3635	0.5772	0.3521	0.7138	0.5661	0.2225	0.7147	0.2983
Mo	0.45307	0.35787	0.52242	-0.40532	-0.12379	-0.23389	-0.49575	0.57232	-0.51548	-0.34227
	0.1885	0.3099	0.1213	0.2452	0.7333	0.5155	0.1451	0.0838	0.1273	0.3330
Nb	-0.01989	0.02091	-0.06595	0.11584	0.43713	-0.06145	0.18041	-0.49576	0.33658	0.24388
	0.9565	0.9543	0.8564	0.7500	0.2065	0.8661	0.6180	0.1451	0.3416	0.4971
Zr	0.00699	0.16035	-0.08785	-0.11117	-0.03048	0.27416	-0.06491	-0.15369	0.03137	0.48059
	0.9847	0.6581	0.8093	0.7598	0.9334	0.4434	0.8586	0.6716	0.9314	0.1597
Y	0.10784	0.22969	0.19523	0.13698	-0.11607	-0.26574	-0.37533	0.03695	-0.26946	0.31142
	0.7668	0.5232	0.5889	0.7059	0.7495	0.4580	0.2852	0.9193	0.4515	0.3811
Sr	-0.73403	-0.61833	-0.76531	0.35656	0.34627	0.76469	0.64151	-0.22775	0.06745	0.89460
	0.0157	0.0567	0.0099	0.3118	0.3270	0.0100	0.0456	0.5269	0.8531	0.0005
Rb	0.40970	0.32375	0.28897	-0.35308	-0.23801	0.06489	-0.16375	-0.27725	0.34171	-0.06878
	0.2397	0.3615	0.4181	0.3169	0.5079	0.8586	0.6512	0.4380	0.3338	0.8502
U	0.00000	0.00000	0.00000	0.00000	0.00000	0.00000	0.00000	0.00000	0.00000	0.00000
	1.0000	1.0000	1.0000	1.0000	1.0000	1.0000	1.0000	1.0000	1.0000	1.0000
Th	0.72664	0.61737	0.79446	-0.62393	-0.78730	-0.43944	-0.83723	0.27719	0.15215	-0.20675
	0.0173	0.0572	0.0060	0.0539	0.0069	0.2038	0.0025	0.4381	0.6748	0.5666
Pb	0.00000	0.00000	0.00000	0.00000	0.00000	0.00000	0.00000	0.00000	0.00000	0.00000
	1.0000	1.0000	1.0000	1.0000	1.0000	1.0000	1.0000	1.0000	1.0000	1.0000
Cr	0.70665	0.60011	0.71224	-0.52536	-0.54202	-0.43876	-0.61457	-0.24016	0.54097	-0.17474
	0.0223	0.0666	0.0208	0.1189	0.1056	0.2046	0.0587	0.5039	0.1064	0.6292
V	0.49874	0.57104	0.48520	-0.07969	-0.28432	-0.44027	-0.50720	-0.52646	0.37234	0.18893
	0.1423	0.0847	0.1552	0.8268	0.4259	0.2029	0.1346	0.1180	0.2893	0.6012
Ba	-0.24972	-0.20891	-0.22165	0.12809	-0.19818	0.34663	-0.02166	0.49085	-0.35577	0.53195
	0.4865	0.5624	0.5383	0.7244	0.5831	0.3265	0.9527	0.1497	0.3130	0.1135
Sc	0.70135	0.63823	0.66914	-0.49670	-0.46828	-0.30891	-0.57891	0.02007	-0.01652	-0.62243
	0.0238	0.0471	0.0343	0.1442	0.1722	0.3851	0.0795	0.9561	0.9639	0.0546
Cl	-0.39777	-0.52688	-0.16499	0.37483	0.33198	-0.08336	0.35946	-0.32765	0.09745	0.09653
	0.2550	0.1176	0.6487	0.2859	0.3487	0.8189	0.3077	0.3554	0.7888	0.7908
F	-0.24398	-0.08797	-0.13647	0.57669	0.38446	-0.35540	0.06540	-0.26495	-0.44958	0.05869
	0.4969	0.8090	0.7070	0.0809	0.2727	0.3135	0.8575	0.4594	0.1924	0.8721

Digitised by the Department of Library Services in support of open access to information, University of Pretoria, 2021.

APPENDIX 22: continued

BENCH C

	SiO_2	TiO_2	Al_2O_3	FeO	MnO	MgO	CaO	Na_2O	K_2O	P_2O_5
Zn	-0.10938	0.07766	0.07529	-0.59766	-0.05840	0.08955	0.06670	0.51569	0.60506	0.34515
	0.7636	0.8311	0.8362	0.0680	0.8727	0.8057	0.8547	0.1271	0.0638	0.3287
Cu	-0.00132	-0.02233	-0.18303	-0.31820	0.09237	0.06632	0.13224	0.54604	-0.14369	0.48220
	0.9971	0.9512	0.6128	0.3702	0.7997	0.8556	0.7157	0.1025	0.6921	0.1581
Ni	-0.65055	-0.66453	-0.44855	-0.06204	0.15845	0.46410	0.60841	0.42074	-0.11148	0.57802
	0.0417	0.0361	0.1935	0.8648	0.6620	0.1766	0.0620	0.2260	0.7592	0.0801
Co	-0.65301	-0.71950	-0.05841	-0.30480	-0.18279	0.50006	0.57772	0.35218	0.03331	0.56702
	0.0406	0.0190	0.8727	0.3918	0.6132	0.1411	0.0803	0.3183	0.9272	0.0874
Ga	0.14937	0.31022	-0.09468	0.52755	0.39192	0.16259	-0.02075	-0.60678	-0.15872	-0.59603
	0.6804	0.3830	0.7947	0.1171	0.2627	0.6536	0.9546	0.0629	0.6614	0.0690
Mo	-0.03997	-0.14345	0.27325	-0.27229	-0.35960	-0.06100	-0.09722	-0.11547	0.58253	-0.17112
	0.9127	0.6926	0.4449	0.4466	0.3074	0.8671	0.7893	0.7508	0.0772	0.6364
Nb	0.60932	0.69264	0.34696	0.29111	-0.01408	-0.35904	-0.54499	-0.57635	-0.00143	-0.75129
	0.0615	0.0264	0.3260	0.4145	0.9692	0.3083	0.1033	0.0812	0.9969	0.0122
Zr	-0.32960	-0.31743	0.31396	-0.75693	-0.49958	0.15847	0.18454	0.63238	0.37927	0.59490
	0.3524	0.3715	0.3770	0.0113	0.1415	0.6619	0.6098	0.0498	0.2797	0.0697
Y	-0.31435	-0.49998	-0.02918	-0.61051	-0.35671	0.06456	0.23626	0.76620	0.06638	0.78740
	0.3764	0.1411	0.9362	0.0608	0.3116	0.8594	0.5111	0.0098	0.8554	0.0069
Sr	-0.77091	-0.68746	-0.18258	-0.63728	-0.10215	0.54701	0.65493	0.80688	0.35821	0.92522
	0.0090	0.0280	0.6137	0.0475	0.7789	0.1018	0.0399	0.0048	0.3095	0.0001
Rb	0.20232	-0.02457	-0.17073	0.49157	0.24021	-0.03234	-0.06837	-0.71199	-0.03180	-0.59792
	0.5751	0.9463	0.6372	0.1490	0.5038	0.9293	0.8511	0.0209	0.9305	0.0679
U	-0.39611	-0.33473	-0.30460	-0.26106	0.11987	0.19275	0.31788	0.46188	0.29127	0.45422
	0.2571	0.3445	0.3921	0.4663	0.7415	0.5937	0.3707	0.1790	0.4142	0.1873
Th	0.48801	0.17081	0.76887	-0.44761	-0.88629	-0.66461	-0.64874	0.00000	0.13135	-0.12497
	0.1524	0.6371	0.0093	0.1946	0.0006	0.0360	0.0424	1.0000	0.7176	0.7309
Pb	0.00000	0.00000	0.00000	0.00000	0.00000	0.00000	0.00000	0.00000	0.00000	0.00000
	1.0000	1.0000	1.0000	1.0000	1.0000	1.0000	1.0000	1.0000	1.0000	1.0000
Cr	0.03568	-0.05384	-0.55993	0.38633	0.55528	0.08807	0.16875	-0.09751	-0.46694	-0.03928
	0.9221	0.8826	0.0923	0.2701	0.0957	0.8088	0.6412	0.7887	0.1736	0.9142
V	0.31987	0.07334	0.13376	-0.17272	-0.23163	-0.38720	-0.27840	0.13724	0.03983	0.17729
	0.3676	0.8404	0.7126	0.6332	0.5196	0.2690	0.4360	0.7054	0.9130	0.6241
Ba	-0.41519	-0.37613	0.22391	-0.77745	-0.48296	0.13887	0.20717	0.76490	0.33233	0.70029
	0.2328	0.2841	0.5340	0.0081	0.1574	0.7020	0.5658	0.0100	0.3481	0.0241
Sc	0.00000	0.00000	0.00000	0.00000	0.00000	0.00000	0.00000	0.00000	0.00000	0.00000
	1.0000	1.0000	1.0000	1.0000	1.0000	1.0000	1.0000	1.0000	1.0000	1.0000
Cl	-0.14840	0.01457	0.77797	-0.47177	-0.68357	0.01458	-0.14337	-0.07458	0.66725	-0.12802
	0.6824	0.9681	0.0081	0.1686	0.0293	0.9681	0.6928	0.8378	0.0350	0.7245
F	-0.02080	0.04791	0.76811	-0.38329	-0.72732	-0.10289	-0.23570	-0.06352	0.35476	-0.10935
	0.9545	0.8954	0.0095	0.2742	0.0171	0.7773	0.5121	0.8616	0.3145	0.7636

BENCH D

	SiO_2	TiO_2	Al_2O_3	FeO	MnO	MgO	CaO	Na_2O	K_2O	P_2O_5
Zn	-0.33839	-0.33489	0.34557	0.34021	-0.50233	-0.67789	-0.18398	-0.17271	0.36688	0.40421
	0.3389	0.3442	0.3280	0.3361	0.1390	0.0312	0.6109	0.6333	0.2970	0.2467
Cu	-0.27481	-0.50833	0.52924	0.05116	-0.26496	0.05655	-0.05612	0.50499	0.77148	0.49572
	0.4422	0.1336	0.1157	0.8884	0.4594	0.8767	0.8776	0.1366	0.0090	0.1451
Ni	-0.00564	0.29602	0.35879	-0.33726	-0.32928	-0.35967	-0.44862	-0.17921	0.25173	-0.12823
	0.9877	0.4063	0.3086	0.3406	0.3529	0.3073	0.1934	0.6203	0.4829	0.7241
Co	-0.56146	-0.15402	-0.02916	0.29330	-0.71407	-0.56675	0.08284	-0.66776	-0.05308	0.28899
	0.0912	0.6710	0.9363	0.4108	0.0204	0.0876	0.8200	0.0349	0.8842	0.4180
Ga	-0.27635	-0.39548	-0.00149	0.32801	-0.15100	-0.00799	0.14381	-0.03337	0.06875	0.21776
	0.4396	0.2580	0.9967	0.3548	0.6771	0.9825	0.6918	0.9271	0.8503	0.5456
Mo	-0.22575	0.23791	-0.19097	0.15948	-0.45883	-0.45789	-0.09083	-0.68930	-0.32336	-0.15867
	0.5306	0.5080	0.5972	0.6599	0.1823	0.1833	0.8029	0.0274	0.3621	0.6615
Nb	0.01551	0.09129	-0.23414	0.23604	0.00000	0.16667	0.05447	-0.12281	-0.22130	-0.15538
	0.9661	0.8020	0.5150	0.5115	1.0000	0.6454	0.8812	0.7354	0.5389	0.6682
Zr	-0.38406	0.07317	-0.11243	0.17101	-0.57072	-0.22762	0.14506	-0.50499	-0.17063	0.32905
	0.2732	0.8408	0.7571	0.6367	0.0849	0.5271	0.6893	0.1366	0.6374	0.3532
Y	0.12073	0.32503	-0.08772	-0.29917	0.03750	0.15421	-0.01279	-0.16650	-0.38989	0.04286
	0.7397	0.3595	0.8096	0.4011	0.9181	0.6706	0.9720	0.6457	0.2654	0.9064
Sr	-0.43965	-0.52721	0.60383	0.14447	-0.55679	-0.42477	-0.07879	0.21590	0.77245	0.75616
	0.2036	0.1174	0.0645	0.6905	0.0946	0.2211	0.8287	0.5491	0.0088	0.0114
Rb	0.38811	0.53060	0.36775	-0.61493	0.10223	0.44663	-0.63666	0.35659	0.30051	-0.62266
	0.2678	0.1146	0.2958	0.0585	0.7787	0.1957	0.0478	0.3118	0.3988	0.0545
U	0.06909	0.24322	0.48449	-0.42682	-0.26392	-0.26047	-0.42113	0.09086	0.32095	0.15987
	0.8496	0.4983	0.1559	0.2186	0.4612	0.4673	0.2255	0.8029	0.3659	0.6591
Th	0.42234	0.58738	-0.03382	-0.60201	0.31655	0.48952	-0.25007	0.22206	-0.22321	-0.48033
	0.2240	0.0739	0.9261	0.0655	0.3729	0.1510	0.4859	0.5375	0.5353	0.1600
Pb	0.00000	0.00000	0.00000	0.00000	0.00000	0.00000	0.00000	0.00000	0.00000	0.00000
	1.0000	1.0000	1.0000	1.0000	1.0000	1.0000	1.0000	1.0000	1.0000	1.0000
Cr	0.42600	0.65630	-0.21223	-0.33529	0.34542	0.49180	-0.14679	-0.05228	-0.28210	-0.57638
	0.2196	0.0393	0.5561	0.3436	0.3283	0.1488	0.6857	0.8860	0.4297	0.0811
V	0.17757	0.17512	0.02185	0.03731	0.07751	-0.15475	-0.06701	0.26129	0.04402	0.11633
	0.6236	0.6284	0.9522	0.9185	0.8315	0.6695	0.8541	0.4659	0.9039	0.7489
Ba	-0.32719	-0.48855	0.74052	0.04663	-0.50268	-0.46477	-0.26099	0.32879	0.83431	0.69177
	0.3561	0.1519	0.0143	0.8982	0.1387	0.1759	0.4664	0.3536	0.0027	0.0267
Sc	0.39900	0.21282	-0.22361	-0.15281	0.50483	0.38236	0.00481	0.11086	-0.27934	-0.44930
	0.2534	0.5550	0.5346	0.6734	0.1367	0.2755	0.9895	0.7604	0.4344	0.1927
Cl	-0.81255	-0.77416	-0.23481	0.79185	-0.60477	-0.65175	0.62163	-0.52560	-0.04858	0.77405
	0.0043	0.0086	0.5138	0.0063	0.0640	0.0412	0.0550	0.1187	0.8940	0.0086
F	-0.42739	-0.20285	-0.02986	0.30765	-0.52162	-0.42373	0.08310	-0.47055	-0.11845	0.32647
	0.2180	0.5741	0.9347	0.3872	0.1220	0.2224	0.8195	0.1699	0.7445	0.3572

Digitised by the Department of Library Services in support of open access to information, University of Pretoria, 2021.

APPENDIX 22: continued

B E N C H E

	SiO_2	TiO_2	Al_2O_3	FeO	MnO	MgO	CaO	Na_2O	K_2O	P_2O_5
Zn	-0.15849	-0.06591	0.53337	-0.49302	0.40002	0.12759	0.27791	0.64908	0.12401	0.59065
	0.6619	0.8564	0.1124	0.1476	0.2520	0.7254	0.4369	0.0423	0.7329	0.0722
Cu	-0.26744	-0.28142	0.17434	-0.06023	0.23702	0.09804	0.11482	0.15335	0.55668	0.39591
	0.4550	0.4309	0.6300	0.8687	0.5097	0.7876	0.7521	0.6723	0.0946	0.2574
Ni	-0.23717	-0.16041	0.09435	-0.32490	0.29215	0.17673	0.44561	0.55533	0.02911	0.66496
	0.5094	0.6580	0.7954	0.3597	0.4127	0.6253	0.1968	0.0956	0.9364	0.0359
Co	-0.61829	-0.30903	0.13230	-0.71597	0.77785	0.70784	0.84660	0.35810	0.01911	0.61057
	0.0567	0.3849	0.7156	0.0199	0.0081	0.0220	0.0020	0.3096	0.9582	0.0608
Ga	-0.20053	-0.04674	0.28225	-0.28458	0.22345	0.37676	0.13250	-0.51805	0.00460	-0.39299
	0.5786	0.8980	0.4295	0.4255	0.5349	0.2832	0.7152	0.1251	0.9899	0.2612
Mo	-0.09223	0.05922	-0.04711	-0.30102	0.35460	0.30212	0.38886	0.22943	-0.44508	0.14945
	0.7999	0.8709	0.8972	0.3980	0.3147	0.3962	0.2667	0.5237	0.1974	0.6803
Nb	0.26728	0.41836	0.33260	-0.07552	-0.10477	0.03336	-0.22470	-0.56811	-0.25655	-0.74229
	0.4553	0.2289	0.3477	0.8357	0.7733	0.9271	0.5325	0.0867	0.4743	0.0139
Zr	-0.37342	0.05813	0.31587	-0.80995	0.68849	0.53509	0.66542	0.36626	0.00000	0.53108
	0.2878	0.8733	0.3739	0.0045	0.0277	0.1110	0.0357	0.2979	1.0000	0.1142
Y	-0.15418	0.17388	-0.09494	-0.37044	0.39843	0.18756	0.48473	0.67580	0.09584	0.70628
	0.6706	0.6309	0.7942	0.2920	0.2541	0.6038	0.1556	0.0320	0.7923	0.0224
Sr	-0.57559	-0.56065	0.04208	-0.33948	0.48315	0.29513	0.53492	0.66287	0.49102	0.94108
	0.0817	0.0918	0.9081	0.3372	0.1572	0.4078	0.1111	0.0367	0.1495	0.0001
Rb	0.59835	0.45872	-0.06153	0.74655	-0.63387	-0.61661	-0.54875	-0.04557	0.20894	-0.28761
	0.0676	0.1824	0.8659	0.0131	0.0491	0.0576	0.1005	0.9005	0.5624	0.4204
U	-0.32261	-0.33679	0.04134	-0.16549	0.37879	0.16194	0.42169	0.69653	0.29737	0.83370
	0.3633	0.3413	0.9097	0.6477	0.2804	0.6549	0.2248	0.0252	0.4040	0.0027
Th	0.39002	0.71460	-0.02619	-0.26205	0.00000	-0.01696	0.03045	0.08492	-0.59218	-0.15465
	0.2652	0.0202	0.9427	0.4645	1.0000	0.9629	0.9334	0.8156	0.0713	0.6697
Pb	0.49073	0.21484	-0.32886	0.94988	-0.66667	-0.60703	-0.58755	-0.07189	0.26096	-0.32424
	0.1498	0.5511	0.3535	0.0001	0.0353	0.0627	0.0741	0.8436	0.4665	0.3607
Cr	-0.03137	0.07475	0.05716	0.37864	0.17140	0.06780	0.05243	0.05809	0.60735	-0.03680
	0.9314	0.8374	0.8754	0.2806	0.6359	0.8524	0.8856	0.8734	0.0626	0.9196
V	0.06965	0.07633	-0.31661	0.29378	0.13942	0.20560	0.11354	-0.22446	-0.37220	-0.36153
	0.8484	0.8340	0.3728	0.4100	0.7009	0.5688	0.7548	0.5330	0.2895	0.3047
Ba	-0.57237	-0.53897	-0.04754	-0.32536	0.40545	0.23358	0.51294	0.65635	0.55272	0.98589
	0.0838	0.1079	0.8962	0.3590	0.2451	0.5160	0.1295	0.0393	0.0975	0.0001
Sc	0.11002	-0.03476	-0.22205	0.54024	-0.34151	-0.36567	-0.29697	0.03399	0.60725	0.13283
	0.7622	0.9241	0.5375	0.1069	0.3341	0.2987	0.4047	0.9257	0.0626	0.7145
Cl	-0.60275	-0.55673	0.05950	-0.57345	0.50984	0.52271	0.63744	0.20299	-0.07480	0.53118
	0.0651	0.0946	0.8703	0.0831	0.1322	0.1211	0.0474	0.5738	0.8373	0.1141
F	-0.40447	0.01009	0.13317	-0.59953	0.77767	0.67385	0.78730	0.38331	-0.06913	0.44254
	0.2463	0.9779	0.7138	0.0670	0.0081	0.0326	0.0069	0.2742	0.8495	0.2003

B E N C H F

	SiO_2	TiO_2	Al_2O_3	FeO	MnO	MgO	CaO	Na_2O	K_2O	P_2O_5
Zn	-0.00413	0.08562	-0.04696	0.28160	0.55563	0.08556	0.32483	-0.44721	-0.17589	0.56441
	0.9923	0.8402	0.9121	0.4992	0.1528	0.8404	0.4324	0.2666	0.6769	0.1450
Cu	0.09971	0.06042	0.29422	-0.30944	0.21822	0.28365	0.17631	-0.21822	0.61687	0.07792
	0.8143	0.8870	0.4793	0.4558	0.6036	0.4960	0.6762	0.6036	0.1033	0.8545
Ni	-0.22452	0.04439	0.15587	0.39549	0.40699	0.54373	0.47011	-0.45222	0.08110	0.03376
	0.5930	0.9169	0.7124	0.3321	0.3170	0.1636	0.2398	0.2606	0.8486	0.9367
Co	-0.30170	0.17696	0.06931	0.54343	0.39016	0.26110	0.35132	-0.33127	-0.32110	0.24350
	0.4677	0.6751	0.8705	0.1639	0.3393	0.5322	0.3935	0.4228	0.4380	0.5612
Ga	-0.43155	-0.01654	-0.13487	-0.49847	-0.20312	-0.38827	-0.34495	-0.03584	-0.25894	0.13691
	0.2857	0.9690	0.7502	0.2086	0.6295	0.3418	0.4027	0.9328	0.5357	0.7465
Mo	-0.16622	0.27441	0.14750	0.69284	0.36012	0.28573	0.41264	-0.09822	-0.34730	0.31138
	0.6940	0.5107	0.7274	0.0568	0.3809	0.4927	0.3096	0.8170	0.3993	0.4528
Nb	-0.08042	0.50293	0.29317	-0.03888	0.19839	-0.35787	-0.12976	0.14171	-0.18694	0.56763
	0.8499	0.2040	0.4810	0.9272	0.6377	0.3841	0.7594	0.7378	0.6576	0.1422
Zr	-0.02688	0.55896	0.24534	0.30147	0.17408	-0.24005	0.09231	0.36493	-0.40956	0.75401
	0.9496	0.1498	0.5581	0.4681	0.6801	0.5669	0.8279	0.3741	0.3136	0.0307
Y	-0.07463	0.56971	0.23693	0.30965	0.29608	-0.29476	0.04607	0.16449	-0.42398	0.73899
	0.8606	0.1404	0.5721	0.4555	0.4764	0.4785	0.9137	0.6971	0.2952	0.0362
Sr	-0.38341	-0.00614	0.05510	0.23396	0.53829	0.54349	0.58522	-0.61702	-0.03150	0.41812
	0.3485	0.9885	0.8969	0.5771	0.1687	0.1638	0.1275	0.1032	0.9410	0.3026
Rb	0.47407	0.17613	0.27786	-0.58648	-0.17066	-0.52819	-0.64655	0.17066	0.63115	-0.39334
	0.2353	0.6765	0.5052	0.1265	0.6862	0.1784	0.0832	0.6862	0.0933	0.3350
U	-0.06346	-0.03224	0.03450	0.59650	0.32026	0.50550	0.45067	-0.32026	-0.03894	-0.09356
	0.8813	0.9396	0.9354	0.1185	0.4393	0.2013	0.2624	0.4393	0.9271	0.8256
Th	-0.40419	0.21462	-0.01170	0.11764	0.14452	-0.27910	-0.17126	-0.26013	-0.41380	0.13417
	0.3206	0.6098	0.9781	0.7815	0.7328	0.5032	0.6851	0.5338	0.3081	0.7514
Pb	0.31563	0.02453	0.18506	-0.29326	-0.19487	-0.26537	-0.44785	0.19487	0.38107	-0.50817
	0.4463	0.9540	0.6609	0.4809	0.6438	0.5253	0.2658	0.6438	0.3517	0.1985
Cr	0.54594	0.94703	0.77512	0.36728	0.60226	-0.27266	0.03271	0.27375	0.23133	0.71334
	0.1616	0.0004	0.0239	0.3708	0.1141	0.5135	0.9387	0.5118	0.5815	0.0470
V	0.20509	0.75653	0.44278	0.44636	0.41292	-0.33111	0.02174	0.26277	-0.25102	0.71813
	0.6261	0.0298	0.2719	0.2676	0.3093	0.4231	0.9593	0.5295	0.5487	0.0448
Ba	0.07486	0.26486	0.46174	0.40584	0.81287	0.57140	0.54324	-0.62125	0.42623	0.23564
	0.8602	0.5261	0.2494	0.3185	0.0142	0.1390	0.1641	0.1002	0.2923	0.5743
Sc	0.46206	0.70325	0.52573	0.26262	0.43370	-0.24161	0.02035	0.18188	0.20880	0.55452
	0.2490	0.0517	0.1808	0.5298	0.2830	0.5643	0.9619	0.6664	0.6197	0.1538
Cl	-0.06404	0.44159	0.27555	0.72849	0.66799	0.31463	0.59376	-0.18120	-0.30440	0.76825
	0.8803	0.2734	0.5089	0.0404	0.0702	0.4478	0.1207	0.6676	0.4635	0.0260
F	-0.18449	0.47591	0.16975	0.28589	0.26839	-0.20484	0.10821	0.10958	-0.46308	0.72377
	0.6619	0.2332	0.6878	0.4925	0.5204	0.6265	0.7987	0.7962	0.2479	0.0424

Digitised by the Department of Library Services in support of open access to information, University of Pretoria, 2021.

APPENDIX 23: Pearson correlation matrix for trace element vs. trace element concentrations of all unaffected coals. Matrices are given separately for eaxh seam bench A to F. Sample GZ is incorporated in the matrix for bench A.

B E N C H A

	Zn	Cu	Ni	Co	Ga	Mo	Nb	Zr	Y	Sr	Rb	U	Th	Pb	Cr	V	Ba	Sc	Cl	F
Zn	1.00000	0.00000	-0.18573	-0.00698	-0.65739	0.29559	-0.19583	0.18724	0.13999	0.71255	-0.59598	0.56365	-0.13082	0.00000	0.40144	-0.06105	0.26951	-0.01946	0.34070	-0.11957
	0.0000	1.0000	0.5845	0.9837	0.0279	0.3775	0.5639	0.5814	0.6814	0.0139	0.0530	0.0709	0.7014	1.0000	0.2211	0.8585	0.4229	0.9547	0.3052	0.7262
Cu	0.00000	0.00000	0.00000	0.00000	0.00000	0.00000	0.00000	0.00000	0.00000	0.00000	0.00000	0.00000	0.00000	0.00000	0.00000	0.00000	0.00000	0.00000	0.00000	0.00000
	1.0000	1.0000	1.0000	1.0000	1.0000	1.0000	1.0000	1.0000	1.0000	1.0000	1.0000	1.0000	1.0000	1.0000	1.0000	1.0000	1.0000	1.0000	1.0000	1.0000
Ni	-0.18573	0.00000	1.00000	0.76834	-0.36944	0.54669	-0.05315	0.05459	0.09498	-0.06092	-0.03652	0.34151	0.08210	0.00000	-0.54165	-0.38614	-0.44727	-0.41257	0.14687	0.26944
	0.5845	1.0000	0.0000	0.0057	0.2635	0.0818	0.8767	0.8733	0.7812	0.8588	0.9151	0.3040	0.8104	1.0000	0.0853	0.2408	0.1678	0.2073	0.6665	0.4230
Co	-0.00698	0.00000	0.76834	1.00000	-0.17267	0.63951	0.21034	0.55624	0.69664	0.04033	0.32506	0.14201	0.46131	0.00000	-0.08368	-0.26183	-0.27076	-0.39710	0.44268	0.62082
	0.9837	1.0000	0.0057	0.0000	0.6117	0.0341	0.5347	0.0756	0.0172	0.9063	0.3294	0.6770	0.1532	1.0000	0.8068	0.4367	0.4207	0.2266	0.1727	0.0415
Ga	-0.65739	0.00000	-0.36944	-0.17267	1.00000	-0.53453	0.53609	0.22191	0.17071	-0.49123	0.82203	-0.88037	0.31108	0.00000	0.29415	0.28901	0.14432	0.39585	-0.23840	0.34608
	0.0279	1.0000	0.2635	0.6117	0.0000	0.0903	0.0892	0.5120	0.6158	0.1249	0.0019	0.0003	0.3518	1.0000	0.3799	0.3887	0.6720	0.2282	0.4802	0.2972
Mo	0.29559	0.00000	0.54669	0.63951	-0.53453	1.00000	-0.02998	0.36232	0.45013	0.21053	-0.14818	0.42607	0.44226	0.00000	-0.01050	-0.49284	0.07042	-0.24424	0.30399	0.49236
	0.3775	1.0000	0.0818	0.0341	0.0903	0.0000	0.9303	0.2735	0.1648	0.5343	0.6637	0.1913	0.1732	1.0000	0.9756	0.1235	0.8370	0.4692	0.3634	0.1239
Nb	-0.19583	0.00000	-0.05315	0.21034	0.53609	-0.02998	1.00000	0.70075	0.37499	-0.39186	0.66595	-0.58729	0.64803	0.00000	0.53950	0.41228	0.08307	0.04652	0.11521	0.66859
	0.5639	1.0000	0.8767	0.5347	0.0892	0.9303	0.0000	0.0163	0.2558	0.2333	0.0253	0.0575	0.0311	1.0000	0.0867	0.2077	0.8081	0.8920	0.7359	0.0245
Zr	0.18724	0.00000	0.05459	0.55624	0.22191	0.36232	0.70075	1.00000	0.80134	0.14341	0.48493	-0.29931	0.84937	0.00000	0.61813	0.15309	0.29123	-0.01888	0.48325	0.68287
	0.5814	1.0000	0.8733	0.0756	0.5120	0.2735	0.0163	0.0000	0.0030	0.6740	0.1306	0.3712	0.0009	1.0000	0.0427	0.6531	0.3849	0.9561	0.1321	0.0206
Y	0.13999	0.00000	0.09498	0.69664	0.17071	0.45013	0.37499	0.80134	1.00000	0.04694	0.54323	-0.24776	0.67733	0.00000	0.50259	0.02713	0.04479	-0.16434	0.58648	0.71102
	0.6814	1.0000	0.7812	0.0172	0.6158	0.1648	0.2558	0.0030	0.0000	0.8910	0.0842	0.4626	0.0220	1.0000	0.1151	0.9369	0.8960	0.6292	0.0579	0.0142
Sr	0.71255	0.00000	-0.06092	0.04033	-0.49123	0.21053	-0.39186	0.14341	0.04694	1.00000	-0.47777	0.63405	-0.13754	0.00000	-0.00371	-0.45010	0.60560	0.22430	-0.00885	-0.26588
	0.0139	1.0000	0.8588	0.9063	0.1249	0.5343	0.2333	0.6740	0.8910	0.0000	0.1372	0.0362	0.6867	1.0000	0.9914	0.1648	0.0483	0.5073	0.9794	0.4294
Rb	-0.59598	0.00000	-0.03652	0.32506	0.82203	-0.14818	0.66595	0.48493	0.54323	-0.47777	1.00000	-0.68960	0.52604	0.00000	0.23187	0.14600	0.02444	0.12145	-0.06815	0.67009
	0.0530	1.0000	0.9151	0.3294	0.0019	0.6637	0.0253	0.1306	0.0842	0.1372	0.0000	0.0189	0.0965	1.0000	0.4927	0.6684	0.9431	0.7220	0.8422	0.0241
U	0.56365	0.00000	0.34151	0.14201	-0.88037	0.42607	-0.58729	-0.29931	-0.24776	0.63405	-0.68960	1.00000	-0.37662	0.00000	-0.44847	-0.52930	0.08353	-0.14844	-0.13607	-0.35202
	0.0709	1.0000	0.3040	0.6770	0.0003	0.1913	0.0575	0.3712	0.4626	0.0362	0.0189	0.0000	0.2536	1.0000	0.1665	0.0941	0.8071	0.6631	0.6900	0.2884
Th	-0.13082	0.00000	0.08210	0.46131	0.31108	0.44226	0.64803	0.84937	0.67733	-0.13754	0.52604	-0.37662	1.00000	0.00000	0.49530	0.11562	0.25242	0.03028	0.32207	0.68631
	0.7014	1.0000	0.8104	0.1532	0.3518	0.1732	0.0311	0.0009	0.0220	0.6867	0.0965	0.2536	0.0000	1.0000	0.1213	0.7350	0.4540	0.9296	0.3341	0.0197
Pb	0.00000	0.00000	0.00000	0.00000	0.00000	0.00000	0.00000	0.00000	0.00000	0.00000	0.00000	0.00000	0.00000	0.00000	0.00000	0.00000	0.00000	0.00000	0.00000	0.00000
	1.0000	1.0000	1.0000	1.0000	1.0000	1.0000	1.0000	1.0000	1.0000	1.0000	1.0000	1.0000	1.0000	1.0000	1.0000	1.0000	1.0000	1.0000	1.0000	1.0000
Cr	0.40144	0.00000	-0.54165	-0.08368	0.29415	-0.01050	0.53950	0.61813	0.50259	-0.00371	0.23187	-0.44847	0.49530	0.00000	1.00000	0.49271	0.28639	0.28813	0.43762	0.44082
	0.2211	1.0000	0.0853	0.8068	0.3799	0.9756	0.0867	0.0427	0.1151	0.9914	0.4927	0.1665	0.1213	1.0000	0.0000	0.1236	0.3932	0.3902	0.1783	0.1748
V	-0.06105	0.00000	-0.38614	-0.26183	0.28901	-0.49284	0.41228	0.15309	0.02713	-0.45010	0.14600	-0.52930	0.11562	0.00000	0.49271	1.00000	-0.30164	-0.04059	0.49338	-0.11384
	0.8585	1.0000	0.2408	0.4367	0.3887	0.1235	0.2077	0.6531	0.9369	0.1648	0.6684	0.0941	0.7350	1.0000	0.1236	0.0000	0.3673	0.9057	0.1230	0.7389
Ba	0.26951	0.00000	-0.44727	-0.27076	0.14432	0.07042	0.08307	0.29123	0.04479	0.60560	0.02444	0.08353	0.25242	0.00000	0.28639	-0.30164	1.00000	0.71645	-0.34218	0.06477
	0.4229	1.0000	0.1678	0.4207	0.6720	0.8370	0.8081	0.3849	0.8960	0.0483	0.9431	0.8071	0.4540	1.0000	0.3932	0.3673	0.0000	0.0131	0.3030	0.8499
Sc	-0.01946	0.00000	-0.41257	-0.39710	0.39585	-0.24424	0.04652	-0.01888	-0.16434	0.22430	0.12145	-0.14844	0.03028	0.00000	0.28813	-0.04059	0.71645	1.00000	-0.38448	0.06716
	0.9547	1.0000	0.2073	0.2266	0.2282	0.4692	0.8920	0.9561	0.6292	0.5073	0.7220	0.6631	0.9296	1.0000	0.3902	0.9057	0.0131	0.0000	0.2430	0.8445
Cl	0.34070	0.00000	0.14687	0.44268	-0.23840	0.30399	0.11521	0.48325	0.58648	-0.00885	-0.06815	-0.13607	0.32207	0.00000	0.43762	0.49338	-0.34218	-0.38448	1.00000	0.18038
	0.3052	1.0000	0.6665	0.1727	0.4802	0.3634	0.7359	0.1321	0.0579	0.9794	0.8422	0.6900	0.3341	1.0000	0.1783	0.1230	0.3030	0.2430	0.0000	0.5956
F	-0.11957	0.00000	0.26944	0.62082	0.34608	0.49236	0.66859	0.68287	0.71102	-0.26588	0.67009	-0.35202	0.68631	0.00000	0.44082	-0.11384	0.06477	0.06716	0.18038	1.00000
	0.7262	1.0000	0.4230	0.0415	0.2972	0.1239	0.0245	0.0206	0.0142	0.4294	0.0241	0.2884	0.0197	1.0000	0.1748	0.7389	0.8499	0.8445	0.5956	0.0000

Digitised by the Department of Library Services in support of open access to information, University of Pretoria, 2021.

APPENDIX 23:

B E N C H B

	Zn	Cu	Ni	Co	Ga	Mo	Nb	Zr	Y	Sr	Rb	U	Th	Pb	Cr	V	Ba	Sc	Cl	F
Zn	1.00000	0.00000	0.12995	0.58996	0.25276	-0.22281	0.28983	-0.28166	-0.16567	-0.06332	-0.41504	0.00000	-0.82220	0.00000	-0.58149	-0.31483	-0.45591	-0.27327	0.27170	0.57744
	0.0000	1.0000	0.7205	0.0726	0.4811	0.5361	0.4166	0.4305	0.6474	0.8620	0.2330	1.0000	0.0035	1.0000	0.0779	0.3756	0.1854	0.4449	0.4476	0.0805
Cu	0.00000	0.00000	0.00000	0.00000	0.00000	0.00000	0.00000	0.00000	0.00000	0.00000	0.00000	0.00000	0.00000	0.00000	0.00000	0.00000	0.00000	0.00000	0.00000	0.00000
	1.0000	1.0000	1.0000	1.0000	1.0000	1.0000	1.0000	1.0000	1.0000	1.0000	1.0000	1.0000	1.0000	1.0000	1.0000	1.0000	1.0000	1.0000	1.0000	1.0000
Ni	0.12995	0.00000	1.00000	0.59609	-0.53366	0.08189	-0.78176	0.08637	0.35329	0.01762	-0.65965	0.00000	-0.06637	0.00000	-0.58996	-0.37877	0.26160	0.27759	-0.10463	0.59415
	0.7205	1.0000	0.0000	0.0690	0.1121	0.8221	0.0076	0.8125	0.3166	0.9615	0.0380	1.0000	0.8555	1.0000	0.0726	0.2804	0.4653	0.4374	0.7736	0.0701
Co	0.58996	0.00000	0.59609	1.00000	-0.09171	0.27740	-0.03967	0.18690	0.55480	0.15140	-0.63759	0.00000	-0.31572	0.00000	-0.56185	-0.09045	0.16389	-0.12956	0.12914	0.82442
	0.0726	1.0000	0.0690	0.0000	0.8011	0.4378	0.9134	0.6051	0.0960	0.6763	0.0473	1.0000	0.3742	1.0000	0.0910	0.8038	0.6510	0.7213	0.7222	0.0033
Ga	0.25276	0.00000	-0.53366	-0.09171	1.00000	-0.20780	0.59028	0.27500	0.03332	0.25319	0.33431	0.00000	-0.35703	0.00000	0.00786	0.38338	-0.01522	-0.27602	-0.28898	0.04749
	0.4811	1.0000	0.1121	0.8011	0.0000	0.5646	0.0724	0.4419	0.9272	0.4803	0.3451	1.0000	0.3112	1.0000	0.9828	0.2741	0.9667	0.4401	0.4180	0.8963
Mo	-0.22281	0.00000	0.08189	0.27740	-0.20780	1.00000	-0.04919	0.20000	0.42395	-0.29000	0.11104	0.00000	0.54422	0.00000	0.19144	0.14118	0.41556	0.32755	-0.36674	-0.15710
	0.5361	1.0000	0.8221	0.4378	0.5646	0.0000	0.8926	0.5796	0.2221	0.4163	0.7601	1.0000	0.1039	1.0000	0.5962	0.6972	0.2323	0.3555	0.2972	0.6647
Nb	0.28983	0.00000	-0.78176	-0.03967	0.59028	-0.04919	1.00000	-0.10502	-0.04832	-0.00070	0.34680	0.00000	-0.17499	0.00000	0.38729	0.50620	-0.30393	-0.47239	0.35890	-0.05993
	0.4166	1.0000	0.0076	0.9134	0.0724	0.8926	0.0000	0.7728	0.8945	0.9985	0.3262	1.0000	0.6287	1.0000	0.2688	0.1355	0.3932	0.1680	0.3085	0.8694
Zr	-0.28166	0.00000	0.08637	0.18690	0.27500	0.20000	-0.10502	1.00000	0.68449	0.62150	0.00900	0.00000	0.27103	0.00000	-0.00067	0.43146	0.52676	0.22579	-0.59591	0.11549
	0.4305	1.0000	0.8125	0.6051	0.4419	0.5796	0.7728	0.0000	0.0290	0.0551	0.9803	1.0000	0.4488	1.0000	0.9985	0.2131	0.1177	0.5305	0.0691	0.7507
Y	-0.16567	0.00000	0.35329	0.55480	0.03332	0.42395	-0.04832	0.68449	1.00000	0.25270	-0.38077	0.00000	0.39118	0.00000	-0.00622	0.52211	0.57610	0.04141	-0.32780	0.49960
	0.6474	1.0000	0.3166	0.0960	0.9272	0.2221	0.8945	0.0290	0.0000	0.4812	0.2777	1.0000	0.2637	1.0000	0.9864	0.1216	0.0813	0.9096	0.3551	0.1415
Sr	-0.06332	0.00000	0.01762	0.15140	0.25319	-0.29000	-0.00070	0.62150	0.25270	1.00000	-0.13723	0.00000	-0.29541	0.00000	-0.38589	-0.05256	0.52468	-0.42821	-0.03989	0.07908
	0.8620	1.0000	0.9615	0.6763	0.4803	0.4163	0.9985	0.0551	0.4812	0.0000	0.7054	1.0000	0.4073	1.0000	0.2707	0.8853	0.1195	0.2170	0.9129	0.8281
Rb	-0.41504	0.00000	-0.65965	-0.63759	0.33431	0.11104	0.34680	0.00900	-0.38077	-0.13723	1.00000	0.00000	0.30720	0.00000	0.68382	0.39961	-0.18495	0.31800	-0.10621	-0.67916
	0.2330	1.0000	0.0380	0.0473	0.3451	0.7601	0.3262	0.9803	0.2777	0.7054	0.0000	1.0000	0.3879	1.0000	0.0292	0.2526	0.6090	0.3706	0.7703	0.0308
U	0.00000	0.00000	0.00000	0.00000	0.00000	0.00000	0.00000	0.00000	0.00000	0.00000	0.00000	0.00000	0.00000	0.00000	0.00000	0.00000	0.00000	0.00000	0.00000	0.00000
	1.0000	1.0000	1.0000	1.0000	1.0000	1.0000	1.0000	1.0000	1.0000	1.0000	1.0000	1.0000	1.0000	1.0000	1.0000	1.0000	1.0000	1.0000	1.0000	1.0000
Th	-0.82220	0.00000	-0.06637	-0.31572	-0.35703	0.54422	-0.17499	0.27103	0.39118	-0.29541	0.30720	0.00000	1.00000	0.00000	0.73273	0.51788	0.25799	0.49606	-0.28548	-0.36108
	0.0035	1.0000	0.8555	0.3742	0.3112	0.1039	0.6287	0.4488	0.2637	0.4073	0.3879	1.0000	0.0000	1.0000	0.0159	0.1252	0.4717	0.1448	0.4240	0.3053
Pb	0.00000	0.00000	0.00000	0.00000	0.00000	0.00000	0.00000	0.00000	0.00000	0.00000	0.00000	0.00000	0.00000	0.00000	0.00000	0.00000	0.00000	0.00000	0.00000	0.00000
	1.0000	1.0000	1.0000	1.0000	1.0000	1.0000	1.0000	1.0000	1.0000	1.0000	1.0000	1.0000	1.0000	1.0000	1.0000	1.0000	1.0000	1.0000	1.0000	1.0000
Cr	-0.58149	0.00000	-0.58996	-0.56185	0.00786	0.19144	0.38729	-0.00067	-0.00622	-0.38589	0.68382	0.00000	0.73273	0.00000	1.00000	0.72182	-0.25550	0.32140	0.05833	-0.47807
	0.0779	1.0000	0.0726	0.0910	0.9828	0.5962	0.2688	0.9985	0.9864	0.2707	0.0292	1.0000	0.0159	1.0000	0.0000	0.0184	0.4762	0.3652	0.8728	0.1622
V	-0.31483	0.00000	-0.37877	-0.09045	0.38338	0.14118	0.50620	0.43146	0.52211	-0.05256	0.39961	0.00000	0.51788	0.00000	0.72182	1.00000	-0.02376	0.18222	-0.11930	0.05706
	0.3756	1.0000	0.2804	0.8038	0.2741	0.6972	0.1355	0.2131	0.1216	0.8853	0.2526	1.0000	0.1252	1.0000	0.0184	0.0000	0.9480	0.6144	0.7427	0.8756
Ba	-0.45591	0.00000	0.26160	0.16389	-0.01522	0.41556	-0.30393	0.52676	0.57610	0.52468	-0.18495	0.00000	0.25799	0.00000	-0.25550	-0.02376	1.00000	-0.19650	-0.43821	-0.07930
	0.1854	1.0000	0.4653	0.6510	0.9667	0.2323	0.3932	0.1177	0.0813	0.1195	0.6090	1.0000	0.4717	1.0000	0.4762	0.9480	0.0000	0.5864	0.2053	0.8276
Sc	-0.27327	0.00000	0.27759	-0.12956	-0.27602	0.32755	-0.47239	0.22579	0.04141	-0.42821	0.31800	0.00000	0.49606	0.00000	0.32140	0.18222	-0.19650	1.00000	-0.49360	-0.13031
	0.4449	1.0000	0.4374	0.7213	0.4401	0.3555	0.1680	0.5305	0.9096	0.2170	0.3706	1.0000	0.1448	1.0000	0.3652	0.6144	0.5864	0.0000	0.1471	0.7197
Cl	0.27170	0.00000	-0.10463	0.12914	-0.28898	-0.36674	0.35890	-0.59591	-0.32780	-0.03989	-0.10621	0.00000	-0.28548	0.00000	0.05833	-0.11930	-0.43821	-0.49360	1.00000	0.18475
	0.4476	1.0000	0.7736	0.7222	0.4180	0.2972	0.3085	0.0691	0.3551	0.9129	0.7703	1.0000	0.4240	1.0000	0.8728	0.7427	0.2053	0.1471	0.0000	0.6094
F	0.57744	0.00000	0.59415	0.82442	0.04749	-0.15710	-0.05993	0.11549	0.49960	0.07908	-0.67916	0.00000	-0.36108	0.00000	-0.47807	0.05706	-0.07930	-0.13031	0.18475	1.00000
	0.0805	1.0000	0.0701	0.0033	0.8963	0.6647	0.8694	0.7507	0.1415	0.8281	0.0308	1.0000	0.3053	1.0000	0.1622	0.8756	0.8276	0.7197	0.6094	0.0000

Digitised by the Department of Library Services in support of open access to information, University of Pretoria, 2021.

APPENDIX 23: continued

B E N C H C

	Zn	Cu	Ni	Co	Ga	Mo	Nb	Zr	Y	Sr	Rb	U	Th	Pb	Cr	V	Ba	Sc	Cl	F
Zn	1.00000	0.55938	-0.28211	-0.18574	0.00527	0.30450	0.19470	0.46779	0.19865	0.36116	-0.16689	0.16917	-0.12327	0.00000	-0.24054	0.15774	0.26202	0.00000	0.12843	-0.09090
	0.0000	0.0927	0.4297	0.6074	0.9885	0.3923	0.5899	0.1728	0.5822	0.3052	0.6449	0.6404	0.7344	1.0000	0.5032	0.6634	0.4646	1.0000	0.7236	0.8028
Cu	0.55938	1.00000	-0.21668	0.11574	0.06363	-0.32109	0.12342	0.54519	0.43904	0.33557	-0.37348	-0.32109	-0.03441	0.00000	-0.06010	0.33844	0.20959	0.00000	-0.27676	-0.13285
	0.0927	0.0000	0.5476	0.7502	0.8614	0.3657	0.7341	0.1031	0.2043	0.3432	0.2878	0.3657	0.9248	1.0000	0.8690	0.3388	0.5611	1.0000	0.4389	0.7145
Ni	-0.28211	-0.21668	1.00000	0.72796	-0.65748	0.07061	-0.90563	0.21034	0.56000	0.62718	-0.25472	0.69202	-0.14983	0.00000	0.12676	-0.29370	0.51707	0.00000	-0.06441	-0.10876
	0.4297	0.5476	0.0000	0.0170	0.0388	0.8463	0.0003	0.5597	0.0923	0.0523	0.4776	0.0266	0.6795	1.0000	0.7271	0.4101	0.1259	1.0000	0.8597	0.7649
Co	-0.18574	0.11574	0.72796	1.00000	-0.55403	0.07625	-0.65670	0.65982	0.74615	0.70198	-0.37221	0.17791	0.20427	0.00000	-0.31480	-0.01169	0.59614	0.00000	0.29056	0.34336
	0.6074	0.7502	0.0170	0.0000	0.0966	0.8342	0.0391	0.0379	0.0132	0.0236	0.2895	0.6229	0.5713	1.0000	0.3757	0.9744	0.0689	1.0000	0.4154	0.3314
Ga	0.00527	0.06363	-0.65748	-0.55403	1.00000	-0.25950	0.75049	-0.45865	-0.77225	-0.54517	0.37002	-0.64875	-0.45883	0.00000	0.15862	-0.21292	-0.65284	0.00000	-0.12712	-0.06944
	0.9885	0.8614	0.0388	0.0966	0.0000	0.4691	0.0124	0.1825	0.0088	0.1031	0.2926	0.0424	0.1823	1.0000	0.6616	0.5548	0.0407	1.0000	0.7264	0.8488
Mo	0.30450	-0.32109	0.07061	0.07625	-0.25950	1.00000	0.07340	0.20744	0.15081	0.02600	0.44961	0.33333	0.31255	0.00000	-0.48255	0.14058	0.02349	0.00000	0.46718	0.16165
	0.3923	0.3657	0.8463	0.8342	0.4691	0.0000	0.8403	0.5652	0.6775	0.9432	0.1923	0.3466	0.3793	1.0000	0.1578	0.6985	0.9486	1.0000	0.1734	0.6555
Nb	0.19470	0.12342	-0.90563	-0.65670	0.75049	0.07340	1.00000	-0.23528	-0.61793	-0.72922	0.36208	-0.70956	0.08390	0.00000	-0.19836	0.11933	-0.61156	0.00000	0.12427	0.13886
	0.5899	0.7341	0.0003	0.0391	0.0124	0.8403	0.0000	0.5129	0.0569	0.0167	0.3039	0.0215	0.8178	1.0000	0.5828	0.7427	0.0603	1.0000	0.7323	0.7020
Zr	0.46779	0.54519	0.21034	0.65982	-0.45865	0.20744	-0.23528	1.00000	0.81231	0.71103	-0.60392	-0.00593	0.43380	0.00000	-0.64219	0.20470	0.76108	0.00000	0.51409	0.53413
	0.1728	0.1031	0.5597	0.0379	0.1825	0.5652	0.5129	0.0000	0.0043	0.0211	0.0645	0.9870	0.2104	1.0000	0.0453	0.5705	0.0106	1.0000	0.1285	0.1117
Y	0.19865	0.43904	0.56000	0.74615	-0.77225	0.15081	-0.61793	0.81231	1.00000	0.76715	-0.51143	0.28486	0.40221	0.00000	-0.36871	0.33048	0.74089	0.00000	0.12692	0.19739
	0.5822	0.2043	0.0923	0.0132	0.0088	0.6775	0.0569	0.0043	0.0000	0.0096	0.1308	0.4250	0.2492	1.0000	0.2944	0.3510	0.0142	1.0000	0.7268	0.5847
Sr	0.36116	0.33557	0.62718	0.70198	-0.54517	0.02600	-0.72922	0.71103	0.76715	1.00000	-0.58436	0.45184	-0.09729	0.00000	-0.23594	0.01295	0.79342	0.00000	0.18213	0.13733
	0.3052	0.3432	0.0523	0.0236	0.1031	0.9432	0.0167	0.0211	0.0096	0.0000	0.0761	0.1899	0.7892	1.0000	0.5117	0.9717	0.0062	1.0000	0.6146	0.7052
Rb	-0.16689	-0.37348	-0.25472	-0.37221	0.37002	0.44961	0.36208	-0.60392	-0.51143	-0.58436	1.00000	-0.06423	-0.15830	0.00000	0.22316	0.15564	-0.79897	0.00000	-0.26470	-0.42637
	0.6449	0.2878	0.4776	0.2895	0.2926	0.1923	0.3039	0.0645	0.1308	0.0761	0.0000	0.8601	0.6623	1.0000	0.5354	0.6677	0.0056	1.0000	0.4599	0.2192
U	0.16917	-0.32109	0.69202	0.17791	-0.64875	0.33333	-0.70956	-0.00593	0.28486	0.45184	-0.06423	1.00000	-0.22325	0.00000	0.26809	-0.26839	0.40436	0.00000	-0.10398	-0.37761
	0.6404	0.3657	0.0266	0.6229	0.0424	0.3466	0.0215	0.9870	0.4250	0.1899	0.8601	0.0000	0.5353	1.0000	0.4539	0.4534	0.2464	1.0000	0.7750	0.2820
Th	-0.12327	-0.03441	-0.14983	0.20427	-0.45883	0.31255	0.08390	0.43380	0.40221	-0.09729	-0.15830	-0.22325	1.00000	0.00000	-0.53721	0.40127	0.29932	0.00000	0.50651	0.61703
	0.7344	0.9248	0.6795	0.5713	0.1823	0.3793	0.8178	0.2104	0.2492	0.7892	0.6623	0.5353	0.0000	1.0000	0.1093	0.2504	0.4008	1.0000	0.1352	0.0574
Pb	0.00000	0.00000	0.00000	0.00000	0.00000	0.00000	0.00000	0.00000	0.00000	0.00000	0.00000	0.00000	0.00000	0.00000	0.00000	0.00000	0.00000	0.00000	0.00000	0.00000
	1.0000	1.0000	1.0000	1.0000	1.0000	1.0000	1.0000	1.0000	1.0000	1.0000	1.0000	1.0000	1.0000	1.0000	1.0000	1.0000	1.0000	1.0000	1.0000	1.0000
Cr	-0.24054	-0.06010	0.12676	-0.31480	0.15862	-0.48255	-0.19836	-0.64219	-0.36871	-0.23594	0.22316	0.26809	-0.53721	0.00000	1.00000	-0.40004	-0.27343	0.00000	-0.79433	-0.77489
	0.5032	0.8690	0.7271	0.3757	0.6616	0.1578	0.5828	0.0453	0.2944	0.5117	0.5354	0.4539	0.1093	1.0000	0.0000	0.2520	0.4446	1.0000	0.0061	0.0085
V	0.15774	0.33844	-0.29370	-0.01169	-0.21292	0.14058	0.11933	0.20470	0.33048	0.01295	0.15564	-0.26839	0.40127	0.00000	-0.40004	1.00000	-0.20397	0.00000	-0.09119	-0.02050
	0.6634	0.3388	0.4101	0.9744	0.5548	0.6985	0.7427	0.5705	0.3510	0.9717	0.6677	0.4534	0.2504	1.0000	0.2520	0.0000	0.5719	1.0000	0.8022	0.9552
Ba	0.26202	0.20959	0.51707	0.59614	-0.65284	0.02349	-0.61156	0.76108	0.74089	0.79342	-0.79897	0.40436	0.29932	0.00000	-0.27343	-0.20397	1.00000	0.00000	0.41517	0.43136
	0.4646	0.5611	0.1259	0.0689	0.0407	0.9486	0.0603	0.0106	0.0142	0.0062	0.0056	0.2464	0.4008	1.0000	0.4446	0.5719	0.0000	1.0000	0.2328	0.2132
Sc	0.00000	0.00000	0.00000	0.00000	0.00000	0.00000	0.00000	0.00000	0.00000	0.00000	0.00000	0.00000	0.00000	0.00000	0.00000	0.00000	0.00000	0.00000	0.00000	0.00000
	1.0000	1.0000	1.0000	1.0000	1.0000	1.0000	1.0000	1.0000	1.0000	1.0000	1.0000	1.0000	1.0000	1.0000	1.0000	1.0000	1.0000	1.0000	1.0000	1.0000
Cl	0.12843	-0.27676	-0.06441	0.29056	-0.12712	0.46718	0.12427	0.51409	0.12692	0.18213	-0.26470	-0.10398	0.50651	0.00000	-0.79433	-0.09119	0.41517	0.00000	1.00000	0.90041
	0.7236	0.4389	0.8597	0.4154	0.7264	0.1734	0.7323	0.1285	0.7268	0.6146	0.4599	0.7750	0.1352	1.0000	0.0061	0.8022	0.2328	1.0000	0.0000	0.0004
F	-0.09090	-0.13285	-0.10876	0.34336	-0.06944	0.16165	0.13886	0.53413	0.19739	0.13733	-0.42637	-0.37761	0.61703	0.00000	-0.77489	-0.02050	0.43136	0.00000	0.90041	1.00000
	0.8028	0.7145	0.7649	0.3314	0.8488	0.6555	0.7020	0.1117	0.5847	0.7052	0.2192	0.2820	0.0574	1.0000	0.0085	0.9552	0.2132	1.0000	0.0004	0.0000

Digitised by the Department of Library Services in support of open access to information, University of Pretoria, 2021.

APPENDIX 23: continued

B E N C H D

	Zn	Cu	Ni	Co	Ga	Mo	Nb	Zr	Y	Sr	Rb	U	Th	Pb	Cr	V	Ba	Sc	Cl	F
Zn	1.00000	0.07394	0.08604	0.58533	0.60562	0.44390	0.40761	0.47047	0.20095	0.40363	-0.27143	-0.01040	-0.61334	0.00000	-0.03615	0.00913	0.48532	-0.57679	0.46930	0.73586
	0.0000	0.8391	0.8132	0.0755	0.0635	0.1988	0.2423	0.1700	0.5778	0.2474	0.4481	0.9773	0.0593	1.0000	0.9210	0.9800	0.1551	0.0809	0.1712	0.0153
Cu	0.07394	1.00000	-0.21679	-0.30297	0.18861	-0.63487	-0.05644	-0.14889	-0.37759	0.75547	0.22055	0.08638	-0.13979	0.00000	-0.37981	0.14224	0.76047	-0.18490	0.01798	-0.20759
	0.8391	0.0000	0.5474	0.3948	0.6018	0.0486	0.8769	0.6814	0.2820	0.0115	0.5403	0.8124	0.7001	1.0000	0.2790	0.6951	0.0107	0.6091	0.9607	0.5650
Ni	0.08604	-0.21679	1.00000	0.54947	-0.58632	0.50017	-0.63533	0.28780	0.15324	0.24956	0.22426	0.81420	0.32894	0.00000	-0.00388	0.07760	0.22774	-0.39735	-0.01025	0.06785
	0.8132	0.5474	0.0000	0.0999	0.0748	0.1410	0.0484	0.4200	0.6726	0.4868	0.5334	0.0041	0.3534	1.0000	0.9915	0.8313	0.5269	0.2555	0.9776	0.8523
Co	0.58533	-0.30297	0.54947	1.00000	0.12897	0.84694	-0.04474	0.77635	0.49306	0.22717	-0.25702	0.39061	-0.15006	0.00000	-0.16141	-0.17232	0.21929	-0.60372	0.61670	0.81646
	0.0755	0.3948	0.0999	0.0000	0.7225	0.0020	0.9023	0.0083	0.1476	0.5279	0.4735	0.2644	0.6790	1.0000	0.6560	0.6340	0.5427	0.0646	0.0576	0.0040
Ga	0.60562	0.18861	-0.58632	0.12897	1.00000	0.04454	0.78768	0.18183	0.22086	-0.00936	-0.11624	-0.61989	-0.46726	0.00000	0.09500	-0.26066	0.08565	-0.22196	0.23773	0.59011
	0.0635	0.6018	0.0748	0.7225	0.0000	0.9028	0.0068	0.6151	0.5398	0.9795	0.7491	0.0559	0.1733	1.0000	0.7940	0.4670	0.8140	0.5377	0.5084	0.0725
Mo	0.44390	-0.63487	0.50017	0.84694	0.04454	1.00000	0.15707	0.65466	0.47751	-0.21083	-0.04690	0.26356	0.04496	0.00000	0.03962	-0.08496	-0.15634	-0.34234	0.29244	0.72889
	0.1988	0.0486	0.1410	0.0020	0.9028	0.0000	0.6648	0.0400	0.1628	0.5588	0.8976	0.4619	0.9019	1.0000	0.9135	0.8155	0.6662	0.3329	0.4122	0.0168
Nb	0.40761	-0.05644	-0.63533	-0.04474	0.78768	0.15707	1.00000	0.22844	0.23109	-0.31522	0.07999	-0.61649	-0.24769	0.00000	0.34291	0.01179	-0.20874	0.00000	-0.10092	0.45363
	0.2423	0.8769	0.0484	0.9023	0.0068	0.6648	0.0000	0.5256	0.5206	0.3750	0.8261	0.0577	0.4902	1.0000	0.3320	0.9742	0.5628	1.0000	0.7815	0.1879
Zr	0.47047	-0.14889	0.28780	0.77635	0.18183	0.65466	0.22844	1.00000	0.74460	0.26527	-0.14425	0.41712	0.03871	0.00000	0.06483	0.16618	0.24336	-0.66732	0.38382	0.78406
	0.1700	0.6814	0.4200	0.0083	0.6151	0.0400	0.5256	0.0000	0.0135	0.4589	0.6909	0.2304	0.9154	1.0000	0.8588	0.6464	0.4981	0.0350	0.2735	0.0073
Y	0.20095	-0.37759	0.15324	0.49306	0.22086	0.47751	0.23109	0.74460	1.00000	-0.13193	-0.03450	0.27248	0.30018	0.00000	0.32062	-0.02132	-0.09974	-0.43350	0.02407	0.63803
	0.5778	0.2820	0.6726	0.1476	0.5398	0.1628	0.5206	0.0135	0.0000	0.7164	0.9246	0.4463	0.3994	1.0000	0.3664	0.9534	0.7840	0.2107	0.9474	0.0471
Sr	0.40363	0.75547	0.24956	0.22717	-0.00936	-0.21083	-0.31522	0.26527	-0.13193	1.00000	-0.11977	0.50696	-0.29617	0.00000	-0.45614	0.20672	0.96252	-0.52332	0.39101	0.11023
	0.2474	0.0115	0.4868	0.5279	0.9795	0.5588	0.3750	0.4589	0.7164	0.0000	0.7417	0.1348	0.4060	1.0000	0.1852	0.5666	0.0001	0.1206	0.2639	0.7618
Rb	-0.27143	0.22055	0.22426	-0.25702	-0.11624	-0.04690	0.07999	-0.14425	-0.03450	-0.11977	1.00000	0.22241	0.67955	0.00000	0.22700	0.13622	0.00207	0.02342	-0.78748	-0.24385
	0.4481	0.5403	0.5334	0.4735	0.7491	0.8976	0.8261	0.6909	0.9246	0.7417	0.0000	0.5368	0.0307	1.0000	0.5283	0.7075	0.9955	0.9488	0.0068	0.4972
U	-0.01040	0.08638	0.81420	0.39061	-0.61989	0.26356	-0.61649	0.41712	0.27248	0.50696	0.22241	1.00000	0.41492	0.00000	-0.22925	0.26836	0.50580	-0.38795	-0.03796	0.05201
	0.9773	0.8124	0.0041	0.2644	0.0559	0.4619	0.0577	0.2304	0.4463	0.1348	0.5368	0.0000	0.2331	1.0000	0.5241	0.4534	0.1358	0.2680	0.9171	0.8865
Th	-0.61334	-0.13979	0.32894	-0.15006	-0.46726	0.04496	-0.24769	0.03871	0.30018	-0.29617	0.67955	0.41492	1.00000	0.00000	0.19916	0.32833	-0.26830	-0.05842	-0.59944	-0.26702
	0.0593	0.7001	0.3534	0.6790	0.1733	0.9019	0.4902	0.9154	0.3994	0.4060	0.0307	0.2331	0.0000	1.0000	0.5812	0.3543	0.4535	0.8727	0.0670	0.4558
Pb	0.00000	0.00000	0.00000	0.00000	0.00000	0.00000	0.00000	0.00000	0.00000	0.00000	0.00000	0.00000	0.00000	0.00000	0.00000	0.00000	0.00000	0.00000	0.00000	0.00000
	1.0000	1.0000	1.0000	1.0000	1.0000	1.0000	1.0000	1.0000	1.0000	1.0000	1.0000	1.0000	1.0000	1.0000	1.0000	1.0000	1.0000	1.0000	1.0000	1.0000
Cr	-0.03615	-0.37981	-0.00388	-0.16141	0.09500	0.03962	0.34291	0.06483	0.32062	-0.45614	0.22700	-0.22925	0.19916	0.00000	1.00000	0.15061	-0.51059	-0.09232	-0.52513	-0.11215
	0.9210	0.2790	0.9915	0.6560	0.7940	0.9135	0.3320	0.8588	0.3664	0.1852	0.5283	0.5241	0.5812	1.0000	0.0000	0.6779	0.1315	0.7998	0.1191	0.7577
V	0.00913	0.14224	0.07760	-0.17232	-0.26066	-0.08496	0.01179	0.16618	-0.02132	0.20672	0.13622	0.26836	0.32833	0.00000	0.15061	1.00000	0.18030	-0.43466	-0.15543	-0.18729
	0.9800	0.6951	0.8313	0.6340	0.4670	0.8155	0.9742	0.6464	0.9534	0.5666	0.7075	0.4534	0.3543	1.0000	0.6779	0.0000	0.6182	0.2094	0.6681	0.6044
Ba	0.48532	0.76047	0.22774	0.21929	0.08565	-0.15634	-0.20874	0.24336	-0.09974	0.96252	0.00207	0.50580	-0.26830	0.00000	-0.51059	0.18030	1.00000	-0.49118	0.30199	0.19321
	0.1551	0.0107	0.5269	0.5427	0.8140	0.6662	0.5628	0.4981	0.7840	0.0001	0.9955	0.1358	0.4535	1.0000	0.1315	0.6182	0.0000	0.1494	0.3964	0.5928
Sc	-0.57679	-0.18490	-0.39735	-0.60372	-0.22196	-0.34234	0.00000	-0.66732	-0.43350	-0.52332	0.02342	-0.38795	-0.05842	0.00000	-0.09232	-0.43466	-0.49118	1.00000	-0.35743	-0.52306
	0.0809	0.6091	0.2555	0.0646	0.5377	0.3329	1.0000	0.0350	0.2107	0.1206	0.9488	0.2680	0.8727	1.0000	0.7998	0.2094	0.1494	0.0000	0.3106	0.1208
Cl	0.46930	0.01798	-0.01025	0.61670	0.23773	0.29244	-0.10092	0.38382	0.02407	0.39101	-0.78748	-0.03796	-0.59944	0.00000	-0.52513	-0.15543	0.30199	-0.35743	1.00000	0.53077
	0.1712	0.9607	0.9776	0.0576	0.5084	0.4122	0.7815	0.2735	0.9474	0.2639	0.0068	0.9171	0.0670	1.0000	0.1191	0.6681	0.3964	0.3106	0.0000	0.1144
F	0.73586	-0.20759	0.06785	0.81646	0.59011	0.72889	0.45363	0.78406	0.63803	0.11023	-0.24385	0.05201	-0.26702	0.00000	-0.11215	-0.18729	0.19321	-0.52306	0.53077	1.00000
	0.0153	0.5650	0.8523	0.0040	0.0725	0.0168	0.1879	0.0073	0.0471	0. [illegible]	0.4972	0.8865	0.4558	1.0000	0.7577	0.6044	0.5928	0.1208	0.1144	0.0000

Digitised by the Department of Library Services in support of open access to information, University of Pretoria, 2021.

APPENDIX 23: continued

B E N C H E

	Zn	Cu	Ni	Co	Ga	Mo	Nb	Zr	Y	Sr	Rb	U	Th	Pb	Cr	V	Ba	Sc	Cl	F
Zn	1.00000	0.35216	0.47211	0.61604	-0.08087	0.29513	-0.26001	0.64349	0.39219	0.71685	-0.54736	0.65470	-0.18751	-0.64765	0.09888	-0.23790	0.58323	-0.36930	0.47218	0.55169
	0.0000	0.3183	0.1683	0.0579	0.8242	0.4078	0.4681	0.0447	0.2623	0.0196	0.1015	0.0399	0.6039	0.0429	0.7858	0.5081	0.0768	0.2936	0.1682	0.0983
Cu	0.35216	1.00000	-0.22223	-0.01418	0.34426	-0.62067	-0.06386	0.20453	-0.06636	0.47368	-0.14022	0.27407	-0.47597	-0.15802	0.43178	-0.54871	0.43741	0.57285	-0.19130	-0.05529
	0.3183	0.0000	0.5372	0.9690	0.3300	0.0555	0.8609	0.5708	0.8555	0.1667	0.6992	0.4435	0.1644	0.6628	0.2127	0.1005	0.2062	0.0835	0.5965	0.8794
Ni	0.47211	-0.22223	1.00000	0.73540	-0.64066	0.74574	-0.69310	0.52057	0.76789	0.59749	-0.10336	0.81161	0.25682	-0.30800	-0.34335	0.20760	0.60698	-0.35411	0.78321	0.62482
	0.1683	0.5372	0.0000	0.0154	0.0460	0.0133	0.0263	0.1229	0.0095	0.0681	0.7763	0.0044	0.4738	0.3866	0.3314	0.5650	0.0628	0.3154	0.0074	0.0534
Co	0.61604	-0.01418	0.73540	1.00000	-0.03510	0.63490	-0.28747	0.82300	0.61275	0.63219	-0.58155	0.61374	0.12663	-0.74295	-0.10329	0.09826	0.56743	-0.56234	0.83386	0.92029
	0.0579	0.9690	0.0154	0.0000	0.9233	0.0486	0.4206	0.0034	0.0596	0.0499	0.0778	0.0591	0.7274	0.0138	0.7765	0.7871	0.0871	0.0906	0.0027	0.0002
Ga	-0.08087	0.34426	-0.64066	-0.03510	1.00000	-0.49980	0.81827	0.15954	-0.50851	-0.29147	-0.31475	-0.58358	-0.13931	-0.33518	0.31186	-0.30695	-0.35319	-0.01272	-0.27387	0.03508
	0.8242	0.3300	0.0460	0.9233	0.0000	0.1413	0.0038	0.6598	0.1334	0.4139	0.3757	0.0765	0.7011	0.3438	0.3804	0.3883	0.3168	0.9722	0.4439	0.9234
Mo	0.29513	-0.62067	0.74574	0.63490	-0.49980	1.00000	-0.34947	0.34055	0.47467	0.15988	-0.23053	0.45245	0.36517	-0.32733	-0.34196	0.67428	0.07997	-0.77678	0.70661	0.63558
	0.4078	0.0555	0.0133	0.0486	0.1413	0.0000	0.3223	0.3356	0.1657	0.6591	0.5217	0.1892	0.2995	0.3559	0.3335	0.0325	0.8262	0.0082	0.0223	0.0483
Nb	-0.26001	-0.06386	-0.69310	-0.28747	0.81827	-0.34947	1.00000	0.00000	-0.49382	-0.70956	0.02530	-0.83788	0.18859	-0.07982	0.28438	-0.10171	-0.74017	-0.11953	-0.52016	-0.09213
	0.4681	0.8609	0.0263	0.4206	0.0038	0.3223	0.0000	1.0000	0.1469	0.0215	0.9447	0.0025	0.6018	0.8265	0.4258	0.7798	0.0144	0.7422	0.1233	0.8002
Zr	0.64349	0.20453	0.52057	0.82300	0.15954	0.34055	0.00000	1.00000	0.69064	0.46386	-0.41895	0.40751	0.36869	-0.77519	0.01618	-0.24129	0.45554	-0.34084	0.46396	0.84507
	0.0447	0.5708	0.1229	0.0034	0.6598	0.3356	1.0000	0.0000	0.0270	0.1769	0.2282	0.2424	0.2945	0.0084	0.9646	0.5019	0.1858	0.3352	0.1768	0.0021
Y	0.39219	-0.06636	0.76789	0.61275	-0.50851	0.47467	-0.49382	0.69064	1.00000	0.49407	0.05461	0.61141	0.51728	-0.22972	-0.07383	-0.06368	0.59417	-0.06110	0.37154	0.65160
	0.2623	0.8555	0.0095	0.0596	0.1334	0.1657	0.1469	0.0270	0.0000	0.1467	0.8809	0.0604	0.1257	0.5232	0.8394	0.8613	0.0701	0.8668	0.2905	0.0412
Sr	0.71685	0.47368	0.59749	0.63219	-0.29147	0.15988	-0.70956	0.46386	0.49407	1.00000	-0.46533	0.86678	-0.40426	-0.41171	0.02816	-0.28579	0.96209	0.01127	0.61132	0.43047
	0.0196	0.1667	0.0681	0.0499	0.4139	0.6591	0.0215	0.1769	0.1467	0.0000	0.1753	0.0012	0.2466	0.2371	0.9384	0.4234	0.0001	0.9753	0.0604	0.2143
Rb	-0.54736	-0.14022	-0.10336	-0.58155	-0.31475	-0.23053	0.02530	-0.41895	0.05461	-0.46533	1.00000	-0.20219	0.29950	0.84515	0.24005	0.13153	-0.33052	0.59947	-0.60431	-0.39872
	0.1015	0.6992	0.7763	0.0778	0.3757	0.5217	0.9447	0.2282	0.8809	0.1753	0.0000	0.5753	0.4005	0.0021	0.5041	0.7172	0.3509	0.0670	0.0642	0.2537
U	0.65470	0.27407	0.81161	0.61374	-0.58358	0.45245	-0.83788	0.40751	0.61141	0.86678	-0.20219	1.00000	-0.16485	-0.25253	-0.05662	0.07834	0.80990	-0.06390	0.64259	0.48834
	0.0399	0.4435	0.0044	0.0591	0.0765	0.1892	0.0025	0.2424	0.0604	0.0012	0.5753	0.0000	0.6490	0.4815	0.8765	0.8297	0.0045	0.8608	0.0451	0.1521
Th	-0.18751	-0.47597	0.25682	0.12663	-0.13931	0.36517	0.18859	0.36869	0.51728	-0.40426	0.29950	-0.16485	1.00000	-0.06562	-0.34900	0.13405	-0.29982	-0.20171	-0.07363	0.32704
	0.6039	0.1644	0.4738	0.7274	0.7011	0.2995	0.6018	0.2945	0.1257	0.2466	0.4005	0.6490	0.0000	0.8571	0.3229	0.7120	0.4000	0.5763	0.8398	0.3563
Pb	-0.64765	-0.15802	-0.30800	-0.74295	-0.33518	-0.32733	-0.07982	-0.77519	-0.22972	-0.41171	0.84515	-0.25253	-0.06562	1.00000	0.27750	0.20967	-0.31823	0.62173	-0.62788	-0.62037
	0.0429	0.6628	0.3866	0.0138	0.3438	0.3559	0.8265	0.0084	0.5232	0.2371	0.0021	0.4815	0.8571	0.0000	0.4376	0.5610	0.3702	0.0550	0.0519	0.0557
Cr	0.09888	0.43178	-0.34335	-0.10329	0.31186	-0.34196	0.28438	0.01618	-0.07383	0.02816	0.24005	-0.05662	-0.34900	0.27750	1.00000	0.01238	-0.02651	0.36407	-0.45653	0.10485
	0.7858	0.2127	0.3314	0.7765	0.3804	0.3335	0.4258	0.9646	0.8394	0.9384	0.5041	0.8765	0.3229	0.4376	0.0000	0.9729	0.9421	0.3010	0.1847	0.7731
V	-0.23790	-0.54871	0.20760	0.09826	-0.30695	0.67428	-0.10171	-0.24129	-0.06368	-0.28579	0.13153	0.07834	0.13405	0.20967	0.01238	1.00000	-0.40014	-0.43559	0.21959	0.21793
	0.5081	0.1005	0.5650	0.7871	0.3883	0.0325	0.7798	0.5019	0.8613	0.4234	0.7172	0.8297	0.7120	0.5610	0.9729	0.0000	0.2519	0.2083	0.5421	0.5453
Ba	0.58323	0.43741	0.60698	0.56743	-0.35319	0.07997	-0.74017	0.45554	0.59417	0.96209	-0.33052	0.80990	-0.29982	-0.31823	-0.02651	-0.40014	1.00000	0.15260	0.54196	0.35433
	0.0768	0.2062	0.0628	0.0871	0.3168	0.8262	0.0144	0.1858	0.0701	0.0001	0.3509	0.0045	0.4000	0.3702	0.9421	0.2519	0.0000	0.6739	0.1056	0.3151
Sc	-0.36930	0.57285	-0.35411	-0.56234	-0.01272	-0.77678	-0.11953	-0.34084	-0.06110	0.01127	0.59947	-0.06390	-0.20171	0.62173	0.36407	-0.43559	0.15260	1.00000	-0.62662	-0.53055
	0.2936	0.0835	0.3154	0.0906	0.9722	0.0082	0.7422	0.3352	0.8668	0.9753	0.0670	0.8608	0.5763	0.0550	0.3010	0.2083	0.6739	0.0000	0.0525	0.1146
Cl	0.47218	-0.19130	0.78321	0.83386	-0.27387	0.70661	-0.52016	0.46396	0.37154	0.61132	-0.60431	0.64259	-0.07363	-0.62788	-0.45653	0.21959	0.54196	-0.62662	1.00000	0.59681
	0.1682	0.5965	0.0074	0.0027	0.4439	0.0223	0.1233	0.1768	0.2905	0.0604	0.0642	0.0451	0.8398	0.0519	0.1847	0.5421	0.1056	0.0525	0.0000	0.0685
F	0.55169	-0.05529	0.62482	0.92029	0.03508	0.63558	-0.09213	0.84507	0.65160	0.43047	-0.39872	0.48834	0.32704	-0.62037	0.10485	0.21793	0.35433	-0.53055	0.59681	1.00000
	0.0983	0.8794	0.0534	0.0002	0.9234	0.0483	0.8002	0.0021	0.0412	0.2143	0.2537	0.1521	0.3563	0.0557	0.7731	0.5453	0.3151	0.1146	0.0685	0.0000

Digitised by the Department of Library Services in support of open access to information, University of Pretoria, 2021.

APPENDIX 23: continued

BENCH F

	Zn	Cu	Ni	Co	Ga	Mo	Nb	Zr	Y	Sr	Rb	U	Th	Pb	Cr	V	Ba	Sc	Cl	F
Zn	1.00000	-0.15082	-0.10847	0.12420	-0.12192	0.04392	0.07029	0.14454	0.31029	0.28582	-0.20584	0.03906	0.06933	-0.41462	0.26934	0.32456	0.22087	0.35550	0.48543	0.26207
	0.0000	0.7215	0.7982	0.7695	0.7736	0.9177	0.8686	0.7327	0.4545	0.4926	0.6248	0.9268	0.8704	0.3071	0.5189	0.4328	0.5991	0.3875	0.2227	0.5307
Cu	-0.15082	1.00000	0.26644	-0.19759	0.22683	-0.32149	0.09277	-0.08357	-0.17229	0.50366	0.26069	-0.20966	-0.24598	-0.21262	0.00978	-0.31128	0.35771	0.15570	-0.16465	-0.10548
	0.7215	0.0000	0.5236	0.6391	0.5891	0.4375	0.8271	0.8440	0.6833	0.2032	0.5329	0.6183	0.5570	0.6132	0.9817	0.4530	0.3843	0.7127	0.6968	0.8037
Ni	-0.10847	0.26644	1.00000	0.83391	-0.19937	0.75061	-0.04998	0.05581	0.12943	0.71054	-0.42447	0.79292	0.54505	-0.43181	0.05605	0.09591	0.76504	0.17272	0.50375	0.17716
	0.7982	0.5236	0.0000	0.0101	0.6360	0.0319	0.9064	0.8956	0.7600	0.0482	0.2945	0.0189	0.1624	0.2854	0.8951	0.8213	0.0270	0.6825	0.2031	0.6747
Co	0.12420	-0.19759	0.83391	1.00000	-0.10423	0.96089	0.19340	0.38437	0.51874	0.58542	-0.60430	0.76385	0.82918	-0.47770	0.28525	0.51233	0.59525	0.27962	0.77542	0.52818
	0.7695	0.6391	0.0101	0.0000	0.8060	0.0001	0.6463	0.3471	0.1878	0.1273	0.1126	0.0274	0.0109	0.2312	0.4935	0.1942	0.1195	0.5024	0.0238	0.1784
Ga	-0.12192	0.22683	-0.19937	-0.10423	1.00000	-0.17485	0.81980	0.49119	0.45516	0.27598	-0.07137	-0.67728	0.27455	0.05821	0.14576	0.20811	-0.11080	-0.23519	0.07067	0.54627
	0.7736	0.5891	0.6360	0.8060	0.0000	0.6788	0.0127	0.2164	0.2571	0.5082	0.8666	0.0650	0.5105	0.8911	0.7305	0.6209	0.7939	0.5750	0.8679	0.1613
Mo	0.04392	-0.32149	0.75061	0.96089	-0.17485	1.00000	0.18650	0.45885	0.54282	0.45060	-0.66489	0.75490	0.74092	-0.42745	0.32313	0.57023	0.47975	0.26245	0.79499	0.54541
	0.9177	0.4375	0.0319	0.0001	0.6788	0.0000	0.6583	0.2528	0.1645	0.2625	0.0720	0.0304	0.0355	0.2908	0.4350	0.1400	0.2290	0.5300	0.0184	0.1621
Nb	0.07029	0.09277	-0.04998	0.19340	0.81980	0.18650	1.00000	0.82349	0.82793	0.33536	-0.16929	-0.46290	0.49395	-0.08284	0.65383	0.70215	0.09864	0.20341	0.49230	0.85841
	0.8686	0.8271	0.9064	0.6463	0.0127	0.6583	0.0000	0.0120	0.0111	0.4168	0.6886	0.2481	0.2135	0.8454	0.0786	0.0522	0.8162	0.6290	0.2152	0.0064
Zr	0.14454	-0.08357	0.05581	0.38437	0.49119	0.45885	0.82349	1.00000	0.95296	0.30925	-0.43728	-0.18274	0.50506	-0.46714	0.65969	0.84337	-0.04863	0.44353	0.68482	0.95944
	0.7327	0.8440	0.8956	0.3471	0.2164	0.2528	0.0120	0.0000	0.0003	0.4561	0.2786	0.6649	0.2017	0.2432	0.0751	0.0085	0.9090	0.2710	0.0609	0.0002
Y	0.31029	-0.17229	0.12943	0.51874	0.45516	0.54282	0.82793	0.95296	1.00000	0.35710	-0.40424	-0.07112	0.67891	-0.44875	0.73684	0.92989	0.10047	0.51364	0.77297	0.98313
	0.4545	0.6833	0.7600	0.1878	0.2571	0.1645	0.0111	0.0003	0.0000	0.3852	0.3206	0.8671	0.0641	0.2647	0.0370	0.0008	0.8129	0.1929	0.0245	0.0001
Sr	0.28582	0.50366	0.71054	0.58542	0.27598	0.45060	0.33536	0.30925	0.35710	1.00000	-0.56157	0.28449	0.39085	-0.62255	0.11689	0.15057	0.71824	0.10449	0.64450	0.46097
	0.4926	0.2032	0.0482	0.1273	0.5082	0.2625	0.4168	0.4561	0.3852	0.0000	0.1475	0.4947	0.3384	0.0993	0.7828	0.7219	0.0448	0.8055	0.0845	0.2503
Rb	-0.20584	0.26069	-0.42447	-0.60430	-0.07137	-0.66489	-0.16929	-0.43728	-0.40424	-0.56157	1.00000	-0.38259	-0.30090	0.56538	0.11807	-0.23063	-0.19187	0.21250	-0.71494	-0.50492
	0.6248	0.5329	0.2945	0.1126	0.8666	0.0720	0.6886	0.2786	0.3206	0.1475	0.0000	0.3496	0.4689	0.1442	0.7807	0.5827	0.6490	0.6134	0.0462	0.2019
U	0.03906	-0.20966	0.79292	0.76385	-0.67728	0.75490	-0.46290	-0.18274	-0.07112	0.28449	-0.38259	1.00000	0.38878	-0.31204	-0.06695	0.04809	0.53360	0.17474	0.39755	-0.09380
	0.9268	0.6183	0.0189	0.0274	0.0650	0.0304	0.2481	0.6649	0.8671	0.4947	0.3496	0.0000	0.3412	0.4518	0.8748	0.9100	0.1732	0.6790	0.3294	0.8251
Th	0.06933	-0.24598	0.54505	0.82918	0.27455	0.74092	0.49395	0.50506	0.67891	0.39085	-0.30090	0.38878	1.00000	-0.27599	0.42080	0.65099	0.36255	0.31663	0.59259	0.66337
	0.8704	0.5570	0.1624	0.0109	0.5105	0.0355	0.2135	0.2017	0.0641	0.3384	0.4689	0.3412	0.0000	0.5082	0.2992	0.0804	0.3774	0.4448	0.1216	0.0729
Pb	-0.41462	-0.21262	-0.43181	-0.47770	0.05821	-0.42745	-0.08284	-0.46714	-0.44875	-0.62255	0.56538	-0.31204	-0.27599	1.00000	-0.07081	-0.26822	-0.13040	-0.46620	-0.55495	-0.48002
	0.3071	0.6132	0.2854	0.2312	0.8911	0.2908	0.8454	0.2432	0.2647	0.0993	0.1442	0.4518	0.5082	0.0000	0.8677	0.5207	0.7583	0.2443	0.1534	0.2287
Cr	0.26934	0.00978	0.05605	0.28525	0.14576	0.32313	0.65383	0.65969	0.73684	0.11689	0.11807	-0.06695	0.42080	-0.07081	1.00000	0.87815	0.30751	0.74141	0.56096	0.64455
	0.5189	0.9817	0.8951	0.4935	0.7305	0.4350	0.0786	0.0751	0.0370	0.7828	0.7807	0.8748	0.2992	0.8677	0.0000	0.0041	0.4587	0.0353	0.1480	0.0845
V	0.32456	-0.31128	0.09591	0.51233	0.20811	0.57023	0.70215	0.84337	0.92989	0.15057	-0.23063	0.04809	0.65099	-0.26822	0.87815	1.00000	0.14790	0.63966	0.74180	0.85690
	0.4328	0.4530	0.8213	0.1942	0.6209	0.1400	0.0522	0.0085	0.0008	0.7219	0.5827	0.9100	0.0804	0.5207	0.0041	0.0000	0.7267	0.0876	0.0351	0.0066
Ba	0.22087	0.35771	0.76504	0.59525	-0.11080	0.47975	0.09864	-0.04863	0.10047	0.71824	-0.19187	0.53360	0.36255	-0.13040	0.30751	0.14790	1.00000	0.17436	0.53342	0.12544
	0.5991	0.3843	0.0270	0.1195	0.7939	0.2290	0.8162	0.9090	0.8129	0.0448	0.6490	0.1732	0.3774	0.7583	0.4587	0.7267	0.0000	0.6796	0.1734	0.7672
Sc	0.35550	0.15570	0.17272	0.27962	-0.23519	0.26245	0.20341	0.44353	0.5[illegible]364	0.10449	0.21250	0.17474	0.31663	-0.46620	0.74141	0.63966	0.17436	1.00000	0.37242	0.39185
	0.3875	0.7127	0.6825	0.5024	0.5750	0.5300	0.6290	0.2710	0.[illegible]929	0.8055	0.6134	0.6790	0.4448	0.2443	0.0353	0.0876	0.6796	0.0000	0.3636	0.3370
Cl	0.48543	-0.16465	0.50375	0.77542	0.07067	0.79499	0.49230	0.68482	0.7[illegible]297	0.64450	-0.71494	0.39755	0.59259	-0.55495	0.56096	0.74180	0.53342	0.37242	1.00000	0.78543
	0.2227	0.6968	0.2031	0.0238	0.8679	0.0184	0.2152	0.0609	0.0245	0.0845	0.0462	0.3294	0.1216	0.1534	0.1480	0.0351	0.1734	0.3636	0.0000	0.0209
F	0.26207	-0.10548	0.17716	0.52818	0.54627	0.54541	0.85841	0.95944	0.98313	0.46097	-0.50492	-0.09380	0.66337	-0.48002	0.64455	0.85690	0.12544	0.39185	0.78543	1.00000
	0.5307	0.8037	0.6747	0.1784	0.1613	0.1621	0.0064	0.0002	0.0001	0.2503	0.2019	0.8251	0.0729	0.2287	0.0845	0.0066	0.7672	0.3370	0.0209	0.0000

Digitised by the Department of Library Services in support of open access to information, University of Pretoria, 2021.